

A STUDY OF THE INFLUENCE OF ROLLING GEOMETRY UPON  
TEXTURE AND DRAWABILITY OF RIMMED STEEL STRIP

by

ISMAIL HAMED GADO B.Sc., M.Sc.

OCTOBER 1976

Submitted for the degree of Doctor of  
Philosophy of the University of Aston  
in Birmingham.

621.77123 GAD  
212805 11 JAN 1978

## SYNOPSIS

The influence of seven different rolling schedules upon R values and textures of cold rolled and of subsequently annealed rimmed steel strip has been studied. The effect of increasing the annealing time upon R value and texture was also examined. R value measured in a tensile test was related to the corresponding texture determined by inverse and (110) pole figures.

The seven rolling schedules consisted of three constant roll gap schedules, in which roll gaps of 0.001 in/pass, 0.005 in/pass and 0.02 in/pass were kept constant during the cold rolling process. The other three rolling schedules involved constant geometry and were designed to maintain constant shear plane angles of  $55^\circ$ ,  $45^\circ$  and  $35^\circ$  to the strip surface, from one pass to the next. The seventh rolling schedule represented a pendulum mill schedule.

Measurements of R values revealed that R values of the cold rolled materials were very low but improved after annealing. The longer the annealing time the more the R values became dependent upon the rolling schedules and total rolling reductions. However, after 6 hrs annealing, R values of strips previously cold rolled using constant roll gap schedules increased with the magnitude of the roll gap and with the total rolling reduction to a maximum and thereafter decreased. On the other hand, R values of corresponding strips cold rolled using controlled geometry schedules increased with decreasing the shear plane angle and remained constant when the total rolling reduction was increased. R values of equivalent strips cold rolled by the pendulum rolling schedule decreased with increasing the total rolling reductions.

The cold rolling textures observed were typical of b.c.c. iron with  $\langle 110 \rangle$  direction parallel to the rolling direction and  $\{111\}$  planes parallel to the rolling plane. For a given total rolling reduction, intensities of the  $\{100\}$  and  $\{111\}$  planes were dependent upon the rolling schedules and total rolling reduction. Rolling with constant roll gap was associated with a decrease in the  $\{100\}$  intensity and an increase in the  $\{111\}$  intensity with increasing the total rolling reduction up to certain reduction then increased and decreased respectively. The total rolling reduction corresponding to the minimum  $\{100\}$  and maximum  $\{111\}$  intensities increased with increasing the magnitude of roll gap. As a result of rolling with constant geometry schedules, intensity of the  $\{100\}$  and  $\{111\}$  planes remained constant with increasing the rolling reduction but their intensities increased and decreased respectively with increasing the shear plane angle. When rolling on the pendulum mill, intensities of the  $\{100\}$  and  $\{111\}$  planes increased and decreased respectively with increasing the total rolling reduction.

Annealing for 0.5 hr was associated with a significant decrease in the  $\{100\}$  and  $\{111\}$  intensities. Increasing the annealing time resulted in a further decrease in the  $\{100\}$  intensity and an increase in the  $\{111\}$  intensity. The relative intensities of the  $\{100\}$  and  $\{111\}$  planes varied with the rolling schedules and with increasing the total rolling reduction in the same manner as for the cold rolled material already described.

## CONTENTS

	Page
1. INTRODUCTION	1
2. LITERATURE REVIEW	
2.1 The geometry of cold rolling	4
2.2 Theories of cold rolling texture formation in b.c.c. polycrystalline metals	7
2.3 Theories of annealing texture formation in b.c.c. polycrystalline metals	12
2.4 The relationship between texture and R value	15
2.5 The relationship between R value and the L.D.R.	22
2.6 Effects of the processing factors upon texture and R value	
2.6.1 The effect of hot rolling	26
2.6.2 The effect of cold rolling	29
2.6.3 The effect of subcritical isothermal annealing	33
3. SCOPE OF THE PRESENT STUDY	38
4. EXPERIMENTAL PROCEDURE	
4.1 Introduction	40
4.2 Cold rolling	40
4.2.1 The constant geometry schedules	41
4.2.2 The constant roll gap schedules	43
4.2.3 The pendulum schedule	45
4.3 Annealing of the cold rolled strips	47
4.4 Measurement of R value	48
4.5 Examination of preferred orientation	51
4.5.1 Direct pole figures	52
4.5.2 Inverse pole figures	54

	Page
5. EXPERIMENTAL RESULTS	
5.1 Introduction	59
5.2 Examination of the initial material	59
5.3 Measurement of R value	
5.3.1 The cold rolled materials	63
5.3.2 The annealed materials	64
5.4 Examination of texture	
5.4.1 The cold rolled materials	67
5.4.2 The annealed materials	75
5.5 Crystal Reorientation after tensile extension	82
6. DISCUSSION	
6.1 Introduction	94
6.2 Texture of the initial material	94
6.3 The effect of cold rolling procedures upon the development of cold rolling textures	97
6.4 The effect of cold rolling textures and annealing time upon the development of the annealing texture	102
6.5 The relationship between processing texture and R value	104
6.6 The relationship between crystal reorientation after tensile extension and R value	110
6.7 The cold rolling geometry	120
7. SUMMARY AND CONCLUSIONS	124
8. APPENDICES	
REFERENCES	
ACKNOWLEDGEMENTS	

## 1. INTRODUCTION

It is generally known that deep drawability of steel sheets depends upon the number, nature and distribution of non-metallic inclusions which arise during smelting and casting operations. These considerations are excluded in the case of rimmed steel which is the material to be studied in the present project. However, there are still a number of possibilities influencing the deep drawing capacity of the final strip in hot rolling, cold rolling and annealing. It is of interest to this project to establish to what degree cold rolling and annealing may influence texture and R value of rimmed steel strip.

Deep drawability of rimmed steel strip is governed by anisotropic behaviour originating from crystallographic preferred orientation. The degree of plastic anisotropy is measured by the strain ratio or R value. A high strain ratio is indicative of good deep drawing capacity and vice-versa. Good drawability is associated with high intensities of {111} planes and low intensities of {100} planes parallel to the strip surface. It is to be expected that the increase in R value corresponds to a similar increase in the {111} texture intensity. On the contrary, it was reported<sup>(1)</sup> that R value of rimmed steel strip increased to a maximum at 70% total reduction, thereafter decreased with further rolling reduction, while intensity of the {111} planes continued to increase as shown in fig. 1.1 and fig. 1.2. Recently<sup>(2)</sup>, it was shown that R value of rimmed steel strip increased when rolling with constant heavy draughts and by increasing the total rolling reduction to a maximum at 75% then decreased. The reduction in R value after 75% total reduction was related to the reduction in the {111}/{100} relative intensities.

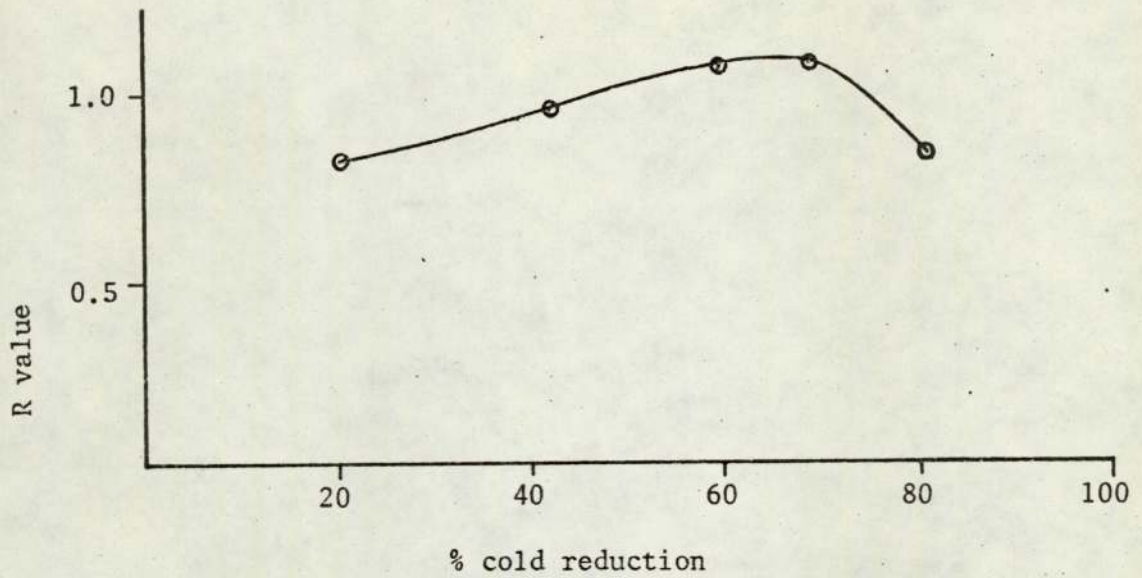


Fig. 1.1 The influence of the amount of cold reduction upon R value of a rimmed steel strip<sup>(1)</sup>.

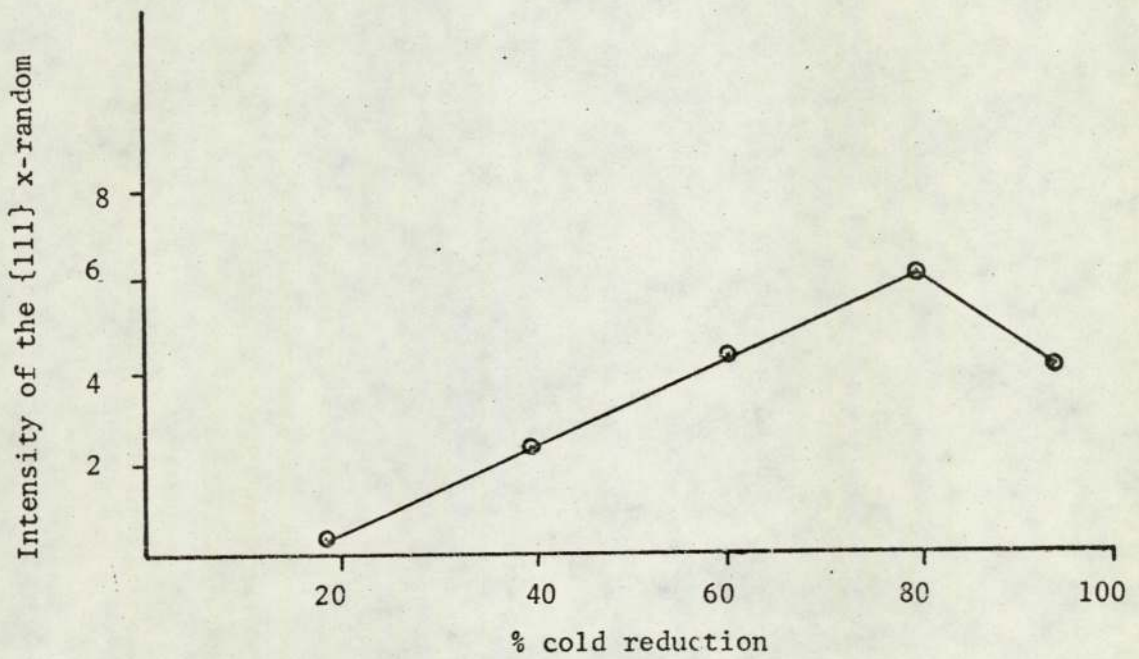


Fig. 1.2 The influence of the amount of cold reduction upon intensity of the {111} x random<sup>(1)</sup>.

Ideally, cold rolling can be regarded as a combination of tension in the rolling direction and compression normal to the rolling plane. By cold rolling, therefore, it is possible to develop mostly tensional texture or mostly compression texture or a combination of both, depending upon the mode of deformation, which is defined by the magnitude of the rolling draughts. Furthermore, by using constant draughts throughout the whole rolling operation, the percentage reduction per pass increases from one pass to the next. As a result, the mode of deformation varies with the progress of rolling, and texture is developed under varying rolling conditions. After heavy reduction, the high percentage reduction per pass might be an important factor contributing to the formation of more {100} texture leading to a reduction in R value.

Controlling the geometry of deformation, during cold rolling is, therefore, necessary in order to control the mode of deformation, texture and hence R value. In the present study, coils of rimmed steel were cold rolled according to three constant geometry schedules in which the shear plane angle is maintained constant from one pass to the next. Using the 2 high mill, reductions per pass equivalent to shear plane angles of  $55^\circ$ ,  $45^\circ$  and  $35^\circ$  corresponding to the previous rolling schedules were used. In order to demonstrate the difference between rolling with constant geometry and rolling with constant roll gap, coils of the same material were cold rolled using light, medium and heavy roll gap. Yet another set of the same coils was cold rolled using the pendulum mill. The effect of these seven rolling schedules upon texture and R value was studied. Since texture developed after annealing is dependent upon texture of the matrix in which it is formed as well as the annealing time, effect of the latter upon texture and R value was also studied.

Since R value is measured in a tensile test, a knowledge of the behaviour of the material under investigation to tensile strain is fundamental. This is necessary to explain the reduction in R value after heavy rolling reduction in constant roll gap schedules and shows how this reduction can be avoided. Crystal reorientation after tensile extension was therefore examined.

2. LITERATURE REVIEW

## 2.1 THE GEOMETRY OF COLD ROLLING

Controlling the geometry of deformation during cold rolling received little attention in the literature though it was noted by Crane and Alexander<sup>(3)</sup> that the rolling condition in the deformation zone is significant to the development of cold rolling texture. Dillamore and Roberts<sup>(4)</sup> concur at least for cold rolling condition close to sticking friction. They used the slip line field of a compression test to illustrate the relative orientation of maximum resolved shear stress axes through the thickness of a strip. They indicated that under both low and high friction conditions (not reaching the sticking friction) the stress distribution at the surface is not altered on passing through the neutral point, as shown in fig. 2.1.1.

For a material between the surface and centre of a strip, the stress system on the exit side of the neutral point is a mirror image of the stress system on the entry side. However, the stress systems at the centre are similar regardless of the cold rolling condition but varied at the surface according to the rolling condition. They assumed also that texture developed during cold rolling is dependent upon the amount of deformation occurring on either side of the neutral point. A parameter P was therefore invoked to calculate the percentage deformation per pass on either side of the neutral point as follows:

$$P = 50 - \left[ \frac{1}{\mu} \left( \frac{R}{2D} \right)^{\frac{1}{2}} - \frac{1}{\mu 2} \left( \frac{R}{4D} \right) \right] \times 100 \quad 2.1.1$$

where  $\mu$  is the coefficient of friction, R is the rolling draught and D is the roll diameter. According to equation 2.1.1, increasing the rolling draughts decrease the amount of deformation after the neutral point, for all values of the coefficient of friction.

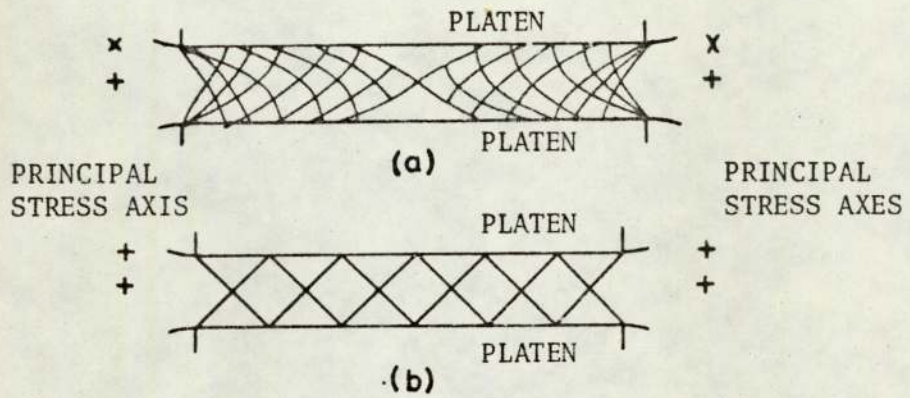


Fig. 2.1.1 Shows the slip line fields for (a) completely rough-platens; strip thickness: platen breadth 1:6.6, (b) zero friction; strip thickness: platen breadth 1:6. (4)

Crane and Alexander<sup>(3)</sup> in discussion were critical of the approach of Dillamore and Roberts<sup>(4)</sup> in that by cold rolling of an aluminium strip to 96% total reduction using 0.04 in/p rolling draughts, the percentage reduction per pass varied from 8% to 80%. The effect of the zone of deformation, however, had varied considerably within that range and maintaining a constant geometry of deformation was therefore necessary to control texture developed. Tucker<sup>(5)</sup> was critical of Dillamore and Roberts' treatment<sup>(4)</sup> because of the failure to maintain the rolling direction accurately from one pass to the next. Hellewell<sup>(2)</sup> reported that the mirror image condition for stable orientations which was suggested by Dillamore and Roberts<sup>(4)</sup> is only applicable if deformation on either side of the neutral point was equal. However, texture developed during cold rolling using light draughts where the deformation is equal on either side of the neutral point, may be accounted for on the basis of mirror image condition. During cold rolling using heavy draughts the majority of deformation occurs on the entry side of the neutral point provided the friction conditions do not approach the sticking friction. Therefore, the mirror image condition does not apply during cold rolling using heavy draughts. According to Hellewell<sup>(2)</sup> texture developed by cold rolling using light draughts varied from surface to centre while texture developed by heavy rolling draughts was homogeneous through the thickness of the strip. This is contrary to what was expected from Dillamore and Roberts' treatment<sup>(4)</sup>. Hellewell<sup>(2)</sup> on the other hand confirmed their observation that texture developed at the strip centre was independent of the cold rolling condition.

More recently, Vandermeer and Ogles<sup>(6)</sup> defined the rolling geometry by a new parameter  $\frac{1}{t_m}$  given by the following equation:

$$\frac{l}{t_m} = (D)^{\frac{1}{2}} \frac{(t_N - t_x)^{\frac{1}{2}}}{\frac{1}{2}(t_N + t_x)} \quad 2.1.2$$

where  $l$  is the length in the rolling direction of the geometrical zone of deformation,  $t_m$  is the average thickness of that zone,  $D$  is the radius of the work rolls,  $t_N$  and  $t_x$  are the entry and exit thicknesses respectively. The parameter  $\frac{l}{t}$  although it was related to texture segregation in niobium is not satisfactory to control the geometry of deformation during cold rolling, since the  $\frac{l}{t_m}$  parameter is likely to increase with the total rolling reduction.

Mathur and Backofen<sup>(76)</sup> pointed out that the geometry of the deformation zone is an important factor contributing to the state of strain during cold rolling. An index of such geometry is the ratio of the mean zone thickness,  $T_N$ , to the zone contact length,  $L$ , or  $\Delta = T_N/L$ . For strip rolling

$$\Delta \approx \frac{T_N}{4DR} (2 - R) \quad 2.1.3$$

where  $D$  is the roll diameter and  $R$  is the rolling draught.  $R = 1 - (T_x/T_N)$ ,  $T_x$  and  $T_N$  being the exit and entry thicknesses. The index  $\Delta$  tends to be near 1 because the horizontally directed friction forces must be large enough for the rolls to bite and deliver the well-lubricated strip. Cold rolling cannot usually be carried out with  $\Delta$  much higher than unity. It was shown that texture and  $R$  value responded to the change in  $\Delta$ .

Yeomans and Richards<sup>(7)</sup> related the geometry of deformation during cold rolling to the relative magnitudes of principal strains for all infinitesimally small increments of the total strains. Since rolling is a combination of tension in the rolling direction and compression normal to the rolling plane, they assumed that crystallographic slip during cold

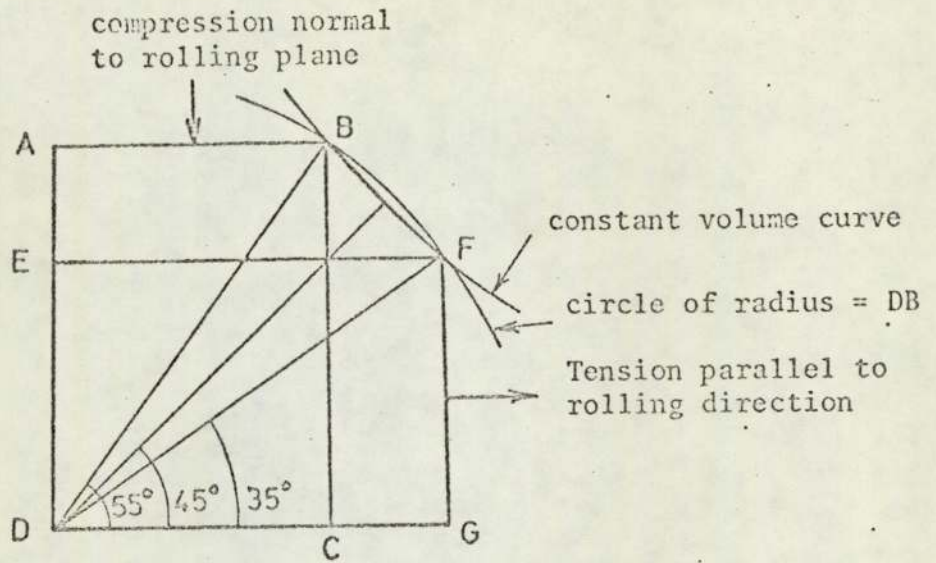


Fig. 2.1.2 Shows that during rolling, a rectangular element ABCD deforms by simple tension from the commencement of deformation, by slip on planes of maximum resolved shear stresses, in the nearest closed packed direction to the direction inclined  $54^{\circ} 44'$  to the rolling direction. With progressive increasing strain, the operative slip planes continue to rotate towards the  $45^{\circ}$  position until the  $35^{\circ}$  position is reached where deformation occurs mostly by compression, without changing the length of the diagonals DB and DF.

rolling is operative over an angular range around the  $45^\circ$  angle to the stress axes (see Appendix I). The extreme limits of that angular range correspond to the most favourably orientated crystallographic plane to slip in the directions inclined  $54^\circ 44'$  and  $35^\circ 16'$  to the tension and compression axes. Furthermore, tension and compression components are conjugately related, hence equal extension could be affected by equal shear on conjugate systems. Thus in cold rolling, it would be expected that the operative slip components would switch from that corresponding to tension to that of compression depending upon the magnitude of the rolling draughts. This is illustrated in fig. 2.1.2.

## 2.2 THEORIES OF COLD ROLLING TEXTURE FORMATION IN b.c.c.

### POLYCRYSTALLINE METALS

All explanations put forward to account for the origin of cold rolling texture in b.c.c. polycrystalline metals are based on the assumption that plastic deformation occurs by a process of crystallographic slip on the  $\{110\}$ ,  $\{112\}$  and  $\{123\}$  close-packed planes in the  $\langle 111 \rangle$  close-packed direction. Since there is a total of 48 slip systems, each has a slip component acting along all possible slip planes, slip occurs only on the slip system which has the maximum resolved shear stress. As Mises<sup>(8)</sup> and Taylor<sup>(9)</sup> assumed, five slip systems must operate simultaneously in order to preserve the external form of the material and maintain cohesion at the grain boundaries. Several objections to Taylor's analysis<sup>(9)</sup> arose on the grounds that it assumes a homogeneous deformation and that the active slip systems were to be

determined by the condition of least shear. Bishop and Hill<sup>(10)</sup>, however, introduced the principle of maximum shear strain and considered that although deformation is known to be inhomogeneous, it may be regarded as sufficiently homogeneous for consideration of the problem of texture formation.

Boas and Schmid<sup>(11)</sup>, and Pickus and Mathewson<sup>(12)</sup> relaxed the Taylor's treatment<sup>(9)</sup> by assuming that unequal participation of the three most favourable slip systems brings the deformation axes to symmetrical end positions, where the resolved shear stresses are equal and the rotations cancel out. The most favourable system to slip is that for which the Schmid factor<sup>(13)</sup> defined by the product of the resolved shear stress and the cosine of the angle between the slip direction and direction in which free flow may occur, is highest. No explanation was given as to how the other crystals reach that position. More recently<sup>(14)</sup>, it was reported that at room temperature, no unique slip system was operative in the early stages of deformation. Some slip systems, having low resolved shear stresses were observed, while some slip systems with high resolved shear stress were missing. There was, therefore, a breakdown of the Schmid law.

In all assumptions that slip occurs on many slip systems simultaneously, the stress within a grain or part of a grain must be such as to give equal resolved shear stresses in all the operative slip systems. No explanation was given to the means by which the most favourable system or systems can withstand resolved shear stresses greater than the critical value until the resolved shear stresses on less favourable systems have reached the critical value for slip. Calnan and Clews<sup>(15)</sup> overcame this problem by introducing in each crystal an effective stress,

$T_e$ , which because of the constraints by neighbouring grains is so orientated on several systems simultaneously. When an increasing applied stress,  $T_a$ , is applied to the polycrystalline aggregate, the effective stress (initially coincident with  $T_a$ ) moves away from  $T_a$  so that  $T_e$  which is resolved on the most favourable system is always less than the critical value for slip. Using this treatment, Calnan and Clews<sup>(15)</sup> determined the tension and compression textures.  $\langle 110 \rangle$  texture with spread towards  $\langle 311 \rangle$  was predicted as the tension texture, while a duplex of  $\langle 100 \rangle + \langle 111 \rangle$  texture was predicted for the compression texture with the  $\langle 111 \rangle$  component predominating. Although the Calnan and Clews treatment assumes inhomogeneous deformation, it is complicated when applying to the b.c.c. structures, since the resolved shear stresses on the three families of slip planes have to be taken into consideration.

Dillamore and Roberts<sup>(16)</sup> assumed that multiple slip operates only in the vicinity of the grain boundary, while one or two slip systems only are operative in the grain body. Their assumption is supported by an earlier experimental observation by Clareborough and Hargreaves<sup>(17)</sup> that this is so. Accordingly slip rotations in the grain body should be more rapid and dominant relative to multiple slip in the boundary. Dillamore and Roberts<sup>(16)</sup>, therefore, assumed that deformation of individual grains in polycrystalline material is closely similar to the deformation of single crystals of the same orientation. Slip rotation during rolling was considered to be due to a biaxial stress system. Viewed in this light, the determination of the b.c.c. rolling texture was simplified and a spread of orientation between  $\{112\}\langle 110 \rangle$  and  $\{110\}\langle 110 \rangle$  was predicted. It was also noted<sup>(16)</sup> that the  $\{112\}\langle 111 \rangle$  and

{123}<111> slip systems are geometrically equivalent to different proportions of primary and cross slips on the {110}<110> systems. Each primary system has two available cross slip systems one of which must always sustain some component of the applied stress. Tucker<sup>(18)</sup> was critical of cross slip in that it is enhanced by failure to keep the rolling direction accurately from one pass to the next. Taylor and Christian<sup>(14)</sup> reported that cross slip in b.c.c. polycrystalline metals is difficult to initiate at low temperature because of the high stresses needed to move individual screw dislocations.

The foregoing analyses of texture formation presuppose that slip elements are known and derive the mode of deformation from texture. This helps to account for texture developed but does not help to control it. Yeomans and Richards<sup>(7)</sup>, however, firstly assumed the mode of deformation then identified the slip system and texture from the magnitude of the principal strains, i.e. in reverse of other theories. Accordingly, the operative slip systems are uniquely defined by the mode of deformation, such as deformation in uniaxial extension, uniaxial compression and pure rolling. Each of the previous modes of deformation is characterised by the relative magnitudes of the principal strains for all infinitesimally small increments of the total strain. Thus, an incremental uniaxial plastic extension in length is associated with equivalent contractions in width and thickness of a rectangular specimen, on the assumption of no change in width. It was, therefore, concluded (see Appendix I) that deformation as occurred by slip is accompanied by rotation of the slip planes of maximum resolved shear stresses in the close packed direction which is nearest to the direction inclined  $54^{\circ}44'$  to the tension axis.

Similarly, for an incremental uniaxial compression, the contraction in thickness is equivalent to elongations in both width and length, and the most favourable slip systems are those corresponding to the planes of maximum resolved shear stresses and in close packed directions which are nearest to the  $54^{\circ}44'$  to the compression axis. In pure rolling where the incremental strain parallel to the rolling direction is equivalent in magnitude to the contraction in strip thickness and the strain in the transverse direction is zero, the operative slip systems are those of maximum resolved shear stresses in the close packed direction lying nearest to the  $45^{\circ}$  to the shear axes, that is  $45^{\circ}$  to the strip surface.

According to Yeomans and Richards<sup>(7)</sup> the crystallographic rotations during the early stages of cold rolling of a randomly orientated material tend to move the  $\langle 111 \rangle$  slip direction towards the compression axis until the  $\{100\}\langle 110 \rangle$  orientation is formed. This rotation brings the four  $\langle 111 \rangle$  directions into symmetrical positions with respect to the rolling direction and the perpendicular direction. The symmetrical arrangements of the  $\langle 111 \rangle$  slip directions defines the operative  $\{112\}$  slip plane, the pole of which lies on the tension axis, as shown in fig. 2.2.1. It would appear then that the stability of the  $\{112\}\langle 110 \rangle$  orientation arises from the fact that the  $\langle 110 \rangle$  direction lies between both the compression and tension circles. Therefore if slip is only operative on the  $\{112\}$  slip planes, it would result in sharpening of the  $\{112\}\langle 110 \rangle$  texture with increasing the amount of cold rolling.

With further increase in the rolling reduction, rotation of  $11^{\circ}$  around the rolling direction brings the  $\{123\}$  into equilibrium position to allow for further deformation, as shown in Fig. 2.2.2. This is

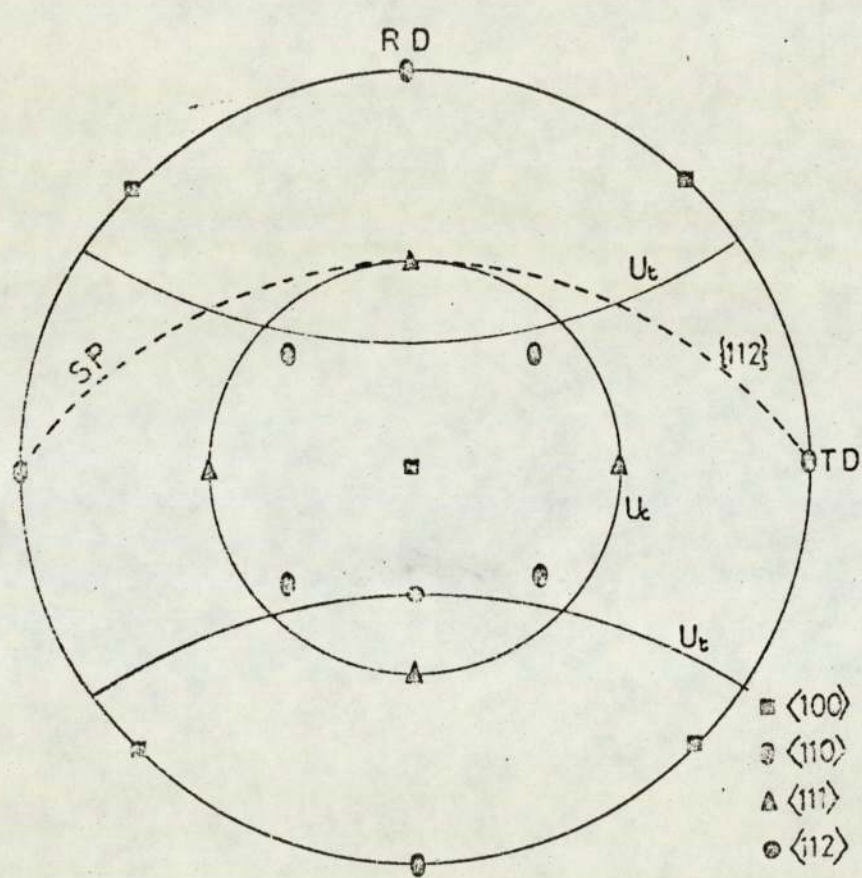


Fig. 2.2.1. Ideal  $\{100\}\langle 110\rangle$  texture, with four  $\langle 111\rangle$  slip directions on  $U_c$  and the pole of the  $\{112\}$  slip plane on  $U_T$ .

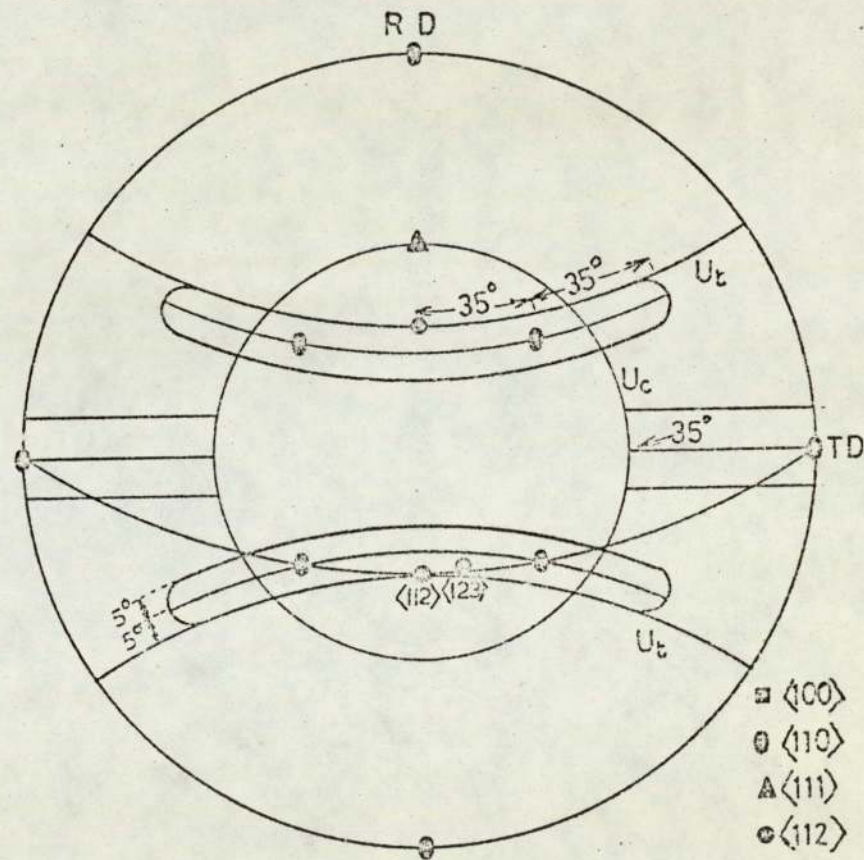


Fig. 2.2.2. Predicted spread in  $\{110\}$  pole figure due to the rotation of  $\{123\}$  poles about  $\langle 111\rangle$  slip direction and  $\{110\}$  poles about the rolling direction to equilibrium or symmetrical positions.

equivalent to fixing the operative slip direction on  $U_c$  and allowing some rotation around it. In the ideal  $\{100\}\langle 110\rangle$  orientation, four poles of the principal  $\{110\}$  slip planes are symmetrically situated around the rolling direction. Rotation of  $\pm 5^\circ$  of the  $\{110\}$  poles on the  $U_t$  circle around the rolling direction account for the  $\{311\}\langle 110\rangle$  orientation. On the other hand, rotation about the rolling direction on the compression circle results in the formation of the  $\{111\}\langle 110\rangle$  orientation, as shown in Fig. 2.2.3. In the  $\{111\}\langle 110\rangle$  texture, rotation of the six  $\{110\}$  poles about the strip normal result in the  $\{111\}\langle 112\rangle$  orientation, as shown in Fig. 2.2.4.

In the  $\{111\}\langle 112\rangle$  orientation, the six  $\{110\}$  and three  $\{100\}$  poles are symmetrical about the strip normal. Furthermore, one of the  $\{112\}$  poles is coincident with the  $\{100\}$  slip planes. Slip can then occur on the  $\{100\}$  planes, if the critical resolved shear stress on these planes is reached. This results in the formation of the  $\{100\}\langle 110\rangle$  orientation. Yeomans and Richards' analysis of the cold rolling texture can be used to select certain modes of deformation and to control texture developed.

## 2.3 THEORIES OF ANNEALING TEXTURE FORMATION IN b.c.c.

### POLYCRYSTALLINE METALS

The origin of annealing texture has been subject of controversy over the relative importance of nucleation and growth as controlling factors. No attempts will be made here to review the historical development of the subject, but emphasis will be placed on the cold rolling and annealing variables which influence the recrystallization texture produced.

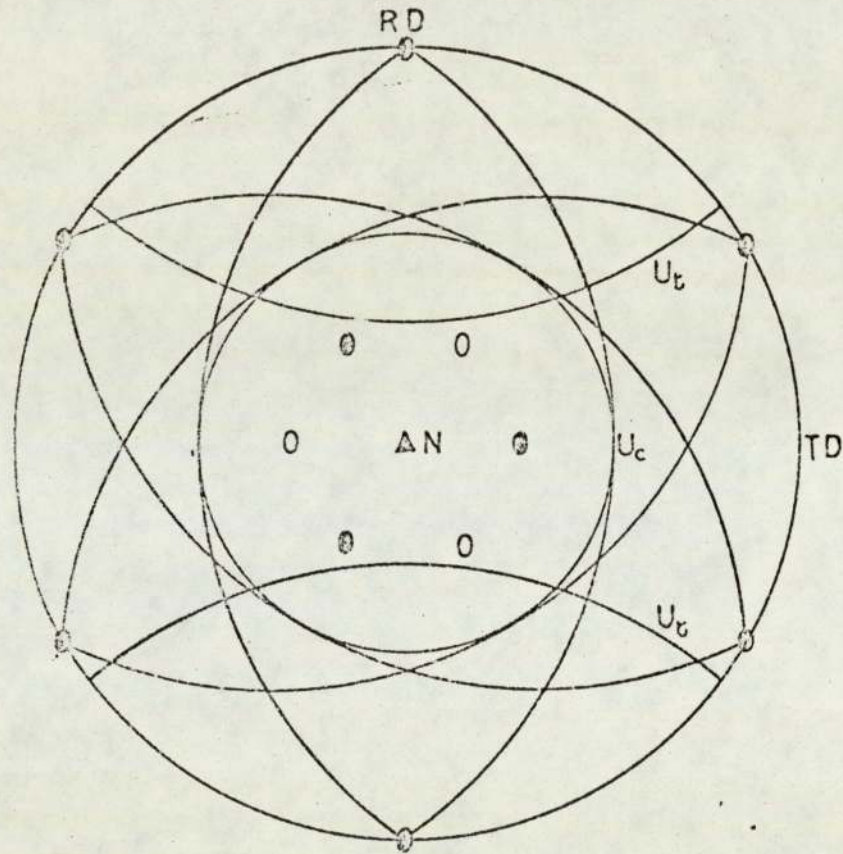


Fig. 2.2.3 Ideal  $\{111\}\langle 110\rangle$  texture, with six  $\{110\}$  slip planes tangential to  $U_c$ .

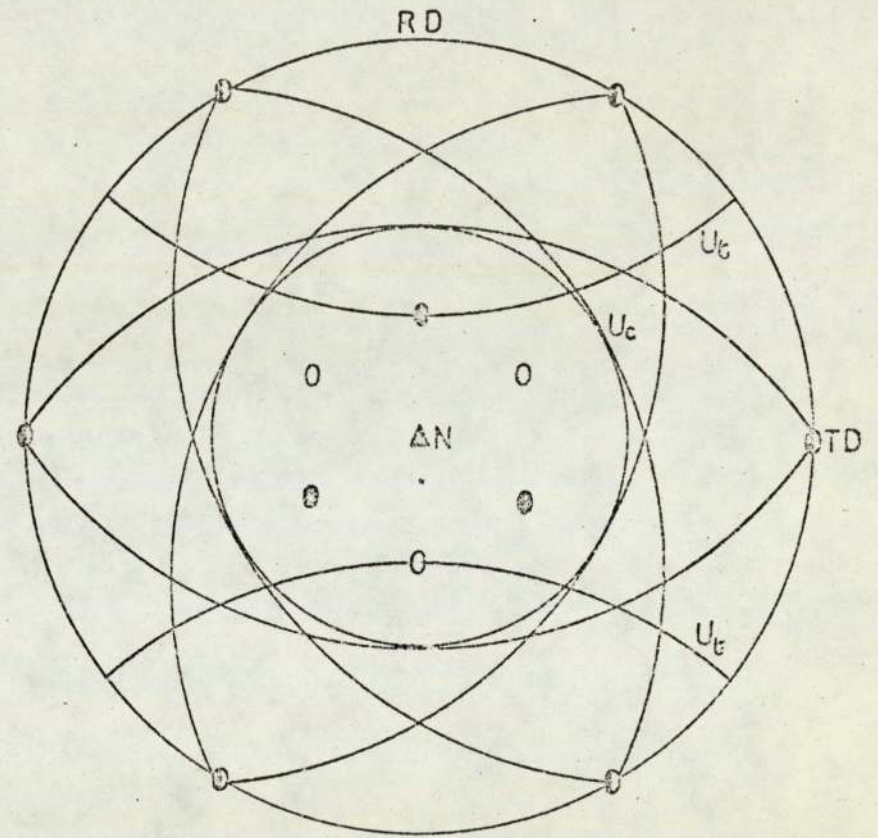


Fig. 2.2.4. Ideal  $\{111\}\langle 112\rangle$  texture, obtained from  $\{111\}\langle 110\rangle$  by  $30^\circ$  rotation about N. The six  $\{110\}$  planes are still tangential to  $U_c$ .

During recrystallisation of a heavily deformed steel the formation of a viable nucleus depends on the driving force available for sub-grain growth which is dependent upon the amount of stored energy of deformation. Since the sequence of increasing the stored energy corresponds to the total amount of dislocation motion which had taken place<sup>(19)</sup>, the ease of nucleation is therefore orientation-sensitive fig. 2.3.1. Within the major texture components, the stored energy increased in the order of the {100}<011>, {211}<011>, {111}<UVW> and {110}<011> orientations as shown in Fig. 2.3.1. During recrystallisation anneal, the {011} and {111} texture components should nucleate first and therefore have the longest time to grow before impingement occurs. The very low density of the {011} planes in the cold worked metals, however, means that it is unlikely ever to become strong after recrystallisation. The least favoured orientation is the {100}, and this was predicted to disappear on annealing. Orientation determination on recrystallised grains during recrystallisation of rimmed steel confirmed the predominance of the {111} planes<sup>(2,20)</sup>.

During normal grain growth, the relatively strong texture components in the primary recrystallisation, are strengthened at the expense of the neighbouring weak components, and the density between different components are sometimes redistributed. In the case of rimmed steel, the relatively strong {111} in the primary recrystallisation texture, is strengthened during normal grain growth at the expense of the weak {100} texture. In the absence of second phase particles, the growth of the large grain is defined by the equation<sup>(21)</sup>

$$\frac{dR}{dt} = k \left( \frac{1}{R_{cr}} - \frac{1}{R} \right) \quad 2.3.1$$

where R is the radius of the growing grains and  $R_{cr}$  is the

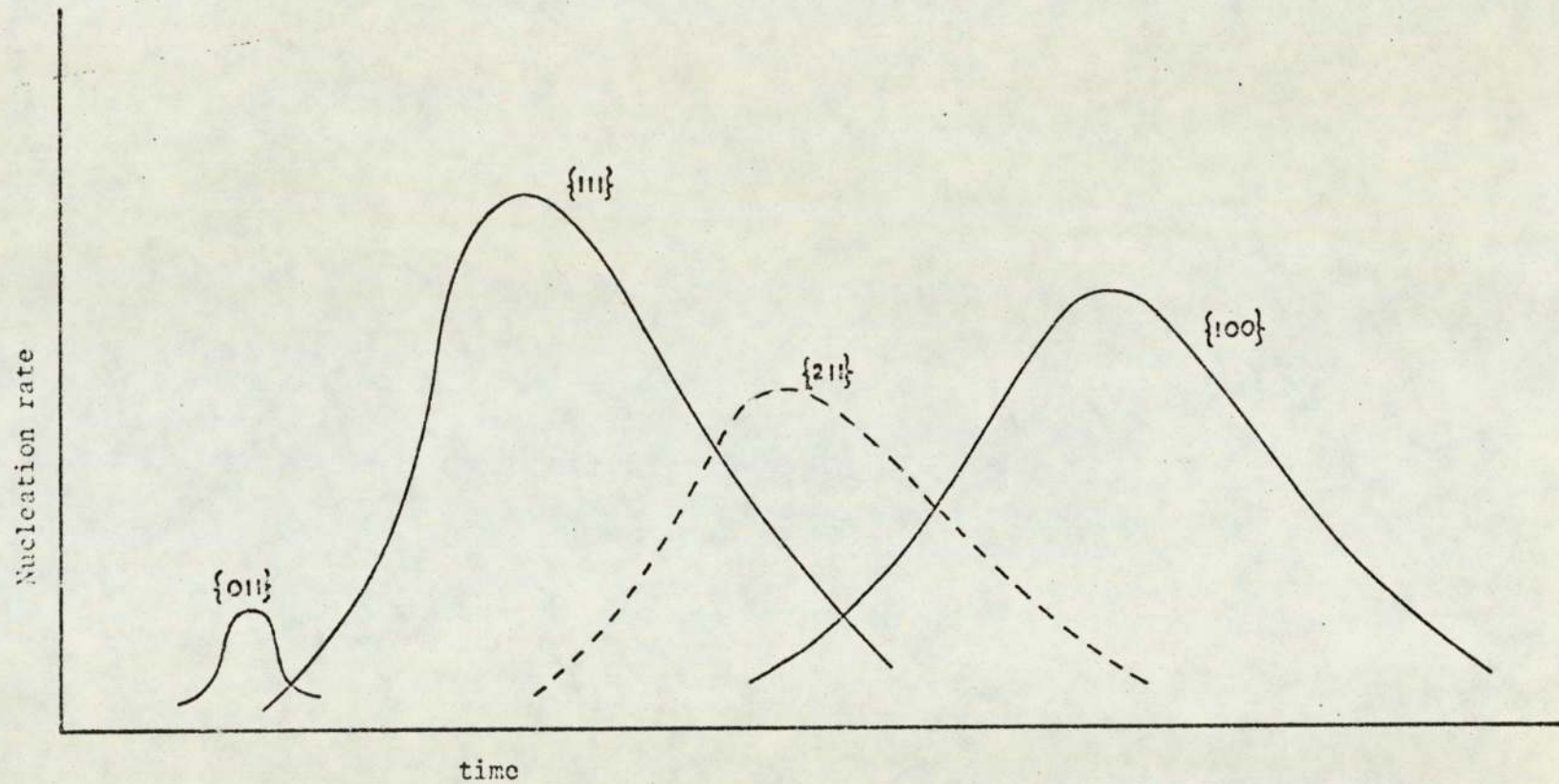


Fig. 2.3.1 Schematic representation of the dependence of the nucleation rate upon orientation in the cold worked iron.

characteristic or average grain size. Grains which are bigger than  $R_{cr}$  grow, while those which are smaller shrink and disappear. The difference in grain size of the grains determines which grains nucleate first and have the longest time to grow. The {111} texture, is, therefore, enhanced by normal grain growth, while the {100} texture is weakened. When effective second phase particles are present, a constant reaction to the movement of grain boundaries is developed. The grain growth rate is now given by the equation<sup>(21)</sup>,

$$\frac{dR}{dT} = k \left( \frac{1}{R_{cr}} - \frac{1}{R} \right) \pm Z \quad 2.3.2$$

where  $Z$  is a reaction term due to the particles which always acts to decrease the absolute value of  $\frac{dR}{dT}$ . The effect of increasing the particle reaction  $Z$  is to limit the range of growing grains to a smaller fraction of those of the largest sizes. Therefore, only much larger grains than the average size can grow while those of grain size about average are inhibited from growing. Eventually, the growth will slow down and stop in the presence of inhibiting particles. A limiting case is reached when normal grain growth is no longer possible and abnormal grain growth (secondary recrystallisation) starts. If, however, the particles were progressively removed by decarburization, normal grain growth may continue. The {111} texture components which have now increased in size continue to grow selectively during further normal grain growth<sup>(19)</sup>.

In isothermal annealing, therefore, texture developed after annealing is dependent upon the cold rolling texture and the annealing time.

#### 2.4 THE RELATIONSHIP BETWEEN TEXTURE AND R VALUE

It is evident that R value, being a measure of plastic anisotropy, should be related to crystallographic texture. Burns and Heyer<sup>(22)</sup> have studied the effect of three major orientations in b.c.c. steel, namely the  $\{001\}\langle 110\rangle$ ,  $\{110\}\langle 001\rangle$  and  $\{111\}\langle 110\rangle$  orientations upon the strain ratio, on the basis that deformation in b.c.c. steel occurs by slip on four  $\langle 111\rangle$  directions. Since each of the four slip directions is common to three  $\{110\}$ , three  $\{112\}$  and six  $\{123\}$ , a total of 48 slip systems is expected. Since it is impracticable to decide which system of the 48 systems is to operate during deformation, it was assumed, from the stand-point of relative changes in the dimensions of cross section of a simple tensile test piece, that it is not necessary to know which plane becomes an active slip plane. It was then concluded that the relative width to thickness strains are dependent upon the slip direction only, the operative slip direction being that of maximum shear stress. Thus, when a sheet with  $(100)[110]$  orientation is extended in the rolling direction, the favourable  $[111]$  slip directions  $A_1$  and  $A_3$  are at an angle of  $35^\circ$  to the specimen axis, hence  $10^\circ$  from the direction of maximum shear stress Fig. 2.4.1. Accordingly, slip occurs in the  $A_1$  and  $A_3$  directions resulting in a greater reduction in thickness than in width. Such a specimen should have a very low strain ratio, approaching zero as the specimen ideally possesses this orientation. In the case of a sheet with  $\{110\}\langle 001\rangle$  texture, all the four slip directions of the type  $[111]$  are at the same angle  $55^\circ$  to the direction of tension in the rolling direction and at  $10^\circ$  to the direction of maximum shear as in Fig. 2.4.2. Hence the width strain should be the same as the thickness strain, resulting in a strain ratio of unity. Finally, in a sheet having the

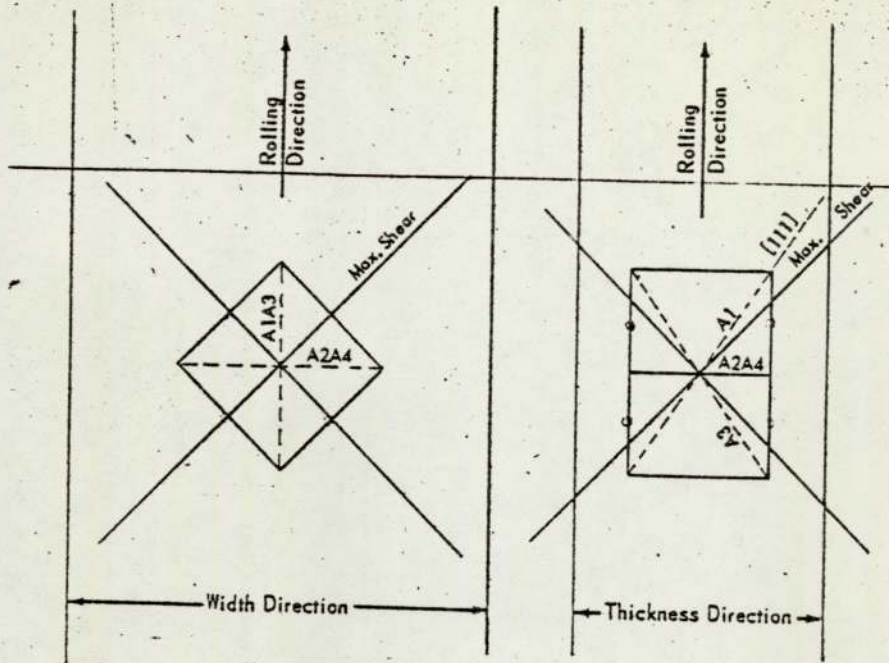


Fig.2.4.1 shows the behaviour of a specimen with cube-on face orientation  $(100)[011]$  under the influence of an uniaxial extension in the rolling direction<sup>(22)</sup>.

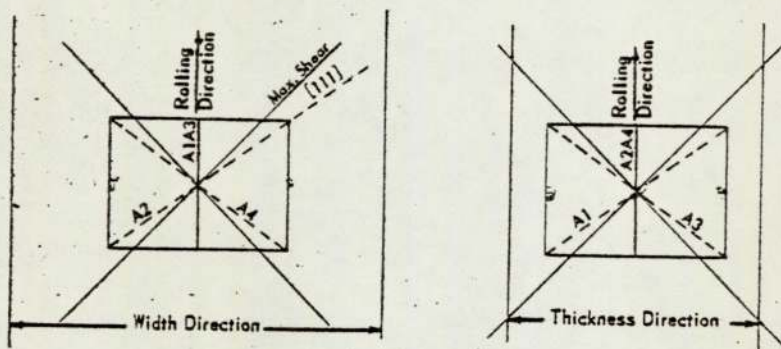


Fig. 2.4.2. shows the behaviour of a specimen with cube-on edge texture  $(110)[001]$  under the influence of an uniaxial extension in the rolling direction<sup>(22)</sup>.

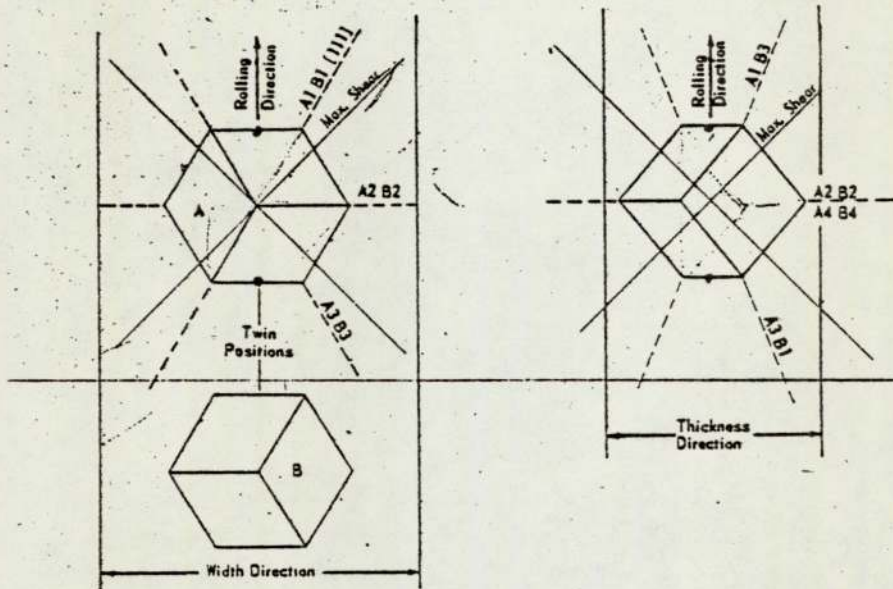


Fig. 2.4.3. shows the behaviour of a specimen with cube-on-corner texture (111)[110] under the influence of an uniaxial extension in the rolling direction<sup>(22)</sup>.

twinned orientation (111)[110], the preferred [111] slip directions  $A_1$  and  $A_3$  are at an angle  $35\frac{1}{2}^\circ$  to the axis of the specimen, if extended in the rolling direction as shown in Fig. 2.4.3. Hence the width strain will be higher than the thickness strain resulting in a strain ratio greater than unity.

The foregoing analysis was based on the assumption that in pulling a strip, the width strain  $\epsilon_w$  and thickness strain  $\epsilon_t$  caused by a strain  $\gamma$  in a particular slip direction at angles  $\lambda_w$  and  $\lambda_t$  to the width and thickness directions respectively is given by the equations

$$\epsilon_w = \gamma \text{Cos } \lambda_w \quad 2.4.1$$

and

$$\epsilon_t = \gamma \text{Cos } \lambda_t \quad 2.4.2$$

The correct relation for resolving the crystallographic shear strains into linear strains are given by the Schmid law<sup>(13)</sup>

$$\epsilon_w = \gamma \text{Cos } \lambda_w \cdot \text{Cos } \phi_w \quad 2.4.3$$

$$\epsilon_t = \gamma \text{Cos } \lambda_t \cdot \text{Cos } \phi_t \quad 2.4.4$$

where  $\phi_w$  and  $\phi_t$  are the angles between the slip-plane normal and the width and thickness directions. Furthermore, no attempt was made to account for the varying amounts of slip on different systems within a grain. Hosford and Backofen<sup>(23)</sup> devised a method relating R value to texture. This method is a follow up of the Taylor's criterion<sup>(9)</sup> which was later modified by Bishop and Hill<sup>(10)</sup> for calculating the tensile (or compressive) stress-strain curves of randomly orientated polycrystals from the stress-strain curves of single crystals. In Taylor's analysis<sup>(9)</sup> it

was assumed that during plastic deformation, the five operative slip systems are those which have the minimum value of a parameter  $M$  given by  $\frac{d\gamma}{d\epsilon_x}$ , where  $d\gamma$  is the sum of the incremental shear strains on all of the active slip systems needed to produce an increment of tensile strain  $d\epsilon_x$ . Since slip occurs on five systems simultaneously, an average  $\bar{M}$  was used to describe the aggregate over-all texture. Minimum  $\bar{M}$  values, obtained for a number of orientations in the unit stereographic triangle were found to be  $\bar{M} = 3.06$ .

The total shear strain increment  $d\gamma$  was then related to the stress  $\sigma_x$  required for a grain to flow with axial symmetry by assuming that in order to activate slip, a shear stress  $\tau$  would be the same for all systems. Therefore, the work expended in slip throughout a unit volume of a material becomes  $dW = \tau d\gamma$  which must be identical to the work per unit volume done by the applied stress in producing the extension. Hence

$$dw = \sigma_x d\epsilon_x = \tau d\gamma \quad 2.4.5$$

and

$$\frac{\sigma_x}{\tau} = \frac{d\gamma}{d\epsilon_x} = M = \frac{dw}{\tau d\epsilon_x} \quad 2.4.6$$

Equation 2.4.6 is a multiple slip analogy of the Schmid's law<sup>(13)</sup> in which

$$\frac{\sigma_x}{\tau} = \frac{d\gamma}{d\epsilon_x} = \frac{1}{\cos\lambda\cos\phi} \quad 2.4.7$$

where  $\lambda$  and  $\phi$  are the angles between  $x$  and slip direction and slip plane normal respectively.

Several objections to Taylor's analysis<sup>(9)</sup> were reported since it was assumed that deformation is homogeneous and the active slip systems

were determined by the condition of minimum shear strain. In addition, many possible combinations of slip systems were overlooked during the calculation of M. Bishop and Hill<sup>(10)</sup>, however, devised a more thorough analysis to calculate M in grains of various orientations. They assumed that simultaneous slip on five or more systems can occur only when the critical stress for slip,  $\tau$ , is reached on these systems without being exceeded on any others. Bishop and Hill<sup>(10)</sup> showed that this condition is satisfied only with a limited number of stress states or combinations of the terms

$$\begin{aligned} A &= \frac{(\sigma_2 - \sigma_3)}{\sqrt{6} \cdot \tau} & F &= \frac{\sigma_{23}}{\sqrt{6} \cdot \tau} \\ B &= \frac{(\sigma_3 - \sigma_1)}{\sqrt{6} \cdot \tau} & G &= \frac{\sigma_{31}}{\sqrt{6} \cdot \tau} \\ C &= \frac{(\sigma_1 - \sigma_2)}{\sqrt{6} \cdot \tau} & H &= \frac{\sigma_{12}}{\sqrt{6} \cdot \tau} \end{aligned}$$

where the stresses  $\sigma$  are taken with reference to the cube axes of the crystal. The actual values of these terms are 0,  $\pm\frac{1}{2}$ ,  $\pm 1$ .

By expanding equation 2.4.6. and substituting the constant volume relationship  $d\epsilon_3 = -(d\epsilon_1 + d\epsilon_2)$  a formula for calculating M was derived hence,

$$M = \frac{1}{\tau} \left[ (\sigma_1 - \sigma_3) \frac{d\epsilon_1}{d\epsilon_x} + (\sigma_2 - \sigma_3) \frac{d\epsilon_2}{d\epsilon_x} + 2\sigma_{23} \frac{d\epsilon_{23}}{d\epsilon_x} + 2\sigma_{31} \frac{d\epsilon_{31}}{d\epsilon_x} + 2\sigma_{12} \frac{d\epsilon_{12}}{d\epsilon_x} \right] \quad 2.4.8$$

or

$$M = \sqrt{6} \left[ -B \frac{d\epsilon_1}{d\epsilon_x} + A \frac{d\epsilon_2}{d\epsilon_x} + 2F \frac{d\epsilon_{23}}{d\epsilon_x} + 2G \frac{d\epsilon_{31}}{d\epsilon_x} + 2H \frac{d\epsilon_{12}}{d\epsilon_x} \right] \quad 2.4.9$$

The parameter M is evaluated for a given orientation (of cube axes

relative to specimen axes) and for a specified shape change, defined by the ratios of the strain components along the specimen axes. This was carried out in three steps.

1. The strain components along the specimen axes, x, y and z were resolved into components along the cube axes of the crystal, 1,2 and 3 with the expression, for  $d\epsilon_1$

$$d\epsilon_1 = l_{1x}^2 d\epsilon_x + l_{1y}^2 d\epsilon_y + l_{1z}^2 d\epsilon_z + l_{1y} l_{1z} d\epsilon_{yz} + l_{1z} l_{1x} d\epsilon_{zx} + l_{1x} l_{1y} d\epsilon_{xy}$$

and similar formulations for the other normal and shear strain components, the  $l$  term is the cosines of the angles between the cube axes and the specimen axes.

2. The relationship between  $d\epsilon_x$ ,  $d\epsilon_y$ ,  $d\epsilon_{yz}$ ,  $d\epsilon_{xy}$  and  $d\epsilon_{xz}$  was assumed to be known for axially symmetric flow, the strains along the cube axes were found relative to  $d\epsilon_x$  to be

$$\frac{d\epsilon_1}{d\epsilon_x} = l_{1x}^2 - \frac{1}{2} l_{1y}^2 - \frac{1}{2} l_{1z}^2, \text{ etc. for other components}$$

3. Finally, equation 2.4.9 was evaluated for each possible combination of A, B, C, F, G and H. The largest result was selected as the appropriate M value according to the principal of maximum virtual work.

The foregoing analysis was broadened by Hosford and Backofen<sup>(23)</sup> to include the anisotropy of yielding in textured sheets as measured by the width to thickness strain ratio  $R = \frac{d\epsilon_y}{d\epsilon_z}$  in a simple tensile test. In order to do that, it was assumed that if the tensile axis, x, is taken parallel to one of the principal axes of anisotropy, hence,

$d\epsilon_{yz} = d\epsilon_{zx} = d\epsilon_{xy} = 0$  and the  $d\epsilon_y$  and  $d\epsilon_z$  were incorporated in a

parameter  $r$  given by

$$r = \frac{d\epsilon_y}{d\epsilon_y + d\epsilon_z} = \frac{R}{R+1}$$

By applying the constant volume equation  $d\epsilon_x = -(d\epsilon_y + d\epsilon_z)$

Therefore  $d\epsilon_y = -rd\epsilon_x$ ;  $d\epsilon_z = -(1-r)d\epsilon_x$

The ratios  $\frac{d\epsilon_1}{d\epsilon_x}$ ,  $\frac{d\epsilon_2}{d\epsilon_x}$ ,  $\frac{d\epsilon_{23}}{d\epsilon_x}$ ,  $\frac{d\epsilon_{31}}{d\epsilon_x}$  and  $\frac{d\epsilon_{12}}{d\epsilon_x}$  in equation 2.4.9 were then

expressed in terms of the parameter  $r$  as follows

$$\frac{d\epsilon_1}{d\epsilon_x} = l_{1x}^2 - rl_{1y}^2 - (1-r)l_{1z}^2 \quad \text{etc.}$$

By assuming different values of  $r$  and calculating the corresponding values of  $M$  from equation 2.4.9,  $M$ .Vs. $r$  plot was drawn (figure 2.4.4). The values of  $M$  and  $r$  at the minimum of the plot identify the relative strength  $\frac{\sigma_x}{\tau}$  and the strain ratio  $R = \frac{r}{1-r}$ . The  $M$ .Vs. $r$  curve for a material consisting of several textural components  $a, b, \dots$  was found from the weighted average.

$$M = f_a M_a + f_b M_b + \dots$$

where  $f_a$  and  $f_b$  are the volume fractions of components  $a, b$ .

The minimum will occur when

$$\frac{dM}{dr} = f_a \frac{dM_a}{dr} + f_b \frac{dM_b}{dr} + \dots$$

If only (111) and (100) orientations were present, the minimum  $M$  would occur when

$$\frac{dM}{dr} = f\{100\} \frac{dM\{100\}}{dr} + f\{111\} \frac{dM\{111\}}{dr} = 0$$

At  $R = 1.5$

$$\frac{dM\{100\}}{dr} = 0.9 \quad \text{and} \quad \frac{dM\{111\}}{dr} = -0.2$$

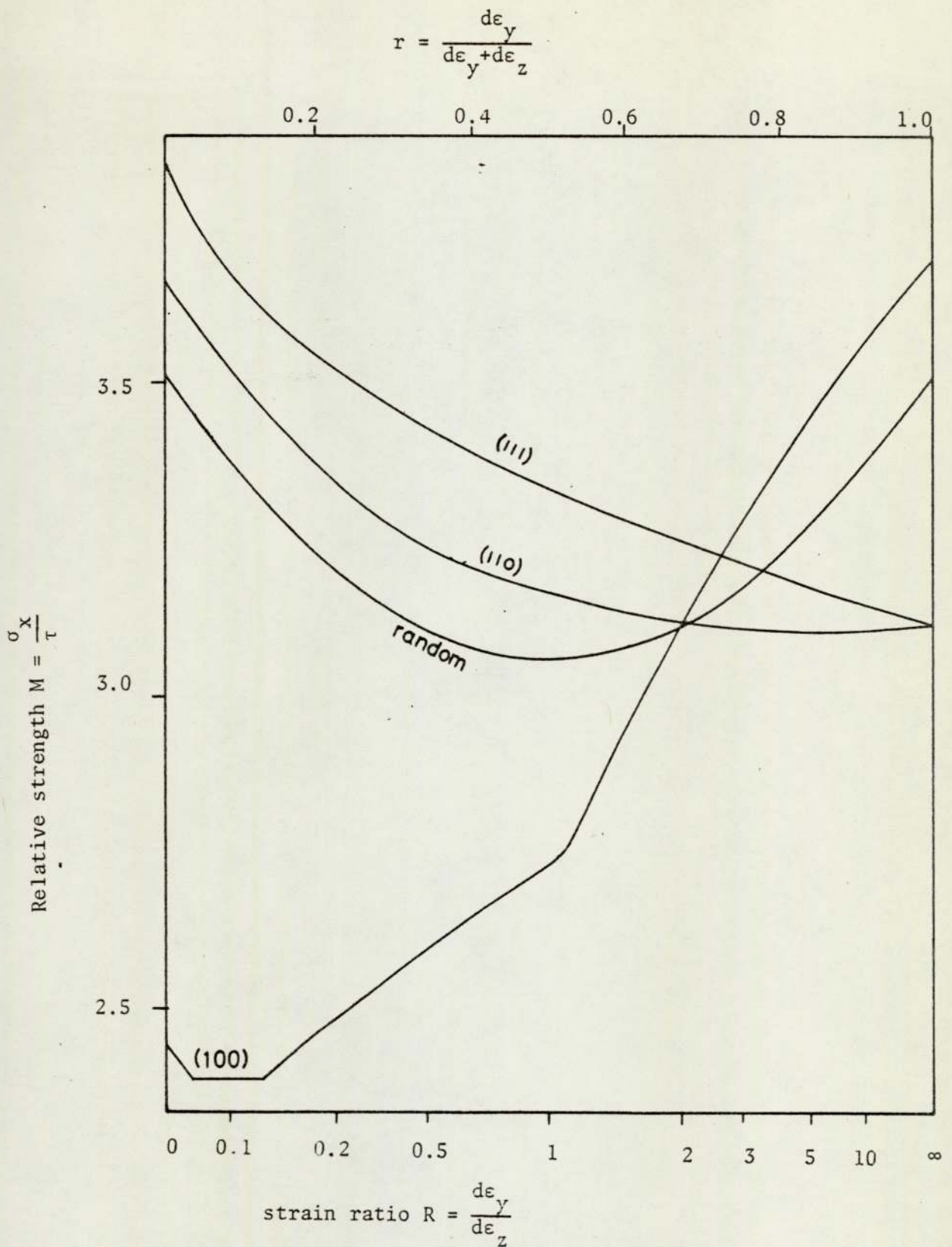


Fig. 2.4.4.  $M$  vs  $r(R)$  curves for textures which are rotationally symmetric about the sheet normal. Curves are shown for sheets in which (111), (110) and (100) are parallel to the rolling plane, and also for a randomly orientated sheet<sup>(23)</sup>.

There the effect of a twofold increase in the amount of {100} material would balance the effect of a ninefold increase in the amount of {111} at an  $\bar{R}$  level of about 1.5.

Fukuda<sup>(24)</sup> reported that if is necessary to examine more than the two orientations {100} and {111} to establish a correlation between  $\bar{R}$  value and texture. A new parameter including the {332} and {311} planes because of their relative preponderance in the recrystallisation texture together with the {100} and {111} textures was defined by

$$P = \frac{I\{111\} + I\{332\}}{I\{100\} + I\{311\}}$$

where I is the intensity of the corresponding {hkℓ} reflection relative to a random sample. The {332} orientation was reported to contribute to high R values whereas {311} texture results in lower R values because of its rotation to {100} orientation only during tensile strain with behaviour like crystals of {100} texture. The rotation of {411} texture to the {100} texture during tensile strain was also found to decrease R value<sup>(25)</sup>. The incidence of {311} texture in heavily rolled and annealed steel was attributed later to its high stored energy rather than to its predominance<sup>(26,27)</sup>.

Although the precise relationship between R value and texture is not fully established yet, it is clear that all different analyses generally lead to similar results, that a texture with {111} planes parallel to the plane of the sheet will give high R value. Also {100} planes parallel to the plane of the sheet will contribute to low R value.

## 2.5 THE RELATIONSHIP BETWEEN R VALUE AND THE L.D.R.

Several theories of anisotropy plasticity have been proposed, but their application has been limited and only the theory of Hill<sup>(28)</sup> has received appreciable attention. By analogy with Huber-Mises<sup>(8)</sup> yield criterion for isotropic behaviour, Hill defined a plastic potential or effective stress for anisotropy behaviour by assuming that the uniaxial yield stress varies with direction.

Whiteley<sup>(29)</sup> using an analysis by Hu<sup>(30)</sup> based on Hill's theory of anisotropy plasticity<sup>(28)</sup> and applying a correction factor to account for frictional forces<sup>(31)</sup>, has carried out an analysis of the punch load required during drawing for the case of an anisotropy material, in order to study the relationship between the L.D.R. and R value. The total punch load required to draw a blank of diameter D was shown to be

$$P_{\text{tot}} = (1 + \eta)\pi.d.t. \frac{\sqrt{\alpha_{33}}}{G}.k.\ln \left(\frac{D}{d}\right) \quad 2.5.1$$

where  $\alpha_{33}$  and G are anisotropy parameters,  $\eta$  is a friction parameter, D is the initial blank diameter, d is the final cup diameter, t is the thickness of the blank and k is the effective strength. The parameter  $\eta$  is constant for certain conditions of geometry and friction.

The maximum diameter of a blank that can be drawn is limited by the maximum punch load which can be supported by the material forming the wall of the cup. It was further shown that the maximum punch load is given by

$$P_{\text{max}} = \pi.d.t. \frac{\sqrt{\alpha_{22}}}{G}.k \quad 2.5.2$$

where  $\alpha_{22}$  is another anisotropic parameter. At the critical blank

diameter equations 2.5.1 and 2.5.2 must be equal, so that the limiting drawing ratio is given by

$$\ln\left(\frac{D}{d}\right)_{\max} = \frac{1}{(1+\eta)} \frac{\sqrt{\alpha_{22}}}{\sqrt{\alpha_{33}}} \quad 2.5.3$$

Equation 2.5.3 indicates that for certain conditions of geometry and lubrication, the limiting drawing ratio is governed by the anisotropy parameters of the sheet and is independent of the effective strength of material.

Whiteley<sup>(29)</sup> extended his analysis to express the anisotropy parameters  $\alpha_{22}$  and  $\alpha_{33}$  and  $G$  in terms of  $R$  value. Assuming a material with normal anisotropy  $R$  it was shown that

$$P_{\text{tot}} = (1+\eta) \cdot \pi \cdot d \cdot t \frac{\sqrt{(2+2\bar{R})}}{\sqrt{(1+2\bar{R})}} \cdot k \cdot \ln\left(\frac{D}{d}\right) \quad 2.5.4$$

$$P_{\text{max}} = \pi \cdot d \cdot t \cdot \frac{\sqrt{(1+\bar{R})^2}}{1+2\bar{R}} \cdot k \quad 2.5.5$$

Equating equation 2.5.4 and 2.5.5 then gives

$$\ln\left(\frac{D}{d}\right)_{\max} = \frac{1}{1+\eta} \frac{\sqrt{1+\bar{R}}}{\sqrt{2}} \quad 2.5.6$$

Rigorously the analysis applies to what might be best termed pure radial drawing with no bending and unbending around tool radii, in flat-bottom cup drawing of ductile metals. This restriction, as indicated by Hosford and Backofen<sup>(23)</sup> does not seriously limit the implication of the analysis. Work hardening was also neglected.

Whiteley<sup>(29)</sup> demonstrated experimentally the dependence of  $(D/d)$  on  $\bar{R}$  for a series of material with average of  $\bar{R}$  value from 0.58 to 1.62. This range was extended by Lloyd<sup>(32)</sup> to  $\bar{R} = 3.8$  for titanium

and reported a remarkably high D/d of 2.75. Wright<sup>(33)</sup> and Lilet<sup>(34)</sup> have demonstrated that slightly better correlation with deep drawing tests may be obtained by using  $R_{\min}$  instead of  $R_{\text{average}}$ . Atkinson and Maclean<sup>(35)</sup> found that the drawability of low carbon steels correlated more closely with  $R_{\text{average}}$  than with maximum or minimum values.

Hosford and Backofen<sup>(23)</sup> have also studied the relationship between drawability and R value by applying the Hill's theory<sup>(28)</sup> to sheet materials assuming rotational symmetry about the sheet normal and in the absence of the Bauschinger effect. Hill's yield criterion then becomes:

$$(\sigma_y - \sigma_z)^2 + (\sigma_z - \sigma_x)^2 + \bar{R}(\sigma_x - \sigma_y)^2 = 2Z^2 \quad 2.5.7$$

where  $Z = X \sqrt{\frac{1+\bar{R}}{2}}$  2.5.8

and  $d\epsilon_x : d\epsilon_y : d\epsilon_z = (\bar{R}+1)\sigma_x - \sigma_y - \sigma_z : (\bar{R}+1)\sigma_y - \sigma_x - \sigma_z : 2\sigma_z - \sigma_x - \sigma_y$  2.5.9

where x and y are the directions of principal stress in the plane of the sheet and Z is the sheet normal. X, Y and Z are the uniaxial yield stresses in the x, y and z directions. R is the R value.

For loading in the plane of the sheet  $\sigma_z = 0$ , and equations 2.5.7 and 2.5.9 become

$$\sigma_x^2 + \sigma_y^2 - \sigma_x \sigma_y \left(\frac{2\bar{R}}{\bar{R}+1}\right) = X^2 \quad 2.5.10$$

and

$$d\epsilon_x : d\epsilon_y : d\epsilon_z = (\bar{R}+1)\sigma_x - \sigma_y : (\bar{R}+1)\sigma_y - \sigma_x : -(\sigma_x + \sigma_y) \quad 2.5.11$$

putting  $\alpha = \frac{\sigma_y}{\sigma_x}$  in equation 2.5.10 therefore,

$$\sigma_x^2 \left[ 1 + \alpha^2 - \alpha \left(\frac{2\bar{R}}{\bar{R}+1}\right) \right] = X^2 \quad 2.5.12$$

By varying the values of  $R$  and  $\alpha$  in the yield condition (equation 2.5.12) a figure representing the anisotropy yield loci is drawn as in figure 2.5.1. In this figure  $R = 1, 2, 3, 5$ ,  $\alpha = 1, \frac{R}{R+1}$  and  $-1$  and the intersection of the loading path (dashed line) with the appropriate locus represent the beginning of yielding and identifies the stress ratio for a state of plane strain.

In deep drawing of a flat-bottomed cup, there are two regions of special importance. These are the flange where deformation occurs and force requirement originates, and the cup wall which must support the necessary forces without tearing. Therefore, for maximum drawability in ductile metals, the wall strength should be as high as possible relative to that of the flange, so that the largest reduction can be accomplished before wall failure by necking. The drawing limit must be governed by and increased with the ratio  $\beta$  of the two planes strengths.

$$B = \frac{\sigma_x(\text{wall}, d\epsilon_y = 0)}{\sigma_y(\text{flange } d\epsilon_z = 0)} \quad 2.5.13$$

Reference to the anisotropy yield loci figure 2.5.1 indicates that although both the flange and wall yield under conditions of plane strains, the axis of zero strain is different as in figure 2.5.2. Yielding in the cup wall occurs under plane strain of  $d\epsilon_y = 0$  and stress ratio  $\alpha = \frac{R}{R+1}$ . Therefore, the wall strength increases for  $R > 1$  i.e. increases with  $R$  value. In the cup flange, where the plane strain components  $d\epsilon_z = 0$ , some softening is the result of  $R > 1$  i.e. the flange strength decreases with  $R$  value. Therefore, the deep drawability of a strip increases with  $R$  value.

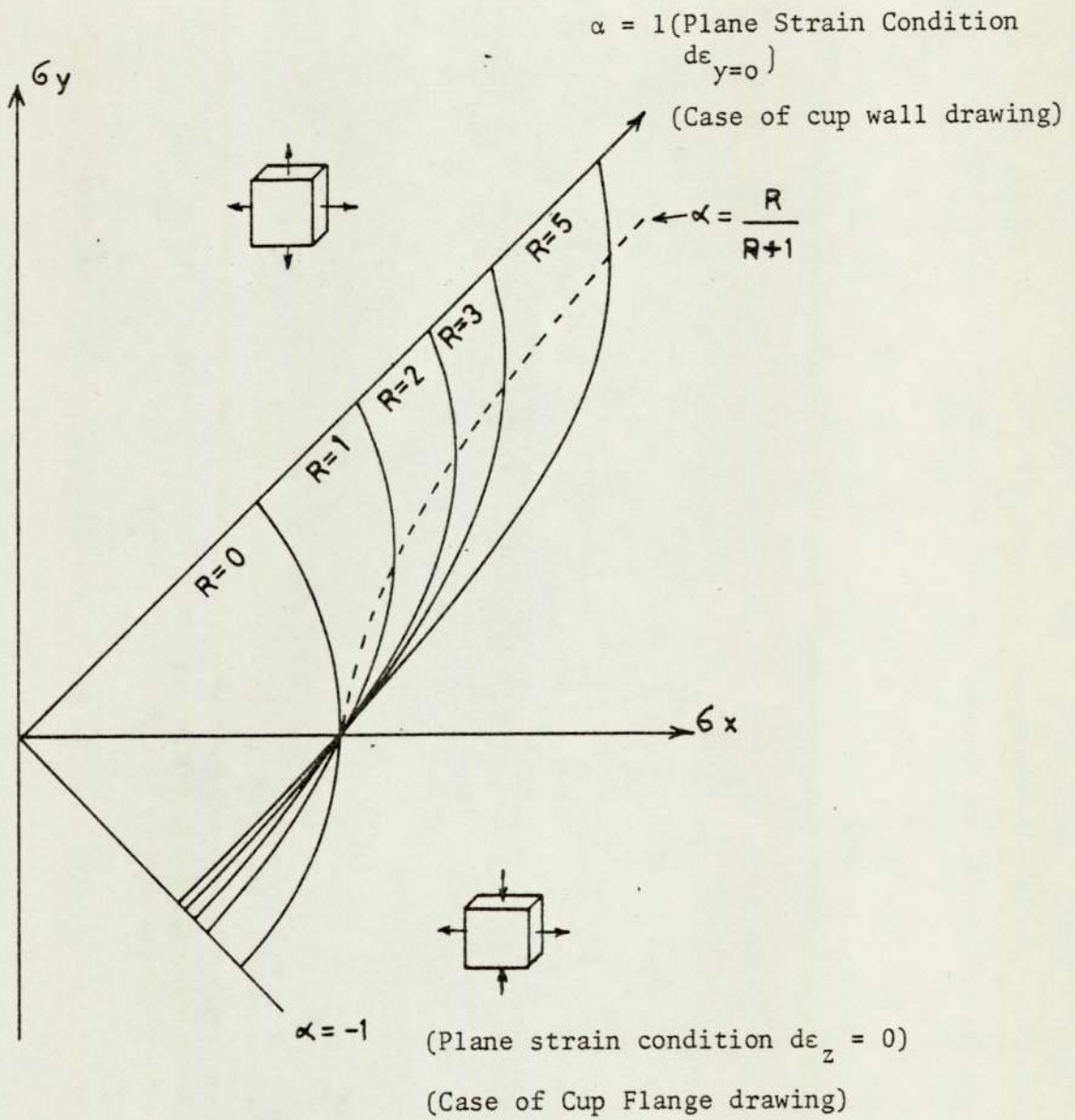


Fig. 2.5.1. Shows the plane stress yield loci for sheets with textures that are rotationally symmetric about the thickness direction  $z$ . Values of  $R$  indicate the degree of anisotropy. The stress ratio,  $\alpha = \frac{\sigma_y}{\sigma_x}$  corresponding to various loading conditions (23).

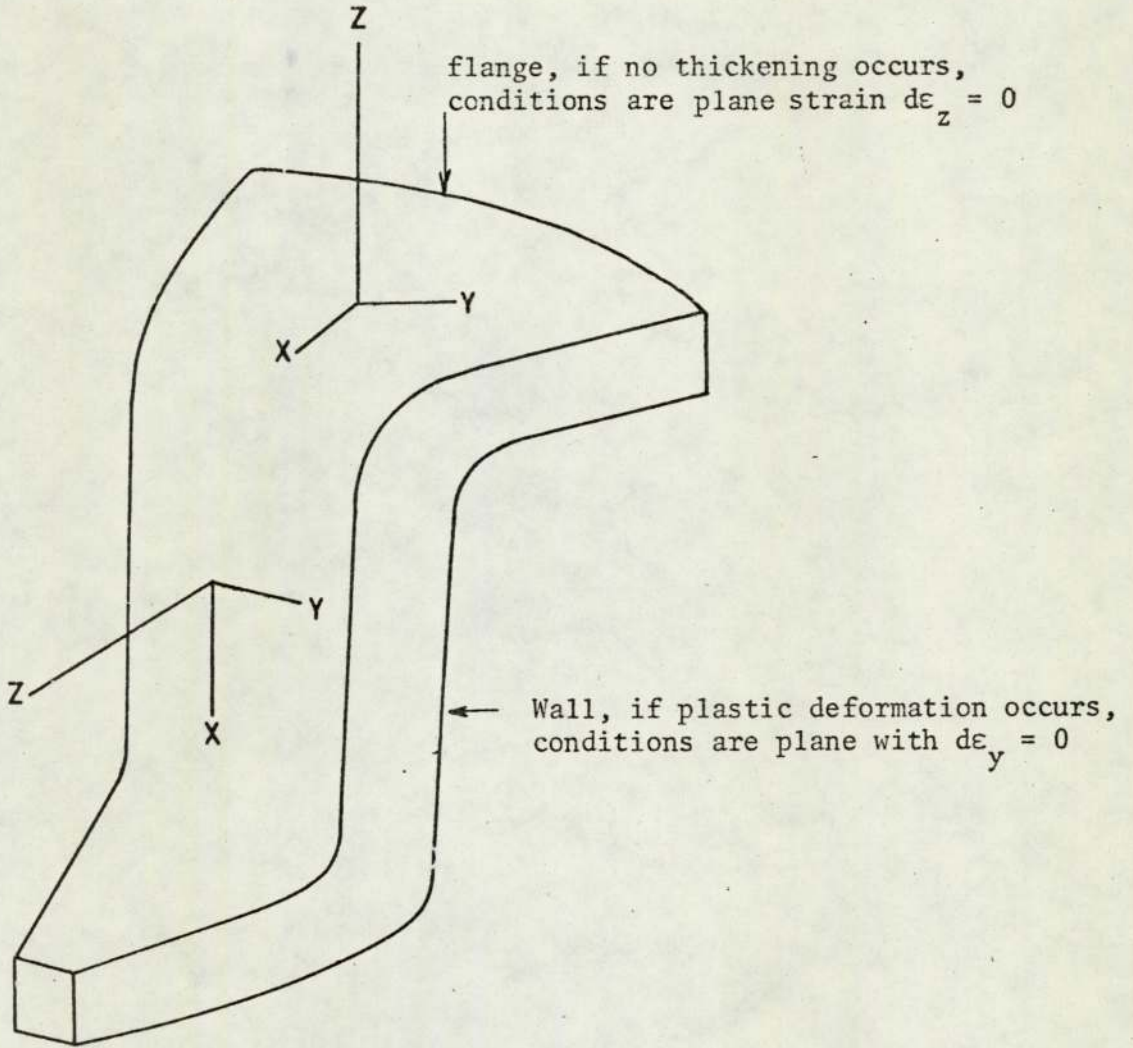


Fig. 2.5.2 shows the plane strain axes in the flange and the wall of a flat bottomed cup. The shape change in the flange is often nearly one of the plane strain,  $d\epsilon_z = 0$ . In the wall only plane strain flow,  $d\epsilon_y = 0$ , can occur because the punch prevents a decrease of wall circumference<sup>(23)</sup>.

## 2.6 EFFECTS OF THE PROCESSING FACTORS UPON TEXTURE AND R VALUE OF RIMMED STEEL STRIP

Rimmed steel strip is manufactured by casting refined steel into ingots of rectangular cross section where solidification occurs producing the characteristic rim and core ingot zones. The zones contribute to rimmed steel's unique properties primarily as a consequence of almost pure iron-inclusion-free-rim zone. The slab ingot is reheated and hot rolled, usually above the  $A_3$  temperature, firstly in a reversing slab mill and then in a tandem mill. The hot band at  $950^\circ\text{C}$  is water sprayed and subsequently coiled at a temperature between  $700^\circ\text{C}$  and  $600^\circ\text{C}$ . The coiled hot band is air cooled and pickled to remove scale. The steel sheet is then cold rolled using a 3 stand tandem mill with 500 mm diameter. The rimmed steel strip is then annealed to render the sheet ductile. The strip is finally temper rolled to improve the surface finish.

Properties of the final rimmed steel strip should depend upon the previous production cycle in addition to the chemical composition of the material. Effect of the latter is reviewed by Rosenstock, Kläner and Schmidtman<sup>(36)</sup> and it is not within the scope of the present review. However, the effects of hot rolling, cold rolling and annealing upon R value and texture of the final strip will be only considered in this review.

### 2.6.1 The effect of hot rolling

Angele and McGarity<sup>(37)</sup> were the first to report that too high hot rolling temperature (i.e.  $>975^\circ$ ) resulted in an over large grain size and hence orange peeling in the fabricated components.

On the other hand, too low hot rolling temperature (i.e.  $<900^{\circ}\text{C}$ ) can lead to poor drawability as a result of too small grain size and unsuitable texture. Hot rolling of rimmed steel is usually carried out at  $950^{\circ}\text{C}$  to produce the suitable grain size necessary to balance the properties of ductility and resistance to orange peeling. Hoff and Masing<sup>(38)</sup> recommended that the finishing temperature for low carbon steel should be somewhat just below the  $A_3$  temperature. More recently<sup>(39)</sup> it was shown that at a hot rolling finishing temperature of  $875^{\circ}\text{C}$ , which is about  $30^{\circ}\text{C}$  above the  $A_{r3}$  of rimmed steel, and spray exit temperatures between  $500^{\circ}\text{C}$  and  $600^{\circ}\text{C}$ , the hot band grain size was a minimum. This was increased when hot rolling was finished at  $775^{\circ}\text{C}$ . Rimmed steel slab hot rolled during dynamic recrystallisation, followed by spray quenching was found<sup>(39)</sup> to contain carbides mainly of the cementite form. On the other hand, hot rolling, when static recrystallisation occurred, resulted in carbides mainly of the form of degenerate pearlite. It was also reported<sup>(39)</sup> that high R value is associated with an optimum hot finishing temperature and low spray exit temperature.

Richards and Ormay<sup>(40)</sup> classified the hot rolling texture of low carbon steel into two general types. Either a relatively weak texture varies slightly from surface to centre when hot rolling above the  $A_3$  temperature, or a relatively strong texture varies considerably from surface to centre when hot rolling below the  $A_3$  temperature. They further stated that the hot rolling texture is not beneficial as the segregation is not favourable for high R values. Nagashima et al<sup>(41)</sup> hot rolled two rimmed steel bands in two different ways, in the first, hot rolling was finished at  $830^{\circ}\text{C}$  and the hot band was then coiled at

620°C. In the second, the finishing and coiling temperatures were 805°C and 550°C respectively. The surface texture in both specimens were essentially the same and was described as  $\{110\}\langle UVW \rangle$  plus  $\{112\}\langle 111 \rangle$ . The centre texture varied from one specimen to the other being of the type  $\{100\}\langle 110 \rangle$  with spread towards the  $\{112\}\langle 110 \rangle$  in the case of the first specimen. In the second specimen, the centre texture was derived from the first texture as a reinforcement of the  $\{100\}\langle 110 \rangle$  component. The centre texture was related to the surface texture by 30° rotation about the transverse direction. This rotation was reported by the same authors<sup>(41)</sup> not to be sufficient to rationalise perfectly the relationship between the two textures. This was attributed to a recrystallisation mechanism operating during hot rolling.

Jones and Walker<sup>(42)</sup> indicated that in the surface texture of specimens that had and had not undergone recrystallisation during hot rolling was identical and was described to be of the  $\{110\}\langle 112 \rangle$  type. On the other hand, the centre texture of the two specimens were different. The main texture components in the recrystallised specimen were  $(100)[011]$  with a weak  $(111)[\bar{1}\bar{1}2]$  and  $(112)[\bar{1}10]$  components, while that of the unrecrystallised specimen was  $(112)[\bar{1}10]$  only. These results are in good agreement with a previous work<sup>(43)</sup> in which it was shown that, during hot rolling, only the mid-plane thickness region of the sample is deformed under rolling condition that is not influenced by surface friction effect.

### 2.6.2 The effect of cold rolling

The room temperature cold rolling texture of rimmed steel strip has been commonly described in terms of two sets of end orientations. The first includes  $\{100\}\langle 110\rangle$ ,  $\{111\}\langle 110\rangle$ ,  $\{113\}\langle 110\rangle$  and  $\{112\}\langle 110\rangle$  orientations with the  $\langle 110\rangle$  directions parallel to the rolling direction. The second end orientation is the  $\{111\}\langle 112\rangle$  texture component with the  $\{111\}$  plane parallel to the rolling plane<sup>(44)</sup>. In some cases the  $\{111\}$  texture has been observed as a minor component<sup>(45)</sup>. Haessner and Weik<sup>(46)</sup> described the cold rolling texture by a fibre texture distributed about the  $\langle 110\rangle$  axis lying  $35^\circ$  from the sheet normal on the rolling direction radius in a pole figure. The cold rolling texture of rimmed steel was also described by the  $\{100\}\langle 110\rangle$  and the  $\{112\}\langle 110\rangle$  component, but the  $\{111\}\langle 110\rangle$  component did not appear frequently while the  $\{111\}\langle 112\rangle$  was recorded<sup>(47)</sup>. Texture of rimmed steel strip was also described in terms of tension and compression texture<sup>(48)</sup>.  $\langle 110\rangle$  texture with spread towards the  $\langle 311\rangle$  component was predicted for tension texture and a duplex  $\{100\} + \{111\}$  texture with the  $\{111\}$  predominating as a compression texture.

Since plastic strains generated during rolling are felt differently at different depths through the thickness of the sheet<sup>(49)</sup> the texture developed should vary from surface to centre. Texture developed during cold rolling is therefore dependent upon the rolling variables such as lubrication, rolling draughts and total rolling reduction. The effect of lubrication upon texture was demonstrated<sup>(50)</sup> by processing two steel strips in two different ways. Steel A was rolled with palm oil lubrication and heavy reductions at each pass.

The magnitude of the rolling draughts was not indicated but it was stated that 75% reduction was achieved in a total of five passes. This represents an average draught of approximately 0.011 in/p. Steel B was rolled without lubrication and light reductions were given per pass. Inverse pole density indicated that steel A exhibited an homogeneous texture while steel B displayed a pronounced texture segregation. Stickels<sup>(51)</sup> carried out an almost parallel study but sample B was lubricated instead of sample A. This time sample A gave the composite texture, which, therefore, resulted from rolling under severe friction condition. The surface textures were of the shear type<sup>(52,53)</sup>, containing the components  $\{112\}\langle 111\rangle$ ,  $\{110\}\langle 001\rangle$ ,  $\{110\}\langle 112\rangle$  and  $\{110\}\langle 111\rangle$ . The centre texture was related to the surface texture by  $90^\circ$  rotation about the transverse axis. Held and Stickels<sup>(50,51)</sup> had, by dry rolling, created severe friction conditions, apparently induced shear type strain in the surface of their metals.

Dillamore and Roberts<sup>(4)</sup> indicated that rolling draughts were also important parameters as heavy draughts contribute to the increase of the friction forces. Hellewell<sup>(2)</sup> has shown that at certain total rolling reduction, the mid plane texture was independent of the magnitude of the rolling draughts and was typical of b.c.c. steel texture, namely, two partial  $\langle 110\rangle$  RD and  $\{111\}$  RP fibre textures. The main difference in texture was observed in the surface layer when rolling with either dry or lubricated rolls and with draughts classified by light, medium and heavy respectively. Rolling with the heaviest possible draughts and rolls dusted with magnesium had a different effect upon the surface texture. Rolling with light draughts developed type I texture, a predominantly  $\langle 110\rangle$  RD texture, which changed

progressively towards the common medial plane texture. With heavy draughts, type III texture was developed, which was a dominant  $\{111\}$  RP. An intermediate texture, type II was developed with medium draughts. Type IV texture developed by rolling with dusted magnesia was described by a  $\{110\}\langle 112\rangle$  rolling texture.

The development of texture with increasingly total rolling reduction was described by Haessner and Weik<sup>(46)</sup>, in terms of three components. Starting from a textureless material, after 30% deformation, two components were present. Component A represents  $\{100\}\langle 011\rangle$  orientation and B is a fibre component with a  $\langle 110\rangle$  fibre axis  $35^\circ$  from the sheet normal on the rolling direction radius of the pole figure. B was much stronger than A. Above 60% deformation, a third component C was found, which was described as a limited fibre texture of increasing spread around the rolling direction as axis. Moller and Stablein<sup>(54)</sup> conducted a similar study to that of Haessner and Weik<sup>(46)</sup>. Texture was also described in terms of three components. Component  $W_1$  is equivalent to C<sup>(46)</sup>,  $W_2$  is a fibre component with a  $\langle 111\rangle$  pole parallel to the sheet normal, and  $W_3$  is a complete fibre component with a  $\langle 100\rangle$  fibre axis parallel to the sheet normal and would include A. Starting from an almost random material, these components were present at 48, 73 and 92% reduction. Spread in the component  $W_1$  increased with increasing the total rolling reduction.

Bennewitz<sup>(55)</sup> followed the effect of increasing the total rolling reduction upon texture developed in two sheets of low and 3% silicon steels exhibiting a similar starting texture described by a  $\{100\}\langle 011\rangle$  at the sheet mid plane and a proportion of  $\{110\}\langle 001\rangle$  orientation at

the sheet surface. It was found that the  $\{100\}\langle 011\rangle$  orientation initially rotated about the rolling direction to  $\{112\}\langle 110\rangle$  while the  $\{110\}\langle 001\rangle$  material rotated about the transverse direction to  $\{554\}\langle 225\rangle$  which is close to  $\{111\}\langle 112\rangle$  orientation and subsequently rotated to  $\{112\}\langle 110\rangle$ . The  $\{112\}\langle 110\rangle$  component in either of the above cases subsequently rotated about the rolling direction to  $\{001\}\langle 110\rangle$  or  $\{111\}\langle 110\rangle$ . The breaking up of the  $\{112\}\langle 110\rangle$  orientation increased with increasing the total rolling reduction. The rolling texture of steel at 60% reduction was described in terms of two fibre textures, in fibre texture A, the texture components  $\{554\}\langle 225\rangle$  and  $\{112\}\langle 110\rangle$  were predominant while fibre texture B which contained the  $\{001\}\langle 110\rangle$  and  $\{111\}\langle 110\rangle$  as a minor texture. With further reduction fibre texture B became more prominent until after 95% cold reduction, the common orientation  $\{112\}\langle 110\rangle$  became most intense. Subsequent rolling caused rotation to the stable end orientation  $\{113\}\langle 110\rangle$ . Fibre texture A was close to that embodied in the B texture component of Haessner and Weik<sup>(46)</sup> and the  $W_2$  component previously described by Möller and Stablein<sup>(54)</sup>. The rotation of the fibre texture components A and B described by Bennewitz<sup>(55)</sup> is schematically represented on one quadrant of a (110) pole figure shown in figure 2.6.2.1.

The components  $\{111\}\langle 110\rangle$  and  $\{100\}\langle 110\rangle$  of fibre texture B are in agreement with the predictions of Calnan and Clews<sup>(15)</sup>, although fibre texture A is not adequately accounted for. The development and subsequent breaking up of the  $\{112\}\langle 110\rangle$  orientation was also suggested by Dillamore and Roberts<sup>(16)</sup>. Takechi et al.<sup>(41)</sup>, considered it impossible to distinguish between the  $\{111\}\langle 112\rangle$  and  $\{554\}\langle 225\rangle$  which are only  $6^\circ$  apart, because of the spread in rolling textures. Also, pole density data<sup>(56)</sup> does not lead to the identical description of

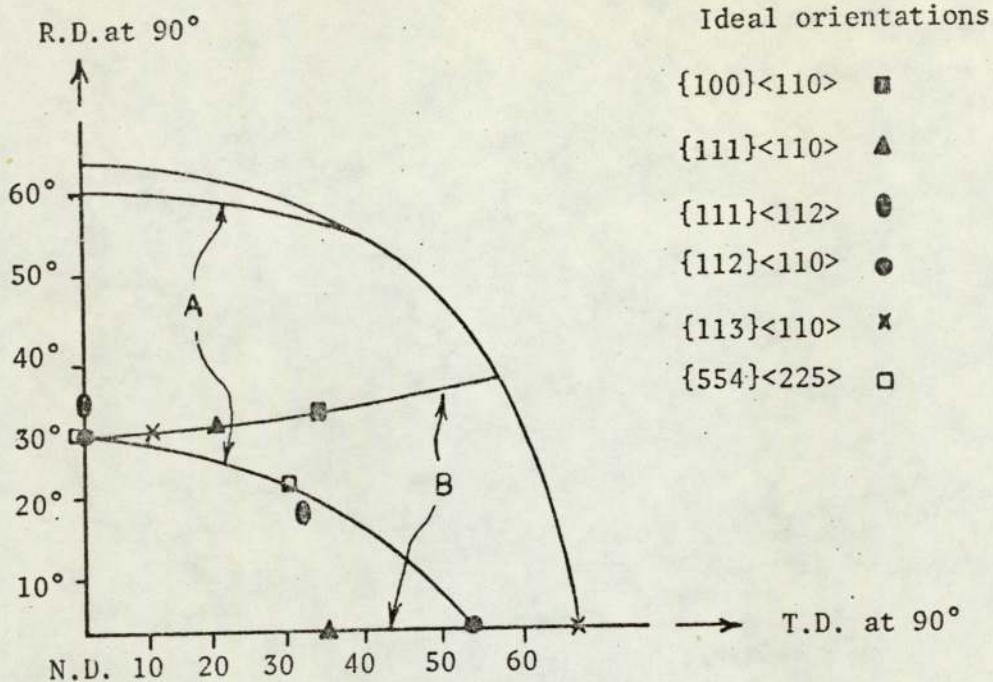


Fig. 2.6.2.1. One quadrant of (110) pole figure showing locus of (110) poles for ideal fibre textures A and B<sup>(55)</sup>.

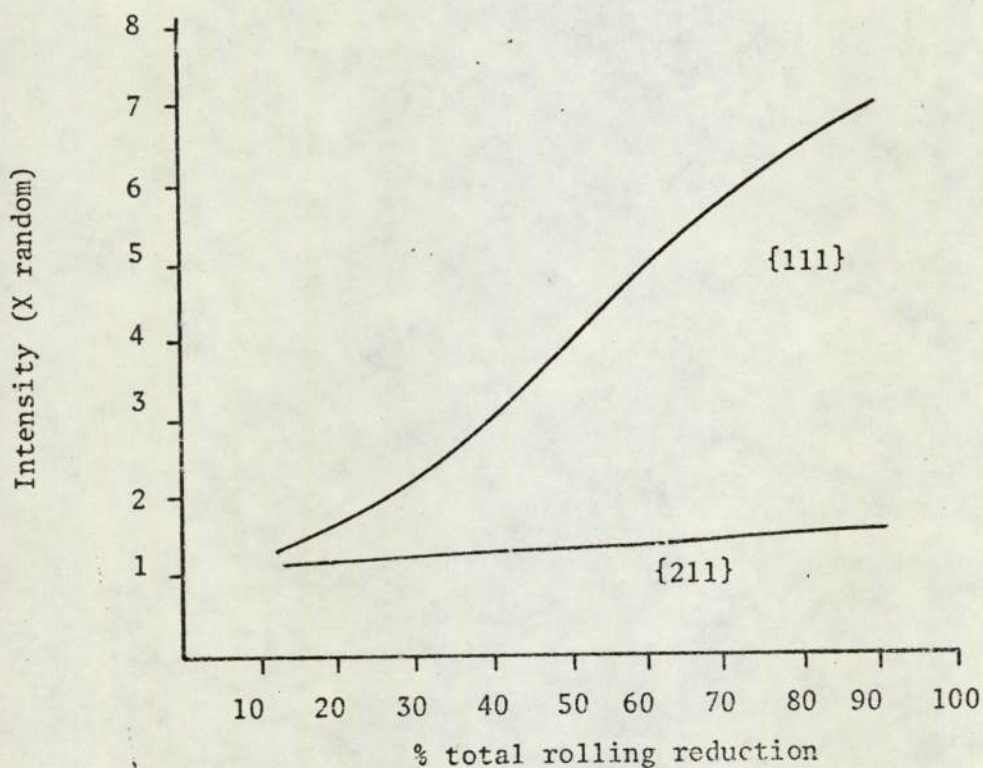


Fig. 2.6.2.2. The effect of total rolling reduction prior to annealing upon the {111} and {211} texture of the as cold rolled low carbon steel strip<sup>(56)</sup>.

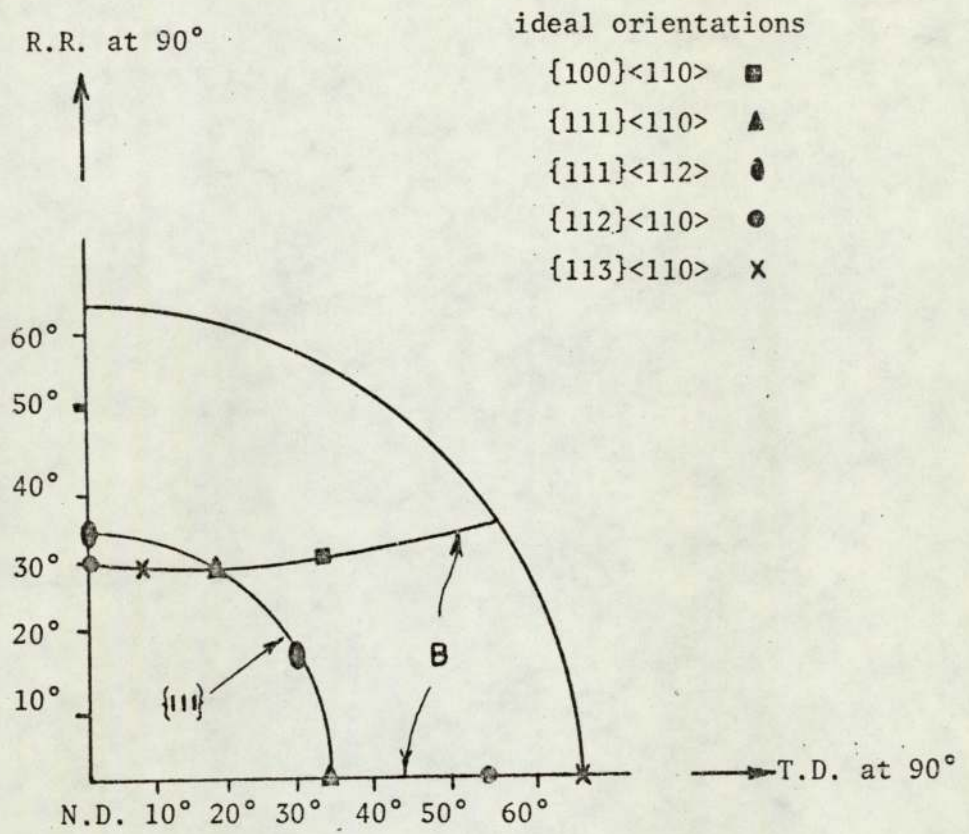


Fig. 2.6.2.3. One quadrant of (110) pole figure showing locus poles of {110} poles for ideal fibre texture B with {111} planes parallel to sheet plane<sup>(40)</sup>.

rolling texture as outlined above<sup>(55)</sup>. Fig.2.6.2.2<sup>(56)</sup> illustrates the change in density of crystal planes parallel to the plane of the sheet with increasing the cold reduction. The {111} planes increased rapidly with cold reduction, whereas {112} planes were constant over that range, and only of approximately 1.5 random intensity. This conflicts with the proposed stable end orientation, at least at 95% reduction, of the {112}<110> texture as had previously been deduced from the examination of pole figures<sup>(55)</sup>. Fibre texture B was retained, but fibre texture A was replaced by a texture with {111} planes parallel to the sheet plane as shown in figure 2.6.2.3.<sup>(40)</sup> In this case, the orientation {111}<110> was common to both textures. The similarity between figure 2.6.2.1 and figure 2.6.2.3. is apparent.

### 2.6.3 The effect of subcritical isothermal annealing

Whitely and Wise<sup>(58)</sup>, examined the effect of cold rolling reduction upon the  $\bar{R}$  values of annealed low carbon steel sheets. The outcome of their study was that R value increased with increasing the rolling reduction to  $\bar{R}_{\max}$  at 70% rolling reduction and thereafter decreased with further increase in rolling reduction as shown in figure 2.6.3.1. The recrystallisation textures were also measured over a range of total rolling reduction. This revealed the coincidence of a minimum {100} and a maximum {111} orientation at  $R_{\max}$  as shown in figure 2.6.3.2. Atkinson et al.<sup>(59)</sup> observed also  $\bar{R}_{\max}$  at 70%, but were unable to confirm any systematic correlation between the total rolling reduction and the {111} and {100} texture intensity. They further indicated that intensity of {100} poles was less than random

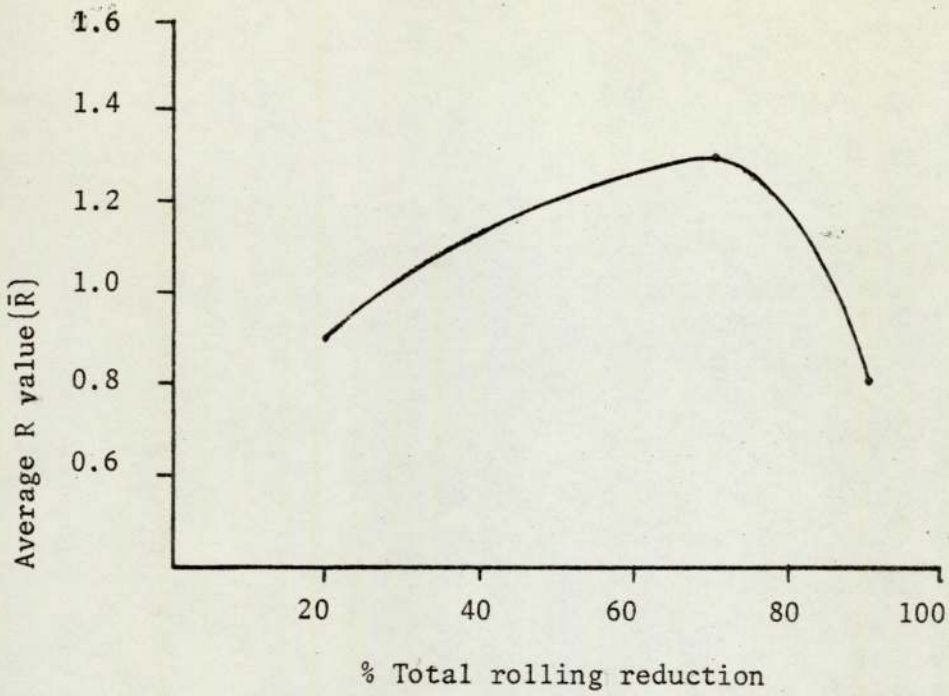


Fig. 2.6.3.1. Influence of percentage total rolling reduction, upon  $\bar{R}$  value of the annealed aluminium killed low carbon steel strip<sup>(58)</sup>.

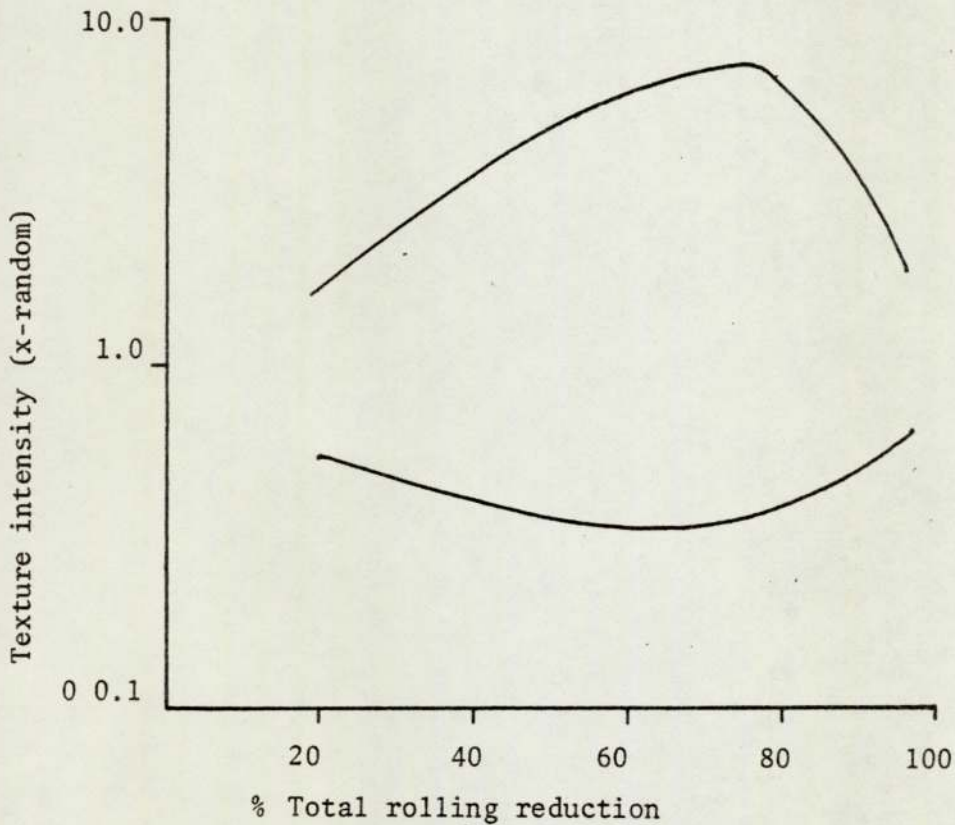


Fig. 2.6.3.2. Influence of the total rolling reduction upon the {111} and {100} texture components of the annealed aluminium killed low carbon steel strip<sup>(58)</sup>.

and questioned whether the {100} planes are capable of reducing  $\bar{R}$  value after 70% rolling reduction. Held<sup>(50)</sup> was able to change the rolling reduction at which  $\bar{R}_{\max}$  occurred by altering the cold rolling conditions so as to produce texture segregation. A "skin zone texture" developed at moderate rolling reductions and had a very high {111}/{100} relative intensity ratio. The texture ratio was intensified and increased in relative thickness to the control zone with increased cold reduction. As the reduction coincides with  $\bar{R}_{\max}$ , corresponding to 40% in this case, the skin zone dominates and results in the subsequent reduction in  $\bar{R}$  value. Furthermore, steel processed to give a homogeneous texture did not exhibit a distinctive  $\bar{R}_{\max}$  up to 88% cold reduction.

A more recent study has been performed<sup>(2)</sup> on the effect of cold rolling variables upon texture and R value of rimmed steel. It was shown that the recrystallisation texture may be described as a partial fibre texture containing the {111}RP + <110> RD components. The through-thickness texture segregation observed after cold rolling was reported<sup>(2)</sup> to be retained after annealing. The relative proportions of texture components, the degree of texture segregation and hence R value were shown to be dependent upon lubrication, rolling draughts and total rolling reduction. For a constant total rolling reduction texture segregation was minimum and R value was higher when rolling with heavy draughts and oil lubrication. Also, the total cold rolling reduction corresponding to  $R_{\max}$  increased when rolling with lubricated rolls and heavy draughts. Analysis of texture using (110) pole figures<sup>(2)</sup> indicated that {111} RP partial fibre texture promotes high R value, whereas <110> RD partial fibre texture results in relatively low R values.  $\bar{R}_{\max}$  was, therefore, associated with a balance between {111} RP and <110> RD textures. This balance is disturbed by texture segregation such that <110> RD texture predominates at variable total rolling reductions.

Mathur and Backofen<sup>(76)</sup> studied the effect of the deformation geometry as defined by the ratio between the height to length of the deformation zone or  $\Delta$ , upon the cold rolling and recrystallization textures of killed steel strip. It was found that for  $\Delta < 1$  texture developed was uniform through the thickness of the strip over a wide range of total rolling reduction. An inversion in intensity of the  $\{111\}$  rolling plane occurred after 98% total rolling reduction. The inversion was attributed to the formation of shear bands as an outgrowth of diminished strain hardening capacity. The formation of shear bands at the edge of the strip, where the hydrostatic part of the roll gap stress is substantially reduced, result in shear cracks at the edge. Edge cracks are therefore a symptom of localised flow which may modify a previously stabilised texture.

As  $\Delta$  became  $> 1$ , texture gradients appeared at the surface. Since the strain-hardening rate drops down at the surface, texture inversion is most apparent at the surface. On increasing  $\Delta$ , the imposed strain for inversion decreased and the inversion occurred at lower total rolling reduction. Intensity of the  $\{111\}$  and  $\{100\}$  components decreased and increased respectively when  $\Delta$  was increased.

Normally, the short heat treatment of the isothermal annealing results in a product that is too hard and insufficiently ductile for forming operations, mainly because the fast heating rate results in a finer grain size than slow heating<sup>(60)</sup>. In work published by Kuznetsov<sup>(61)</sup> and Keller<sup>(62)</sup>, claims were made that high heating rate

followed by fast cooling can give soft products free from quench ageing. According to Mohri<sup>(63)</sup> an effective soaking time of about 15 seconds is sufficient for almost complete recrystallisation. The effective soaking time was defined as the total time a steel specimen is above the lowest temperature at which the first strain free grains appear.

Garber<sup>(64)</sup> reasoned that the greatest softening could be made by quenching from the annealing temperature and subjecting the material to a subsequent age-softening or over-ageing treatment in a separate operation. An annealing cycle including heating rapidly to 700°C immediately quenching to 300°C and over-ageing for 30 minutes was, therefore, recommended. On cooling rapidly from 700°C to the room temperature the ferrite becomes super-saturated with carbon. After quenching, the carbon atoms came out of solution in clusters or sub-precipitates, i.e. groups of carbon atoms concentrating in local regions, distorting the  $\alpha$ Fe lattice and producing material of increased hardness. However, when higher ageing temperature was employed, the carbon atoms came out of solution as discrete precipitates of carbide, or deposited on existing carbides without the distortion of the  $\alpha$ Fe lattice and the structure became relatively softer. Dewsnap<sup>(60)</sup> studying the effect of the Garber's annealing cycle<sup>(64)</sup> upon R value of rimmed steel indicated that R values remained constant up to 50% reduction. When the total reduction was then increased the trend was towards a steady increase in R values up to 80% total rolling reduction where a sharp drop in R value occurred. The results contrast with the work of Whitely and Wise<sup>(58)</sup> on batch annealed specimens. Hellewell<sup>(2)</sup> reported that the total rolling reduction corresponding to  $R_{\max}$  was increased when intragranular cementite was

precipitated during an overageing treatment at 300°C. R values were also improved.

Haessner and Weik<sup>(46)</sup> studied the recrystallisation textures in rolled carbonyl iron. They adjusted the recrystallisation temperature to compensate for the degree of cold reduction so that recrystallisation was complete in all cases in one to two hours. After annealing for a few minutes, the rolling texture sharpened then diminished in intensity as the annealing time increased. Stickels<sup>(65)</sup> studied the textural changes resulting when 90% cold rolled electrolytic iron specimens were isothermally annealed at 700°C for 5 sec to 68 hrs then rapidly cooled. It was observed that primary recrystallisation was complete in 5 secs and normal grain growth occurred up to 16 hrs followed by abnormal recrystallisation (secondary recrystallisation) between 16 hrs and 68 hrs. The recrystallisation texture was classified as follows:

1. At 5 secs, a duplex fibre texture was evident. The dominant fibre texture was that with a  $\langle 110 \rangle$  fibre axis in the rolling direction and planes  $\{001\}$ ,  $\{112\}$  and  $\{111\}$  parallel to the rolling plane. The second fibre texture was described by  $\langle 111 \rangle$  fibre axis parallel to the rolling plane and included the orientations  $\{111\}\langle 110 \rangle$  and  $\{111\}\langle 112 \rangle$
2. From 5 secs through to 10 mins the special texture near  $\{322\}\langle 226 \rangle$  was formed by elimination of textural components near  $\{112\}\langle 110 \rangle$ .
3. After 4 hrs annealing the texture began to disappear reverting back to a texture consisting primarily of  $\{111\}\langle 110 \rangle$  and  $\{112\}\langle 110 \rangle$  components.
4. After 16 hrs annealing, texture was mainly  $\{111\}\langle 110 \rangle$  and  $\{112\}\langle 110 \rangle$ .

### 3. SCOPE OF THE PRESENT STUDY

A critical look at the literature indicates that there is still need for a closer study of the factors influencing the deep drawability of rimmed steel in order to overcome specific inadequacies in the quality of the finally annealed strip. Drawability is controlled by a degree of plastic anisotropy which is related to texture developed during the processing cycle. Since the annealing texture is related to the cold rolling texture, texture is mainly established during cold rolling. The present study was therefore, designed to study the the effect of cold rolling variables upon the texture of rimmed steel strip with a view to improving its deep drawability.

The experimental work was performed on an industrially processed rimmed steel coil (0.25 in thick and 2 ins wide). It had been hot rolled on a 3 stand tandem mill finishing at 900°C. It was water sprayed,coiled, then air cooled. It was then cold rolled from 0.324 in to 0.25 in, sub-critically annealed at 700°C for 3 hrs then furnace cooled. The chemical composition was 0.056%C, 0.039%Mn, 0.035%S, 0.01%P and 0.018%Al. Narrow coils had to be used because the pendulum mill, which is one of two mills used in the present study for cold rolling, is only suitable for cold rolling of up to 2 inch wide coils. In order to make a strict comparison between the suitability of the pendulum mill and the 2 high mill for strip production from the standpoint of texture and anisotropy the same material had to be used throughout.

The investigation was planned in four sections:

#### (1) Examination of the initial material

Texture of the initial material and its possible influence upon the cold rolling texture was examined. General information with regard to the micro-structure and grain size was provided in order to ascertain that the micro-structure is in agreement with the hot rolling condition.

(2) Examination of the cold rolled strips

The object of this section was firstly, to study the effect of seven rolling schedules upon R value and texture. Secondly, to study the effect of increasing the total rolling reduction upon texture developed by each of the seven rolling schedules.

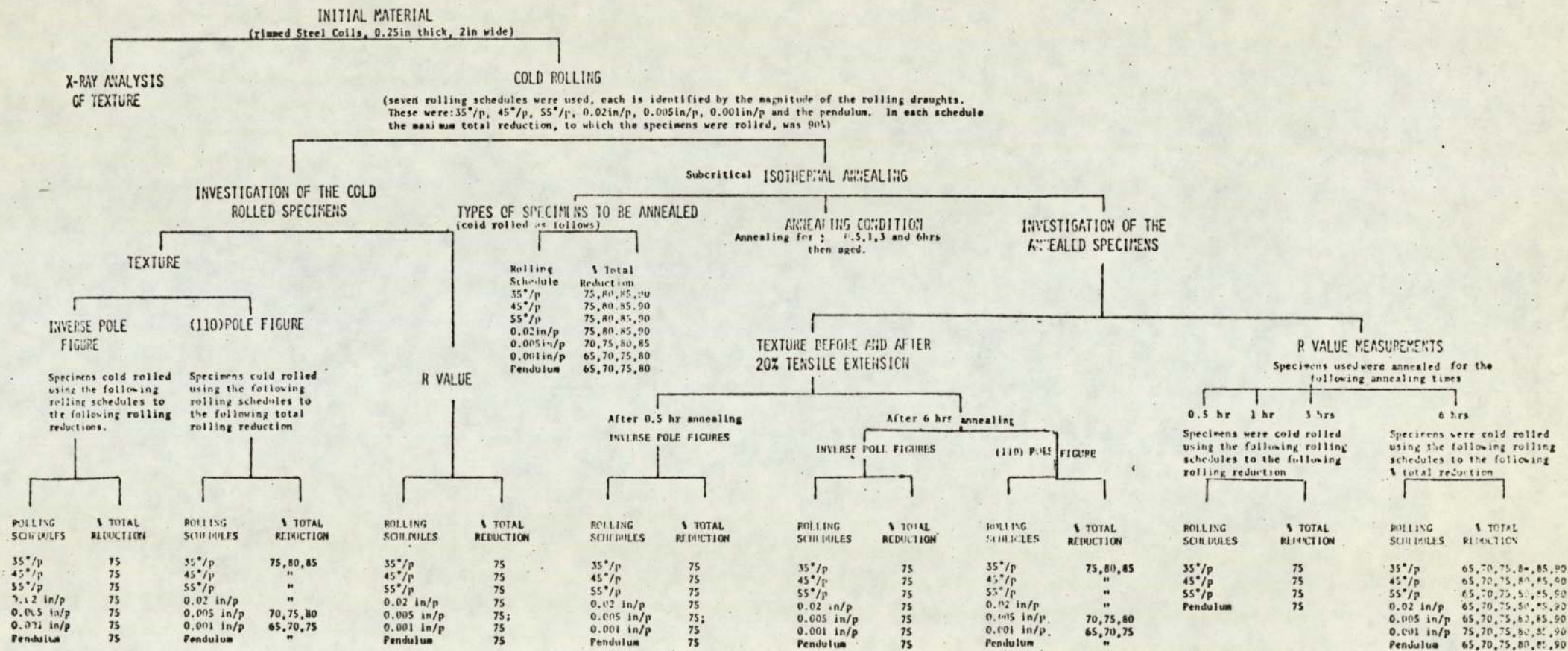
(3) Examination of the annealed strips

R value and texture were examined after annealing for different periods in order to establish the effect of annealing time. The effect of increasing the total rolling reduction upon R value and texture was examined in order to explain clearly the sharp drop in R value after heavy reductions in terms of preferred orientation.

(4) Examination of crystal reorientation after tensile strain

Texture was examined also after 20% tensile extension to monitor the modification of rimmed steel recrystallisation texture by tensile strain. This section was designed to explain the probable difference in R values of specimens processed in accordance with the seven rolling schedules.

#### 4. EXPERIMENTAL PROCEDURE



#### 4.1 INTRODUCTION

The experimental procedure of the present study included cold rolling of the initial material, annealing of the cold rolled strips, measurements of R value and examination of texture. Cold rolling was performed on the 2 high and pendulum mills. During cold rolling using the first mill, six rolling schedules were applied, either to keep a constant shear plane, or to keep a constant roll gap from one pass to the next. Details of those schedules together with the pendulum schedule are given in this section. Samples from the cold rolled strips were taken for R values and texture measurements. Corresponding samples were also taken for annealing. Annealing was carried out isothermally for different periods. R value and texture were then measured. Finally, textures of the tensile test pieces were examined after R value measurements. A full account of the experimental procedure is illustrated in figure 4.1.

#### 4.2 COLD ROLLING OF THE INITIAL MATERIAL

Seven sets of samples, cut from the initial rimmed steel coils, were selected for cold rolling at room temperature. Each set of samples was cold rolled according to certain rolling schedule. In the first type of rolling schedule, the roll gap varied from one pass to the next in order to keep a constant shear plane angle, and this was called the controlled geometry schedule. In the second type of rolling schedule, the roll gap was kept constant during the whole rolling operation and this was called constant roll gap schedule. The third type of rolling schedule was characterised by small strokes per pass and involved the pendulum rolling schedule.

#### 4.2.1 The Controlled geometry schedules

In these schedules, cold rolling was performed unidirectionally on a 2 high mill of 476 in roll diameter and rolls speed of 20 r.p.m. The rolls and the specimens were lubricated by mineral oil and were allowed to cool down to the room temperature after each pass. Measurements of thickness were taken after each pass to ensure that the required draught is accurately observed during rolling. The basis of calculating the rolling draughts is described as follows:

Consider a sheet bcde, figure 4.2.1 of initial thickness  $T_N$ , rolled to thickness  $T_x$ , with work roll diameter  $D$  and a reduction per pass  $R$ . If  $\frac{R}{2}$  is small then bcde may be considered a rectangular element in which the angle bcde is  $\theta$ . Therefore,

$$\text{Tan}\theta = \frac{T_x}{a} \quad 4.2.1.1$$

but

$$\begin{aligned} a^2 &= \left(\frac{1}{2}D\right)^2 - \left(\frac{1}{2}D - \frac{1}{2}R\right)^2 \\ &= \frac{D^2}{4} - \frac{D^2}{4} - \frac{R^2}{4} + \frac{DR}{2} \end{aligned}$$

Hence 
$$a^2 = \frac{DR}{2} - \frac{R^2}{4}$$

for small reduction per pass, hence

$$a^2 = \frac{DR}{2} \quad 4.2.1.2$$

Substitute from equation 4.2.1.2. into equation 4.2.1.1.

$$\text{Tan}\theta = \frac{T_x}{\frac{\sqrt{DR}}{\sqrt{2}}} \quad 4.2.1.3$$

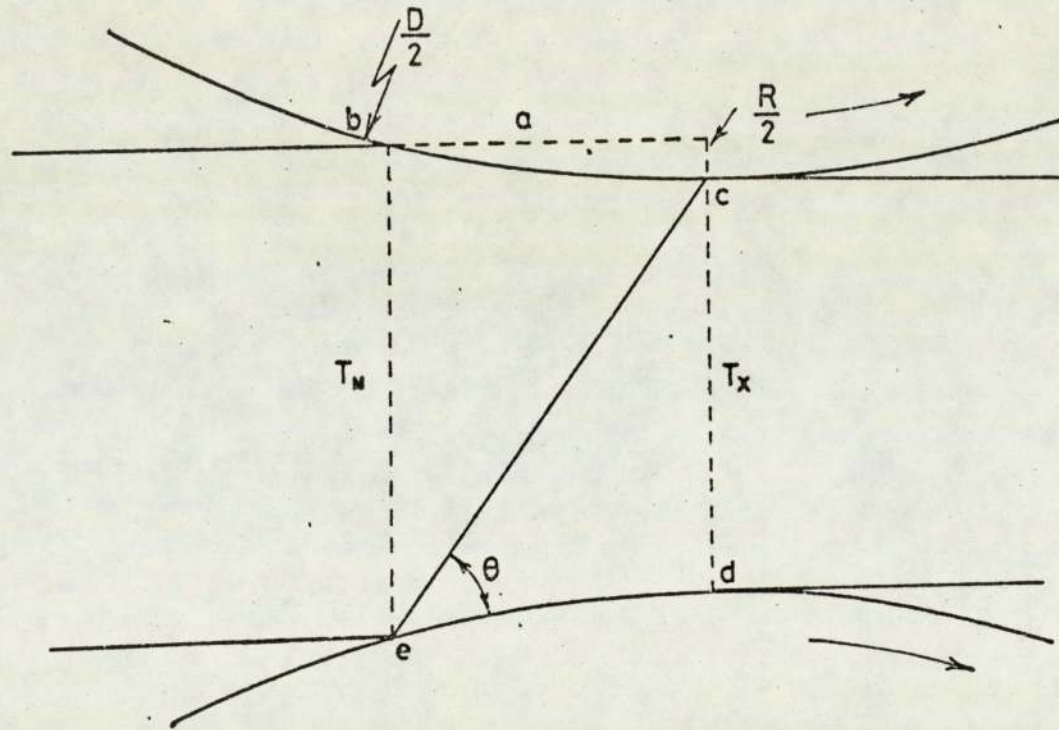


Fig. 4.2.1. Shows an element  $bcde$  being rolled to a thickness  $T_x$  with work roll diameter  $D$  and a reduction per pass  $R$ .

From Yeomans and Richards' assumption<sup>(7)</sup> for cold rolling texture formation, crystallographic slip during cold rolling is operative in each crystal on the most favourable systems over an angular range about the 45° angle to the specimen surface. Assuming rolling to be equivalent to tension in the rolling direction and compression normal to the rolling plane, the extreme limits of that angular range for the most favourably orientated planes to slip should be such that the most favourable slip directions inclined initially at 54° 44' and finally at 35° 16' to the tension axis and inversely with respect to the compression axis.

Replacing  $\theta$  in equation 4.2.1.3 by the angles 54° 44', 45° and 35° 16' resulted in three formulae corresponding to three rolling programmes. The roll gap corresponding to the three rolling schedules were calculated as follows:-

Substitute for  $\theta$  by 54° 44' in equation 4.2.1.3 therefore,

$$\tan \theta = \frac{T_x \sqrt{2}}{\sqrt{DR}} = \sqrt{2} \quad 4.2.1.4$$

The exit thickness  $T_x$  can be derived from the entry thickness  $T_N$  and the roll gap R, hence

$$T_N = T_x + R$$

Therefore,

$$T_x = T_N - R$$

From equations 4.2.1.5 and 4.2.1.4, therefore

$$R = \frac{T_N^2}{D+2T_N} \quad 4.2.1.6$$

Equation 4.2.1.6 was used for calculating the roll gap (R) corresponding to 55° shear plane angle per each pass.

Substitute for  $\theta$  by  $45^\circ$  and  $T_x$  by  $T_N$  in equation 4.2.1.3, therefore

$$R = \frac{2T_N^2}{D+4T_N} \quad 4.2.1.7$$

Equation 4.2.1.7 was used for calculating the roll gap corresponding to the  $45^\circ$  per pass rolling schedule.

Substitute for  $\theta$  by  $35^\circ 16'$  and  $T_x$  by  $T_N$  in equation 4.2.1.3 therefore,

$$R = \frac{4T_N^2}{D+8T_N} \quad 4.2.1.8$$

This equation was used to calculate the roll gap corresponding to the  $35^\circ$  per pass rolling schedule.

The draughts were calculated using a computer programme (Appendix II) the output of which is shown in Appendices III, IV and V.

The ratios between the number of passes required to reach 90% total reduction using tensional, pure and compressive rolling draughts were 4:2:1 respectively as shown in Table 4.2.1.

#### 4.2.2 The constant roll gap schedules

The same 2 high mill was used for unidirectional cold rolling under the same lubrication condition. Thickness was also measured after each pass. Three rolling schedules were used to reach total reductions similar to those in the previous schedules. The first

TABLE 4.2.1 shows the number of passes used to reach 90% total reduction in the three controlled geometry schedules.

% Total rolling Reduction	No of passes used in the 55°/p schedule.	No of passes used in the 45°/p schedule	No of passes used in the 35°/p schedule
70	45	23	11
80	77	39	20
90	174	87	44

schedule was characterised by light draughts of the order of 0.001 in/pass. The second and third schedules were described as medium and heavy draughts of the order of 0.005 in/pass and 0.02 in/p respectively. The number of passes used to affect total reduction up to 90% are shown in Table 4.2.2.

#### 4.2.3 The Pendulum Rolling Schedule

The pendulum mill<sup>(66)</sup> used in the present investigation, is an incremental rolling method for producing thin strip from thick sheets in one operation. The process is shown diagrammatically in figure 4.2.3. The ingoing sheet is forced by feed rolls into a gap formed by converging paths of two work rolls which are moved forwards and backwards. The work rolls are freely rotatable, each being supported by two rows of backing rolls. These are rotated by frictional contact with the strip which forces the sheet into the roll gap at certain speed and merges at higher speed. The rolls oscillate over paths corresponding to the reduction zones. The average relative speed of the rolls is fairly high and continuously changing during the cycle. The roll path in a rigid system is circular and the overrun of the rolls on the outgoing side increases the rolls gap at the extreme of the travel. Reduction of the load at this point results in partial release of the strain in the system, diagrammatically shown as the displacement of the pendulum pivot. The rolls then travel on parallel paths for part of the stroke and remain loaded. Deformation of the strip during rolling takes place by both strokes of the cycle.

TABLE 4.2.2 shows the number of passes used to reach 90% total rolling reduction in the three controlled draughts schedules.

% Total rolling Reduction	No. of passes used in light rolling	No. of passes used in medium rolling	No. of passed used in heavy rolling
70	176	36	10
80	189	41	12
90	226	46	14

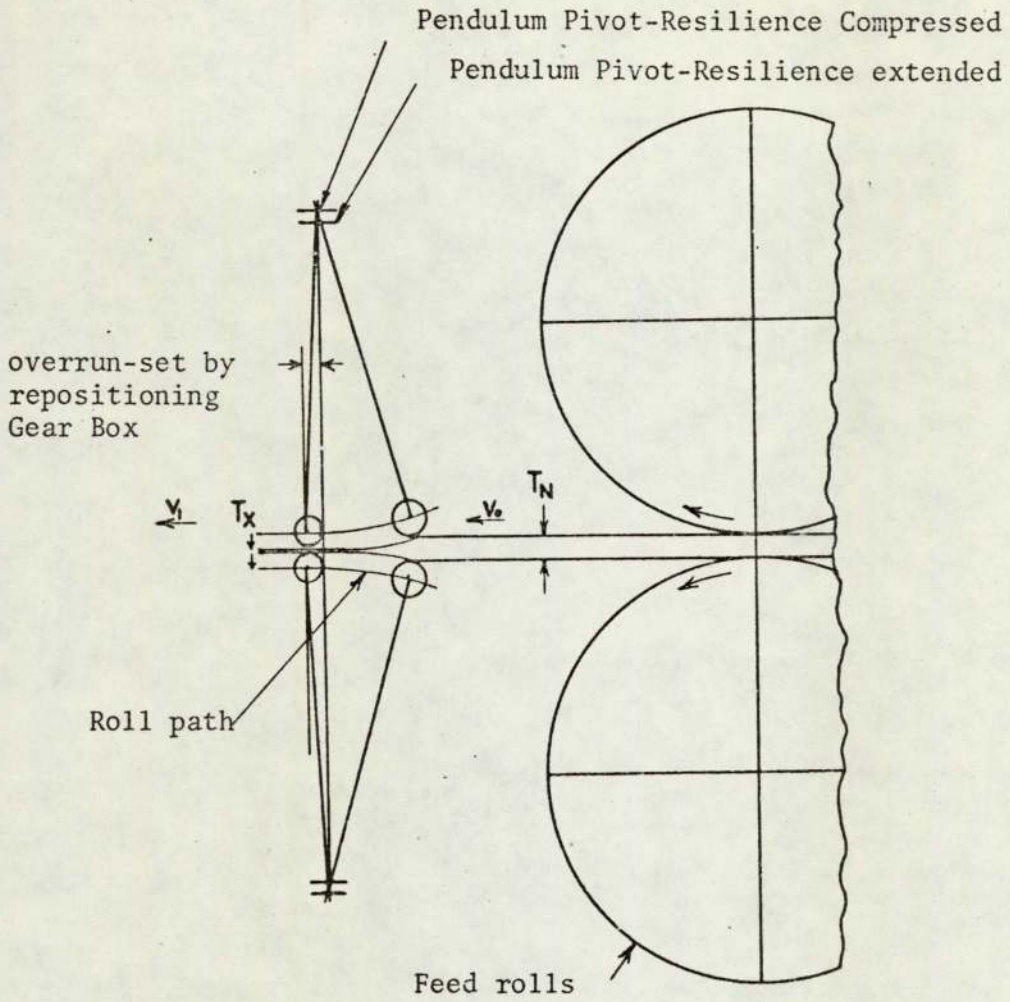


Fig. 4.2.3. Diagrammatic arrangement of the pendulum process<sup>(66)</sup>.

An experimental pendulum mill with 2 ins.-wide rolls was used in the present study. The rolling procedures started by entering the initial rimmed steel coil between two rolls, the gap between them being sufficient to admit the material to be rolled. The gap was then closed until the oscillating rolls started to exert adequate pressure on the metal to form a wedge shaped zone. The thin end of the wedge was approximately the thickness required. This was produced by rolling a stationary or slowly moving coil and applying a small reduction during the stroke. In a successful start, a 0.5 - 5% reduction is adequate to form the wedge zone after a few seconds of rolling. The rolls oscillate over paths corresponding to the reduction zone at a fairly high speed gradually reducing the material in thickness. The specimen was cooled during rolling by a special fluid and the required reduction was reached in one operation by many small strokes. Total rolling reductions corresponding to those affected by the two high mill were taken for examination.

#### 4.3 ANNEALING OF THE COLD ROLLED STRIPS

All specimens to be annealed (figure 4.1) were wrapped in thin copper foils. In addition, two protective strips of 0.02in. in thickness taken from the same cold rolled strip were placed on both sides of each specimen to be annealed, directly under the copper foil. This arrangement formed a sandwich in which the specimen to be annealed occupied the centre, surrounded by two unwanted strips and all wrapped in copper foil. This technique was shown<sup>(2,40)</sup> to reduce oxidation and decarburisation during the annealing cycle.

The specimens were then placed in the centre of an electrically heated muffle furnace, at  $700^{\circ}\text{C} \pm 5^{\circ}\text{C}$ , for periods of 0.5, 1, 3 and 6 hrs, then air cooled to room temperature. They were then overaged at  $300^{\circ}\text{C}$  for one hour and furnace cooled.

#### 4.4 MEASUREMENT OF R VALUE

The strain ratio or R value<sup>(67)</sup> is measured by the ratio of width to thickness strains in a tensile test. Since thickness strains are very small, a more practical relationship based on the constancy of volume criterion is given by the formula:

$$R = \frac{\ln\left(\frac{w_0}{w}\right)}{\ln\left(\frac{w_0}{\ell_0 w_0}\right)} \quad 4.4.1$$

where  $w_0$  and  $\ell_0$  are the initial width and length of the parallel gauge portion respectively.  $w$  and  $\ell$  are the width and length after tensile extension respectively.

Complete isotropy occurs when  $R = 1$  in all directions of the strip. When there is preferred orientation  $R$  may be  $\neq 1$  and will usually vary with the direction of testing in the plane of the sheet. If  $R$  value is infinite the thickness strain will be zero and a maximum resistance to thinning is to be expected. Conversely, if  $R = 0$ , deformation occurs mostly in the thickness direction and thinning should, therefore, occur very easily. Neither of these extremes is realised in practice.

Whiteley<sup>(29)</sup> differentiated between two types of anisotropy.

Normal anisotropy which measures the difference in properties in the

normal direction and an average value parallel to the strip surface, and planar anisotropy which indicates the difference in properties in various directions within the plane of the strip. Normal anisotropy is measured by the average strain ratio "R" value. It is, therefore, indicative of the ability of a strip to resist thinning. Planar anisotropy, on the other hand, is measured by the difference between the maximum and minimum strain ratio measured in various directions within the plane of a strip. It is associated with the earing behaviour of a strip during deep drawing. In general, if planar anisotropy is present, the strain ratio will vary considerably with direction of measurement and the average strain ratio used to describe the degree of anisotropy is defined by the relationship.

$$\bar{R} = \frac{1}{4}(R_0 + 2R_{45} + R_{90}) \quad 4.4.2$$

where the suffixes 0, 45 and 90 refer to the angle between the strip rolling direction and tensile axis.

In the present study, R values were measured in the rolling direction only, before and after annealing, using a Hounsfield tensometer, at a constant strain rate of  $4 \times 10^{-4}$ /sec. Prior to testing, blanks were machined to tensile test pieces, according to B.S.18.1962 (figure 4.4.1) except with regard to the total specimen length. The specification states that the length of the test piece should be 8 in. but test pieces of 6.5 in. were adopted since it was most conveniently suitable for the strip thickness with the minimum wastage of material whilst still allowing sufficient area for gripping purposes. The test pieces were machined by milling at high speed using a light cut each time to reduce the work

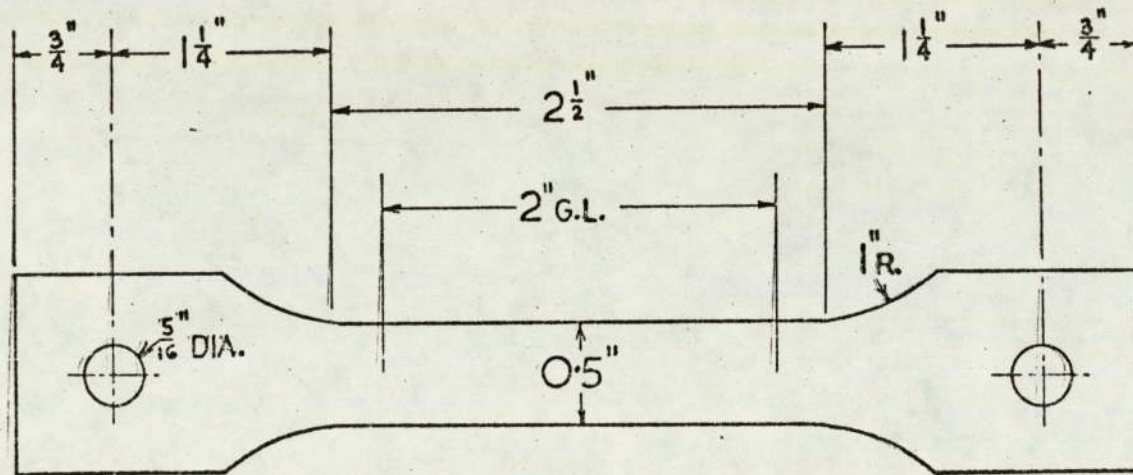


Fig. 4.4.1 A Standard tensile test piece

hardening effect upon the edges of the test pieces. The 2 in. gauge length portion was finally dressed by hand with a fine emery cloth.

In order to measure  $R_0$  value, a 2 in. gauge length was marked on the parallel portion of the tensile test piece. Each test piece was preloaded to 0.05 ton (in the region of the elastic limit) in an attempt to correctly position the specimen in the Hounsfield tensometer axis, then the load was reduced to 0.01 ton for measurements of width and thickness. Four measurements of width were made using a micrometer in the portion bounded by the gauge length and the average width was recorded. The gauge length was measured using a travelling microscope.

Measurement of  $R_0$  values before annealing were made on 7 sets of specimens rolled to 75% total reduction, using the rolling schedules, 35°/p, 45°/p, 55°/p, 0.02 in/p, 0.002 in/p, 0.001 in/p and pendulum. It was observed that the specimens accommodated a maximum tensile extension of only 2% at which a slight indication of necking occurred. The test was quickly stopped before fracture, and the gauge length, width and thickness were recorded.

$R_0$  values of the annealed specimens were measured after 20% tensile extension, firstly, for certain rolling reduction and different annealing time and, secondly, for certain annealing time and a range of total rolling reductions (fig. 4.1). In the first case, four sets of specimens cold rolled to 75% total reduction using rolling draughts of 35°/p, 45°/p, 55°/p and pendulum were selected. Each was annealed for 0.5, 1, 3 and 6 hrs at 700°C and the corresponding  $R_0$  values were measured.

In the second case, seven sets of specimens, corresponding to the seven rolling schedules, each with six different total rolling reductions of 65, 70, 75, 80, 85 and 90% were annealed for 6 hours only and their  $R_0$  values were then measured. All  $R_0$  values were calculated using equation 4.4.1.

#### 4.5 EXAMINATION OF PREFERRED ORIENTATION

Direct and inverse pole figures were used for examination of texture. A direct pole figure is a statistical distribution diagram of a given crystallographic pole relative to a suitable reference axes. In the case of rolling, the plane of a direct pole figure represents the rolling plane, the N-S axis represents the rolling direction and W-E axis is the transverse direction.

Inverse pole figures provide a quantitative distribution of pole density plots compared with the equivalent densities of a random sample relative to a single reference axis which is the sheet normal.  $\{xyz\}$  texture indicates that the  $\{xyz\}$  planes are parallel to the sheet surface. Noting the importance of the sheet normal with regard to normal anisotropy, the crystallographic direction  $\langle uvw \rangle$  parallel to the rolling direction is not considered in the description. That is, when normal anisotropy is to be considered, it is only necessary to specify the planes parallel to the sheet surface without specifying a direction parallel to the rolling direction as in direct pole figures. The sheet then may be considered to be equivalent to a fibre with the fibre axis parallel to the sheet normal.

##### 4.5.1 Direct pole figures

A number of X-ray methods for plotting direct pole figures are

available<sup>(57)</sup>. Conventionally, two geometries of specimen arrangements relative to the incident and diffracted beam are used, these being the transmission and reflection methods. For the transmission method the counter is arranged to measure the intensity of the diffracted beam transmitted through the sheet, whilst in the reflection method the intensity of the diffracted beam reflected from the surface of a true specimen is measured. Both techniques are necessary to obtain a complete pole figure, as absorption in the first, and defocusing in the second, limit the angle of specimens rotation over which accurate determination of direct pole figures can be made.

Difficulties arose in constructing a complete pole figure using two different techniques and a method was therefore devised to plot a complete pole figure using the reflection method only<sup>(77,78)</sup>. Later, Halland, Engler and Powers<sup>(79)</sup> developed a method of plotting one quadrant of the pole figure from the reflection data at three orthogonally cut specimens for description of texture. This was modified<sup>(80)</sup> to plot a complete pole figure from 0 to 180 degrees along longitude and latitude lines with corrections for backaround and intensity loss due to geometric defocusing. Texture of a sheet can be completely defined by means of the orientation distribution function<sup>(81)</sup> which can be calculated from the information provided by several pole figures.

For the purpose of this project, sufficient information can be obtained by using the reflection method described by Schultz<sup>(68)</sup> in which a thick specimen rather than a costly prepared thin specimen is required.

A Siemens X-ray generator with a cobalt target operating at 35kv and a filament current of 15 mA was employed in conjunction with a

texture goniometer and an electric pulse height discriminator. The X-ray tube aperture was set at 2 mm. in height and 2 mm. in width. The texture goniometer ring was set at  $26^\circ$  incident angle for determination of (110) pole figure. The incident beam was filtered using an iron filter to remove the  $K_\beta$  and some of the white radiations. Intensity of the diffracted beam was measured by a proportional counter situated at  $52^\circ$  and operating at 1.9 kv. The counter slit was set at 3 mm. in height and 2 mm. in width. The proportional counter is especially suited for detection of a relatively low energy radiation such as cobalt radiation because of its low background and high energy resolution. The pulse height discriminator was set at a maximum pulse rate of  $4 \times 10^4$  counts/sec and statistical error of 1.5%.

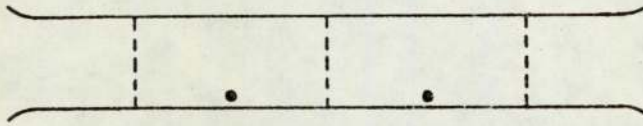
As a preliminary measure the diameter of the pole figure was scanned (radial scan) in order to have a quick idea about the specimen texture and to choose the suitable maximum pulse rate to keep the maximum line intensity of the diffracted beam within the range of the recorder chart. A complete analysis of texture was then carried out by scanning the pole figure from  $0^\circ$  to  $75^\circ$  along a spiral with a pitch of  $5^\circ$ . A random sample was then scanned in order to determine the one random level, the multiples of which are used to determine the levels 2, 3, 4...etc. of a textured specimen. The data from the recorded chart was then transferred onto a pole figure spiral which represented intensity levels as a function of the inclination angle within the range  $0^\circ$  to  $75^\circ$  studied.

The initial material, cold rolled strips and annealed strips before and after tensile extension were examined according to the foregoing procedure. Specifications of specimens examined are illustrated in figure 4.1. It is sufficient to mention here that in all cases one

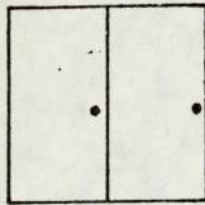
inch square specimens cut from the middle of the mother strips were used. In order to measure texture after tensile extension, two pieces of 1" x 0.5" were cut from adjacent parts of the 0.5" parallel portion width of the tensile pieces after tensile extension, then mounted together in a cold setting plastic, as shown in figure 4.5.1. Textures of all specimens were measured at 0.004 in. below the surface. Texture analysis was limited to the surface only, since it has been shown recently<sup>(2)</sup> that for a certain total rolling reduction, the mid-plane texture was independent of the rolling schedule. The main difference in texture was apparent in the surface plane with gradual transition from surface to centre texture. For the purpose of the present project, therefore, the effect of the seven rolling schedules upon texture can be revealed by examining the surface texture only. This procedure precludes the possibility of making exact correlations between texture and mechanical properties. Thinning to the surface plane to be examined was done by blocking off one face of the specimens with lacomit (except those mounted in cold setting) and alternate grinding and etching of the other face in a solution of nitric acid (one part conc. nitric acid in three parts water). Etching was necessary to remove the distorted surface layers. Textures of all specimens were determined relative to a random sample which was prepared by filing a piece of rimmed steel into a powder. The filed powder was then made into a one inch square sample by mounting in a corresponding size of X-ray specimen holder using cold setting mounting adhesive.

#### 4.5.2 Inverse pole figures

In an inverse pole figure technique, the specimen mounted on a specimen holder with its surface normal to the diffractometer axis is caused to rotate about the sheet normal to allow similar areas of the specimen to be examined. By simultaneously changing the incidence and



(a)



(b)

Fig. 4.5.1 Section from a standard tensile test piece after 20% tensile extension (a) shows the areas selected, (b) construction of the one in. square specimen required for X-ray examination.

diffraction angles, the diffraction intensities of a number of planes of a specimen and the corresponding planes of a random sample are measured. The line intensities received from the specimen planes are related to those received from the corresponding planes of a random sample by a parameter P given by the Mueller equation<sup>(91)</sup>

$$P = \frac{I_{\{hkl\}}}{IR_{\{hkl\}}} \frac{1}{h} \sum \frac{I_{\{hkl\}}}{IR_{\{hkl\}}} \quad 4.5.2$$

where  $I_{\{hkl\}}$  and  $IR_{\{hkl\}}$  are the integrated line intensities in a specimen and a random sample respectively.  $\sum I_{\{hkl\}}$  and  $\sum IR_{\{hkl\}}$  are the sums of the integrated line intensities of the specimen and random sample respectively.  $n$  is the number of crystallographic planes examined. The inverse pole figure technique<sup>(69,82)</sup> yields a quantitative measure of pole densities relative to a particular specimen direction. A multiaxial inverse pole figure has been used to identify the crystallographic direction and planes by plotting inverse pole figures in the normal, rolling and transverse directions<sup>(83,84)</sup>. This does not define sheet texture completely. Nevertheless, an inverse pole figure in the normal direction of a sheet provides useful information concerning the relationship between texture and normal anisotropy.

A Philips X-ray generator with a molybdenum target, operating at 40 kv and a filament current of 20 mA was used in the present study for inverse pole figure determination according to Harris's technique<sup>(69)</sup>. A short wave length radiation such as molybdenum radiation was used in order to increase the number of reflections so that inverse pole figures are as accurate as possible. The incident beam was filtered by a zirconium filter in order to filter out the  $k\beta$  and some of the white radiation. Intensities of eight diffracted beams corresponding to eight crystallographic planes were measured by a scintillation counter operating at

0.82 kv, at diffraction angles up to  $75^\circ$  from the plane of the sheet, as measured by a goniometer. A scintillation counter is suited for detection of  $M_oK_\alpha$  radiation because of its high energy response at  $M_oK_\beta$  wavelength. The goniometer was connected to a pulse height discrimination and a Canberra DATINUM Control unit. The pulse height discrimination was set at attenuation 4x, time constant 0.4 sec. base line 9 volts and window 10 volts. The Canberra DATINUM unit was used to control the goniometer in order to scan for peak position over a wide range of Bragg angles and to step scan across the eight sets of diffraction lines in order to measure their integrated intensities. This control over the goniometer was achieved by coordinating a data acquisition and a control function with an operational programme. Determination of inverse pole figures was carried out according to the following procedures:

(1) The random sample was scanned over a range of  $80^\circ$  between  $10^\circ$  and  $90^\circ$  for two reasons, firstly, to confirm that it is perfectly random and secondly to locate the positions and intensities of the eight diffraction lines to be examined, namely the  $\{110\}$ ,  $\{200\}$ ,  $\{211\}$ ,  $\{310\}$ ,  $\{222\}$ ,  $\{321\}$ ,  $\{411\}$  and  $\{332\}$ . A specimen in the cold rolled condition and another in the annealed condition were also scanned over the same range as the random samples to determine the peak intensities and spread of the eight diffraction lines of both specimens. This was necessary to design a step scanning programme.

(2) In order to design an operational programme to step scan across the eight sets of planes to be examined and count their integrated intensity, it was taken into consideration that the background intensity will be counted with the peak intensity itself. Therefore, counting was carried out over a range of angles at low speed of  $2^\circ$  per minute with the peak placed within that range. This range varied from the cold rolled strips

to the annealed strips and the random sample and sometimes from one peak to the next depending upon the peak spread as shown in Table 4.5.2. After the peak was scanned, the goniometer was made to move at a higher speed of  $8^\circ/\text{min}$  to the next diffraction line to be scanned by the aid of the operational programme. The diffraction line was then step scanned at a lower speed of  $2^\circ/\text{min}$  and so on until intensities of the eight diffraction lines were scanned.

(3) The integrated intensity data of the 8 sets of planes of all specimens together with the corresponding 8 sets of planes of the random sample, all punched on a suitably coded tape every 4 seconds were stored in the computer via an input signal printed in the beginning of each tape.

(4) A computer programme (Appendix VI) was used to calculate P values of the eight sets of planes by comparing their integrated intensities with the corresponding integrated intensities taken from the same diffraction lines of the random sample.

Specifications of specimens examined by inverse pole figure technique are shown in figure 4.1. Texture was measured at 0.004 in. below the surface and thinning to that depth was carried out as described in (110) pole figure technique (4.5.1).

TABLE 4.5.2. Illustrates the crystallographic plane, Bragg's angles and the range scanned during determination of inverse pole figure.

{hkl}	BRAGG ANGLES	RANGES SCANNED IN THE CASE OF			
		The as-cold rolled strips		The random sample and the annealed strips	
		From	To	From	To
110	20.15	19.40	20.90	19.30	21.30*
200	28.67	27.70	29.70	27.95	29.45
211	35.30	34.30	36.30	34.55	36.05
310	46.08	45.57	47.07	45.57	47.07
222	50.80	50.16	51.66	50.16	51.66
321	55.15	54.65	56.65	54.65	56.65
310	63.33	62.45	64.45	62.45	64.45
411					
332	70.80	69.92	71.92	69.92	71.92

\* Examination of the diffraction lines of the random sample, cold rolled and annealed strips indicated that the {110} diffraction intensity was very weak in the case of the cold rolled strips, except the pendulum, and strong in the case of the random sample, strips cold rolled by the pendulum and strips in the annealed condition. Therefore, the diffraction intensity of the {110} planes of the cold rolled strip was scanned over a narrower range. Examining the background intensity before and after the {110} peak of the cold rolled strips indicated that the full peak has been scanned.

## 5. EXPERIMENTAL RESULTS

## 5.1 INTRODUCTION

The experimental results of the present study are presented in four sections. The first section includes a description of the initial material's surface and centre textures. General information concerning the microstructure, grain size and chemical composition is also provided.

The second section illustrates the effect of seven rolling schedules upon  $R_0$  values of strips cold rolled to 75% total reduction, firstly, in the cold rolled condition and, secondly, after annealing for different periods followed by an overageing treatment. The effect of the seven rolling schedules upon  $R_0$  values of strips cold rolled to 65, 70, 75, 80, 85 and 90% total reductions, annealed for 6 hours only then aged is also illustrated.

In the third section, the cold rolling texture of materials cold rolled to 75% using each rolling schedule is described by inverse and (110) pole figures. Texture of materials cold rolled to a range of different total reductions is described in terms of (110) pole figures only. The corresponding texture developed after 0.5 hour and 6 hours annealing at 700°C will also be given in this section.

Finally, reorientation of materials cold rolled to a range of total rolling reduction, annealed for 0.5 hr and 6 hrs, aged then subjected to 20% tensile extension is examined in Section Four.

## 5.2 EXAMINATION OF THE INITIAL MATERIAL

Examination of the initial material's microstructure by optical microscopy revealed that it is a typical low carbon steel microstructure. It is characterised by equiaxed ferrites of 25-30  $\mu$  grain size and fine

carbide dispersions of cementite. A micrograph showing the microstructure of the initial material is shown in figure 5.2.1. The chemical composition of the initial material is listed in Table 5.2.1.

It was necessary to establish, firstly, that the random sample used for P value measurements is perfectly random. However, measurements of the integrated intensities of eight crystallographic reflections of the random sample was compared with the calculated relative intensities of corresponding planes of a perfectly random steel sample. The comparison confirmed that the random sample used in the present study is perfectly random as shown in Table 5.2.2.

Measurements of P values of 8 crystallographic planes of the initial material indicated that the {110} planes were dominant at the surface while the {100} planes were dominant at the centre. P values of the {100} and {111} planes varied slightly from surface to centre, as shown in figure 5.2.2. and Table 5.2.3.

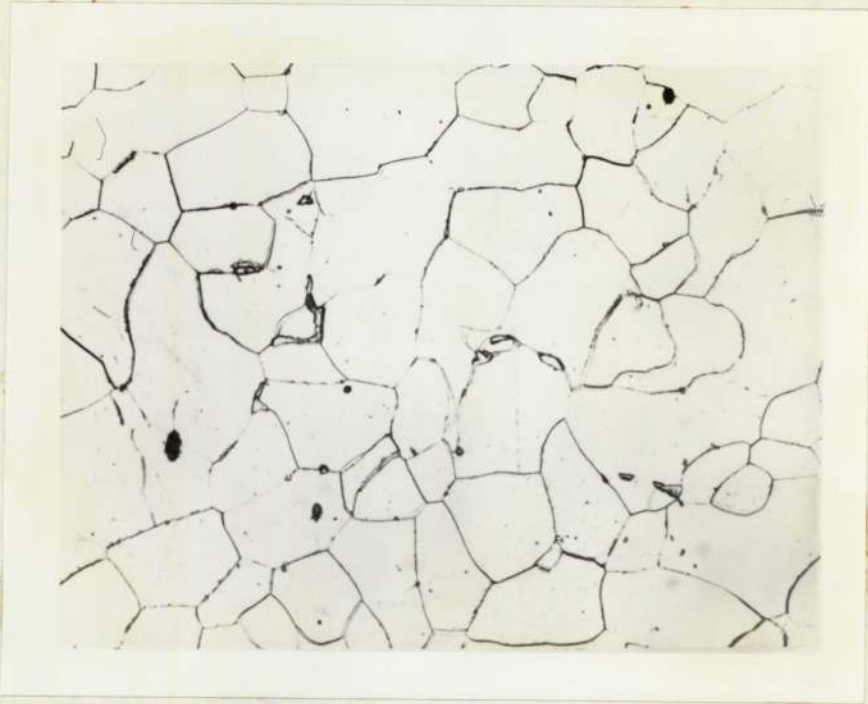


Fig. 5.2.1. A micrograph of the initial material showing equiaxed ferrites of 30  $\mu$  grain size, and fine carbide dispersions of cementite (X 500)

Table 5.2.1. A comparison between chemical composition as determined in the present project and that provided by the supplier.

Element	C	Mn	S	AL	O <sub>2</sub>	P	N <sub>2</sub>
Weight % (Measured)	0.05	0.35	0.028	0.014	0.015	0.014	0.003
Weight % (Supplied)	0.056	0.39	0.035	0.018	Not Supplied	0.01	Not Supplied

{hkl}	calculated relative integrated intensity	Measured integrated intensity
110	100	99.8
200	20	20.5
211	30	30.3
310	11.3	11.5
222	2.5	2.7
321	10.9	11.0
330	4.3	4.5
411		
332	1.8	2.0

Table 5.2.2. Measured integrated intensities of 8 crystallographic Bragg reflections of a rimmed steel random sample compared with the calculated relative integrated intensity of corresponding planes of a steel random sample.

Relative integrated intensity was calculated from the equation<sup>(85)</sup>

$$I = [F]_p^2 \left[ \frac{1 + \cos^2 2\theta}{\sin^2 \theta \cos \theta} \right] e^{-2M}$$

where F is the structure factor, P is the multiplicity factor,  $\left[ \frac{1 + \cos^2 2\theta}{\sin^2 \theta \cos \theta} \right]$  is the Lorentz polarisation factor, and  $e^{-2M}$  is the temperature factor.

No.	$2\theta^\circ$	{hkl}	P values (surface)	P values (centre)
1	20.14	110	1.12	0.70
2	28.67	200	1.05	1.27
3	35.25	211	0.97	1.15
4	46.03	310	0.75	0.72
5	50.50	222	1.00	0.95
6	55.00	321	0.87	1.06
7	63.00	330 411	1.12 0.18	0.70 0.67
8	70.50	332	0.93	0.77

Table 5.2.3. P values of the initial material

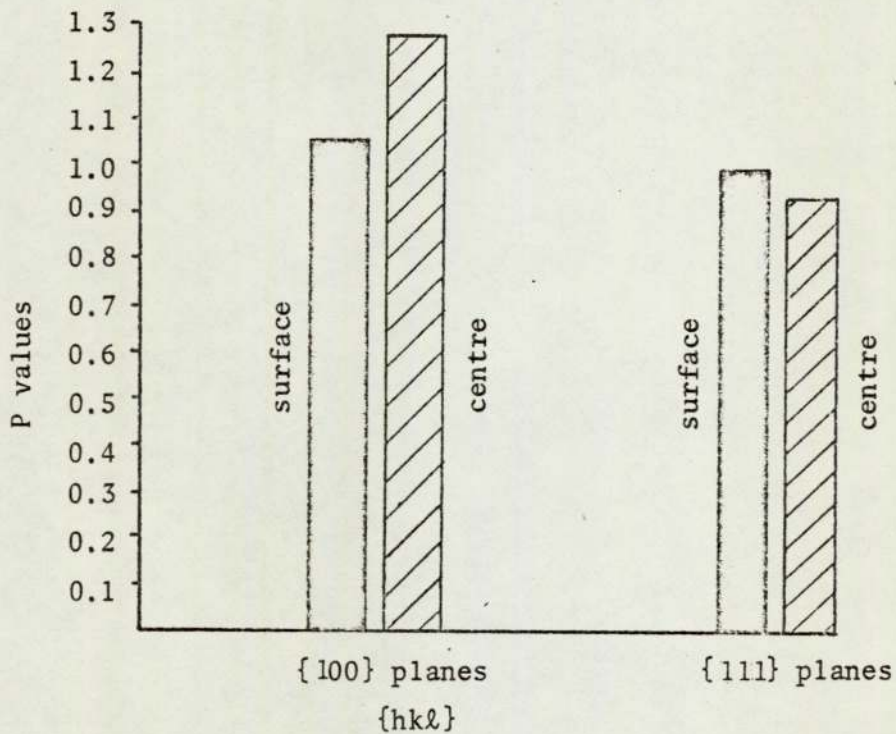


Fig. 5.2.2. The variation in the P values of the {111} and {100} planes at the surface and centre of the initial material.

### 5.3 Measurement of $R_0$ values

#### 5.3.1 The cold rolled materials

$R_0$  values of the cold rolled materials were very low ranging between 0.35 and 0.16 in the case of material rolled by the 35°/p and Pendulum schedules respectively. The experimental error in  $R_0$  value ( $\delta R$ ) due to the uncertainty in measurements of width and gauge length was calculated according to the equation

$$R = \frac{R_0+1}{\ln(\ell/\ell_0)} \left[ (R_0+1) \left( \frac{\delta W}{W} + \frac{\delta W_0}{W_0} \right) + R \left( \frac{\delta \ell}{\ell} + \frac{\delta \ell_0}{\ell_0} \right) \right]$$

where

$\ell_0$  is the gauge length before ten.ext.(2.0")

$\ell$  is the gauge length after 2% ten.ext. (2.04")

$\delta \ell$  is the error in the gauge length measurement (0.001")

$W_0$  is the width before tensile ext. (0.5")

$W$  is the width after 2% tensile ext.

$\delta$  is the error in measurement of width (0.0005")

Table 5.3.1 shows the variation in  $R_0$  value  $\pm \delta R$  with the seven rolling schedules

Rolling schedules	$R_0$ values	$\delta R$
35°/p	0.35	$\pm 19$
45°/p	0.31	$\pm 18$
55°/p	0.27	$\pm 18$
0.02 in/p	0.24	$\pm 0.17$
0.005 in/p	0.22	$\pm 0.17$
0.001 in/p	0.20	$\pm 0.16$
Pendulum	0.16	$\pm 0.14$

The variations in  $R_0 \pm \delta R$  with the rolling schedules are also shown in Fig. 5.3.1.

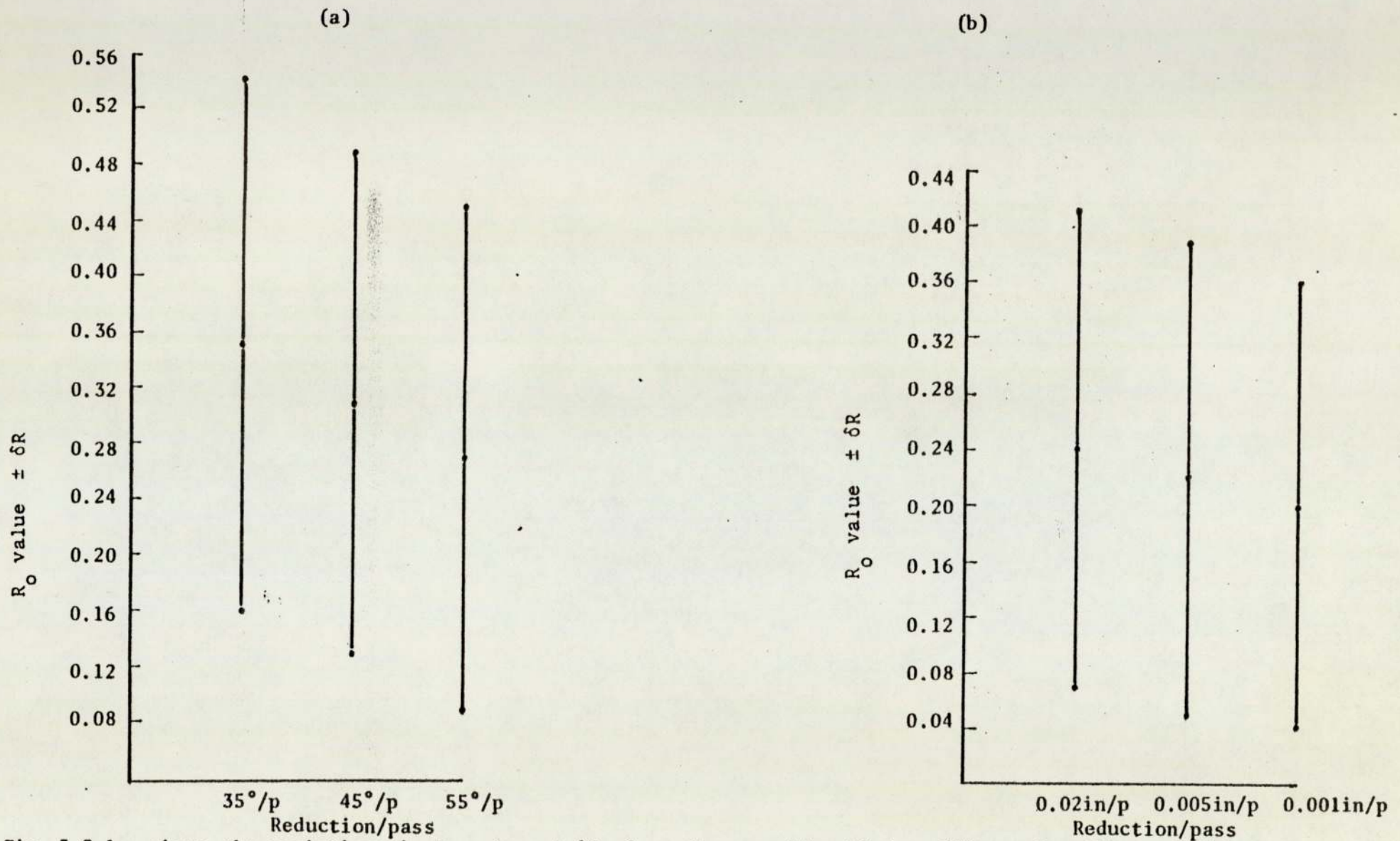


Fig. 5.3.1. shows the variations in  $R_o$  values  $\pm \delta R$  of specimens cold rolled to 75% total rolling schedules using the 35°/p, 45°/p and 55°/p schedule (a), and the 0.02 in/p, 0.005 in/p and 0.001 in/p schedules (b).

### 5.3.2 The annealed materials

#### (a) R values of materials cold rolled to 75% total reduction then annealed for different annealing times

Measurements of R values of specimens cold rolled to 75% using the 35°/p, 45°/p, 55°/p and pendulum schedules, annealed for 0.5, 1, 3 and 6 hrs then aged, indicated a significant improvement in  $R_0$  values by increasing the annealing time, as shown in figure 5.3.2a. The results indicate also that  $R_0$  value was dependent upon the rolling procedure especially after longer annealing time.

Annealing for half an hour resulted in slightly higher  $R_0$  value when rolling with reduction per pass equivalent to 35° relative to rolling with 45°, 55° and pendulum. After 6 hrs annealing, the difference in R value was apparent. The increase in  $R_0$  value of specimens cold rolled using 35°/p, for example, was equivalent to 59% in comparison with 19% in the case of specimens cold rolled by the pendulum mill. A full presentation of the variation in  $R_0$  value after 0.5 and 6 hrs annealing with the 35°/p, 45°/p, 55°/p and pendulum rolling schedules is listed in Table 5.3.2a.

#### (b) $R_0$ values of materials cold rolled to a range of total reductions then annealed for 6 hrs

$R_0$  values of specimens cold rolled to 65, 70, 75, 80, 85 and 90% total reductions, according to the rolling schedules 35°/p, 45°/p, 55°/p, 0.02 in/p, 0.005 in/p, 0.001 in/p and pendulum, annealed for 6 hrs then aged are shown in figure 5.3.2b. It is evident that the behaviour of  $R_0$  values when increasing the total rolling reduction within the range studied was dependent upon the

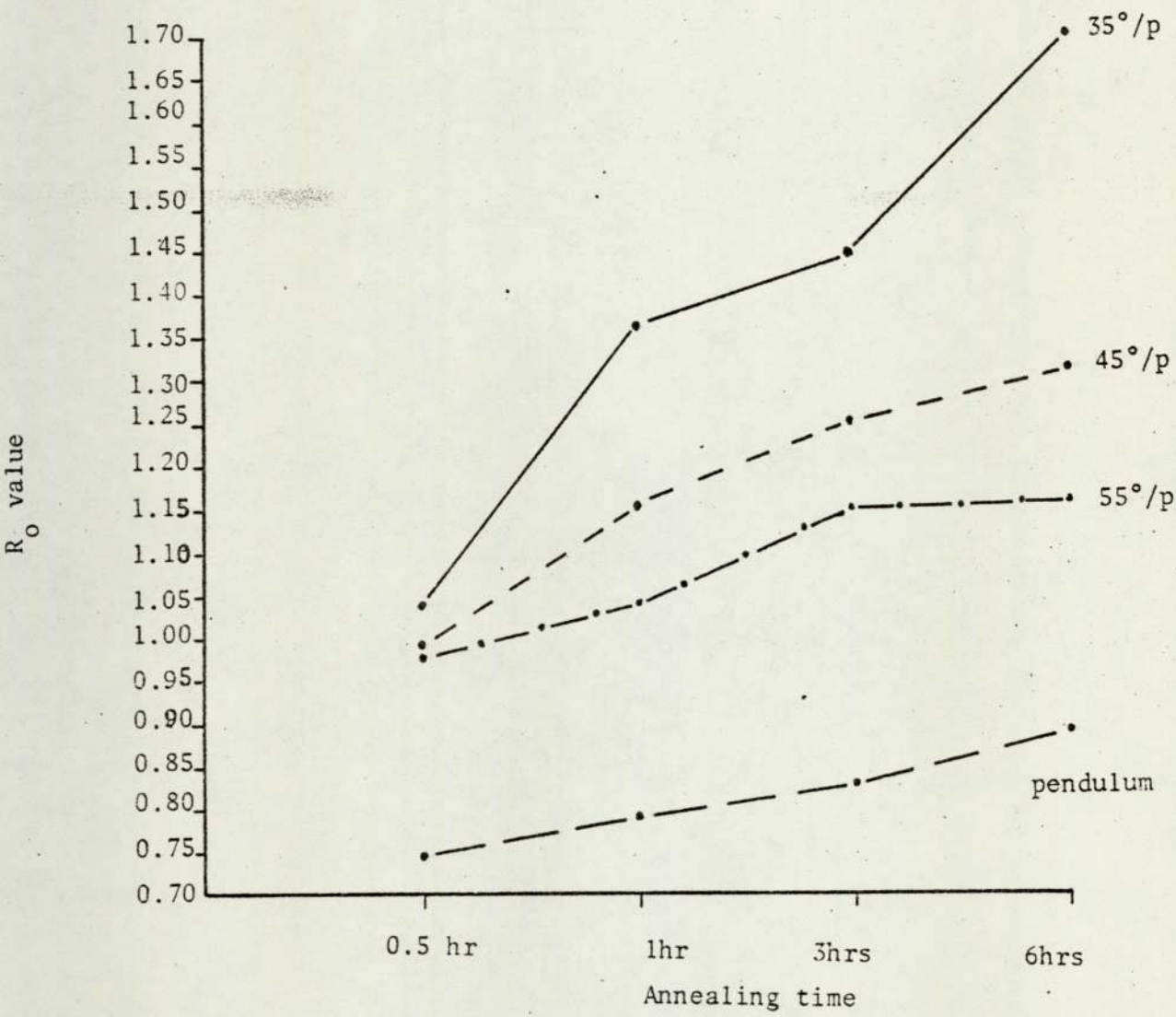


Fig. 5.3.2.a. Shows the effect of increasing the annealing time before a final overageing treatment upon  $R_o$  values of specimens cold rolled to 75% total reduction, using 35°/p, 45°/p, 55°/p and pendulum rolling schedules.

Table 5.3.2a. Illustrates the effect of increasing the annealing time upon  $R_0$  values of specimens cold rolled to 75% total reduction, using 35°/p, 45°/p, 55°/p and pendulum rolling schedules.

Rolling schedules	$R_0$ values measured after the following annealing times				% increase in $R_0$ values after 6 hrs annealing relative to 0.5 hour annealing
	annealing times				
	0.5 hr	0.5 hr	3 hrs	6 hrs	
35°/p	1.041	1.362	1.424	1.653	58.8%
45°/p	0.982	1.153	1.233	1.324	34.8%
55°/p	0.968	1.037	1.176	1.221	26.1%
Pendulum	0.740	0.790	0.820	0.880	18.9%

rolling procedures. This behaviour may be classified into three categories corresponding to constant geometry, constant roll gap and pendulum rolling schedules.

In constant geometry rolling schedules, no change in  $R_o$  value with increasing the total rolling reduction was observed, but  $R_o$  value was dependent upon the rolling schedule. It is apparent from figure 5.3.2b that  $R_o$  value has significantly increased with decreasing the shear plane angle. For example,  $R_o$  value increased from 1.22 to 1.33 to 1.65 when rolling with  $55^\circ/p$ ,  $45^\circ/p$  and  $35^\circ/p$  respectively and remained constant within the range of total reduction studied.

Specimens cold rolled using constant roll gap schedules are characterised by an increase in  $R_o$  value when increasing the total rolling reductions up to a critical value at which  $R_o$  value decreased with further increase in rolling reduction. The total rolling reduction corresponding to the maximum  $R_o$  value was dependent upon the magnitude of the roll gap. These  $R_{o \text{ max}}$  coincide with 70, 75 and 80% total reduction when rolling with 0.001 in/p, 0.005 in/p and 0.02 in/p respectively. The magnitudes of the maximum  $R_o$  values increased by increasing the roll gap.

The pendulum mill schedule, on the other hand, had a completely different effect upon  $R_o$  values at higher total rolling reductions. This is apparent in figure 5.3.2b from the continuous decrease in  $R_o$  value when the total rolling reduction was increased from 65% to 90%.

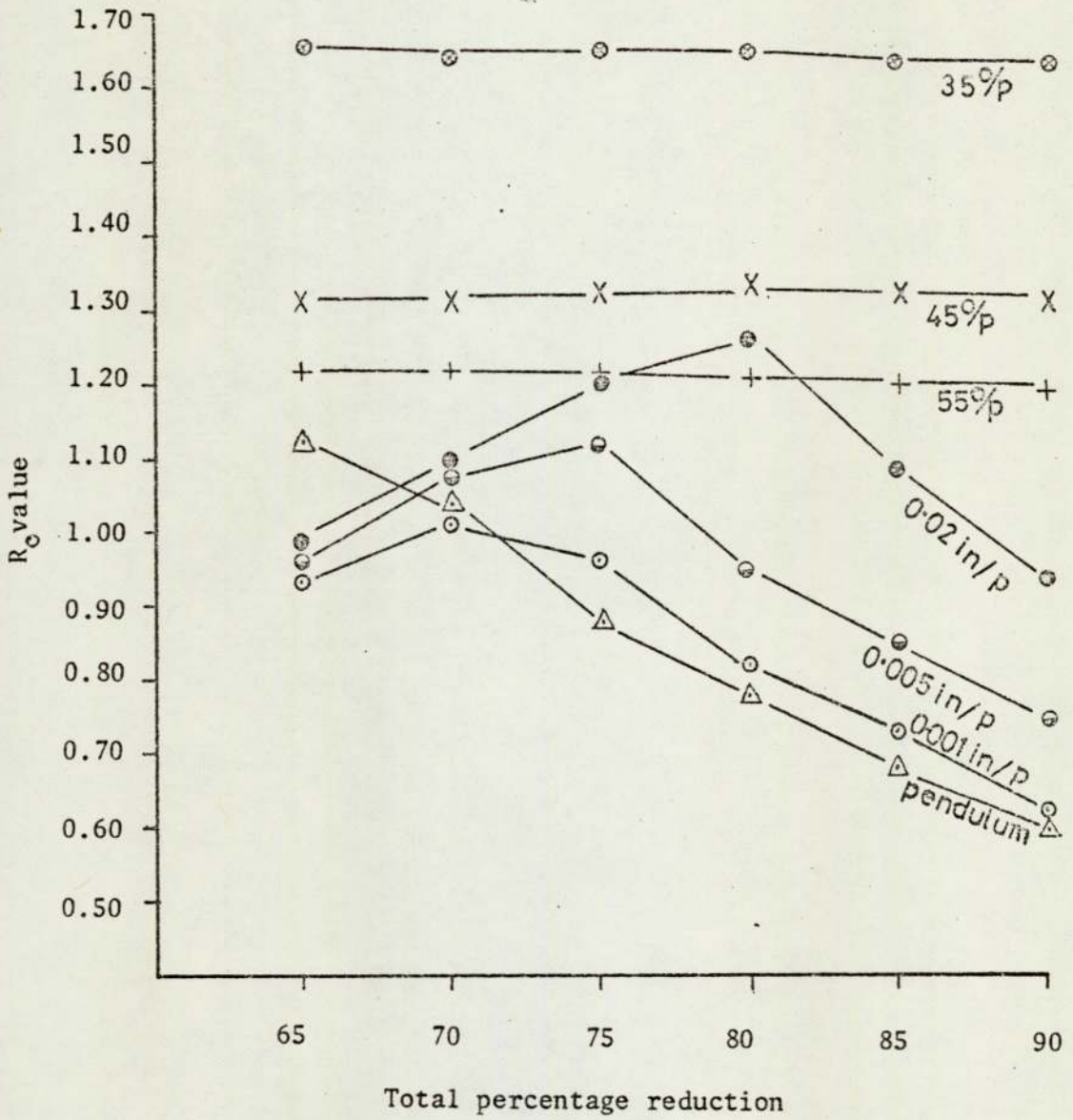


Fig. 5.3.2.b. Illustrates the effect of seven rolling schedules upon  $R_0$  values of specimen cold rolled to a range of total reductions, annealed for 6 hrs then aged.

## 5.4 EXAMINATION OF TEXTURE

### 5.4.1 The cold rolled materials

#### (a) Texture developed by controlled geometry rolling schedules

Measurements of P values of specimens cold rolled to 75% total reduction using reductions per pass equivalent to 35°, 45° and 55° indicated that crystals with {111} crystallographic planes parallel to the surface were predominant, as shown in Table 5.4.1.1a. The {100}, {211} and {332} P values were the next most highest depending upon the rolling schedule, while the {110} orientation was a minor component. It is also apparent from Table 5.4.1.1 that textures of specimens cold rolled using the 35°/p schedule had the highest {111} and the lowest {100} P values in comparison with texture of specimens cold rolled using the 45°/p and 55°/p schedules. A slight reduction in the P values of the {211} and {332} planes is also evident when the shear plane angle was decreased. On the other hand, P values of the {310}, {321} and {411} increased by decreasing the shear plane angle.

Analysis of the (110) pole figures of specimens cold rolled to 75, 80 and 85% total reductions using the 35°/p, 45°/p and 55°/p schedules with reference to the ideal (110) pole figure shown in figure 5.4.1.1 indicated that texture developed was typical of b.c.c. iron texture. It can be described by two partial fibre textures with  $\langle 110 \rangle$  direction parallel to the rolling direction and {111} plane parallel to the rolling plane, that is  $\langle 111 \rangle$  RD and {111} RP respectively. The main texture components were the {112} $\langle 110 \rangle$  {113} $\langle 110 \rangle$ , {111} $\langle 110 \rangle$ , {100} $\langle 110 \rangle$  and {111} $\langle 112 \rangle$  components, as

No	{hkl}	P VALUES		
		35°/p	45°/p	55°/p
(1)	110	0.05	0.06	0.06
(2)	200	2.20	2.48	2.61
(3)	211	1.59	1.44	1.41
(4)	310	0.10	0.11	0.13
(5)	222	3.49	3.37	3.26
(6)	321	0.09	0.12	0.14
(7)	330	0.05	0.06	0.06
	411	0.09	0.10	0.11
(8)	332	0.34	0.26	0.22

(a)

No	{hkl}	P VALUES		
		0.02in/p	0.005in/p	0.001in/p
(1)	110	0.07	0.07	0.07
(2)	200	2.70	2.80	3.01
(3)	211	1.39	1.33	1.27
(4)	310	0.22	0.25	0.29
(5)	222	3.01	2.92	2.72
(6)	321	0.18	0.20	0.23
(7)	330	0.07	0.07	0.07
	411	0.17	0.19	0.22
(8)	332	0.19	0.15	0.10

(b)

No	{hkl}	P Values Pendulum
(1)	110	0.27
(2)	200	3.20
(3)	211	0.91
(4)	310	0.31
(5)	222	2.39
(6)	321	0.30
(7)	330	0.27
	411	0.29
(8)	332	0.06

(c)

Table 5.4.1.1. P values of specimens cold rolled to 75% (a) using the 35°/p, 45°/p, 55°/p schedules, (b) using the 0.02 in/p, 0.005 on/p, 0.001 in/p schedules and (c) using the pendulum schedules.

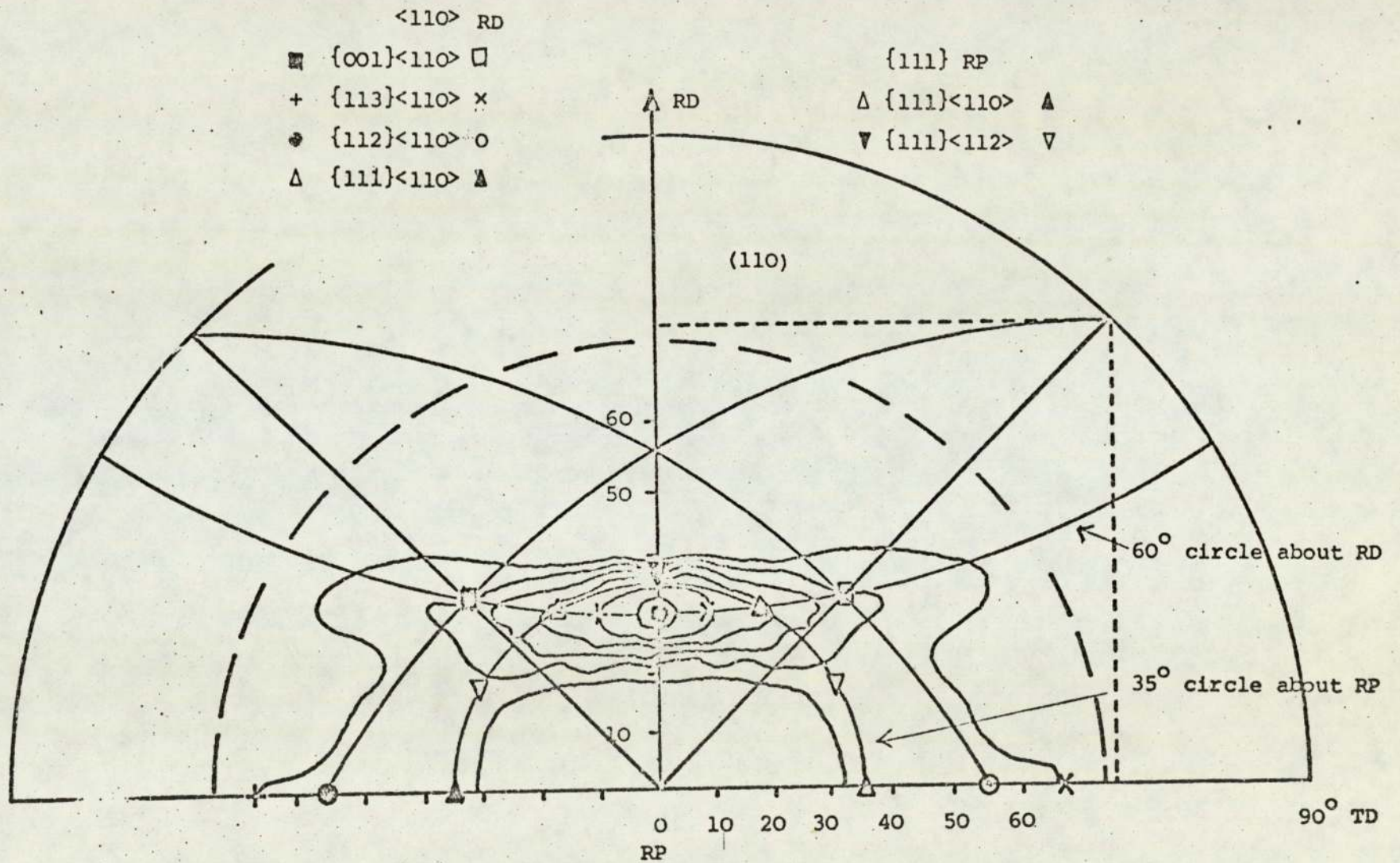


Fig. 5.4.1.1. (110) ideal orientation in b.c.c. steel.

illustrated in (110) pole figures shown in figure 5.4.1.2 (a,b,c), figure 5.4.1.3 (a,b,c) and figure 5.4.1.4 (a,b,c).

After 75% total rolling reduction, texture developed by the 35°/p schedule was the strongest and the most concentrated about the 30° and 35° circles from the sheet normal along the sheet normal - rolling direction radius of the pole figure. A gradual reduction in texture intensity and more spread towards the {100}<110> component in the sequence of rolling with 45°/p and 55°/p schedules was also evident.

Texture of specimens cold rolled using the 35°/p schedule had relatively higher {112}<110> and {111}<112> components and a relatively lower {100}<110> component. Reductions in the {112}<110> and {111}<112> components and an increase in the {100}<110> component occurred when rolling with the 45°/p and 55°/p schedules respectively.

Increasing the total rolling reduction to 80% using the 35°/p schedule resulted in an increase in the {112}<110> intensity, while intensities of the {113}<110>, {100}<110> and {111}<112> remained constant. With increasing the total rolling reduction to 85% using the same rolling schedule intensity of the {112}<110> increased furthermore and intensities of the {113}<110>, {100}<110> and {111}<112> again remained constant, as shown in figure 5.4.1.2., (a,b,c). A similar behaviour is evident when examining the (110) pole figure of specimens cold rolled to 75%, 80% and 85% using the 45°/p and 55°/p rolling schedules shown in figure 5.4.1.3 (a,b,c) and figure 5.4.1.4 (a,b,c) respectively.

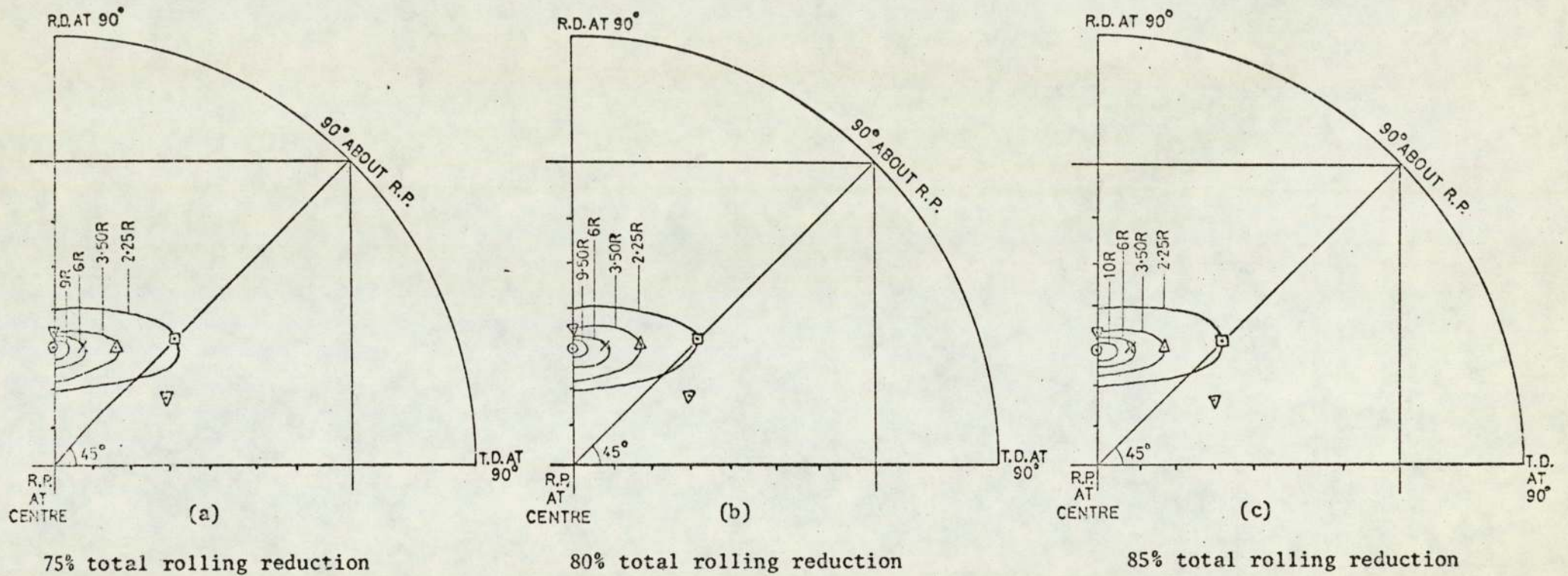


Fig. 5.4.1.2. One quadrant of (110) pole figures of specimens cold rolled using the 35°/p schedule.

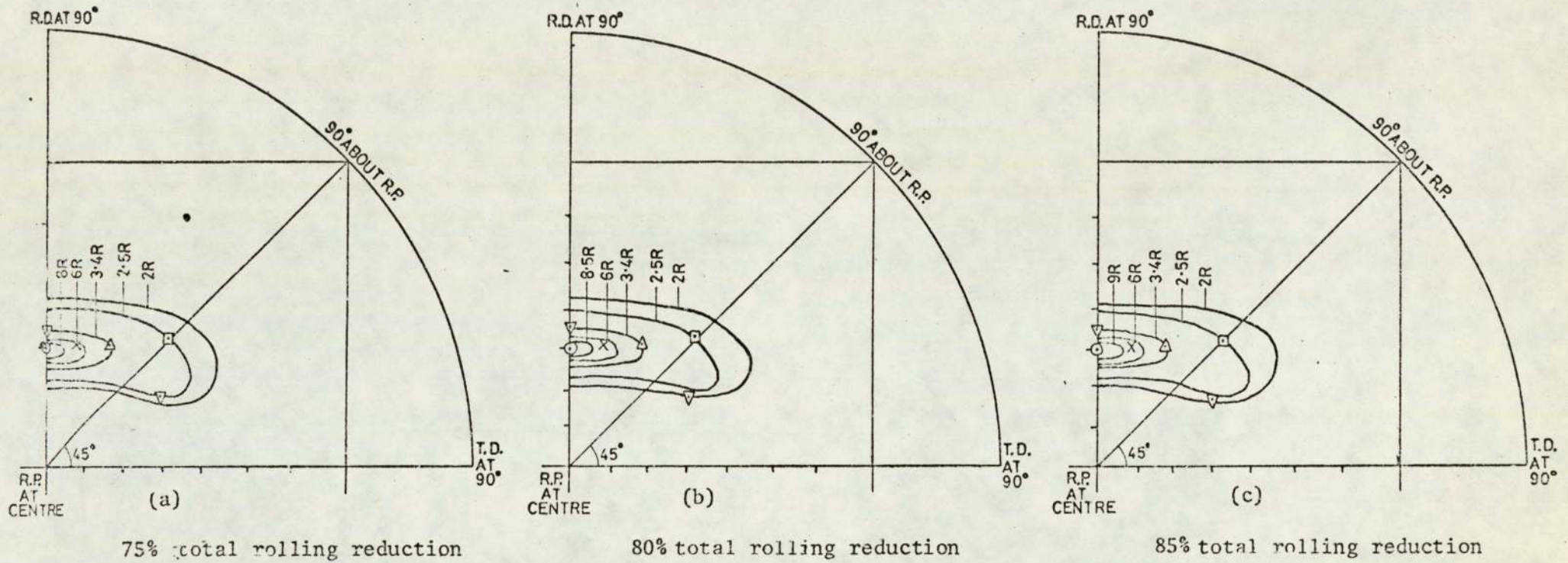


Fig. 5.4.1.3. One quadrant of (110) pole figures of specimens cold rolled using the 45°/p rolling schedule.

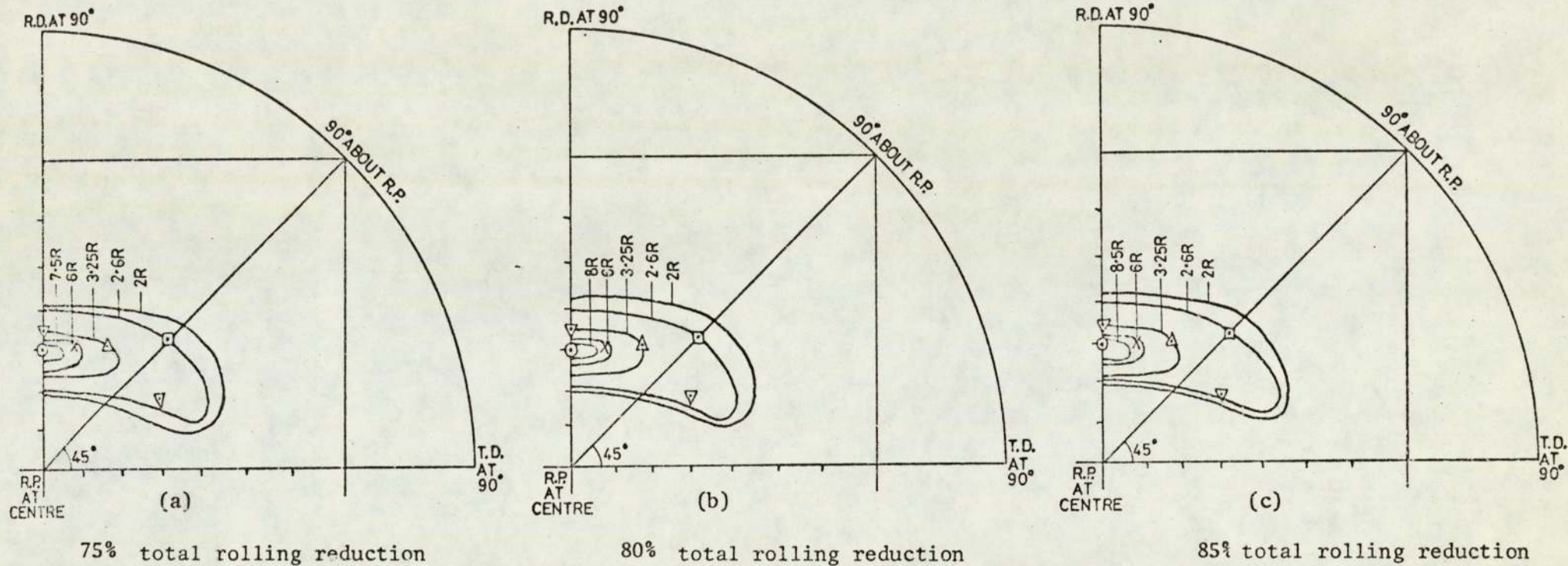


Fig. 5.4.1.4. One quadrant of (110) pole figure of specimens cold rolled using the  $55^\circ/p$  rolling schedule.

(b) Texture developed by constant roll gap schedules

P values of specimen cold rolled to 75% total reduction using roll gaps of the order of 0.02 in/p, 0.005 in/p and 0.001 in/p are listed in Table 5.4.1.1. The results indicate that the {111} and {100} orientations are the most intense while the {110} orientation is the weakest. The {211} and {332} are the next strongly aligned parallel to the strip surface. It is to be noted also that P values of the {111} and {100} planes decreased and increased respectively by decreasing the magnitude of the roll gap. There is also a slight reduction in the {211} and {332}, P values and slight increase in the {310}, {321} and {411} P values after decreasing the magnitude of the roll gap.

(110) pole figures of specimens cold rolled using the 0.02 in/p, 0.005 in/p and 0.001 in/p schedules indicated that the major texture components were the {112}<110>, {113}<110>, {111}<110>, {100}<110> and {111}<112>, as shown in figure 5.4.1.5.(a,b,c), figure 5.4.1.6.(a,b,c) and figure 5.4.1.7.(a,b,c). It is also evident that intensities of the {111}<112> and {100}<110> components increased and decreased respectively up to certain total rolling reduction depending upon each rolling schedule. Further increase in the total rolling reduction resulted in a reduction in intensity of the first component and an increase in intensity of the second component.

In the (110) pole figures of specimen cold rolled to 75% using the 0.02 in/p rolling schedule, intensity of the {111}<112> component increased and intensity of the {100}<110> component decreased when increasing the total rolling reduction to 80%, as shown in figure

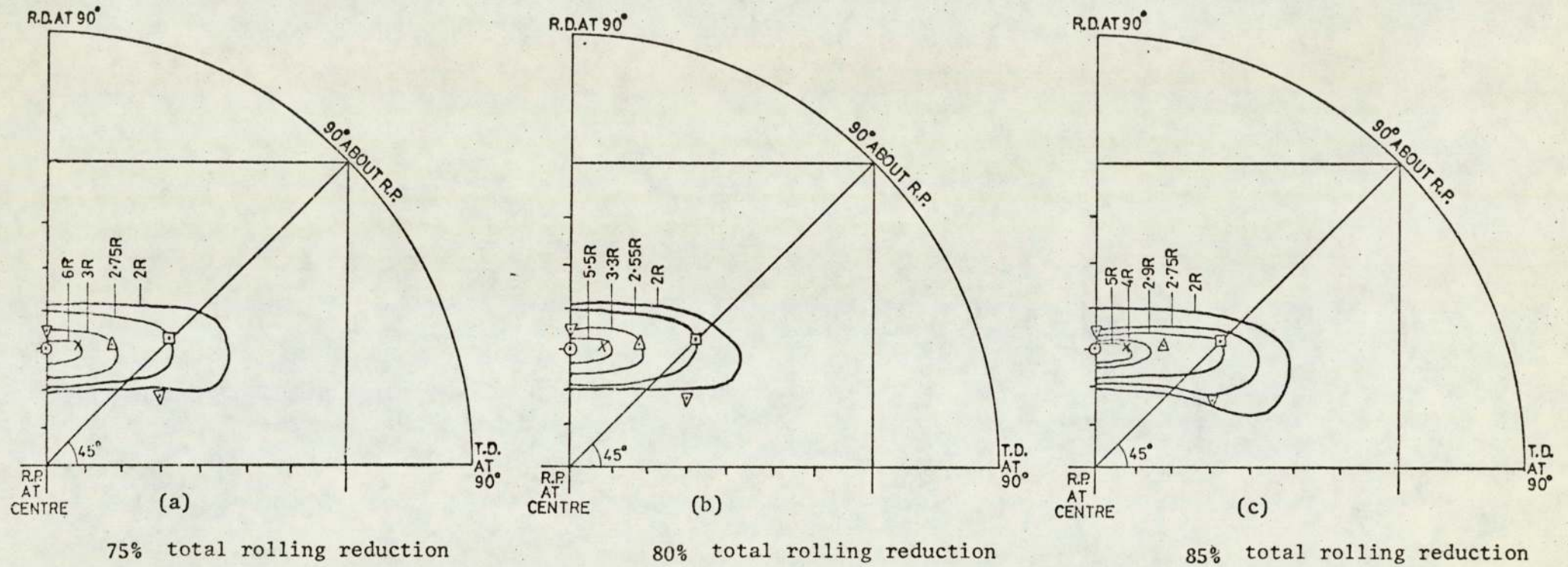


Fig. 5.4.1.5. One quadrant of (110) pole figures of specimens cold rolled using the 0.02 in/p rolling schedule .

5.4.1.5. Increasing the total rolling reduction to 85% was associated with a reduction in the  $\{111\}\langle 112 \rangle$  and an increase in the  $\{100\}\langle 110 \rangle$  texture intensities as shown in the same figures. Intensities of the  $\{112\}\langle 110 \rangle$  and  $\{113\}\langle 110 \rangle$  components decreased with increasing the rolling reduction within the range 75% to 85%.

(110) pole figures of specimens cold rolled using 0.005 in/p rolling draughts revealed a similar behaviour to (110) pole figures of specimens cold rolled using the 0.02 in/p schedule, except the maximum  $\{111\}\langle 112 \rangle$  and the minimum  $\{100\}\langle 110 \rangle$  components were lower and higher respectively and coincided with 75% total rolling reduction, as shown in figure 5.4.1.6 (a,b,c). The maximum intensity of the  $\{111\}\langle 112 \rangle$  component and minimum intensity of the  $\{100\}\langle 110 \rangle$  component of specimens cold rolled using the 0.001 in/p schedule corresponded to 70% total reduction as shown in figure 5.4.1.7 (a,b,c). In all (110) pole figures of specimens cold rolled using the 0.005 in/p and 0.001 in/p rolling schedules, intensities of the  $\{111\}\langle 112 \rangle$  components were lower before and after the total rolling reductions coinciding with the maximum  $\{111\}\langle 112 \rangle$  intensity. Intensities of the  $\{100\}\langle 110 \rangle$  components were higher before and after the total rolling reduction corresponding to the minimum  $\{100\}\langle 110 \rangle$  intensities in (110) pole figures of both schedules. Intensities of the  $\{112\}\langle 110 \rangle$  component developed by rolling with 0.005 in/p and 0.001 in.p, on the other hand, increased after increasing the total rolling reduction, which is contrary to rolling with 0.002 in/p rolling schedule. Common to these three rolling schedules, intensity of the  $\{113\}\langle 110 \rangle$  component remained unchanged with increasing the total rolling reduction.

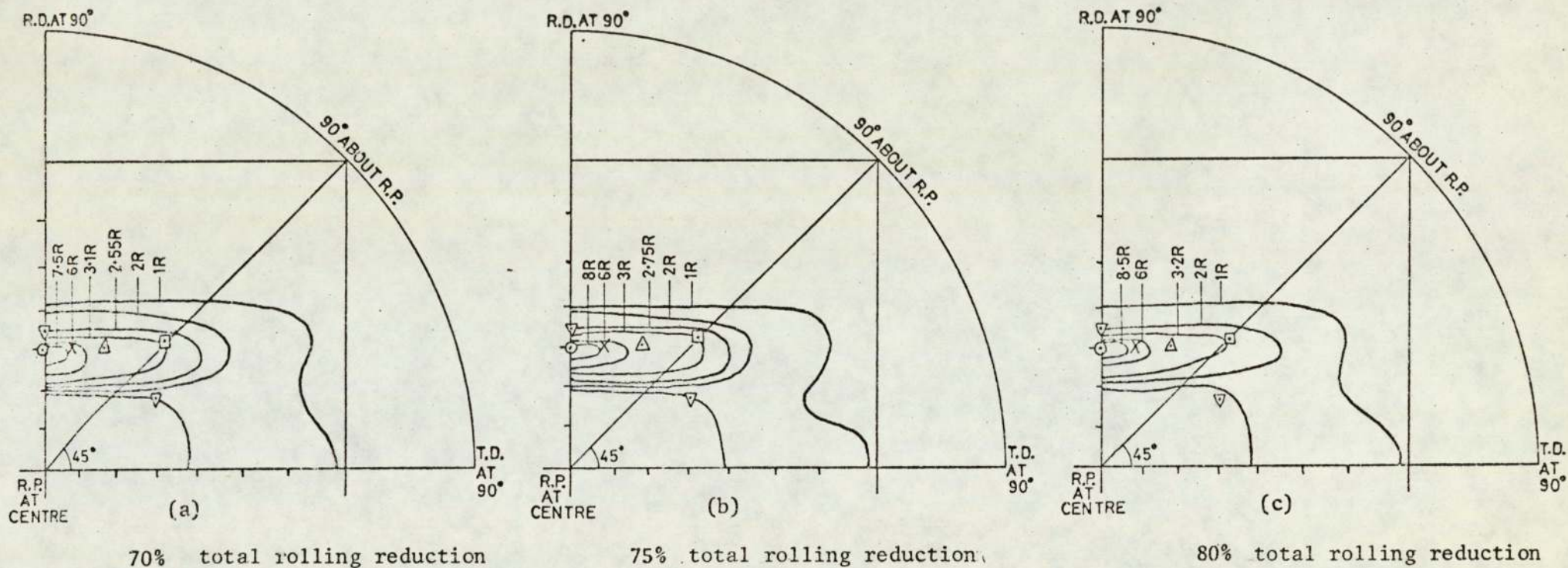


Fig. 5.4.1.6. One quadrant of (110) pole figure of specimens cold rolled using the 0.005 in/p rolling schedule.

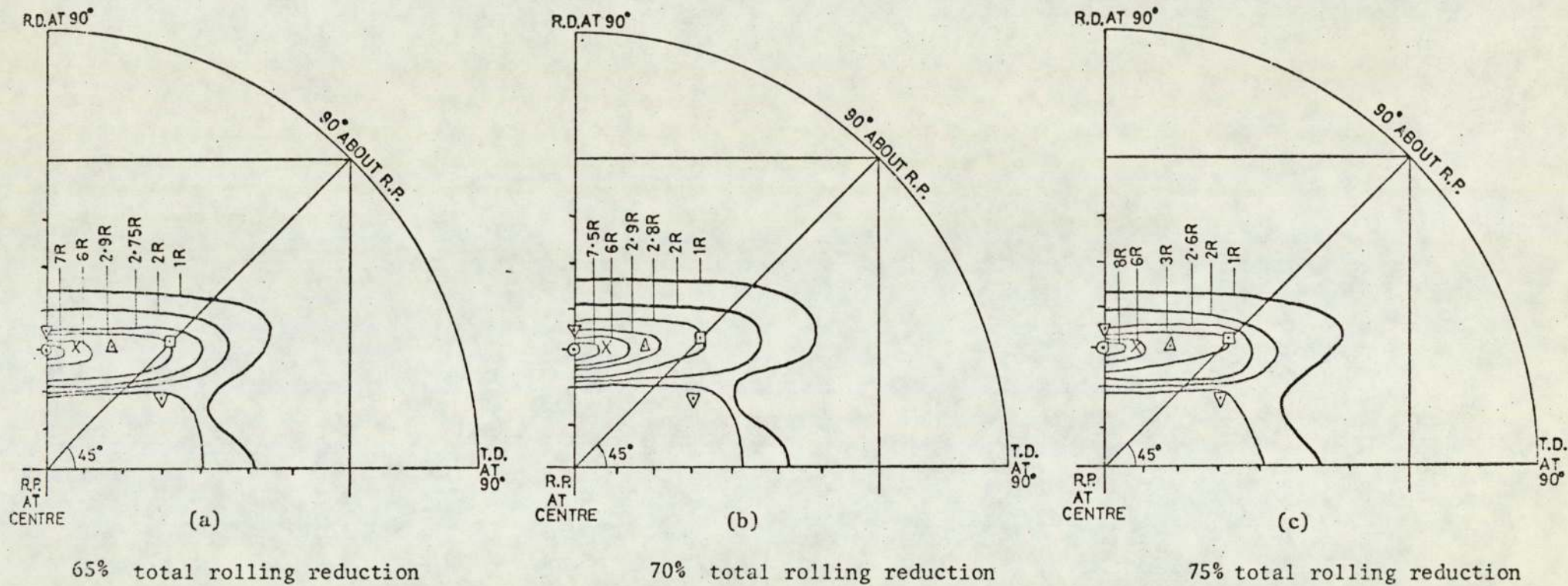


Fig. 5.4.1.7. One quadrant of (110) pole figure of specimens cold rolled using the 0.001 in/p rolling schedule.

For a given total rolling reduction texture spread increased by decreasing the magnitude of the roll gap. Texture spread increased also after increasing the total rolling reduction for a certain rolling schedule.

(c) Texture developed by the pendulum rolling schedule

Textures of specimens cold rolled to 75% using the pendulum mill is illustrated in terms of P values of eight crystallographic planes in Table 5.4.1.1. Contrary to constant geometry and roll gap schedules, crystals with {100} planes were the most predominantly aligned parallel to the strip surface, while the {111} planes were the next intense. Also P value of the {110} plane increased in comparison with P values of the same plane developed by constant geometry and roll gap schedules, but it was still relatively low. Instead, the {332} orientation was the minor component. P value of the {211} decreased and P values of the {310}, {321} and {411} increased as a result of pendulum rolling.

Considering (110) pole figure of specimen cold rolled to 65% total reduction using the pendulum mill, figure 5.4.1.8a, it is evident that the major texture components were the {112}<110>, {113}<110>, {100}<110>, {111}<110> and {111}<112> with the {112}<110> and {113}<110> predominating. In comparison with (110) pole figures of specimens cold rolled using constant geometry and roll gap schedules, intensities of the {112}<110>, {113}<110> and {111}<112> components decreased and intensity of the {100}<110> component increased when rolling with the pendulum mill. Texture spread has also increased.

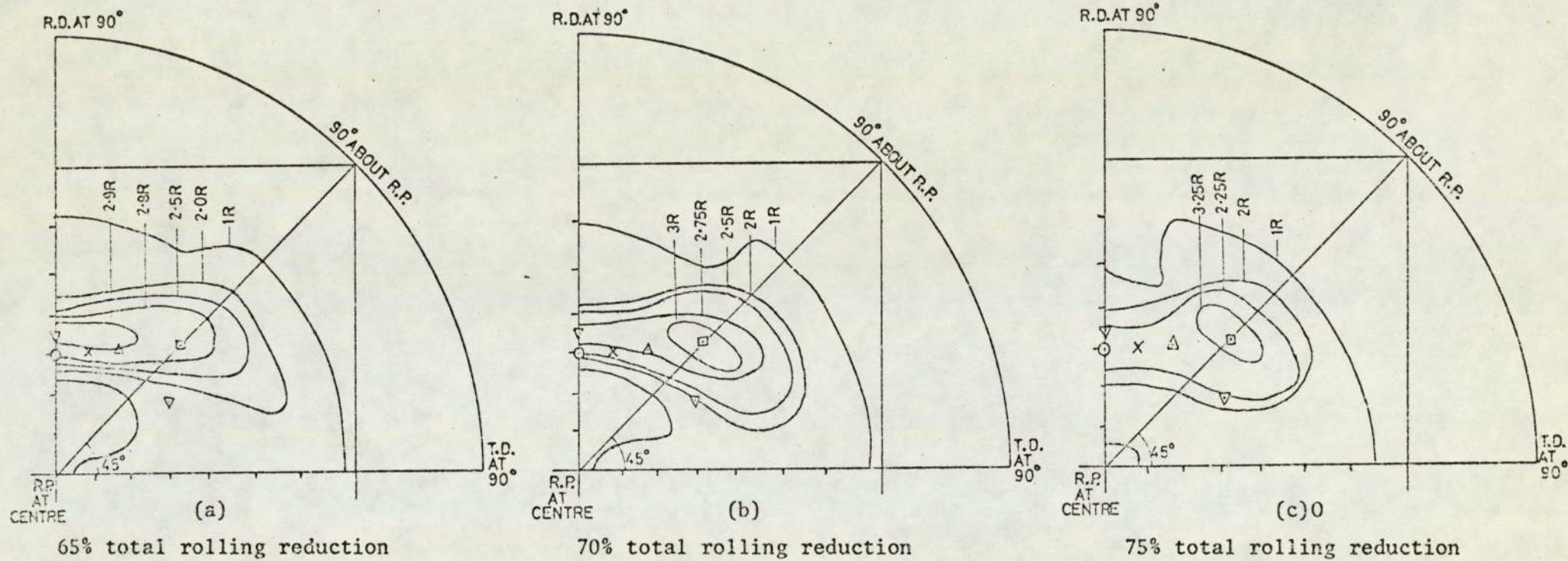


Fig. 5.4.1.8. One quadrant of (110) pole figures of specimens cold rolled using the pendulum rolling schedule.

With increasing the total rolling reduction to 70%, the  $\{100\}\langle 110\rangle$  component became dominant while intensities of the  $\{112\}\langle 110\rangle$ ,  $\{113\}\langle 110\rangle$  and  $\{111\}\langle 112\rangle$  orientations, as shown in figure 5.4.1.8b decreased. Further increase in the total rolling reduction to 75% was associated with intensification of the  $\{100\}\langle 110\rangle$  component and deterioration of the  $\{112\}\langle 110\rangle$ ,  $\{113\}\langle 110\rangle$ , and  $\{111\}\langle 112\rangle$  intensities, as shown in figure 5.4.1.8c. Texture spread increased further towards the  $60^\circ$  circle about the sheet normal towards the rolling and the transverse directions especially at the random intensity range.

(d) General observations on R value and texture of the cold rolled materials

Texture of specimens cold rolled using the  $35^\circ/p$  schedule to 75% total reduction was characterised by higher  $\{111\}$ ,  $\{211\}$  and  $\{332\}$  P values and lower  $\{100\}$ ,  $\{310\}$ ,  $\{411\}$  and  $\{321\}$  P values in comparison with texture developed by the other six rolling schedules. In contrast texture of specimens cold rolled by the pendulum mill to the same total rolling reduction consisted of lower  $\{111\}$ ,  $\{211\}$  and  $\{332\}$  and higher  $\{100\}$ ,  $\{310\}$ ,  $\{411\}$ ,  $\{321\}$  and  $\{110\}$  P values. With regard to texture of specimens cold rolled to 75% using the  $45^\circ/p$ ,  $55^\circ/p$ , 0.02 in/p, 0.005 in/p and 0.001 in/p rolling draughts gradual reductions in the P values of the  $\{111\}$ ,  $\{211\}$  and  $\{332\}$  and gradual increase in the P values of the  $\{100\}$ ,  $\{310\}$ ,  $\{411\}$  and  $\{321\}$  planes were observed.

With reference to all (110) pole figures of specimens cold rolled to 75% using the  $35^\circ/p$ ,  $45^\circ/p$ ,  $55^\circ/p$ , 0.02 in/p, 0.005 in/p, 0.001 in/p and pendulum rolling schedules, intensity of the  $\{112\}\langle 110\rangle$  and  $\{100\}\langle 110\rangle$  increased and intensity of the  $\{111\}\langle 112\rangle$  decreased in the same sequence

of the rolling schedules. The  $\{113\}\langle 110 \rangle$  texture component has not changed with altering the rolling schedules except when rolling with the 0.02 in/p and pendulum schedule where it was significantly decreased.

Inverse and (110) pole figure are therefore consistent with  $R_0$  value measurements in that higher  $R_0$  values are associated with a higher proportion of  $\{111\}$  and a lower proportion of  $\{100\}$  planes parallel to the strip surface. Accordingly, texture of specimens cold rolled using  $35^\circ/p$  schedule contributed to higher  $R_0$  value while texture of specimens cold rolled by the pendulum mill resulted in lower  $R_0$  values. The reduction in  $R_0$  values when rolling with  $45^\circ/p$ ,  $55^\circ/p$ , 0.02 in/p, 0.005 in/p, 0.001 in/p, was accompanied by corresponding reductions in the  $\{111\}$  and increases in the  $\{100\}$  intensities respectively. The high proportion of the  $\{100\}$  orientation in the cold rolling texture has counteracted the ability of the  $\{111\}$  orientation to improve  $R_0$  value. Consequently  $R_0$  values of the cold rolled materials were very low. It is to be noted also that the intensification of the  $\{100\}$  component and the reduction of the  $\{111\}$  intensity, after certain total rolling reduction, is responsible for the decrease in  $R_0$  value when rolling with constant roll gap and pendulum rolling schedules. A constant ratio of the two components, as occurred when rolling with controlled geometry schedules, is associated with constant  $R_0$  value at heavy rolling reduction.

#### 5.4.2 The annealed materials

(a) Texture of materials cold rolled to 75% total reduction then annealed for 0.5 hrs and 6 hrs.

Textures of specimens cold rolled to 75% total reduction, using the 35°/p, 45°/p, 55°/p, 0.02 in/p, 0.005 in/p, 0.001 in/p and pendulum rolling schedules, annealed for half an hour then aged are shown in Table 5.4.2.1 in terms of P values of eight crystallographic planes. Considering the {111} and {100} textures, which are most important with regard to R value, it is clear that their P values did not change significantly when changing the rolling procedures. This is consistent with  $R_0$  value measurements after half an hour annealing in that slight variations in the {111}/{100} ratio is corresponding to slight variation in R value.

In comparing P values of the cold rolled materials given in Table 5.4.1.1. with P values of the same specimens after half an hour annealing listed in Table 5.4.2.1. it is apparent that annealing resulted in reductions of the {100}, {211} and {111} P values, depending upon the rolling schedules i.e. the cold rolling texture. On the other hand, annealing increased the {110}, {310}, {321}, {411} and {332} P values, also depending upon the rolling schedules. The reduction in the {100} P values after half an hour annealing contributed to the improvement in  $R_0$  value of the annealed strip in comparison with  $R_0$  value prior to annealing. Presumably, the reduction in P values of the {111} planes after half an hour annealing was responsible for the relatively low  $R_0$  value of specimens annealed to that period.

No	{hkℓ}	P VALUES		
		35°/p	45°/p	55°/p
(1)	110	0.64	0.62	0.60
(2)	200	0.50	0.53	0.55
(3)	211	0.90	0.87	0.84
(4)	310	0.76	0.81	0.83
(5)	222	2.20	2.18	2.18
(6)	321	0.89	0.90	0.92
(7)	330	0.64	0.62	0.60
	411	0.56	0.59	0.62
(8)	332	0.92	0.89	0.86

(a)

No	{hkℓ}	P VALUES		
		0.02in/p	0.005in/p	0.001in/p
(1)	110	0.58	0.55	0.53
(2)	200	0.55	0.57	0.58
(3)	211	0.82	0.79	0.76
(4)	310	0.86	0.90	0.93
(5)	222	2.15	2.14	2.13
(6)	321	0.94	0.96	0.98
(7)	330	0.58	0.55	0.53
	411	0.67	0.72	0.78
(8)	332	0.84	0.80	0.76

(b)

No	{hkℓ}	P Values Pendulum
(1)	110	0.51
(2)	200	0.61
(3)	211	0.70
(4)	310	
(5)	222	2.01
(6)	321	1.10
(7)	330	0.51
	411	0.86
(8)	332	0.71

(c)

Table 5.4.2.1. P values of specimens cold rolled to 75% using the 35°/p, 45°/p, 55°/p (a) 0.02 in/p, 0.005 in/p, 0.001 in/p, (b) and pendulum, (c) schedules annealed for 0.5hr then aged.

No	{hkℓ}	P VALUES		
		35°/p	45°/p	55°/p
(1)	110	0.88	0.85	0.82
(2)	200	0.42	0.48	0.55
(3)	211	1.03	1.00	0.97
(4)	310	0.19	0.27	0.34
(5)	222	3.16	3.00	2.81
(6)	321	0.15	0.21	0.34
(7)	330	0.88	0.85	0.82
	411	0.11	0.18	0.25
(8)	332	1.17	1.15	1.13

(a)

No	{hkℓ}	P VALUES		
		0.02in/p	0.005in/p	0.001in/p
(1)	110	0.80	0.76	0.69
(2)	200	0.51	0.53	0.56
(3)	211	0.89	0.85	0.78
(4)	310	0.40	0.49	0.70
(5)	222	2.76	2.66	2.46
(6)	321	0.40	0.46	0.57
(7)	330	0.80	0.76	0.69
	411	0.34	0.41	0.51
(8)	332	1.09	1.07	1.04

(b)

No	{hkℓ}	P Values Pendulum
(1)	110	0.65
(2)	200	0.58
(3)	211	0.64
(4)	310	0.78
(5)	222	2.28
(6)	321	0.76
(7)	330	0.65
	411	0.71
(8)	332	0.95

(c)

Table 5.4.2.2. P values of specimens cold rolled to 75% using the 35°/p, 45°/p, 55°/p (a) 0.02 in/p, 0.005 in/p, 0.001 in/p, (b) and pendulum, (c) schedules annealed for 6 hrs then aged.

Increasing the annealing time from half an hour to six hours was accompanied by an increase in the  $\{111\}$  P value and a decrease in the  $\{100\}$  P value, depending upon the rolling schedules. There were also increases in the  $\{110\}$ ,  $\{211\}$  and  $\{322\}$  P values and decreases in the  $\{310\}$  and  $\{411\}$  P values. A list of P values of eight crystallographic planes of specimens cold rolled to 75% using the  $35^\circ/p$ ,  $45^\circ/p$ ,  $55^\circ/p$ , 0.02 in/p, 0.005 in/p, 0.001 in/p and pendulum rolling schedules, annealed for 6 hours then aged is given in Table 5.4.2.2. According to Table 5.4.2.2, P values of the  $\{100\}$ ,  $\{310\}$ ,  $\{321\}$  and  $\{411\}$  increased and the P values of the  $\{110\}$ ,  $\{211\}$ ,  $\{111\}$  and  $\{332\}$  decreased from one rolling schedule to the next in the same order of the previous rolling schedules. The variations in the  $\{111\}$  and  $\{100\}$  P values before and after half an hour and six hours annealing are summarised in figure 5.4.2.1 and figure 5.4.2.2.

According to (110) pole figures of specimens cold rolled to 75% total reduction using the controlled geometry rolling schedules, texture developed after 6 hours annealing consisted of two partial fibre textures described by  $\langle 110 \rangle$  direction parallel to the rolling direction and  $\{111\}$  plane parallel to the rolling plane, as shown in figure 5.4.2.3 figure 5.4.2.4 and figure 5.4.2.5. The  $\langle 110 \rangle$  direction is common to the  $\{112\}$ ,  $\{113\}$ ,  $\{111\}$  and  $\{100\}$  planes and  $\{111\}$  planes in the  $\langle 112 \rangle$  direction. Intensities of the  $\{112\}\langle 110 \rangle$ ,  $\{113\}\langle 110 \rangle$  and  $\{111\}\langle 112 \rangle$  decreased and intensity of the  $\{100\}\langle 110 \rangle$  component increased when increasing the angle between the specimen and rolls.

Texture of specimens cold rolled to 75% using controlled roll gap rolling schedules annealed for 6 hrs then aged consisted of the same texture components developed by controlled geometry rolling but

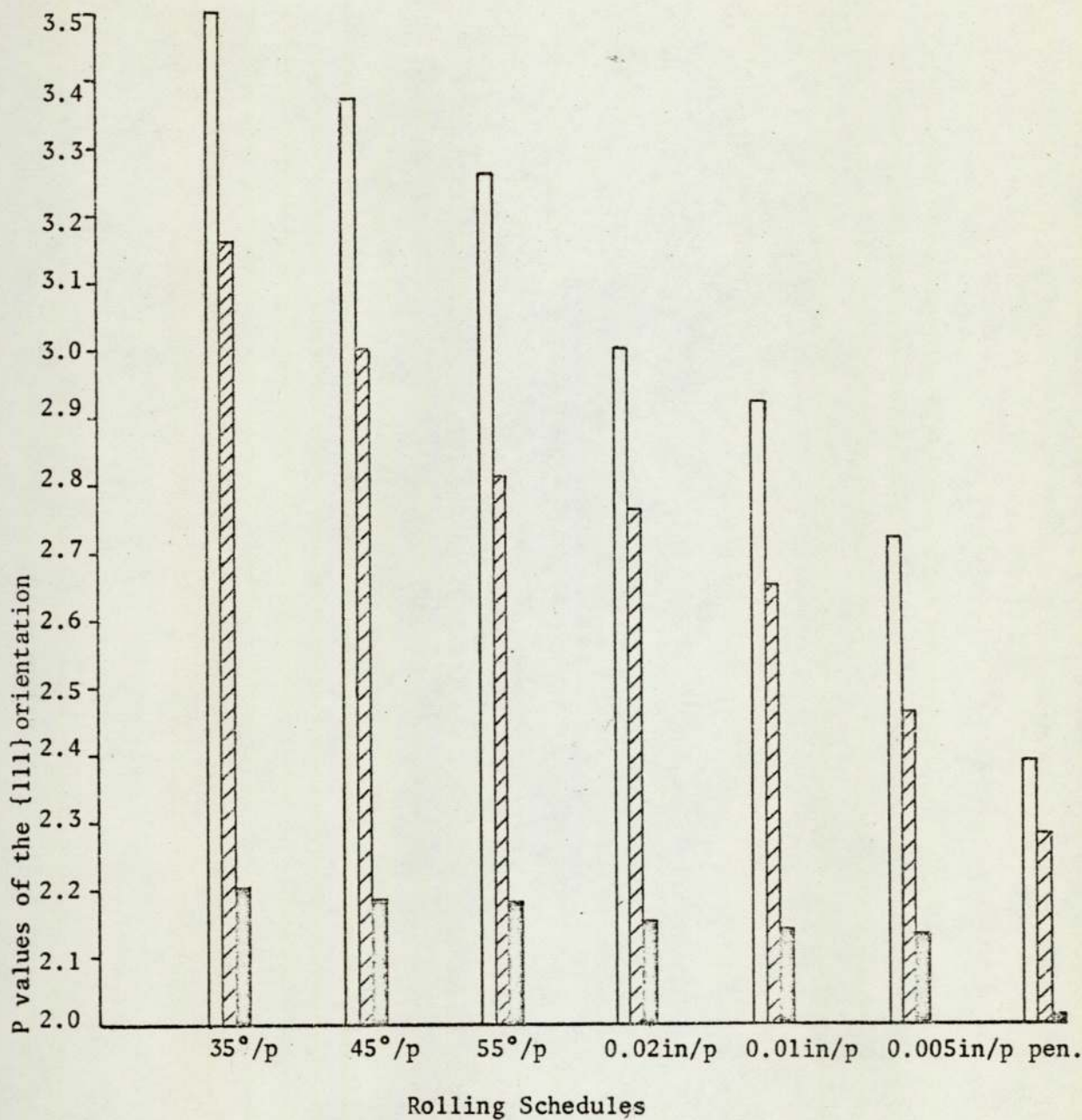


Fig. 5.4.2.1. Shows the variations in P values of the {111} planes with the 35°/p, 45°/p, 55°/p, 0.02 in/p, 0.005 in/p, 0.001 in/p and pendulum rolling schedules prior to annealing (□) and after annealing for 6 hrs (▨) and 0.5 hr (■).

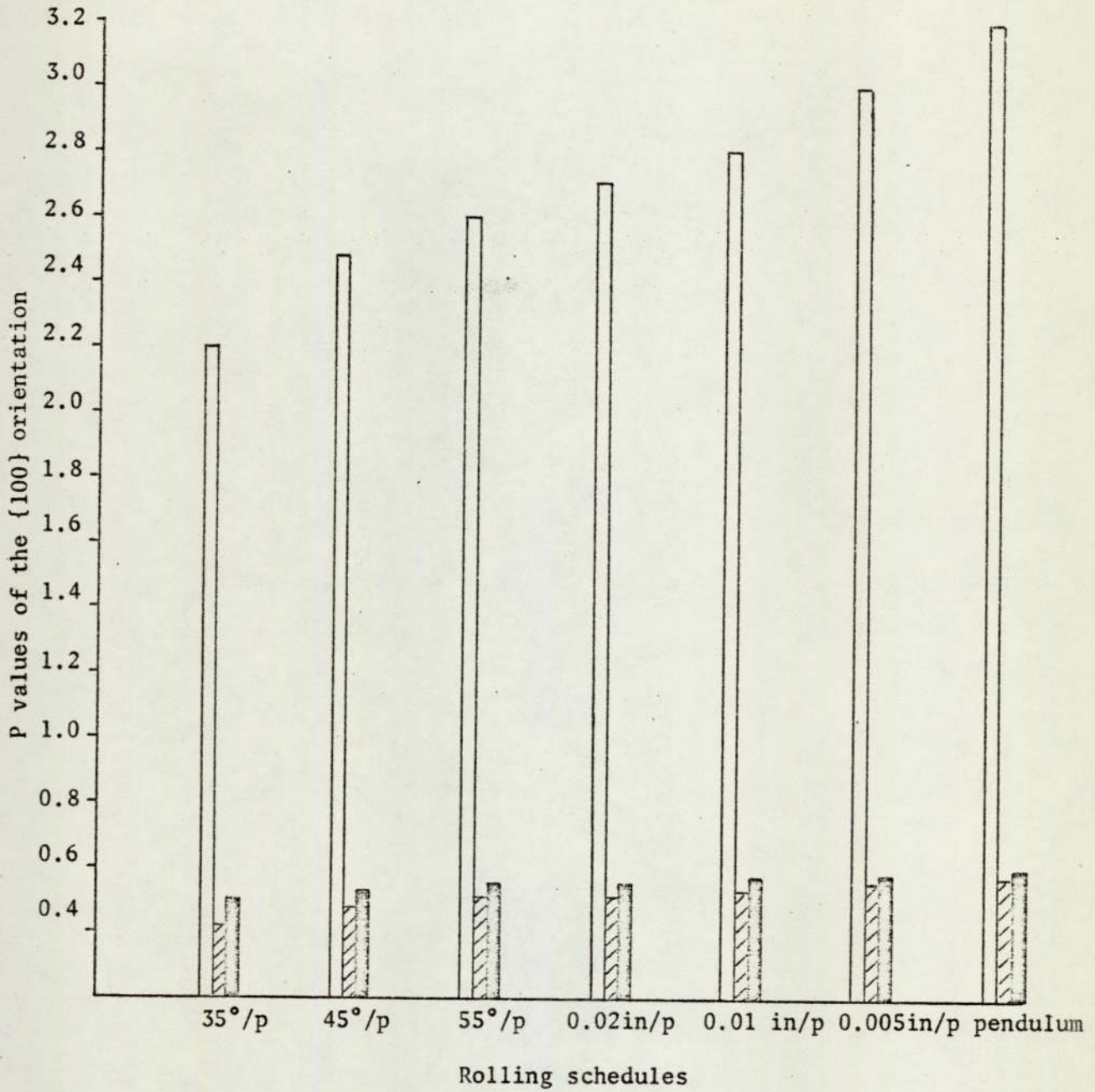


Fig. 5.4.2.2. Shows the variations in the {100} P values with the 35°/p, 45°/p, 55°/p, 0.02in/p, 0.005 in/p, 0.001 in/p and pendulum, prior to annealing (□) after 6 hrs annealing (▨) and 0.5 hr annealing (■).

texture intensities were different, as illustrated in figure 5.4.2.6, figure 5.4.2.7 and figure 5.4.2.8. In comparison with controlled geometry rolling intensities of the  $\{112\}\langle 110\rangle$ ,  $\{113\}\langle 110\rangle$  and  $\{111\}\langle 112\rangle$  components were lower and intensity of the  $\{100\}\langle 110\rangle$  component was higher when rolling with constant roll gap schedules. With reference to the magnitude of roll gap, intensities of the  $\{112\}\langle 110\rangle$ ,  $\{113\}\langle 110\rangle$  and  $\{100\}\langle 110\rangle$  decreased and intensities of the  $\{111\}\langle 112\rangle$  increased with increasing the roll gap.

(110) pole figures of specimens cold rolled to 75% using the pendulum mill, annealed for 6 hrs then aged revealed a weaker partial fibre texture in comparison with texture developed by controlled geometry and roll gap rolling schedules, as shown in figure 5.4.2.9c. Texture is characterised by more  $\{100\}\langle 110\rangle$  component and less  $\{112\}\langle 110\rangle$ ,  $\{113\}\langle 110\rangle$  and  $\{111\}\langle 112\rangle$  relative to the previous rolling schedules.

Texture spread after 75% total rolling reduction and 6 hrs annealing was dependent upon the rolling schedules, being sharper when rolling with  $35^\circ/p$  rolling schedule. However, texture spread increased when rolling with  $45^\circ/p$ ,  $55^\circ/p$ , 0.02 in/p, 0.005 in/p, 0.001 in/p and pendulum rolling schedules respectively.

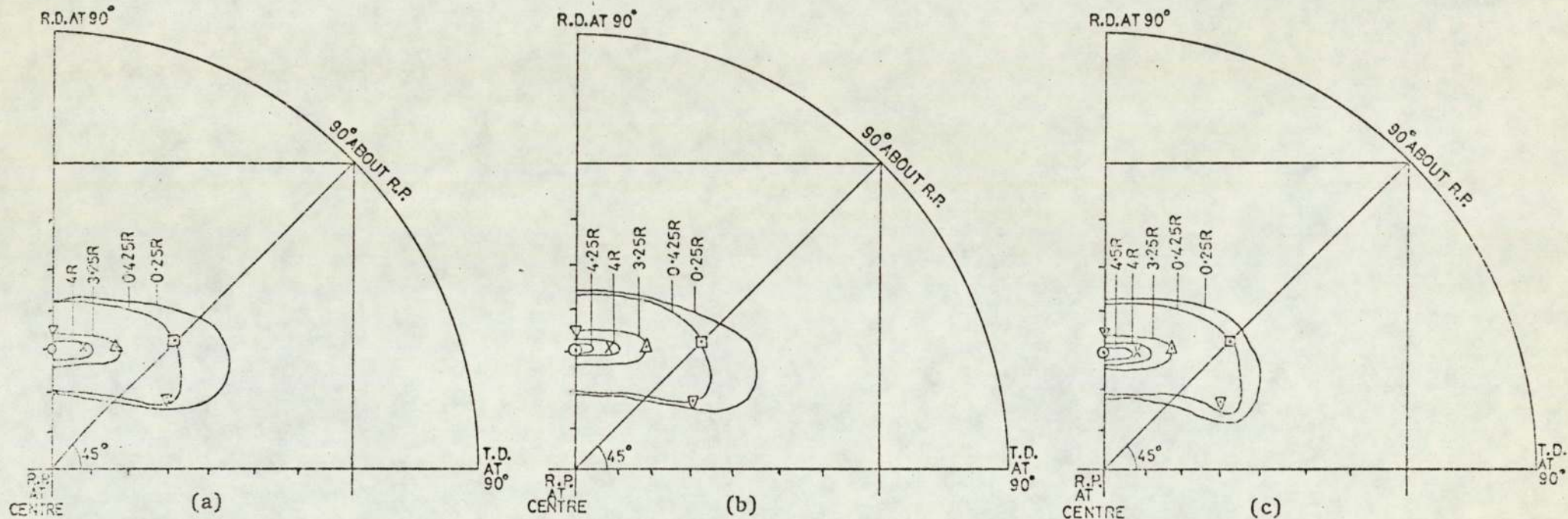
Comparing (110) pole figures of specimens cold rolled to 75% using the previous rolling schedules with the corresponding (110) pole figures prior to annealing, it was revealed that texture intensity decreased significantly but texture components were similar to the cold rolling texture components. Intensities of the  $\{112\}\langle 110\rangle$ ,  $\{113\}\langle 110\rangle$  and  $\{100\}\langle 110\rangle$  components were the most affected by annealing while the  $\{111\}\langle 112\rangle$  components were less affected.

Rolling with  $35^\circ/p$  then annealing for 6 hours is associated with more  $\{111\}$  planes and less  $\{100\}$  planes parallel to the surface and is therefore favoured for higher R value. This is consistent with the R value measurements.

(b) Texture of materials cold rolled to a range of total reductions then annealed for 6 hrs only

In order to demonstrate the effect of increasing the total rolling reduction prior to annealing upon texture developed after annealing, (110) pole figures of specimens cold rolled to different rolling reductions depended upon each rolling schedule, annealed for 6 hrs then aged were examined. (110) pole figures of specimens cold rolled to 75, 80 and 85% using the controlled geometry rolling schedules are shown in figure 5.4.2.3 (a,b,c), figure 5.4.2.4 (a,b,c) and figure 5.4.2.5 (a,b,c). It is evident from figure 5.4.2.3 (a,b,c) that during rolling with  $35^\circ/p$  rolling schedule, intensities of the  $\{100\}\langle 110 \rangle$  and  $\{111\}\langle 112 \rangle$  remained constant regardless of increasing the total reduction. On the other hand, intensities of the  $\{112\}\langle 110 \rangle$  and  $\{113\}\langle 110 \rangle$  continued to increase. Texture developed by the  $45^\circ/p$  and  $55^\circ/p$  behaved in the same manner except intensities of the  $\{112\}$ ,  $\{113\}$  and  $\{111\}$  components increased and intensity of the  $\{100\}$  component decreased when decreasing the shear plane angle. The behaviour of the cold rolling texture developed by controlled geometry rolling schedules was therefore, preserved after annealing.

Like the cold rolling texture developed by controlled roll gap rolling schedules, intensity of the  $\{100\}\langle 110 \rangle$  component decreased and



75% total rolling reduction + 6 hrs  
annealing

80% total rolling reduction + 6 hrs  
annealing

85% total rolling reduction + 6 hrs  
annealing

Fig. 5.4.2.3. One quadrant of (110) pole figures of specimens cold rolled using the 35°/p schedule,  
annealed for 6 hrs then aged.

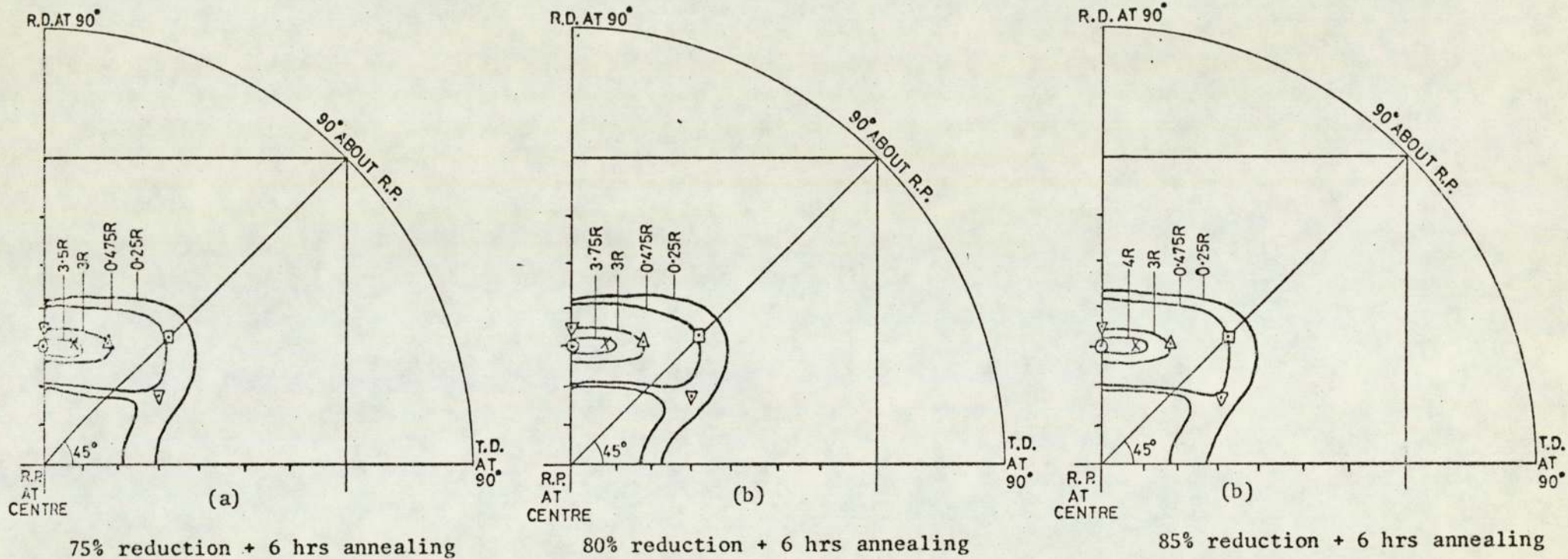
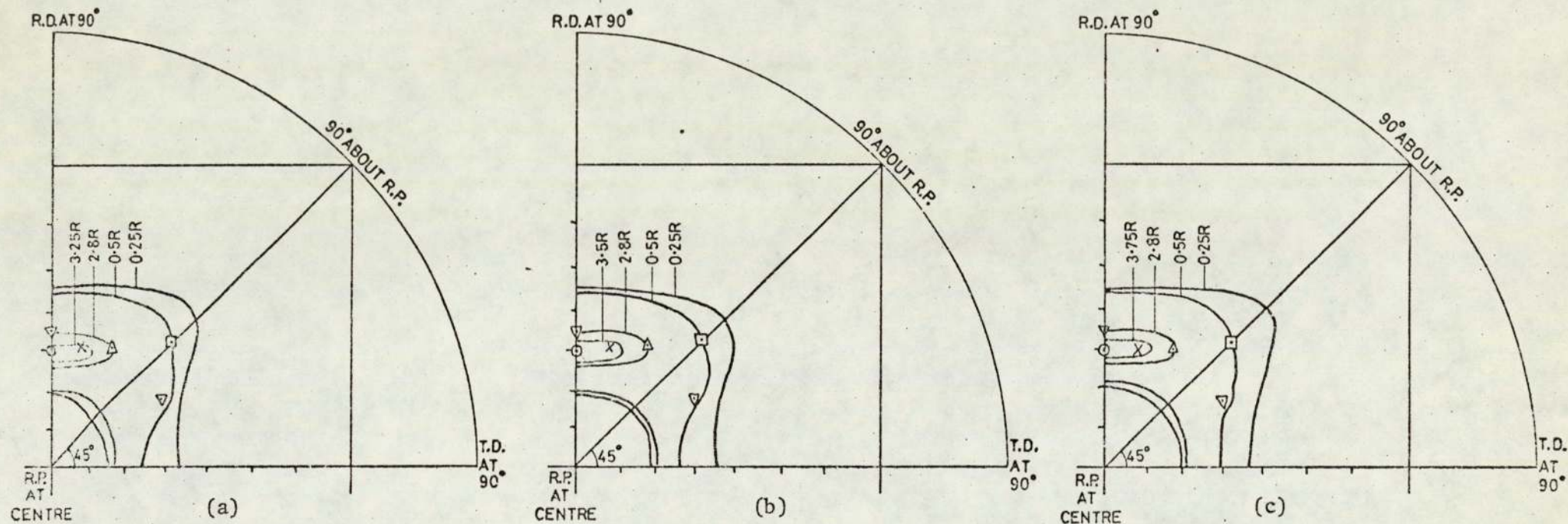


Fig. 5.4.2.4. One quadrant of (110) pole figures of specimens cold rolled using the 45°/p schedule, annealed for 6 hrs then aged.



75% total rolling reduction  
+ 6 hrs annealing

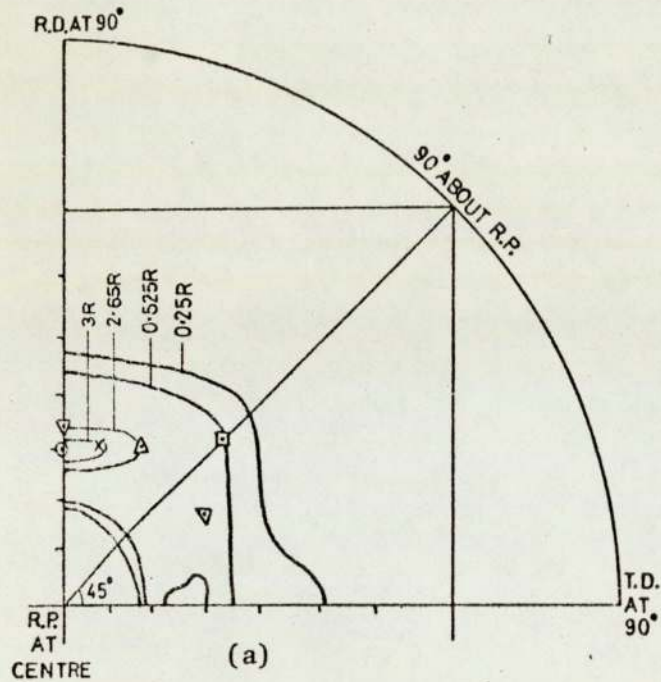
80% total rolling reduction  
+ 6 hrs annealing

85% total rolling reduction  
+ 6 hrs annealing

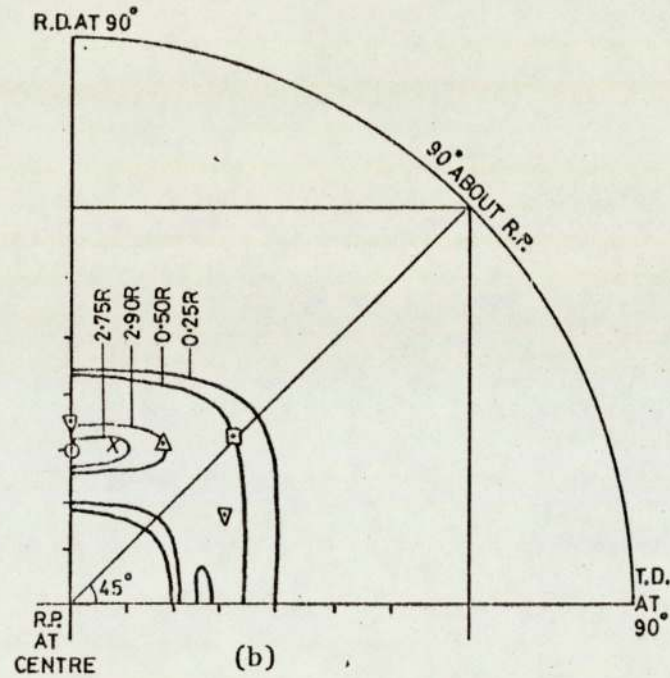
Fig. 5.4.2.5. One quadrant of (110) pole figures of specimens cold rolled using the 55°/p schedule, annealed for 6 hrs then aged.

intensity of the  $\{111\}\langle 112 \rangle$  component increased, after annealing up to certain rolling reductions depended upon each rolling schedule. Further increase in the total reduction resulted in an increase in intensity of the first component and a decrease in intensity of the second component as shown in figure 5.4.2.5 (a,b,c), figure 5.4.2.6 (a,b,c) and figure 5.4.2.7 (a,b,c). In the case of specimens cold rolled using 0.02 in/p rolling schedule, intensities of the  $\{100\}\langle 110 \rangle$ ,  $\{112\}\langle 110 \rangle$  and  $\{113\}\langle 110 \rangle$  components decreased and intensities of the  $\{111\}\langle 112 \rangle$  components increased with increasing the total rolling reduction from 75% to 80%. With increasing the total rolling reduction to 85% intensity of the  $\{100\}\langle 110 \rangle$  component increased and intensities of the  $\{111\}\langle 112 \rangle$  components decreased, while intensities of the  $\{112\}\langle 110 \rangle$  and  $\{113\}\langle 110 \rangle$  components continued to decrease, as shown in figure 5.4.2.5 (a,b,c).

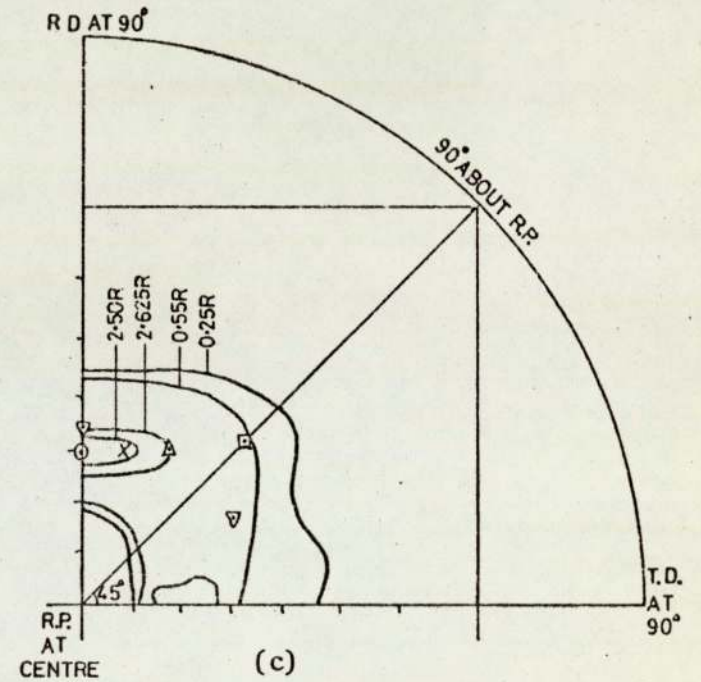
Considering figure 5.4.2.6 (a,b,c) and figure 5.4.2.7 (a,b,c), it is apparent that intensities of the  $\{100\}\langle 110 \rangle$  and  $\{111\}\langle 112 \rangle$  components followed the same behaviour pattern when rolling with 0.005 in/p to 70, 75 and 80% and when rolling with 0.001 in/p schedule to 65, 70 and 75%, except the minimum  $\{100\}\langle 110 \rangle$  and maximum  $\{111\}\langle 112 \rangle$  coincided with lower total reductions. These total reductions corresponded to 75% and 70% when rolling with 0.005 in/p and 0.001 in/p draughts respectively. Contrary to rolling with 0.02 in/p schedule intensities of the  $\{112\}\langle 110 \rangle$  and  $\{113\}\langle 110 \rangle$  continued to increase with increasing the total rolling reduction.



75% Total rolling reduction  
+ 6 hrs annealing

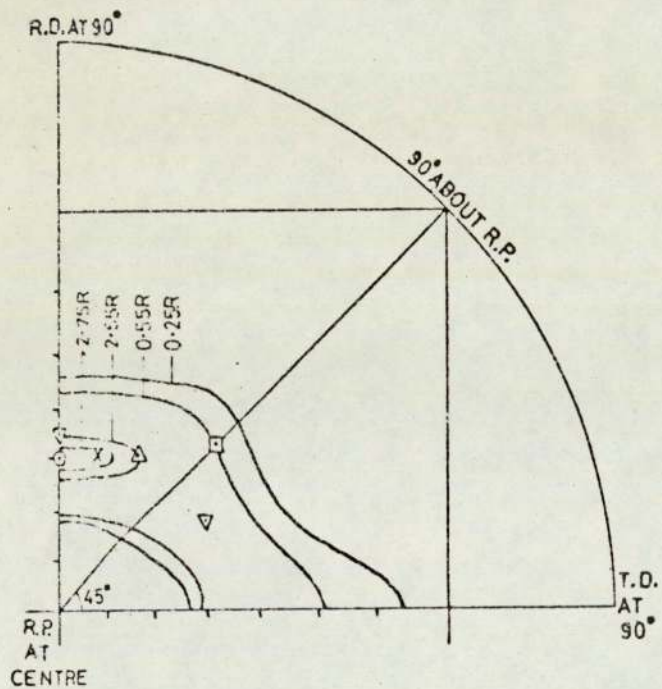


80% Total rolling reduction  
+ 6 hrs annealing

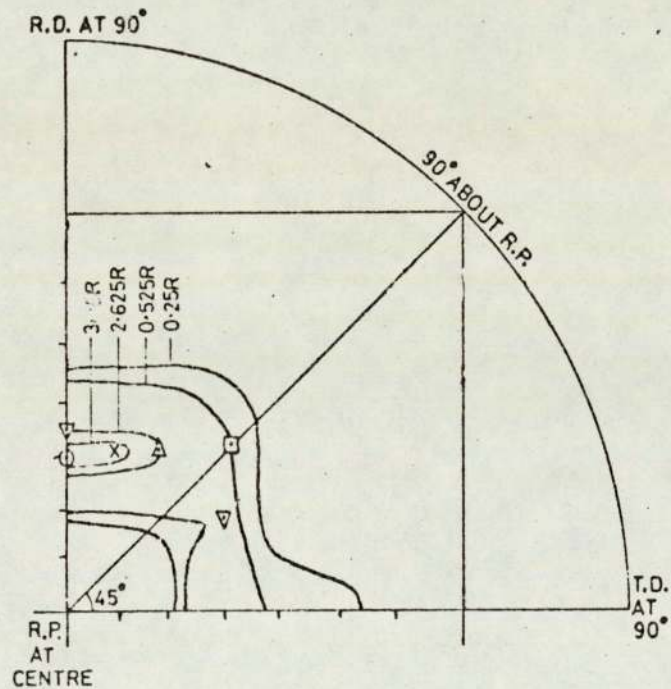


85% Total rolling reduction  
+ 6 hrs annealing

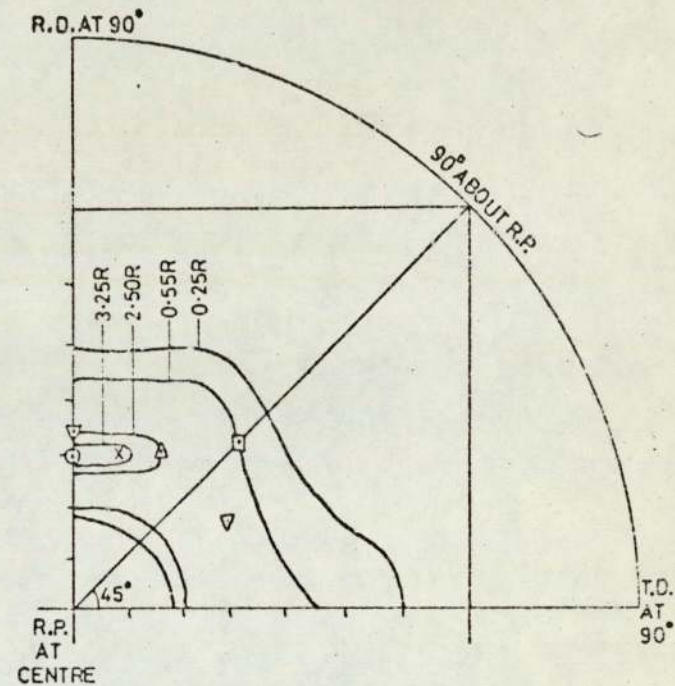
Fig. 5.4.2.6. One quadrant of (110) pole figures of specimens cold rolled using the 0.02 in/p schedule , annealed for 6 hrs then aged.



(a) 70% Total Rolling Reduction  
+ 6 hrs annealing



(b) 75% Total Rolling Reduction  
+ 6 hrs annealing



(c) 80% Total Rolling Reduction  
+ 6 hrs annealing

Fig.5.4.2.7. One quadrant of (110) pole figures of specimens cold rolled using the 0.005 in/p schedule, annealed for 6 hrs then aged.

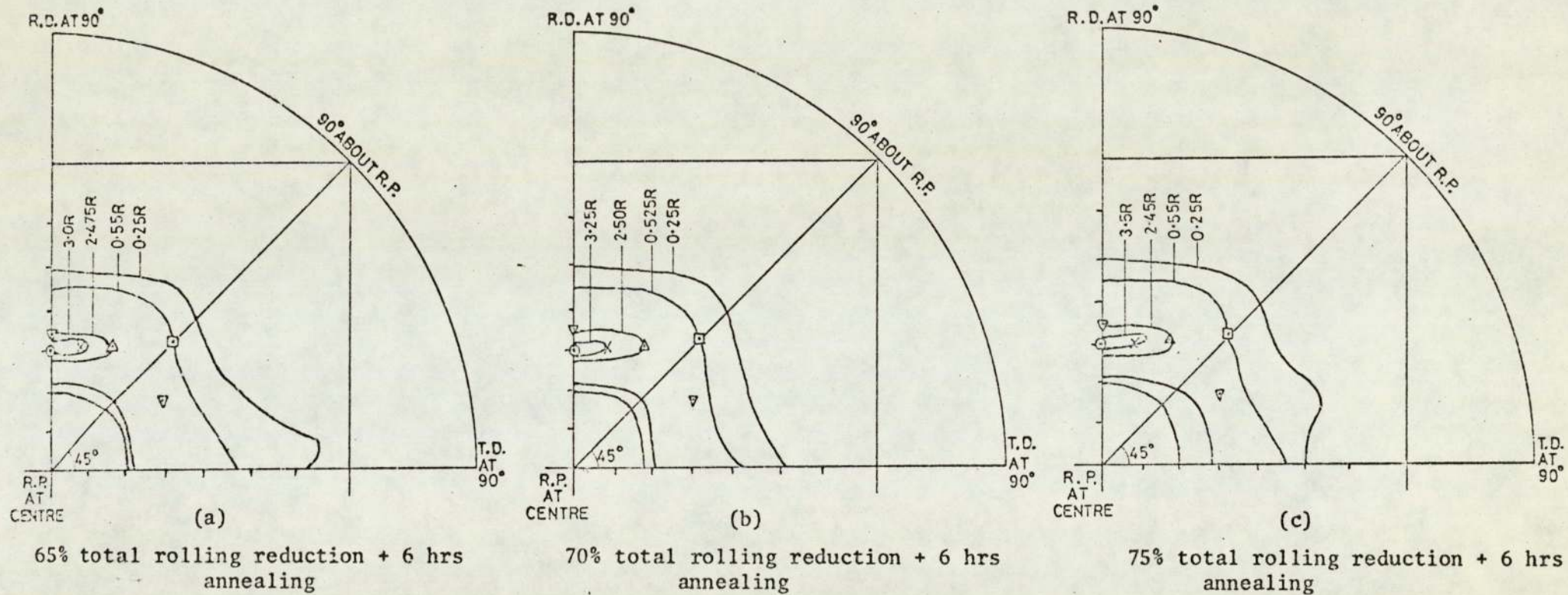


Fig. 5.4.2.8. One quadrant of (110) pole figures of specimens cold rolled using the 0.001 in/p schedule, annealed for 6 hrs then aged.

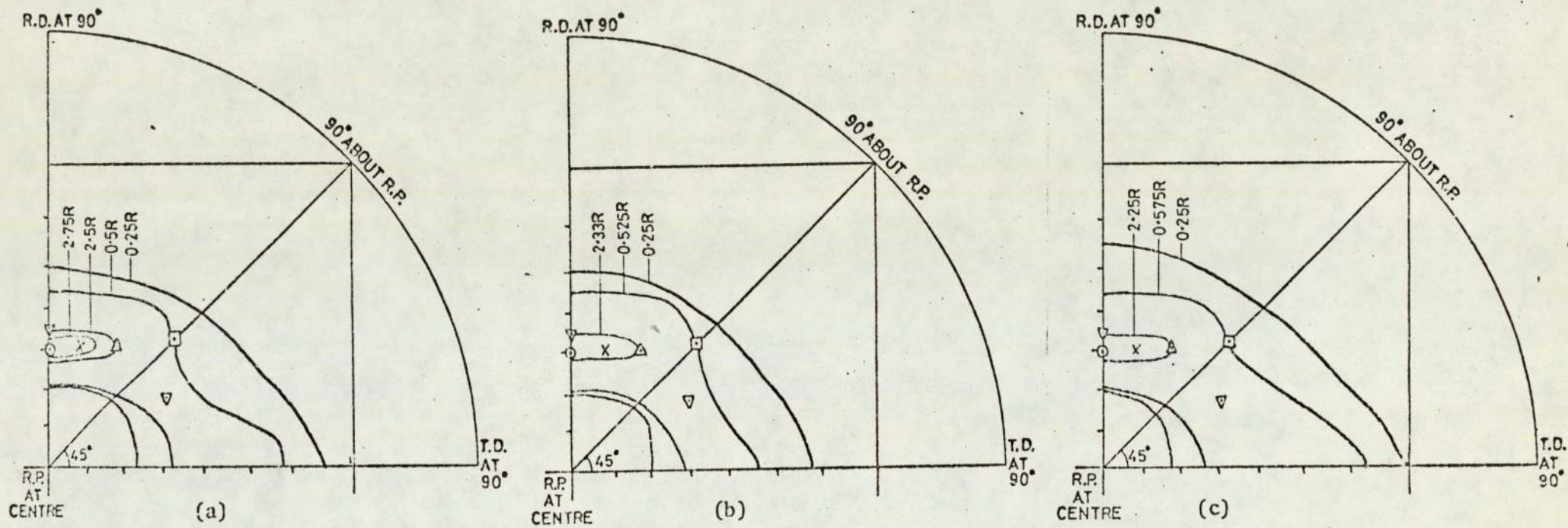
(110) pole figures of specimens cold rolled by the pendulum to 65% 70% and 75%, annealed for 6 hrs then aged figure 5.4.2.9 (a,b,c) revealed that increasing the total reduction from 65% to 70% was associated with an increase in the  $\{100\}\langle 110\rangle$  intensity and decreases in the  $\{111\}\langle 112\rangle$ ,  $\{112\}\langle 110\rangle$  and  $\{113\}\langle 110\rangle$  intensities. Increasing the total rolling reduction to 75% resulted in further increase in intensity of the first component and decreases in intensities of the second components, as shown in figure 5.4.2.9c.

#### 5.5 CRYSTAL REORIENTATION AFTER TENSILE EXTENSION

The reorientation of crystals after tensile extension is dealt with in this section in two parts. The first part is concerned with the reorientation of crystals of specimens cold rolled to 75%, annealed for different times, aged and then subjected to 20% tensile extension. In the second part, crystals reorientation of specimens cold rolled to different total rolling reductions, , annealed for 6 hrs, aged then subjected to 20% tensile extension is described.

##### (a) Reorientation of crystals of materials cold rolled to 75% total reduction then annealed for 0.5 and 6 hrs

Measurements of P values of specimens cold rolled to 75% using the 35°/p, 45°/p, 55°/p, 0.02 in/p, 0.005 in/p, 0.001 in/p and pendulum rolling schedules, annealed for 0.5 hr, aged then subjected to 20% tensile extension are listed in Table 5.5.a.1. Accordingly, P values of the  $\{110\}$ ,  $\{211\}$ ,  $\{111\}$  and  $\{332\}$  planes decreased when altering the rolling schedules in the same sequence as the previous schedules. P values of the  $\{100\}$ ,  $\{310\}$ ,  $\{321\}$  and  $\{411\}$  planes increased in the same previous order of rolling schedules.



65% Total rolling reduction +  
6 hrs annealing

70% Total rolling reduction +  
6 hrs annealing

75% Total rolling reduction  
6 hrs annealing

Fig. 5.4.2.9. One quadrant of (110) pole figures of specimens cold rolled using the pendulum schedule, annealed for 6 hrs then aged.

No	{hkℓ}	P VALUES		
		35°/p	45°/p	55°/p
(1)	110	0.57	0.56	0.55
(2)	200	0.62	0.67	0.71
(3)	211	1.11	1.07	1.01
(4)	310	0.68	0.70	0.71
(5)	222	1.92	1.87	1.81
(6)	321	0.97	1.05	1.15
(7)	330	0.57	0.56	0.55
	411	0.49	0.50	0.52
(8)	332	1.08	1.02	0.98

(a)

No	{hkℓ}	P VALUES		
		0.02in/p	0.005in/p	0.001in/p
(1)	110	0.54	0.52	0.51
(2)	200	0.78	0.83	0.91
(3)	211	0.98	0.94	0.89
(4)	310	0.72	0.75	0.76
(5)	222	1.73	1.69	1.66
(6)	321	1.24	1.30	1.35
(7)	330	0.54	0.52	0.51
	411	0.53	0.55	0.57
(8)	332	0.94	0.89	0.84

(b)

No	{hkℓ}	P Values Pendulum
(1)	110	0.49
(2)	200	1.11
(3)	211	0.82
(4)	310	0.80
(5)	222	1.39
(6)	321	1.50
(7)	330	0.49
	411	0.61
(8)	332	0.77

(c)

Table 5.5. a.1. P values of specimens cold rolled to 75% using the 35°/p, 45°/p, 55°/p (a) 0.02 in/p, 0.005 in/p, 0.001 in/p, (b) and pendulum, (c) schedules annealed for 0.5hr, aged, then subjected to 20% tensile extension.

The significance of P values after tensile extension listed in the previous table is apparent when compared with the corresponding P values before tensile extension in Table 5.4.2.1. Thus, it was concluded that the {111} P values decreased after tensile extension depending upon the rolling schedules. The magnitude of such reductions increased when using the 35°/p, 45°/p, 55°/p, 0.02 in/p, 0.005 in/p, 0.001 in/p and pendulum respectively, as shown in Table 5.5.a.2. For instance, the reduction in the {111} P values after tensile extension was equal to 0.3 and 0.67 when rolling with 35°/p and pendulum. P values of the {100} planes, on the other hand, increased after tensile extension in the same previous order of rolling schedules as shown in Table 5.5.a.3. The difference in P values of the {100} planes before and after tensile extension varied between 0.12 and 0.50 when rolling with 35°/p and pendulum rolling schedules. P values of the {110}, {310} and {411} planes slightly decreased, while P values of the {211}, {321} and {332} planes slightly increased after tensile extension, depending upon the rolling schedules.

Measurements of P values of specimens cold rolled to the same previous rolling reduction using the same rolling schedules, but annealed for 6 hrs, aged then subjected to 20% tensile extension are shown in Table 5.5.a.4. The differences in P values of the {111} and {100} planes before and after tensile extension were more significant than the difference in P values of corresponding planes after half an hour annealing. P values of the {111} planes, for example, decreased by 0.18 when rolling with 35°/p schedule in comparison with 0.56 when rolling with the pendulum schedule. Differences in P values before

ROLLING SCHEDULES	P VALUES		DIFFERENCES
	Before tensile extension	After tensile extension	
35°/p	2.20	1.90	0.30
45°/p	2.18	1.86	0.32
55°/p	2.17	1.81	0.36
0.02 in/p	2.15	1.73	0.42
0.005 in/p	2.14	1.69	0.45
0.001 in/p	2.13	1.65	0.48
Pendulum	2.06	1.39	0.67

Table 5.5.a.2. A summary of the differences in the  $\{111\}$  P values of specimen cold rolled to 75%, using the 35°/p, 45°/p, 55°/p, 0.02 in/p, 0.005 in/p, 0.001 in/p and pendulum schedules, annealed for 0.5 hr, aged, before and after 20% tensile extension.

ROLLING SCHEDULES	P VALUES		DIFFERENCES
	Before tensile extension	After tensile extension	
35°/p	0.50	0.62	0.12
45°/p	0.53	0.67	0.14
55°/p	0.54	0.71	0.17
0.02 in/p	0.55	0.77	0.22
0.005 in/p	0.57	0.83	0.26
0.001 in/p	0.58	0.91	0.33
Pendulum	0.61	1.11	0.50

Table 5 5.a. 3 A summary of the differences in the {100} P values of specimen cold rolled to 75%, using the 35°/p, 45°/p, 55°/p, 0.02 in/p, 0.005 in/p, 0.001 in/p and pendulum schedules, annealed for 0.5 hr, aged, before and after 20% tensile extension.

No	{hkl}	P VALUES		
		35°/p	45°/p	55°/p
(1)	110	0.75	0.74	0.73
(2)	200	0.45	0.54	0.59
(3)	211	1.30	1.25	1.20
(4)	310	0.13	0.20	0.25
(5)	222	2.98	2.77	2.56
(6)	321	0.17	0.26	0.44
(7)	330	0.75	0.74	0.73
	411	0.08	0.15	0.21
(8)	332	1.38	1.35	1.28

(a)

No	{hkl}	P VALUES		
		0.02in/p	0.005in/p	0.001in/p
(1)	110	0.72	0.70	0.69
(2)	200	0.62	0.68	0.74
(3)	211	1.11	1.04	0.95
(4)	310	0.30	0.37	0.55
(5)	222	2.43	2.30	2.00
(6)	321	0.59	0.67	0.81
(7)	330	0.72	0.70	0.69
	411	0.29	0.35	0.43
(8)	332	1.22	1.17	1.12

(b)

No	{hkl}	P Values Pendulum
(1)	110	0.63
(2)	200	0.78
(3)	211	0.77
(4)	310	0.70
(5)	222	1.62
(6)	321	1.21
(7)	330	0.63
	411	0.63
(8)	332	1.01

(a)

Table 5.5. a 4. P values of specimens cold rolled to 75% using the 35°/p, 45°/p, 55°/p (a) 0.02 in/p, 0.005 in/p, 0.001 in/p, (b) and pendulum, (c) schedules annealed for 6 hrs aged, then subjected to 20% tensile extension.

and after tensile extension in the case of specimens cold rolled to the same previous total rolling reduction using the  $45^\circ/p$ ,  $55^\circ/p$ , 0.02 in/p, 0.005 in/p and 0.001 in/p, increased in the same order rolling schedules as shown in Table 5.5.a.5. The difference in P values of the {100} planes increased with altering schedules in the same order of previous rolling schedules as shown in Table 5.5.a.6. Tensile extension was accompanied also with a slight gradual reduction in the P values of the {110}, {211} and {322} planes and a gradual slight increase in the P values of the {310}, {321} and {411} planes. This is evident when comparing Table 5.4.2.2 with Table 5.5.a.4.

Crystals reorientation of specimens cold rolled to 75% using the previous rolling schedules, annealed for 6 hrs, aged then subjected to 20% tensile extension is described in (110) pole figures shown in figure 5.5.b.1, figure 5.5.b.2, figure 5.5.b.3, figure 5.5.b.6, figure 5.5.b.<sup>7</sup>, figure 5.5.b.<sup>8</sup>, and figure 5.5.b.9. Analysis of these figures indicated that intensities of the {112}<110>, {113}<110> and {111}<112> decreased while intensity of the {100}<110> component increased with the rolling schedules in the same order. The effect of tensile extension upon crystals orientation is clear when comparing corresponding (110) pole figures before and after tensile extension. However, the difference in intensities of the {111}<112> before and after tensile extension was relatively small when rolling with  $35^\circ/p$  and increased when rolling with  $45^\circ/p$ ,  $55^\circ/p$ , 0.02 in/p, 0.005 in/p, 0.001 in/p and pendulum respectively. The difference in the {100}<110> intensity increased in the same sequence as the previous rolling schedules.

ROLLING SCHEDULES	P VALUES		DIFFERENCES
	Before tensile extension	After tensile extension	
35°/p	3.16	2.98	0.18
45°/p	3.00	2.77	0.23
55°/p	2.80	2.56	0.24
0.02 in/p	2.76	2.42	0.34
0.005 in/p	2.65	2.30	0.35
0.001 in/p	2.46	2.00	0.46
Pendulum	2.28	1.62	0.56

Table 5.5.a.5. A summary of the differences in the {111} P values of specimen cold rolled to 75%, using the 35°/p, 45°/p, 55°/p, 0.02 in/p, 0.005 in/p, 0.001 in/p and pendulum schedules, annealed for 6 hr, aged, before and after 20% tensile extension.

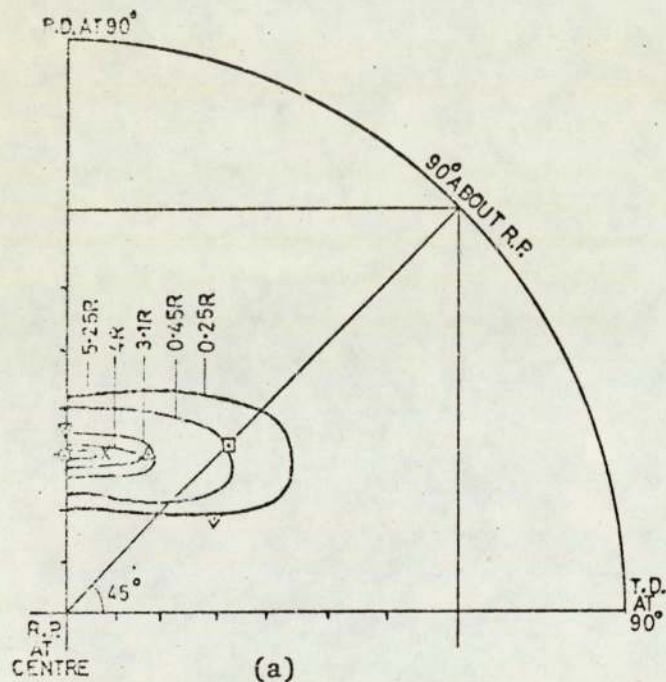
ROLLING SCHEDULES	P VALUES		DIFFERENCES
	Before tensile extension	After tensile extension	
35°/p	0.42	0.45	0.03
45°/p	0.48	0.54	0.04
55°/p	0.51	0.59	0.08
0.02 in/p	0.51	0.62	0.11
0.005 in/p	0.53	0.68	0.15
0.001 in/p	0.56	0.74	0.18
Pendulum	0.58	0.78	0.20

Table 5.5. a.6. A summary of the differences in the {100} P values of specimen cold rolled to 75%, using the 35°/p, 45°/p, 55°/p, 0.02 in/p, 0.005 in/p, 0.001 in/p and pendulum schedules, annealed for 6 hrs aged, before and after 20% tensile extension.

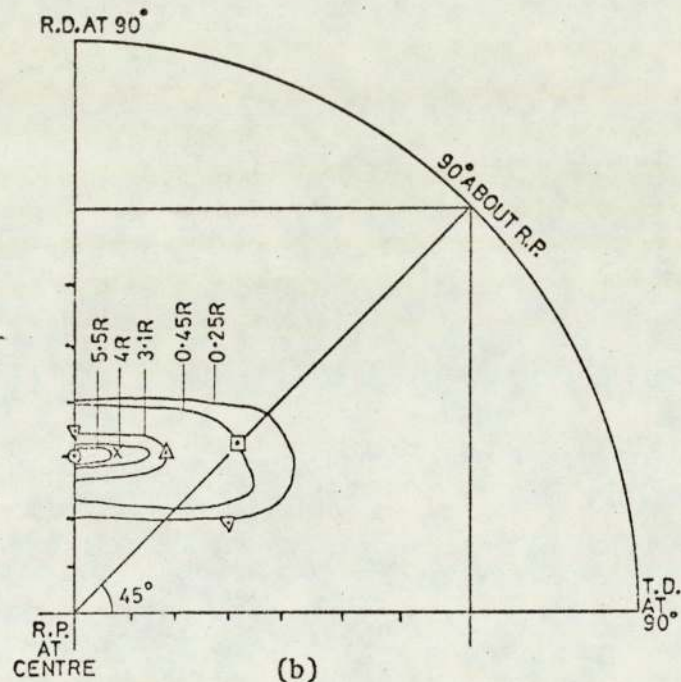
Crystals reorientation accompanying tensile extension is clearly dependent upon the rolling schedules and annealing time. A high reduction in the  $\{111\}$  and a high increase in the  $\{100\}$  after tensile extension is indicative of through-thickness shear and hence low R value. On the other hand a small reduction in the  $\{111\}$  and a small increase in the  $\{100\}$  indicates through-strip plane shear and hence high R value. Accordingly, rolling with  $35^\circ/p$  rolling schedule and 6 hrs annealing are favoured for higher R values. Inverse and (110) pole figures are therefore consistent with R value measurements.

(b) Reorientation of crystals of materials cold rolled to a range of total rolling reductions then annealed for 6 hrs.

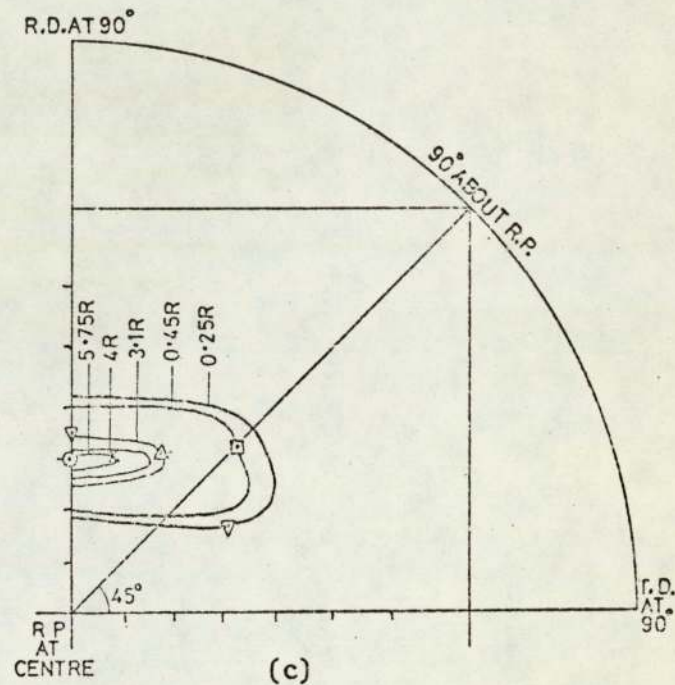
Textures of specimens cold rolled to 75%, 80% and 85% using  $35^\circ/p$ ,  $45^\circ/p$  and  $55^\circ/p$ , annealed for 6 hrs, aged then subjected to 20% extension are shown in (110) pole figures, figure 5.5.b.1 (a,b,c), figure 5.5.b.2 (a,b,c) and figure 5.5.b.3 (a,b,c). It follows that the major texture components of these specimens consisted of the  $\{112\}\langle 110\rangle$ ,  $\{113\}\langle 110\rangle$ ,  $\{111\}\langle 112\rangle$  and  $\{100\}\langle 110\rangle$  components. Intensities of the  $\{112\}\langle 110\rangle$ ,  $\{113\}\langle 110\rangle$  components increased with increasing the total rolling reduction but intensities of the  $\{111\}\langle 112\rangle$  and  $\{100\}\langle 110\rangle$  components remained constant. With reference to the corresponding (110) pole figures before tensile extension figure 5.4.2.3, figure 5.4.2.4 and figure 5.4.2.5., it is apparent that the difference in intensities of the  $\{111\}\langle 112\rangle$  and  $\{100\}\langle 110\rangle$  before and after tensile extension was also constant within the same range of total rolling reductions, as shown in figure 5.5.b.4 and figure 5.5.b.5.



75% total rolling reduction + 6 hrs annealing + 20% tensile extension



80% total rolling reduction + 6 hrs annealing + 20% tensile extension



85% total rolling reduction + 6 hrs annealing + 20% tensile extension.

Fig. 5.5.b.1. One quadrant of (110) pole figures of specimens cold rolling using the 35°/p schedule, annealed for 6 hrs, aged then subjected to 20% tensile extension.

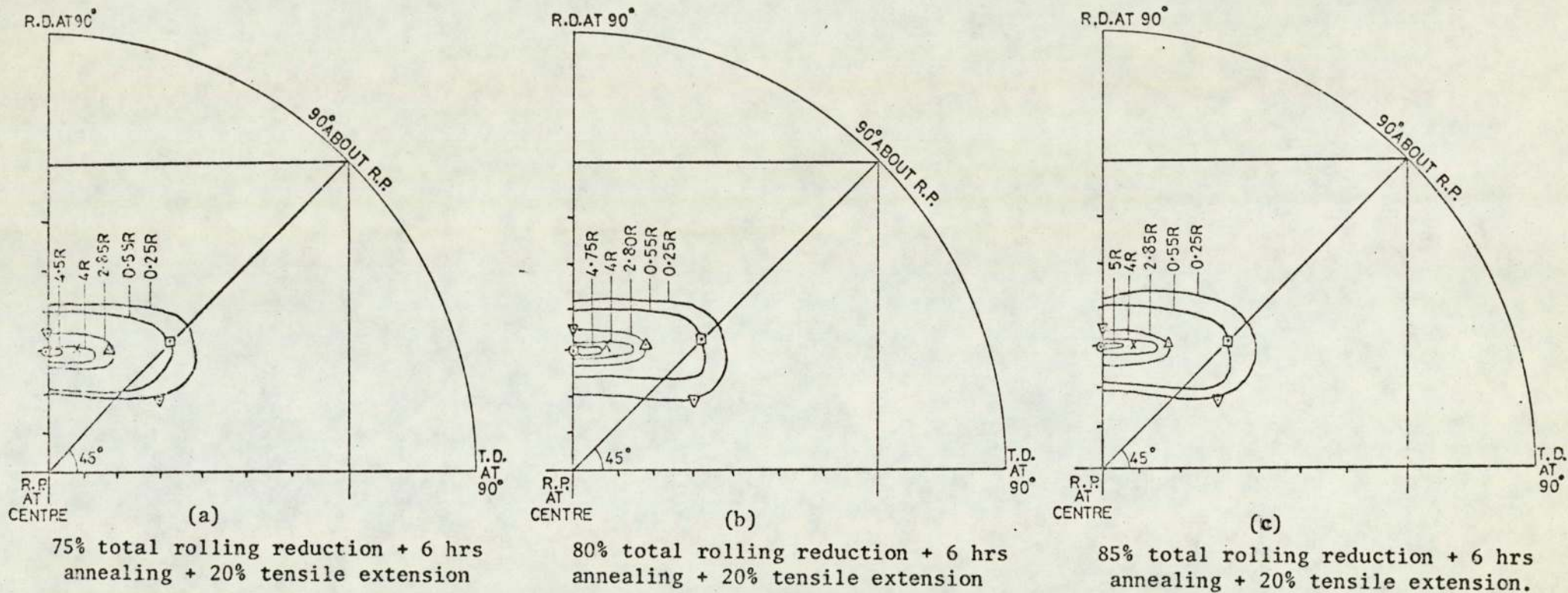


Fig. 5.5.b.2. One quadrant of (110) pole figures of specimens cold rolled using the 45°/p schedule, annealed for 6 hrs, aged then subjected to 20% tensile extension.

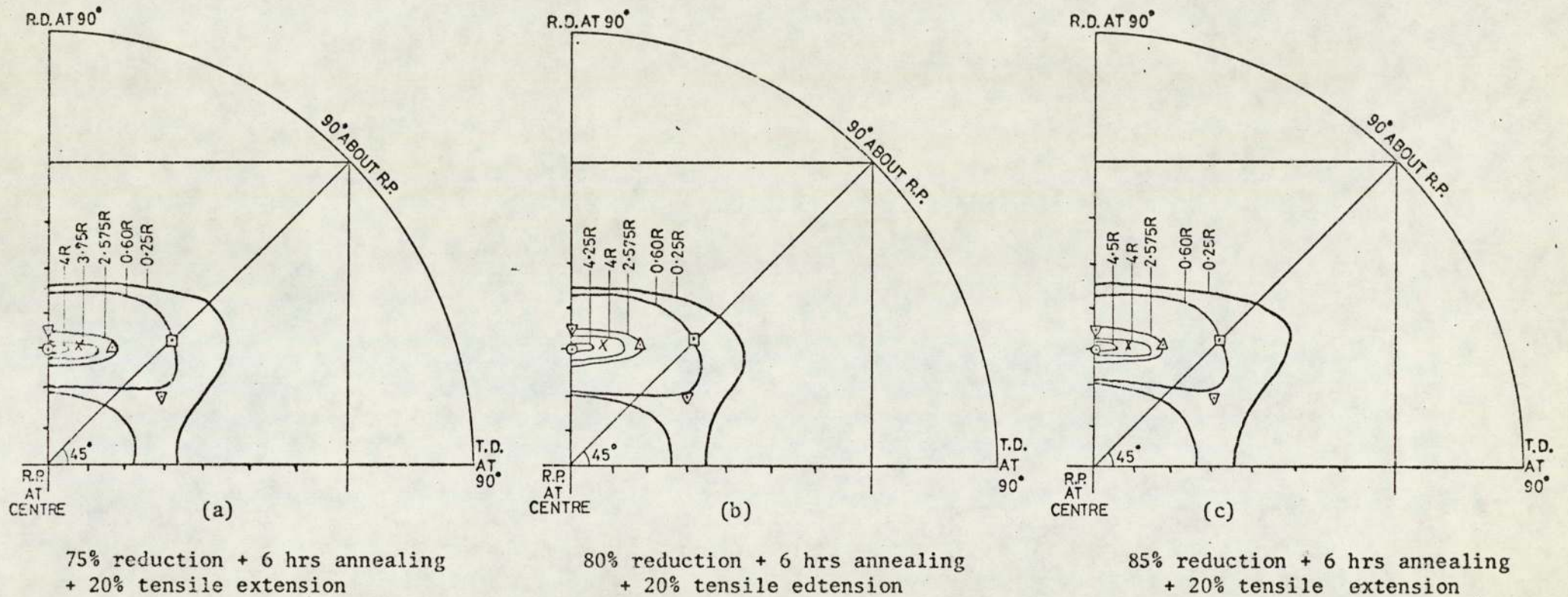


Fig. 5.5.b.3. One quadrant of (110) pole figures of specimens cold rolled using the 55°/p schedule, annealed for 6 hrs, aged then subjected to 20% tensile extension

Difference in {111} intensities X random before and after tensile extension

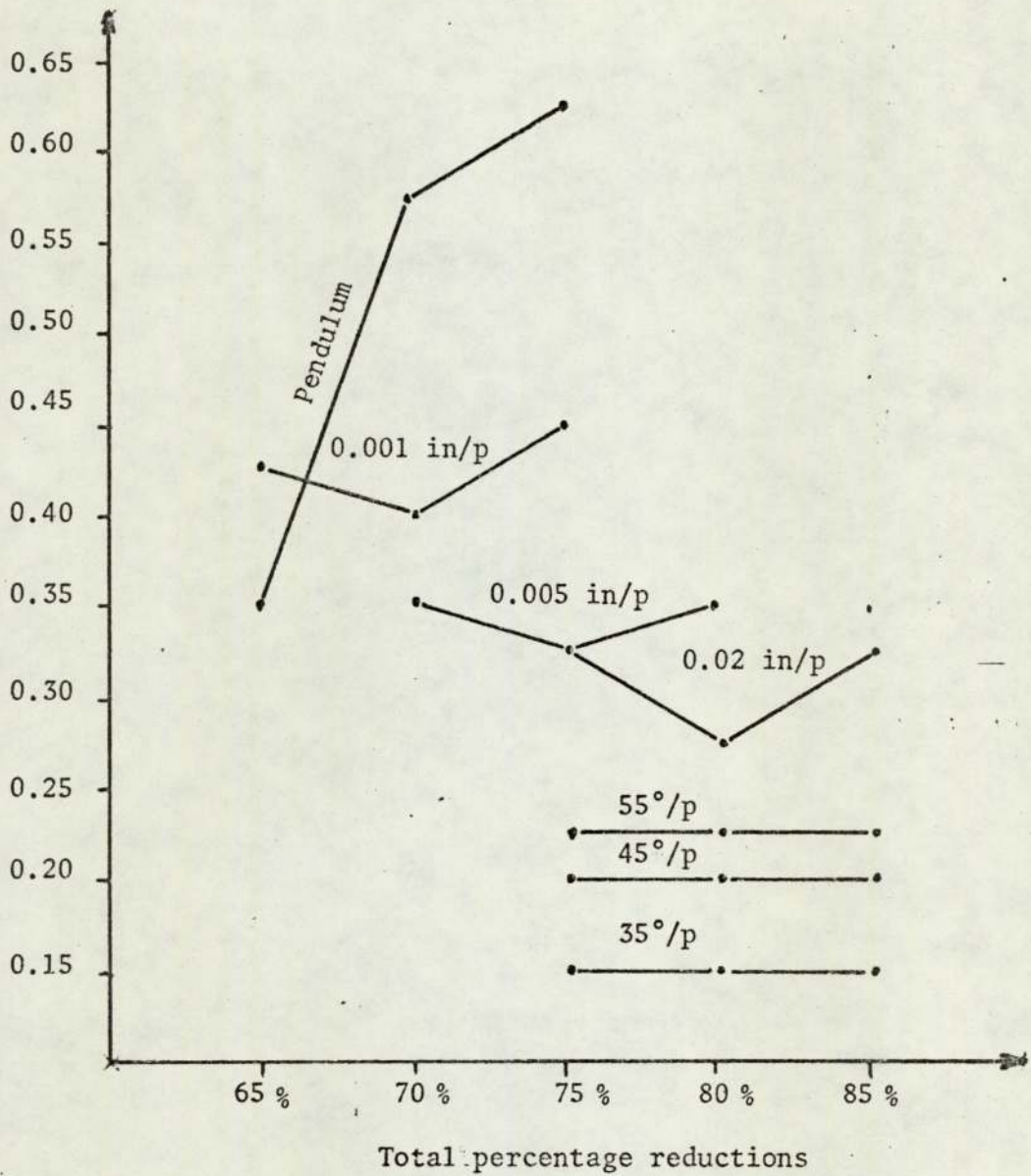


Fig. 5.5.b.4 The decrease in the {111} intensities after tensile extension in the case of specimens cold rolled to a range of total rolling reductions between 65% and 85% depending upon the rolling schedules, annealed for 6 hrs then aged.

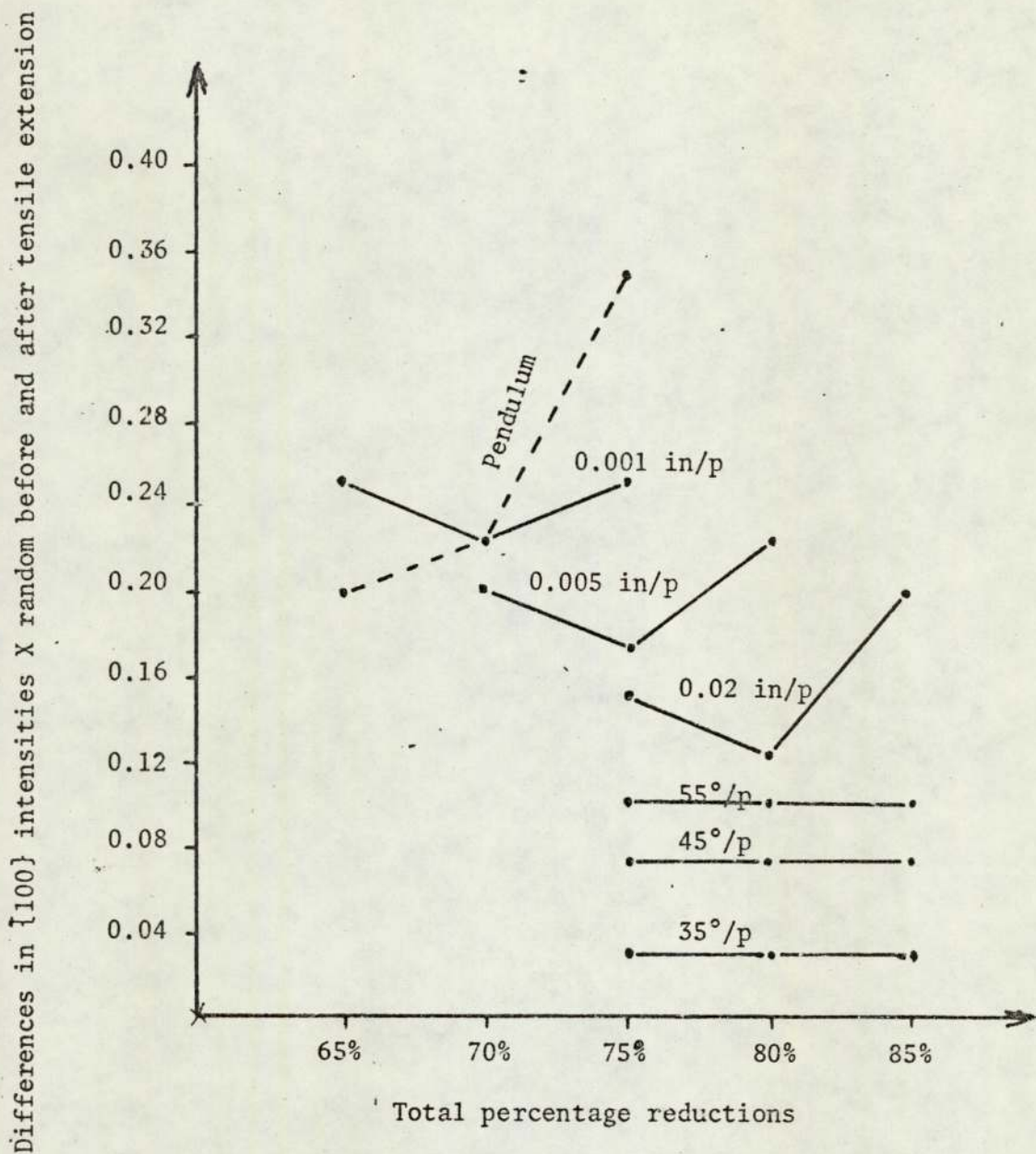
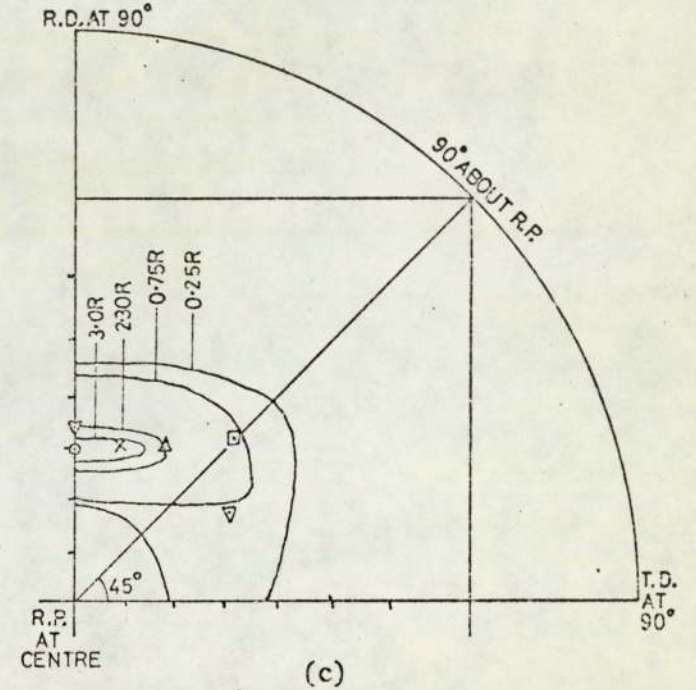
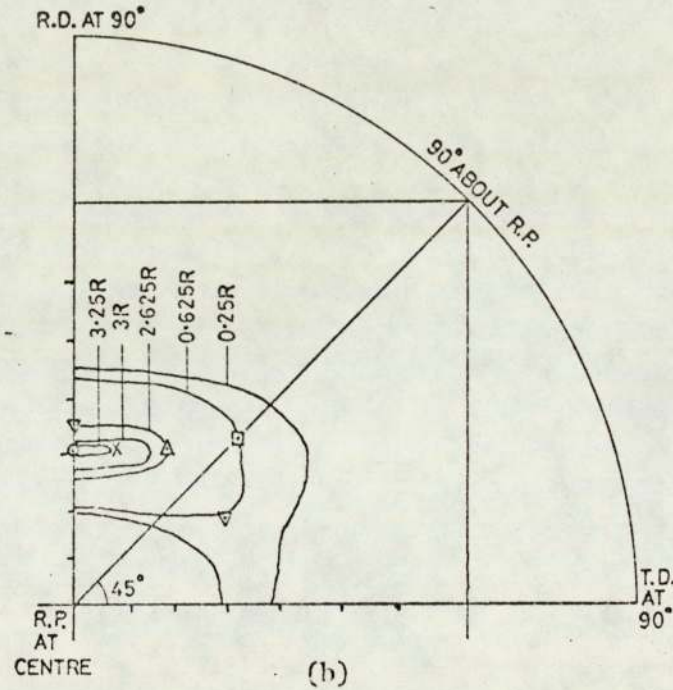
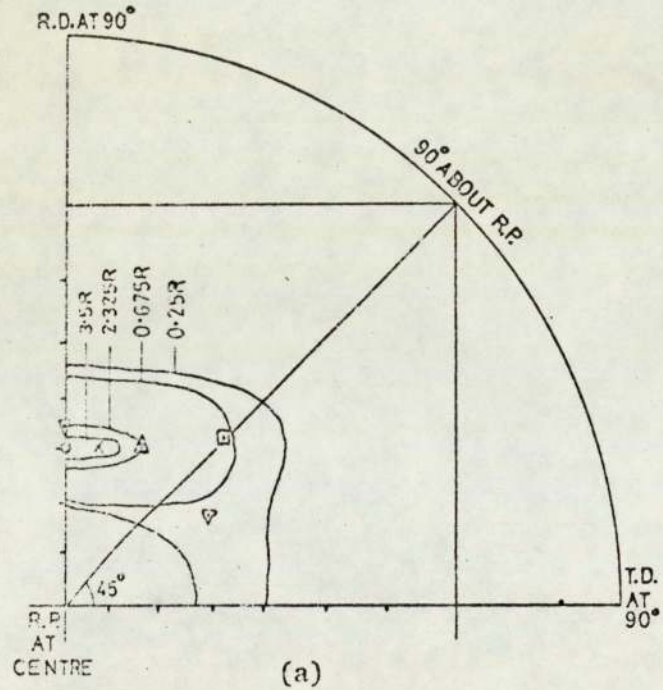


Fig. 5.5.b.5 The increase in the {100} intensities after tensile extension in the case of specimens cold rolled to a range of total reductions, between 65% and 85% depending upon the rolling schedules, annealed for 6 hrs, then aged.

(110) pole figures of specimens cold rolled to 75, 80 and 85% reductions using the 0.02 in/p schedule, annealed for 6 hrs, aged then subjected to 20% extension are shown in figure 5.5.b.6 (a,b,c). According to these figures, intensities of the  $\{111\}\langle 112\rangle$  increased and intensity of the  $\{100\}\langle 110\rangle$  decreased with increasing the total rolling reduction from 75% to 80% then decreased and increased respectively with further increase in rolling reduction. A similar behaviour was also evident when examining (110) pole figures of specimens cold rolled to 70, 75 and 80% using 0.005 in/p rolling schedule and 65, 70 and 75% using 0.001 in/p rolling schedule all annealed for 6 hrs, aged then subjected to 20% tensile extension. These figures are shown in figure 5.5.b.7 (a,b,c) and figure 5.5.b.8 (a,b,c). In the case of rolling with 0.02 in/p rolling schedule intensities of the  $\{112\}\langle 110\rangle$  and  $\{113\}\langle 110\rangle$  decreased with increasing the total rolling reduction. On the contrary, intensities of these components increased with increasing the total rolling reduction when rolling with 0.001 in/p and 0.005 in/p rolling schedules.

By comparing the previous figures with the corresponding (110) pole figures before tensile extension, the difference in intensities of the  $\{111\}\langle 112\rangle$  and  $\{100\}\langle 110\rangle$  components before and after tensile extension was calculated. However, difference in the  $\{111\}\langle 112\rangle$  and  $\{100\}\langle 110\rangle$  intensities before and after tensile extension increased and decreased respectively when increasing the rolling reduction in the same order as their intensity. The maximum increase in the  $\{111\}$  intensity and the minimum decrease in the  $\{100\}$  intensity after tensile extension coincided with 80%, 75% and 70% total reduction when rolling with

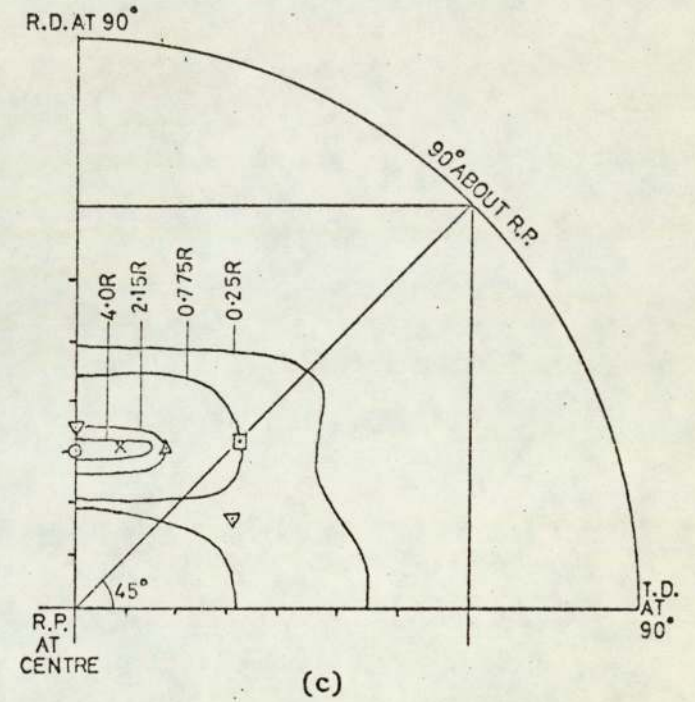
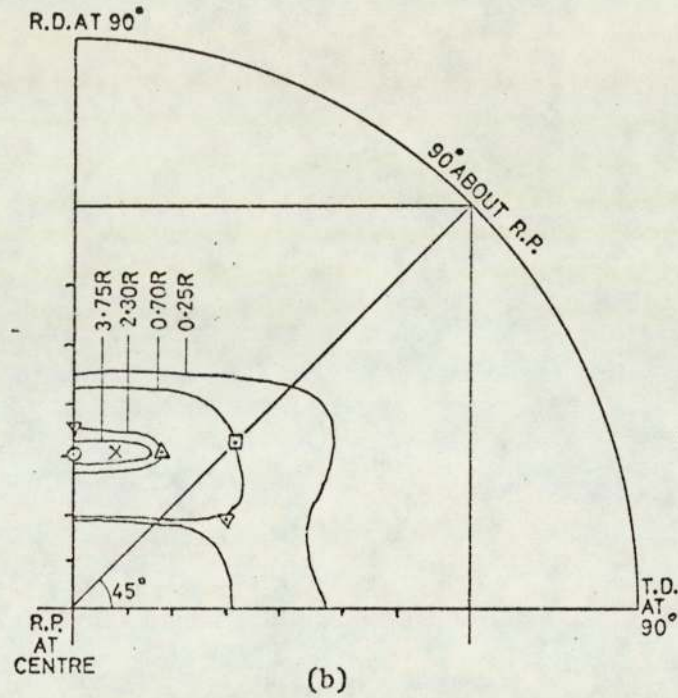
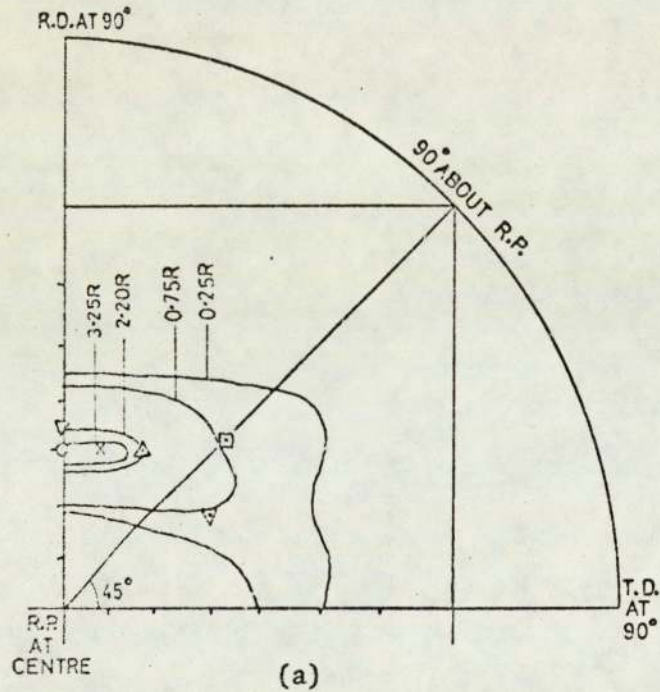


75% total rolling reduction + 6 hrs annealing + 20% tensile extension.

80% total rolling reduction + 6 hrs annealing + 20% tensile extension

85% total rolling reduction + 6 hrs annealing + 20% tensile extension.

Fig. 5.5.b.6. One quadrant of (110) pole figures of specimens cold rolled using the 0.02 in/p schedule, annealed for 6 hrs, aged then subjected to 20% tensile extension.

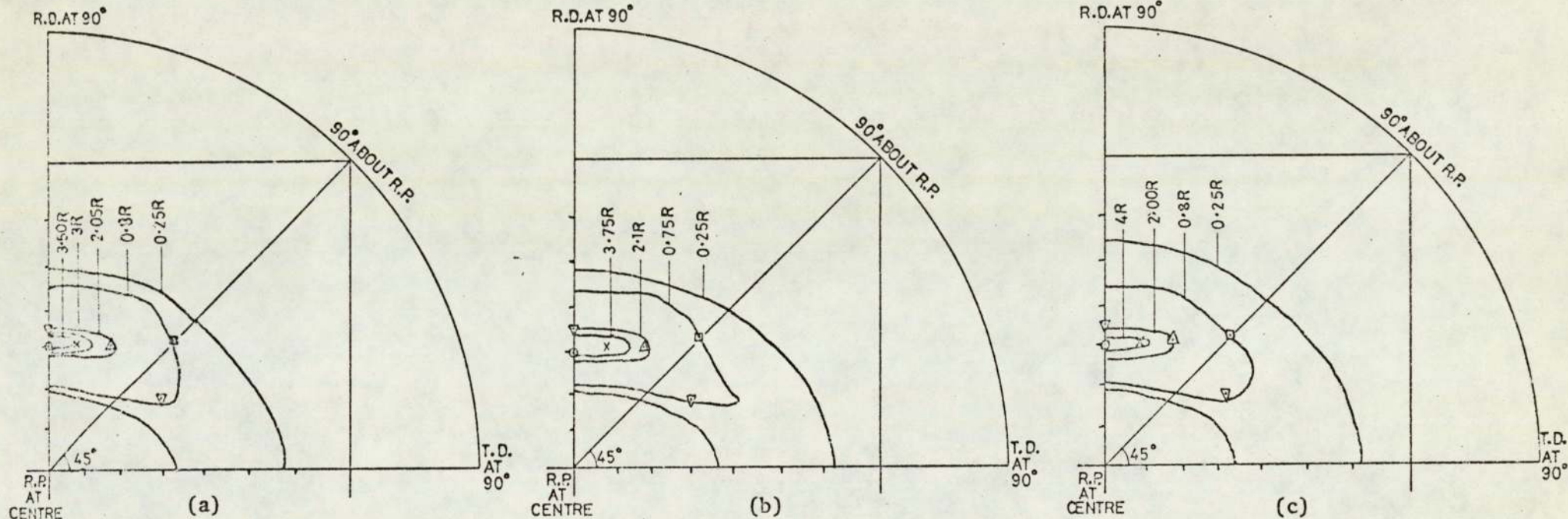


70% total rolling reduction + 6 hrs  
annealing + 20% tensile extension

75% total rolling reduction + 6 hrs  
annealing + 20% tensile extension

80% total rolling reduction + 6 hrs  
annealing + 20% tensile extension.

Fig. 5.5.b.7. One quadrant of (110) pole figures of specimens cold rolled using the 0.005 in/p schedule, annealed for 6 hrs, aged then subjected to 20% tensile extension.



65% total rolling + 6 hrs annealing + 20% tensile extension

70% total rolling reduction + 6 hrs annealing + 20% tensile extension

75% total rolling reduction + 6 hrs annealing + 20% tensile extension.

Fig. 5.5.b.8. One quadrant of (110) pole figures of specimens cold rolled using the 0.001 in/p schedule , annealed for 6 hrs then subjected to 20% tensile extension.

0.02 in/p, 0.005 in/p and 0.001 in/p rolling schedule respectively. This is demonstrated in figure 5.5.b.4 and figure 5.5.b.5.

(110) pole figures of specimens cold rolled to 65, 70 and 75% using the pendulum mill, annealed for 6 hrs, aged then subjected to 20% tensile extension are shown in figure 5.5.b.9. (a,b,c). It is apparent that intensity of the  $\{112\}\langle 110\rangle$ ,  $\{113\}\langle 110\rangle$  and  $\{111\}\langle 112\rangle$  increased with increasing the total rolling reduction while intensity of the  $\{100\}\langle 110\rangle$  continued to increase. By calculating the difference in intensities of corresponding  $\{111\}$  and  $\{100\}$  components before and after tensile extension it appeared that the decrease in the  $\{111\}$  intensity and increase in the  $\{100\}$  intensity after tensile extension was enhanced when increasing the total rolling reduction as shown in figure 5.5.b.4 and figure 5.5.b.5.

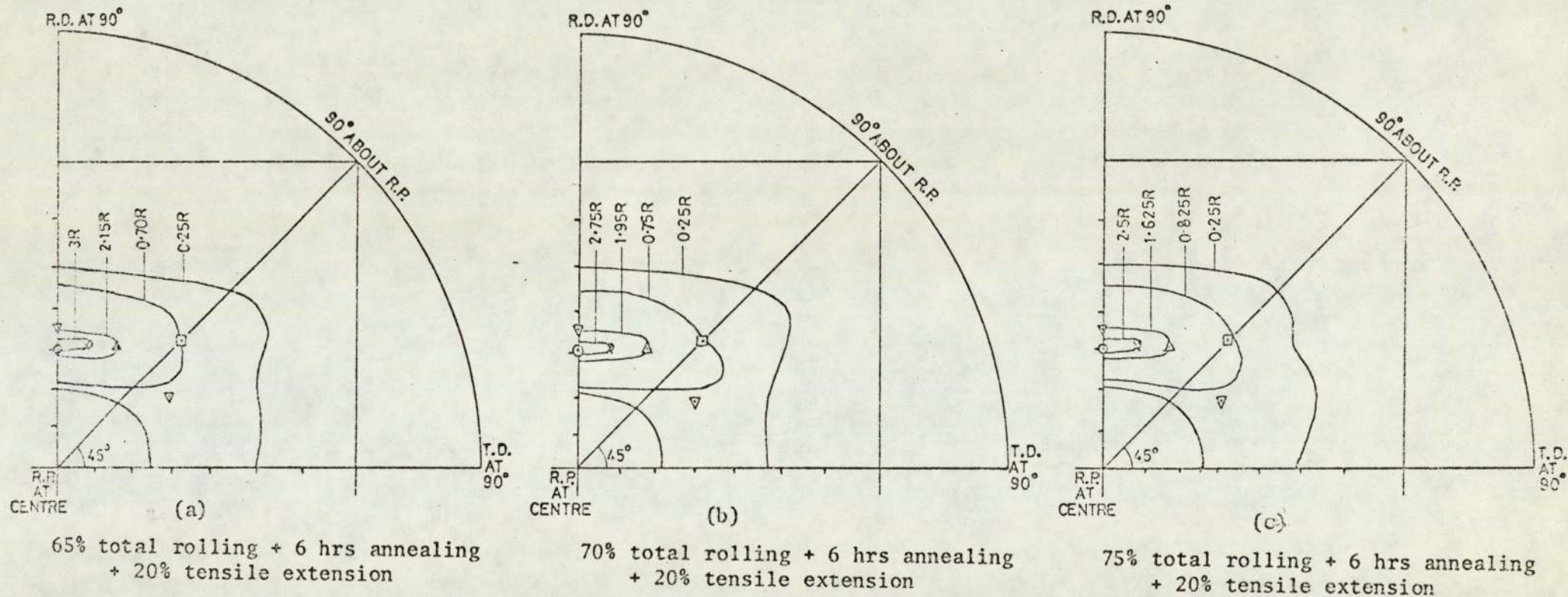


Fig. 5.5.b.9. One quadrant of (110) pole figures of specimens cold rolled using the pendulum schedule, annealed for 6 hrs, aged then subjected to 20% tensile extension.

## 6. DISCUSSION

## 6.1 INTRODUCTION

The results of the present investigation will be discussed in the order presented in the experimental results. It will be shown that the 25% total rolling reduction given to the initial material had no significant influence upon its final texture. The development of cold rolling and annealing textures will be accounted for. Texture before and after tensile extension is related to R value by the  $\frac{\{111\}}{\{100\}}$  texture ratio. The significance of the cold rolling geometry in the control of texture and R value is considered.

## 6.2 TEXTURE OF THE INITIAL MATERIAL

Deformation of low carbon steel, during hot rolling above the  $A_3$  temperature where austenite is the stable phase, occurs in a manner similar to that of high stacking fault f.c.c. metals at room temperature under similar friction condition<sup>(4)</sup>. Texture developed at that temperature should correspond to a weak f.c.c. pure metal and exhibit surface to centre segregation similar to that observed in copper and aluminium at room temperature under high frictions. A weak texture is to be expected since dynamic recrystallisation during hot rolling above the  $A_3$  temperature prohibits the formation of a strong austenitic texture. Phase transformation as dynamic recrystallisation occurs also reduced texture intensity in the ferritic phase<sup>(71)</sup>.

The surface and centre textures of ferritic steel were derived from the austenitic texture<sup>(42)</sup>, using the K-S transformation (G.Kurdjumov and G.Sachs, Z.Physik, 1930, 64, 325). Accordingly, the relationship between the transformed ferrite and the parent austenite can be described as follows:

- $\{101\}_\alpha$  orientation results from both  $\{100\}_\gamma$  and  $\{111\}_\gamma$  orientations<sup>(42,85)</sup>
- $\{100\}_\alpha$  orientation results from  $\{100\}_\gamma$  and  $\{110\}_\gamma$ <sup>(42,85)</sup>
- $\{111\}_\alpha$  orientation results from  $\{201\}_\gamma$  orientation<sup>(85)</sup>
- $\{112\}_\alpha$  orientation results from  $\{101\}_\gamma$  orientation<sup>(85)</sup>
- $\{312\}_\alpha$  orientation results from  $\{211\}_\gamma$  orientation<sup>(85)</sup>

The surface texture of the austenitic phase is expected to be a mixture of the  $\{100\}\langle 011\rangle$  and  $\{111\}\langle 110\rangle$  orientations, the latter being the prominent when rolling under high friction condition. Applying the above transformations, the  $\{110\}_\alpha$  orientation is the main ferritic texture at the sheet surface. Since the  $\{201\}_\gamma$  and  $\{101\}_\gamma$  orientations are of low intensities, therefore, the  $\{111\}_\alpha$  and  $\{112\}_\alpha$  orientation are expected to be of low intensity also. At the sheet mid-plane, the austenitic texture is expected to be a mixture of  $\{110\}\langle 112\rangle$  and  $\{112\}\langle 111\rangle$  orientations with the former predominating. Therefore, the  $\{100\}_\alpha$  is dominant at the centre of the sheet followed by the  $\{112\}_\alpha$  orientation. The  $\{111\}_\gamma$  and  $\{100\}_\gamma$  orientations, on the other hand, are of low intensity which results in a weak  $\{110\}_\alpha$  at the sheet mid-plane.

The observed texture of the initial material was weak but corresponded approximately with the predicted ferrite texture<sup>(70)</sup> as shown in Table 6.2.1. The surface texture however, is characterised by a higher ratio of  $\{110\}$  and lower ratio of  $\{112\}$  planes parallel to the surface. At the centre, intensity of the  $\{100\}$  was higher and intensity of the  $\{110\}$  planes was lower. The terms higher and lower refer to the relative magnitude of each texture component to each other. On the whole, texture of the initial material was relatively weak. This is in agreement with the previous measurements of texture of hot band rimmed steel<sup>(40,85)</sup>.

Texture components	Measured texture intensity X random	Predicted relative texture intensity
{110}	1.12	high
{100}	1.05	medium
{111}	1.00	low
{112}	0.97	low

(a) surface texture

Texture Components	Measured texture intensity X random	Predicted relative texture intensity
{100}	1.27	high
{112}	1.15	high
{123}	1.06	medium
{110}	0.70	low

(b) centre texture

Table 6.2.1. Illustrates the agreement between the surface and centre textures measured in the present study and the corresponding texture predicted<sup>(70)</sup>.

{hkl}	P values of the mid plane of the initial rimmed steel material used in the present study.	P values of the mid plane of a hot band rimmed steel abstracted from previous study
{110}	0.70	0.68
{200}	1.27	1.30
{211}	1.15	1.11
{310}	0.72	0.90
{222}	0.95	0.93
{321}	1.06	0.95
{411}	0.67	not given
{332}	0.77	0.98

Table 6.2.2. P values of the centre of the initial material used in the present study compared with the corresponding P values of the centre of a hot rolled rimmed steel band abstracted from the work of Hellewell<sup>(85)</sup>.

P values of the initial material mid-plane measured in the present study were comparable with the corresponding P values of a hot rolled rimmed steel band abstracted from the work of Hellewell<sup>(85)</sup> as shown in Table 6.2.2. It was, therefore, concluded that the 25% total cold rolling reduction and the annealing cycle previously given to the present initial material had no influence upon the final texture. This is also in agreement with a study by Thomson and Baker<sup>(72)</sup> in which it was stated that cold rolling of a hot rimmed steel band to a total reduction up to 40% had no effect upon its final texture.

### 6.3 THE EFFECT OF COLD ROLLING PROCEDURES UPON THE DEVELOPMENT OF COLD ROLLING TEXTURES

Development of the cold rolling texture is accounted for here on the basis of a theory<sup>(7)</sup> which has not found a wide-spread acceptance. Alternative approaches are possible<sup>(16,92)</sup>.

Analysis of (110) pole figures (section 5.4) revealed that texture developed after cold rolling was dependent upon the rolling procedures. After certain rolling reduction, intensities of the {112}<110> and {111}<112> orientations decreased when increasing the shear plane angle, decreasing the roll gap and using the pendulum mill. Conversely, intensity of the {100}<110> orientation increased with altering the rolling procedures in the previous order. This is shown in figure 6.3.1.(a,b,c) derived from (110) pole figures of the cold rolled materials (figure 5.e.1.2(a,b,c), figure 5.4.1.3(a,b,c), figure 5.4.1.4(a,b,c), figure 5.4.1.5(a,b,c), figure 5.4.1.6(a,b,c), figure 5.4.1.7(a,b,c) and figure 5.4.1.8(a,b,c)).

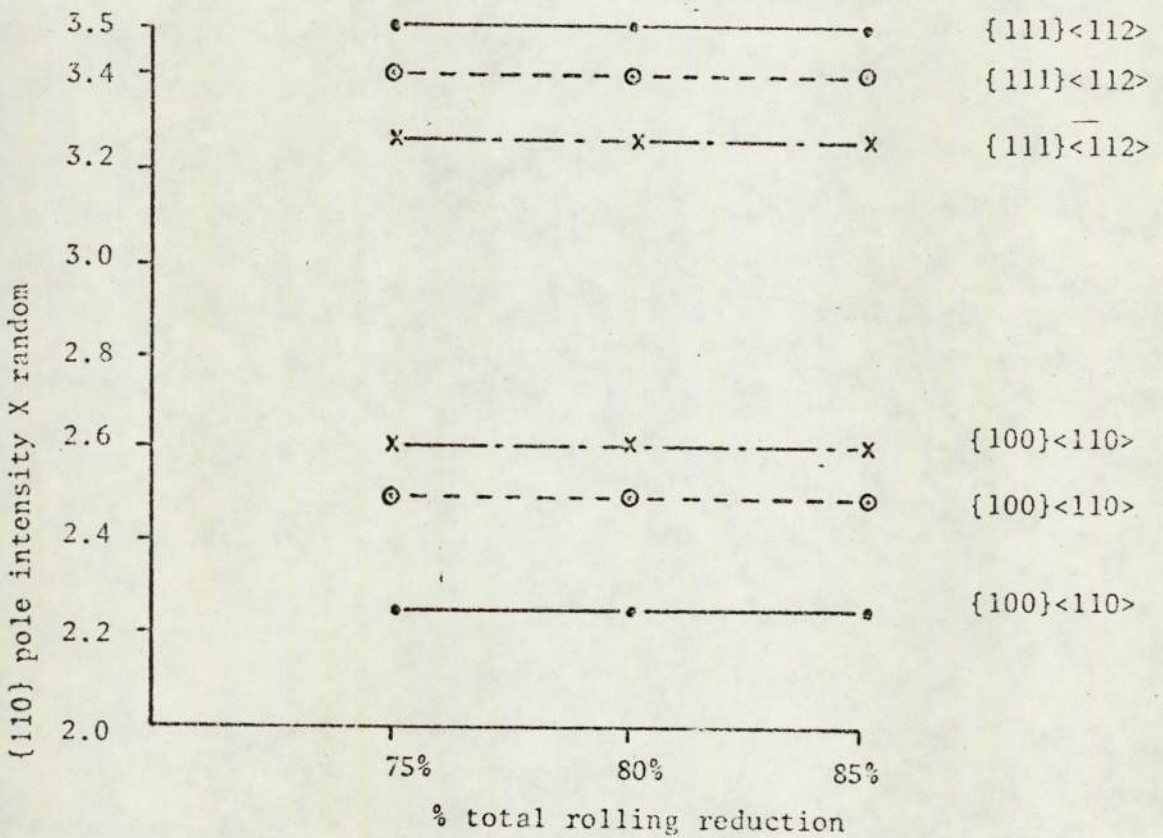
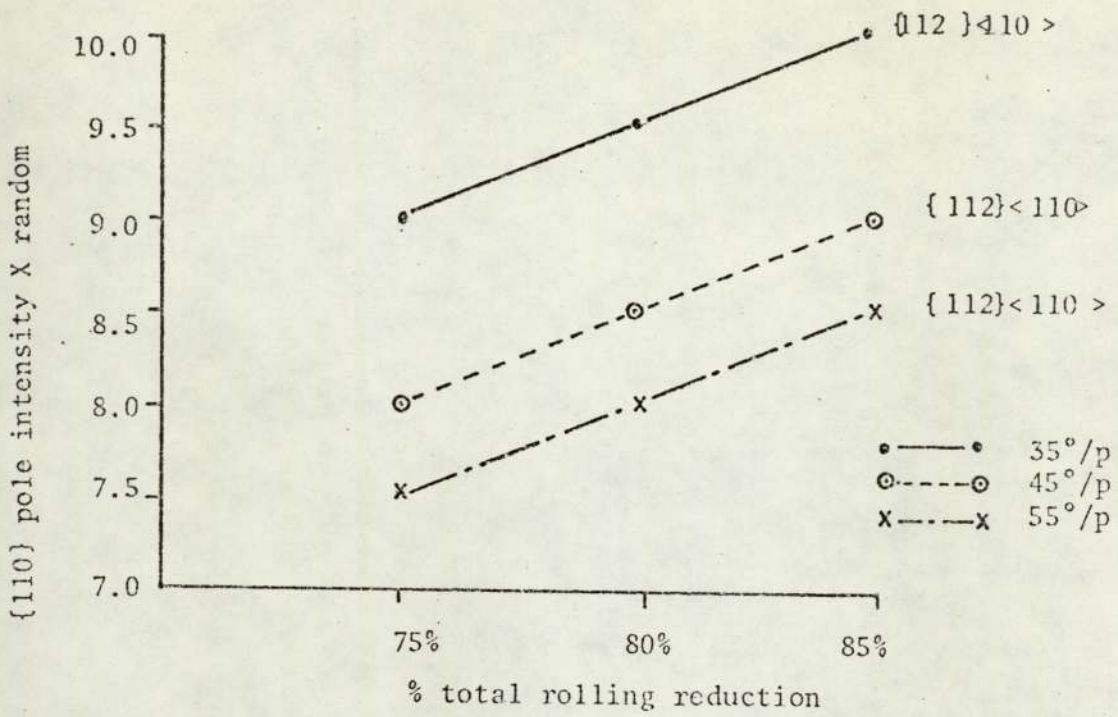


Fig.6.3.1.a Shows the variations in the {110} pole intensity at the ideal orientations  $\{112\}\langle 110 \rangle$ ,  $\{111\}\langle 112 \rangle$  and  $\{100\}\langle 110 \rangle$  with increasing the total rolling reduction using the 35°/p (●—●), 45°/p (⊙---⊙) and 55°/p (x-·-·-x) rolling schedules.

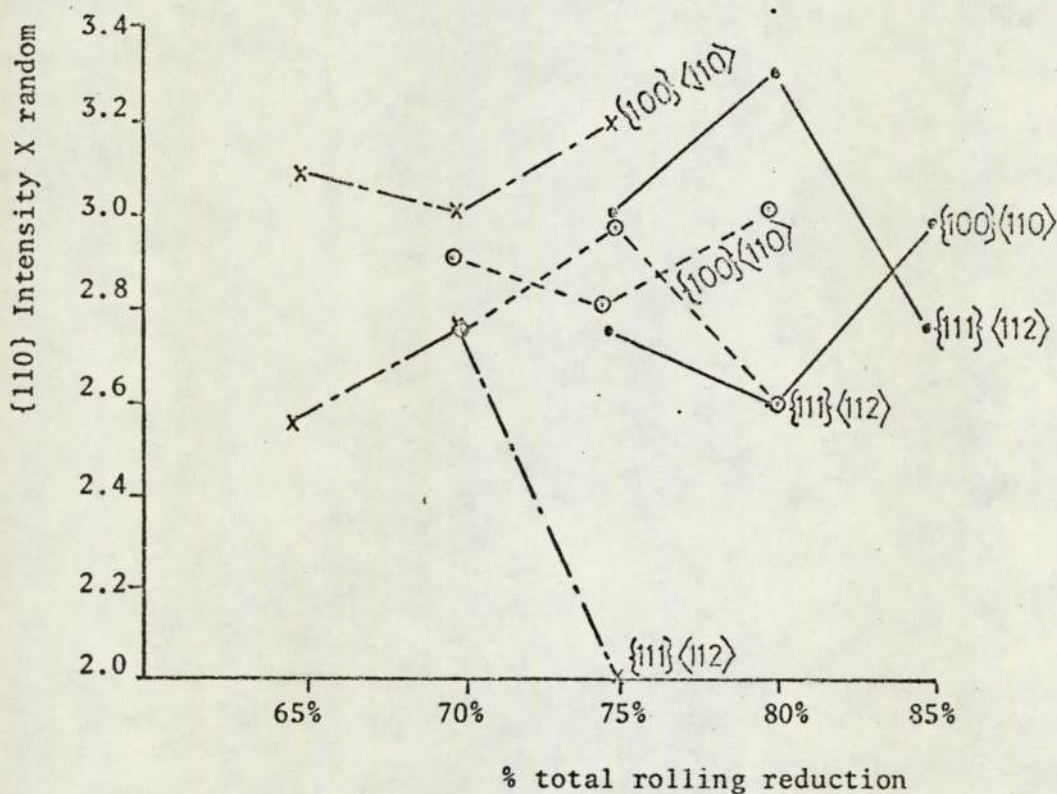
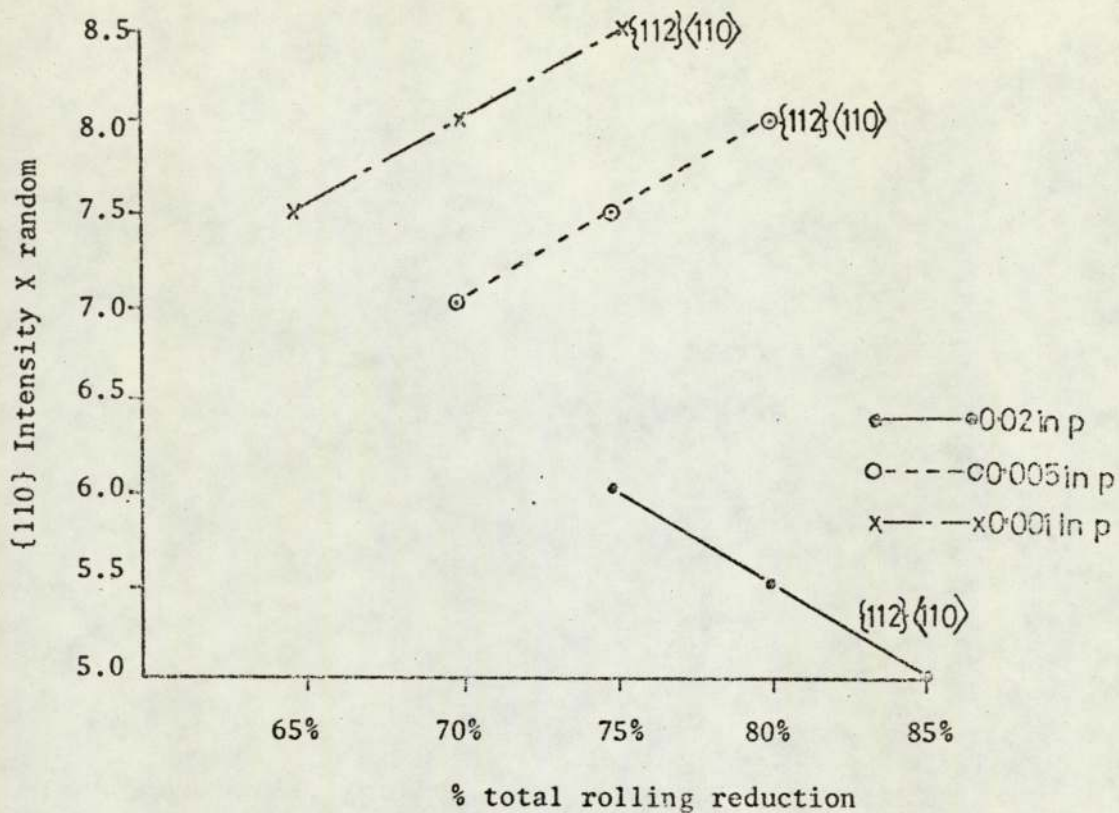


Fig. 6.3.1.b. Shows the variation in the {110} pole intensity at the ideal orientations {112}<110>, {111}<112> and {100}<110> with increasing the total rolling reduction using the 0.02 in/p (•—•), 0.005 in/p (⊙---⊙) and the 0.001 in/p (x---x) rolling schedules.

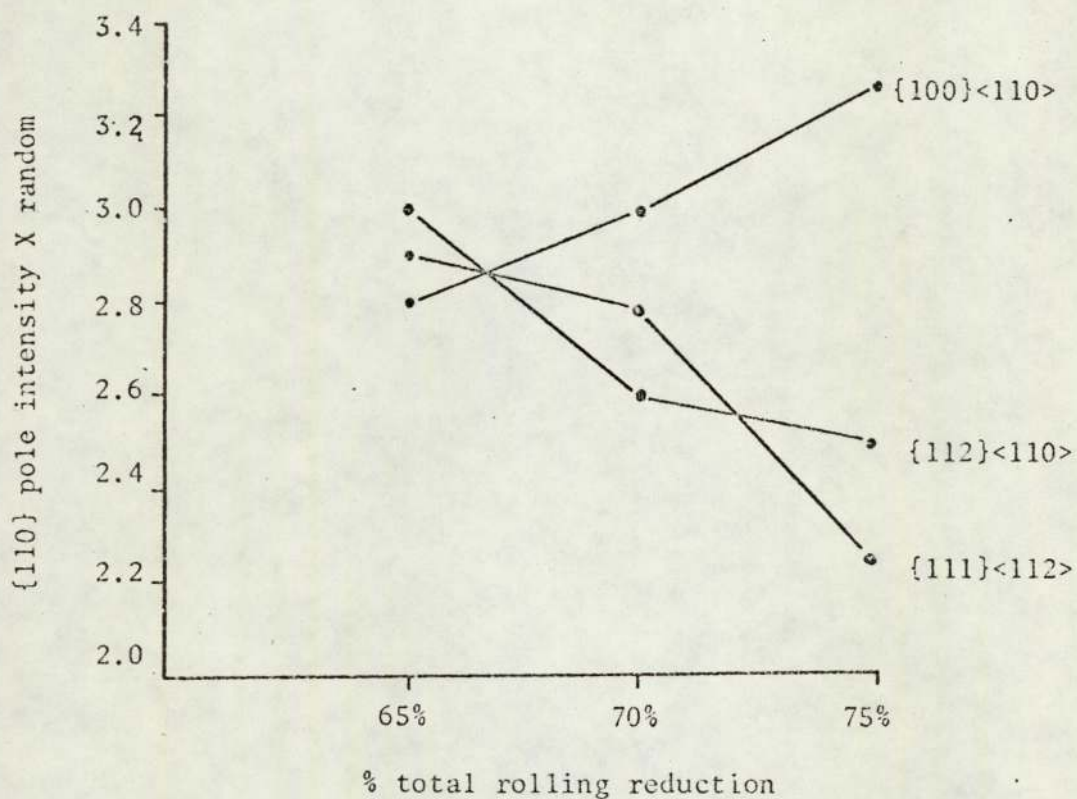


Fig. 6.3.1.c Shows the variation in the {110} pole intensity at the ideal orientations {112}<110>, {111}<112> and {100}<110> with increasing the total rolling reduction using the pendulum mill.

Cold rolling textures can be looked upon as symmetrically stable orientations under a biaxial stress system, compression normal to the rolling plane and tension in the rolling direction<sup>(7)</sup>. Furthermore, the crystallographic rotations during cold rolling can be represented stereographically by  $54^{\circ} 44'$  around the rolling direction and around the strip normal<sup>(7)</sup> as shown in figure 2.2.1. Accordingly in the early stages of cold rolling of a randomly orientated material, the  $\langle 111 \rangle$  slip direction rotates towards the rolling direction and stable on the  $54^{\circ} 44'$  around the strip normal. The  $\{110\}$  slip planes maintain contact with the compression circle likewise. The slip plane normal therefore, is stable on the tension circle and  $35^{\circ} 16'$  from the strip normal, figure 2.2.1. On this basis the  $\{100\}\langle 110 \rangle$  orientation is formed in the initial stages of cold rolling. In the  $\{100\}\langle 110 \rangle$  orientation figure 2.2.1, the  $\{111\}$  slip directions are symmetrically disposed around the rolling direction and the  $\{112\}$  pole lies on the tension circle. The  $\{112\}$  planes therefore, are active slip planes resulting in the formation of the  $\{112\}\langle 110 \rangle$  orientation. In addition the  $\{123\}$  slip planes which lie near the  $\{112\}$  slip planes as shown in figure 2.2.2. rotate around the  $\langle 111 \rangle$  direction to form the  $\{113\}\langle 110 \rangle$  orientation. Also, the four  $\{100\}$  poles rotate around the rolling direction to form the  $\{111\}\langle 110 \rangle$  orientation, figure 2.2.3. The  $\{111\}\langle 110 \rangle$  orientation rotates around the strip normal so as the  $\{110\}$  poles lie in the rolling direction and form the  $\{111\}\langle 112 \rangle$  orientation as in figure 2.2.4.

In a randomly orientated material where orientation of crystals may vary from one crystal to the next, deformation occurs by slip on those systems which lie parallel or near to the  $35^{\circ}$  and  $55^{\circ}$  from the

stress axes. The  $\{211\}$  poles lie  $35^\circ$  from the strip normal and the  $\{110\}$  poles rotate to the  $35^\circ$  position from the strip normal to form the  $\{111\}\langle 112 \rangle$  orientation. As a result, more  $\{112\}\langle 110 \rangle$  and  $\{111\}\langle 112 \rangle$  orientations are formed during cold rolling using the  $35^\circ/p$  rolling schedule in comparison with the  $45^\circ/p$  and  $55^\circ/p$  rolling schedules. During cold rolling using constant roll gap rolling schedules, the shear plane angle varies continuously, as shown in figure 6.3.2., to or away from the  $35^\circ$  position. Accordingly, less  $\{112\}\langle 110 \rangle$  and  $\{111\}\langle 112 \rangle$  orientations are formed during cold rolling using constant roll gap schedules. During cold rolling using the pendulum mill, the direction of rolling was reversed at the end of each stroke by reversing the stroke direction end for end before proceeding with the next stroke. Cold rolling using the pendulum mill is therefore equivalent to reverse rolling, see figure 6.3.3. Since the  $\{100\}\langle 110 \rangle$  component is the only texture component with four fold symmetry around the sheet normal, the development of the  $\{100\}\langle 110 \rangle$  component is enhanced at the expense of the  $\{112\}\langle 110 \rangle$  and  $\{111\}\langle 112 \rangle$  components during cold rolling using the pendulum mill.

During cold rolling using controlled geometry rolling schedules the rolling draughts and the percentage reduction per pass were very small after 75% total reduction (see Appendix III, IV and V). On increasing the total rolling reduction to 85% intensity of the  $\{112\}\langle 110 \rangle$  orientation increased while intensities of the  $\{111\}\langle 112 \rangle$  and  $\{100\}\langle 110 \rangle$  orientations remained constant (figure 6.3.1a).

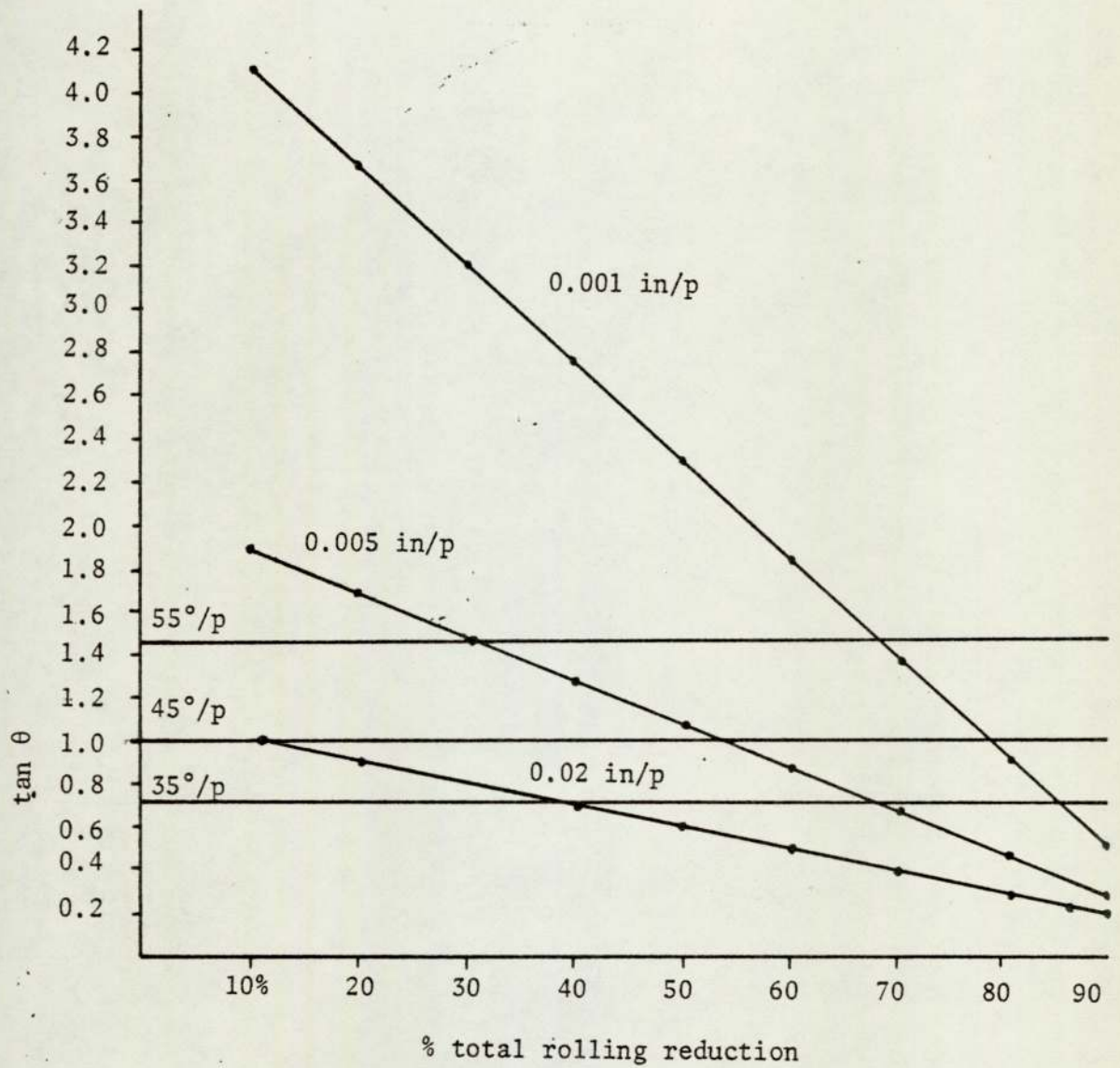


Fig. 6.3.2. The variation in  $\tan \theta$  versus the percentage total rolling reduction in the case of six rolling schedules,  $\theta$  is the shear angle in the material undergoing deformation.

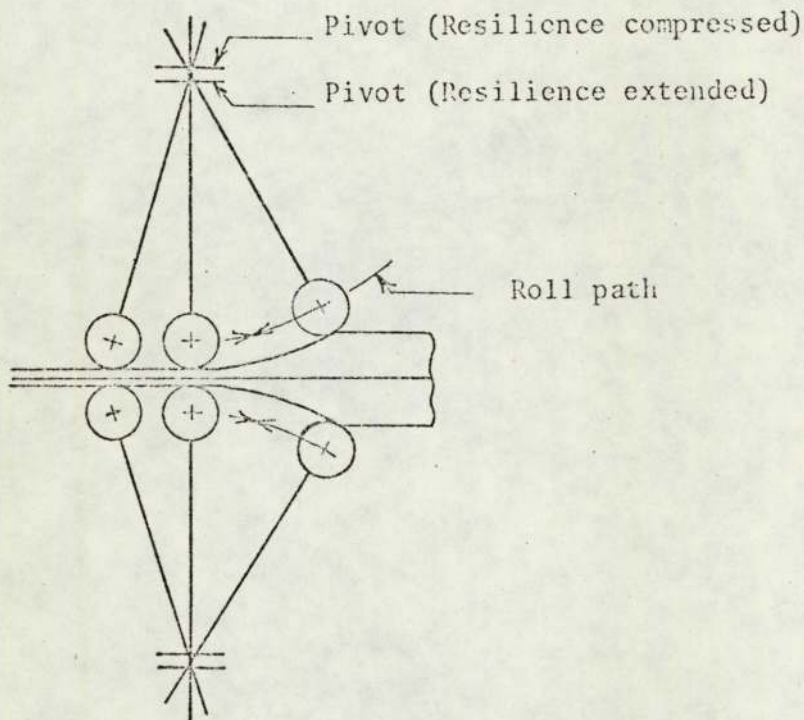


Fig. 6.3.3. A schematic representation of the pendulum cycle in which the rolls reverse their direction at the end of each stroke.

As cold rolling proceeds using 0.001 in/p rolling draughts, the angle  $\theta$  continues to decrease as shown in figure 6.3.2. towards the  $35^\circ$  position. This resulted in increasing the intensity of the  $\{112\}\langle 110\rangle$  and  $\{111\}\langle 112\rangle$  orientations at the expense of the  $\{100\}\langle 110\rangle$  orientation. After 70% total reduction, the percentage reduction per pass increased and the critical resolved shear stress on the  $\{100\}$  slip planes increased<sup>(7)</sup> so that the  $\{100\}$  planes become active slip planes. Accordingly the  $\{111\}\langle 112\rangle$  component rotates to the  $\{100\}\langle 110\rangle$  orientation and results in an increase in intensity of the second component at the expense of the first. During cold rolling using 0.005 in/p rolling draughts the percentage reduction per pass is higher. This increases the critical resolved shear stress on the  $\{100\}$  planes<sup>(7)</sup> which results in rotation of the  $\{112\}\langle 110\rangle$  component to the  $\{111\}\langle 112\rangle$  orientation. As a result, the reduction in intensity of the  $\{111\}\langle 112\rangle$  component is more noticeable after 75% total rolling reduction. Such a total rolling reduction is coincident with a stage at which the rotation of the  $\{112\}\langle 110\rangle$  component to the  $\{111\}\langle 112\rangle$  component is less than rotation of the second component to the  $\{100\}\langle 110\rangle$  orientation. In cold rolling using 0.02 in/p rolling draughts the situation is different in that the percentage reduction per pass is much higher and more  $\{112\}\langle 110\rangle$  orientation rotates to the  $\{111\}\langle 112\rangle$  orientation. Accordingly, intensity of the  $\{112\}\langle 110\rangle$  orientation decreased on increasing the total rolling reduction and the reduction in intensity of the  $\{111\}\langle 112\rangle$  occurred after higher total reductions (80%).

During cold rolling using the pendulum mill the deformation temperature and the coefficient of friction increased on increasing the total rolling reduction<sup>(66)</sup>. This can only increase the amount of {100}<110> orientation after heavy total rolling reduction as in figure 6.3.1.c. This is consistent with the previous analysis of cold rolling texture developed by conventional reverse rolling of b.c.c. metals<sup>(4,7,30,46)</sup>.

#### 6.4 THE EFFECT OF COLD ROLLING TEXTURE AND ANNEALING TIME UPON THE DEVELOPMENT OF THE ANNEALING TEXTURE

Analysis of the annealing texture after 0.5 hr annealing indicated a significant reduction in P value of the {100} component depending upon the rolling schedules. P values of the {111} component decreased also but remained dominant in the annealing texture, as shown in Table 5.4.2.1, figure 5.4.2.1 and figure 5.4.2.2. There was also an increase in intensity of the {110} orientation. The reduction in intensity of the {100} component after 0.5 hr annealing is due to its low stored energy of deformation<sup>(19)</sup>. On the same basis, the predominance of the {111} component in the annealing texture is to be expected because of its relatively high stored energy and its preponderance in the cold rolling texture. Although the stored energy of the {110} planes is higher than that of the {111} planes<sup>(19)</sup>, it is unlikely to dominate the annealing texture because of its low proportion in the cold rolling texture. The relatively low proportion of the {211}, {310}, {321}, {411}, and {332} planes in the annealing texture is also attributed to their low stored energies and proportions in the cold rolling texture.

Increasing the annealing time from 0.5 hr to 6 hrs was accompanied by an increase and a decrease in P values of the {111} and {100} orientations respectively. This is shown in Table 5.4.2.2, figure 5.4.2.1, and figure 5.4.2.2. The increase in P values of the {111} component after 6 hrs annealing in comparison with annealing for 0.5 hr is due to the normal growth of the {111} planes which are relatively strong in the primary recrystallisation texture at the expense of the weak {100} planes. With reference to the cold rolling texture, Table

5.4.1.1, P values of the {111} and {100} orientations of materials cold rolled to 75% using the 35°/p, 45°/p, 55°/p, 0.02 in/p, 0.005 in/p, 0.001 in/p and pendulum schedules decreased and increased respectively in that order. Accordingly, the growth of the {111} and {100} components after 6 hrs annealing varied with the rolling schedules in the same order of their magnitude in the cold rolling texture. After 6 hrs annealing, however, more {111} and less {100} components were developed on annealing of materials cold rolled using the 35°/p rolling schedules. In comparison less {111} and more {100} orientations were developed when materials cold rolled using the 45°/p, 55°/p, 0.02 in/p, 0.005 in/p, 0.001 in/p and pendulum schedules were annealed.

With reference to (110) pole figures of materials cold rolled to a range of total rolling reductions, figure 5.4.2.3 to figure 5.4.2.9, intensities of the {111} and {100} orientations depended upon the total rolling reductions. The growth of the {111} and {100} planes during annealing is, therefore, dependent upon the total rolling reduction prior to annealing. Accordingly, the variations in intensities of the {111} and {100} components after 6 hrs annealing with the total rolling reduction followed the same pattern as for prior to annealing though intensity of the {100} operation was greatly reduced. This is evident in figure 5.4.1.2 to figure 5.4.1.8 and figure 5.4.2.3 to figure 5.4.2.9.

## 6.5 THE RELATIONSHIP BETWEEN PROCESSING, TEXTURE AND R VALUE

It is well recognised that the average plastic strain ratio  $\bar{R}$  can be related to a texture parameter of the form  $\{111\}/\{100\}$ <sup>(87)</sup> as shown in figure 6.5.1. The theoretical reasons for this relationship have been given<sup>(23)</sup>. Because of the limited material width,  $\bar{R}$ , was not measured in the present investigation and  $R_0$  values only were obtained. For the materials investigated, there is also a good correlation between  $R_0$  value and the  $\{111\}/\{100\}$  texture parameter as shown in figure 6.5.2.

The measurements of the  $\{111\}/\{100\}$  ratios of materials cold rolled to 75% total rolling reductions using the 35°/p, 45°/p, 55°/p, 0.02 in/p, 0.005 in/p, 0.001 in/p and pendulum rolling schedules are shown in Table 6.5.1. The  $\{111\}/\{100\}$  ratios of the cold rolled materials are very low and below unity in the case of material cold rolled by the pendulum mill. These low values of the texture parameter are related to the very low  $R_0$  values of materials in the cold rolled conditions shown in figure 5.3.1. The  $\{111\}/\{100\}$  texture ratio decreased on increasing the shear plane angle, decreasing the roll gap and the lowest value of all is obtained by the pendulum schedule. Because of the experimental difficulty encountered in measuring  $R_0$  values of materials with very limited ductility, it was not possible to correlate these changes in texture parameter with changes in  $R_0$  value at these levels. Measurements of the  $\{111\}/\{100\}$  ratios after 75%, 80% and 85% total rolling reduction using the 35°/p schedule revealed no change in the texture parameter, as shown in figure 6.5.3. A similar observation is also evident in the case of materials cold rolled to the same total reductions using the 45°/p and 55°/p schedules. Cold rolling using the 0.02 in/p, 0.005 in/p and 0.001 in/p schedules resulted in increasing  $\{111\}/\{100\}$

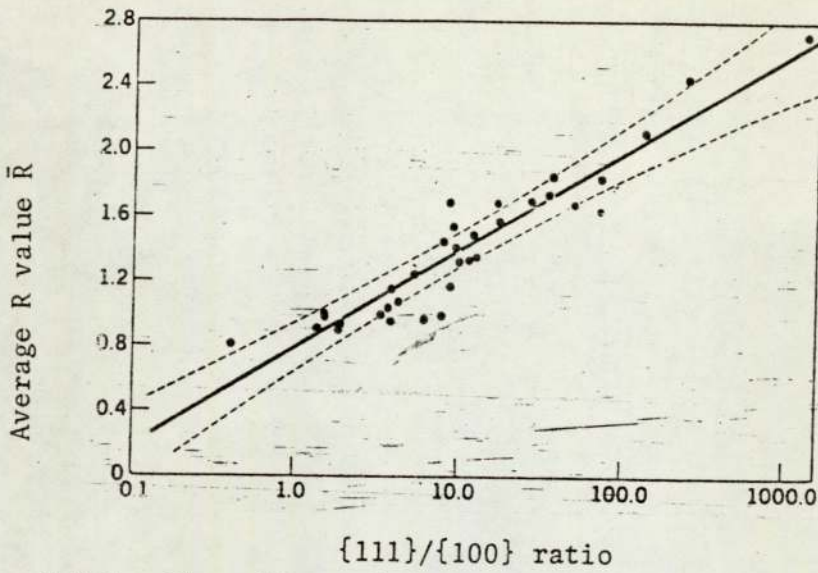


Fig. 6.5.1. The effect of the ratio of the intensity of the (111) component to the intensity of the (001) component on the average R value strain ratio of low-carbon steel.

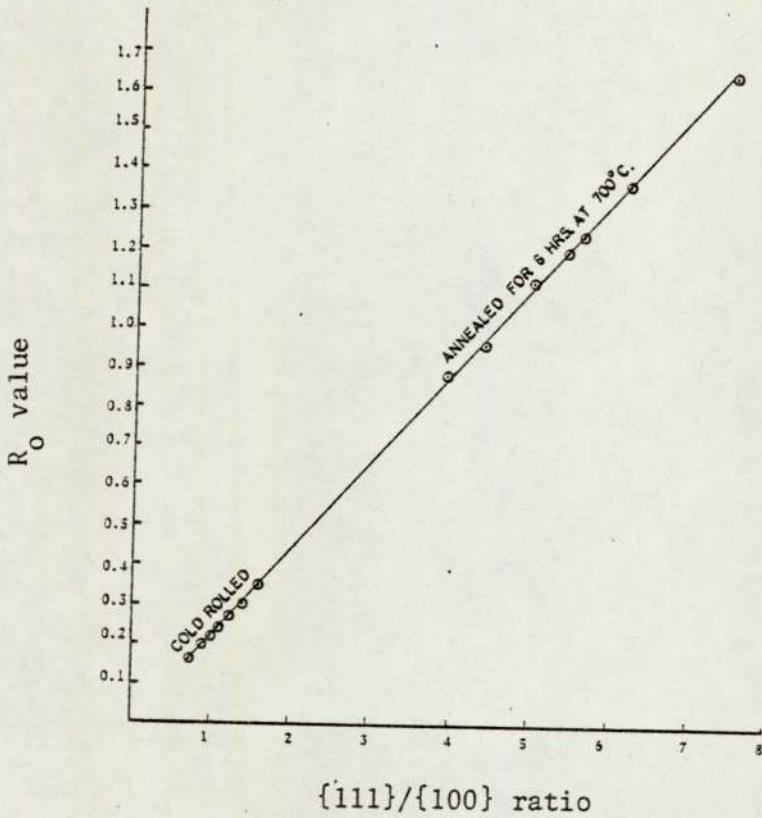


Fig. 6.5.2. The effect of the ratio {111}/{100} texture intensity upon  $R_0$  value measured in the present study.

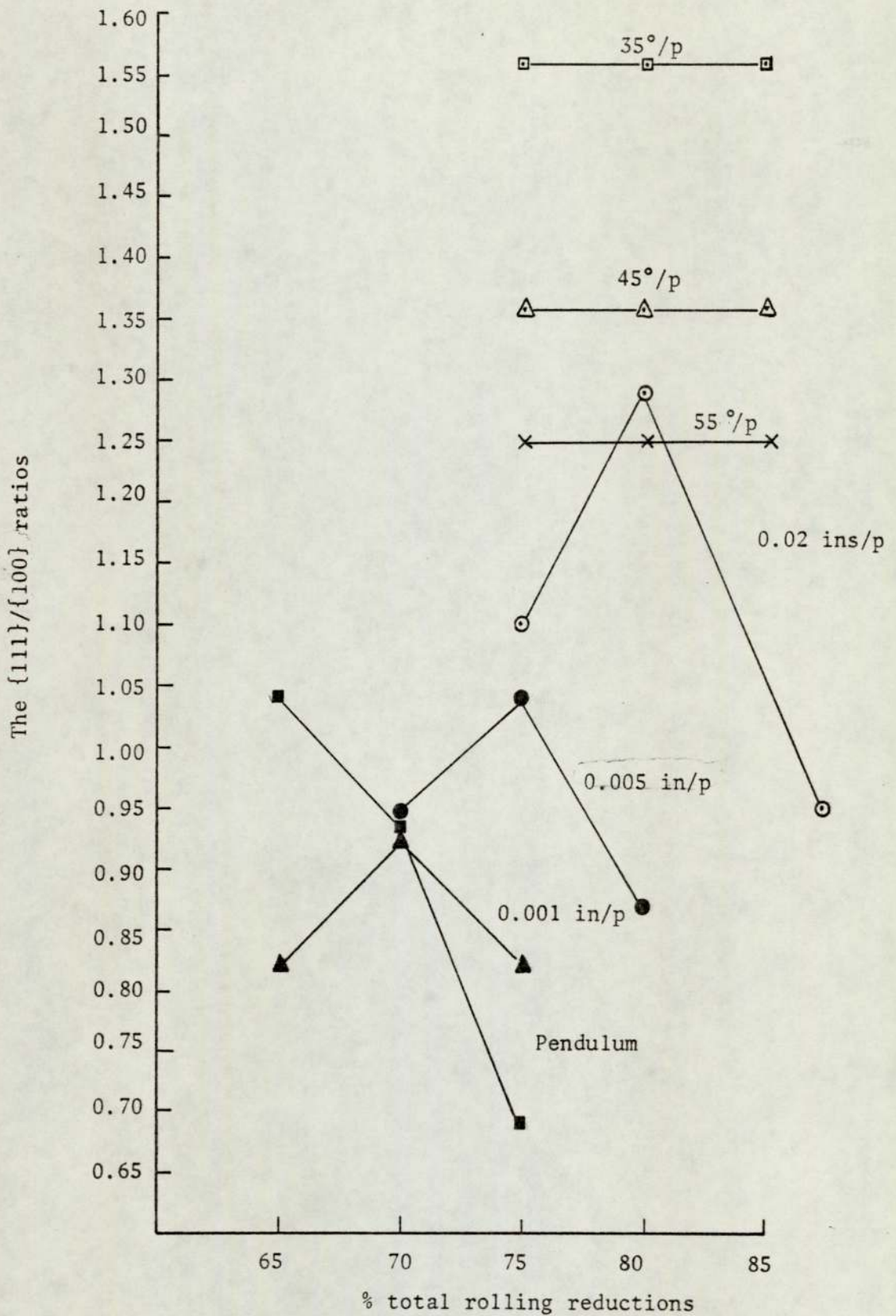


Fig. 6.5.3. The variations in the  $\{111\}/\{100\}$  ratios of materials cold rolled using the seven rolling schedules versus the percentage total rolling reduction

Rolling schedules	P values		{111}/{100} ratios
	{111} Planes	{100} Planes	
35°/p	3.49	2.20	1.59
45°/p	3.37	2.48	1.36
55°/p	3.26	2.60	1.25
0.02 in/p	3.01	2.71	1.11
0.005 in/p	2.92	2.81	1.04
0.001 in/p	2.72	3.01	0.90
Pendulum	2.39	3.20	0.75

Table 6.5.1. The variations in the {111}/{100} ratios and  $R_0$  values of materials cold rolled to 75% total reduction using the 35°/p, 45°/p, 55°/p, 0.02 in/p, 0.005 in.p, 0.001 in/p and pendulum schedules.

ratios with increasing total rolling reduction to a maximum at 80%, 75% and 70% respectively. In the case of materials cold rolled by the pendulum schedule, the  $\{111\}/\{100\}$  ratios decreased on increasing the total rolling reductions from 65% to 75%.

In order to demonstrate the significance of the reductions in intensity of the  $\{111\}$  and  $\{100\}$  components after 0.5 hr isothermal annealing at 700°C upon  $R_o$  value, the  $\{111\}/\{100\}$  ratios were measured and are listed in Table 6.5.2. By comparing Table 6.5.1 and Table 6.5.2, it is evident that the  $\{111\}/\{100\}$  ratios increased significantly after annealing. The improvement in the  $R_o$  values after annealing (see figure 5.3.2.a) is due to the relatively large reduction in P value of the  $\{100\}$  component.

The increase and decrease in P values of the  $\{111\}$  and  $\{100\}$  components respectively on increasing the annealing time from 0.5 hr to 6 hrs resulted in a significant increase in the  $\{111\}/\{100\}$  ratios of all materials. The magnitudes of the increases in the  $\{111\}/\{100\}$  ratios together with the percentage increase in their ratios are listed in Table 6.5.3. Accordingly, increasing the annealing time from 0.5 hr to 6 hrs resulted in 59% increase in the  $\{111\}/\{100\}$  ratio of a material previously cold rolled to 75% using the 35°/p rolling schedule. The corresponding values are 50%, 41% and 19% in the case of the materials cold rolled using the 45°/p, 55°/p and pendulum schedules. The increase in  $R_o$  value with increasing the annealing time is closely related to the increase in the corresponding  $\{111\}/\{100\}$  ratios. The variations in the  $\{111\}/\{100\}$  ratios of materials cold rolled to ranges of total rolling reductions using the 35°/p, 45°/p, 55°/p, 0.02 in/p,

Rolling schedules	P. values		{111}/{100} ratios
	{111} Planes	{100} Planes	
35°/p	2.20	0.50	4.39
45°/p	2.18	0.52	4.15
55°/p	2.17	0.54	3.98
0.02 in/p	2.15	0.55	3.89
0.005 in/p	2.14	0.57	3.74
0.001 in/p	2.14	0.58	3.66
Pendulum	2.01	0.61	3.31

Table 6.5.2. The variations in the {111}/{100} ratios and  $R_o$  values of materials cold rolled using the 35°/p, 45°/p, 55°/p and pendulum rolling schedules to 75% total reduction, annealed for 0.5 hr then aged.

Rolling Schedules	The $\frac{\{111\}}{\{100\}}$ ratios after 6 hrs annealing	The $\frac{\{111\}}{\{100\}}$ ratios after 0.5 hr annealing	% increase
35°/p	7.47	4.39	69
45°/p	6.22	4.15	50
55°/p	5.60	3.98	41
0.02 in/p	5.39	3.89	40
0.005 in/p	4.99	3.74	34
0.001 in/p	4.37	3.66	20
Pendulum	3.95	3.31	19

Table 6.5.3. The percentage increase in the  $\{111\}/\{100\}$  ratios after 6 hrs annealing in comparison with 0.5 hr annealing, the materials previously cold rolled to 75% total reduction using the 35°/p, 45°/p, 55°/p, 0.02 in/p, 0.005 in/p, 0.001 in/p and pendulum rolling schedules.

0.005 in/p, 0.001 in/p and pendulum schedules, annealed for 6 hrs then aged are shown in figure 6.5.4. It is evident that the variations in the  $\{111\}/\{100\}$  ratios correspond with the variations in  $R_0$  values (see figure 5.3.2.6).

An interesting comparison can be made between the present work and an earlier investigation by Mathur and Backofen<sup>(76)</sup>. These latter authors varied the deformation geometry by carrying out cold rolling and deep drawing with dies of varying angle. They characterised their deformation zone geometry by a term  $\Delta$  equivalent to the ratio between the entry thickness  $T_N$  and the roll diameter  $D$  which was used in the present study. They observed an effect of  $\Delta$  on the development of cold worked texture and also on the recrystallisation texture of Al killed steel. It was observed also that the microscopic shearing was associated with high  $\Delta$  geometry and that the occurrence of such shearing led to a reduction in the amount of the  $\{111\}$  component. Accordingly, repeated low  $\Delta$  reductions with possible intermediate annealing to restore work hardening capacity and further reduce the tendency for microscopic shearing was suggested as a process route for sheets with a high porportion of  $\{111\}$  oriented material. They were unable to associate the proportion of the  $\{100\}$  material with macro-shearing and their final statement regarding the effect of deformation geometry on  $\bar{R}$  value of finished sheet was inclusive. However, their results suggest a decreasing ratio of  $\{111\}/\{100\}$  as  $\Delta$  increases between 1 and 4 which is in agreement with the present observations.

The rolling schedules used in the present study can be expressed in terms of  $\Delta$  as shown in Table 6.5.4.

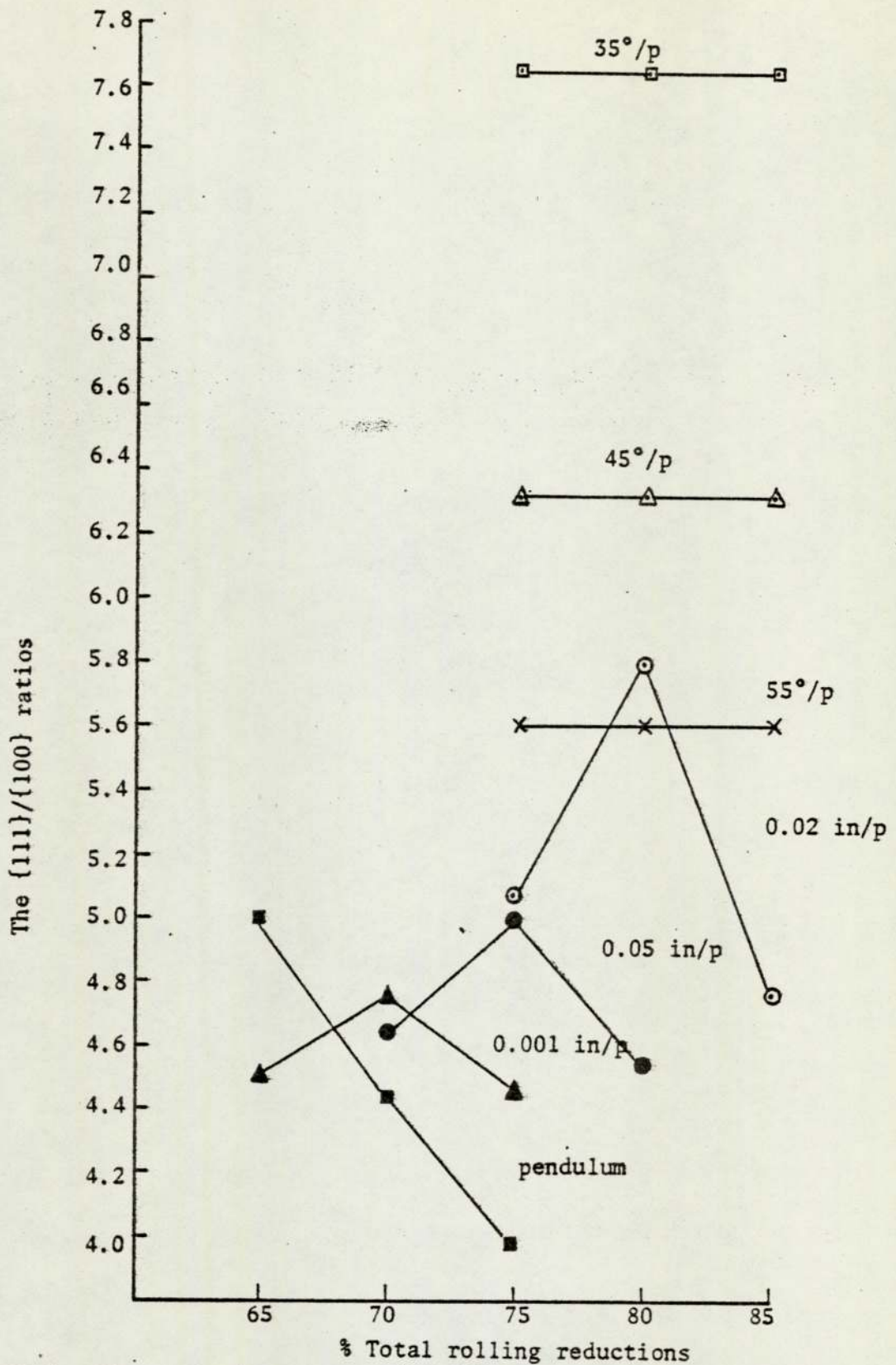


Fig. 6.5.4. The variations in the {111}/{100} ratios of materials cold rolled using the seven rolling schedules, annealed for 6 hrs then aged versus the total rolling reduction.

Table 6.5.4 shows the magnitude of  $\Delta$  at the beginning of rolling and after 90% total rolling reduction versus the constant geometry and constant roll gap schedules.

Rolling Schedules	$\Delta = T_N/D$	
	at the beginning of rolling	after 90% total rolling reduction
35°/p shear angle	0.7	0.7
45°/p shear angle	1.0	1.0
55°/p shear angle	1.4	1.4
0.02 in/p roll gap	0.8	0.14
0.005 in/p roll gap	1.6	0.18
0.001 in/p roll gap	3.5	0.35

Because of the varying geometry in the constant roll gap schedules, it is not possible to make a direct comparison with the results of Mathur and Backofen. On the other hand, deformation carried out with constant geometry demonstrates that a  $\Delta$  value of 0.7 leads to the production of sheets with a significantly higher ratio of  $\{111\}/\{100\}$ , and therefore a higher  $R_0$  value than those obtained, the higher  $\Delta$  values of 1.0 and 1.4.

The effects of the total rolling reduction were noted by Mathur and Backofen and they were also studied in the present work. Mathur and Backofen observed that the peak value of the  $\{111\}/\{100\}$  ratio occurred at high total reduction when  $\Delta$  was equal to 1 and at lower

total reductions as  $\Delta$  increased. It should be noted, however, that Mathur and Backofen measured only the  $\{111\}$  and  $\{100\}$  intensities and therefore their textural information was not as complete as that obtained in the present study. In the present investigation, it was observed that both the  $\{111\}/\{100\}$  texture ratio and  $R_0$  value were independent of the total rolling reduction over the range from 65% to 90% in the case of constant geometry schedules. On the other hand, the total reduction for a peak value of  $\{111\}/\{100\}$  and  $R_0$  decreased as the reduction per pass decreased for the constant roll gap schedules.

The evidence all points to the considerable importance of the deformation zone geometry in controlling the texture development in rolled and annealed low carbon steel. It suggests also that texture gradients arising from the frictional effects are not so important as they affect only a relatively small volume fraction of the sheet thickness.

Finally, of course, the annealing cycle itself can have a major influence on the development of the recrystallisation texture. Two annealing procedures were used in the present work and the beneficial effect of increasing the annealing time in order to promote the normal grain growth was demonstrated.

#### 6.6 THE RELATIONSHIP BETWEEN CRYSTAL REORIENTATION AFTER TENSILE EXTENSION AND R VALUE

As mentioned at the start of section 6.3, the rotations accompanying deformation can be analysed in various ways, and the method of analysis presented here is based on a particular viewpoint<sup>(7)</sup>.

According to (110) pole figures of materials cold rolled to 75% total reduction, annealed for 6 hrs, aged then subjected to 20% tensile extension intensities of the {112}, {113} and {100} planes of the <110> direction increased while intensity of the {111}<112> decreased after tensile extension. This is shown in figure 5.5.2.1 to figure 5.5.2.7. The increase and decrease in intensities of the {100} and {111} planes after tensile extension were dependent upon the rolling schedules. This indicates that crystals reorientation accompanying tensile extension resulted from different rotation mechanisms as shown in figure 6.6.1. The first mechanism decreases the texture intensity about the sheet normal resulting in increasing the intensities of the {112}, {113}, {100} planes of the <110> direction. The second mechanism accompanies the first and occurs by rotation away from the {111}<112> component resulting in a reduction in its intensity. The third mechanism occurs at the same time as the first and second and can be represented by rotation about the <110> rolling direction. This results in decreasing the intensity of the {111} planes parallel to the plane of the sheet and increasing the intensity of the {100} planes.

Measurements of P values of the {111} planes of materials cold rolled to 75% using the 35°/p, 45°/p, 55°/p, 0.02 in/p, 0.005 in/p, 0.001 in/p and pendulum schedules indicated that the {111} planes are not strongly represented in the 0.5 hr annealing texture (see Table 5.5.1.1). It is therefore rational that the third mechanism dominates resulting in a big reduction in P value of the {111} planes and a big increase in P value of the {100} planes after tensile extension. This is shown in Table 6.6.1. Since P values of the {111} planes decreased towards cold rolling using the pendulum mill, type 3 rotation becomes

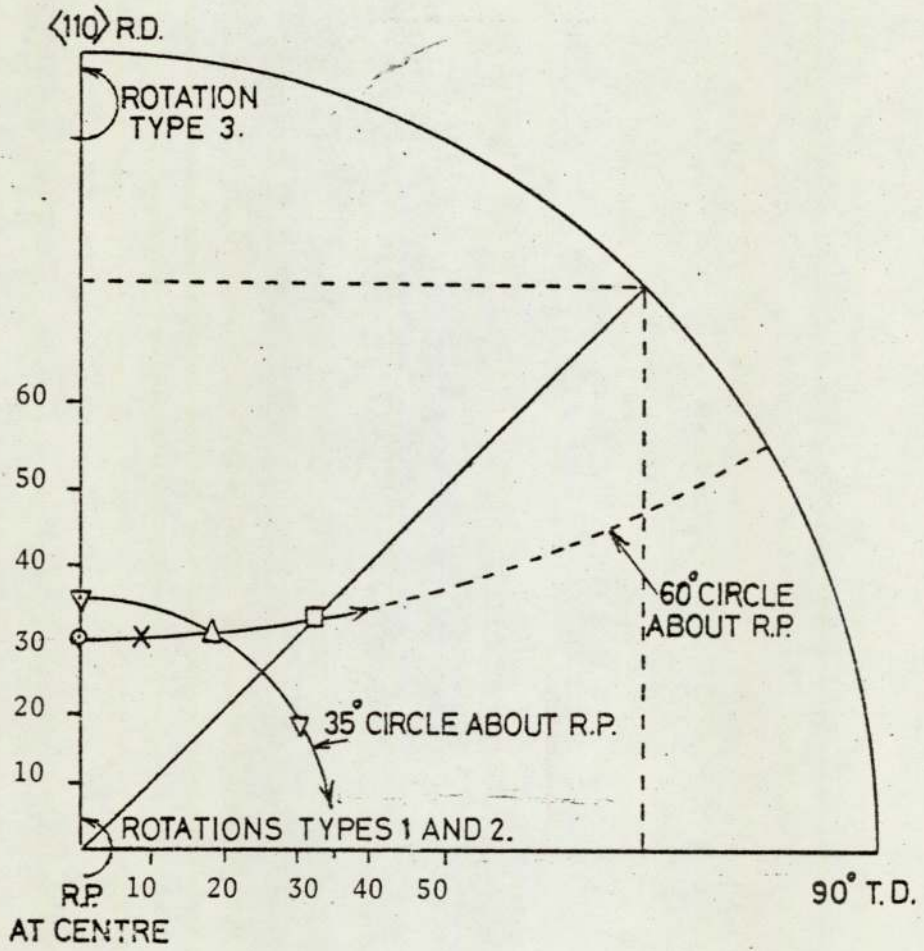


Fig. 6.6.1. Reorientation of (110) pole figure as a result of rotation of partial fibre textures  $\langle 110 \rangle \text{RD}$  and  $\langle 111 \rangle \text{RP}$  accompanying tensile strain.

more effective in the same direction. This resulted in more reduction and more increase in P values of the {111} and {100} planes in the order of the previous rolling schedules as shown in Table 5.5.1.1. Accordingly the corresponding {111}/{100} ratios decreased by increasing the angle  $\theta$  between the material and rolls, decreasing the rolling schedules and cold rolling using the pendulum mill as shown in Table 6.6.2. The difference in the {111}/{100} ratio before and after tensile extension decreased with altering the rolling procedure from 1.29 when cold rolling using 35°/p rolling schedules to 2.06 in the case of the pendulum mill. A big reduction in the {111}/{100} ratio as in the case of materials cold rolled by the pendulum indicates a through-thickness shear which results in more reduction in thickness than in width and hence low R values. On the other hand, a small reduction in the {111}/{100} ratio as in the case of material cold rolled using 35°/p rolling schedules indicates a through width shear. This results in more reduction in width than in thickness and higher R value.

Texture of materials annealed for 6 hrs were characterised by more {111} and less {100} planes parallel to the surface (Table 5.4.2.2.) in comparison with texture of materials annealed for 0.5 hr (Table 5.4.2.1). However, the reduction and increase in P values of the {111} and {100} planes of the first material were less relative to those annealed for 0.5 hr. This resulted in less reduction in the {111}/{100} ratios of materials annealed for 6 hrs after tensile extension as shown in Table 6.6.3 and Table 6.6.4 which indicates an improvement in R value after 6 hrs annealing.

Rolling Schedules	$P_{\{111\}}$	$P_{\{100\}}$	$P_{\{111\}}/P_{\{100\}}$
35°/p	1.92	0.62	3.10
45°/p	1.87	0.67	2.81
55°/p	1.81	0.70	2.57
0.02 in/p	1.73	0.78	2.24
0.005 in/p	1.69	0.83	2.04
0.001 in/p	1.66	0.91	1.82
Pendulum	1.39	1.11	1.25

Table 6.6.1. shows the  $\{111\}/\{100\}$  ratios of materials cold rolled for 75% total reduction, annealed for 0.5hr, aged, then subjected to 20% tensile extension as a function of the seven rolling schedules.

Rolling Schedules	$P_{\{111\}}/P_{\{100\}}$ (before ten.ext.)	$P_{\{111\}}/P_{\{100\}}$ (after ten.ext.)	Difference
35°/p	4.39	3.10	1.29
45°/p	4.15	2.81	1.34
55°/p	3.98	2.57	1.41
0.02 in/p	3.89	2.24	1.65
0.005 in/p	3.74	2.04	1.70
0.001 in/p	3.66	1.82	1.84
Pendulum	3.31	1.25	2.06

Table 6.6.2. shows the difference in the  $\{111\}/\{100\}$  ratios before and after 20% tensile extension of materials cold rolled to 75% total reduction using the seven rolling schedules, annealed for 0.5hrs then aged.

In the 6 hrs annealing texture of materials cold rolled using constant geometry rolling schedules, P values of the {111} and {100} planes increased and decreased respectively with decreasing the shear plane angle " $\theta$ " (Table 5.5.1.4.). Accordingly, the reduction and increase in P values of the {111} and {100} planes, after tensile extension, increased with increasing the angle  $\theta$ . The corresponding {111}/{100} ratios decreased also in the same order as shown in Table 6.6.3. The reduction in the {111}/{100} ratio after tensile extension increased on increasing the angle  $\theta$  as shown in Table 6.6.4. However, the reduction in thickness after tensile extension increases with increasing the angle  $\theta$  and therefore the R value decreases in this order. (figure 5.3.2). On increasing the total rolling reduction from 75% to 85%, the reduction in the {111}/{100} ratio after tensile extension remained constant as in figure 6.6.2 and figure 6.6.3. This indicates a constant R value when increasing the total rolling reduction.

In constant roll gap rolling schedules, the 6 hrs annealing texture contained less {111} and more {100} planes in comparison with constant geometry schedules. This resulted in more reductions in the {111} and more increases in the {100} P values after tensile extension, i.e. less {111}/{100} ratios as shown in Table 6.6.3. The corresponding reductions in the {111}/{100} ratios after tensile extension were relatively higher as shown in Table 6.6.4. This is in agreement with the relatively low R values in the case of materials previously cold rolled using constant roll gap schedules. The {111}/{100} ratios of materials cold rolled to 65%, 70% and 75%; 70%, 75% and 80%; and 75%, 80% and 85% using the 0.001 in/p, 0.005 in/p and 0.02 in/p respectively, annealed for 6 hrs, aged then subjected to 20% tensile extension are shown in figure 6.6.2.

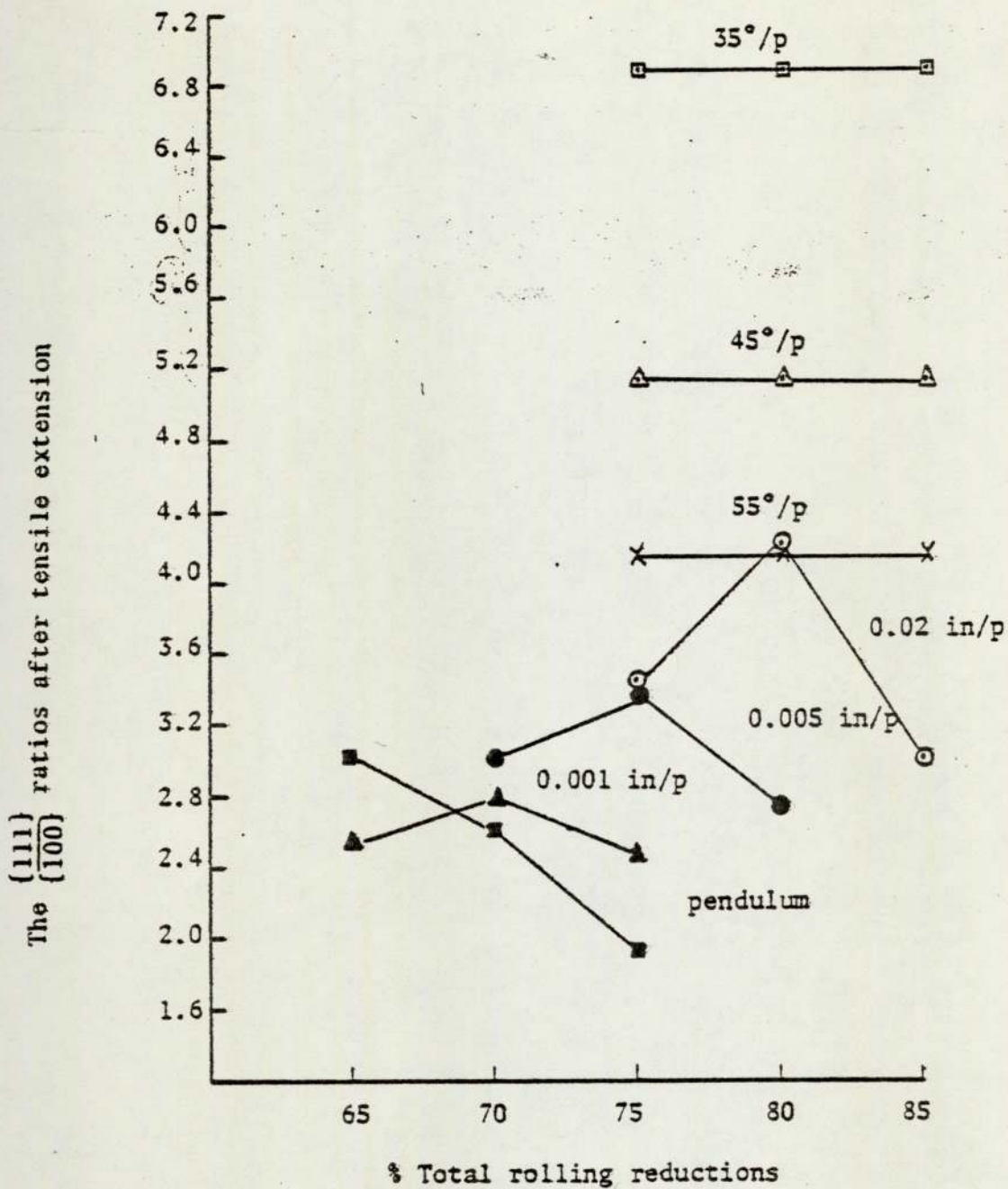


Fig. 6.6.2. The variation in the {111}/{100} ratios of materials cold rolled using the seven rolling schedules, annealed for 6 hrs aged then subjected to 20% tensile extension versus the total rolling reduction.

Rolling Schedules	$P_{\{111\}}$	$P_{\{100\}}$	$P_{\{111\}}/P_{\{100\}}$
35°/p	2.98	0.45	6.62
45°/p	2.77	0.54	5.13
55°/p	2.56	0.59	4.31
0.02 in/p	2.43	0.62	3.89
0.005 in/p	2.30	0.68	3.37
0.001 in/p	2.00	0.74	2.70
Pendulum	1.62	0.78	2.08

Table 6.6. 3. shows the  $\{111\}/\{100\}$  ratios of materials cold rolled for 75% total reduction, annealed for 6 hrs, aged then subjected to 20% tensile extension as a function of the seven rolling schedules.

Rolling Schedules	$P_{\{111\}}/P_{\{100\}}$ (before ten.ext.)	$P_{\{111\}}/P_{\{100\}}$ (after ten.ext.)	Difference
35°/p	7.47	6.62	0.85
45°/p	6.22	5.13	1.09
55°/p	5.60	4.31	1.29
0.02 in/p	5.39	3.89	1.50
0.005 in/p	4.99	3.37	1.62
0.001 in/p	4.37	2.70	1.63
Pendulum	3.95	2.08	1.87

Table 6.6.4. shows the difference in the  $\{111\}/\{100\}$  ratios before and after 20% tensile extension of materials cold rolled to 75% total reduction using the seven rolling schedules, annealed for 6 hrs then aged.

It is evident that the  $\{111\}/\{100\}$  ratios increased on increasing the total rolling reduction to a maximum at 70%, 75% and 80% total reduction in the case of material cold rolled using the 0.001 in/p, 0.005 in/p and 0.02 in/p rolling schedules. On the other hand, the reduction in the  $\{111\}/\{100\}$  ratios after tensile extension were minimum at 70%, 75% and 80%. On either side of the critical total rolling reduction the reduction in the  $\{111\}/\{100\}$  ratios were higher. R values of these materials increased on increasing the total rolling reduction to a maximum corresponding to a minimum reduction in the  $\{111\}/\{100\}$  ratios.

The 6 hrs annealing texture of material cold rolled to 75% using the pendulum mill contained less  $\{111\}$  and more  $\{100\}$  planes in comparison with controlled geometry and draughts rolling schedules, (see Table 5.5.1.4.). Accordingly, more reduction in intensity of the  $\{111\}$  and more increase in intensity of the  $\{100\}$  planes occurred after tensile strain. The corresponding  $\{111\}/\{100\}$  ratios were small in comparison with constant geometry and roll gap schedules, as shown in Table 6.6.3. The reductions in such ratios after tensile strain were higher as shown in Table 6.6.4. This indicates more reduction in thickness than in width and hence low R value. With reference to figure 6.6.2 the  $\{111\}/\{100\}$  ratios of materials cold rolled to 65%, 70% and 75% total reductions decreased with increasing the total rolling reduction. As a result, the thickness strain increased and hence R value decreased with increasing the total rolling reduction.

## 6.7 THE COLD ROLLING GEOMETRY

In the rolling process the arc of contact and hence the roll load increases with increasing roll diameter, rolling draughts and with decreasing the shear angle  $\theta$  (Section 4.2.1). During cold rolling using constant geometry schedules, the shear angle  $\theta$  was kept constant with the progress of rolling by reducing the rolling draughts from one pass to the next. This confines the deformation to certain zones in which crystallographic slip occurs under the same rolling condition. Three equations were therefore, derived (Section 4.2.1) in order to calculate the roll gap required to maintain  $55^\circ$ ,  $45^\circ$  and  $35^\circ$  shear angle during the rolling operations. These equations were based on the assumptions that the material in the roll gap is rectangular and that the entry thickness was equal to the difference between the exit of the previous pass and the next roll gap. A more accurate calculation is possible by considering the entry thickness to be equal to the difference between the average exit thickness and the roll gap.

Cold rolling to 80% total rolling reduction using the  $55^\circ/p$  and  $45^\circ/p$  schedules was reached in 77 and 39 passes respectively. In comparison, 20 passes were required by the  $35^\circ/p$  schedule to affect the same total rolling reduction. Besides being less favourable for high R value cold rolling by the  $55^\circ/p$  and  $45^\circ/p$  is not practicable relative to the  $35^\circ/p$  schedule. The number of passes corresponding to the  $35^\circ/p$  schedule is reduced to a certain extent by increasing the initial material thickness and decreasing the roll diameter. Decreasing the roll diameter is necessary<sup>(86)</sup> to decrease the amount of energy dissipated by the frictional losses, to decrease energy consumption and to improve the mill efficiency during cold rolling. The frictional losses were minimised

by reducing the rolling draughts. Following Orowan<sup>(75)</sup> cold rolling using lubricated, polished rolls and a small percentage reduction per pass is characterised by a low friction coefficient. The small draughts during the later stages of constant geometry schedules would therefore be associated with low frictional losses. Furthermore, cold rolling using the same percentage reduction per pass as in constant geometry schedules ensures that cold rolling was carried out under the frictional condition during each pass. The difficulty involved in using the present schedules on industrial scale is the high number of passes required to affect a heavy total rolling reduction.

With reference to Mathur and Backofen<sup>(76)</sup>, the deformation geometry ' $\Delta$ ' is determined by the material thickness, the roll diameter and the rolling draughts. In the present study, the rolling geometry is related to the previous variables together with a shear plane angle which is related to the deformation modes. The practical limitation involved in using Mathur and Backofen findings, and also the present work in strip rolling is that in order to keep a constant geometry the rolling draughts became very small and difficult to control. Nevertheless, the present study agrees with Mathur and Backofen in that the rolling geometry is an important factor in the control of texture and R value. Furthermore, the rolling draughts must be reduced with the progress of rolling in order to maintain a constant geometry.

In constant roll gap schedules, where the roll gap was kept constant during cold rolling, the percentage reduction per pass increased with the progress of rolling. The percentage reduction per pass, for example, increased from 8% at the beginning of rolling to 80% after 90% total

reduction using the 0.02 in/p schedules. Hence, as rolling proceeds and the material is reduced in thickness, the roll load varies from one pass to the next. The deformation during cold rolling occurs under different rolling geometry. In addition the energy dissipated and hence energy consumption is increased relative to a schedule involving small draughts. During cold rolling using constant roll gap schedules, the shear plane angle  $\theta$  decreases with increasing the roll gap and the total reductions as shown in figure 6.3.2.

Measurements of width of materials cold rolled using constant geometry and constant roll gap schedules revealed that the spread in width increased with decreasing the shear angle and increasing the roll gap.

In the pendulum schedule, the initial material is forced by feed rolls into a gap formed by converging paths of two work rolls. The rolls move backwards and forwards at about 2000 cycles/min. at very high speed reaching 400 ft/min. The entry strip moves at a low speed of 2 ft/min. and leaves the mill with a speed of 20 ft/min. Deformation of the strip takes place during both the up and down strokes of the cycle. The amount of reduction per stroke is small in comparison with that in conventional rolling, but the total reduction in the whole operation (many strokes) is a lot higher.

Since the percentage reduction per each operation of the pendulum schedule may be ten or twenty times greater than that in a conventional mill, the temperature rise during rolling is much higher and its effect on the strip properties is more important. Although the temperature distribution in the reduction zone is not known, it is locally high for

a very short period of time<sup>(66)</sup>. Empirical data related to the variation of the energy of deformation of annealed low carbon steel strip with the strain rate (rolling speed) at ambient temperature, indicated that deformation becomes more and more dependent upon the strain rate as it increases<sup>(88,89)</sup>. Holloman and Zener<sup>(90)</sup> pointed out that the yield strength is doubled by a thousandfold increase in the strain rate. The strip during the pendulum rolling schedule is at much higher temperature than ambient, and the resistance to deformation does not rise with the speed of deformation because of the temperature effect. Increasing the speed of deformation on the other hand, will reduce the effectiveness of cooling and temperature is bound to rise more with increasing the total reduction throughout the rolling operation, provided that the cooling condition remains unchanged.

The pendulum mill process in terms of conventional rolling mills is therefore equivalent to reverse rolling at high speed. Instead of reversing the direction of rolling by turning the strip end for end after each pass before re-entering the rolls as in conventional rolling, the direction of rolling in the pendulum process is reversed by reversing the direction of the pendulum oscillation after each stroke. A schematic representation of the pendulum cycle is shown in figure 6.3.3.

7. SUMMARY AND CONCLUSIONS

1. Texture of the initial material was relatively weak but similar to texture of the hot rolled rimmed steel band. This indicates that the interstage anneal given to the initially cold rolled material has not significantly affected the final texture.

2. Texture developed during cold rolling depended upon the rolling procedures as follows:

(a) Cold rolling using constant geometry schedules were characterised by higher proportions of the  $\{100\}\langle 110 \rangle$  orientation relative to the constant roll gap and pendulum schedules. On increasing the total rolling reduction, using the controlled geometry schedules intensity of the  $\{112\}\langle 110 \rangle$  orientation increased while intensity of the  $\{111\}\langle 112 \rangle$  and  $\{100\}\langle 110 \rangle$  orientations remained constant.

(b) In constant roll gap schedules, the percentage reduction per pass increases with the progress of rolling. As a result, the  $\{111\}\langle 112 \rangle$  component rotates to the  $\{100\}\langle 110 \rangle$  component. This contributes to the reduction in intensity of the  $\{111\}\langle 112 \rangle$  orientation after certain total rolling reduction. During cold rolling using the 0.02 in/p schedule the percentage reduction per pass is higher relative to the 0.005 in/p and 0.001 in/p schedules. Accordingly, one  $\{112\}\langle 110 \rangle$  component rotates to the  $\{111\}\langle 112 \rangle$  which results in a decrease in intensity of the first component and an increase in intensity of the second when cold rolling using the 0.002 in/p schedule. Therefore, the critical total rolling reduction at which there is a turn over in intensities of the  $\{111\}\langle 112 \rangle$  and  $\{100\}\langle 110 \rangle$  orientations, decreases with decreasing the magnitude of the roll gap.

(c) Cold rolling using the pendulum schedule is equivalent to reverse rolling at high speed. It therefore, favours the development of more  $\{100\}\langle 110\rangle$  orientation since it is the only component with four fold symmetry around the rolling direction. Intensity of the  $\{100\}\langle 110\rangle$  orientation was therefore increased with the progress of rolling at the expense of the  $\{111\}\langle 112\rangle$  and  $\{112\}\langle 110\rangle$  components.

3. The low  $R_0$  values of the cold rolled materials is due to the relatively high proportion of the  $\{100\}$  oriented material in the cold rolled texture. The improvement in  $R_0$  values after 0.5 hr annealing is due to the big reduction in intensity of the  $\{100\}$  component. The increase in  $R_0$  value after 6 hrs annealing is attributed to the normal growth of the  $\{111\}$  oriented materials at the expense of the  $\{100\}$  component. The annealing texture developed is dependent upon texture of the matrix in which they grow. However,  $R_0$  value and texture developed after annealing varied with the total rolling reduction in the same manner as the cold rolling texture. Cold rolling using the  $35^\circ/p$  followed by annealing for 6 hrs then ageing resulted in higher  $\{111\}\langle 100\rangle$  texture ratio and hence higher  $R_0$  value in comparison with cold rolling using the  $45^\circ/p$ ,  $55^\circ/p$ , 0.02 in/p, 0.005 in/p, 0.001 in/p and pendulum schedules respectively. Furthermore, the  $\{111\}/\{100\}$  texture ratio and  $R_0$  value remained constant when the total rolling reduction was increased using the  $35^\circ/p$ ,  $45^\circ/p$  and  $55^\circ/p$  schedules. On the other hand, materials cold rolled using the 0.02 in/p, 0.005 in/p and 0.001 in/p schedules exhibited a maximum  $\{111\}/\{100\}$  ratio and a maximum  $R_0$  value at 80%, 75% and 70% total reduction respectively. The  $\{111\}/\{100\}$  ratio and  $R_0$  value of materials cold rolled using the pendulum mill schedule continued to decrease with increasing the total rolling reduction.

4. There is a linear relationship between  $R_0$  value and the  $\{111\}/\{100\}$  texture parameter.

5. Crystal orientation during subsequent tensile elongation is dependent upon the relative proportion of the  $\{111\}$  and  $\{100\}$  components in the texture prior to tensile extension. Texture of material cold rolled by the  $35^\circ/p$  schedule which is associated with high  $\{111\}/\{100\}$  ratio in the cold rolled and annealed condition changed only slightly after tensile extension. On the contrary texture of material cold rolled by the pendulum schedule which is characterised by a low  $\{111\}/\{100\}$  ratio, altered significantly during tensile extension.

6. The rolling geometry is an important factor in the control of texture and R value. It is defined by the rolling draughts, the material thickness, the roll diameter and a shear plane angle. For certain work roll diameter, the rolling draughts must be reduced with the progress of rolling in order to keep a constant geometry of deformation. Cold rolling using the  $35^\circ/p$  shear plane angle is favoured for a high  $\{111\}/\{100\}$  ratio and a high  $R_0$  value.

8. APPENDICES

## APPENDIX I

### CALCULATION OF THE SHEAR ANGLES IN PLASTIC DEFORMATION

The relative magnitudes of principal strains associated with an incremental strain by extension, compression and rolling was used to define the direction of extension and compression during plastic deformation. These directions were related to the direction of applied stress by an angle depending upon each mode of deformation as follows.

#### (a) Uniaxial extension

In a simple plastic extension, each incremental strain along the strain axis is associated with a strain of half the amount and of opposite sense in the transverse directions, on the assumption of no change in volume. Thus, an incremental plastic extension  $e$  in a direction  $OX$ , figure 10.1a, is accompanied by a contraction equivalent to  $\frac{1}{2}e$  in the  $OY$  and  $OZ$  directions. Considering a unit length in the direction  $OX$ , extended to a length  $(1 + e)$ . Let  $OP$  be the direction of zero extension in the  $XY$  plane making an angle  $\theta$  with the axis  $OX$ . Let the length of  $PX = L$ . Thus  $PX$  is contracted from  $L$  to  $L(1 - \frac{1}{2}e)$ . Therefore,

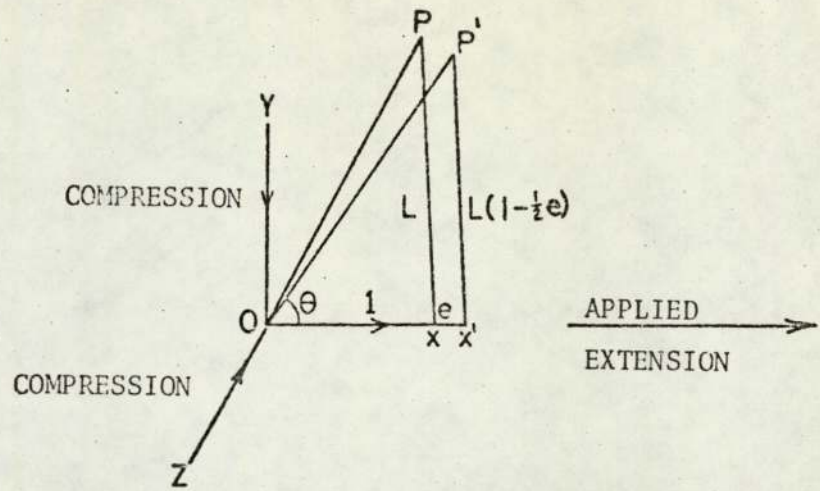
$$\begin{aligned}\overline{OP}^2 &= \overline{OX}^2 + \overline{PX}^2 \\ &= 1 + L^2\end{aligned}\quad \text{(before extension)}$$

and

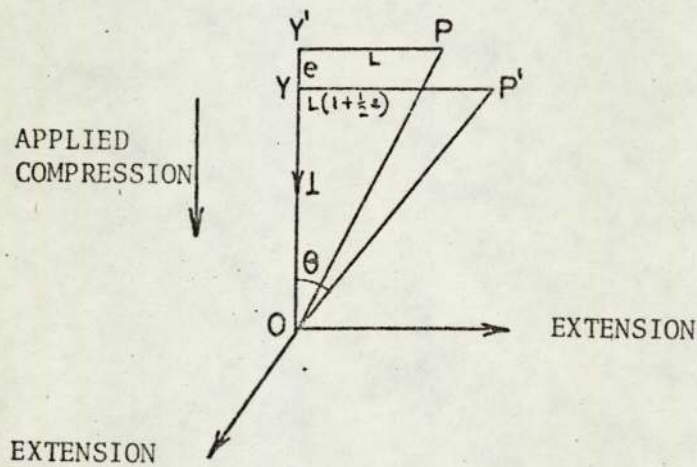
$$= (1+e)^2 + L^2(1 - \frac{1}{2}e)^2 \quad \text{(after extension)}$$

Therefore

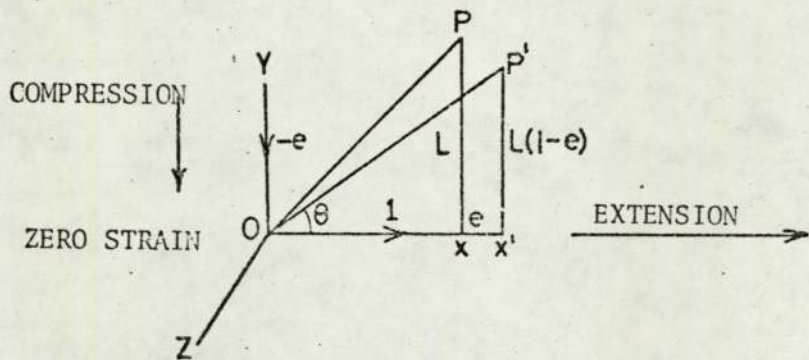
$$1 + L^2 = 1 + 2e + e^2 + L^2 - eL^2 + e^2L^2/4$$



(a) Tension parallel to OX



(b) Compression parallel to OY



(c) Rolling with tension component parallel to OX and compression component parallel to OY.

Fig. 10.1 Illustration of the incremental principal strain in plastic deformation by (a) tension, (b) compression, and (c) rolling.

Hence

$$L^2(1 - e/4)e = (2 + e)e$$

Accordingly

$$L^2 = \frac{2 + e}{1 - e/4}$$

For infinitesimally small  $e$ , hence,

$$L = \pm \sqrt{2}$$

Therefore

$$\text{Cot}\theta = \pm \sqrt{2}$$

That is

$$\theta = \pm 54^\circ 44'$$

(b) Uniaxial compression

This case is analogous to that of uniaxial extension but the incremental plastic extension- $e$  in the OY direction is accompanied by an extension of  $\frac{1}{2}e$  in the OX and OZ directions. Following the previous analysis the angle between the unextended direction OP and the compression axis is equivalent to  $54^\circ 44'$ , as shown in figure 10.I.b.

(c) Pure rolling

In the case of rolling, a small extension in the direction of OX (length) is accompanied by an equal contraction in OY (thickness) without change in OZ (width), on the assumption of constant volume. The angle between OP and OX directions, figure 10.I.c can be calculated as follows:

Considering a unit of unextended length OX, extended to a length  $(1 + e)$ . Let the strain in the direction OP in the XY plane be zero

and let  $PX = L$  then

$$\begin{aligned}\overline{OP}^2 &= \overline{OX}^2 + \overline{PX}^2 \\ &= 1 + L^2\end{aligned}\quad \text{(before extension)}$$

And

$$= (1 + e)^2 + L^2(1 - e)^2 \quad \text{(after extension)}$$

Hence

$$= 1 + 2e + e^2 + L^2 - 2eL^2 + e^2L^2$$

Therefore

$$L^2 = \frac{2 + e}{2 - e}$$

For infinitesimally small  $e$ , hence

$$L^2 = 1$$

That is

$$L = \pm 1$$

And

$$\text{Cot } \theta = \pm 1$$

$$\theta = \pm 45^\circ$$

APPENDIX II. A Computer programme for calculation of controlled  
geometry rolling draughts

```
0001      LIST (LP)
0002      PROGRAM (FXXX)
0003      INPUT 1 = CR0
0004      INPUT 3 = TR0
0005      INPUT 5 = CR1
0006      OUTPUT 2 = LP0
0007      OUTPUT 6 = LP1
0008      COMPRESS INTEGER AND LOGICAL
0009      COMPACT
0010      TRACE 2
0011      END
0012      TRACE 1
0013      READ FROM (CR)
0001      MASTER
0002      L = 0
0003      10 READ (1,60) THETA
0004      L = L + 1
0005      WRITE (2,80) THETA
0006      RAD = (3.14159*THETA)/180
0007      Z=TAN(RAD)
0008      TE=0.2500
0009      D=4.745
0010      20 R=(2.0*TE*TE)/(D*Z*Z+2.0*TE)
0011      PRCNT=(0.2500-TE)/0.2500*100
0012      TE=(TE-R)
0013      WRITE(2,70)R, TE, PRCNT
0014      IF(TE.GT.0.0088) GO TO 20
0015      IF(L.LT.3) GO TO 10
0016      60 FORMAT(F0.0)
0017      70 FORMAT(3(10X,F10.7))
0018      80 FORMAT(///,15X,7H THETA =,F10.5,
0019      1 //,15X,1HR,15X,7HNEXT TE,15X,5HPRCNT,/)
0020      STOP
0021      END
```

APPENDIX III. The calculated rolling draughts and % reduction per pass required to maintain a constant angle of 35° between the material rolled and rolls during cold rolling of the initial material to 90% total reduction.

R	NEXT TE	PRCNT
0.0432355	0.2067645	0.0000000
0.0304860	0.1762785	17.2942001
0.0226513	0.1536273	29.4885853
0.0174929	0.1361344	38.5490876
0.0139164	0.1222180	45.5462313
0.0113351	0.1108829	51.1128005
0.0094110	0.1014719	55.6468300
0.0079385	0.0935335	59.4112245
0.0067865	0.0867470	62.5866172
0.0058683	0.0808787	65.3012165
0.0051246	0.0757540	67.6485385
0.0045139	0.0712401	69.6983976
0.0040062	0.0672338	71.5039683
0.0035796	0.0636542	73.1064638
0.0032177	0.0604365	74.5383202
0.0029081	0.0575284	75.8254152
0.0026411	0.0548873	76.9886455
0.0024092	0.0524781	78.0450707
0.0022066	0.0502715	79.0087549
0.0020285	0.0482430	79.8913970
0.0018712	0.0463718	80.7028073
0.0017314	0.0446404	81.4512744
0.0016068	0.0430336	82.1438489
0.0014951	0.0415384	82.7865660
0.0013947	0.0401437	83.3846225
0.0013041	0.0388396	83.9425172
0.0012221	0.0376175	84.4641641
0.0011475	0.0364700	84.9529847
0.0010796	0.0353905	85.4119830
0.0010175	0.0343730	85.8438675
0.0009606	0.0334124	86.2508018
0.0009084	0.0325040	86.6350477
0.0008603	0.0316437	86.9984007
0.0008159	0.0308278	87.3425196
0.0007749	0.0300529	87.6688924
0.0007369	0.0293159	87.9788571
0.0007016	0.0286143	88.2736210
0.0006688	0.0279455	88.5542753
0.0006383	0.0273072	88.8218095
0.0006098	0.0266974	89.0771226
0.0005831	0.0261143	89.3210333
0.0005582	0.0255561	89.5542887
0.0005348	0.0250212	89.7775722
0.0005129	0.0245083	89.9915098
0.0004923	0.0240160	90.1966763

APPENDIX IV. The calculated rolling draughts and % reduction per pass required to maintain a constant angle of 45° between the material rolled and rolls during cold rolling of the initial material to 90% total reduction

R	NEXT TE	PRCNT
0.0236072	0.2263928	0.0000000
0.0195335	0.2068593	9.4428933
0.0164305	0.1904288	17.2562933
0.0140124	0.1764163	23.8284834
0.0120916	0.1643247	29.4334620
0.0105404	0.1537843	34.2701078
0.0092697	0.1445146	38.4862719
0.0082157	0.1362989	42.1941575
0.0073318	0.1289670	45.4804524
0.0065833	0.1223837	48.4131916
0.0059438	0.1164399	51.0465186
0.0053932	0.1110466	53.4240583
0.0049157	0.1061309	55.5813531
0.0044990	0.1016319	57.5476523
0.0041331	0.0974988	59.3472450
0.0038100	0.0936888	61.0004698
0.0035235	0.0901653	62.5244858
0.0032680	0.0868973	63.9338709
0.0030394	0.0838578	65.2410895
0.0028340	0.0810238	66.4568622
0.0026487	0.0783751	67.5904603
0.0024810	0.0758941	68.6499427
0.0023288	0.0735654	69.6423480
0.0021901	0.0713753	70.5738507
0.0020635	0.0693118	71.4498904
0.0019475	0.0673643	72.2752772
0.0018411	0.0655232	73.0542810
0.0017431	0.0637801	73.7907045
0.0016528	0.0621274	74.4879461
0.0015693	0.0605581	75.1490519
0.0014919	0.0590662	75.7767600
0.0014202	0.0576460	76.3735389
0.0013535	0.0562924	76.9416196
0.0012914	0.0550010	77.4830235
0.0012335	0.0537675	77.9995867
0.0011794	0.0525882	78.4929804
0.0011287	0.0514594	78.9647293
0.0010813	0.0503781	79.4162271
0.0010368	0.0493413	79.8487504
0.0009950	0.0483463	80.2634707
0.0009557	0.0473907	80.6614651
0.0009186	0.0464721	81.0437253
0.0008837	0.0455884	81.4111663
0.0008507	0.0447377	81.7646336
0.0008195	0.0439182	82.1049093
0.0007900	0.0431282	82.4327184
0.0007621	0.0423660	82.7487337
0.0007356	0.0416304	83.0535804
0.0007105	0.0409199	83.3478403
0.0006867	0.0402332	83.6320554
0.0006640	0.0395691	83.9067316

APPENDIX IV. continued

0.0006425	0.0389267	84.1723410
0.0006219	0.0383048	84.4293254
0.0006024	0.0377024	84.6780980
0.0005837	0.0371187	84.9190464
0.0005659	0.0365527	85.1525339
0.0005489	0.0360038	85.3789019
0.0005327	0.0354711	85.5984709
0.0005171	0.0349540	85.8115429
0.0005023	0.0344517	86.0184019
0.0004881	0.0339637	86.2193159
0.0004744	0.0334892	86.4145375
0.0004613	0.0330279	86.6043051
0.0004488	0.0325791	86.7886443
0.0004368	0.0321423	86.9683682
0.0004252	0.0317171	87.1430784
0.0004141	0.0313030	87.3131661
0.0004034	0.0308995	87.4788122
0.0003932	0.0305064	87.6401886
0.0003833	0.0301231	87.7974581
0.0003738	0.0297493	87.9507757
0.0003646	0.0293847	88.1002884
0.0003558	0.0290289	88.2461361
0.0003473	0.0286816	88.3884520
0.0003391	0.0283425	88.5273628
0.0003311	0.0280114	88.6629892
0.0003235	0.0276879	88.7954464
0.0003161	0.0273718	88.9248442
0.0003090	0.0270628	89.0512874
0.0003021	0.0267607	89.1748761
0.0002954	0.0264653	89.2957057
0.0002890	0.0261764	89.4138677
0.0002827	0.0258937	89.5294495
0.0002767	0.0256170	89.6425346
0.0002708	0.0253462	89.7532032
0.0002652	0.0250810	89.8615317
0.0002597	0.0248214	89.9675938
0.0002543	0.0245670	90.0714597

APPENDIX V. The calculated rolling draughts and % reduction per pass required to maintain a constant angle of 54°44' between the material rolled and rolls during cold rolling of the initial material to 90%

total reduction.

<u>R</u>	<u>NEXT TF</u>	<u>PRCNT</u>
0.0123905	0.2376095	0.0000000
0.0112203	0.2263891	4.9562128
0.0102084	0.2161807	9.4443439
0.0093275	0.2068532	13.5277139
0.0085559	0.1982973	17.2587153
0.0078762	0.1904211	20.6810723
0.0072745	0.1831466	23.8315623
0.0067391	0.1764075	26.7413427
0.0062608	0.1701468	29.4369852
0.0058316	0.1643152	31.9412893
0.0054451	0.1588701	34.2739287
0.0050958	0.1537743	36.4519693
0.0047791	0.1489952	38.4902877
0.0044910	0.1445043	40.4019107
0.0042282	0.1402761	42.1982948
0.0039878	0.1362884	43.8895555
0.0037673	0.1325211	45.4846583
0.0035646	0.1289564	46.9915770
0.0033779	0.1255785	48.4174279
0.0032054	0.1223731	49.7685812
0.0030459	0.1193272	51.0507572
0.0028979	0.1164293	52.2691064
0.0027605	0.1136688	53.4282789
0.0026326	0.1110361	54.5324839
0.0025135	0.1085227	55.5855408
0.0024022	0.1061205	56.5909229
0.0022981	0.1038224	57.5517961
0.0022007	0.1016217	58.4710521
0.0021094	0.0995123	59.3513373
0.0020236	0.0974887	60.1950785
0.0019429	0.0955458	61.0045050
0.0018670	0.0936788	61.7816684
0.0017954	0.0918834	62.5284601
0.0017279	0.0901555	63.2466263
0.0016641	0.0884914	63.9377820
0.0016038	0.0868877	64.6034228
0.0015467	0.0853410	65.2449359
0.0014926	0.0838484	65.8636100
0.0014413	0.0824071	66.4606433
0.0013926	0.0810146	67.0371517
0.0013463	0.0796683	67.5941758
0.0013023	0.0783660	68.1326870
0.0012604	0.0771056	68.6535931
0.0012205	0.0758852	69.1577435
0.0011824	0.0747027	69.6459339
0.0011462	0.0735566	70.1189104
0.0011115	0.0724450	70.5773732
0.0010784	0.0713666	71.0219802
0.0010468	0.0703198	71.4533504
0.0010165	0.0693033	71.8720660
0.0009876	0.0683158	72.2786760

APPENDIX V. continued

0.0009598	0.0673560	72.6736978
0.0009332	0.0664227	73.0576198
0.0009077	0.0655150	73.4309034
0.0008832	0.0646318	73.7939848
0.0008597	0.0637721	74.1472766
0.0008372	0.0629349	74.4911694
0.0008155	0.0621195	74.8260333
0.0007946	0.0613248	75.1522195
0.0007745	0.0605503	75.4700607
0.0007552	0.0597951	75.7798733
0.0007366	0.0590585	76.0819577
0.0007187	0.0583398	76.3765994
0.0007014	0.0576384	76.6640702
0.0006847	0.0569537	76.9446288
0.0006687	0.0562850	77.2185213
0.0006531	0.0556319	77.4859827
0.0006382	0.0549938	77.7472368
0.0006237	0.0543701	78.0024973
0.0006097	0.0537604	78.2519680
0.0005962	0.0531642	78.4958437
0.0005831	0.0525811	78.7343106
0.0005704	0.0520107	78.9675466
0.0005582	0.0514525	79.1957220
0.0005463	0.0509062	79.4189997
0.0005349	0.0503713	79.6375357
0.0005237	0.0498476	79.8514796
0.0005130	0.0493346	80.0609744
0.0005025	0.0488321	80.2661576
0.0004924	0.0483397	80.4671609
0.0004825	0.0478572	80.6641108
0.0004730	0.0473842	80.8571286
0.0004637	0.0469204	81.0463310
0.0004548	0.0464657	81.2318299
0.0004460	0.0460196	81.4137331
0.0004375	0.0455821	81.5921441
0.0004293	0.0451528	81.7671625
0.0004213	0.0447315	81.9388842
0.0004135	0.0443180	82.1074014
0.0004059	0.0439121	82.2728030
0.0003986	0.0435135	82.4351746
0.0003914	0.0431221	82.5945987
0.0003844	0.0427377	82.7511549
0.0003776	0.0423601	82.9049199
0.0003710	0.0419891	83.0559676
0.0003646	0.0416245	83.2043694
0.0003583	0.0412662	83.3501943
0.0003522	0.0409141	83.4935088
0.0003462	0.0405672	83.6343772
0.0003404	0.0402274	83.7728616
0.0003347	0.0398927	83.9090219
0.0003292	0.0395635	84.0429162
0.0003238	0.0392397	84.1746006
0.0003186	0.0389211	84.3041294

APPENDIX V. continued

0.0003134	0.0386077	84.4315551
0.0003084	0.0382993	84.5569284
0.0003035	0.0379957	84.6802986
0.0002988	0.0376970	84.8017133
0.0002941	0.0374029	84.9212185
0.0002895	0.0371133	85.0388591
0.0002851	0.0368282	85.1546783
0.0002808	0.0365475	85.2687181
0.0002765	0.0362709	85.3810192
0.0002724	0.0359986	85.4916210
0.0002683	0.0357303	85.6005618
0.0002643	0.0354660	85.7078788
0.0002604	0.0352055	85.8136079
0.0002566	0.0349489	85.9177843
0.0002529	0.0346960	86.0204418
0.0002493	0.0344467	86.1216134
0.0002457	0.0342009	86.2213311
0.0002423	0.0339587	86.3196262
0.0002388	0.0337198	86.4165286
0.0002355	0.0334843	86.5120680
0.0002322	0.0332521	86.6062728
0.0002290	0.0330230	86.6991708
0.0002259	0.0327971	86.7907890
0.0002228	0.0325743	86.8811537
0.0002198	0.0323544	86.9702904
0.0002169	0.0321376	87.0582240
0.0002140	0.0319236	87.1449787
0.0002112	0.0317124	87.2305780
0.0002084	0.0315040	87.3150449
0.0002057	0.0312983	87.3984016
0.0002030	0.0310955	87.4806700
0.0002004	0.0308949	87.5618712
0.0001978	0.0306971	87.6420258
0.0001953	0.0305018	87.7211540
0.0001928	0.0303090	87.7992752
0.0001904	0.0301186	87.8764088
0.0001880	0.0299305	87.9525731
0.0001857	0.0297448	88.0277865
0.0001834	0.0295614	88.1020665
0.0001812	0.0293803	88.1754305
0.0001790	0.0292013	88.2478954
0.0001768	0.0290245	88.3194774
0.0001747	0.0288499	88.3901927
0.0001726	0.0286773	88.4600570
0.0001705	0.0285068	88.5290854
0.0001685	0.0283383	88.5972929
0.0001665	0.0281717	88.6646941
0.0001646	0.0280072	88.7313031
0.0001627	0.0278445	88.7971339
0.0001608	0.0276837	88.8622000
0.0001589	0.0275248	88.9265146
0.0001571	0.0273676	88.9900908
0.0001553	0.0272123	89.0529411
0.0001536	0.0270587	89.1150779

APPENDIX V. continued

0.0001519	0.0269069	89.1765133
0.0001502	0.0267567	89.2372591
0.0001485	0.0266082	89.2973269
0.0001469	0.0264613	89.3567279
0.0001453	0.0263161	89.4154731
0.0001437	0.0261724	89.4735735
0.0001421	0.0260303	89.5310394
0.0001406	0.0258897	89.5878814
0.0001391	0.0257507	89.6441094
0.0001376	0.0256131	89.6997334
0.0001361	0.0254770	89.7547630
0.0001347	0.0253423	89.8092078
0.0001333	0.0252091	89.8630770
0.0001319	0.0250772	89.9163796
0.0001305	0.0249467	89.9691247
0.0001291	0.0248176	90.0213208

APPENDIX VI. The computer programme used to calculate the P values of eight sets of  
crystallographic planes

```
LIST (LP)  
PROGRAM (FXYX)  
INPUT 1 = CR0  
INPUT 3 = IP0  
INPUT 5 = CR1  
OUTPUT 2 = IP0  
OUTPUT 4 = IP1  
COMPACT  
END
```

```
MASTER INVPGLEFIGST  
INTEGER TYPE,X,Y  
COMMON CURVE(2,20), M,N
```

```
DEPARTMENT OF METALLURGY, UNIVERSITY OF ASTON IN BIRMINGHAM  
THIS PROGRAM CALCULATES LINE INTENSITY RATIOS FROM A SERIES OF  
STRINGS OF PULSE COUNTS. IT ALLOWS FOR BACKGROUND AND ALSO  
TESTS FOR ERRORS IN THE DATA.  
DATA IS INPUT AS A SERIES OF INTEGER NUMBERS. EACH CURVE IS  
TERMINATED WITH A NEGATIVE INTEGER. EACH SERIES OF CURVES(SAMPLE  
AND RANDOM) IS TERMINATED WITH AN ADDITIONAL NEGATIVE INTEGER.  
FINALLY, THE WHOLE RUN IS TERMINATED WITH YET ANOTHER NEGATIVE  
INTEGER.
```

```
51 TYPE=1  
M=0  
SIGMA=0  
52 M=M+1  
70 READ(3,200)X  
200 FORMAT(13X,16)
```

APPENDIX VI. continued

```

IF(X)53,70,54
54 CURVE(TYPF,M)=TOTAL(X,TYPE )
WRITE(2,500)M
500 FORMAT(12)
GO TO 52
53 IF(TYPF-1)55,55,56
55 MA=M
TYPF=2
M=0
GO TO 52
56 IF(M.EQ.MA)GO TO 57
WRITE(2,151)
151 FORMAT(/56H THERE ARE DIFFERENT NUMBERS OF SAMPLE AND RANDOM CURVE
15)
GO TO 60
57 MA=MA-1
SIGMA=0
DO 58 M=1,MA
CURVE(1,M)=CURVE(1,M)/CURVE(2,M)
IF(N.F0.5000)GO TO 60
58 SIGMA=SIGMA+CURVE(1,M)
SIGMA=SIGMA/MA
WRITE(2,152)
152 FORMAT(/////40H LINE NUMBER RANDOM VALUE P,VALUE/)
DO 59 M=1,MA
CURVE(2,M)=CURVE(1,M)/SIGMA
59 WRITE(2,153)M,CURVE(1,M),CURVE(2,M)
153 FORMAT(/16,F16.4,F17.4)
READ(3,200)Y
IF(X)60,61,61
61 TYPF=1
M=1
SIGMA=0
GO TO 54
60 STOP
END

```

APPENDIX VI. continued

```

FUNCTION TOTAL(Y,TYPE )
DIMENSION X(1000),CURVE(2,20)
COMMON CURVE ,M,N
REAL MEAN
INTEGER Y,TYPE,ADD,TOP,ROT,X

C
C FUNCTION TO TEST AND TOTAL POINTS FROM TAPE PRODUCED BY X-RAY SCAN
C

XSQ=0
ADD=0
SIGSTART=0
SIGEND=0
N=2

SUMX=Y
X(1)=Y
1 LAST=X(N-1)
30 READ(3,201)X(N)
201 FORMAT(13X,16)
IF(X(N))2,30,3
3 IF(ABS(X(N)-LAST)-6000)4,5,5
5 IF(TYPE-1)6,6,7
6 WRITE(2,101)M, LAST, X(N)
101 FORMAT(/20H SAMPLE CURVE NUMBER,12,20H HAS ADJACENT VALUES,15,4H A
1ND,15)
GO TO 4
7 WRITE(2,102)M, LAST, X(N)
102 FORMAT(/20H RANDOM CURVE NUMBER,12,20H HAS ADJACENT VALUES,15,4H A
1ND,15)
4 SUMX=SUMX+X(N)
N=N+1
GO TO 1
2 DO 9 J=1,20
SIGSTART=SIGSTART+X(J)

```

APPENDIX VI. continued

```

9     XSQ=YSQ+FLOAT(Y(J))*FLOAT(X(J))
      N=N-1
      DO 10 J=21,24
10     ADD=ADD+Y(J)
      IF((0.25*ADD-0.05*SIGSTART)-0.318*SQRT(XSQ-0.05*SIGSTART*
1SIGSTART))11,11,12
12 IF(TYPE-1)13,13,14
13 WRITE(2,103)M
103 FORMAT(/20H SAMPLE CURVE NUMBER,12,60H APPEARS TO HAVE TOO LITTLE
1BACKGROUND SCAN AT THE BEGINNING)
      GO TO 11
14 WRITE(2,104)M
104 FORMAT(/20H RANDOM CURVE NUMBER,12,60H APPEARS TO HAVE TOO LITTLE
1BACKGROUND SCAN AT THE BEGINNING)
11 XSQ=0
      ADD=0
      DO 16 J=N-19,N
          SIGEND=SIGEND+X(J)
16     XSQ=XSQ+FLOAT(X(J))*FLOAT(X(J))
      DO 17 J=N-23,N-20
          ADD=ADD+Y(J)
          IF((0.25*ADD-0.05*SIGEND)-0.318*SQRT(XSQ-0.05*SIGEND*SIGEND))
118,18,17
17 IF(TYPE-1)19,19,20
19 WRITE(2,105)M
105 FORMAT(/20H SAMPLE CURVE NUMBER,12,54H APPEARS TO HAVE TOO LITTLE
1BACKGROUND SCAN AT THE END)
      GO TO 18
20 WRITE(2,106)M
106 FORMAT(/20H RANDOM CURVE NUMBER,12,54H APPEARS TO HAVE TOO LITTLE
1BACKGROUND SCAN AT THE END)
18 CONTINUE
22 TOTAL=SUMX-(SIGSTART+SIGEND)*0.125*N
      RETURN
      END

```

## REFERENCES

1. R.L.Whitely, D.E.Wise and D.J. Blickwede, *Steet Metal Industries* 1961, 38, 349.
2. B.N.Hellewell, T.Ll.Richards, *Metals Technology*, 1974, 1, 265.
3. F.A.Crane and J.M.Alexander, *J.Ins.Metals*, 1963/4, 92, 382.
4. I.L.Dillamore and W.T.Roberts, *J.Ins.Metals*, 1963/4, 92, 193.
5. G.E.Tucker, *Acta Met.*, 1964, 12, 1094.
6. R.A.Vandermeer and J.C.Ogle, *Trans.Met.Soc.AIME*, 1969, 245, 1511.
7. D.E.Yeomans and T.Ll.Richards, *Acta Cryst.* 1954, 7, 663.
8. R.V.Mises, *Z.Angew.Math.Mech.* 1928, 8, 161.
9. G.I.Taylor, *J.Ins.Metals*, 1938, 62, 307.
10. J.F.W.Bishop and R.Hill, *Phil.Mag.* 1951, 42, 414 and 1953, 44, 51.
11. W.Boas and E.Schmid, *Z.Tech.Physics*, 1931, 12, 71.
12. M.R.Pickus and E.H.Mathewson, *J.Ins.Metals*, 1939, 54, 237.
13. E.Schmid and W.Boas, *Plasticity of Crystals*, F.A.Hughes and Co.Ltd. London. 1950, 60 and 105.
14. G.I.Taylor and J.W.Christian, *Phil.Mag.* 1967, 15, 893.
15. E.A.Calnan and C.J.B.Clews, *Phil.Mag.* 1951, 42, 616.
16. I.L.Dillamore and W.T.Roberts, *Acta Met.*, 1964, 12, 281.
17. L.Clareborough and M.E.Hargreaves, *Prog.Metal Phys.* 1958, 8, 1.
18. G.E.G.Tucker, *Acta Met.*, 1964, 12, 1094.
19. I.L.Dillamore, C.J.E.Smith and T.W.Watson, *Met.Sci.J.* 1967, 1, 49.
20. I.L.Dillamore and W.B. Hutchinson, *Proc.I.C.S.T.I.S.*, *Suppl. Trans. I.S.I.J.*, 1971, 11, 877.
21. M.Hillert, *Acta Met.* 1965, 13, 227.

22. R.S.Burns and R.H.Heyer, Sheet Metal Ind., 1958, 35, 261.
23. W.F.Hosford and W.A.Backofen, 9th Sagamore ~~ordance~~ of Material Research Conf., 1962, 28 - 31 Aug.
24. M.Fukuda, Trans.Jap. I.S.I., 1968, 8, 68.
25. S.Nagashima, H.Takechi and H.Kato, Texture in Research and Practice, Proc. ~~Claustal~~ Zellerfeld Symposium, 1968, Oct 2-5.
26. P.N.Richards and K.Ormay, Trans.Met.Soc.A.I.M.E., 1969, 245, 715.
27. T.M.Thomson and J.M.Baker, <sup>J. Aust. I. M.,</sup> ~~J. Ins. I. M.~~, 1969, 14, 84.
28. R.Hill, Mathematical Theory of Plasticity, Oxford Univ. press, London, 1950, 315.
29. R.L.Whiteley, Trans.A.S.M., 1960, 52, 154.
30. L.W.Hu, J.App.Mechanics, 1956, 23, 444.
31. J.Willis, Deep Drawing, Butterworth Publication Ltd., London, 1954, 28.
32. D.H.Lloyd, Sheet Metal Ind., 1962, 39, 82.
33. J.C.Wright, Sheet Metal Ind., 1962, 39, 887.
34. I.Lilet, Sheet Metal Ind., 1966, 43, 949.
35. M.Atkinson and I.M.Maclean, I.D.D.R.G. Colloquium, London, 1964.
36. H.G.Rosenstock, H.F.Kläner and E.Schmidtman, Archiv fur das Eisenhüttenwesen, 1962, 33, 281.
37. J.E.Angele and W.F.McGarity, Trans.Amer.Soc.Mech.Eng. 1937, 5, 433.
38. H.Hoff and G.Masing, Stahl und Eisenhüttenwesen, 1956, 76, 1442.
39. S.D.Bhole, W.T.Roberts and D.V.Wilson, I.S.I./I.O.M.Meeting, 1973, Nov. 14 - 15. Met. Sci., 1974, 8, 277.
40. P.N.Richards and M.K.Ormay, J.Iron and Steel Ins., 1969, 239, 1857.
41. S.Nagashima, H.Takechi and H.Kato, Trans.Met.Soc.A.I.M.E., 1968, 242, 56.

42. A.Jones and B.Walker, ~~S.I./I.O.M. Meeting~~, <sup>Metals Technology</sup>, 1973, Nov.14 - 15.
43. P.N.Richards, J.Iron & Steel Ins., 1969, 207, 1333.
44. C.S.Barrett, Structure of Metals, McGraw Hill, N.Y. (2nd Edition).
45. G.Pomey and C.Crussard, Rev.Met., 1955, 52, 401.
46. F.Haessner and H.Weik, Arch. Eisenhüttenwesen, 1956, 27, 153.
47. J.Pugh and W.R.Wibbard, Trans.Am.Soc.Metals, 1956, 48, 526.
48. E.A.Calnan and C.J.B.Clews, Phil.Mag. 1950, 41, 1085.
49. L.R.Underwood, The Rolling of Metals, Chapman and Hall, London, 1958.
50. J.F.Held Trans.Met.Soc.A.I.M.E., 1967, 239, 573.
51. C.A.Stickels, Trans.Met.Soc.A.I.M.E., 1967, 239, 1857.
52. R.O.Williams, Trans.Met.Soc.A.I.M.E., 1962, 224, 129.
53. W.A.Backofen and B.B.Hundy, Trans.Met.Soc.A.I.M.E., 1953, 197, 61.
54. H.Möller and H.Stablein, Arch. Eisenhüttenwesen, 1958, 29, 377
55. J.Bennewitz, Arch. Eisenhüttenwesen, 1962, 33, 393.
56. S.Nagashima, H.Takechi and H.Kato, Texture in Research and  
Practice, Proc.Clausthal Zellerfeld Sym. 1968, Oct. 2 - 5.
57. I.L.Dillamore and W.T.Roberts, Metallurgical Review, 1965, 10, 39.
58. R.Whitely and D.Wise, 4th Mech.Working Conf. A.I.M.E., Chicago,  
1962, Jan.
59. M.Atkinson, P.G.Brooks, A.O'Connor and T.G.Philips, Sheet Metal  
Ind., 1963, 40, 57.
60. R.F.Dewsnap, I.S.I. Special Report, 1963, 79, 112.
61. B.A.Kuznetsov, Metalloved. Term obra.Met. 1958, 2, 28.
62. J.D.Keller, A.I.S.E.Convention, Buffalo, N.Y., 1958, Apr.
63. A.F.Mohri, A.I.S.I. Convention, N.Y., 1956, May 23.
64. S.Garber, J.Iron and Steel Ins., 1962, 200, 460.
65. C.A.Stickels, Trans.Met.Soc. A.I.M.E., 1965, 233, 1550.

66. K.Saxl, Proc.Ins.Mech.Eng., 1964/5, 179.
67. W.T.Lankford, S.C.Snyder and J.A.Bauscher, Trans.Am.Soc.Metals,  
1950, 42, 1197.
68. L.Schultz.App.Phys., 1949, 20, 1030.
69. G.B.Harris, Phil.Mag. 43, 113.
70. G.Kurdjumov and S.Sachs, Z.Phys., 1930, 64, 325.
71. M.Gensamer and P.A.Vukmanic, Trans.Met.Soc. A.I.M.E.,1937, 125,  
507.
72. T.R.Thomson and J.M.Baker, J.Aus.I.M., 1969, 14, 84.
73. T.J.Lewis, The University of Aston in Birmingham, Ph.D.Thesis,1971.
74. R.J.Bentz and W.L.Roberts, Iron and Steel Eng., 1964, March, 101.
75. E.D.Orowan, Proc.Inst.Mech.Eng., 1943, 50, 140.
76. P.S.Mathur and W.A.Backofen, Met.Trans.1973, 4, 643.
77. J.T.Norton, J.Appl.Phys., 1948, 19, 1176.
78. M.Field and M.E.Merchant, J.Appl.Phys. 1949, 20, 741.
79. J.R.Holland, N.Engler and W.Powers, Editor W.Mueller, Advances in  
X ray Analysis, 1960, 4, 74.
80. J.J.Klappholz, S.Waxmann and C.Feno, Advances in X ray Analysis,  
1972, 15, 365.
81. H.J.Bunge and W.T.Roberts, J.App.Crystallography, 1969, 2, 116.
82. L.K.Jetter, C.McHargue and R.O.Williams, J.Appl.Phys. 1956, 27,368.
83. R.O. Williams, A.I.M.E. Trans, 1968, 242, 105.
84. C.Feng, Advances in X ray Analysis, 1972, 15, 489.
85. B.N.Hellewell, Ph.D.Thesis, The University of Aston in Birmingham,  
1971.
86. R.J.Benz and W.L.Roberts, Iron & Steel Eng., 1964, March, 101.

87. J.F.Held, Mechanical Working and Steel Processing IV, A.I.M.E. Conference, 1966, p.3.
88. F.A.Witt and W.L.Roberts, 5th Annual Conf. of the Mech.Working Committee, Iron and Steel Div. A.I.M.E., 1963, Jun.
89. W.C.F.Hessenburg and R.B.Smith, J.Iron and Steel Inst., 1951, June.
90. J.H.Hollomon and C.Zener, J.App.Physics, 1944, 15, 22.
91. M.H.Mueller, W.P.Chernock and P.A.Beck, Trans. of the Metallurgical Society of A.I.M.E., 1958, Feb., 39.
92. I.L.Dillamore and H.Katoh, Metal Science, 1974, 8, 73.

## ACKNOWLEDGEMENTS

The author would like to express his gratitude to the late Dr. T.Ll. Richards and Mr. D. Green for the encouragement and advice received during the present investigation.

Dr. W.T. Roberts has been especially helpful by his supervision during the preparation of the final manuscript and his help is greatly appreciated.

The guidance and discussion of Professor I.L. Dillamore and Professor J.T. Barnby are also acknowledged.

My thanks also to Mrs. G.M. Gado and Mr. H.J. Hyde for their help during the preparation of this thesis.

A STUDY OF THE INFLUENCE OF ROLLING GEOMETRY UPON  
TEXTURE AND DRAWABILITY OF RIMMED STEEL STRIP

by

ISMAIL HAMED GADO B.Sc., M.Sc.

OCTOBER 1976

Submitted for the degree of Doctor of  
Philosophy of the University of Aston  
in Birmingham.

621.77123 GAD  
212805 11 JAN 1978

## SYNOPSIS

The influence of seven different rolling schedules upon R values and textures of cold rolled and of subsequently annealed rimmed steel strip has been studied. The effect of increasing the annealing time upon R value and texture was also examined. R value measured in a tensile test was related to the corresponding texture determined by inverse and (110) pole figures.

The seven rolling schedules consisted of three constant roll gap schedules, in which roll gaps of 0.001 in/pass, 0.005 in/pass and 0.02 in/pass were kept constant during the cold rolling process. The other three rolling schedules involved constant geometry and were designed to maintain constant shear plane angles of  $55^\circ$ ,  $45^\circ$  and  $35^\circ$  to the strip surface, from one pass to the next. The seventh rolling schedule represented a pendulum mill schedule.

Measurements of R values revealed that R values of the cold rolled materials were very low but improved after annealing. The longer the annealing time the more the R values became dependent upon the rolling schedules and total rolling reductions. However, after 6 hrs annealing, R values of strips previously cold rolled using constant roll gap schedules increased with the magnitude of the roll gap and with the total rolling reduction to a maximum and thereafter decreased. On the other hand, R values of corresponding strips cold rolled using controlled geometry schedules increased with decreasing the shear plane angle and remained constant when the total rolling reduction was increased. R values of equivalent strips cold rolled by the pendulum rolling schedule decreased with increasing the total rolling reductions.

The cold rolling textures observed were typical of b.c.c. iron with  $\langle 110 \rangle$  direction parallel to the rolling direction and  $\{111\}$  planes parallel to the rolling plane. For a given total rolling reduction, intensities of the  $\{100\}$  and  $\{111\}$  planes were dependent upon the rolling schedules and total rolling reduction. Rolling with constant roll gap was associated with a decrease in the  $\{100\}$  intensity and an increase in the  $\{111\}$  intensity with increasing the total rolling reduction up to certain reduction then increased and decreased respectively. The total rolling reduction corresponding to the minimum  $\{100\}$  and maximum  $\{111\}$  intensities increased with increasing the magnitude of roll gap. As a result of rolling with constant geometry schedules, intensity of the  $\{100\}$  and  $\{111\}$  planes remained constant with increasing the rolling reduction but their intensities increased and decreased respectively with increasing the shear plane angle. When rolling on the pendulum mill, intensities of the  $\{100\}$  and  $\{111\}$  planes increased and decreased respectively with increasing the total rolling reduction.

Annealing for 0.5 hr was associated with a significant decrease in the  $\{100\}$  and  $\{111\}$  intensities. Increasing the annealing time resulted in a further decrease in the  $\{100\}$  intensity and an increase in the  $\{111\}$  intensity. The relative intensities of the  $\{100\}$  and  $\{111\}$  planes varied with the rolling schedules and with increasing the total rolling reduction in the same manner as for the cold rolled material already described.

## CONTENTS

	Page
1. INTRODUCTION	1
2. LITERATURE REVIEW	
2.1 The geometry of cold rolling	4
2.2 Theories of cold rolling texture formation in b.c.c. polycrystalline metals	7
2.3 Theories of annealing texture formation in b.c.c. polycrystalline metals	12
2.4 The relationship between texture and R value	15
2.5 The relationship between R value and the L.D.R.	22
2.6 Effects of the processing factors upon texture and R value	
2.6.1 The effect of hot rolling	26
2.6.2 The effect of cold rolling	29
2.6.3 The effect of subcritical isothermal annealing	33
3. SCOPE OF THE PRESENT STUDY	38
4. EXPERIMENTAL PROCEDURE	
4.1 Introduction	40
4.2 Cold rolling	40
4.2.1 The constant geometry schedules	41
4.2.2 The constant roll gap schedules	43
4.2.3 The pendulum schedule	45
4.3 Annealing of the cold rolled strips	47
4.4 Measurement of R value	48
4.5 Examination of preferred orientation	51
4.5.1 Direct pole figures	52
4.5.2 Inverse pole figures	54

	Page
5. EXPERIMENTAL RESULTS	
5.1 Introduction	59
5.2 Examination of the initial material	59
5.3 Measurement of R value	
5.3.1 The cold rolled materials	63
5.3.2 The annealed materials	64
5.4 Examination of texture	
5.4.1 The cold rolled materials	67
5.4.2 The annealed materials	75
5.5 Crystal Reorientation after tensile extension	82
6. DISCUSSION	
6.1 Introduction	94
6.2 Texture of the initial material	94
6.3 The effect of cold rolling procedures upon the development of cold rolling textures	97
6.4 The effect of cold rolling textures and annealing time upon the development of the annealing texture	102
6.5 The relationship between processing texture and R value	104
6.6 The relationship between crystal reorientation after tensile extension and R value	110
6.7 The cold rolling geometry	120
7. SUMMARY AND CONCLUSIONS	124
8. APPENDICES	
REFERENCES	
ACKNOWLEDGEMENTS	

## 1. INTRODUCTION

It is generally known that deep drawability of steel sheets depends upon the number, nature and distribution of non-metallic inclusions which arise during smelting and casting operations. These considerations are excluded in the case of rimmed steel which is the material to be studied in the present project. However, there are still a number of possibilities influencing the deep drawing capacity of the final strip in hot rolling, cold rolling and annealing. It is of interest to this project to establish to what degree cold rolling and annealing may influence texture and R value of rimmed steel strip.

Deep drawability of rimmed steel strip is governed by anisotropic behaviour originating from crystallographic preferred orientation. The degree of plastic anisotropy is measured by the strain ratio or R value. A high strain ratio is indicative of good deep drawing capacity and vice-versa. Good drawability is associated with high intensities of  $\{111\}$  planes and low intensities of  $\{100\}$  planes parallel to the strip surface. It is to be expected that the increase in R value corresponds to a similar increase in the  $\{111\}$  texture intensity. On the contrary, it was reported<sup>(1)</sup> that R value of rimmed steel strip increased to a maximum at 70% total reduction, thereafter decreased with further rolling reduction, while intensity of the  $\{111\}$  planes continued to increase as shown in fig. 1.1 and fig. 1.2. Recently<sup>(2)</sup>, it was shown that R value of rimmed steel strip increased when rolling with constant heavy draughts and by increasing the total rolling reduction to a maximum at 75% then decreased. The reduction in R value after 75% total reduction was related to the reduction in the  $\{111\}/\{100\}$  relative intensities.

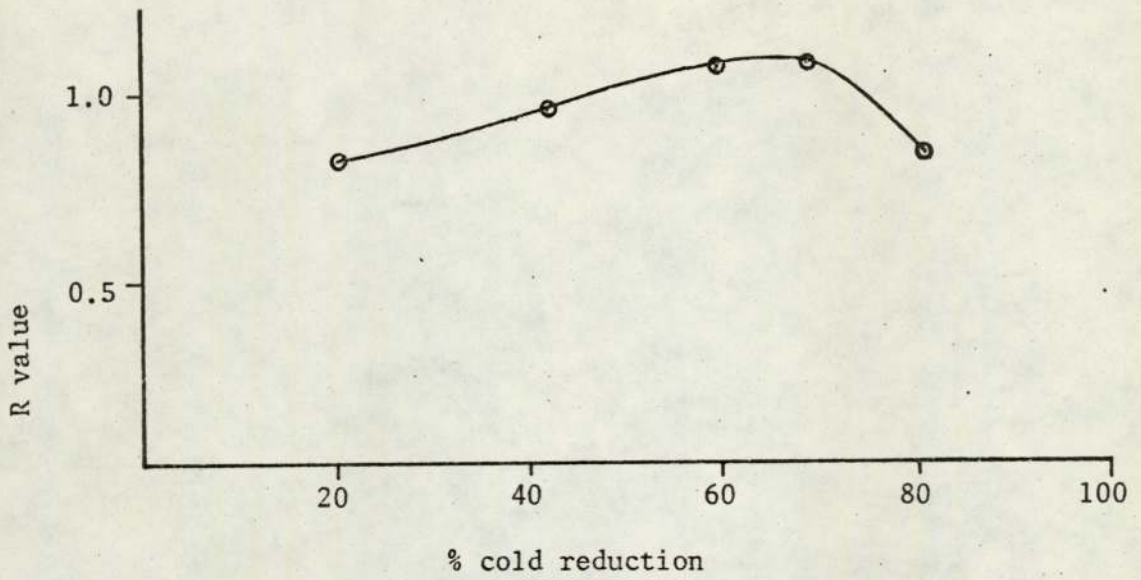


Fig. 1.1 The influence of the amount of cold reduction upon R value of a rimmed steel strip<sup>(1)</sup>.

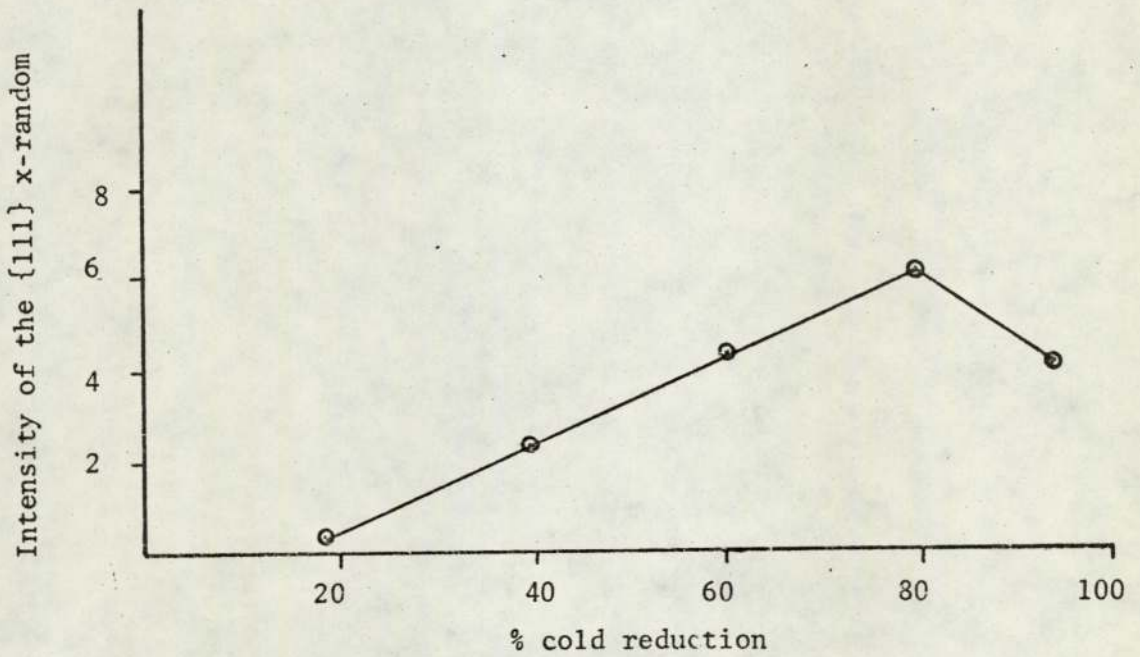


Fig. 1.2 The influence of the amount of cold reduction upon intensity of the {111} x random<sup>(1)</sup>.

Ideally, cold rolling can be regarded as a combination of tension in the rolling direction and compression normal to the rolling plane. By cold rolling, therefore, it is possible to develop mostly tensional texture or mostly compression texture or a combination of both, depending upon the mode of deformation, which is defined by the magnitude of the rolling draughts. Furthermore, by using constant draughts throughout the whole rolling operation, the percentage reduction per pass increases from one pass to the next. As a result, the mode of deformation varies with the progress of rolling, and texture is developed under varying rolling conditions. After heavy reduction, the high percentage reduction per pass might be an important factor contributing to the formation of more {100} texture leading to a reduction in R value.

Controlling the geometry of deformation, during cold rolling is, therefore, necessary in order to control the mode of deformation, texture and hence R value. In the present study, coils of rimmed steel were cold rolled according to three constant geometry schedules in which the shear plane angle is maintained constant from one pass to the next. Using the 2 high mill, reductions per pass equivalent to shear plane angles of  $55^\circ$ ,  $45^\circ$  and  $35^\circ$  corresponding to the previous rolling schedules were used. In order to demonstrate the difference between rolling with constant geometry and rolling with constant roll gap, coils of the same material were cold rolled using light, medium and heavy roll gap. Yet another set of the same coils was cold rolled using the pendulum mill. The effect of these seven rolling schedules upon texture and R value was studied. Since texture developed after annealing is dependent upon texture of the matrix in which it is formed as well as the annealing time, effect of the latter upon texture and R value was also studied.

Since R value is measured in a tensile test, a knowledge of the behaviour of the material under investigation to tensile strain is fundamental. This is necessary to explain the reduction in R value after heavy rolling reduction in constant roll gap schedules and shows how this reduction can be avoided. Crystal reorientation after tensile extension was therefore examined.

## 2. LITERATURE REVIEW

## 2.1 THE GEOMETRY OF COLD ROLLING

Controlling the geometry of deformation during cold rolling received little attention in the literature though it was noted by Crane and Alexander<sup>(3)</sup> that the rolling condition in the deformation zone is significant to the development of cold rolling texture. Dillamore and Roberts<sup>(4)</sup> concur at least for cold rolling condition close to sticking friction. They used the slip line field of a compression test to illustrate the relative orientation of maximum resolved shear stress axes through the thickness of a strip. They indicated that under both low and high friction conditions (not reaching the sticking friction) the stress distribution at the surface is not altered on passing through the neutral point, as shown in fig. 2.1.1.

For a material between the surface and centre of a strip, the stress system on the exit side of the neutral point is a mirror image of the stress system on the entry side. However, the stress systems at the centre are similar regardless of the cold rolling condition but varied at the surface according to the rolling condition. They assumed also that texture developed during cold rolling is dependent upon the amount of deformation occurring on either side of the neutral point. A parameter P was therefore invoked to calculate the percentage deformation per pass on either side of the neutral point as follows:

$$P = 50 - \left[ \frac{1}{\mu} \left( \frac{R}{2D} \right)^{\frac{1}{2}} - \frac{1}{\mu 2} \left( \frac{R}{4D} \right) \right] \times 100 \quad 2.1.1$$

where  $\mu$  is the coefficient of friction, R is the rolling draught and D is the roll diameter. According to equation 2.1.1, increasing the rolling draughts decrease the amount of deformation after the neutral point, for all values of the coefficient of friction.

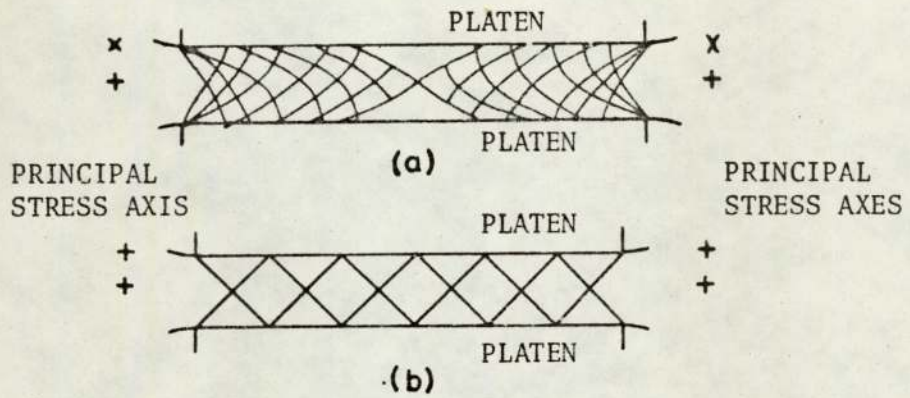


Fig. 2.1.1 Shows the slip line fields for (a) completely rough-platens; strip thickness: platen breadth 1:6.6, (b) zero friction; strip thickness: platen breadth 1:6. (4)

Crane and Alexander<sup>(3)</sup> in discussion were critical of the approach of Dillamore and Roberts<sup>(4)</sup> in that by cold rolling of an aluminium strip to 96% total reduction using 0.04 in/p rolling draughts, the percentage reduction per pass varied from 8% to 80%. The effect of the zone of deformation, however, had varied considerably within that range and maintaining a constant geometry of deformation was therefore necessary to control texture developed. Tucker<sup>(5)</sup> was critical of Dillamore and Roberts' treatment<sup>(4)</sup> because of the failure to maintain the rolling direction accurately from one pass to the next. Hellewell<sup>(2)</sup> reported that the mirror image condition for stable orientations which was suggested by Dillamore and Roberts<sup>(4)</sup> is only applicable if deformation on either side of the neutral point was equal. However, texture developed during cold rolling using light draughts where the deformation is equal on either side of the neutral point, may be accounted for on the basis of mirror image condition. During cold rolling using heavy draughts the majority of deformation occurs on the entry side of the neutral point provided the friction conditions do not approach the sticking friction. Therefore, the mirror image condition does not apply during cold rolling using heavy draughts. According to Hellewell<sup>(2)</sup> texture developed by cold rolling using light draughts varied from surface to centre while texture developed by heavy rolling draughts was homogeneous through the thickness of the strip. This is contrary to what was expected from Dillamore and Roberts' treatment<sup>(4)</sup>. Hellewell<sup>(2)</sup> on the other hand confirmed their observation that texture developed at the strip centre was independent of the cold rolling condition.

More recently, Vandermeer and Ogles<sup>(6)</sup> defined the rolling geometry by a new parameter  $\frac{1}{t_m}$  given by the following equation:

$$\frac{l}{t_m} = (D)^{\frac{1}{2}} \frac{(t_N - t_x)^{\frac{1}{2}}}{\frac{1}{2}(t_N + t_x)} \quad 2.1.2$$

where  $l$  is the length in the rolling direction of the geometrical zone of deformation,  $t_m$  is the average thickness of that zone,  $D$  is the radius of the work rolls,  $t_N$  and  $t_x$  are the entry and exit thicknesses respectively. The parameter  $\frac{l}{t}$  although it was related to texture segregation in niobium is not satisfactory to control the geometry of deformation during cold rolling, since the  $\frac{l}{t_m}$  parameter is likely to increase with the total rolling reduction.

Mathur and Backofen<sup>(76)</sup> pointed out that the geometry of the deformation zone is an important factor contributing to the state of strain during cold rolling. An index of such geometry is the ratio of the mean zone thickness,  $T_N$ , to the zone contact length,  $L$ , or  $\Delta = T_N/L$ . For strip rolling

$$\Delta \approx \frac{T_N}{4DR} (2 - R) \quad 2.1.3$$

where  $D$  is the roll diameter and  $R$  is the rolling draught.  $R = 1 - (T_x/T_N)$ ,  $T_x$  and  $T_N$  being the exit and entry thicknesses. The index  $\Delta$  tends to be near 1 because the horizontally directed friction forces must be large enough for the rolls to bite and deliver the well-lubricated strip. Cold rolling cannot usually be carried out with  $\Delta$  much higher than unity. It was shown that texture and  $R$  value responded to the change in  $\Delta$ .

Yeomans and Richards<sup>(7)</sup> related the geometry of deformation during cold rolling to the relative magnitudes of principal strains for all infinitesimally small increments of the total strains. Since rolling is a combination of tension in the rolling direction and compression normal to the rolling plane, they assumed that crystallographic slip during cold

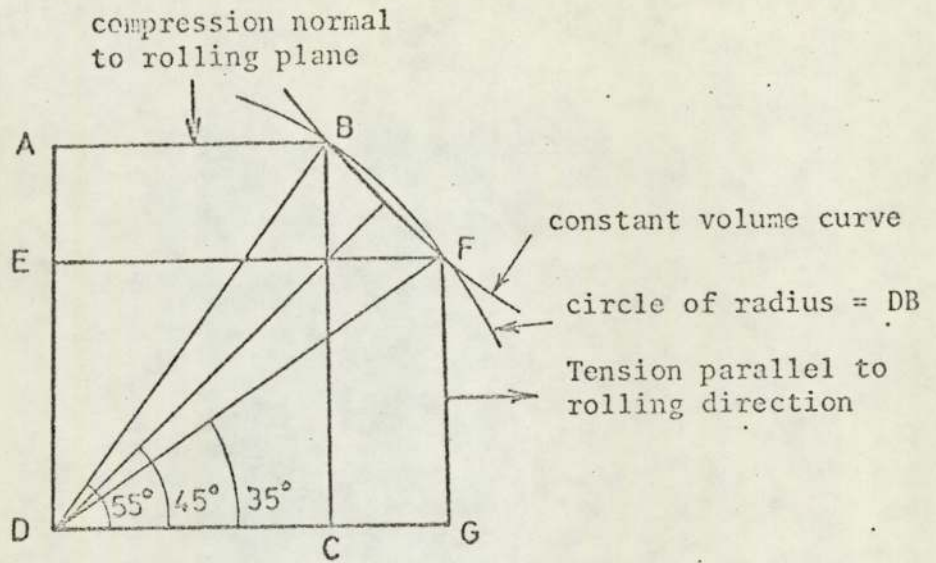


Fig. 2.1.2 Shows that during rolling, a rectangular element ABCD deforms by simple tension from the commencement of deformation, by slip on planes of maximum resolved shear stresses, in the nearest closed packed direction to the direction inclined  $54^{\circ} 44'$  to the rolling direction. With progressive increasing strain, the operative slip planes continue to rotate towards the  $45^{\circ}$  position until the  $35^{\circ}$  position is reached where deformation occurs mostly by compression, without changing the length of the diagonals DB and DF.

rolling is operative over an angular range around the  $45^\circ$  angle to the stress axes (see Appendix I). The extreme limits of that angular range correspond to the most favourably orientated crystallographic plane to slip in the directions inclined  $54^\circ 44'$  and  $35^\circ 16'$  to the tension and compression axes. Furthermore, tension and compression components are conjugately related, hence equal extension could be affected by equal shear on conjugate systems. Thus in cold rolling, it would be expected that the operative slip components would switch from that corresponding to tension to that of compression depending upon the magnitude of the rolling draughts. This is illustrated in fig. 2.1.2.

## 2.2 THEORIES OF COLD ROLLING TEXTURE FORMATION IN b.c.c.

### POLYCRYSTALLINE METALS

All explanations put forward to account for the origin of cold rolling texture in b.c.c. polycrystalline metals are based on the assumption that plastic deformation occurs by a process of crystallographic slip on the  $\{110\}$ ,  $\{112\}$  and  $\{123\}$  close-packed planes in the  $\langle 111 \rangle$  close-packed direction. Since there is a total of 48 slip systems, each has a slip component acting along all possible slip planes, slip occurs only on the slip system which has the maximum resolved shear stress. As Mises<sup>(8)</sup> and Taylor<sup>(9)</sup> assumed, five slip systems must operate simultaneously in order to preserve the external form of the material and maintain cohesion at the grain boundaries. Several objections to Taylor's analysis<sup>(9)</sup> arose on the grounds that it assumes a homogeneous deformation and that the active slip systems were to be

determined by the condition of least shear. Bishop and Hill<sup>(10)</sup>, however, introduced the principle of maximum shear strain and considered that although deformation is known to be inhomogeneous, it may be regarded as sufficiently homogeneous for consideration of the problem of texture formation.

Boas and Schmid<sup>(11)</sup>, and Pickus and Mathewson<sup>(12)</sup> relaxed the Taylor's treatment<sup>(9)</sup> by assuming that unequal participation of the three most favourable slip systems brings the deformation axes to symmetrical end positions, where the resolved shear stresses are equal and the rotations cancel out. The most favourable system to slip is that for which the Schmid factor<sup>(13)</sup> defined by the product of the resolved shear stress and the cosine of the angle between the slip direction and direction in which free flow may occur, is highest. No explanation was given as to how the other crystals reach that position. More recently<sup>(14)</sup>, it was reported that at room temperature, no unique slip system was operative in the early stages of deformation. Some slip systems, having low resolved shear stresses were observed, while some slip systems with high resolved shear stress were missing. There was, therefore, a breakdown of the Schmid law.

In all assumptions that slip occurs on many slip systems simultaneously, the stress within a grain or part of a grain must be such as to give equal resolved shear stresses in all the operative slip systems. No explanation was given to the means by which the most favourable system or systems can withstand resolved shear stresses greater than the critical value until the resolved shear stresses on less favourable systems have reached the critical value for slip. Calnan and Clews<sup>(15)</sup> overcame this problem by introducing in each crystal an effective stress,

$T_e$ , which because of the constraints by neighbouring grains is so orientated on several systems simultaneously. When an increasing applied stress,  $T_a$ , is applied to the polycrystalline aggregate, the effective stress (initially coincident with  $T_a$ ) moves away from  $T_a$  so that  $T_e$  which is resolved on the most favourable system is always less than the critical value for slip. Using this treatment, Calnan and Clews<sup>(15)</sup> determined the tension and compression textures.  $\langle 110 \rangle$  texture with spread towards  $\langle 311 \rangle$  was predicted as the tension texture, while a duplex of  $\langle 100 \rangle + \langle 111 \rangle$  texture was predicted for the compression texture with the  $\langle 111 \rangle$  component predominating. Although the Calnan and Clews treatment assumes inhomogeneous deformation, it is complicated when applying to the b.c.c. structures, since the resolved shear stresses on the three families of slip planes have to be taken into consideration.

Dillamore and Roberts<sup>(16)</sup> assumed that multiple slip operates only in the vicinity of the grain boundary, while one or two slip systems only are operative in the grain body. Their assumption is supported by an earlier experimental observation by Clareborough and Hargreaves<sup>(17)</sup> that this is so. Accordingly slip rotations in the grain body should be more rapid and dominant relative to multiple slip in the boundary. Dillamore and Roberts<sup>(16)</sup>, therefore, assumed that deformation of individual grains in polycrystalline material is closely similar to the deformation of single crystals of the same orientation. Slip rotation during rolling was considered to be due to a biaxial stress system. Viewed in this light, the determination of the b.c.c. rolling texture was simplified and a spread of orientation between  $\{112\}\langle 110 \rangle$  and  $\{110\}\langle 110 \rangle$  was predicted. It was also noted<sup>(16)</sup> that the  $\{112\}\langle 111 \rangle$  and

{123}<111> slip systems are geometrically equivalent to different proportions of primary and cross slips on the {110}<110> systems. Each primary system has two available cross slip systems one of which must always sustain some component of the applied stress. Tucker<sup>(18)</sup> was critical of cross slip in that it is enhanced by failure to keep the rolling direction accurately from one pass to the next. Taylor and Christian<sup>(14)</sup> reported that cross slip in b.c.c. polycrystalline metals is difficult to initiate at low temperature because of the high stresses needed to move individual screw dislocations.

The foregoing analyses of texture formation presuppose that slip elements are known and derive the mode of deformation from texture. This helps to account for texture developed but does not help to control it. Yeomans and Richards<sup>(7)</sup>, however, firstly assumed the mode of deformation then identified the slip system and texture from the magnitude of the principal strains, i.e. in reverse of other theories. Accordingly, the operative slip systems are uniquely defined by the mode of deformation, such as deformation in uniaxial extension, uniaxial compression and pure rolling. Each of the previous modes of deformation is characterised by the relative magnitudes of the principal strains for all infinitesimally small increments of the total strain. Thus, an incremental uniaxial plastic extension in length is associated with equivalent contractions in width and thickness of a rectangular specimen, on the assumption of no change in width. It was, therefore, concluded (see Appendix I) that deformation as occurred by slip is accompanied by rotation of the slip planes of maximum resolved shear stresses in the close packed direction which is nearest to the direction inclined  $54^{\circ}44'$  to the tension axis.

Similarly, for an incremental uniaxial compression, the contraction in thickness is equivalent to elongations in both width and length, and the most favourable slip systems are those corresponding to the planes of maximum resolved shear stresses and in close packed directions which are nearest to the  $54^{\circ}44'$  to the compression axis. In pure rolling where the incremental strain parallel to the rolling direction is equivalent in magnitude to the contraction in strip thickness and the strain in the transverse direction is zero, the operative slip systems are those of maximum resolved shear stresses in the close packed direction lying nearest to the  $45^{\circ}$  to the shear axes, that is  $45^{\circ}$  to the strip surface.

According to Yeomans and Richards<sup>(7)</sup> the crystallographic rotations during the early stages of cold rolling of a randomly orientated material tend to move the  $\langle 111 \rangle$  slip direction towards the compression axis until the  $\{100\}\langle 110 \rangle$  orientation is formed. This rotation brings the four  $\langle 111 \rangle$  directions into symmetrical positions with respect to the rolling direction and the perpendicular direction. The symmetrical arrangements of the  $\langle 111 \rangle$  slip directions defines the operative  $\{112\}$  slip plane, the pole of which lies on the tension axis, as shown in fig. 2.2.1. It would appear then that the stability of the  $\{112\}\langle 110 \rangle$  orientation arises from the fact that the  $\langle 110 \rangle$  direction lies between both the compression and tension circles. Therefore if slip is only operative on the  $\{112\}$  slip planes, it would result in sharpening of the  $\{112\}\langle 110 \rangle$  texture with increasing the amount of cold rolling.

With further increase in the rolling reduction, rotation of  $11^{\circ}$  around the rolling direction brings the  $\{123\}$  into equilibrium position to allow for further deformation, as shown in Fig. 2.2.2. This is

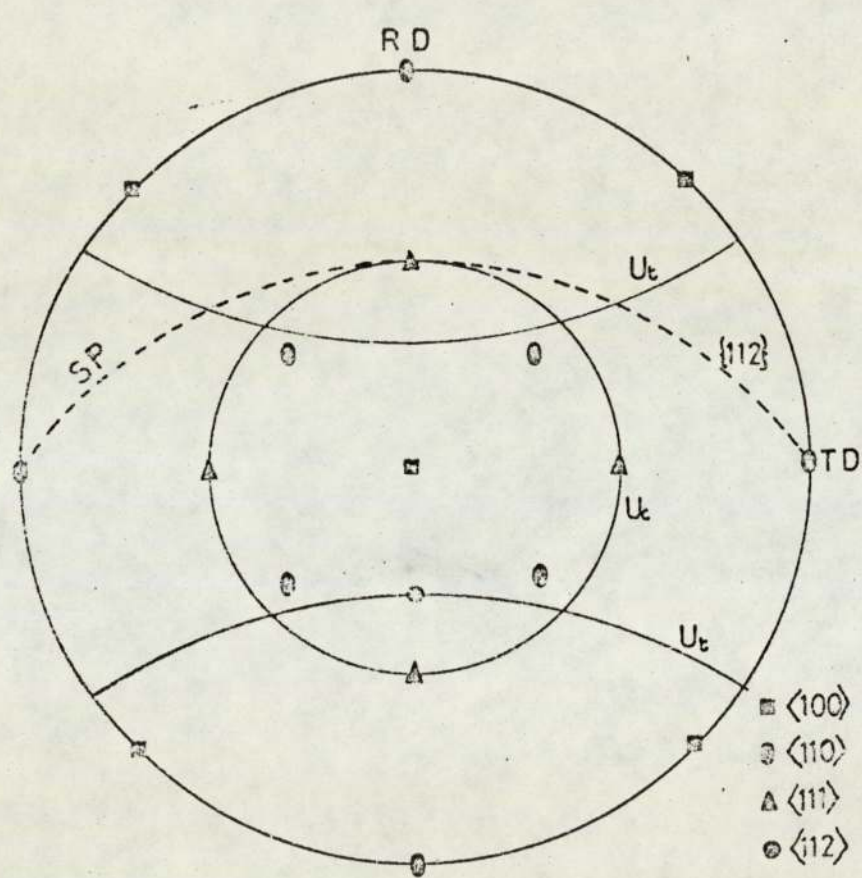


Fig. 2.2.1. Ideal  $\{100\}\langle 110 \rangle$  texture, with four  $\langle 111 \rangle$  slip directions on  $U_c$  and the pole of the  $\{112\}$  slip plane on  $U_t$ .

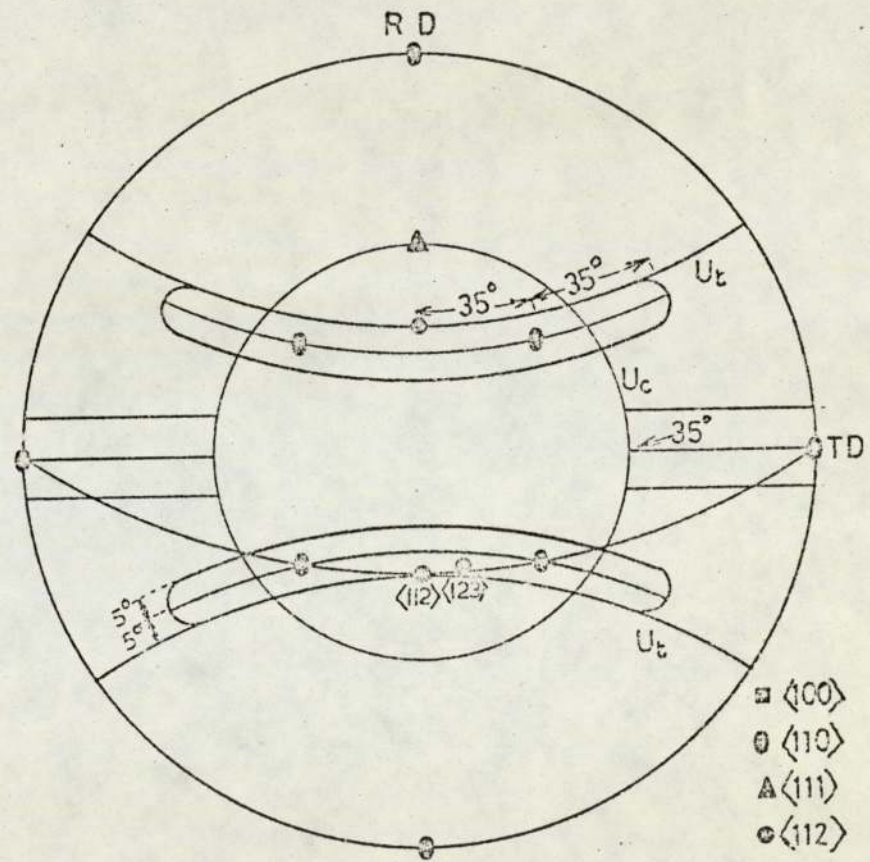


Fig. 2.2.2. Predicted spread in  $\{110\}$  pole figure due to the rotation of  $\{123\}$  poles about  $\langle 111 \rangle$  slip direction and  $\{110\}$  poles about the rolling direction to equilibrium or symmetrical positions.

equivalent to fixing the operative slip direction on  $U_c$  and allowing some rotation around it. In the ideal  $\{100\}\langle 110 \rangle$  orientation, four poles of the principal  $\{110\}$  slip planes are symmetrically situated around the rolling direction. Rotation of  $\pm 5^\circ$  of the  $\{110\}$  poles on the  $U_t$  circle around the rolling direction account for the  $\{311\}\langle 110 \rangle$  orientation. On the other hand, rotation about the rolling direction on the compression circle results in the formation of the  $\{111\}\langle 110 \rangle$  orientation, as shown in Fig. 2.2.3. In the  $\{111\}\langle 110 \rangle$  texture, rotation of the six  $\{110\}$  poles about the strip normal result in the  $\{111\}\langle 112 \rangle$  orientation, as shown in Fig. 2.2.4.

In the  $\{111\}\langle 112 \rangle$  orientation, the six  $\{110\}$  and three  $\{100\}$  poles are symmetrical about the strip normal. Furthermore, one of the  $\{112\}$  poles is coincident with the  $\{100\}$  slip planes. Slip can then occur on the  $\{100\}$  planes, if the critical resolved shear stress on these planes is reached. This results in the formation of the  $\{100\}\langle 110 \rangle$  orientation. Yeomans and Richards' analysis of the cold rolling texture can be used to select certain modes of deformation and to control texture developed.

### 2.3 THEORIES OF ANNEALING TEXTURE FORMATION IN b.c.c.

#### POLYCRYSTALLINE METALS

The origin of annealing texture has been subject of controversy over the relative importance of nucleation and growth as controlling factors. No attempts will be made here to review the historical development of the subject, but emphasis will be placed on the cold rolling and annealing variables which influence the recrystallization texture produced.

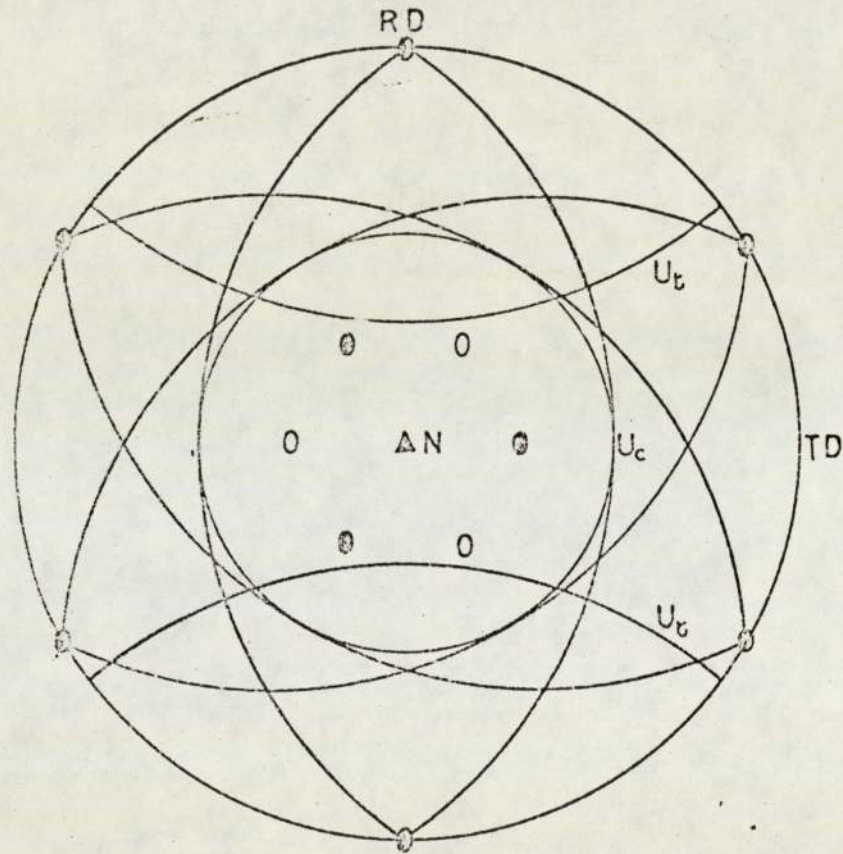


Fig. 2.2.3 Ideal  $\{111\}\langle 110\rangle$  texture, with six  $\{110\}$  slip planes tangential to  $U_c$ .

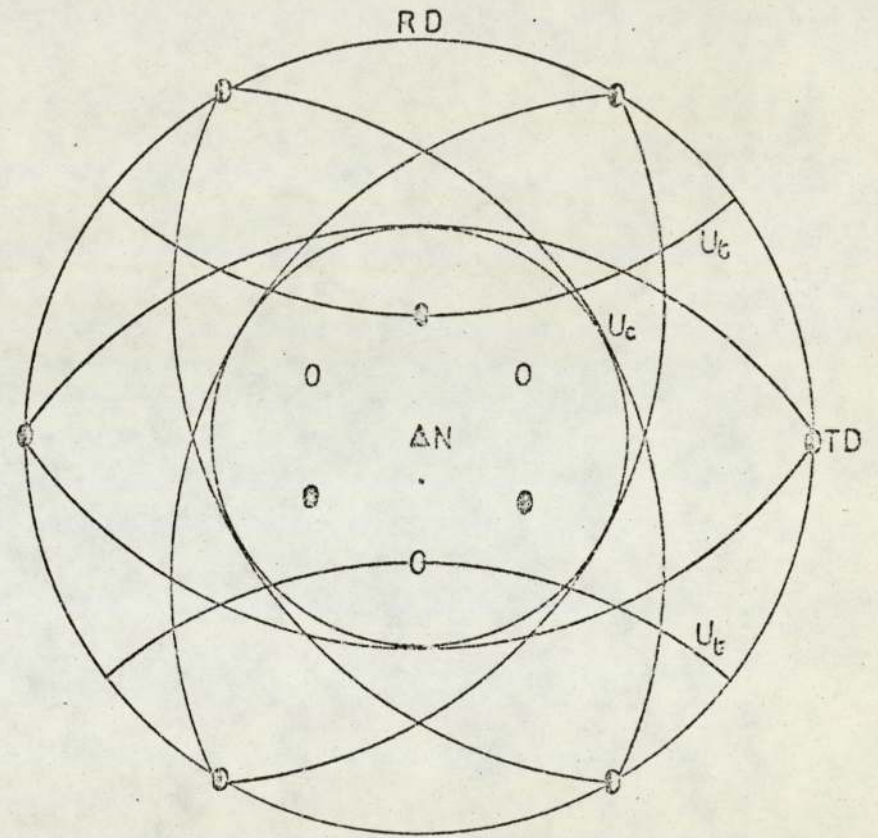


Fig. 2.2.4. Ideal  $\{111\}\langle 112\rangle$  texture, obtained from  $\{111\}\langle 110\rangle$  by  $30^\circ$  rotation about N. The six  $\{110\}$  planes are still tangential to  $U_c$ .

During recrystallisation of a heavily deformed steel the formation of a viable nucleus depends on the driving force available for sub-grain growth which is dependent upon the amount of stored energy of deformation. Since the sequence of increasing the stored energy corresponds to the total amount of dislocation motion which had taken place<sup>(19)</sup>, the ease of nucleation is therefore orientation-sensitive fig. 2.3.1. Within the major texture components, the stored energy increased in the order of the {100}<011>, {211}<011>, {111}<UVW> and {110}<011> orientations as shown in Fig. 2.3.1. During recrystallisation anneal, the {011} and {111} texture components should nucleate first and therefore have the longest time to grow before impingement occurs. The very low density of the {011} planes in the cold worked metals, however, means that it is unlikely ever to become strong after recrystallisation. The least favoured orientation is the {100}, and this was predicted to disappear on annealing. Orientation determination on recrystallised grains during recrystallisation of rimmed steel confirmed the predominance of the {111} planes<sup>(2,20)</sup>.

During normal grain growth, the relatively strong texture components in the primary recrystallisation, are strengthened at the expense of the neighbouring weak components, and the density between different components are sometimes redistributed. In the case of rimmed steel, the relatively strong {111} in the primary recrystallisation texture, is strengthened during normal grain growth at the expense of the weak {100} texture. In the absence of second phase particles, the growth of the large grain is defined by the equation<sup>(21)</sup>

$$\frac{dR}{dt} = k \left( \frac{1}{R_{cr}} - \frac{1}{R} \right) \quad 2.3.1$$

where R is the radius of the growing grains and  $R_{cr}$  is the

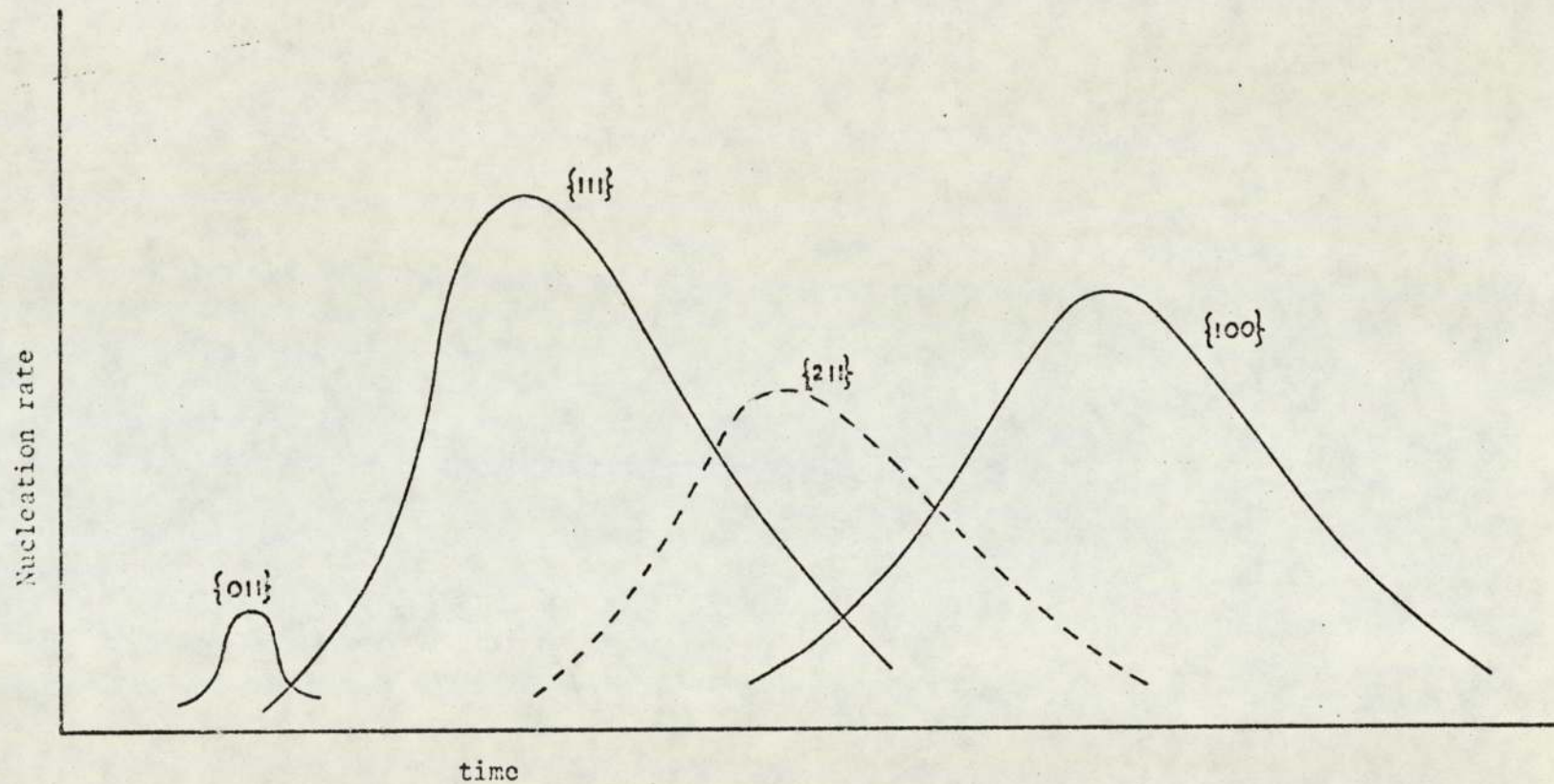


Fig. 2.3.1 Schematic representation of the dependence of the nucleation rate upon orientation in the cold worked iron.

characteristic or average grain size. Grains which are bigger than  $R_{cr}$  grow, while those which are smaller shrink and disappear. The difference in grain size of the grains determines which grains nucleate first and have the longest time to grow. The {111} texture, is, therefore, enhanced by normal grain growth, while the {100} texture is weakened. When effective second phase particles are present, a constant reaction to the movement of grain boundaries is developed. The grain growth rate is now given by the equation<sup>(21)</sup>,

$$\frac{dR}{dT} = k \left( \frac{1}{R_{cr}} - \frac{1}{R} \right) \pm Z \quad 2.3.2$$

where  $Z$  is a reaction term due to the particles which always acts to decrease the absolute value of  $\frac{dR}{dT}$ . The effect of increasing the particle reaction  $Z$  is to limit the range of growing grains to a smaller fraction of those of the largest sizes. Therefore, only much larger grains than the average size can grow while those of grain size about average are inhibited from growing. Eventually, the growth will slow down and stop in the presence of inhibiting particles. A limiting case is reached when normal grain growth is no longer possible and abnormal grain growth (secondary recrystallisation) starts. If, however, the particles were progressively removed by decarburization, normal grain growth may continue. The {111} texture components which have now increased in size continue to grow selectively during further normal grain growth<sup>(19)</sup>.

In isothermal annealing, therefore, texture developed after annealing is dependent upon the cold rolling texture and the annealing time.

#### 2.4 THE RELATIONSHIP BETWEEN TEXTURE AND R VALUE

It is evident that R value, being a measure of plastic anisotropy, should be related to crystallographic texture. Burns and Heyer<sup>(22)</sup> have studied the effect of three major orientations in b.c.c. steel, namely the  $\{001\}\langle 110\rangle$ ,  $\{110\}\langle 001\rangle$  and  $\{111\}\langle 110\rangle$  orientations upon the strain ratio, on the basis that deformation in b.c.c. steel occurs by slip on four  $\langle 111\rangle$  directions. Since each of the four slip directions is common to three  $\{110\}$ , three  $\{112\}$  and six  $\{123\}$ , a total of 48 slip systems is expected. Since it is impracticable to decide which system of the 48 systems is to operate during deformation, it was assumed, from the stand-point of relative changes in the dimensions of cross section of a simple tensile test piece, that it is not necessary to know which plane becomes an active slip plane. It was then concluded that the relative width to thickness strains are dependent upon the slip direction only, the operative slip direction being that of maximum shear stress. Thus, when a sheet with  $(100)[110]$  orientation is extended in the rolling direction, the favourable  $[111]$  slip directions  $A_1$  and  $A_3$  are at an angle of  $35^\circ$  to the specimen axis, hence  $10^\circ$  from the direction of maximum shear stress Fig. 2.4.1. Accordingly, slip occurs in the  $A_1$  and  $A_3$  directions resulting in a greater reduction in thickness than in width. Such a specimen should have a very low strain ratio, approaching zero as the specimen ideally possesses this orientation. In the case of a sheet with  $\{110\}\langle 001\rangle$  texture, all the four slip directions of the type  $[111]$  are at the same angle  $55^\circ$  to the direction of tension in the rolling direction and at  $10^\circ$  to the direction of maximum shear as in Fig. 2.4.2. Hence the width strain should be the same as the thickness strain, resulting in a strain ratio of unity. Finally, in a sheet having the

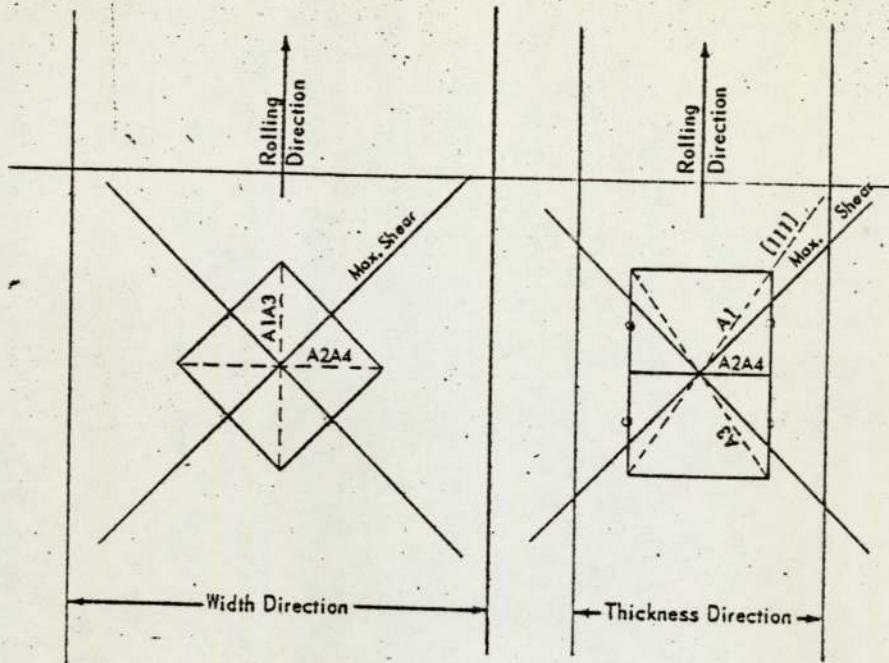


Fig.2.4.1 shows the behaviour of a specimen with cube-on face orientation  $(100)[011]$  under the influence of an uniaxial extension in the rolling direction<sup>(22)</sup>.

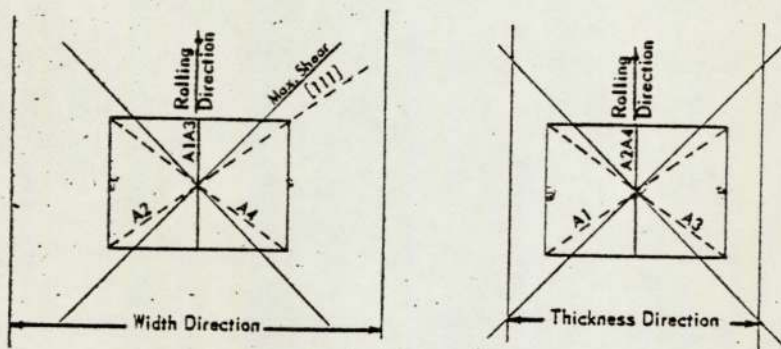


Fig. 2.4.2. shows the behaviour of a specimen with cube-on edge texture  $(110)[001]$  under the influence of an uniaxial extension in the rolling direction<sup>(22)</sup>.

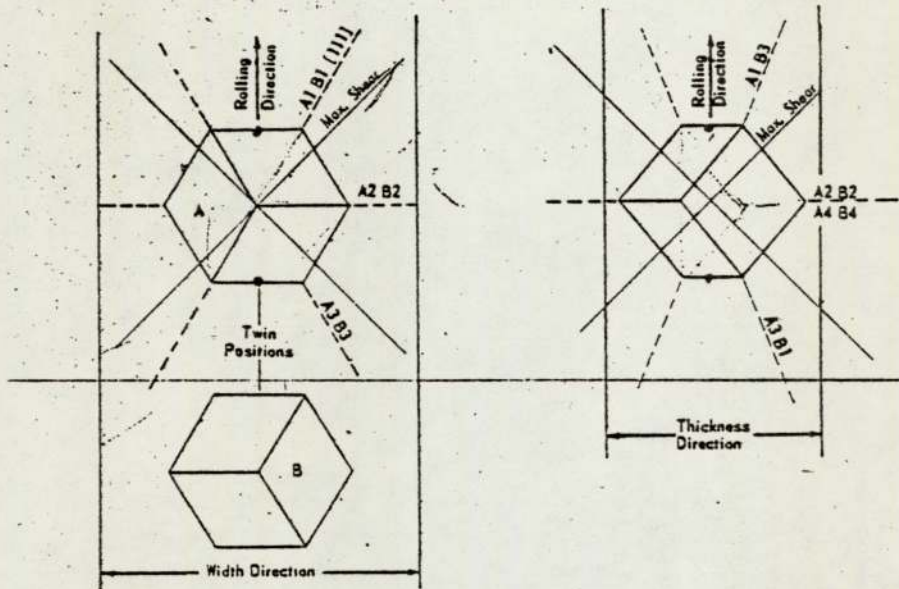


Fig. 2.4.3. shows the behaviour of a specimen with cube-on-corner texture (111)[110] under the influence of an uniaxial extension in the rolling direction<sup>(22)</sup>.

twinned orientation (111)[110], the preferred [111] slip directions  $A_1$  and  $A_3$  are at an angle  $35\frac{1}{2}^\circ$  to the axis of the specimen, if extended in the rolling direction as shown in Fig. 2.4.3. Hence the width strain will be higher than the thickness strain resulting in a strain ratio greater than unity.

The foregoing analysis was based on the assumption that in pulling a strip, the width strain  $\epsilon_w$  and thickness strain  $\epsilon_t$  caused by a strain  $\gamma$  in a particular slip direction at angles  $\lambda_w$  and  $\lambda_t$  to the width and thickness directions respectively is given by the equations

$$\epsilon_w = \gamma \text{Cos } \lambda_w \quad 2.4.1$$

and

$$\epsilon_t = \gamma \text{Cos } \lambda_t \quad 2.4.2$$

The correct relation for resolving the crystallographic shear strains into linear strains are given by the Schmid law<sup>(13)</sup>

$$\epsilon_w = \gamma \text{Cos } \lambda_w \cdot \text{Cos } \phi_w \quad 2.4.3$$

$$\epsilon_t = \gamma \text{Cos } \lambda_t \cdot \text{Cos } \phi_t \quad 2.4.4$$

where  $\phi_w$  and  $\phi_t$  are the angles between the slip-plane normal and the width and thickness directions. Furthermore, no attempt was made to account for the varying amounts of slip on different systems within a grain. Hosford and Backofen<sup>(23)</sup> devised a method relating R value to texture. This method is a follow up of the Taylor's criterion<sup>(9)</sup> which was later modified by Bishop and Hill<sup>(10)</sup> for calculating the tensile (or compressive) stress-strain curves of randomly orientated polycrystals from the stress-strain curves of single crystals. In Taylor's analysis<sup>(9)</sup> it

was assumed that during plastic deformation, the five operative slip systems are those which have the minimum value of a parameter  $M$  given by  $\frac{d\gamma}{d\epsilon_x}$ , where  $d\gamma$  is the sum of the incremental shear strains on all of the active slip systems needed to produce an increment of tensile strain  $d\epsilon_x$ . Since slip occurs on five systems simultaneously, an average  $\bar{M}$  was used to describe the aggregate over-all texture. Minimum  $\bar{M}$  values, obtained for a number of orientations in the unit stereographic triangle were found to be  $\bar{M} = 3.06$ .

The total shear strain increment  $d\gamma$  was then related to the stress  $\sigma_x$  required for a grain to flow with axial symmetry by assuming that in order to activate slip, a shear stress  $\tau$  would be the same for all systems. Therefore, the work expended in slip throughout a unit volume of a material becomes  $dW = \tau d\gamma$  which must be identical to the work per unit volume done by the applied stress in producing the extension. Hence

$$dw = \sigma_x d\epsilon_x = \tau d\gamma \quad 2.4.5$$

and

$$\frac{\sigma_x}{\tau} = \frac{d\gamma}{d\epsilon_x} = M = \frac{dw}{\tau d\epsilon_x} \quad 2.4.6$$

Equation 2.4.6 is a multiple slip analogy of the Schmid's law<sup>(13)</sup> in which

$$\frac{\sigma_x}{\tau} = \frac{d\gamma}{d\epsilon_x} = \frac{1}{\cos\lambda\cos\phi} \quad 2.4.7$$

where  $\lambda$  and  $\phi$  are the angles between  $x$  and slip direction and slip plane normal respectively.

Several objections to Taylor's analysis<sup>(9)</sup> were reported since it was assumed that deformation is homogeneous and the active slip systems

were determined by the condition of minimum shear strain. In addition, many possible combinations of slip systems were overlooked during the calculation of M. Bishop and Hill<sup>(10)</sup>, however, devised a more thorough analysis to calculate M in grains of various orientations. They assumed that simultaneous slip on five or more systems can occur only when the critical stress for slip,  $\tau$ , is reached on these systems without being exceeded on any others. Bishop and Hill<sup>(10)</sup> showed that this condition is satisfied only with a limited number of stress states or combinations of the terms

$$\begin{aligned} A &= \frac{(\sigma_2 - \sigma_3)}{\sqrt{6} \cdot \tau} & F &= \frac{\sigma_{23}}{\sqrt{6} \cdot \tau} \\ B &= \frac{(\sigma_3 - \sigma_1)}{\sqrt{6} \cdot \tau} & G &= \frac{\sigma_{31}}{\sqrt{6} \cdot \tau} \\ C &= \frac{(\sigma_1 - \sigma_2)}{\sqrt{6} \cdot \tau} & H &= \frac{\sigma_{12}}{\sqrt{6} \cdot \tau} \end{aligned}$$

where the stresses  $\sigma$  are taken with reference to the cube axes of the crystal. The actual values of these terms are 0,  $\pm\frac{1}{2}$ ,  $\pm 1$ .

By expanding equation 2.4.6. and substituting the constant volume relationship  $d\epsilon_3 = -(d\epsilon_1 + d\epsilon_2)$  a formula for calculating M was derived hence,

$$M = \frac{1}{\tau} \left[ (\sigma_1 - \sigma_3) \frac{d\epsilon_1}{d\epsilon_x} + (\sigma_2 - \sigma_3) \frac{d\epsilon_2}{d\epsilon_x} + 2\sigma_{23} \frac{d\epsilon_{23}}{d\epsilon_x} + 2\sigma_{31} \frac{d\epsilon_{31}}{d\epsilon_x} + 2\sigma_{12} \frac{d\epsilon_{12}}{d\epsilon_x} \right] \quad 2.4.8$$

or

$$M = \sqrt{6} \left[ -B \frac{d\epsilon_1}{d\epsilon_x} + A \frac{d\epsilon_2}{d\epsilon_x} + 2F \frac{d\epsilon_{23}}{d\epsilon_x} + 2G \frac{d\epsilon_{31}}{d\epsilon_x} + 2H \frac{d\epsilon_{12}}{d\epsilon_x} \right] \quad 2.4.9$$

The parameter M is evaluated for a given orientation (of cube axes

relative to specimen axes) and for a specified shape change, defined by the ratios of the strain components along the specimen axes. This was carried out in three steps.

1. The strain components along the specimen axes, x, y and z were resolved into components along the cube axes of the crystal, 1, 2 and 3 with the expression, for  $d\epsilon_1$

$$d\epsilon_1 = l_{1x}^2 d\epsilon_x + l_{1y}^2 d\epsilon_y + l_{1z}^2 d\epsilon_z + l_{1y} l_{1z} d\epsilon_{yz} + l_{1z} l_{1x} d\epsilon_{zx} + l_{1x} l_{1y} d\epsilon_{xy}$$

and similar formulations for the other normal and shear strain components, the  $l$  term is the cosines of the angles between the cube axes and the specimen axes.

2. The relationship between  $d\epsilon_x$ ,  $d\epsilon_y$ ,  $d\epsilon_{yz}$ ,  $d\epsilon_{xy}$  and  $d\epsilon_{xz}$  was assumed to be known for axially symmetric flow, the strains along the cube axes were found relative to  $d\epsilon_x$  to be

$$\frac{d\epsilon_1}{d\epsilon_x} = l_{1x}^2 - \frac{1}{2} l_{1y}^2 - \frac{1}{2} l_{1z}^2, \text{ etc. for other components}$$

3. Finally, equation 2.4.9 was evaluated for each possible combination of A, B, C, F, G and H. The largest result was selected as the appropriate M value according to the principal of maximum virtual work.

The foregoing analysis was broadened by Hosford and Backofen<sup>(23)</sup> to include the anisotropy of yielding in textured sheets as measured by the width to thickness strain ratio  $R = \frac{d\epsilon_y}{d\epsilon_z}$  in a simple tensile test. In order to do that, it was assumed that if the tensile axis, x, is taken parallel to one of the principal axes of anisotropy, hence,

$d\epsilon_{yz} = d\epsilon_{zx} = d\epsilon_{xy} = 0$  and the  $d\epsilon_y$  and  $d\epsilon_z$  were incorporated in a

parameter  $r$  given by

$$r = \frac{d\epsilon_y}{d\epsilon_y + d\epsilon_z} = \frac{R}{R+1}$$

By applying the constant volume equation  $d\epsilon_x = -(d\epsilon_y + d\epsilon_z)$

Therefore  $d\epsilon_y = -rd\epsilon_x$ ;  $d\epsilon_z = -(1-r)d\epsilon_x$

The ratios  $\frac{d\epsilon_1}{d\epsilon_x}$ ,  $\frac{d\epsilon_2}{d\epsilon_x}$ ,  $\frac{d\epsilon_{23}}{d\epsilon_x}$ ,  $\frac{d\epsilon_{31}}{d\epsilon_x}$  and  $\frac{d\epsilon_{12}}{d\epsilon_x}$  in equation 2.4.9 were then

expressed in terms of the parameter  $r$  as follows

$$\frac{d\epsilon_1}{d\epsilon_x} = l_{1x}^2 - rl_{1y}^2 - (1-r)l_{1z}^2 \quad \text{etc.}$$

By assuming different values of  $r$  and calculating the corresponding values of  $M$  from equation 2.4.9,  $M$ .Vs. $r$  plot was drawn (figure 2.4.4). The values of  $M$  and  $r$  at the minimum of the plot identify the relative strength  $\frac{\sigma_x}{\tau}$  and the strain ratio  $R = \frac{r}{1-r}$ . The  $M$ .Vs. $r$  curve for a material consisting of several textural components  $a, b, \dots$  was found from the weighted average.

$$M = f_a M_a + f_b M_b + \dots$$

where  $f_a$  and  $f_b$  are the volume fractions of components  $a, b$ .

The minimum will occur when

$$\frac{dM}{dr} = f_a \frac{dM_a}{dr} + f_b \frac{dM_b}{dr} + \dots$$

If only (111) and (100) orientations were present, the minimum  $M$  would occur when

$$\frac{dM}{dr} = f\{100\} \frac{dM\{100\}}{dr} + f\{111\} \frac{dM\{111\}}{dr} = 0$$

At  $R = 1.5$

$$\frac{dM\{100\}}{dr} = 0.9 \quad \text{and} \quad \frac{dM\{111\}}{dr} = -0.2$$

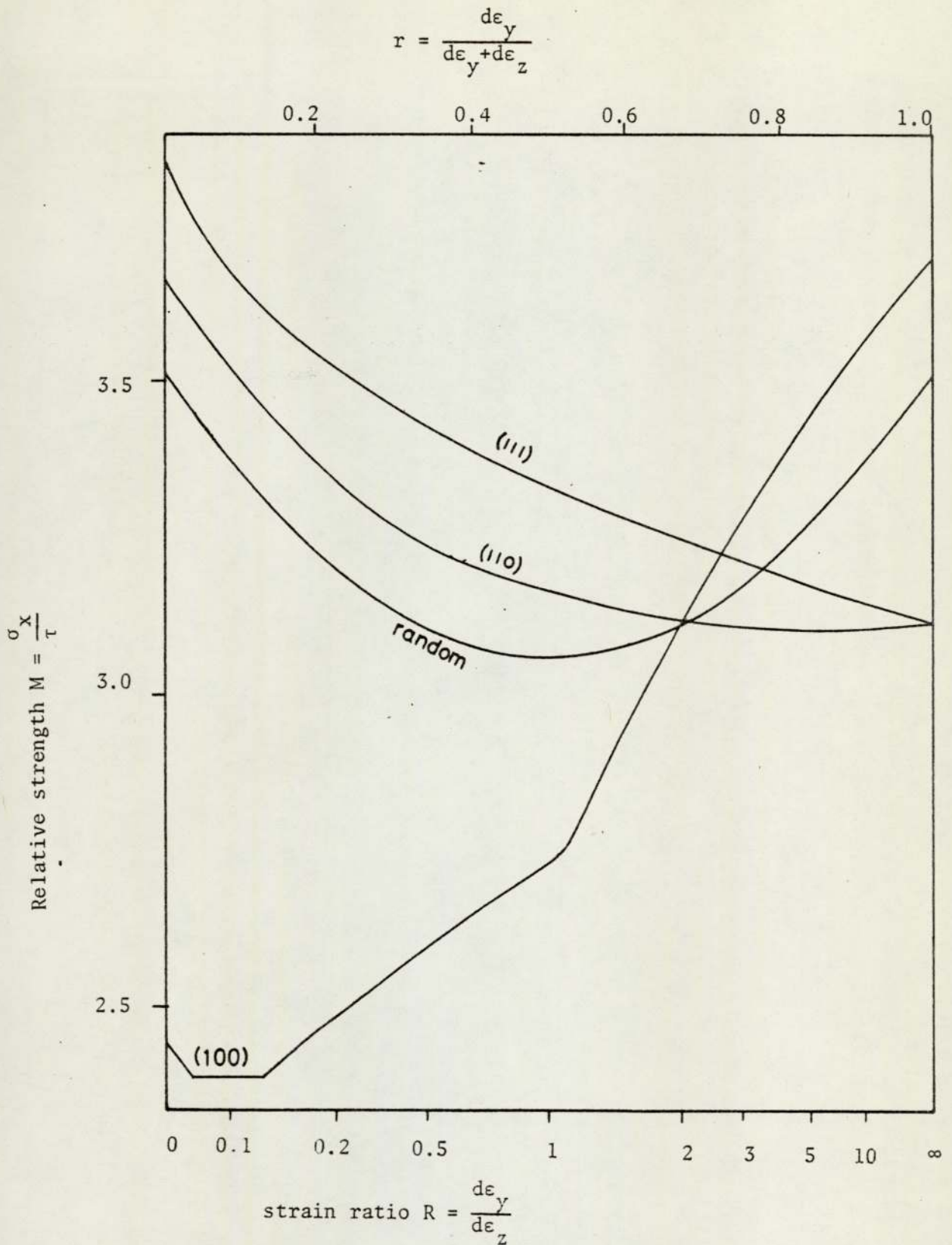


Fig. 2.4.4.  $M$  vs  $r(R)$  curves for textures which are rotationally symmetric about the sheet normal. Curves are shown for sheets in which (111), (110) and (100) are parallel to the rolling plane, and also for a randomly orientated sheet<sup>(23)</sup>.

There the effect of a twofold increase in the amount of {100} material would balance the effect of a ninefold increase in the amount of {111} at an  $\bar{R}$  level of about 1.5.

Fukuda<sup>(24)</sup> reported that if is necessary to examine more than the two orientations {100} and {111} to establish a correlation between  $\bar{R}$  value and texture. A new parameter including the {332} and {311} planes because of their relative preponderance in the recrystallisation texture together with the {100} and {111} textures was defined by

$$P = \frac{I\{111\} + I\{332\}}{I\{100\} + I\{311\}}$$

where I is the intensity of the corresponding {hkℓ} reflection relative to a random sample. The {332} orientation was reported to contribute to high R values whereas {311} texture results in lower R values because of its rotation to {100} orientation only during tensile strain with behaviour like crystals of {100} texture. The rotation of {411} texture to the {100} texture during tensile strain was also found to decrease R value<sup>(25)</sup>. The incidence of {311} texture in heavily rolled and annealed steel was attributed later to its high stored energy rather than to its predominance<sup>(26,27)</sup>.

Although the precise relationship between R value and texture is not fully established yet, it is clear that all different analyses generally lead to similar results, that a texture with {111} planes parallel to the plane of the sheet will give high R value. Also {100} planes parallel to the plane of the sheet will contribute to low R value.

## 2.5 THE RELATIONSHIP BETWEEN R VALUE AND THE L.D.R.

Several theories of anisotropy plasticity have been proposed, but their application has been limited and only the theory of Hill<sup>(28)</sup> has received appreciable attention. By analogy with Huber-Mises<sup>(8)</sup> yield criterion for isotropic behaviour, Hill defined a plastic potential or effective stress for anisotropy behaviour by assuming that the uniaxial yield stress varies with direction.

Whiteley<sup>(29)</sup> using an analysis by Hu<sup>(30)</sup> based on Hill's theory of anisotropy plasticity<sup>(28)</sup> and applying a correction factor to account for frictional forces<sup>(31)</sup>, has carried out an analysis of the punch load required during drawing for the case of an anisotropy material, in order to study the relationship between the L.D.R. and R value. The total punch load required to draw a blank of diameter D was shown to be

$$P_{\text{tot}} = (1 + \eta)\pi.d.t. \frac{\sqrt{\alpha_{33}}}{G}.k.\ln \left(\frac{D}{d}\right) \quad 2.5.1$$

where  $\alpha_{33}$  and G are anisotropy parameters,  $\eta$  is a friction parameter, D is the initial blank diameter, d is the final cup diameter, t is the thickness of the blank and k is the effective strength. The parameter  $\eta$  is constant for certain conditions of geometry and friction.

The maximum diameter of a blank that can be drawn is limited by the maximum punch load which can be supported by the material forming the wall of the cup. It was further shown that the maximum punch load is given by

$$P_{\text{max}} = \pi.d.t. \frac{\sqrt{\alpha_{22}}}{G}.k \quad 2.5.2$$

where  $\alpha_{22}$  is another anisotropic parameter. At the critical blank

diameter equations 2.5.1 and 2.5.2 must be equal, so that the limiting drawing ratio is given by

$$\ln\left(\frac{D}{d}\right)_{\max} = \frac{1}{(1+\eta)} \frac{\sqrt{\alpha_{22}}}{\sqrt{\alpha_{33}}} \quad 2.5.3$$

Equation 2.5.3 indicates that for certain conditions of geometry and lubrication, the limiting drawing ratio is governed by the anisotropy parameters of the sheet and is independent of the effective strength of material.

Whiteley<sup>(29)</sup> extended his analysis to express the anisotropy parameters  $\alpha_{22}$  and  $\alpha_{33}$  and  $G$  in terms of  $R$  value. Assuming a material with normal anisotropy  $R$  it was shown that

$$P_{\text{tot}} = (1+\eta) \cdot \pi \cdot d \cdot t \frac{\sqrt{(2+2\bar{R})}}{\sqrt{(1+2\bar{R})}} \cdot k \cdot \ln\left(\frac{D}{d}\right) \quad 2.5.4$$

$$P_{\text{max}} = \pi \cdot d \cdot t \cdot \frac{\sqrt{(1+\bar{R})^2}}{1+2\bar{R}} \cdot k \quad 2.5.5$$

Equating equation 2.5.4 and 2.5.5 then gives

$$\ln\left(\frac{D}{d}\right)_{\max} = \frac{1}{1+\eta} \frac{\sqrt{1+\bar{R}}}{\sqrt{2}} \quad 2.5.6$$

Rigorously the analysis applies to what might be best termed pure radial drawing with no bending and unbending around tool radii, in flat-bottom cup drawing of ductile metals. This restriction, as indicated by Hosford and Backofen<sup>(23)</sup> does not seriously limit the implication of the analysis. Work hardening was also neglected.

Whiteley<sup>(29)</sup> demonstrated experimentally the dependence of  $(D/d)$  on  $\bar{R}$  for a series of material with average of  $\bar{R}$  value from 0.58 to 1.62. This range was extended by Lloyd<sup>(32)</sup> to  $\bar{R} = 3.8$  for titanium

and reported a remarkably high D/d of 2.75. Wright<sup>(33)</sup> and Lilet<sup>(34)</sup> have demonstrated that slightly better correlation with deep drawing tests may be obtained by using  $R_{\min}$  instead of  $R_{\text{average}}$ . Atkinson and Maclean<sup>(35)</sup> found that the drawability of low carbon steels correlated more closely with R average than with maximum or minimum values.

Hosford and Backofen<sup>(23)</sup> have also studied the relationship between drawability and R value by applying the Hill's theory<sup>(28)</sup> to sheet materials assuming rotational symmetry about the sheet normal and in the absence of the Bauschinger effect. Hill's yield criterion then becomes:

$$(\sigma_y - \sigma_z)^2 + (\sigma_z - \sigma_x)^2 + \bar{R}(\sigma_x - \sigma_y)^2 = 2Z^2 \quad 2.5.7$$

where  $Z = X \sqrt{\frac{1+\bar{R}}{2}}$  2.5.8

and  $d\epsilon_x : d\epsilon_y : d\epsilon_z = (\bar{R}+1)\sigma_x - \sigma_y - \sigma_z : (\bar{R}+1)\sigma_y - \sigma_x - \sigma_z : 2\sigma_z - \sigma_x - \sigma_y$  2.5.9

where x and y are the directions of principal stress in the plane of the sheet and Z is the sheet normal. X, Y and Z are the uniaxial yield stresses in the x, y and z directions. R is the R value.

For loading in the plane of the sheet  $\sigma_z = 0$ , and equations 2.5.7 and 2.5.9 become

$$\sigma_x^2 + \sigma_y^2 - \sigma_x \sigma_y \left(\frac{2\bar{R}}{\bar{R}+1}\right) = X^2 \quad 2.5.10$$

and

$$d\epsilon_x : d\epsilon_y : d\epsilon_z = (\bar{R}+1)\sigma_x - \sigma_y : (\bar{R}+1)\sigma_y - \sigma_x : -(\sigma_x + \sigma_y) \quad 2.5.11$$

putting  $\alpha = \frac{\sigma_y}{\sigma_x}$  in equation 2.5.10 therefore,

$$\sigma_x^2 [1 + \alpha^2 - \alpha \left(\frac{2\bar{R}}{\bar{R}+1}\right)] = X^2 \quad 2.5.12$$

By varying the values of  $R$  and  $\alpha$  in the yield condition (equation 2.5.12) a figure representing the anisotropy yield loci is drawn as in figure 2.5.1. In this figure  $R = 1, 2, 3, 5$ ,  $\alpha = 1, \frac{R}{R+1}$  and  $-1$  and the intersection of the loading path (dashed line) with the appropriate locus represent the beginning of yielding and identifies the stress ratio for a state of plane strain.

In deep drawing of a flat-bottomed cup, there are two regions of special importance. These are the flange where deformation occurs and force requirement originates, and the cup wall which must support the necessary forces without tearing. Therefore, for maximum drawability in ductile metals, the wall strength should be as high as possible relative to that of the flange, so that the largest reduction can be accomplished before wall failure by necking. The drawing limit must be governed by and increased with the ratio  $\beta$  of the two planes strengths.

$$B = \frac{\sigma_x(\text{wall}, d\epsilon_y = 0)}{\sigma_y(\text{flange } d\epsilon_z = 0)} \quad 2.5.13$$

Reference to the anisotropy yield loci figure 2.5.1 indicates that although both the flange and wall yield under conditions of plane strains, the axis of zero strain is different as in figure 2.5.2. Yielding in the cup wall occurs under plane strain of  $d\epsilon_y = 0$  and stress ratio  $\alpha = \frac{R}{R+1}$ . Therefore, the wall strength increases for  $R > 1$  i.e. increases with  $R$  value. In the cup flange, where the plane strain components  $d\epsilon_z = 0$ , some softening is the result of  $R > 1$  i.e. the flange strength decreases with  $R$  value. Therefore, the deep drawability of a strip increases with  $R$  value.

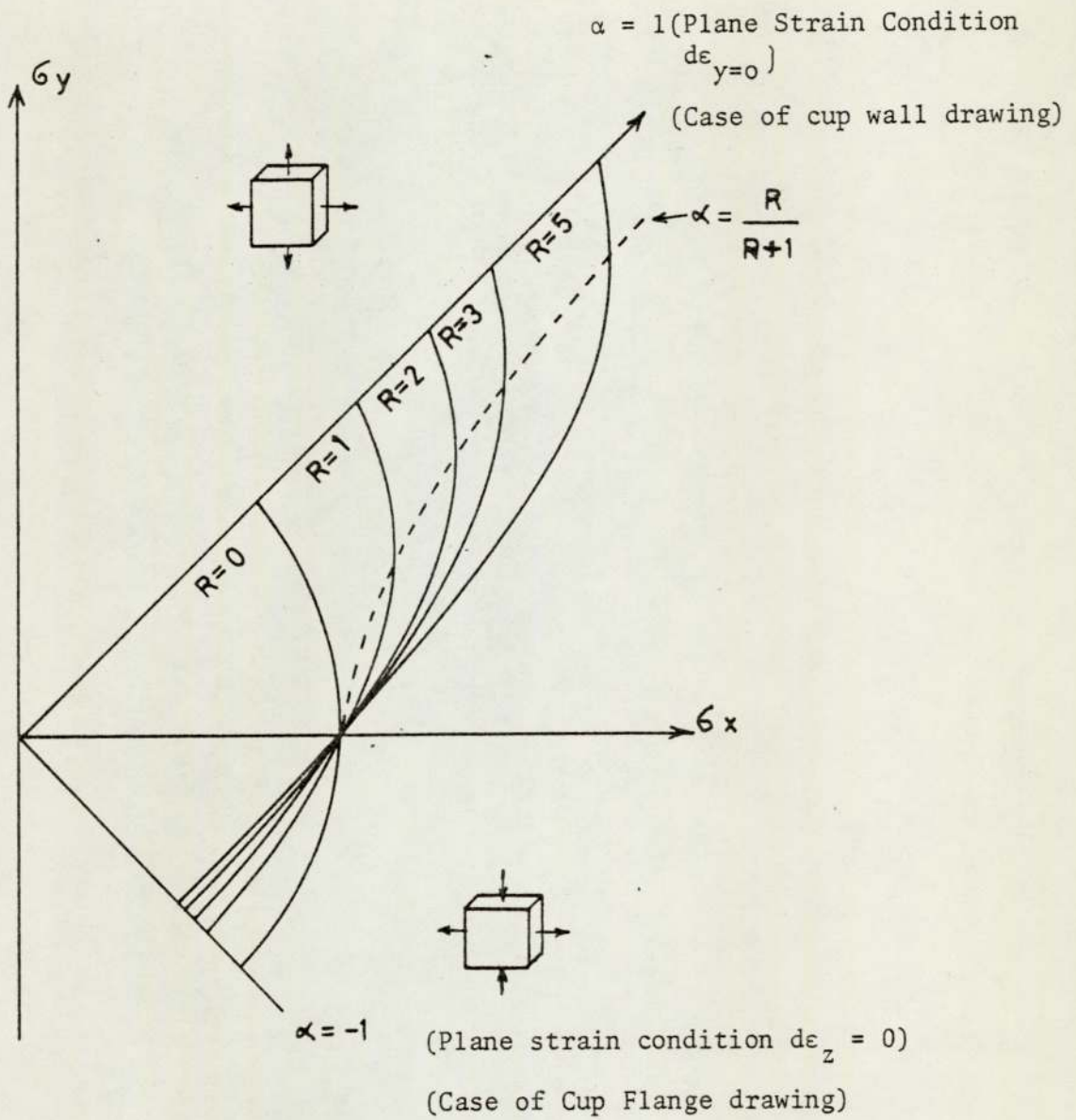


Fig. 2.5.1. Shows the plane stress yield loci for sheets with textures that are rotationally symmetric about the thickness direction  $z$ . Values of  $R$  indicate the degree of anisotropy. The stress ratio,  $\alpha = \frac{\sigma_y}{\sigma_x}$  corresponding to various loading conditions<sup>(23)</sup>.

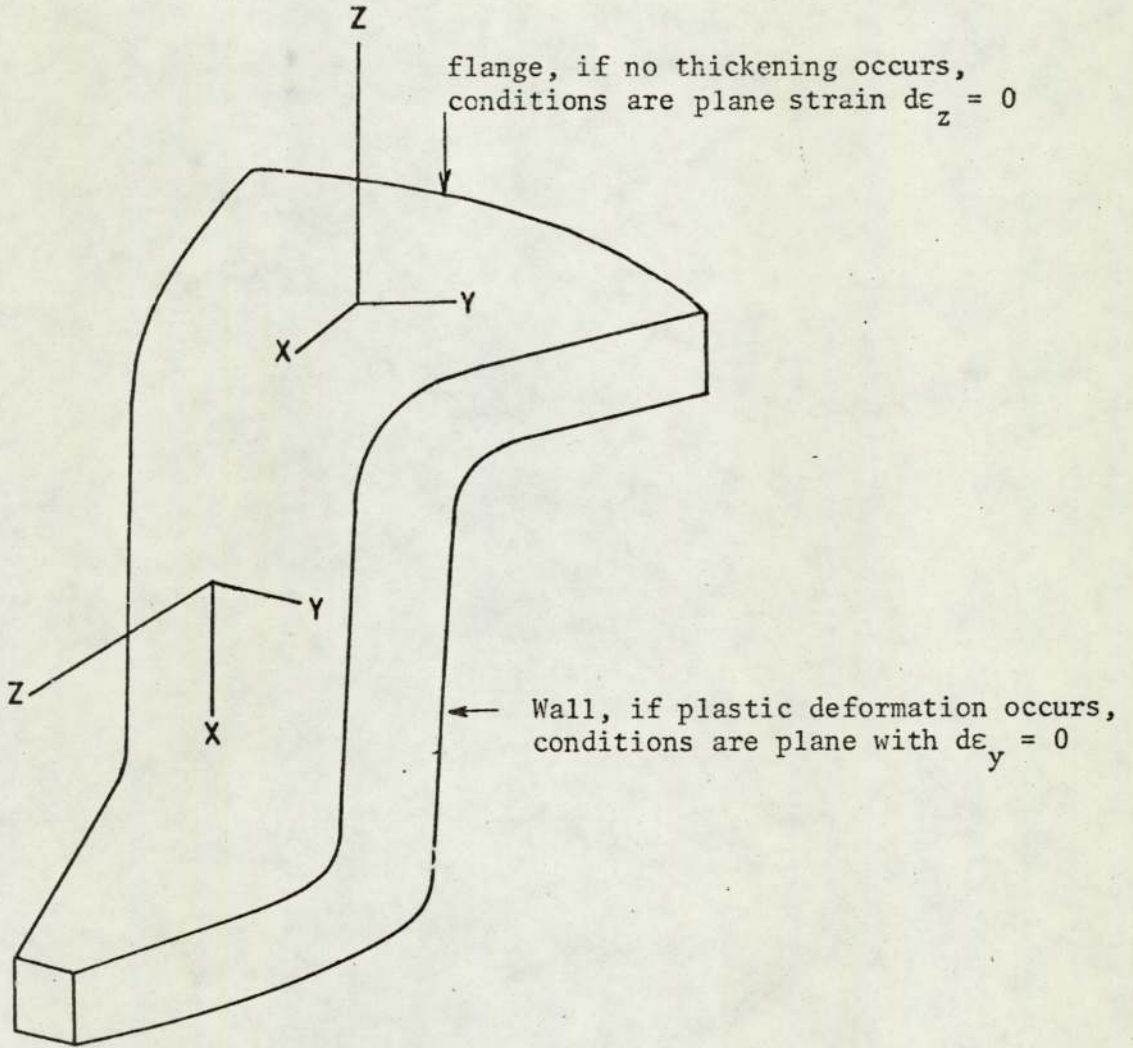


Fig. 2.5.2 shows the plane strain axes in the flange and the wall of a flat bottomed cup. The shape change in the flange is often nearly one of the plane strain,  $d\epsilon_z = 0$ . In the wall only plane strain flow,  $d\epsilon_y = 0$ , can occur because the punch prevents a decrease of wall circumference<sup>(23)</sup>.

## 2.6 EFFECTS OF THE PROCESSING FACTORS UPON TEXTURE AND R VALUE OF RIMMED STEEL STRIP

Rimmed steel strip is manufactured by casting refined steel into ingots of rectangular cross section where solidification occurs producing the characteristic rim and core ingot zones. The zones contribute to rimmed steel's unique properties primarily as a consequence of almost pure iron-inclusion-free-rim zone. The slab ingot is reheated and hot rolled, usually above the  $A_3$  temperature, firstly in a reversing slab mill and then in a tandem mill. The hot band at  $950^\circ\text{C}$  is water sprayed and subsequently coiled at a temperature between  $700^\circ\text{C}$  and  $600^\circ\text{C}$ . The coiled hot band is air cooled and pickled to remove scale. The steel sheet is then cold rolled using a 3 stand tandem mill with 500 mm diameter. The rimmed steel strip is then annealed to render the sheet ductile. The strip is finally temper rolled to improve the surface finish.

Properties of the final rimmed steel strip should depend upon the previous production cycle in addition to the chemical composition of the material. Effect of the latter is reviewed by Rosenstock, Kläner and Schmidtman<sup>(36)</sup> and it is not within the scope of the present review. However, the effects of hot rolling, cold rolling and annealing upon R value and texture of the final strip will be only considered in this review.

### 2.6.1 The effect of hot rolling

Angele and McGarity<sup>(37)</sup> were the first to report that too high hot rolling temperature (i.e.  $>975^\circ$ ) resulted in an over large grain size and hence orange peeling in the fabricated components.

On the other hand, too low hot rolling temperature (i.e.  $<900^{\circ}\text{C}$ ) can lead to poor drawability as a result of too small grain size and unsuitable texture. Hot rolling of rimmed steel is usually carried out at  $950^{\circ}\text{C}$  to produce the suitable grain size necessary to balance the properties of ductility and resistance to orange peeling. Hoff and Masing<sup>(38)</sup> recommended that the finishing temperature for low carbon steel should be somewhat just below the  $A_3$  temperature. More recently<sup>(39)</sup> it was shown that at a hot rolling finishing temperature of  $875^{\circ}\text{C}$ , which is about  $30^{\circ}\text{C}$  above the  $A_{r3}$  of rimmed steel, and spray exit temperatures between  $500^{\circ}\text{C}$  and  $600^{\circ}\text{C}$ , the hot band grain size was a minimum. This was increased when hot rolling was finished at  $775^{\circ}\text{C}$ . Rimmed steel slab hot rolled during dynamic recrystallisation, followed by spray quenching was found<sup>(39)</sup> to contain carbides mainly of the cementite form. On the other hand, hot rolling, when static recrystallisation occurred, resulted in carbides mainly of the form of degenerate pearlite. It was also reported<sup>(39)</sup> that high R value is associated with an optimum hot finishing temperature and low spray exit temperature.

Richards and Ormay<sup>(40)</sup> classified the hot rolling texture of low carbon steel into two general types. Either a relatively weak texture varies slightly from surface to centre when hot rolling above the  $A_3$  temperature, or a relatively strong texture varies considerably from surface to centre when hot rolling below the  $A_3$  temperature. They further stated that the hot rolling texture is not beneficial as the segregation is not favourable for high R values. Nagashima et al<sup>(41)</sup> hot rolled two rimmed steel bands in two different ways, in the first, hot rolling was finished at  $830^{\circ}\text{C}$  and the hot band was then coiled at

620°C. In the second, the finishing and coiling temperatures were 805°C and 550°C respectively. The surface texture in both specimens were essentially the same and was described as  $\{110\}\langle UVW \rangle$  plus  $\{112\}\langle 111 \rangle$ . The centre texture varied from one specimen to the other being of the type  $\{100\}\langle 110 \rangle$  with spread towards the  $\{112\}\langle 110 \rangle$  in the case of the first specimen. In the second specimen, the centre texture was derived from the first texture as a reinforcement of the  $\{100\}\langle 110 \rangle$  component. The centre texture was related to the surface texture by 30° rotation about the transverse direction. This rotation was reported by the same authors<sup>(41)</sup> not to be sufficient to rationalise perfectly the relationship between the two textures. This was attributed to a recrystallisation mechanism operating during hot rolling.

Jones and Walker<sup>(42)</sup> indicated that in the surface texture of specimens that had and had not undergone recrystallisation during hot rolling was identical and was described to be of the  $\{110\}\langle 112 \rangle$  type. On the other hand, the centre texture of the two specimens were different. The main texture components in the recrystallised specimen were  $(100)[011]$  with a weak  $(111)[\bar{1}\bar{1}2]$  and  $(112)[\bar{1}10]$  components, while that of the unrecrystallised specimen was  $(112)[\bar{1}10]$  only. These results are in good agreement with a previous work<sup>(43)</sup> in which it was shown that, during hot rolling, only the mid-plane thickness region of the sample is deformed under rolling condition that is not influenced by surface friction effect.

### 2.6.2 The effect of cold rolling

The room temperature cold rolling texture of rimmed steel strip has been commonly described in terms of two sets of end orientations. The first includes  $\{100\}\langle 110\rangle$ ,  $\{111\}\langle 110\rangle$ ,  $\{113\}\langle 110\rangle$  and  $\{112\}\langle 110\rangle$  orientations with the  $\langle 110\rangle$  directions parallel to the rolling direction. The second end orientation is the  $\{111\}\langle 112\rangle$  texture component with the  $\{111\}$  plane parallel to the rolling plane<sup>(44)</sup>. In some cases the  $\{111\}$  texture has been observed as a minor component<sup>(45)</sup>. Haessner and Weik<sup>(46)</sup> described the cold rolling texture by a fibre texture distributed about the  $\langle 110\rangle$  axis lying  $35^\circ$  from the sheet normal on the rolling direction radius in a pole figure. The cold rolling texture of rimmed steel was also described by the  $\{100\}\langle 110\rangle$  and the  $\{112\}\langle 110\rangle$  component, but the  $\{111\}\langle 110\rangle$  component did not appear frequently while the  $\{111\}\langle 112\rangle$  was recorded<sup>(47)</sup>. Texture of rimmed steel strip was also described in terms of tension and compression texture<sup>(48)</sup>.  $\langle 110\rangle$  texture with spread towards the  $\langle 311\rangle$  component was predicted for tension texture and a duplex  $\{100\} + \{111\}$  texture with the  $\{111\}$  predominating as a compression texture.

Since plastic strains generated during rolling are felt differently at different depths through the thickness of the sheet<sup>(49)</sup> the texture developed should vary from surface to centre. Texture developed during cold rolling is therefore dependent upon the rolling variables such as lubrication, rolling draughts and total rolling reduction. The effect of lubrication upon texture was demonstrated<sup>(50)</sup> by processing two steel strips in two different ways. Steel A was rolled with palm oil lubrication and heavy reductions at each pass.

The magnitude of the rolling draughts was not indicated but it was stated that 75% reduction was achieved in a total of five passes. This represents an average draught of approximately 0.011 in/p. Steel B was rolled without lubrication and light reductions were given per pass. Inverse pole density indicated that steel A exhibited an homogeneous texture while steel B displayed a pronounced texture segregation. Stickels<sup>(51)</sup> carried out an almost parallel study but sample B was lubricated instead of sample A. This time sample A gave the composite texture, which, therefore, resulted from rolling under severe friction condition. The surface textures were of the shear type<sup>(52,53)</sup>, containing the components  $\{112\}\langle 111\rangle$ ,  $\{110\}\langle 001\rangle$ ,  $\{110\}\langle 112\rangle$  and  $\{110\}\langle 111\rangle$ . The centre texture was related to the surface texture by 90° rotation about the transverse axis. Held and Stickels<sup>(50,51)</sup> had, by dry rolling, created severe friction conditions, apparently induced shear type strain in the surface of their metals.

Dillamore and Roberts<sup>(4)</sup> indicated that rolling draughts were also important parameters as heavy draughts contribute to the increase of the friction forces. Hellewell<sup>(2)</sup> has shown that at certain total rolling reduction, the mid plane texture was independent of the magnitude of the rolling draughts and was typical of b.c.c. steel texture, namely, two partial  $\langle 110\rangle$  RD and  $\{111\}$  RP fibre textures. The main difference in texture was observed in the surface layer when rolling with either dry or lubricated rolls and with draughts classified by light, medium and heavy respectively. Rolling with the heaviest possible draughts and rolls dusted with magnesium had a different effect upon the surface texture. Rolling with light draughts developed type I texture, a predominantly  $\langle 110\rangle$  RD texture, which changed

progressively towards the common medial plane texture. With heavy draughts, type III texture was developed, which was a dominant  $\{111\}$  RP. An intermediate texture, type II was developed with medium draughts. Type IV texture developed by rolling with dusted magnesia was described by a  $\{110\}\langle 112\rangle$  rolling texture.

The development of texture with increasingly total rolling reduction was described by Haessner and Weik<sup>(46)</sup>, in terms of three components. Starting from a textureless material, after 30% deformation, two components were present. Component A represents  $\{100\}\langle 011\rangle$  orientation and B is a fibre component with a  $\langle 110\rangle$  fibre axis  $35^\circ$  from the sheet normal on the rolling direction radius of the pole figure. B was much stronger than A. Above 60% deformation, a third component C was found, which was described as a limited fibre texture of increasing spread around the rolling direction as axis. Moller and Stablein<sup>(54)</sup> conducted a similar study to that of Haessner and Weik<sup>(46)</sup>. Texture was also described in terms of three components. Component  $W_1$  is equivalent to C<sup>(46)</sup>,  $W_2$  is a fibre component with a  $\langle 111\rangle$  pole parallel to the sheet normal, and  $W_3$  is a complete fibre component with a  $\langle 100\rangle$  fibre axis parallel to the sheet normal and would include A. Starting from an almost random material, these components were present at 48, 73 and 92% reduction. Spread in the component  $W_1$  increased with increasing the total rolling reduction.

Bennewitz<sup>(55)</sup> followed the effect of increasing the total rolling reduction upon texture developed in two sheets of low and 3% silicon steels exhibiting a similar starting texture described by a  $\{100\}\langle 011\rangle$  at the sheet mid plane and a proportion of  $\{110\}\langle 001\rangle$  orientation at

the sheet surface. It was found that the  $\{100\}\langle 011\rangle$  orientation initially rotated about the rolling direction to  $\{112\}\langle 110\rangle$  while the  $\{110\}\langle 001\rangle$  material rotated about the transverse direction to  $\{554\}\langle 225\rangle$  which is close to  $\{111\}\langle 112\rangle$  orientation and subsequently rotated to  $\{112\}\langle 110\rangle$ . The  $\{112\}\langle 110\rangle$  component in either of the above cases subsequently rotated about the rolling direction to  $\{001\}\langle 110\rangle$  or  $\{111\}\langle 110\rangle$ . The breaking up of the  $\{112\}\langle 110\rangle$  orientation increased with increasing the total rolling reduction. The rolling texture of steel at 60% reduction was described in terms of two fibre textures, in fibre texture A, the texture components  $\{554\}\langle 225\rangle$  and  $\{112\}\langle 110\rangle$  were predominant while fibre texture B which contained the  $\{001\}\langle 110\rangle$  and  $\{111\}\langle 110\rangle$  as a minor texture. With further reduction fibre texture B became more prominent until after 95% cold reduction, the common orientation  $\{112\}\langle 110\rangle$  became most intense. Subsequent rolling caused rotation to the stable end orientation  $\{113\}\langle 110\rangle$ . Fibre texture A was close to that embodied in the B texture component of Haessner and Weik<sup>(46)</sup> and the  $W_2$  component previously described by Möller and Stablein<sup>(54)</sup>. The rotation of the fibre texture components A and B described by Bennewitz<sup>(55)</sup> is schematically represented on one quadrant of a (110) pole figure shown in figure 2.6.2.1.

The components  $\{111\}\langle 110\rangle$  and  $\{100\}\langle 110\rangle$  of fibre texture B are in agreement with the predictions of Calnan and Clews<sup>(15)</sup>, although fibre texture A is not adequately accounted for. The development and subsequent breaking up of the  $\{112\}\langle 110\rangle$  orientation was also suggested by Dillamore and Roberts<sup>(16)</sup>. Takechi et al.<sup>(41)</sup>, considered it impossible to distinguish between the  $\{111\}\langle 112\rangle$  and  $\{554\}\langle 225\rangle$  which are only  $6^\circ$  apart, because of the spread in rolling textures. Also, pole density data<sup>(56)</sup> does not lead to the identical description of

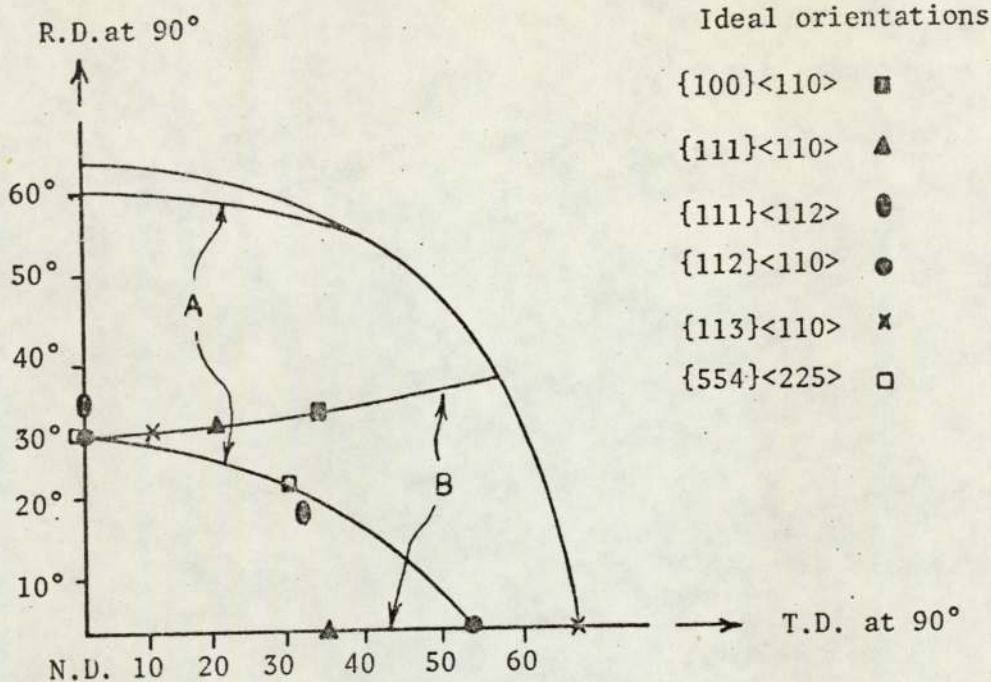


Fig. 2.6.2.1. One quadrant of (110) pole figure showing locus of (110) poles for ideal fibre textures A and B<sup>(55)</sup>.

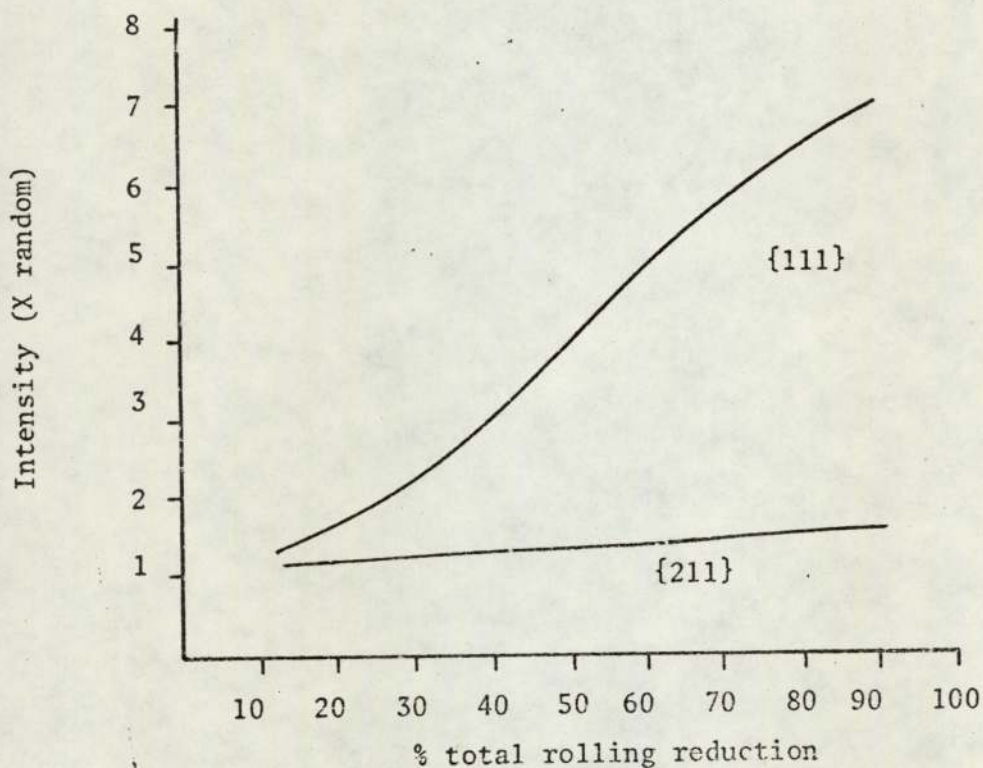


Fig. 2.6.2.2. The effect of total rolling reduction prior to annealing upon the {111} and {211} texture of the as cold rolled low carbon steel strip<sup>(56)</sup>.

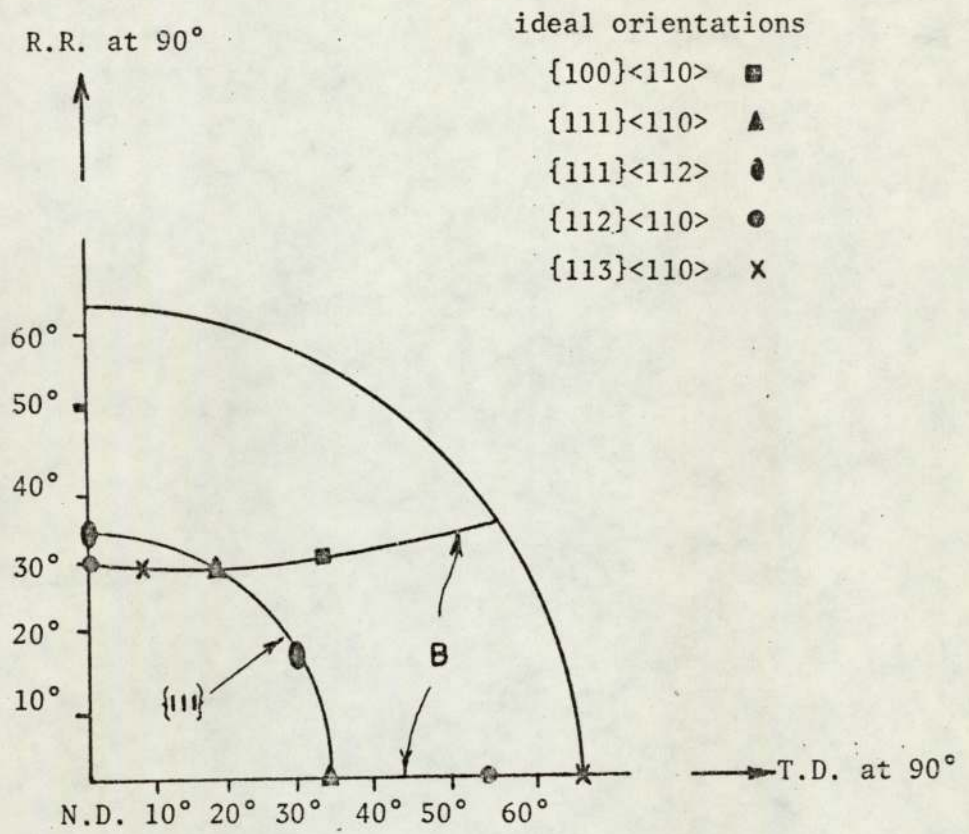


Fig. 2.6.2.3. One quadrant of (110) pole figure showing locus poles of {110} poles for ideal fibre texture B with {111} planes parallel to sheet plane<sup>(40)</sup>.

rolling texture as outlined above<sup>(55)</sup>. Fig.2.6.2.2<sup>(56)</sup> illustrates the change in density of crystal planes parallel to the plane of the sheet with increasing the cold reduction. The {111} planes increased rapidly with cold reduction, whereas {112} planes were constant over that range, and only of approximately 1.5 random intensity. This conflicts with the proposed stable end orientation, at least at 95% reduction, of the {112}<110> texture as had previously been deduced from the examination of pole figures<sup>(55)</sup>. Fibre texture B was retained, but fibre texture A was replaced by a texture with {111} planes parallel to the sheet plane as shown in figure 2.6.2.3.<sup>(40)</sup> In this case, the orientation {111}<110> was common to both textures. The similarity between figure 2.6.2.1 and figure 2.6.2.3. is apparent.

### 2.6.3 The effect of subcritical isothermal annealing

Whitely and Wise<sup>(58)</sup>, examined the effect of cold rolling reduction upon the  $\bar{R}$  values of annealed low carbon steel sheets. The outcome of their study was that R value increased with increasing the rolling reduction to  $\bar{R}_{\max}$  at 70% rolling reduction and thereafter decreased with further increase in rolling reduction as shown in figure 2.6.3.1. The recrystallisation textures were also measured over a range of total rolling reduction. This revealed the coincidence of a minimum {100} and a maximum {111} orientation at  $R_{\max}$  as shown in figure 2.6.3.2. Atkinson et al.<sup>(59)</sup> observed also  $\bar{R}_{\max}$  at 70%, but were unable to confirm any systematic correlation between the total rolling reduction and the {111} and {100} texture intensity. They further indicated that intensity of {100} poles was less than random

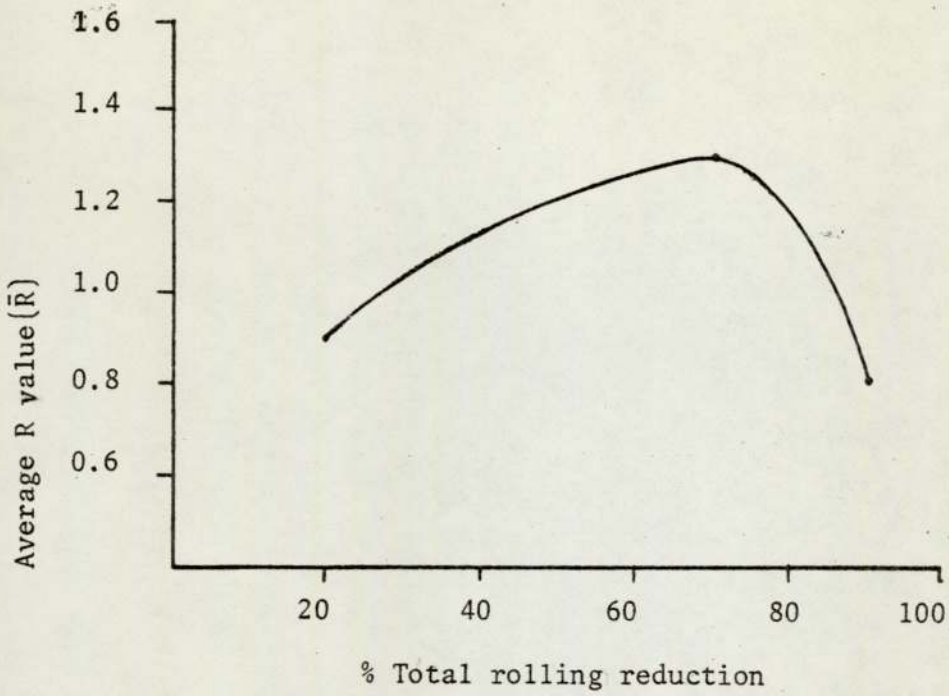


Fig. 2.6.3.1. Influence of percentage total rolling reduction, upon  $\bar{R}$  value of the annealed aluminium killed low carbon steel strip<sup>(58)</sup>.

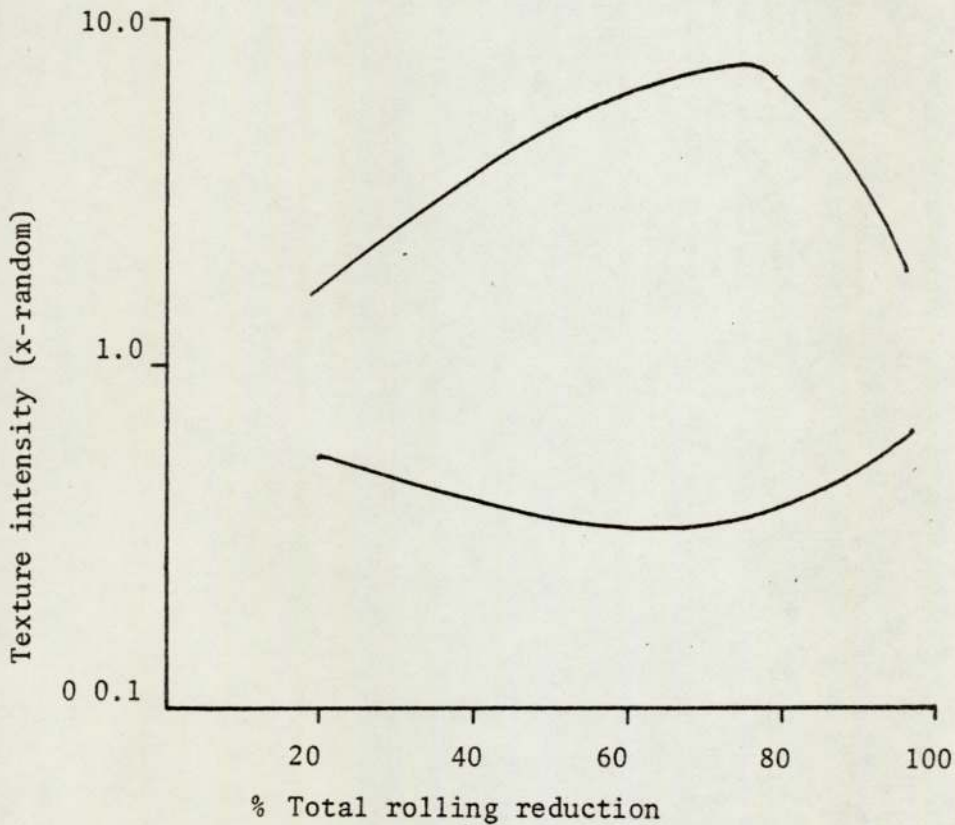


Fig. 2.6.3.2. Influence of the total rolling reduction upon the {111} and {100} texture components of the annealed aluminium killed low carbon steel strip<sup>(58)</sup>.

and questioned whether the {100} planes are capable of reducing  $\bar{R}$  value after 70% rolling reduction. Held<sup>(50)</sup> was able to change the rolling reduction at which  $\bar{R}_{\max}$  occurred by altering the cold rolling conditions so as to produce texture segregation. A "skin zone texture" developed at moderate rolling reductions and had a very high {111}/{100} relative intensity ratio. The texture ratio was intensified and increased in relative thickness to the control zone with increased cold reduction. As the reduction coincides with  $\bar{R}_{\max}$ , corresponding to 40% in this case, the skin zone dominates and results in the subsequent reduction in  $\bar{R}$  value. Furthermore, steel processed to give a homogeneous texture did not exhibit a distinctive  $\bar{R}_{\max}$  up to 88% cold reduction.

A more recent study has been performed<sup>(2)</sup> on the effect of cold rolling variables upon texture and R value of rimmed steel. It was shown that the recrystallisation texture may be described as a partial fibre texture containing the {111}RP + <110> RD components. The through-thickness texture segregation observed after cold rolling was reported<sup>(2)</sup> to be retained after annealing. The relative proportions of texture components, the degree of texture segregation and hence R value were shown to be dependent upon lubrication, rolling draughts and total rolling reduction. For a constant total rolling reduction texture segregation was minimum and R value was higher when rolling with heavy draughts and oil lubrication. Also, the total cold rolling reduction corresponding to  $\bar{R}_{\max}$  increased when rolling with lubricated rolls and heavy draughts. Analysis of texture using (110) pole figures<sup>(2)</sup> indicated that {111} RP partial fibre texture promotes high R value, whereas <110> RD partial fibre texture results in relatively low R values.  $\bar{R}_{\max}$  was, therefore, associated with a balance between {111} RP and <110> RD textures. This balance is disturbed by texture segregation such that <110> RD texture predominates at variable total rolling reductions.

Mathur and Backofen<sup>(76)</sup> studied the effect of the deformation geometry as defined by the ratio between the height to length of the deformation zone or  $\Delta$ , upon the cold rolling and recrystallization textures of killed steel strip. It was found that for  $\Delta < 1$  texture developed was uniform through the thickness of the strip over a wide range of total rolling reduction. An inversion in intensity of the  $\{111\}$  rolling plane occurred after 98% total rolling reduction. The inversion was attributed to the formation of shear bands as an outgrowth of diminished strain hardening capacity. The formation of shear bands at the edge of the strip, where the hydrostatic part of the roll gap stress is substantially reduced, result in shear cracks at the edge. Edge cracks are therefore a symptom of localised flow which may modify a previously stabilised texture.

As  $\Delta$  became  $> 1$ , texture gradients appeared at the surface. Since the strain-hardening rate drops down at the surface, texture inversion is most apparent at the surface. On increasing  $\Delta$ , the imposed strain for inversion decreased and the inversion occurred at lower total rolling reduction. Intensity of the  $\{111\}$  and  $\{100\}$  components decreased and increased respectively when  $\Delta$  was increased.

Normally, the short heat treatment of the isothermal annealing results in a product that is too hard and insufficiently ductile for forming operations, mainly because the fast heating rate results in a finer grain size than slow heating<sup>(60)</sup>. In work published by Kuznetsov<sup>(61)</sup> and Keller<sup>(62)</sup>, claims were made that high heating rate

followed by fast cooling can give soft products free from quench ageing. According to Mohri<sup>(63)</sup> an effective soaking time of about 15 seconds is sufficient for almost complete recrystallisation. The effective soaking time was defined as the total time a steel specimen is above the lowest temperature at which the first strain free grains appear.

Garber<sup>(64)</sup> reasoned that the greatest softening could be made by quenching from the annealing temperature and subjecting the material to a subsequent age-softening or over-ageing treatment in a separate operation. An annealing cycle including heating rapidly to 700°C immediately quenching to 300°C and over-ageing for 30 minutes was, therefore, recommended. On cooling rapidly from 700°C to the room temperature the ferrite becomes super-saturated with carbon. After quenching, the carbon atoms came out of solution in clusters or sub-precipitates, i.e. groups of carbon atoms concentrating in local regions, distorting the  $\alpha$ Fe lattice and producing material of increased hardness. However, when higher ageing temperature was employed, the carbon atoms came out of solution as discrete precipitates of carbide, or deposited on existing carbides without the distortion of the  $\alpha$ Fe lattice and the structure became relatively softer. Dewsnap<sup>(60)</sup> studying the effect of the Garber's annealing cycle<sup>(64)</sup> upon R value of rimmed steel indicated that R values remained constant up to 50% reduction. When the total reduction was then increased the trend was towards a steady increase in R values up to 80% total rolling reduction where a sharp drop in R value occurred. The results contrast with the work of Whitely and Wise<sup>(58)</sup> on batch annealed specimens. Hellewell<sup>(2)</sup> reported that the total rolling reduction corresponding to  $R_{\max}$  was increased when intragranular cementite was

precipitated during an overageing treatment at 300°C. R values were also improved.

Haessner and Weik<sup>(46)</sup> studied the recrystallisation textures in rolled carbonyl iron. They adjusted the recrystallisation temperature to compensate for the degree of cold reduction so that recrystallisation was complete in all cases in one to two hours. After annealing for a few minutes, the rolling texture sharpened then diminished in intensity as the annealing time increased. Stickels<sup>(65)</sup> studied the textural changes resulting when 90% cold rolled electrolytic iron specimens were isothermally annealed at 700°C for 5 sec to 68 hrs then rapidly cooled. It was observed that primary recrystallisation was complete in 5 secs and normal grain growth occurred up to 16 hrs followed by abnormal recrystallisation (secondary recrystallisation) between 16 hrs and 68 hrs. The recrystallisation texture was classified as follows:

1. At 5 secs, a duplex fibre texture was evident. The dominant fibre texture was that with a  $\langle 110 \rangle$  fibre axis in the rolling direction and planes  $\{001\}$ ,  $\{112\}$  and  $\{111\}$  parallel to the rolling plane. The second fibre texture was described by  $\langle 111 \rangle$  fibre axis parallel to the rolling plane and included the orientations  $\{111\}\langle 110 \rangle$  and  $\{111\}\langle 112 \rangle$
2. From 5 secs through to 10 mins the special texture near  $\{322\}\langle 226 \rangle$  was formed by elimination of textural components near  $\{112\}\langle 110 \rangle$ .
3. After 4 hrs annealing the texture began to disappear reverting back to a texture consisting primarily of  $\{111\}\langle 110 \rangle$  and  $\{112\}\langle 110 \rangle$  components.
4. After 16 hrs annealing, texture was mainly  $\{111\}\langle 110 \rangle$  and  $\{112\}\langle 110 \rangle$ .

### 3. SCOPE OF THE PRESENT STUDY

A critical look at the literature indicates that there is still need for a closer study of the factors influencing the deep drawability of rimmed steel in order to overcome specific inadequacies in the quality of the finally annealed strip. Drawability is controlled by a degree of plastic anisotropy which is related to texture developed during the processing cycle. Since the annealing texture is related to the cold rolling texture, texture is mainly established during cold rolling. The present study was therefore, designed to study the the effect of cold rolling variables upon the texture of rimmed steel strip with a view to improving its deep drawability.

The experimental work was performed on an industrially processed rimmed steel coil (0.25 in thick and 2 ins wide). It had been hot rolled on a 3 stand tandem mill finishing at 900°C. It was water sprayed,coiled, then air cooled. It was then cold rolled from 0.324 in to 0.25 in, sub-critically annealed at 700°C for 3 hrs then furnace cooled. The chemical composition was 0.056%C, 0.039%Mn, 0.035%S, 0.01%P and 0.018%Al. Narrow coils had to be used because the pendulum mill, which is one of two mills used in the present study for cold rolling, is only suitable for cold rolling of up to 2 inch wide coils. In order to make a strict comparison between the suitability of the pendulum mill and the 2 high mill for strip production from the standpoint of texture and anisotropy the same material had to be used throughout.

The investigation was planned in four sections:

#### (1) Examination of the initial material

Texture of the initial material and its possible influence upon the cold rolling texture was examined. General information with regard to the micro-structure and grain size was provided in order to ascertain that the micro-structure is in agreement with the hot rolling condition.

(2) Examination of the cold rolled strips

The object of this section was firstly, to study the effect of seven rolling schedules upon R value and texture. Secondly, to study the effect of increasing the total rolling reduction upon texture developed by each of the seven rolling schedules.

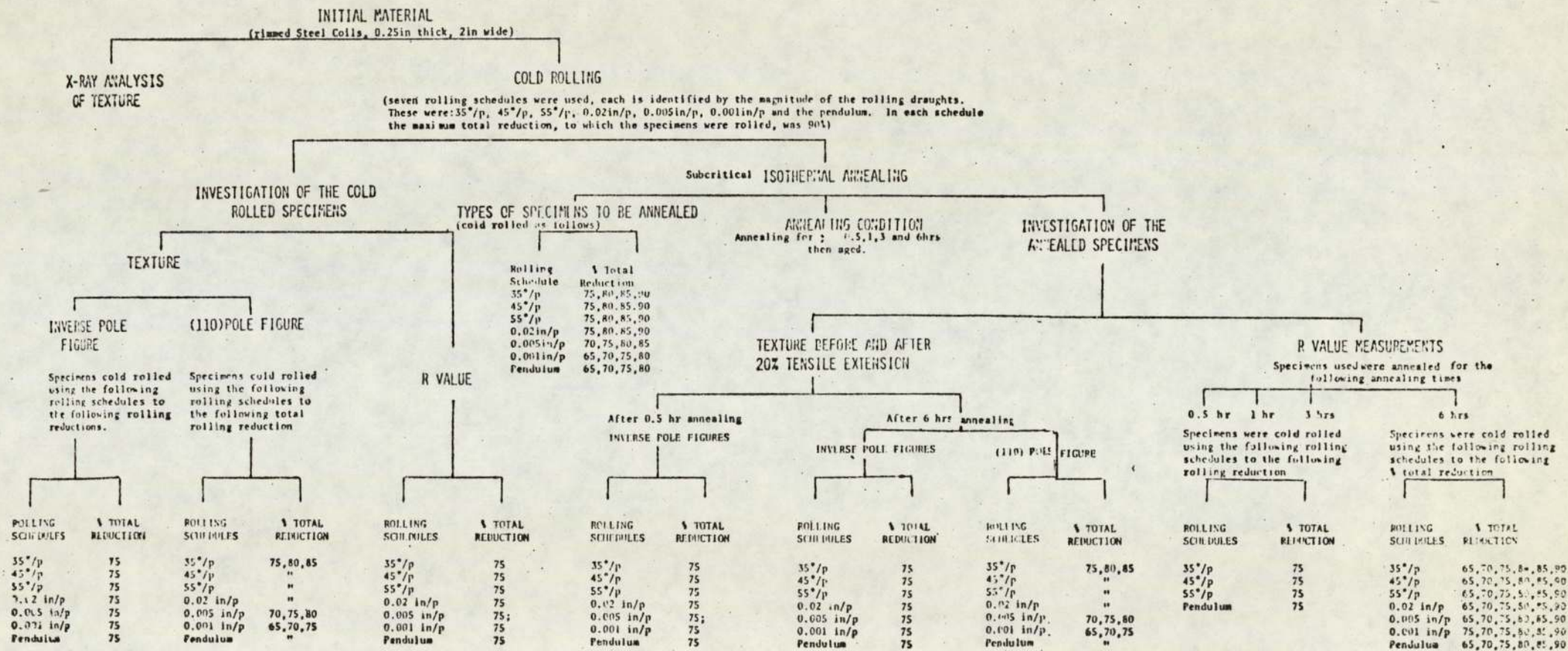
(3) Examination of the annealed strips

R value and texture were examined after annealing for different periods in order to establish the effect of annealing time. The effect of increasing the total rolling reduction upon R value and texture was examined in order to explain clearly the sharp drop in R value after heavy reductions in terms of preferred orientation.

(4) Examination of crystal reorientation after tensile strain

Texture was examined also after 20% tensile extension to monitor the modification of rimmed steel recrystallisation texture by tensile strain. This section was designed to explain the probable difference in R values of specimens processed in accordance with the seven rolling schedules.

#### 4. EXPERIMENTAL PROCEDURE



#### 4.1 INTRODUCTION

The experimental procedure of the present study included cold rolling of the initial material, annealing of the cold rolled strips, measurements of R value and examination of texture. Cold rolling was performed on the 2 high and pendulum mills. During cold rolling using the first mill, six rolling schedules were applied, either to keep a constant shear plane, or to keep a constant roll gap from one pass to the next. Details of those schedules together with the pendulum schedule are given in this section. Samples from the cold rolled strips were taken for R values and texture measurements. Corresponding samples were also taken for annealing. Annealing was carried out isothermally for different periods. R value and texture were then measured. Finally, textures of the tensile test pieces were examined after R value measurements. A full account of the experimental procedure is illustrated in figure 4.1.

#### 4.2 COLD ROLLING OF THE INITIAL MATERIAL

Seven sets of samples, cut from the initial rimmed steel coils, were selected for cold rolling at room temperature. Each set of samples was cold rolled according to certain rolling schedule. In the first type of rolling schedule, the roll gap varied from one pass to the next in order to keep a constant shear plane angle, and this was called the controlled geometry schedule. In the second type of rolling schedule, the roll gap was kept constant during the whole rolling operation and this was called constant roll gap schedule. The third type of rolling schedule was characterised by small strokes per pass and involved the pendulum rolling schedule.

#### 4.2.1 The Controlled geometry schedules

In these schedules, cold rolling was performed unidirectionally on a 2 high mill of 476 in roll diameter and rolls speed of 20 r.p.m. The rolls and the specimens were lubricated by mineral oil and were allowed to cool down to the room temperature after each pass. Measurements of thickness were taken after each pass to ensure that the required draught is accurately observed during rolling. The basis of calculating the rolling draughts is described as follows:

Consider a sheet bcde, figure 4.2.1 of initial thickness  $T_N$ , rolled to thickness  $T_x$ , with work roll diameter  $D$  and a reduction per pass  $R$ . If  $\frac{R}{2}$  is small then bcde may be considered a rectangular element in which the angle bcde is  $\theta$ . Therefore,

$$\text{Tan}\theta = \frac{T_x}{a} \quad 4.2.1.1$$

but

$$\begin{aligned} a^2 &= \left(\frac{1}{2}D\right)^2 - \left(\frac{1}{2}D - \frac{1}{2}R\right)^2 \\ &= \frac{D^2}{4} - \frac{D^2}{4} - \frac{R^2}{4} + \frac{DR}{2} \end{aligned}$$

Hence 
$$a^2 = \frac{DR}{2} - \frac{R^2}{4}$$

for small reduction per pass, hence

$$a^2 = \frac{DR}{2} \quad 4.2.1.2$$

Substitute from equation 4.2.1.2. into equation 4.2.1.1.

$$\text{Tan}\theta = \frac{T_x}{\frac{\sqrt{DR}}{\sqrt{2}}} \quad 4.2.1.3$$

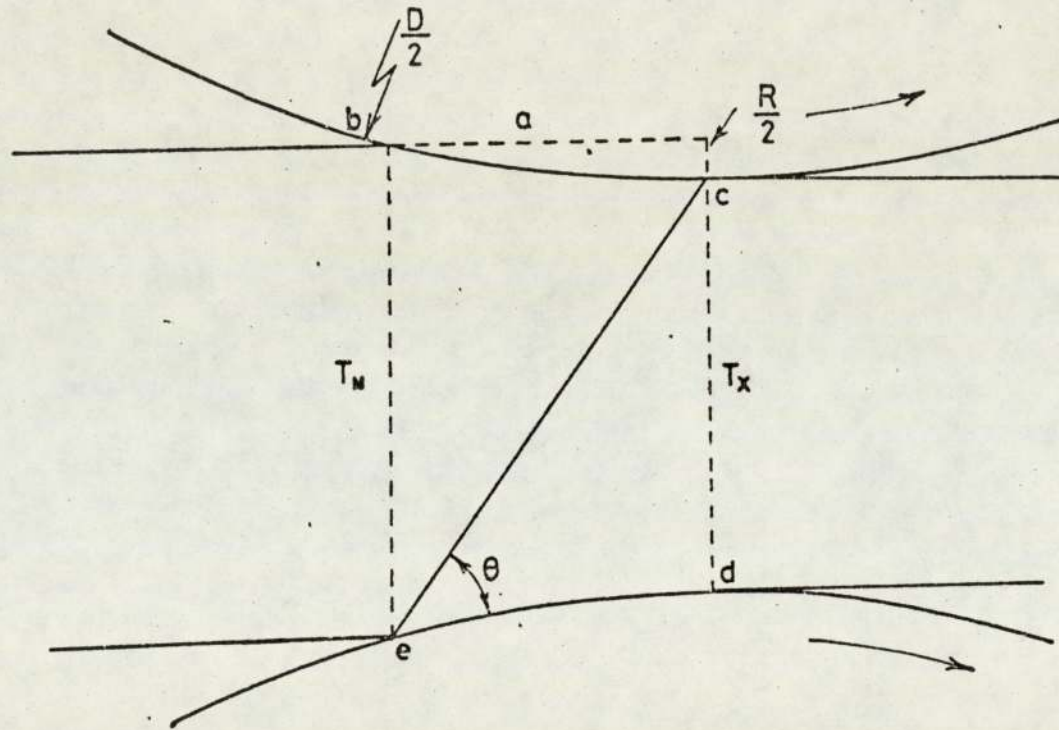


Fig. 4.2.1. Shows an element  $bcde$  being rolled to a thickness  $T_x$  with work roll diameter  $D$  and a reduction per pass  $R$ .

From Yeomans and Richards' assumption<sup>(7)</sup> for cold rolling texture formation, crystallographic slip during cold rolling is operative in each crystal on the most favourable systems over an angular range about the 45° angle to the specimen surface. Assuming rolling to be equivalent to tension in the rolling direction and compression normal to the rolling plane, the extreme limits of that angular range for the most favourably orientated planes to slip should be such that the most favourable slip directions inclined initially at 54° 44' and finally at 35° 16' to the tension axis and inversely with respect to the compression axis.

Replacing  $\theta$  in equation 4.2.1.3 by the angles 54° 44', 45° and 35° 16' resulted in three formulae corresponding to three rolling programmes. The roll gap corresponding to the three rolling schedules were calculated as follows:-

Substitute for  $\theta$  by 54° 44' in equation 4.2.1.3 therefore,

$$\tan \theta = \frac{T_x \sqrt{2}}{\sqrt{DR}} = \sqrt{2} \quad 4.2.1.4$$

The exit thickness  $T_x$  can be derived from the entry thickness  $T_N$  and the roll gap R, hence

$$T_N = T_x + R$$

Therefore,

$$T_x = T_N - R$$

4.2.1.5

From equations 4.2.1.5 and 4.2.1.4, therefore

$$R = \frac{T_N^2}{D+2T_N} \quad 4.2.1.6$$

Equation 4.2.1.6 was used for calculating the roll gap (R) corresponding to 55° shear plane angle per each pass.

Substitute for  $\theta$  by  $45^\circ$  and  $T_x$  by  $T_N$  in equation 4.2.1.3, therefore

$$R = \frac{2T_N^2}{D+4T_N} \quad 4.2.1.7$$

Equation 4.2.1.7 was used for calculating the roll gap corresponding to the  $45^\circ$  per pass rolling schedule.

Substitute for  $\theta$  by  $35^\circ 16'$  and  $T_x$  by  $T_N$  in equation 4.2.1.3 therefore,

$$R = \frac{4T_N^2}{D+8T_N} \quad 4.2.1.8$$

This equation was used to calculate the roll gap corresponding to the  $35^\circ$  per pass rolling schedule.

The draughts were calculated using a computer programme (Appendix II) the output of which is shown in Appendices III, IV and V.

The ratios between the number of passes required to reach 90% total reduction using tensional, pure and compressive rolling draughts were 4:2:1 respectively as shown in Table 4.2.1.

#### 4.2.2 The constant roll gap schedules

The same 2 high mill was used for unidirectional cold rolling under the same lubrication condition. Thickness was also measured after each pass. Three rolling schedules were used to reach total reductions similar to those in the previous schedules. The first

TABLE 4.2.1 shows the number of passes used to reach 90% total reduction in the three controlled geometry schedules.

% Total rolling Reduction	No of passes used in the 55°/p schedule.	No of passes used in the 45°/p schedule	No of passes used in the 35°/p schedule
70	45	23	11
80	77	39	20
90	174	87	44

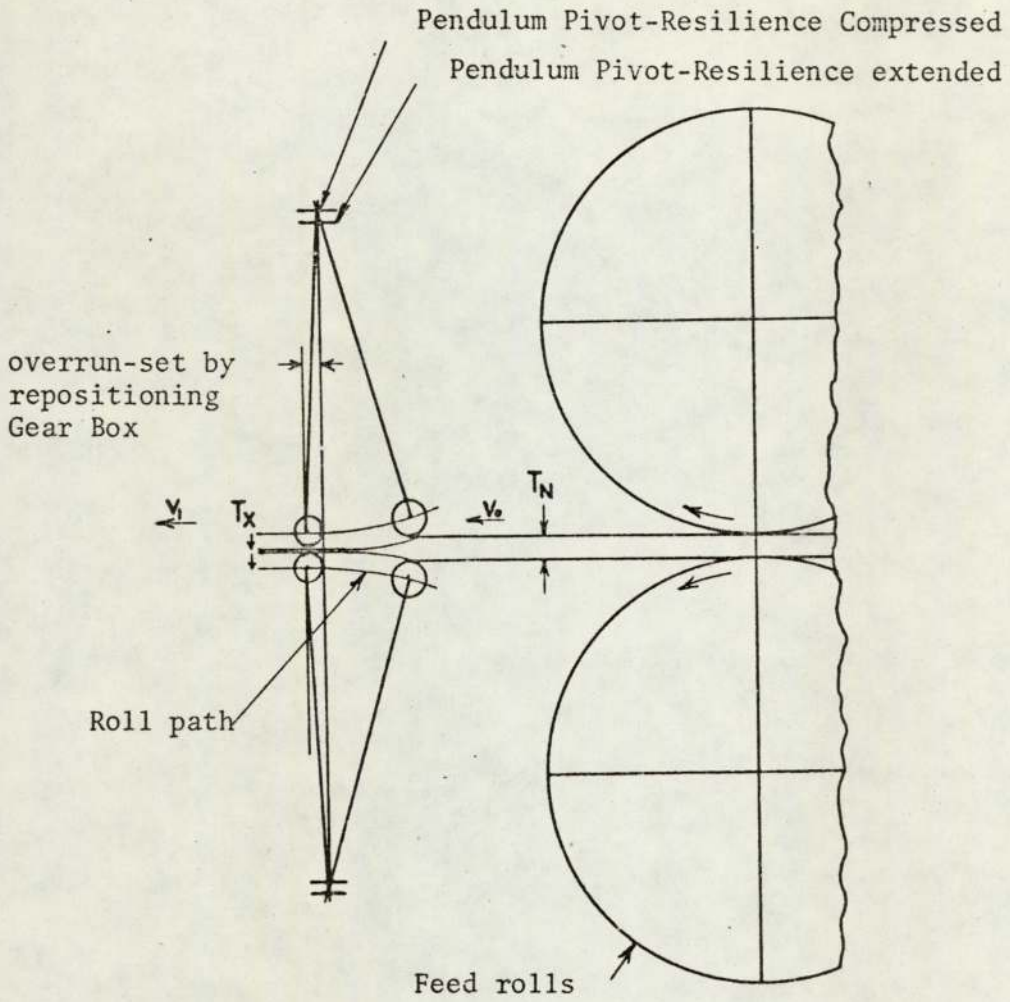
schedule was characterised by light draughts of the order of 0.001 in/pass. The second and third schedules were described as medium and heavy draughts of the order of 0.005 in/pass and 0.02 in/p respectively. The number of passes used to affect total reduction up to 90% are shown in Table 4.2.2.

#### 4.2.3 The Pendulum Rolling Schedule

The pendulum mill<sup>(66)</sup> used in the present investigation, is an incremental rolling method for producing thin strip from thick sheets in one operation. The process is shown diagrammatically in figure 4.2.3. The ingoing sheet is forced by feed rolls into a gap formed by converging paths of two work rolls which are moved forwards and backwards. The work rolls are freely rotatable, each being supported by two rows of backing rolls. These are rotated by frictional contact with the strip which forces the sheet into the roll gap at certain speed and merges at higher speed. The rolls oscillate over paths corresponding to the reduction zones. The average relative speed of the rolls is fairly high and continuously changing during the cycle. The roll path in a rigid system is circular and the overrun of the rolls on the outgoing side increases the rolls gap at the extreme of the travel. Reduction of the load at this point results in partial release of the strain in the system, diagrammatically shown as the displacement of the pendulum pivot. The rolls then travel on parallel paths for part of the stroke and remain loaded. Deformation of the strip during rolling takes place by both strokes of the cycle.

TABLE 4.2.2 shows the number of passes used to reach 90% total rolling reduction in the three controlled draughts schedules.

% Total rolling Reduction	No. of passes used in light rolling	No. of passes used in medium rolling	No. of passed used in heavy rolling
70	176	36	10
80	189	41	12
90	226	46	14



$T_N$  is the entry thickness,  $T_x$  is the exit thickness

$V_o$  is the entry velocity,  $V_1$  is the exit velocity

Fig. 4.2.3. Diagrammatic arrangement of the pendulum process<sup>(66)</sup>.

An experimental pendulum mill with 2 ins.-wide rolls was used in the present study. The rolling procedures started by entering the initial rimmed steel coil between two rolls, the gap between them being sufficient to admit the material to be rolled. The gap was then closed until the oscillating rolls started to exert adequate pressure on the metal to form a wedge shaped zone. The thin end of the wedge was approximately the thickness required. This was produced by rolling a stationary or slowly moving coil and applying a small reduction during the stroke. In a successful start, a 0.5 - 5% reduction is adequate to form the wedge zone after a few seconds of rolling. The rolls oscillate over paths corresponding to the reduction zone at a fairly high speed gradually reducing the material in thickness. The specimen was cooled during rolling by a special fluid and the required reduction was reached in one operation by many small strokes. Total rolling reductions corresponding to those affected by the two high mill were taken for examination.

#### 4.3 ANNEALING OF THE COLD ROLLED STRIPS

All specimens to be annealed (figure 4.1) were wrapped in thin copper foils. In addition, two protective strips of 0.02in. in thickness taken from the same cold rolled strip were placed on both sides of each specimen to be annealed, directly under the copper foil. This arrangement formed a sandwich in which the specimen to be annealed occupied the centre, surrounded by two unwanted strips and all wrapped in copper foil. This technique was shown<sup>(2,40)</sup> to reduce oxidation and decarburisation during the annealing cycle.

The specimens were then placed in the centre of an electrically heated muffle furnace, at  $700^{\circ}\text{C} \pm 5^{\circ}\text{C}$ , for periods of 0.5, 1, 3 and 6 hrs, then air cooled to room temperature. They were then overaged at  $300^{\circ}\text{C}$  for one hour and furnace cooled.

#### 4.4 MEASUREMENT OF R VALUE

The strain ratio or R value<sup>(67)</sup> is measured by the ratio of width to thickness strains in a tensile test. Since thickness strains are very small, a more practical relationship based on the constancy of volume criterion is given by the formula:

$$R = \frac{\ln\left(\frac{w_0}{w}\right)}{\ln\left(\frac{w_0}{\ell_0 w_0}\right)} \quad 4.4.1$$

where  $w_0$  and  $\ell_0$  are the initial width and length of the parallel gauge portion respectively.  $w$  and  $\ell$  are the width and length after tensile extension respectively.

Complete isotropy occurs when  $R = 1$  in all directions of the strip. When there is preferred orientation  $R$  may be  $\neq 1$  and will usually vary with the direction of testing in the plane of the sheet. If  $R$  value is infinite the thickness strain will be zero and a maximum resistance to thinning is to be expected. Conversely, if  $R = 0$ , deformation occurs mostly in the thickness direction and thinning should, therefore, occur very easily. Neither of these extremes is realised in practice.

Whiteley<sup>(29)</sup> differentiated between two types of anisotropy. Normal anisotropy which measures the difference in properties in the

normal direction and an average value parallel to the strip surface, and planar anisotropy which indicates the difference in properties in various directions within the plane of the strip. Normal anisotropy is measured by the average strain ratio "R" value. It is, therefore, indicative of the ability of a strip to resist thinning. Planar anisotropy, on the other hand, is measured by the difference between the maximum and minimum strain ratio measured in various directions within the plane of a strip. It is associated with the earing behaviour of a strip during deep drawing. In general, if planar anisotropy is present, the strain ratio will vary considerably with direction of measurement and the average strain ratio used to describe the degree of anisotropy is defined by the relationship.

$$\bar{R} = \frac{1}{4}(R_0 + 2R_{45} + R_{90}) \quad 4.4.2$$

where the suffixes 0, 45 and 90 refer to the angle between the strip rolling direction and tensile axis.

In the present study, R values were measured in the rolling direction only, before and after annealing, using a Hounsfield tensometer, at a constant strain rate of  $4 \times 10^{-4}$ /sec. Prior to testing, blanks were machined to tensile test pieces, according to B.S.18.1962 (figure 4.4.1) except with regard to the total specimen length. The specification states that the length of the test piece should be 8 in. but test pieces of 6.5 in. were adopted since it was most conveniently suitable for the strip thickness with the minimum wastage of material whilst still allowing sufficient area for gripping purposes. The test pieces were machined by milling at high speed using a light cut each time to reduce the work

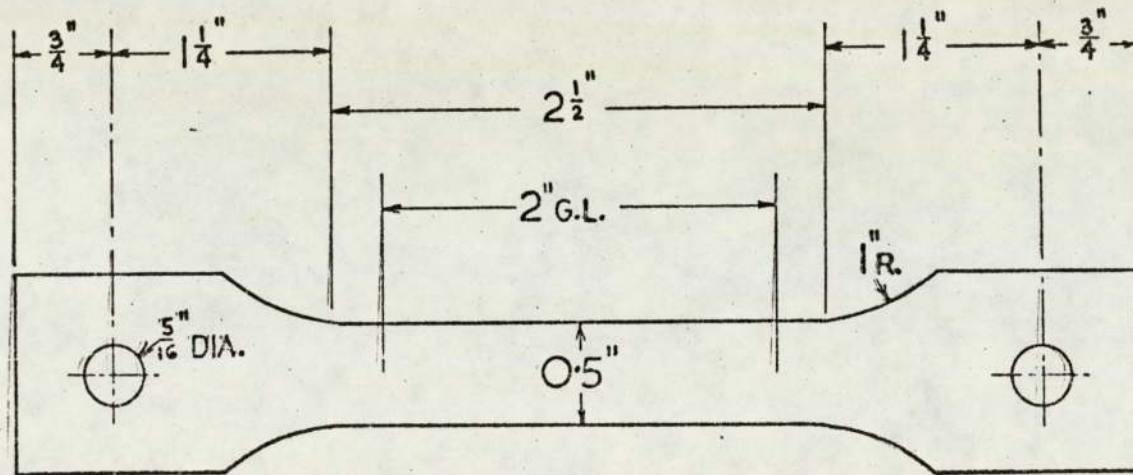


Fig. 4.4.1 A Standard tensile test piece

hardening effect upon the edges of the test pieces. The 2 in. gauge length portion was finally dressed by hand with a fine emery cloth.

In order to measure  $R_0$  value, a 2 in. gauge length was marked on the parallel portion of the tensile test piece. Each test piece was preloaded to 0.05 ton (in the region of the elastic limit) in an attempt to correctly position the specimen in the Hounsfield tensometer axis, then the load was reduced to 0.01 ton for measurements of width and thickness. Four measurements of width were made using a micrometer in the portion bounded by the gauge length and the average width was recorded. The gauge length was measured using a travelling microscope.

Measurement of  $R_0$  values before annealing were made on 7 sets of specimens rolled to 75% total reduction, using the rolling schedules, 35°/p, 45°/p, 55°/p, 0.02 in/p, 0.002 in/p, 0.001 in/p and pendulum. It was observed that the specimens accommodated a maximum tensile extension of only 2% at which a slight indication of necking occurred. The test was quickly stopped before fracture, and the gauge length, width and thickness were recorded.

$R_0$  values of the annealed specimens were measured after 20% tensile extension, firstly, for certain rolling reduction and different annealing time and, secondly, for certain annealing time and a range of total rolling reductions (fig. 4.1). In the first case, four sets of specimens cold rolled to 75% total reduction using rolling draughts of 35°/p, 45°/p, 55°/p and pendulum were selected. Each was annealed for 0.5, 1, 3 and 6 hrs at 700°C and the corresponding  $R_0$  values were measured.

In the second case, seven sets of specimens, corresponding to the seven rolling schedules, each with six different total rolling reductions of 65, 70, 75, 80, 85 and 90% were annealed for 6 hours only and their  $R_0$  values were then measured. All  $R_0$  values were calculated using equation 4.4.1.

#### 4.5 EXAMINATION OF PREFERRED ORIENTATION

Direct and inverse pole figures were used for examination of texture. A direct pole figure is a statistical distribution diagram of a given crystallographic pole relative to a suitable reference axes. In the case of rolling, the plane of a direct pole figure represents the rolling plane, the N-S axis represents the rolling direction and W-E axis is the transverse direction.

Inverse pole figures provide a quantitative distribution of pole density plots compared with the equivalent densities of a random sample relative to a single reference axis which is the sheet normal.  $\{xyz\}$  texture indicates that the  $\{xyz\}$  planes are parallel to the sheet surface. Noting the importance of the sheet normal with regard to normal anisotropy, the crystallographic direction  $\langle uvw \rangle$  parallel to the rolling direction is not considered in the description. That is, when normal anisotropy is to be considered, it is only necessary to specify the planes parallel to the sheet surface without specifying a direction parallel to the rolling direction as in direct pole figures. The sheet then may be considered to be equivalent to a fibre with the fibre axis parallel to the sheet normal.

##### 4.5.1 Direct pole figures

A number of X-ray methods for plotting direct pole figures are

available<sup>(57)</sup>. Conventionally, two geometries of specimen arrangements relative to the incident and diffracted beam are used, these being the transmission and reflection methods. For the transmission method the counter is arranged to measure the intensity of the diffracted beam transmitted through the sheet, whilst in the reflection method the intensity of the diffracted beam reflected from the surface of a true specimen is measured. Both techniques are necessary to obtain a complete pole figure, as absorption in the first, and defocusing in the second, limit the angle of specimens rotation over which accurate determination of direct pole figures can be made.

Difficulties arose in constructing a complete pole figure using two different techniques and a method was therefore devised to plot a complete pole figure using the reflection method only<sup>(77,78)</sup>. Later, Halland, Engler and Powers<sup>(79)</sup> developed a method of plotting one quadrant of the pole figure from the reflection data at three orthogonally cut specimens for description of texture. This was modified<sup>(80)</sup> to plot a complete pole figure from 0 to 180 degrees along longitude and latitude lines with corrections for backaround and intensity loss due to geometric defocusing. Texture of a sheet can be completely defined by means of the orientation distribution function<sup>(81)</sup> which can be calculated from the information provided by several pole figures.

For the purpose of this project, sufficient information can be obtained by using the reflection method described by Schultz<sup>(68)</sup> in which a thick specimen rather than a costly prepared thin specimen is required.

A Siemens X-ray generator with a cobalt target operating at 35kv and a filament current of 15 mA was employed in conjunction with a

texture goniometer and an electric pulse height discriminator. The X-ray tube aperture was set at 2 mm. in height and 2 mm. in width. The texture goniometer ring was set at  $26^\circ$  incident angle for determination of (110) pole figure. The incident beam was filtered using an iron filter to remove the  $K_\beta$  and some of the white radiations. Intensity of the diffracted beam was measured by a proportional counter situated at  $52^\circ$  and operating at 1.9 kv. The counter slit was set at 3 mm. in height and 2 mm. in width. The proportional counter is especially suited for detection of a relatively low energy radiation such as cobalt radiation because of its low background and high energy resolution. The pulse height discriminator was set at a maximum pulse rate of  $4 \times 10^4$  counts/sec and statistical error of 1.5%.

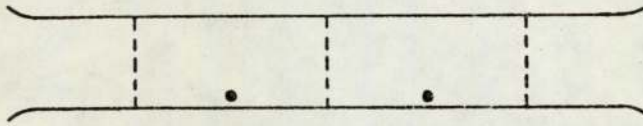
As a preliminary measure the diameter of the pole figure was scanned (radial scan) in order to have a quick idea about the specimen texture and to choose the suitable maximum pulse rate to keep the maximum line intensity of the diffracted beam within the range of the recorder chart. A complete analysis of texture was then carried out by scanning the pole figure from  $0^\circ$  to  $75^\circ$  along a spiral with a pitch of  $5^\circ$ . A random sample was then scanned in order to determine the one random level, the multiples of which are used to determine the levels 2, 3, 4...etc. of a textured specimen. The data from the recorded chart was then transferred onto a pole figure spiral which represented intensity levels as a function of the inclination angle within the range  $0^\circ$  to  $75^\circ$  studied.

The initial material, cold rolled strips and annealed strips before and after tensile extension were examined according to the foregoing procedure. Specifications of specimens examined are illustrated in figure 4.1. It is sufficient to mention here that in all cases one

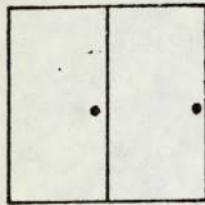
inch square specimens cut from the middle of the mother strips were used. In order to measure texture after tensile extension, two pieces of 1" x 0.5" were cut from adjacent parts of the 0.5" parallel portion width of the tensile pieces after tensile extension, then mounted together in a cold setting plastic, as shown in figure 4.5.1. Textures of all specimens were measured at 0.004 in. below the surface. Texture analysis was limited to the surface only, since it has been shown recently<sup>(2)</sup> that for a certain total rolling reduction, the mid-plane texture was independent of the rolling schedule. The main difference in texture was apparent in the surface plane with gradual transition from surface to centre texture. For the purpose of the present project, therefore, the effect of the seven rolling schedules upon texture can be revealed by examining the surface texture only. This procedure precludes the possibility of making exact correlations between texture and mechanical properties. Thinning to the surface plane to be examined was done by blocking off one face of the specimens with lacomit (except those mounted in cold setting) and alternate grinding and etching of the other face in a solution of nitric acid (one part conc. nitric acid in three parts water). Etching was necessary to remove the distorted surface layers. Textures of all specimens were determined relative to a random sample which was prepared by filing a piece of rimmed steel into a powder. The filed powder was then made into a one inch square sample by mounting in a corresponding size of X-ray specimen holder using cold setting mounting adhesive.

#### 4.5.2 Inverse pole figures

In an inverse pole figure technique, the specimen mounted on a specimen holder with its surface normal to the diffractometer axis is caused to rotate about the sheet normal to allow similar areas of the specimen to be examined. By simultaneously changing the incidence and



(a)



(b)

Fig. 4.5.1 Section from a standard tensile test piece after 20% tensile extension (a) shows the areas selected, (b) construction of the one in. square specimen required for X-ray examination.

diffraction angles, the diffraction intensities of a number of planes of a specimen and the corresponding planes of a random sample are measured. The line intensities received from the specimen planes are related to those received from the corresponding planes of a random sample by a parameter P given by the Mueller equation<sup>(91)</sup>

$$P = \frac{I_{\{hkl\}}}{IR_{\{hkl\}}} \frac{1}{h} \sum \frac{I_{\{hkl\}}}{IR_{\{hkl\}}} \quad 4.5.2$$

where  $I_{\{hkl\}}$  and  $IR_{\{hkl\}}$  are the integrated line intensities in a specimen and a random sample respectively.  $\sum I_{\{hkl\}}$  and  $\sum IR_{\{hkl\}}$  are the sums of the integrated line intensities of the specimen and random sample respectively.  $n$  is the number of crystallographic planes examined. The inverse pole figure technique<sup>(69,82)</sup> yields a quantitative measure of pole densities relative to a particular specimen direction. A multiaxial inverse pole figure has been used to identify the crystallographic direction and planes by plotting inverse pole figures in the normal, rolling and transverse directions<sup>(83,84)</sup>. This does not define sheet texture completely. Nevertheless, an inverse pole figure in the normal direction of a sheet provides useful information concerning the relationship between texture and normal anisotropy.

A Philips X-ray generator with a molybdenum target, operating at 40 kv and a filament current of 20 mA was used in the present study for inverse pole figure determination according to Harris's technique<sup>(69)</sup>. A short wave length radiation such as molybdenum radiation was used in order to increase the number of reflections so that inverse pole figures are as accurate as possible. The incident beam was filtered by a zirconium filter in order to filter out the  $k\beta$  and some of the white radiation. Intensities of eight diffracted beams corresponding to eight crystallographic planes were measured by a scintillation counter operating at

0.82 kv, at diffraction angles up to  $75^\circ$  from the plane of the sheet, as measured by a goniometer. A scintillation counter is suited for detection of  $M_oK_\alpha$  radiation because of its high energy response at  $M_oK_\beta$  wavelength. The goniometer was connected to a pulse height discrimination and a Canberra DATINUM Control unit. The pulse height discrimination was set at attenuation 4x, time constant 0.4 sec. base line 9 volts and window 10 volts. The Canberra DATINUM unit was used to control the goniometer in order to scan for peak position over a wide range of Bragg angles and to step scan across the eight sets of diffraction lines in order to measure their integrated intensities. This control over the goniometer was achieved by coordinating a data acquisition and a control function with an operational programme. Determination of inverse pole figures was carried out according to the following procedures:

(1) The random sample was scanned over a range of  $80^\circ$  between  $10^\circ$  and  $90^\circ$  for two reasons, firstly, to confirm that it is perfectly random and secondly to locate the positions and intensities of the eight diffraction lines to be examined, namely the  $\{110\}$ ,  $\{200\}$ ,  $\{211\}$ ,  $\{310\}$ ,  $\{222\}$ ,  $\{321\}$ ,  $\{411\}$  and  $\{332\}$ . A specimen in the cold rolled condition and another in the annealed condition were also scanned over the same range as the random samples to determine the peak intensities and spread of the eight diffraction lines of both specimens. This was necessary to design a step scanning programme.

(2) In order to design an operational programme to step scan across the eight sets of planes to be examined and count their integrated intensity, it was taken into consideration that the background intensity will be counted with the peak intensity itself. Therefore, counting was carried out over a range of angles at low speed of  $2^\circ$  per minute with the peak placed within that range. This range varied from the cold rolled strips

to the annealed strips and the random sample and sometimes from one peak to the next depending upon the peak spread as shown in Table 4.5.2. After the peak was scanned, the goniometer was made to move at a higher speed of  $8^\circ/\text{min}$  to the next diffraction line to be scanned by the aid of the operational programme. The diffraction line was then step scanned at a lower speed of  $2^\circ/\text{min}$  and so on until intensities of the eight diffraction lines were scanned.

(3) The integrated intensity data of the 8 sets of planes of all specimens together with the corresponding 8 sets of planes of the random sample, all punched on a suitably coded tape every 4 seconds were stored in the computer via an input signal printed in the beginning of each tape.

(4) A computer programme (Appendix VI) was used to calculate P values of the eight sets of planes by comparing their integrated intensities with the corresponding integrated intensities taken from the same diffraction lines of the random sample.

Specifications of specimens examined by inverse pole figure technique are shown in figure 4.1. Texture was measured at 0.004 in. below the surface and thinning to that depth was carried out as described in (110) pole figure technique (4.5.1).

TABLE 4.5.2. Illustrates the crystallographic plane, Bragg's angles and the range scanned during determination of inverse pole figure.

{hkl}	BRAGG ANGLES	RANGES SCANNED IN THE CASE OF			
		The as-cold rolled strips		The random sample and the annealed strips	
		From	To	From	To
110	20.15	19.40	20.90	19.30	21.30*
200	28.67	27.70	29.70	27.95	29.45
211	35.30	34.30	36.30	34.55	36.05
310	46.08	45.57	47.07	45.57	47.07
222	50.80	50.16	51.66	50.16	51.66
321	55.15	54.65	56.65	54.65	56.65
310	63.33	62.45	64.45	62.45	64.45
411					
332	70.80	69.92	71.92	69.92	71.92

\* Examination of the diffraction lines of the random sample, cold rolled and annealed strips indicated that the {110} diffraction intensity was very weak in the case of the cold rolled strips, except the pendulum, and strong in the case of the random sample, strips cold rolled by the pendulum and strips in the annealed condition. Therefore, the diffraction intensity of the {110} planes of the cold rolled strip was scanned over a narrower range. Examining the background intensity before and after the {110} peak of the cold rolled strips indicated that the full peak has been scanned.

## 5. EXPERIMENTAL RESULTS

## 5.1 INTRODUCTION

The experimental results of the present study are presented in four sections. The first section includes a description of the initial material's surface and centre textures. General information concerning the microstructure, grain size and chemical composition is also provided.

The second section illustrates the effect of seven rolling schedules upon  $R_0$  values of strips cold rolled to 75% total reduction, firstly, in the cold rolled condition and, secondly, after annealing for different periods followed by an overageing treatment. The effect of the seven rolling schedules upon  $R_0$  values of strips cold rolled to 65, 70, 75, 80, 85 and 90% total reductions, annealed for 6 hours only then aged is also illustrated.

In the third section, the cold rolling texture of materials cold rolled to 75% using each rolling schedule is described by inverse and (110) pole figures. Texture of materials cold rolled to a range of different total reductions is described in terms of (110) pole figures only. The corresponding texture developed after 0.5 hour and 6 hours annealing at 700°C will also be given in this section.

Finally, reorientation of materials cold rolled to a range of total rolling reduction, annealed for 0.5 hr and 6 hrs, aged then subjected to 20% tensile extension is examined in Section Four.

## 5.2 EXAMINATION OF THE INITIAL MATERIAL

Examination of the initial material's microstructure by optical microscopy revealed that it is a typical low carbon steel microstructure. It is characterised by equiaxed ferrites of 25-30  $\mu$  grain size and fine

carbide dispersions of cementite. A micrograph showing the microstructure of the initial material is shown in figure 5.2.1. The chemical composition of the initial material is listed in Table 5.2.1.

It was necessary to establish, firstly, that the random sample used for P value measurements is perfectly random. However, measurements of the integrated intensities of eight crystallographic reflections of the random sample was compared with the calculated relative intensities of corresponding planes of a perfectly random steel sample. The comparison confirmed that the random sample used in the present study is perfectly random as shown in Table 5.2.2.

Measurements of P values of 8 crystallographic planes of the initial material indicated that the {110} planes were dominant at the surface while the {100} planes were dominant at the centre. P values of the {100} and {111} planes varied slightly from surface to centre, as shown in figure 5.2.2. and Table 5.2.3.

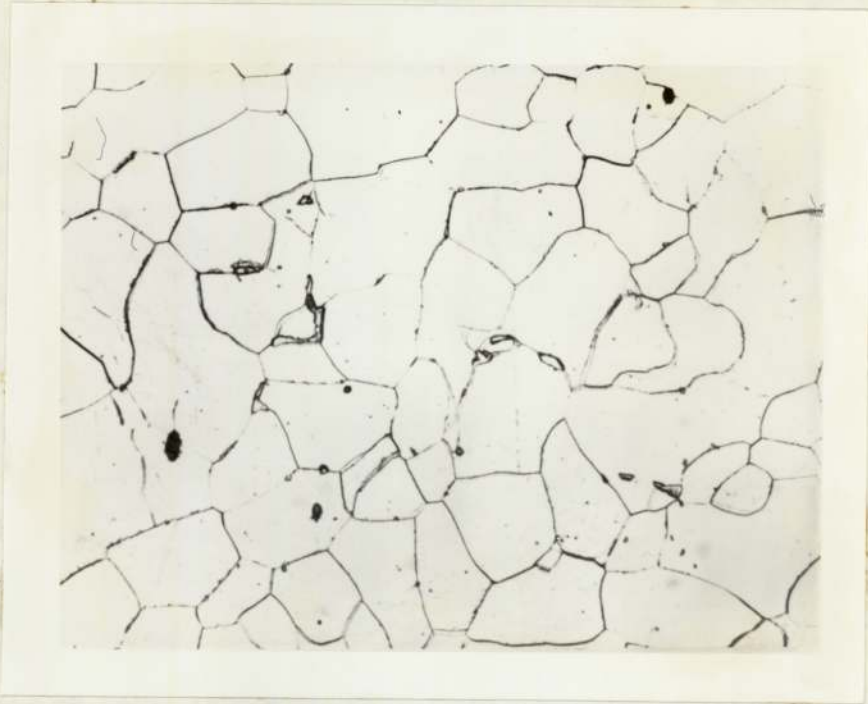


Fig. 5.2.1. A micrograph of the initial material showing equiaxed ferrites of 30  $\mu$  grain size, and fine carbide dispersions of cementite (X 500)

Table 5.2.1. A comparison between chemical composition as determined in the present project and that provided by the supplier.

Element	C	Mn	S	AL	O <sub>2</sub>	P	N <sub>2</sub>
Weight % (Measured)	0.05	0.35	0.028	0.014	0.015	0.014	0.003
Weight % (Supplied)	0.056	0.39	0.035	0.018	Not Supplied	0.01	Not Supplied

{hkl}	calculated relative integrated intensity	Measured integrated intensity
110	100	99.8
200	20	20.5
211	30	30.3
310	11.3	11.5
222	2.5	2.7
321	10.9	11.0
330	4.3	4.5
411		
332	1.8	2.0

Table 5.2.2. Measured integrated intensities of 8 crystallographic Bragg reflections of a rimmed steel random sample compared with the calculated relative integrated intensity of corresponding planes of a steel random sample.

Relative integrated intensity was calculated from the equation<sup>(85)</sup>

$$I = [F]_p^2 \left[ \frac{1 + \cos^2 2\theta}{\sin^2 \theta \cos \theta} \right] e^{-2M}$$

where F is the structure factor, P is the multiplicity factor,  $\left[ \frac{1 + \cos^2 2\theta}{\sin^2 \theta \cos \theta} \right]$  is the Lorentz polarisation factor, and  $e^{-2M}$  is the temperature factor.

No.	$2\theta^\circ$	{hkl}	P values (surface)	P values (centre)
1	20.14	110	1.12	0.70
2	28.67	200	1.05	1.27
3	35.25	211	0.97	1.15
4	46.03	310	0.75	0.72
5	50.50	222	1.00	0.95
6	55.00	321	0.87	1.06
7	63.00	330 411	1.12 0.18	0.70 0.67
8	70.50	332	0.93	0.77

Table 5.2.3. P values of the initial material

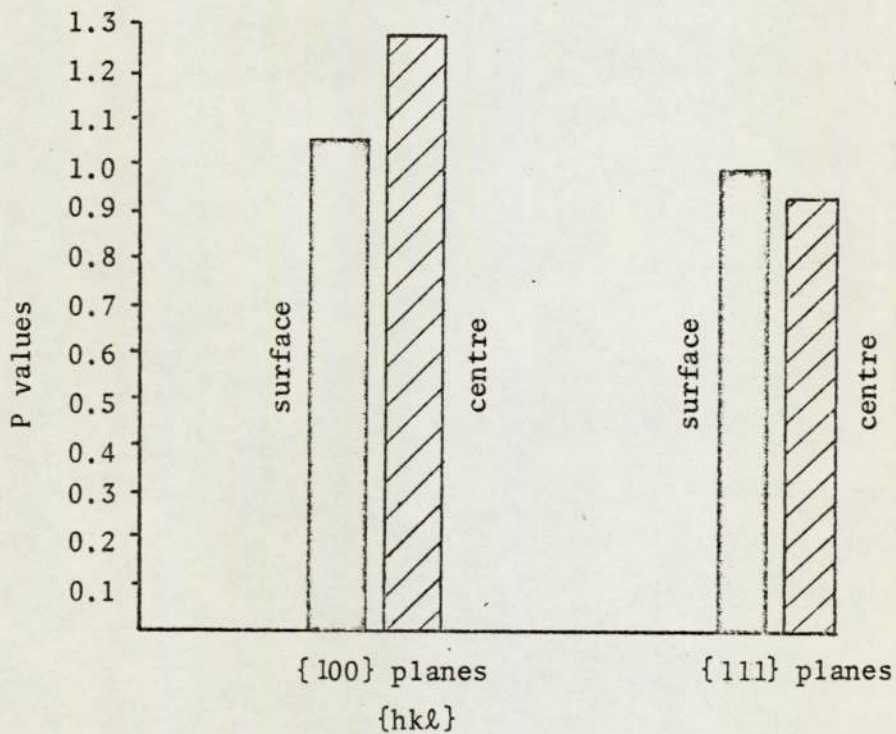


Fig. 5.2.2. The variation in the P values of the {111} and {100} planes at the surface and centre of the initial material.

### 5.3 Measurement of $R_0$ values

#### 5.3.1 The cold rolled materials

$R_0$  values of the cold rolled materials were very low ranging between 0.35 and 0.16 in the case of material rolled by the 35°/p and Pendulum schedules respectively. The experimental error in  $R_0$  value ( $\delta R$ ) due to the uncertainty in measurements of width and gauge length was calculated according to the equation

$$R = \frac{R_0+1}{\ln(\ell/\ell_0)} \left[ (R_0+1) \left( \frac{\delta W}{W} + \frac{\delta W_0}{W_0} \right) + R \left( \frac{\delta \ell}{\ell} + \frac{\delta \ell_0}{\ell_0} \right) \right]$$

where

$\ell_0$  is the gauge length before ten.ext.(2.0")

$\ell$  is the gauge length after 2% ten.ext. (2.04")

$\delta \ell$  is the error in the gauge length measurement (0.001")

$W_0$  is the width before tensile ext. (0.5")

$W$  is the width after 2% tensile ext.

$\delta$  is the error in measurement of width (0.0005")

Table 5.3.1 shows the variation in  $R_0$  value  $\pm \delta R$  with the seven rolling schedules

Rolling schedules	$R_0$ values	$\delta R$
35°/p	0.35	$\pm 19$
45°/p	0.31	$\pm 18$
55°/p	0.27	$\pm 18$
0.02 in/p	0.24	$\pm 0.17$
0.005 in/p	0.22	$\pm 0.17$
0.001 in/p	0.20	$\pm 0.16$
Pendulum	0.16	$\pm 0.14$

The variations in  $R_0 \pm \delta R$  with the rolling schedules are also shown in Fig. 5.3.1.

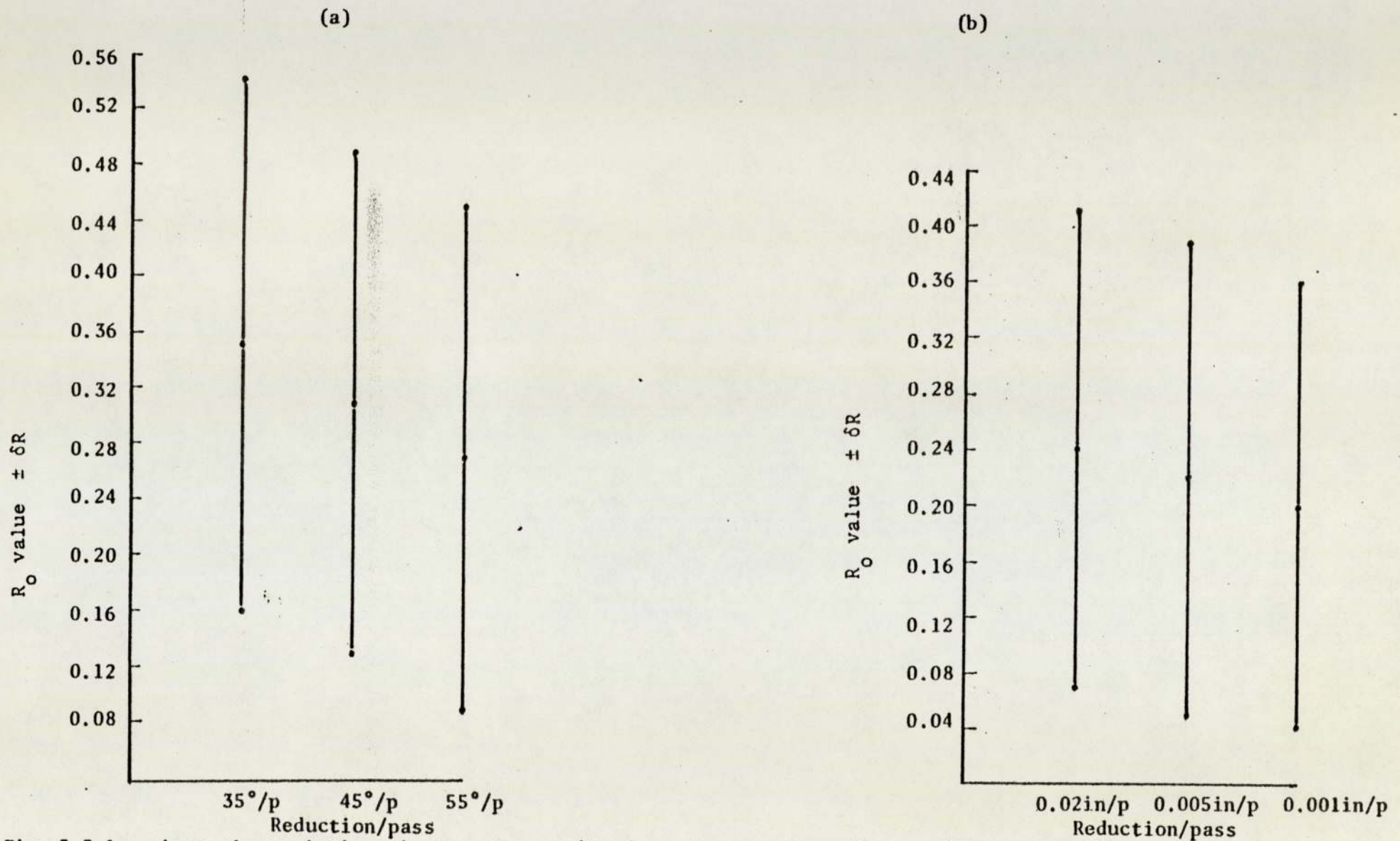


Fig. 5.3.1. shows the variations in  $R_o$  values  $\pm \delta R$  of specimens cold rolled to 75% total rolling schedules using the 35°/p, 45°/p and 55°/p schedule (a), and the 0.02 in/p, 0.005 in/p and 0.001 in/p schedules (b).

### 5.3.2 The annealed materials

#### (a) R values of materials cold rolled to 75% total reduction then annealed for different annealing times

Measurements of R values of specimens cold rolled to 75% using the 35°/p, 45°/p, 55°/p and pendulum schedules, annealed for 0.5, 1, 3 and 6 hrs then aged, indicated a significant improvement in  $R_0$  values by increasing the annealing time, as shown in figure 5.3.2a. The results indicate also that  $R_0$  value was dependent upon the rolling procedure especially after longer annealing time.

Annealing for half an hour resulted in slightly higher  $R_0$  value when rolling with reduction per pass equivalent to 35° relative to rolling with 45°, 55° and pendulum. After 6 hrs annealing, the difference in R value was apparent. The increase in  $R_0$  value of specimens cold rolled using 35°/p, for example, was equivalent to 59% in comparison with 19% in the case of specimens cold rolled by the pendulum mill. A full presentation of the variation in  $R_0$  value after 0.5 and 6 hrs annealing with the 35°/p, 45°/p, 55°/p and pendulum rolling schedules is listed in Table 5.3.2a.

#### (b) $R_0$ values of materials cold rolled to a range of total reductions then annealed for 6 hrs

$R_0$  values of specimens cold rolled to 65, 70, 75, 80, 85 and 90% total reductions, according to the rolling schedules 35°/p, 45°/p, 55°/p, 0.02 in/p, 0.005 in/p, 0.001 in/p and pendulum, annealed for 6 hrs then aged are shown in figure 5.3.2b. It is evident that the behaviour of  $R_0$  values when increasing the total rolling reduction within the range studied was dependent upon the

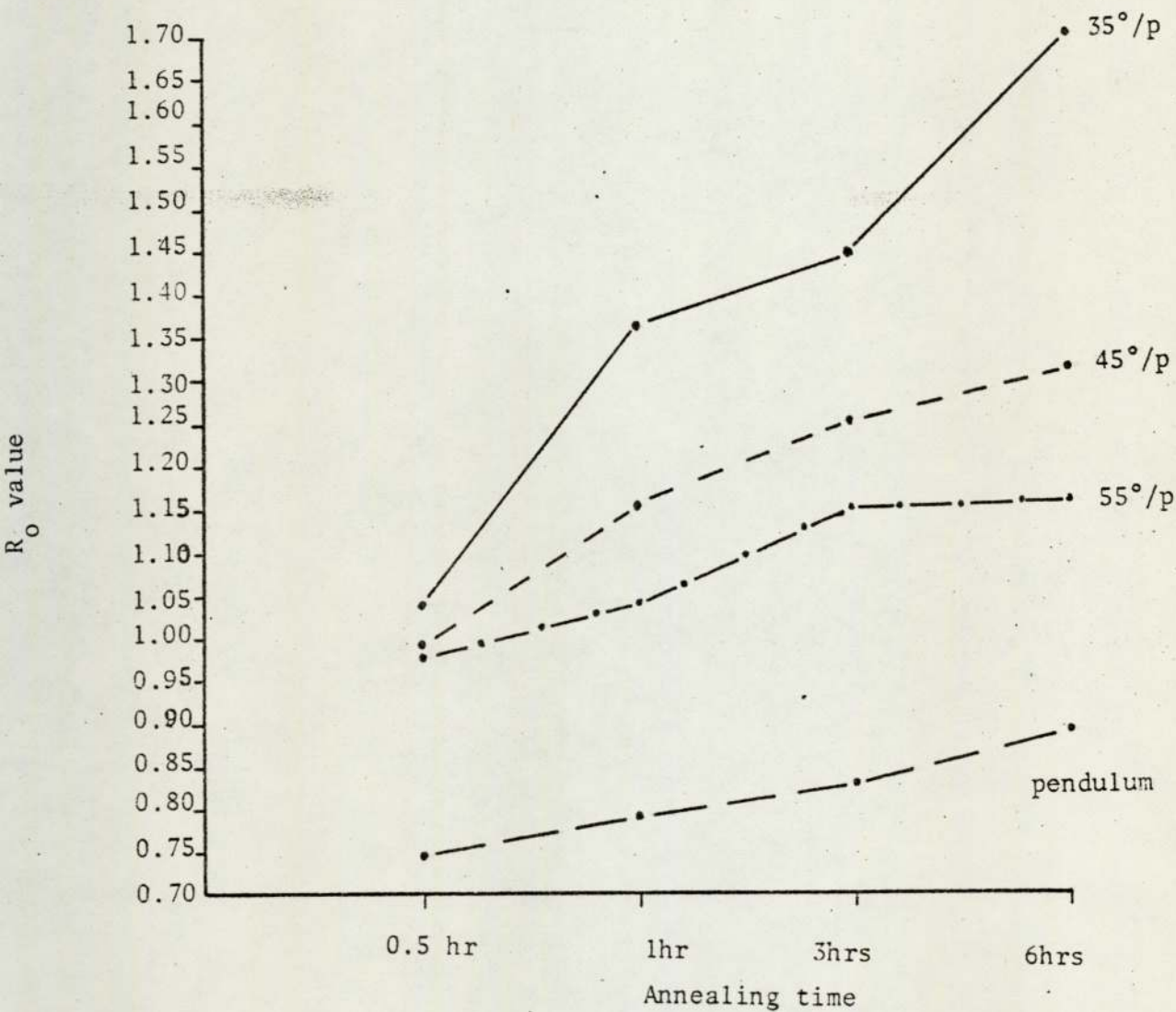


Fig. 5.3.2.a. Shows the effect of increasing the annealing time before a final overageing treatment upon  $R_o$  values of specimens cold rolled to 75% total reduction, using 35°/p, 45°/p, 55°/p and pendulum rolling schedules.

Table 5.3.2a. Illustrates the effect of increasing the annealing time upon  $R_0$  values of specimens cold rolled to 75% total reduction, using 35°/p, 45°/p, 55°/p and pendulum rolling schedules.

Rolling schedules	$R_0$ values measured after the following annealing times				% increase in $R_0$ values after 6 hrs annealing relative to 0.5 hour annealing
	annealing times				
	0.5 hr	0.5 hr	3 hrs	6 hrs	
35°/p	1.041	1.362	1.424	1.653	58.8%
45°/p	0.982	1.153	1.233	1.324	34.8%
55°/p	0.968	1.037	1.176	1.221	26.1%
Pendulum	0.740	0.790	0.820	0.880	18.9%

rolling procedures. This behaviour may be classified into three categories corresponding to constant geometry, constant roll gap and pendulum rolling schedules.

In constant geometry rolling schedules, no change in  $R_o$  value with increasing the total rolling reduction was observed, but  $R_o$  value was dependent upon the rolling schedule. It is apparent from figure 5.3.2b that  $R_o$  value has significantly increased with decreasing the shear plane angle. For example,  $R_o$  value increased from 1.22 to 1.33 to 1.65 when rolling with  $55^\circ/p$ ,  $45^\circ/p$  and  $35^\circ/p$  respectively and remained constant within the range of total reduction studied.

Specimens cold rolled using constant roll gap schedules are characterised by an increase in  $R_o$  value when increasing the total rolling reductions up to a critical value at which  $R_o$  value decreased with further increase in rolling reduction. The total rolling reduction corresponding to the maximum  $R_o$  value was dependent upon the magnitude of the roll gap. These  $R_{o \text{ max}}$  coincide with 70, 75 and 80% total reduction when rolling with 0.001 in/p, 0.005 in/p and 0.02 in/p respectively. The magnitudes of the maximum  $R_o$  values increased by increasing the roll gap.

The pendulum mill schedule, on the other hand, had a completely different effect upon  $R_o$  values at higher total rolling reductions. This is apparent in figure 5.3.2b from the continuous decrease in  $R_o$  value when the total rolling reduction was increased from 65% to 90%.

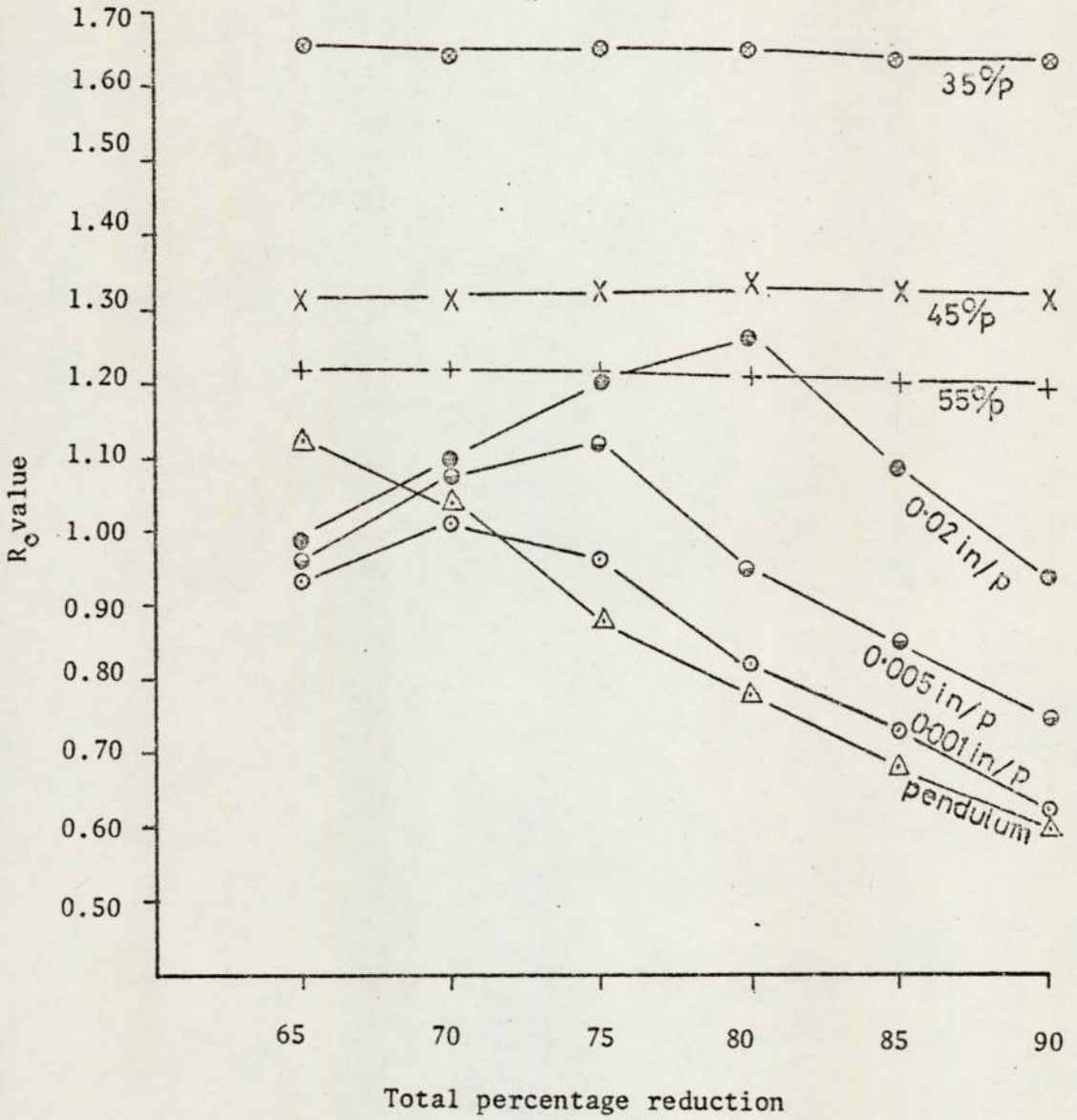


Fig. 5.3.2.b. Illustrates the effect of seven rolling schedules upon  $R_0$  values of specimen cold rolled to a range of total reductions, annealed for 6 hrs then aged.

## 5.4 EXAMINATION OF TEXTURE

### 5.4.1 The cold rolled materials

#### (a) Texture developed by controlled geometry rolling schedules

Measurements of P values of specimens cold rolled to 75% total reduction using reductions per pass equivalent to 35°, 45° and 55° indicated that crystals with {111} crystallographic planes parallel to the surface were predominant, as shown in Table 5.4.1.1a. The {100}, {211} and {332} P values were the next most highest depending upon the rolling schedule, while the {110} orientation was a minor component. It is also apparent from Table 5.4.1.1 that textures of specimens cold rolled using the 35°/p schedule had the highest {111} and the lowest {100} P values in comparison with texture of specimens cold rolled using the 45°/p and 55°/p schedules. A slight reduction in the P values of the {211} and {332} planes is also evident when the shear plane angle was decreased. On the other hand, P values of the {310}, {321} and {411} increased by decreasing the shear plane angle.

Analysis of the (110) pole figures of specimens cold rolled to 75, 80 and 85% total reductions using the 35°/p, 45°/p and 55°/p schedules with reference to the ideal (110) pole figure shown in figure 5.4.1.1 indicated that texture developed was typical of b.c.c. iron texture. It can be described by two partial fibre textures with  $\langle 110 \rangle$  direction parallel to the rolling direction and {111} plane parallel to the rolling plane, that is  $\langle 111 \rangle$  RD and {111} RP respectively. The main texture components were the {112} $\langle 110 \rangle$  {113} $\langle 110 \rangle$ , {111} $\langle 110 \rangle$ , {100} $\langle 110 \rangle$  and {111} $\langle 112 \rangle$  components, as

No	{hkℓ}	P VALUES		
		35°/p	45°/p	55°/p
(1)	110	0.05	0.06	0.06
(2)	200	2.20	2.48	2.61
(3)	211	1.59	1.44	1.41
(4)	310	0.10	0.11	0.13
(5)	222	3.49	3.37	3.26
(6)	321	0.09	0.12	0.14
(7)	330	0.05	0.06	0.06
	411	0.09	0.10	0.11
(8)	332	0.34	0.26	0.22

(a)

No	{hkℓ}	P VALUES		
		0.02in/p	0.005in/p	0.001in/p
(1)	110	0.07	0.07	0.07
(2)	200	2.70	2.80	3.01
(3)	211	1.39	1.33	1.27
(4)	310	0.22	0.25	0.29
(5)	222	3.01	2.92	2.72
(6)	321	0.18	0.20	0.23
(7)	330	0.07	0.07	0.07
	411	0.17	0.19	0.22
(8)	332	0.19	0.15	0.10

(b)

No	{hkℓ}	P Values Pendulum
(1)	110	0.27
(2)	200	3.20
(3)	211	0.91
(4)	310	0.31
(5)	222	2.39
(6)	321	0.30
(7)	330	0.27
	411	0.29
(8)	332	0.06

(c)

Table 5.4.1.1. P values of specimens cold rolled to 75% (a) using the 35°/p, 45°/p, 55°/p schedules, (b) using the 0.02 in/p, 0.005 on/p, 0.001 in/p schedules and (c) using the pendulum schedules.



illustrated in (110) pole figures shown in figure 5.4.1.2 (a,b,c), figure 5.4.1.3 (a,b,c) and figure 5.4.1.4 (a,b,c).

After 75% total rolling reduction, texture developed by the 35°/p schedule was the strongest and the most concentrated about the 30° and 35° circles from the sheet normal along the sheet normal - rolling direction radius of the pole figure. A gradual reduction in texture intensity and more spread towards the {100}<110> component in the sequence of rolling with 45°/p and 55°/p schedules was also evident.

Texture of specimens cold rolled using the 35°/p schedule had relatively higher {112}<110> and {111}<112> components and a relatively lower {100}<110> component. Reductions in the {112}<110> and {111}<112> components and an increase in the {100}<110> component occurred when rolling with the 45°/p and 55°/p schedules respectively.

Increasing the total rolling reduction to 80% using the 35°/p schedule resulted in an increase in the {112}<110> intensity, while intensities of the {113}<110>, {100}<110> and {111}<112> remained constant. With increasing the total rolling reduction to 85% using the same rolling schedule intensity of the {112}<110> increased furthermore and intensities of the {113}<110>, {100}<110> and {111}<112> again remained constant, as shown in figure 5.4.1.2., (a,b,c). A similar behaviour is evident when examining the (110) pole figure of specimens cold rolled to 75%, 80% and 85% using the 45°/p and 55°/p rolling schedules shown in figure 5.4.1.3 (a,b,c) and figure 5.4.1.4 (a,b,c) respectively.

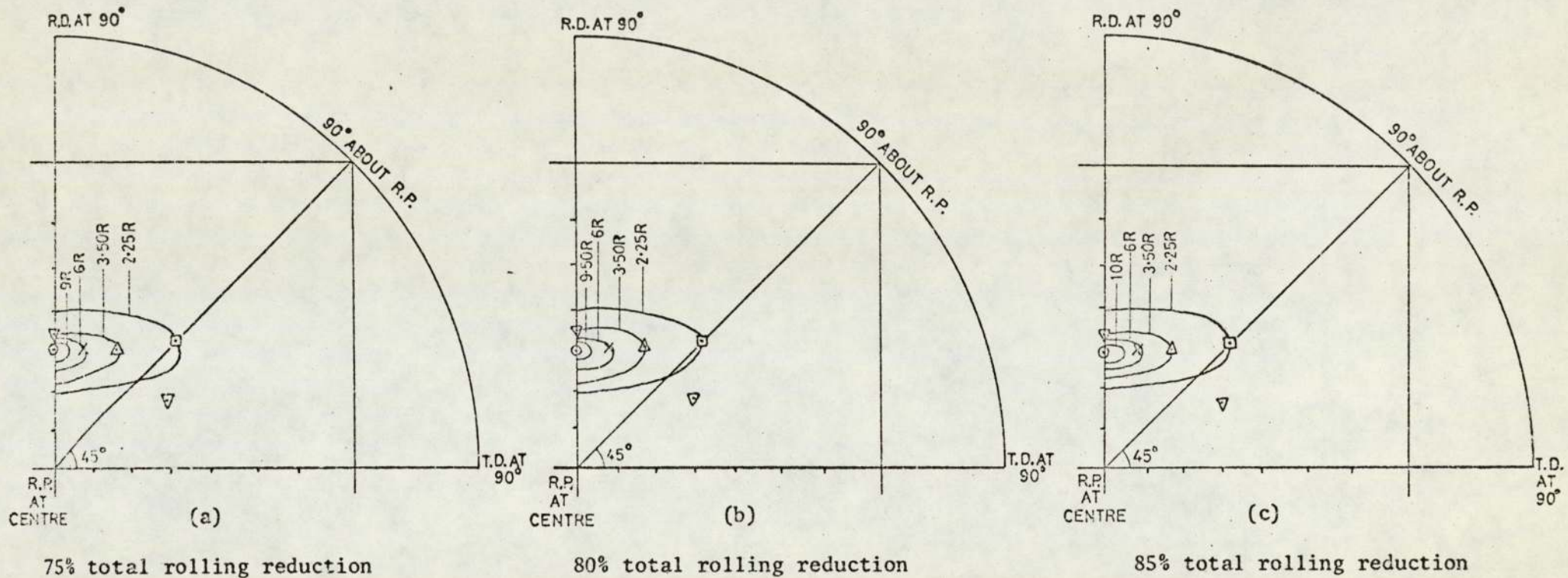


Fig. 5.4.1.2. One quadrant of (110) pole figures of specimens cold rolled using the 35°/p schedule.

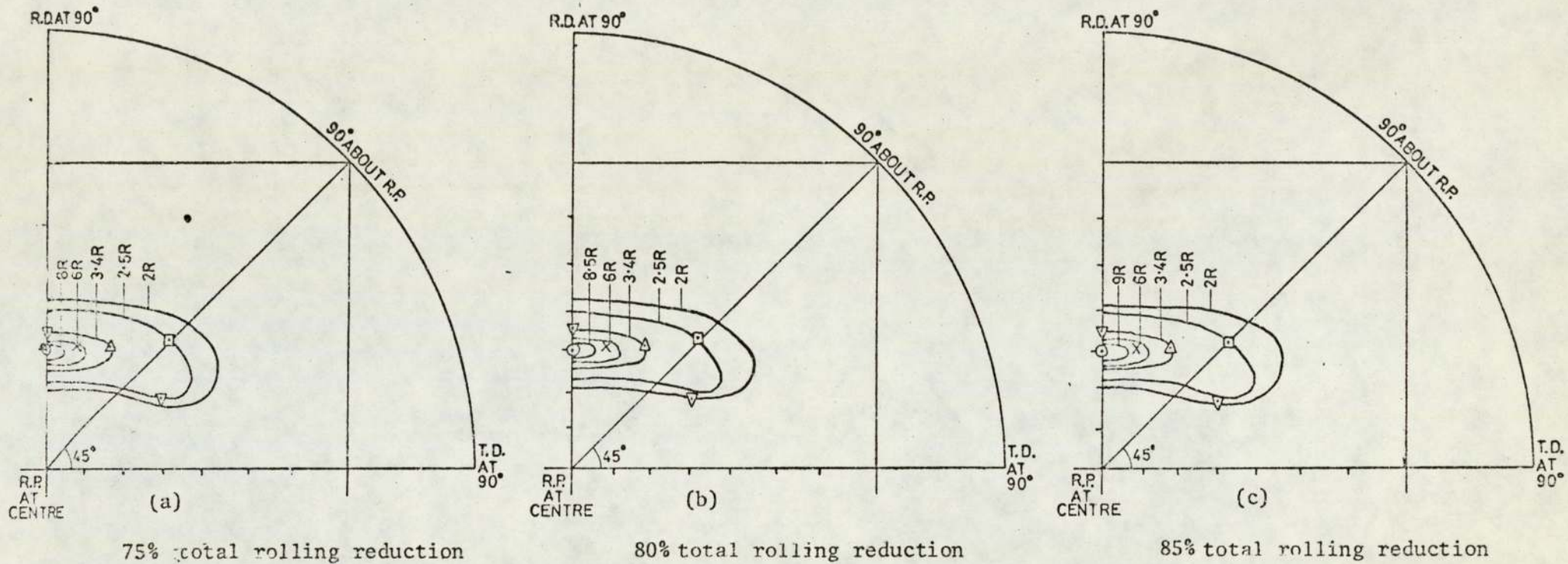


Fig. 5.4.1.3. One quadrant of (110) pole figures of specimens cold rolled using the  $45^\circ/p$  rolling schedule.

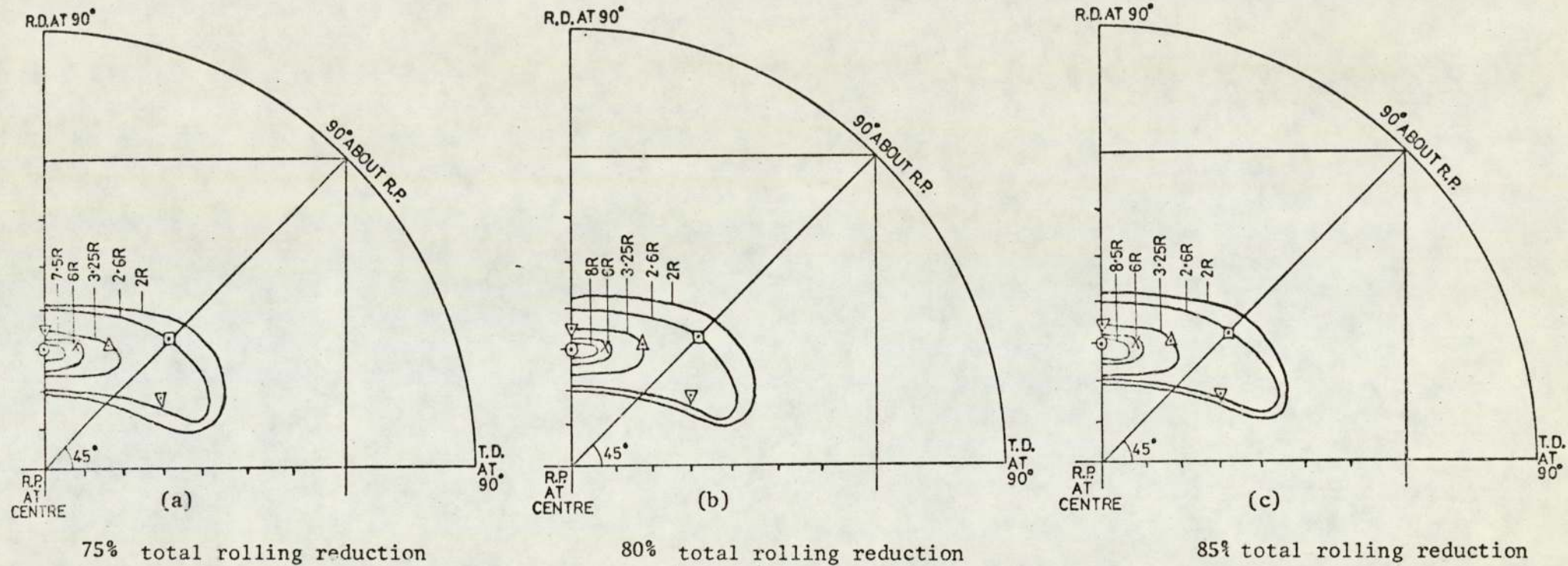


Fig. 5.4.1.4. One quadrant of (110) pole figure of specimens cold rolled using the  $55^\circ/p$  rolling schedule.

(b) Texture developed by constant roll gap schedules

P values of specimen cold rolled to 75% total reduction using roll gaps of the order of 0.02 in/p, 0.005 in/p and 0.001 in/p are listed in Table 5.4.1.1. The results indicate that the {111} and {100} orientations are the most intense while the {110} orientation is the weakest. The {211} and {332} are the next strongly aligned parallel to the strip surface. It is to be noted also that P values of the {111} and {100} planes decreased and increased respectively by decreasing the magnitude of the roll gap. There is also a slight reduction in the {211} and {332}, P values and slight increase in the {310}, {321} and {411} P values after decreasing the magnitude of the roll gap.

(110) pole figures of specimens cold rolled using the 0.02 in/p, 0.005 in/p and 0.001 in/p schedules indicated that the major texture components were the {112}<110>, {113}<110>, {111}<110>, {100}<110> and {111}<112>, as shown in figure 5.4.1.5.(a,b,c), figure 5.4.1.6.(a,b,c) and figure 5.4.1.7.(a,b,c). It is also evident that intensities of the {111}<112> and {100}<110> components increased and decreased respectively up to certain total rolling reduction depending upon each rolling schedule. Further increase in the total rolling reduction resulted in a reduction in intensity of the first component and an increase in intensity of the second component.

In the (110) pole figures of specimen cold rolled to 75% using the 0.02 in/p rolling schedule, intensity of the {111}<112> component increased and intensity of the {100}<110> component decreased when increasing the total rolling reduction to 80%, as shown in figure

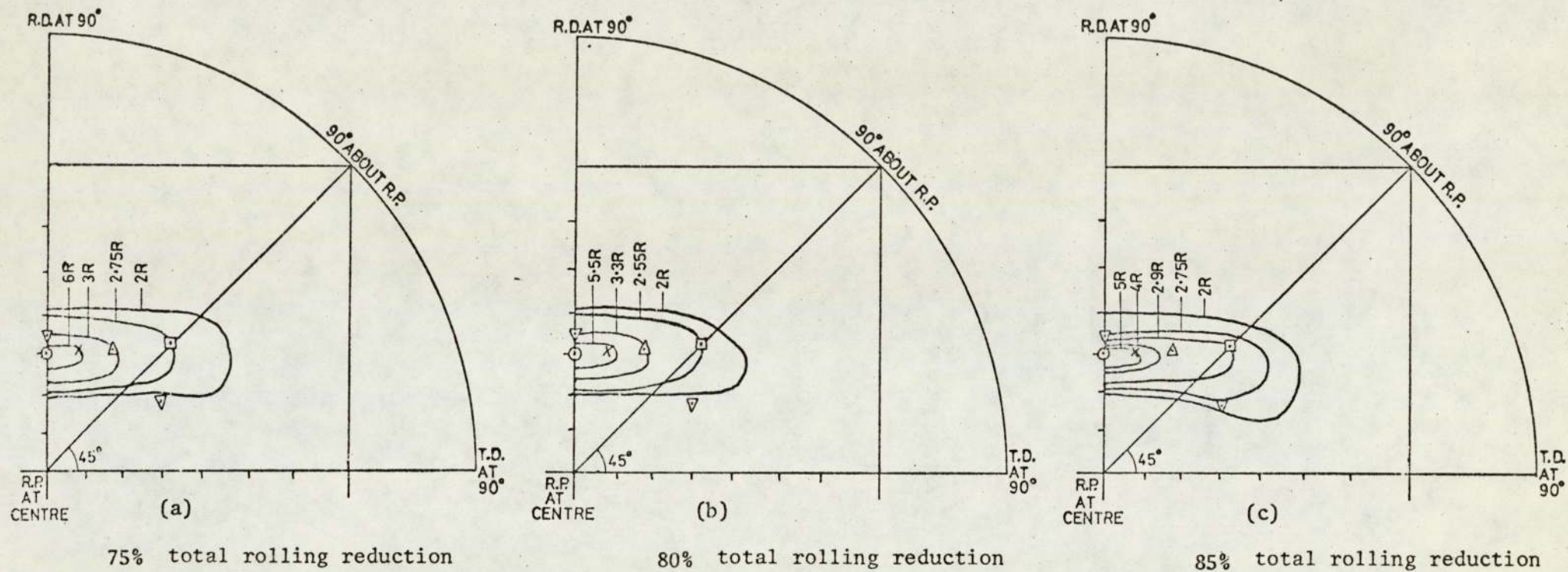


Fig. 5.4.1.5. One quadrant of (110) pole figures of specimens cold rolled using the 0.02 in/p rolling schedule .

5.4.1.5. Increasing the total rolling reduction to 85% was associated with a reduction in the  $\{111\}\langle 112\rangle$  and an increase in the  $\{100\}\langle 110\rangle$  texture intensities as shown in the same figures. Intensities of the  $\{112\}\langle 110\rangle$  and  $\{113\}\langle 110\rangle$  components decreased with increasing the rolling reduction within the range 75% to 85%.

(110) pole figures of specimens cold rolled using 0.005 in/p rolling draughts revealed a similar behaviour to (110) pole figures of specimens cold rolled using the 0.02 in/p schedule, except the maximum  $\{111\}\langle 112\rangle$  and the minimum  $\{100\}\langle 110\rangle$  components were lower and higher respectively and coincided with 75% total rolling reduction, as shown in figure 5.4.1.6 (a,b,c). The maximum intensity of the  $\{111\}\langle 112\rangle$  component and minimum intensity of the  $\{100\}\langle 110\rangle$  component of specimens cold rolled using the 0.001 in/p schedule corresponded to 70% total reduction as shown in figure 5.4.1.7 (a,b,c). In all (110) pole figures of specimens cold rolled using the 0.005 in/p and 0.001 in/p rolling schedules, intensities of the  $\{111\}\langle 112\rangle$  components were lower before and after the total rolling reductions coinciding with the maximum  $\{111\}\langle 112\rangle$  intensity. Intensities of the  $\{100\}\langle 110\rangle$  components were higher before and after the total rolling reduction corresponding to the minimum  $\{100\}\langle 110\rangle$  intensities in (110) pole figures of both schedules. Intensities of the  $\{112\}\langle 110\rangle$  component developed by rolling with 0.005 in/p and 0.001 in.p, on the other hand, increased after increasing the total rolling reduction, which is contrary to rolling with 0.002 in/p rolling schedule. Common to these three rolling schedules, intensity of the  $\{113\}\langle 110\rangle$  component remained unchanged with increasing the total rolling reduction.

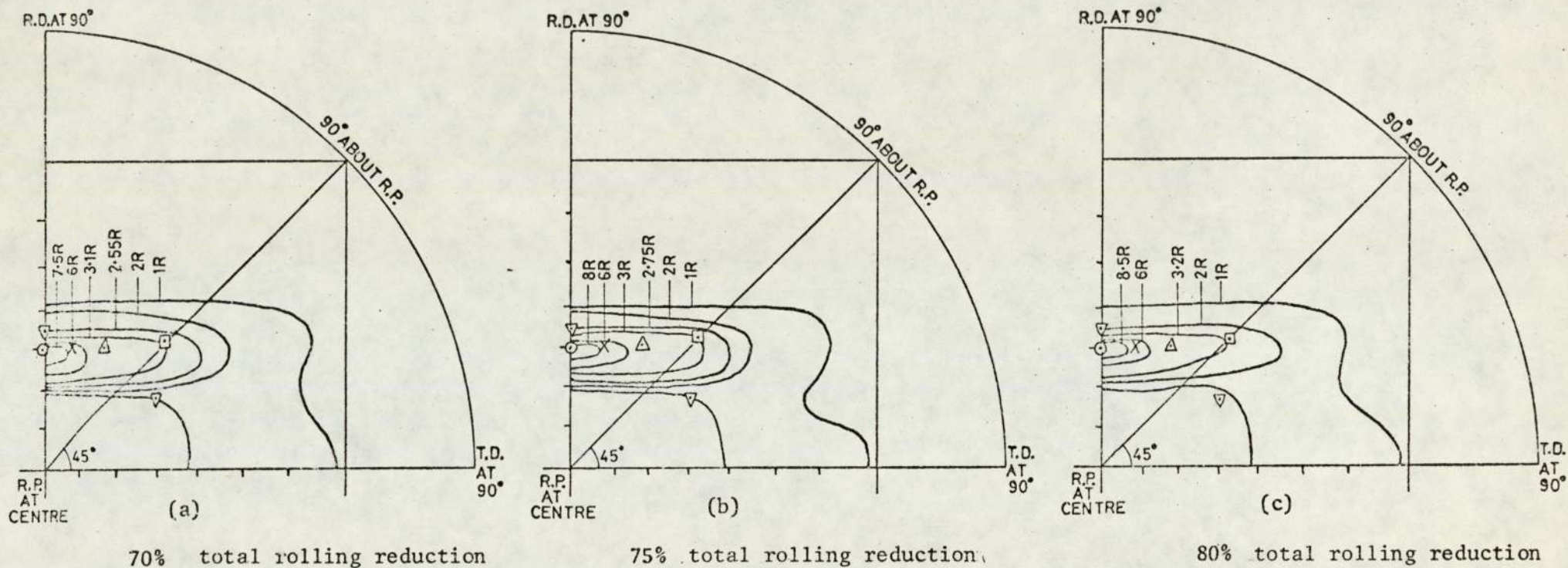


Fig. 5.4.1.6. One quadrant of (110) pole figure of specimens cold rolled using the 0.005 in/p rolling schedule.

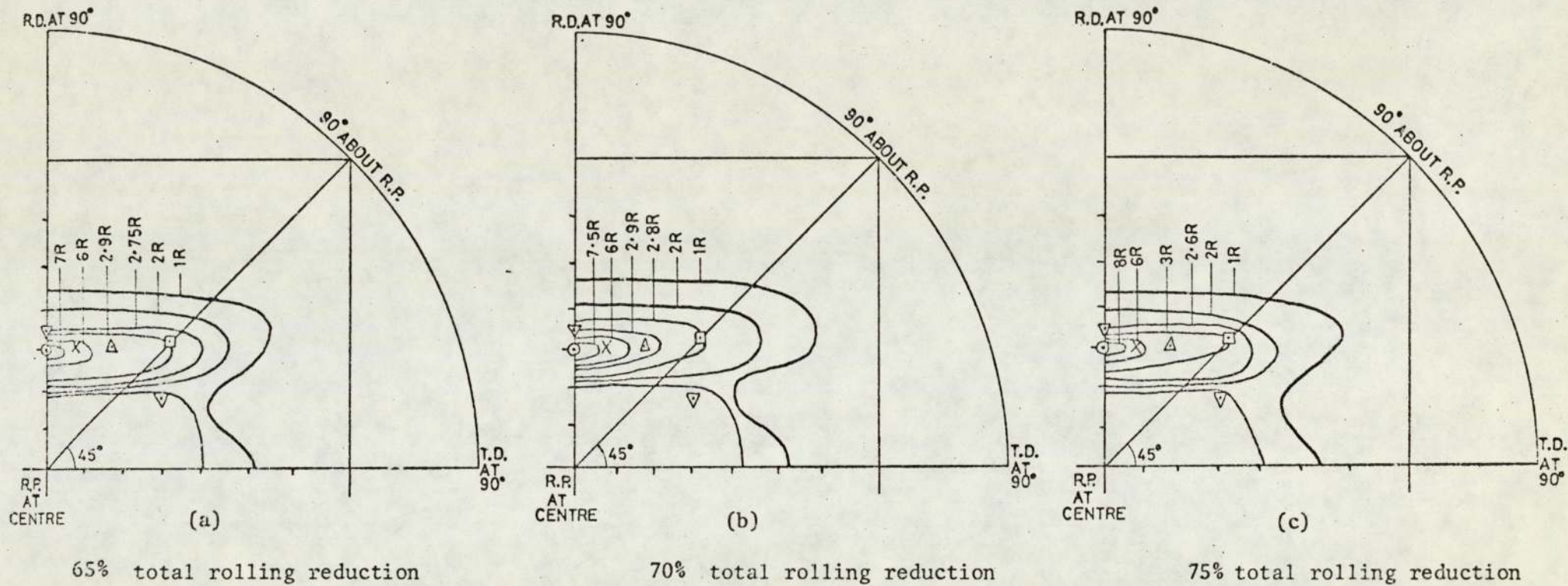


Fig. 5.4.1.7. One quadrant of (110) pole figure of specimens cold rolled using the 0.001 in/p rolling schedule.

For a given total rolling reduction texture spread increased by decreasing the magnitude of the roll gap. Texture spread increased also after increasing the total rolling reduction for a certain rolling schedule.

(c) Texture developed by the pendulum rolling schedule

Textures of specimens cold rolled to 75% using the pendulum mill is illustrated in terms of P values of eight crystallographic planes in Table 5.4.1.1. Contrary to constant geometry and roll gap schedules, crystals with {100} planes were the most predominantly aligned parallel to the strip surface, while the {111} planes were the next intense. Also P value of the {110} plane increased in comparison with P values of the same plane developed by constant geometry and roll gap schedules, but it was still relatively low. Instead, the {332} orientation was the minor component. P value of the {211} decreased and P values of the {310}, {321} and {411} increased as a result of pendulum rolling.

Considering (110) pole figure of specimen cold rolled to 65% total reduction using the pendulum mill, figure 5.4.1.8a, it is evident that the major texture components were the {112}<110>, {113}<110>, {100}<110>, {111}<110> and {111}<112> with the {112}<110> and {113}<110> predominating. In comparison with (110) pole figures of specimens cold rolled using constant geometry and roll gap schedules, intensities of the {112}<110>, {113}<110> and {111}<112> components decreased and intensity of the {100}<110> component increased when rolling with the pendulum mill. Texture spread has also increased.

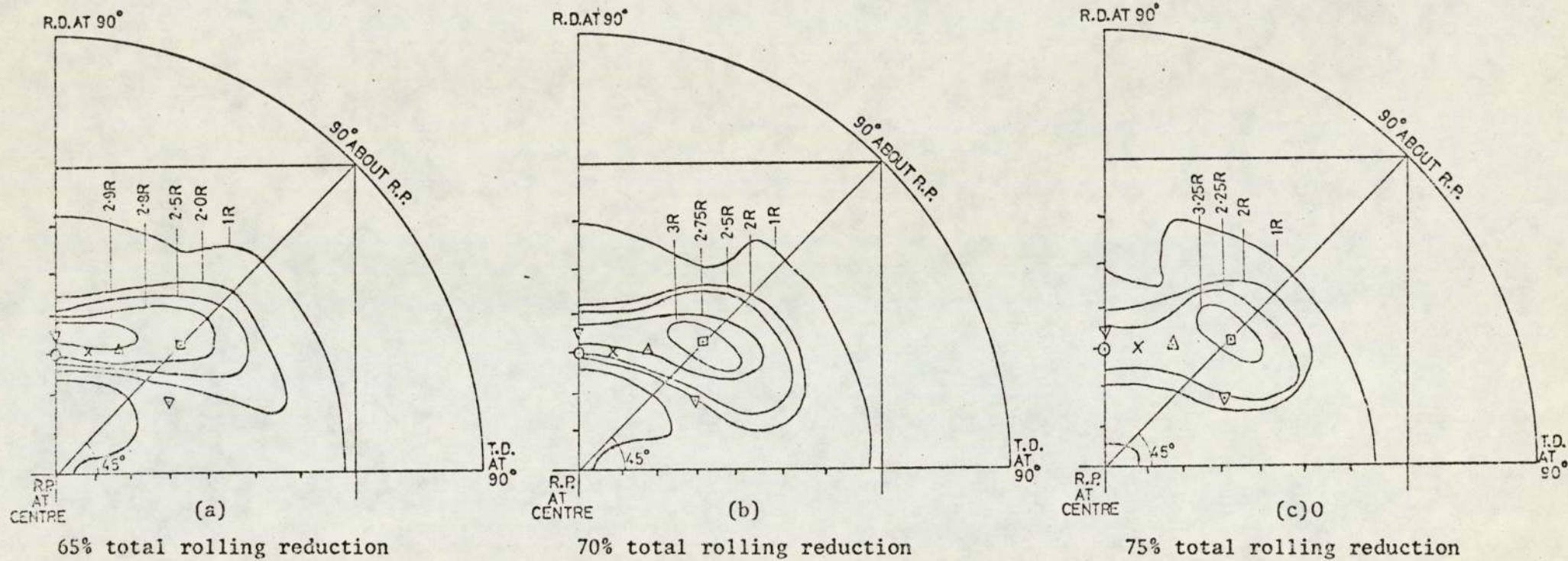


Fig. 5.4.1.8. One quadrant of (110) pole figures of specimens cold rolled using the pendulum rolling schedule.

With increasing the total rolling reduction to 70%, the  $\{100\}\langle 110\rangle$  component became dominant while intensities of the  $\{112\}\langle 110\rangle$ ,  $\{113\}\langle 110\rangle$  and  $\{111\}\langle 112\rangle$  orientations, as shown in figure 5.4.1.8b decreased. Further increase in the total rolling reduction to 75% was associated with intensification of the  $\{100\}\langle 110\rangle$  component and deterioration of the  $\{112\}\langle 110\rangle$ ,  $\{113\}\langle 110\rangle$ , and  $\{111\}\langle 112\rangle$  intensities, as shown in figure 5.4.1.8c. Texture spread increased further towards the  $60^\circ$  circle about the sheet normal towards the rolling and the transverse directions especially at the random intensity range.

(d) General observations on R value and texture of the cold rolled materials

Texture of specimens cold rolled using the  $35^\circ/p$  schedule to 75% total reduction was characterised by higher  $\{111\}$ ,  $\{211\}$  and  $\{332\}$  P values and lower  $\{100\}$ ,  $\{310\}$ ,  $\{411\}$  and  $\{321\}$  P values in comparison with texture developed by the other six rolling schedules. In contrast texture of specimens cold rolled by the pendulum mill to the same total rolling reduction consisted of lower  $\{111\}$ ,  $\{211\}$  and  $\{332\}$  and higher  $\{100\}$ ,  $\{310\}$ ,  $\{411\}$ ,  $\{321\}$  and  $\{110\}$  P values. With regard to texture of specimens cold rolled to 75% using the  $45^\circ/p$ ,  $55^\circ/p$ , 0.02 in/p, 0.005 in/p and 0.001 in/p rolling draughts gradual reductions in the P values of the  $\{111\}$ ,  $\{211\}$  and  $\{332\}$  and gradual increase in the P values of the  $\{100\}$ ,  $\{310\}$ ,  $\{411\}$  and  $\{321\}$  planes were observed.

With reference to all (110) pole figures of specimens cold rolled to 75% using the  $35^\circ/p$ ,  $45^\circ/p$ ,  $55^\circ/p$ , 0.02 in/p, 0.005 in/p, 0.001 in/p and pendulum rolling schedules, intensity of the  $\{112\}\langle 110\rangle$  and  $\{100\}\langle 110\rangle$  increased and intensity of the  $\{111\}\langle 112\rangle$  decreased in the same sequence

of the rolling schedules. The  $\{113\}\langle 110 \rangle$  texture component has not changed with altering the rolling schedules except when rolling with the 0.02 in/p and pendulum schedule where it was significantly decreased.

Inverse and (110) pole figure are therefore consistent with  $R_o$  value measurements in that higher  $R_o$  values are associated with a higher proportion of  $\{111\}$  and a lower proportion of  $\{100\}$  planes parallel to the strip surface. Accordingly, texture of specimens cold rolled using  $35^\circ/p$  schedule contributed to higher  $R_o$  value while texture of specimens cold rolled by the pendulum mill resulted in lower  $R_o$  values. The reduction in  $R_o$  values when rolling with  $45^\circ/p$ ,  $55^\circ/p$ , 0.02 in/p, 0.005 in/p, 0.001 in/p, was accompanied by corresponding reductions in the  $\{111\}$  and increases in the  $\{100\}$  intensities respectively. The high proportion of the  $\{100\}$  orientation in the cold rolling texture has counteracted the ability of the  $\{111\}$  orientation to improve  $R_o$  value. Consequently  $R_o$  values of the cold rolled materials were very low. It is to be noted also that the intensification of the  $\{100\}$  component and the reduction of the  $\{111\}$  intensity, after certain total rolling reduction, is responsible for the decrease in  $R_o$  value when rolling with constant roll gap and pendulum rolling schedules. A constant ratio of the two components, as occurred when rolling with controlled geometry schedules, is associated with constant  $R_o$  value at heavy rolling reduction.

#### 5.4.2 The annealed materials

##### (a) Texture of materials cold rolled to 75% total reduction then annealed for 0.5 hrs and 6 hrs.

Textures of specimens cold rolled to 75% total reduction, using the 35°/p, 45°/p, 55°/p, 0.02 in/p, 0.005 in/p, 0.001 in/p and pendulum rolling schedules, annealed for half an hour then aged are shown in Table 5.4.2.1 in terms of P values of eight crystallographic planes. Considering the {111} and {100} textures, which are most important with regard to R value, it is clear that their P values did not change significantly when changing the rolling procedures. This is consistent with  $R_0$  value measurements after half an hour annealing in that slight variations in the {111}/{100} ratio is corresponding to slight variation in R value.

In comparing P values of the cold rolled materials given in Table 5.4.1.1. with P values of the same specimens after half an hour annealing listed in Table 5.4.2.1. it is apparent that annealing resulted in reductions of the {100}, {211} and {111} P values, depending upon the rolling schedules i.e. the cold rolling texture. On the other hand, annealing increased the {110}, {310}, {321}, {411} and {332} P values, also depending upon the rolling schedules. The reduction in the {100} P values after half an hour annealing contributed to the improvement in  $R_0$  value of the annealed strip in comparison with  $R_0$  value prior to annealing. Presumably, the reduction in P values of the {111} planes after half an hour annealing was responsible for the relatively low  $R_0$  value of specimens annealed to that period.

No	{hkℓ}	P VALUES		
		35°/p	45°/p	55°/p
(1)	110	0.64	0.62	0.60
(2)	200	0.50	0.53	0.55
(3)	211	0.90	0.87	0.84
(4)	310	0.76	0.81	0.83
(5)	222	2.20	2.18	2.18
(6)	321	0.89	0.90	0.92
(7)	330	0.64	0.62	0.60
	411	0.56	0.59	0.62
(8)	332	0.92	0.89	0.86

(a)

No	{hkℓ}	P VALUES		
		0.02in/p	0.005in/p	0.001in/p
(1)	110	0.58	0.55	0.53
(2)	200	0.55	0.57	0.58
(3)	211	0.82	0.79	0.76
(4)	310	0.86	0.90	0.93
(5)	222	2.15	2.14	2.13
(6)	321	0.94	0.96	0.98
(7)	330	0.58	0.55	0.53
	411	0.67	0.72	0.78
(8)	332	0.84	0.80	0.76

(b)

No	{hkℓ}	P Values Pendulum
(1)	110	0.51
(2)	200	0.61
(3)	211	0.70
(4)	310	
(5)	222	2.01
(6)	321	1.10
(7)	330	0.51
	411	0.86
(8)	332	0.71

(c)

Table 5.4.2.1. P values of specimens cold rolled to 75% using the 35°/p, 45°/p, 55°/p (a) 0.02 in/p, 0.005 in/p, 0.001 in/p, (b) and pendulum, (c) schedules annealed for 0.5hr then aged.

No	{hkℓ}	P VALUES		
		35°/p	45°/p	55°/p
(1)	110	0.88	0.85	0.82
(2)	200	0.42	0.48	0.55
(3)	211	1.03	1.00	0.97
(4)	310	0.19	0.27	0.34
(5)	222	3.16	3.00	2.81
(6)	321	0.15	0.21	0.34
(7)	330	0.88	0.85	0.82
	411	0.11	0.18	0.25
(8)	332	1.17	1.15	1.13

(a)

No	{hkℓ}	P VALUES		
		0.02in/p	0.005in/p	0.001in/p
(1)	110	0.80	0.76	0.69
(2)	200	0.51	0.53	0.56
(3)	211	0.89	0.85	0.78
(4)	310	0.40	0.49	0.70
(5)	222	2.76	2.66	2.46
(6)	321	0.40	0.46	0.57
(7)	330	0.80	0.76	0.69
	411	0.34	0.41	0.51
(8)	332	1.09	1.07	1.04

(b)

No	{hkℓ}	P Values Pendulum
(1)	110	0.65
(2)	200	0.58
(3)	211	0.64
(4)	310	0.78
(5)	222	2.28
(6)	321	0.76
(7)	330	0.65
	411	0.71
(8)	332	0.95

(c)

Table 5.4.2.2. P values of specimens cold rolled to 75% using the 35°/p, 45°/p, 55°/p (a) 0.02 in/p, 0.005 in/p, 0.001 in/p, (b) and pendulum, (c) schedules annealed for 6 hrs then aged.

Increasing the annealing time from half an hour to six hours was accompanied by an increase in the  $\{111\}$  P value and a decrease in the  $\{100\}$  P value, depending upon the rolling schedules. There were also increases in the  $\{110\}$ ,  $\{211\}$  and  $\{322\}$  P values and decreases in the  $\{310\}$  and  $\{411\}$  P values. A list of P values of eight crystallographic planes of specimens cold rolled to 75% using the  $35^\circ/p$ ,  $45^\circ/p$ ,  $55^\circ/p$ , 0.02 in/p, 0.005 in/p, 0.001 in/p and pendulum rolling schedules, annealed for 6 hours then aged is given in Table 5.4.2.2. According to Table 5.4.2.2, P values of the  $\{100\}$ ,  $\{310\}$ ,  $\{321\}$  and  $\{411\}$  increased and the P values of the  $\{110\}$ ,  $\{211\}$ ,  $\{111\}$  and  $\{332\}$  decreased from one rolling schedule to the next in the same order of the previous rolling schedules. The variations in the  $\{111\}$  and  $\{100\}$  P values before and after half an hour and six hours annealing are summarised in figure 5.4.2.1 and figure 5.4.2.2.

According to (110) pole figures of specimens cold rolled to 75% total reduction using the controlled geometry rolling schedules, texture developed after 6 hours annealing consisted of two partial fibre textures described by  $\langle 110 \rangle$  direction parallel to the rolling direction and  $\{111\}$  plane parallel to the rolling plane, as shown in figure 5.4.2.3 figure 5.4.2.4 and figure 5.4.2.5. The  $\langle 110 \rangle$  direction is common to the  $\{112\}$ ,  $\{113\}$ ,  $\{111\}$  and  $\{100\}$  planes and  $\{111\}$  planes in the  $\langle 112 \rangle$  direction. Intensities of the  $\{112\}\langle 110 \rangle$ ,  $\{113\}\langle 110 \rangle$  and  $\{111\}\langle 112 \rangle$  decreased and intensity of the  $\{100\}\langle 110 \rangle$  component increased when increasing the angle between the specimen and rolls.

Texture of specimens cold rolled to 75% using controlled roll gap rolling schedules annealed for 6 hrs then aged consisted of the same texture components developed by controlled geometry rolling but

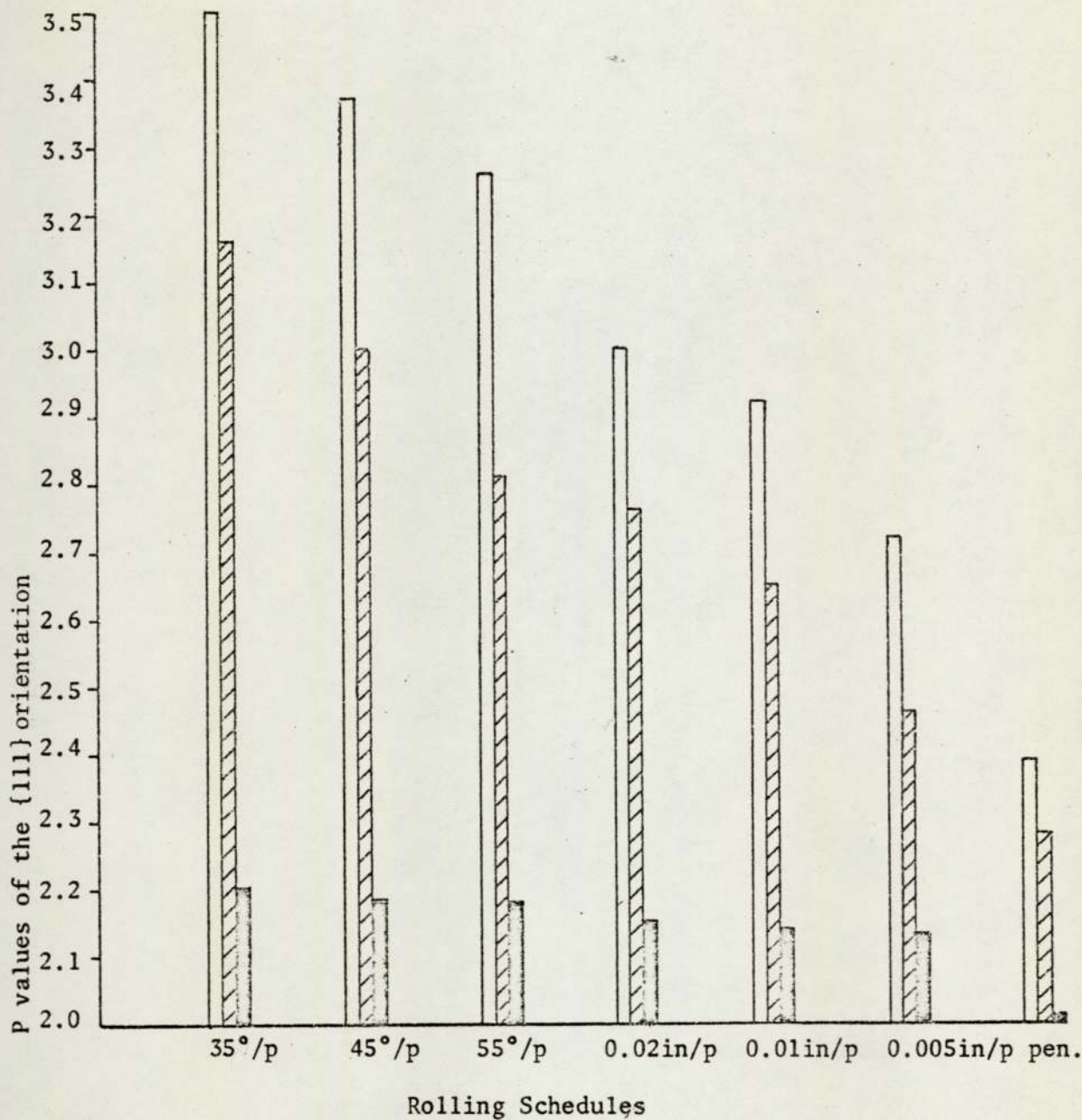


Fig. 5.4.2.1. Shows the variations in P values of the {111} planes with the 35°/p, 45°/p, 55°/p, 0.02 in/p, 0.005 in/p, 0.001 in/p and pendulum rolling schedules prior to annealing (□) and after annealing for 6 hrs (▨) and 0.5 hr (■).

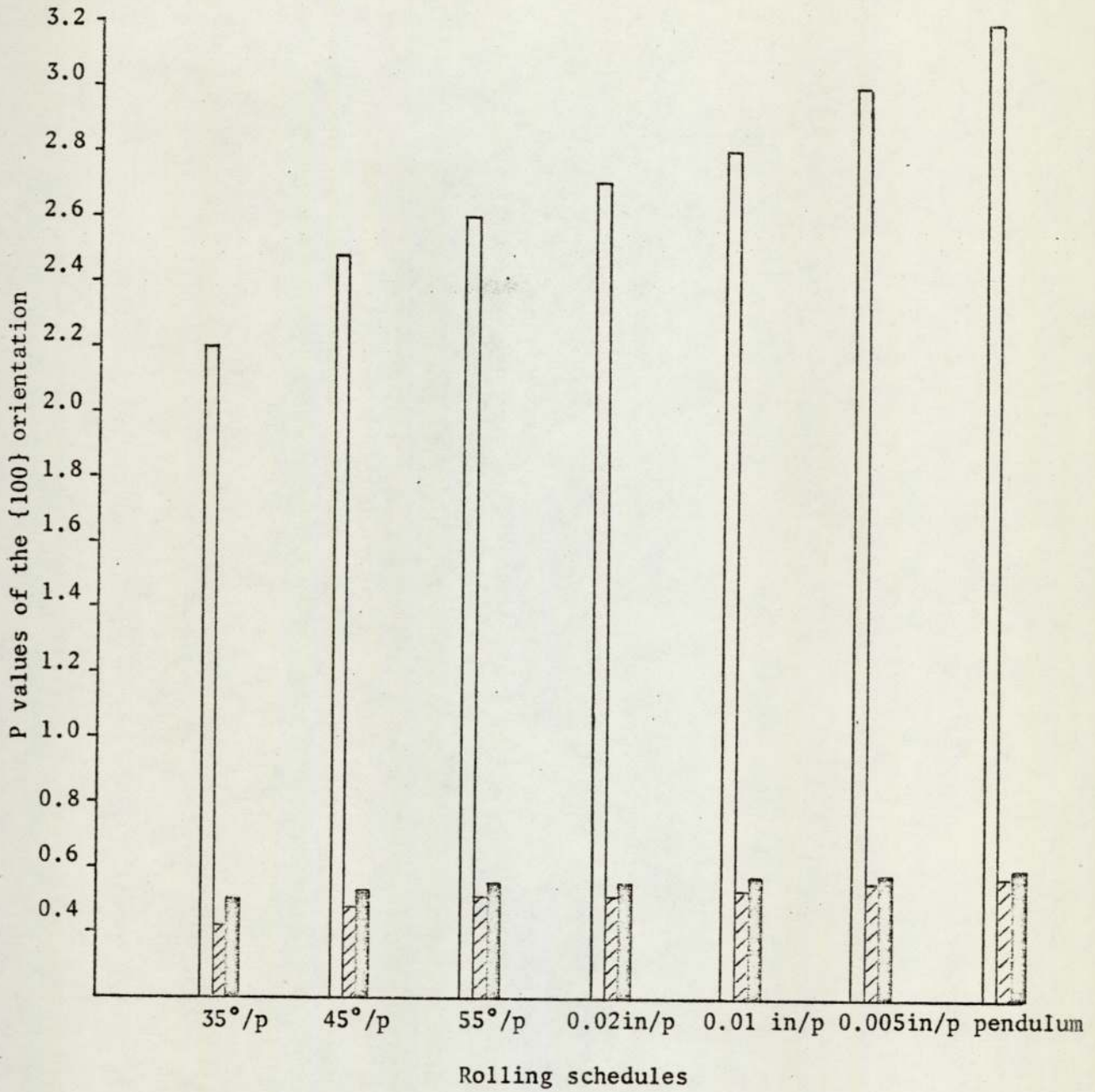


Fig. 5.4.2.2. Shows the variations in the {100} P values with the 35°/p, 45°/p, 55°/p, 0.02in/p, 0.005 in/p, 0.001 in/p and pendulum, prior to annealing (□) after 6 hrs annealing (▨) and 0.5 hr annealing (■).

texture intensities were different, as illustrated in figure 5.4.2.6, figure 5.4.2.7 and figure 5.4.2.8. In comparison with controlled geometry rolling intensities of the  $\{112\}\langle 110\rangle$ ,  $\{113\}\langle 110\rangle$  and  $\{111\}\langle 112\rangle$  components were lower and intensity of the  $\{100\}\langle 110\rangle$  component was higher when rolling with constant roll gap schedules. With reference to the magnitude of roll gap, intensities of the  $\{112\}\langle 110\rangle$ ,  $\{113\}\langle 110\rangle$  and  $\{100\}\langle 110\rangle$  decreased and intensities of the  $\{111\}\langle 112\rangle$  increased with increasing the roll gap.

(110) pole figures of specimens cold rolled to 75% using the pendulum mill, annealed for 6 hrs then aged revealed a weaker partial fibre texture in comparison with texture developed by controlled geometry and roll gap rolling schedules, as shown in figure 5.4.2.9c. Texture is characterised by more  $\{100\}\langle 110\rangle$  component and less  $\{112\}\langle 110\rangle$ ,  $\{113\}\langle 110\rangle$  and  $\{111\}\langle 112\rangle$  relative to the previous rolling schedules.

Texture spread after 75% total rolling reduction and 6 hrs annealing was dependent upon the rolling schedules, being sharper when rolling with  $35^\circ/p$  rolling schedule. However, texture spread increased when rolling with  $45^\circ/p$ ,  $55^\circ/p$ , 0.02 in/p, 0.005 in/p, 0.001 in/p and pendulum rolling schedules respectively.

Comparing (110) pole figures of specimens cold rolled to 75% using the previous rolling schedules with the corresponding (110) pole figures prior to annealing, it was revealed that texture intensity decreased significantly but texture components were similar to the cold rolling texture components. Intensities of the  $\{112\}\langle 110\rangle$ ,  $\{113\}\langle 110\rangle$  and  $\{100\}\langle 110\rangle$  components were the most affected by annealing while the  $\{111\}\langle 112\rangle$  components were less affected.

Rolling with  $35^\circ/p$  then annealing for 6 hours is associated with more  $\{111\}$  planes and less  $\{100\}$  planes parallel to the surface and is therefore favoured for higher R value. This is consistent with the R value measurements.

(b) Texture of materials cold rolled to a range of total reductions then annealed for 6 hrs only

In order to demonstrate the effect of increasing the total rolling reduction prior to annealing upon texture developed after annealing, (110) pole figures of specimens cold rolled to different rolling reductions depended upon each rolling schedule, annealed for 6 hrs then aged were examined. (110) pole figures of specimens cold rolled to 75, 80 and 85% using the controlled geometry rolling schedules are shown in figure 5.4.2.3 (a,b,c), figure 5.4.2.4 (a,b,c) and figure 5.4.2.5 (a,b,c). It is evident from figure 5.4.2.3 (a,b,c) that during rolling with  $35^\circ/p$  rolling schedule, intensities of the  $\{100\}\langle 110 \rangle$  and  $\{111\}\langle 112 \rangle$  remained constant regardless of increasing the total reduction. On the other hand, intensities of the  $\{112\}\langle 110 \rangle$  and  $\{113\}\langle 110 \rangle$  continued to increase. Texture developed by the  $45^\circ/p$  and  $55^\circ/p$  behaved in the same manner except intensities of the  $\{112\}$ ,  $\{113\}$  and  $\{111\}$  components increased and intensity of the  $\{100\}$  component decreased when decreasing the shear plane angle. The behaviour of the cold rolling texture developed by controlled geometry rolling schedules was therefore, preserved after annealing.

Like the cold rolling texture developed by controlled roll gap rolling schedules, intensity of the  $\{100\}\langle 110 \rangle$  component decreased and

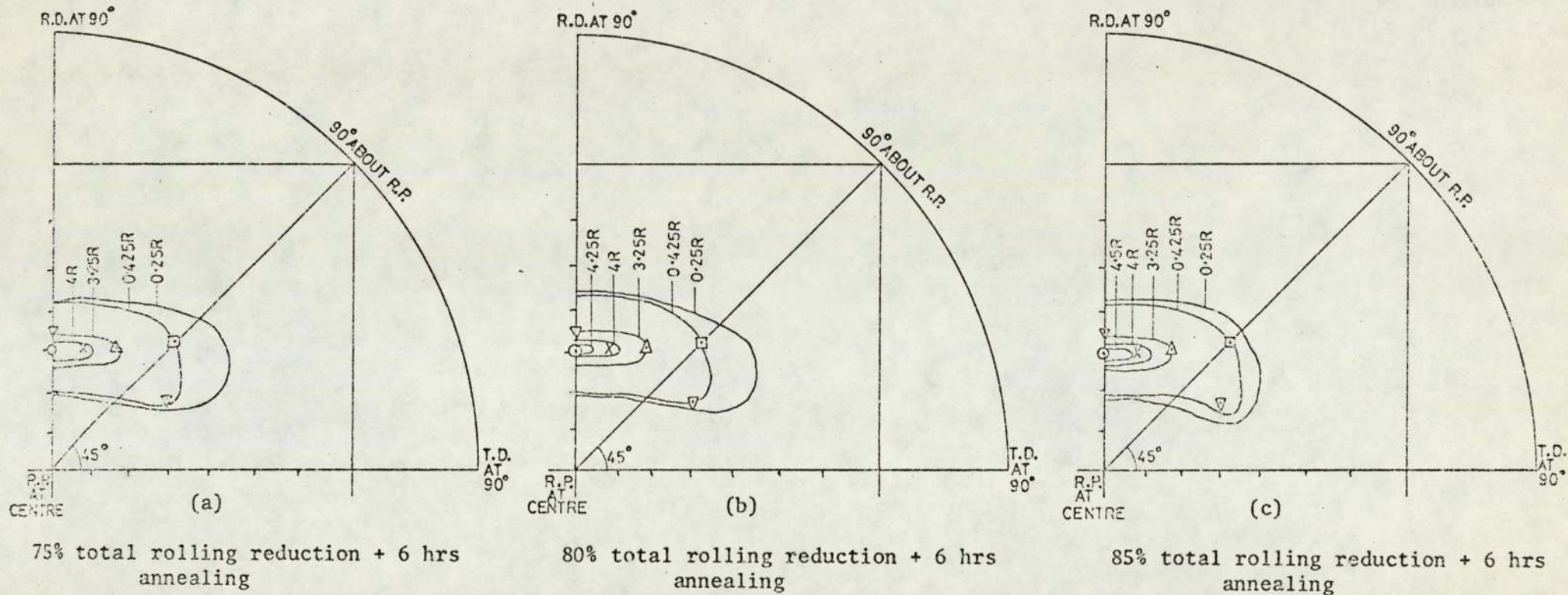


Fig. 5.4.2.3. One quadrant of (110) pole figures of specimens cold rolled using the 35°/p schedule, annealed for 6 hrs then aged.

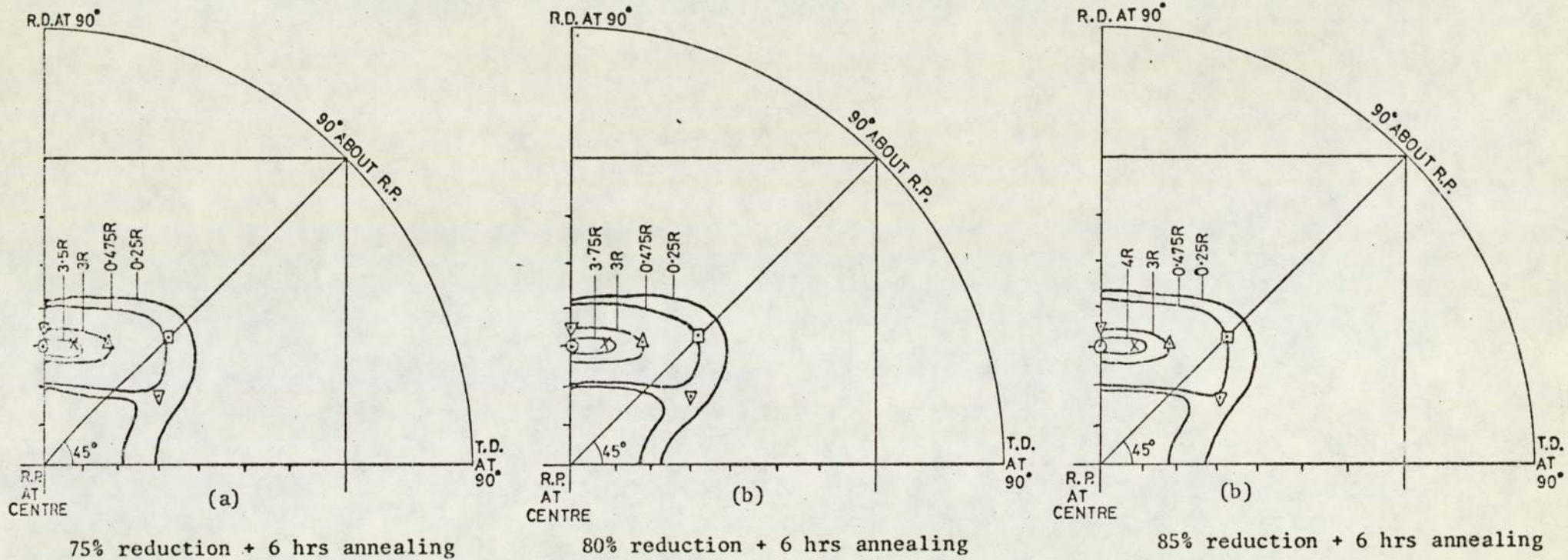
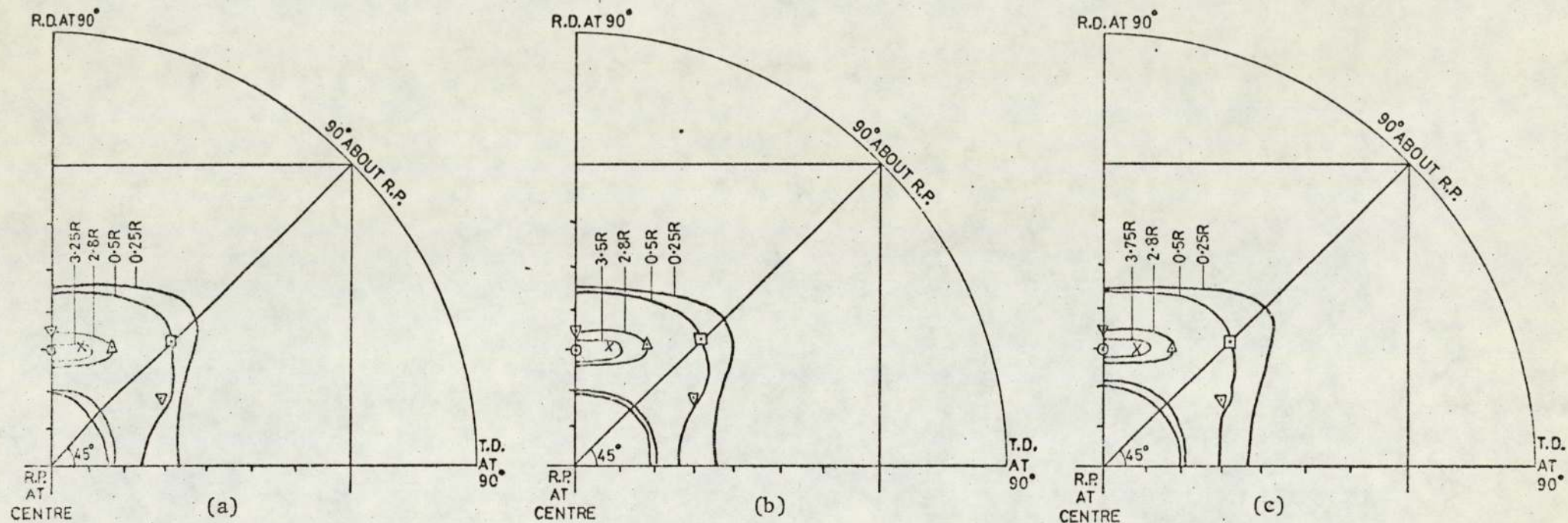


Fig. 5.4.2.4. One quadrant of (110) pole figures of specimens cold rolled using the  $45^\circ/p$  schedule, annealed for 6 hrs then aged.



75% total rolling reduction  
+ 6 hrs annealing

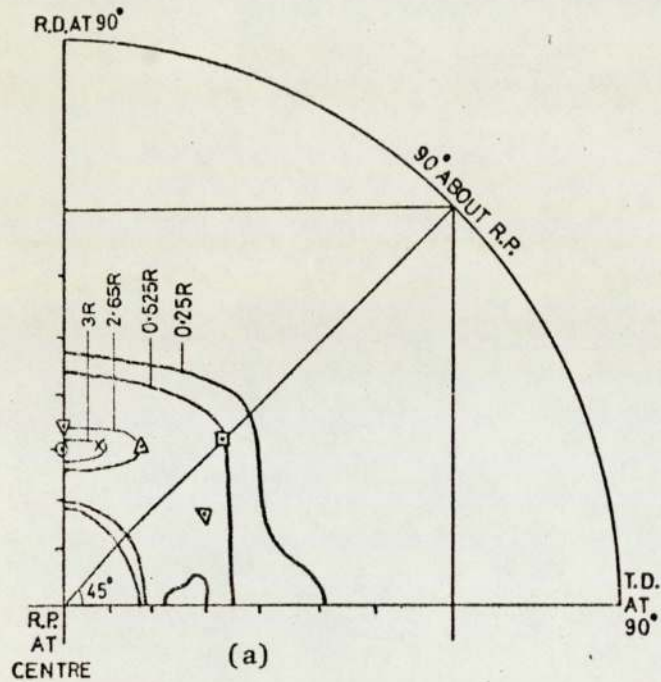
80% total rolling reduction  
+ 6 hrs annealing

85% total rolling reduction  
+ 6 hrs annealing

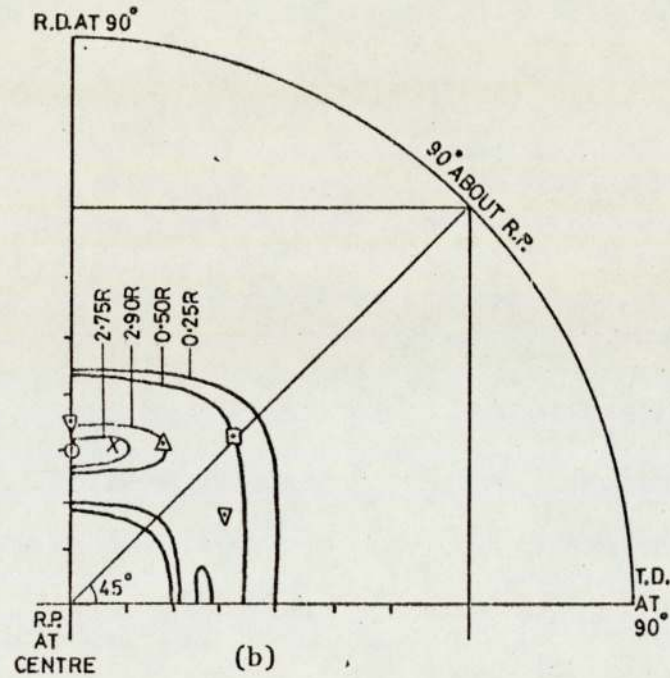
Fig. 5.4.2.5. One quadrant of (110) pole figures of specimens cold rolled using the 55°/p schedule, annealed for 6 hrs then aged.

intensity of the  $\{111\}\langle 112 \rangle$  component increased, after annealing up to certain rolling reductions depended upon each rolling schedule. Further increase in the total reduction resulted in an increase in intensity of the first component and a decrease in intensity of the second component as shown in figure 5.4.2.5 (a,b,c), figure 5.4.2.6 (a,b,c) and figure 5.4.2.7 (a,b,c). In the case of specimens cold rolled using 0.02 in/p rolling schedule, intensities of the  $\{100\}\langle 110 \rangle$ ,  $\{112\}\langle 110 \rangle$  and  $\{113\}\langle 110 \rangle$  components decreased and intensities of the  $\{111\}\langle 112 \rangle$  components increased with increasing the total rolling reduction from 75% to 80%. With increasing the total rolling reduction to 85% intensity of the  $\{100\}\langle 110 \rangle$  component increased and intensities of the  $\{111\}\langle 112 \rangle$  components decreased, while intensities of the  $\{112\}\langle 110 \rangle$  and  $\{113\}\langle 110 \rangle$  components continued to decrease, as shown in figure 5.4.2.5 (a,b,c).

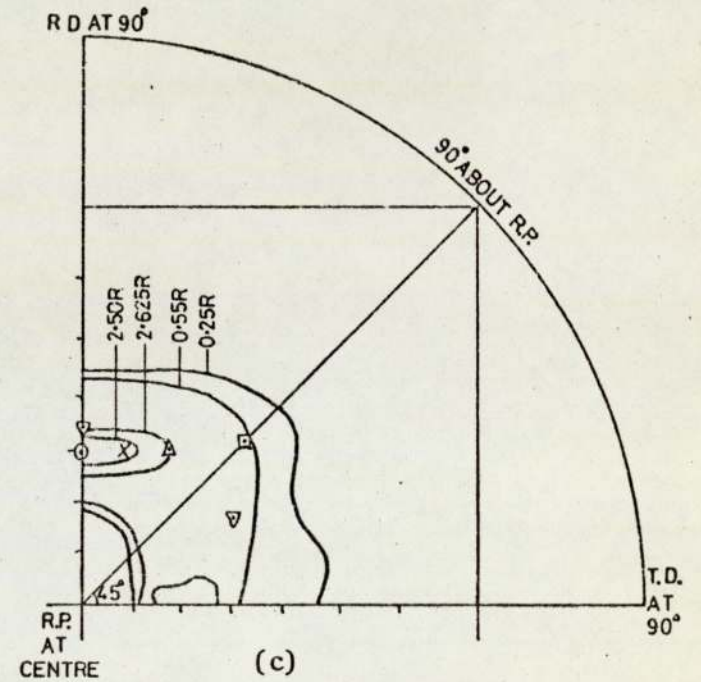
Considering figure 5.4.2.6 (a,b,c) and figure 5.4.2.7 (a,b,c), it is apparent that intensities of the  $\{100\}\langle 110 \rangle$  and  $\{111\}\langle 112 \rangle$  components followed the same behaviour pattern when rolling with 0.005 in/p to 70, 75 and 80% and when rolling with 0.001 in/p schedule to 65, 70 and 75%, except the minimum  $\{100\}\langle 110 \rangle$  and maximum  $\{111\}\langle 112 \rangle$  coincided with lower total reductions. These total reductions corresponded to 75% and 70% when rolling with 0.005 in/p and 0.001 in/p draughts respectively. Contrary to rolling with 0.02 in/p schedule intensities of the  $\{112\}\langle 110 \rangle$  and  $\{113\}\langle 110 \rangle$  continued to increase with increasing the total rolling reduction.



75% Total rolling reduction  
+ 6 hrs annealing

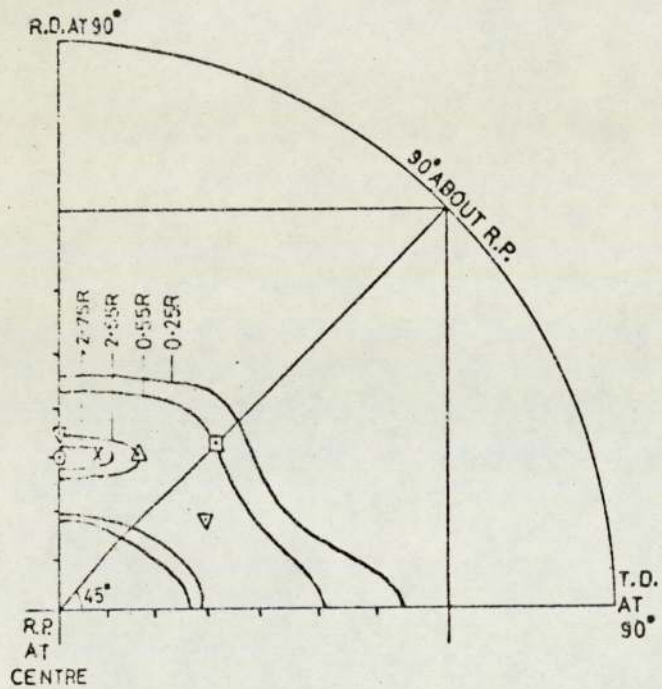


80% Total rolling reduction  
+ 6 hrs annealing

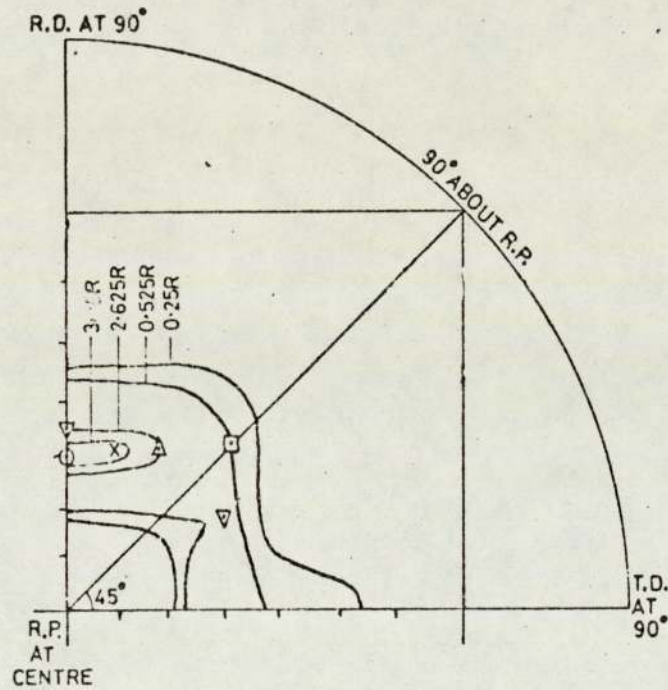


85% Total rolling reduction  
+ 6 hrs annealing

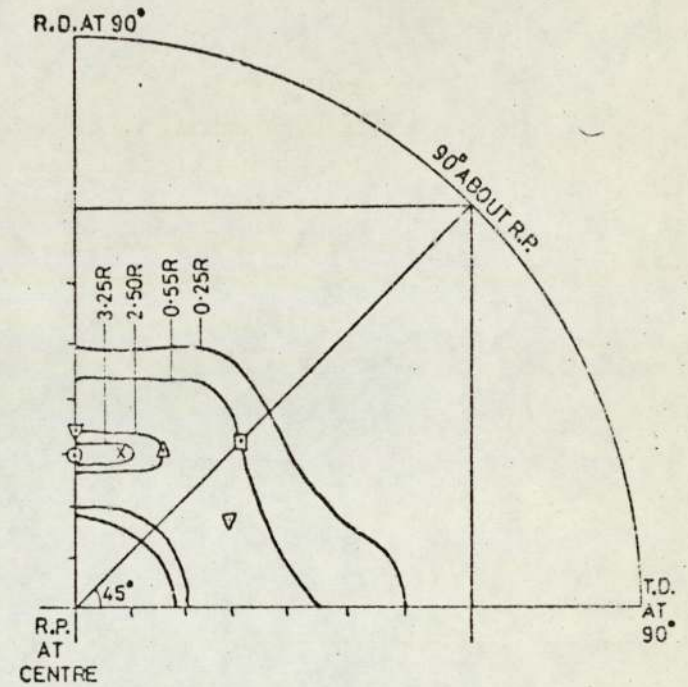
Fig. 5.4.2.6. One quadrant of (110) pole figures of specimens cold rolled using the 0.02 in/p schedule , annealed for 6 hrs then aged.



(a) 70% Total Rolling Reduction  
+ 6 hrs annealing



(b) 75% Total Rolling Reduction  
+ 6 hrs annealing



(c) 80% Total Rolling Reduction  
+ 6 hrs annealing

Fig.5.4.2.7. One quadrant of (110) pole figures of specimens cold rolled using the 0.005 in/p schedule, annealed for 6 hrs then aged.

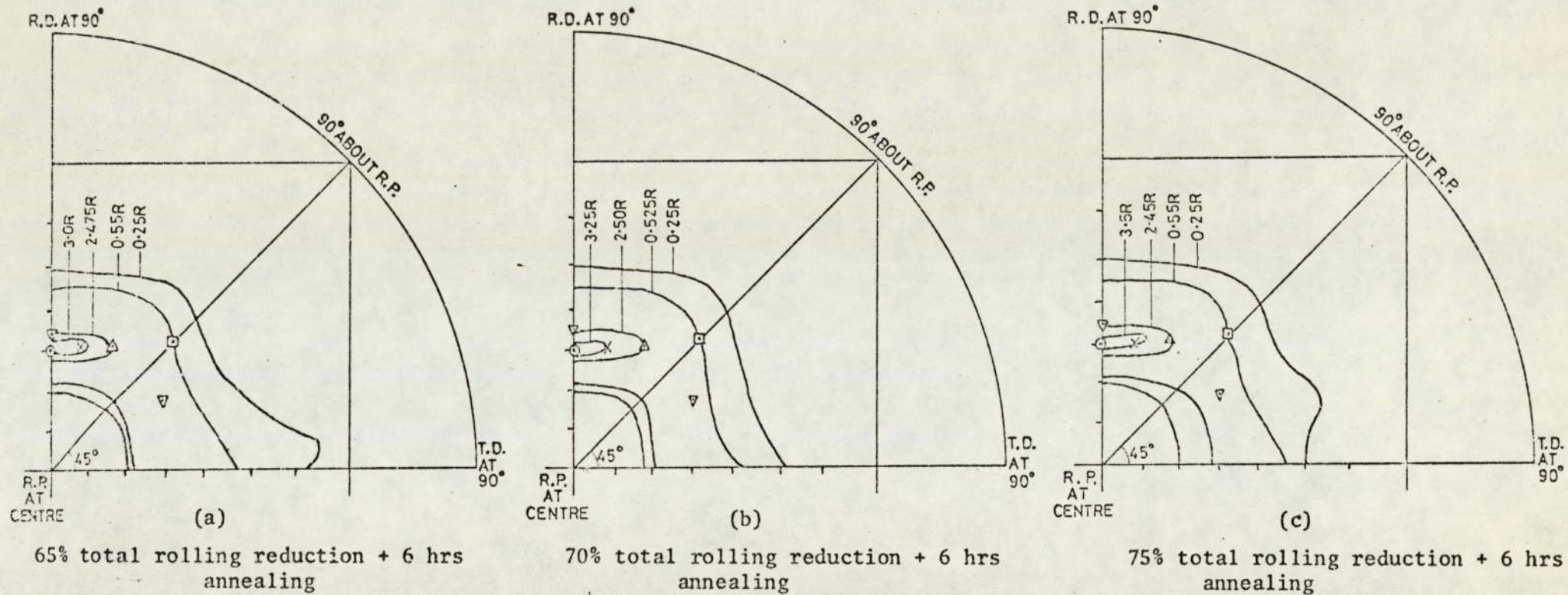


Fig. 5.4.2.8. One quadrant of (110) pole figures of specimens cold rolled using the 0.001 in/p schedule, annealed for 6 hrs then aged.

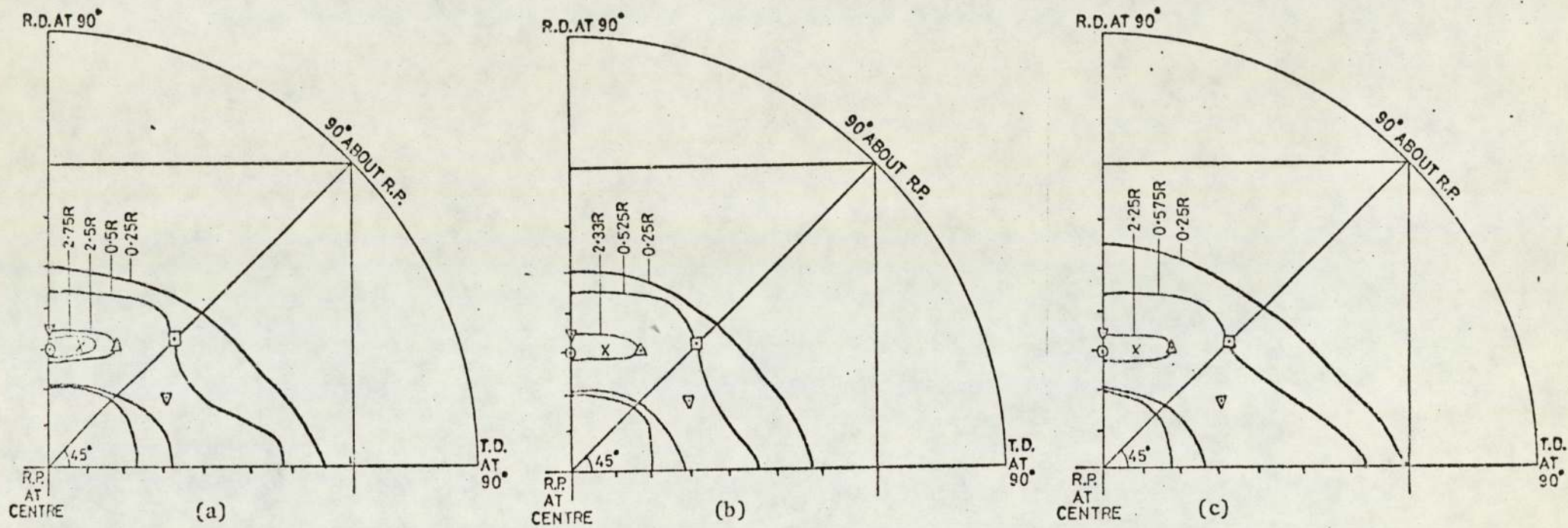
(110) pole figures of specimens cold rolled by the pendulum to 65% 70% and 75%, annealed for 6 hrs then aged figure 5.4.2.9 (a,b,c) revealed that increasing the total reduction from 65% to 70% was associated with an increase in the  $\{100\}\langle 110 \rangle$  intensity and decreases in the  $\{111\}\langle 112 \rangle$ ,  $\{112\}\langle 110 \rangle$  and  $\{113\}\langle 110 \rangle$  intensities. Increasing the total rolling reduction to 75% resulted in further increase in intensity of the first component and decreases in intensities of the second components, as shown in figure 5.4.2.9c.

#### 5.5 CRYSTAL REORIENTATION AFTER TENSILE EXTENSION

The reorientation of crystals after tensile extension is dealt with in this section in two parts. The first part is concerned with the reorientation of crystals of specimens cold rolled to 75%, annealed for different times, aged and then subjected to 20% tensile extension. In the second part, crystals reorientation of specimens cold rolled to different total rolling reductions, , annealed for 6 hrs, aged then subjected to 20% tensile extension is described.

##### (a) Reorientation of crystals of materials cold rolled to 75% total reduction then annealed for 0.5 and 6 hrs

Measurements of P values of specimens cold rolled to 75% using the 35°/p, 45°/p, 55°/p, 0.02 in/p, 0.005 in/p, 0.001 in/p and pendulum rolling schedules, annealed for 0.5 hr, aged then subjected to 20% tensile extension are listed in Table 5.5.a.1. Accordingly, P values of the  $\{110\}$ ,  $\{211\}$ ,  $\{111\}$  and  $\{332\}$  planes decreased when altering the rolling schedules in the same sequence as the previous schedules. P values of the  $\{100\}$ ,  $\{310\}$ ,  $\{321\}$  and  $\{411\}$  planes increased in the same previous order of rolling schedules.



65% Total rolling reduction +  
6 hrs annealing

70% Total rolling reduction +  
6 hrs annealing

75% Total rolling reduction  
6 hrs annealing

Fig. 5.4.2.9. One quadrant of (110) pole figures of specimens cold rolled using the pendulum schedule, annealed for 6 hrs then aged.

No	{hkℓ}	P VALUES		
		35°/p	45°/p	55°/p
(1)	110	0.57	0.56	0.55
(2)	200	0.62	0.67	0.71
(3)	211	1.11	1.07	1.01
(4)	310	0.68	0.70	0.71
(5)	222	1.92	1.87	1.81
(6)	321	0.97	1.05	1.15
(7)	330	0.57	0.56	0.55
	411	0.49	0.50	0.52
(8)	332	1.08	1.02	0.98

(a)

No	{hkℓ}	P VALUES		
		0.02in/p	0.005in/p	0.001in/p
(1)	110	0.54	0.52	0.51
(2)	200	0.78	0.83	0.91
(3)	211	0.98	0.94	0.89
(4)	310	0.72	0.75	0.76
(5)	222	1.73	1.69	1.66
(6)	321	1.24	1.30	1.35
(7)	330	0.54	0.52	0.51
	411	0.53	0.55	0.57
(8)	332	0.94	0.89	0.84

(b)

No	{hkℓ}	P Values Pendulum
(1)	110	0.49
(2)	200	1.11
(3)	211	0.82
(4)	310	0.80
(5)	222	1.39
(6)	321	1.50
(7)	330	0.49
	411	0.61
(8)	332	0.77

(c)

Table 5.5. a.1. P values of specimens cold rolled to 75% using the 35°/p, 45°/p, 55°/p (a) 0.02 in/p, 0.005 in/p, 0.001 in/p, (b) and pendulum, (c) schedules annealed for 0.5hr, aged, then subjected to 20% tensile extension.

The significance of P values after tensile extension listed in the previous table is apparent when compared with the corresponding P values before tensile extension in Table 5.4.2.1. Thus, it was concluded that the {111} P values decreased after tensile extension depending upon the rolling schedules. The magnitude of such reductions increased when using the 35°/p, 45°/p, 55°/p, 0.02 in/p, 0.005 in/p, 0.001 in/p and pendulum respectively, as shown in Table 5.5.a.2. For instance, the reduction in the {111} P values after tensile extension was equal to 0.3 and 0.67 when rolling with 35°/p and pendulum. P values of the {100} planes, on the other hand, increased after tensile extension in the same previous order of rolling schedules as shown in Table 5.5.a.3. The difference in P values of the {100} planes before and after tensile extension varied between 0.12 and 0.50 when rolling with 35°/p and pendulum rolling schedules. P values of the {110}, {310} and {411} planes slightly decreased, while P values of the {211}, {321} and {332} planes slightly increased after tensile extension, depending upon the rolling schedules.

Measurements of P values of specimens cold rolled to the same previous rolling reduction using the same rolling schedules, but annealed for 6 hrs, aged then subjected to 20% tensile extension are shown in Table 5.5.a.4. The differences in P values of the {111} and {100} planes before and after tensile extension were more significant than the difference in P values of corresponding planes after half an hour annealing. P values of the {111} planes, for example, decreased by 0.18 when rolling with 35°/p schedule in comparison with 0.56 when rolling with the pendulum schedule. Differences in P values before

ROLLING SCHEDULES	P VALUES		DIFFERENCES
	Before tensile extension	After tensile extension	
35°/p	2.20	1.90	0.30
45°/p	2.18	1.86	0.32
55°/p	2.17	1.81	0.36
0.02 in/p	2.15	1.73	0.42
0.005 in/p	2.14	1.69	0.45
0.001 in/p	2.13	1.65	0.48
Pendulum	2.06	1.39	0.67

Table 5.5.a.2. A summary of the differences in the  $\{111\}$  P values of specimen cold rolled to 75%, using the 35°/p, 45°/p, 55°/p, 0.02 in/p, 0.005 in/p, 0.001 in/p and pendulum schedules, annealed for 0.5 hr, aged, before and after 20% tensile extension.

ROLLING SCHEDULES	P VALUES		DIFFERENCES
	Before tensile extension	After tensile extension	
35°/p	0.50	0.62	0.12
45°/p	0.53	0.67	0.14
55°/p	0.54	0.71	0.17
0.02 in/p	0.55	0.77	0.22
0.005 in/p	0.57	0.83	0.26
0.001 in/p	0.58	0.91	0.33
Pendulum	0.61	1.11	0.50

Table 5 5.a. 3 A summary of the differences in the {100} P values of specimen cold rolled to 75%, using the 35°/p, 45°/p, 55°/p, 0.02 in/p, 0.005 in/p, 0.001 in/p and pendulum schedules, annealed for 0.5 hr, aged, before and after 20% tensile extension.

No	{hkl}	P VALUES		
		35°/p	45°/p	55°/p
(1)	110	0.75	0.74	0.73
(2)	200	0.45	0.54	0.59
(3)	211	1.30	1.25	1.20
(4)	310	0.13	0.20	0.25
(5)	222	2.98	2.77	2.56
(6)	321	0.17	0.26	0.44
(7)	330	0.75	0.74	0.73
	411	0.08	0.15	0.21
(8)	332	1.38	1.35	1.28

(a)

No	{hkl}	P VALUES		
		0.02in/p	0.005in/p	0.001in/p
(1)	110	0.72	0.70	0.69
(2)	200	0.62	0.68	0.74
(3)	211	1.11	1.04	0.95
(4)	310	0.30	0.37	0.55
(5)	222	2.43	2.30	2.00
(6)	321	0.59	0.67	0.81
(7)	330	0.72	0.70	0.69
	411	0.29	0.35	0.43
(8)	332	1.22	1.17	1.12

(b)

No	{hkl}	P Values Pendulum
(1)	110	0.63
(2)	200	0.78
(3)	211	0.77
(4)	310	0.70
(5)	222	1.62
(6)	321	1.21
(7)	330	0.63
	411	0.63
(8)	332	1.01

(a)

Table 5.5. a 4. P values of specimens cold rolled to 75% using the 35°/p, 45°/p, 55°/p (a) 0.02 in/p, 0.005 in/p, 0.001 in/p, (b) and pendulum, (c) schedules annealed for 6 hrs aged, then subjected to 20% tensile extension.

and after tensile extension in the case of specimens cold rolled to the same previous total rolling reduction using the  $45^\circ/p$ ,  $55^\circ/p$ ,  $0.02$  in/p,  $0.005$  in/p and  $0.001$  in/p, increased in the same order rolling schedules as shown in Table 5.5.a.5. The difference in P values of the  $\{100\}$  planes increased with altering schedules in the same order of previous rolling schedules as shown in Table 5.5.a.6. Tensile extension was accompanied also with a slight gradual reduction in the P values of the  $\{110\}$ ,  $\{211\}$  and  $\{322\}$  planes and a gradual slight increase in the P values of the  $\{310\}$ ,  $\{321\}$  and  $\{411\}$  planes. This is evident when comparing Table 5.4.2.2 with Table 5.5.a.4.

Crystals reorientation of specimens cold rolled to 75% using the previous rolling schedules, annealed for 6 hrs, aged then subjected to 20% tensile extension is described in (110) pole figures shown in figure 5.5.b.1, figure 5.5.b.2, figure 5.5.b.3, figure 5.5.b.6, figure 5.5.b.<sup>7</sup>, figure 5.5.b.<sup>8</sup>, and figure 5.5.b.9. Analysis of these figures indicated that intensities of the  $\{112\}\langle 110\rangle$ ,  $\{113\}\langle 110\rangle$  and  $\{111\}\langle 112\rangle$  decreased while intensity of the  $\{100\}\langle 110\rangle$  component increased with the rolling schedules in the same order. The effect of tensile extension upon crystals orientation is clear when comparing corresponding (110) pole figures before and after tensile extension. However, the difference in intensities of the  $\{111\}\langle 112\rangle$  before and after tensile extension was relatively small when rolling with  $35^\circ/p$  and increased when rolling with  $45^\circ/p$ ,  $55^\circ/p$ ,  $0.02$  in/p,  $0.005$  in/p,  $0.001$  in/p and pendulum respectively. The difference in the  $\{100\}\langle 110\rangle$  intensity increased in the same sequence as the previous rolling schedules.

ROLLING SCHEDULES	P VALUES		DIFFERENCES
	Before tensile extension	After tensile extension	
35°/p	3.16	2.98	0.18
45°/p	3.00	2.77	0.23
55°/p	2.80	2.56	0.24
0.02 in/p	2.76	2.42	0.34
0.005 in/p	2.65	2.30	0.35
0.001 in/p	2.46	2.00	0.46
Pendulum	2.28	1.62	0.56

Table 5.5.a.5. A summary of the differences in the  $\{111\}$  P values of specimen cold rolled to 75%, using the 35°/p, 45°/p, 55°/p, 0.02 in/p, 0.005 in/p, 0.001 in/p and pendulum schedules, annealed for 6 hr, aged, before and after 20% tensile extension.

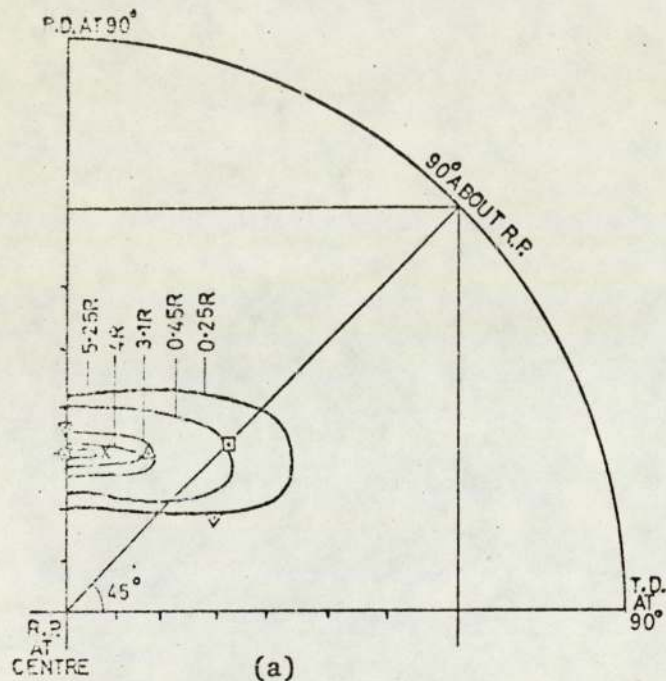
ROLLING SCHEDULES	P VALUES		DIFFERENCES
	Before tensile extension	After tensile extension	
35°/p	0.42	0.45	0.03
45°/p	0.48	0.54	0.04
55°/p	0.51	0.59	0.08
0.02 in/p	0.51	0.62	0.11
0.005 in/p	0.53	0.68	0.15
0.001 in/p	0.56	0.74	0.18
Pendulum	0.58	0.78	0.20

Table 5.5. a.6. A summary of the differences in the {100} P values of specimen cold rolled to 75%, using the 35°/p, 45°/p, 55°/p, 0.02 in/p, 0.005 in/p, 0.001 in/p and pendulum schedules, annealed for 6 hrs aged, before and after 20% tensile extension.

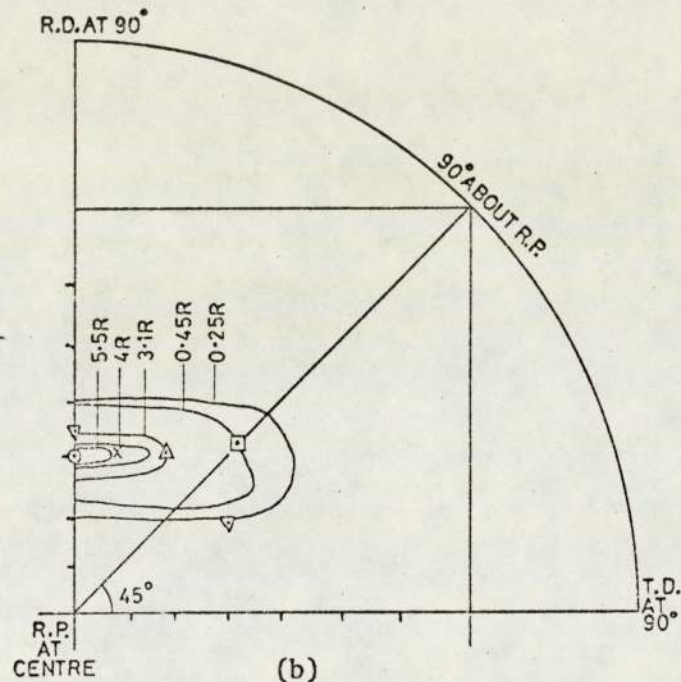
Crystals reorientation accompanying tensile extension is clearly dependent upon the rolling schedules and annealing time. A high reduction in the  $\{111\}$  and a high increase in the  $\{100\}$  after tensile extension is indicative of through-thickness shear and hence low R value. On the other hand a small reduction in the  $\{111\}$  and a small increase in the  $\{100\}$  indicates through-strip plane shear and hence high R value. Accordingly, rolling with  $35^\circ/p$  rolling schedule and 6 hrs annealing are favoured for higher R values. Inverse and (110) pole figures are therefore consistent with R value measurements.

(b) Reorientation of crystals of materials cold rolled to a range of total rolling reductions then annealed for 6 hrs.

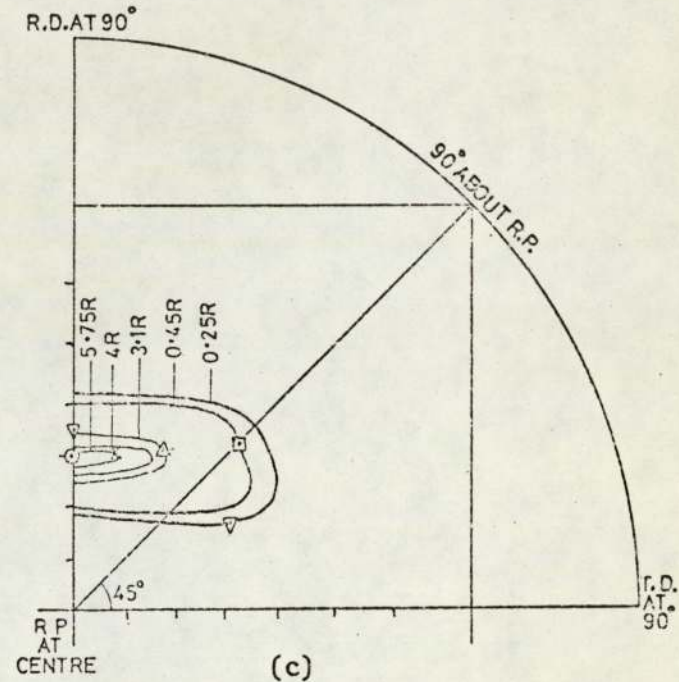
Textures of specimens cold rolled to 75%, 80% and 85% using  $35^\circ/p$ ,  $45^\circ/p$  and  $55^\circ/p$ , annealed for 6 hrs, aged then subjected to 20% extension are shown in (110) pole figures, figure 5.5.b.1 (a,b,c), figure 5.5.b.2 (a,b,c) and figure 5.5.b.3 (a,b,c). It follows that the major texture components of these specimens consisted of the  $\{112\}\langle 110\rangle$ ,  $\{113\}\langle 110\rangle$ ,  $\{111\}\langle 112\rangle$  and  $\{100\}\langle 110\rangle$  components. Intensities of the  $\{112\}\langle 110\rangle$ ,  $\{113\}\langle 110\rangle$  components increased with increasing the total rolling reduction but intensities of the  $\{111\}\langle 112\rangle$  and  $\{100\}\langle 110\rangle$  components remained constant. With reference to the corresponding (110) pole figures before tensile extension figure 5.4.2.3, figure 5.4.2.4 and figure 5.4.2.5., it is apparent that the difference in intensities of the  $\{111\}\langle 112\rangle$  and  $\{100\}\langle 110\rangle$  before and after tensile extension was also constant within the same range of total rolling reductions, as shown in figure 5.5.b.4 and figure 5.5.b.5.



75% total rolling reduction + 6 hrs annealing + 20% tensile extension



80% total rolling reduction + 6 hrs annealing + 20% tensile extension



85% total rolling reduction + 6 hrs annealing + 20% tensile extension.

Fig. 5.5.b.1. One quadrant of (110) pole figures of specimens cold rolling using the 35°/p schedule, annealed for 6 hrs, aged then subjected to 20% tensile extension.

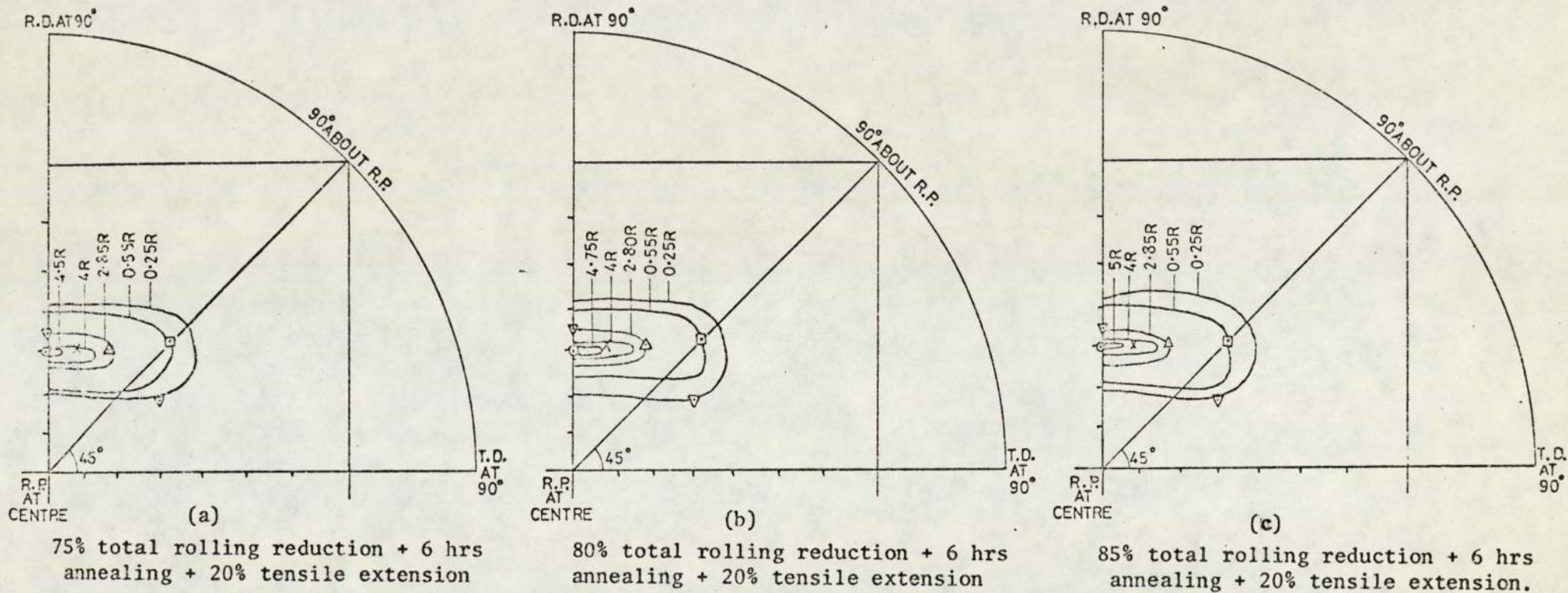


Fig. 5.5.b.2. One quadrant of (110) pole figures of specimens cold rolled using the  $45^\circ/p$  schedule, annealed for 6 hrs, aged then subjected to 20% tensile extension.

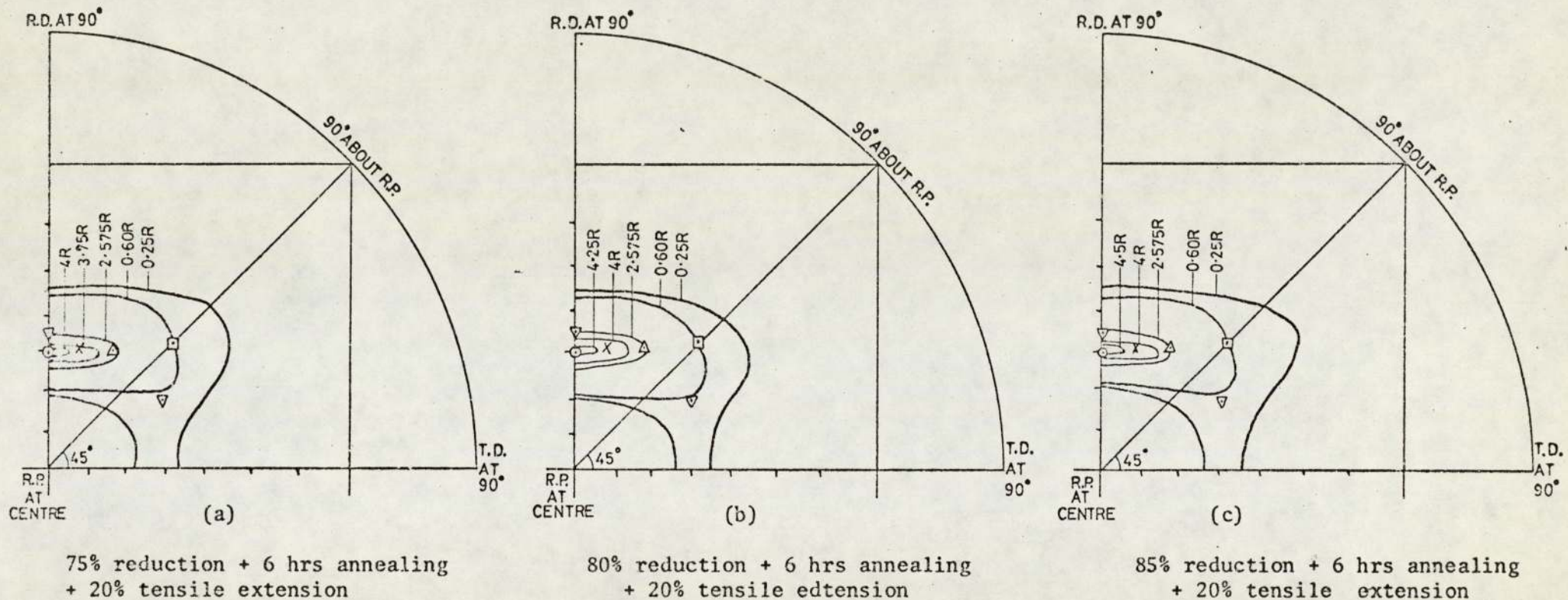


Fig. 5.5.b.3. One quadrant of (110) pole figures of specimens cold rolled using the 55°/p schedule, annealed for 6 hrs, aged then subjected to 20% tensile extension

Difference in {111} intensities X random before and after tensile extension

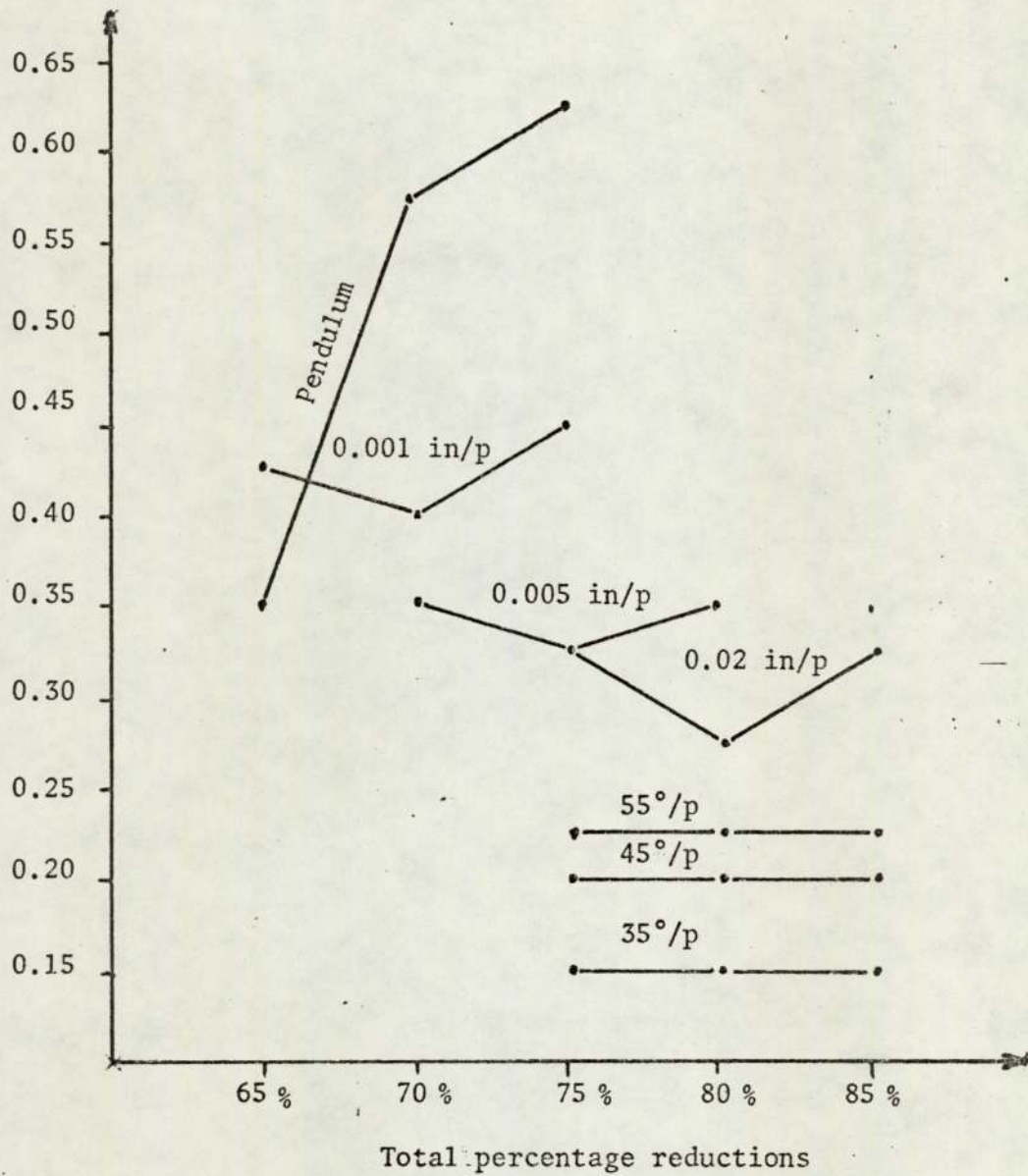


Fig. 5.5.b.4 The decrease in the {111} intensities after tensile extension in the case of specimens cold rolled to a range of total rolling reductions between 65% and 85% depending upon the rolling schedules, annealed for 6 hrs then aged.

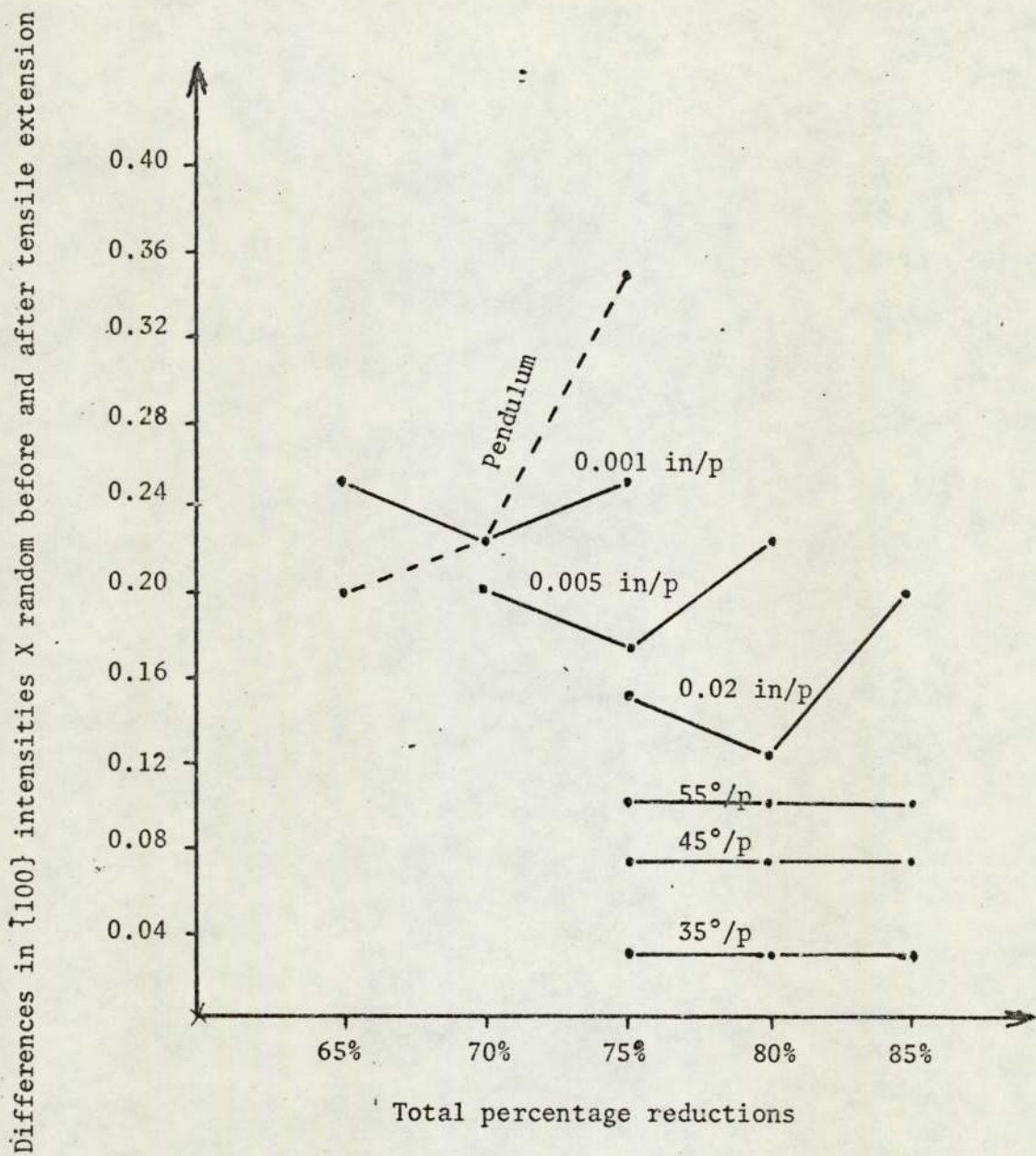
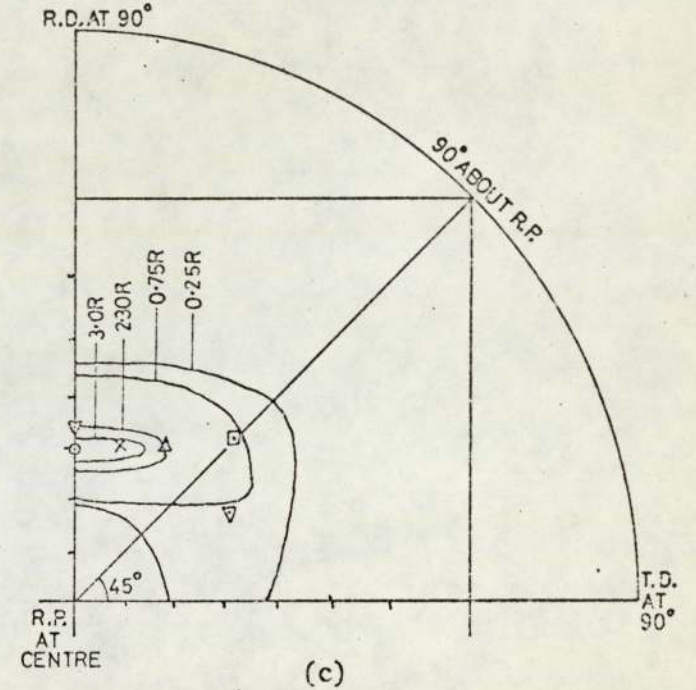
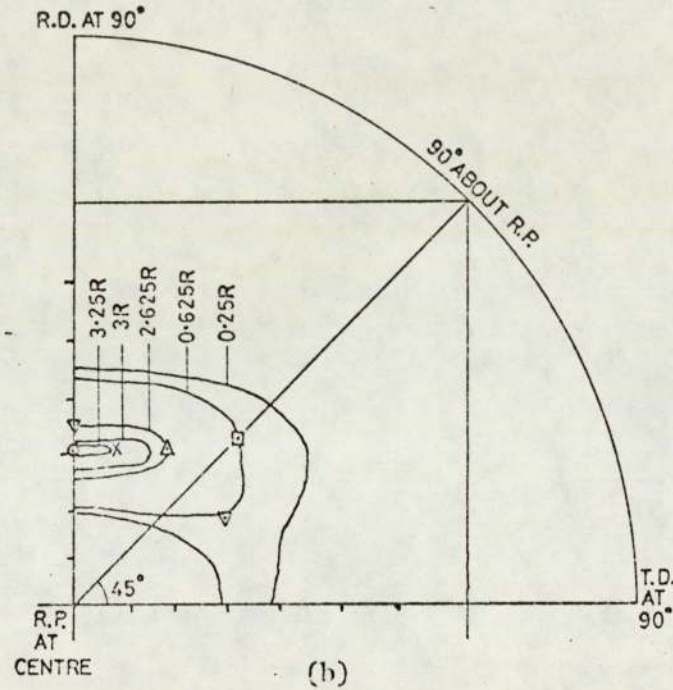
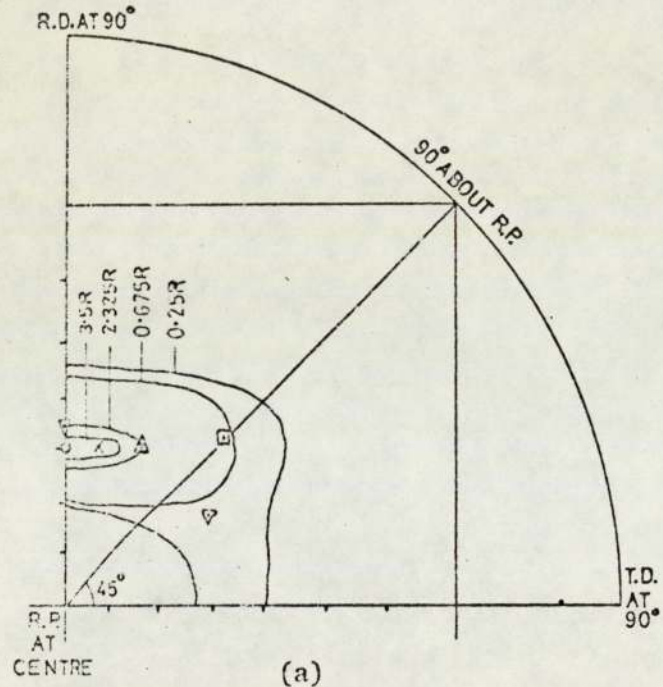


Fig. 5.5.b.5 The increase in the {100} intensities after tensile extension in the case of specimens cold rolled to a range of total reductions, between 65% and 85% depending upon the rolling schedules, annealed for 6 hrs, then aged.

(110) pole figures of specimens cold rolled to 75, 80 and 85% reductions using the 0.02 in/p schedule, annealed for 6 hrs, aged then subjected to 20% extension are shown in figure 5.5.b.6 (a,b,c). According to these figures, intensities of the  $\{111\}\langle 112\rangle$  increased and intensity of the  $\{100\}\langle 110\rangle$  decreased with increasing the total rolling reduction from 75% to 80% then decreased and increased respectively with further increase in rolling reduction. A similar behaviour was also evident when examining (110) pole figures of specimens cold rolled to 70, 75 and 80% using 0.005 in/p rolling schedule and 65, 70 and 75% using 0.001 in/p rolling schedule all annealed for 6 hrs, aged then subjected to 20% tensile extension. These figures are shown in figure 5.5.b.7 (a,b,c) and figure 5.5.b.8 (a,b,c). In the case of rolling with 0.02 in/p rolling schedule intensities of the  $\{112\}\langle 110\rangle$  and  $\{113\}\langle 110\rangle$  decreased with increasing the total rolling reduction. On the contrary, intensities of these components increased with increasing the total rolling reduction when rolling with 0.001 in/p and 0.005 in/p rolling schedules.

By comparing the previous figures with the corresponding (110) pole figures before tensile extension, the difference in intensities of the  $\{111\}\langle 112\rangle$  and  $\{100\}\langle 110\rangle$  components before and after tensile extension was calculated. However, difference in the  $\{111\}\langle 112\rangle$  and  $\{100\}\langle 110\rangle$  intensities before and after tensile extension increased and decreased respectively when increasing the rolling reduction in the same order as their intensity. The maximum increase in the  $\{111\}$  intensity and the minimum decrease in the  $\{100\}$  intensity after tensile extension coincided with 80%, 75% and 70% total reduction when rolling with

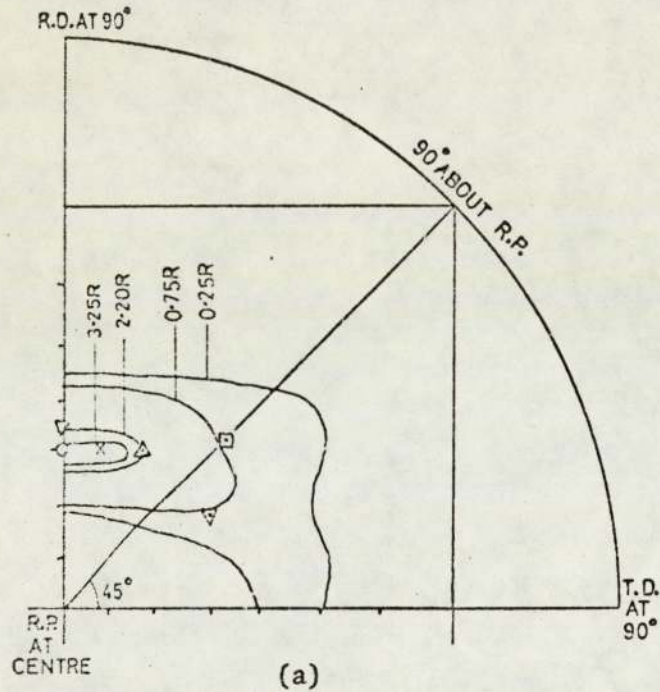


75% total rolling reduction + 6 hrs  
annealing + 20% tensile extension.

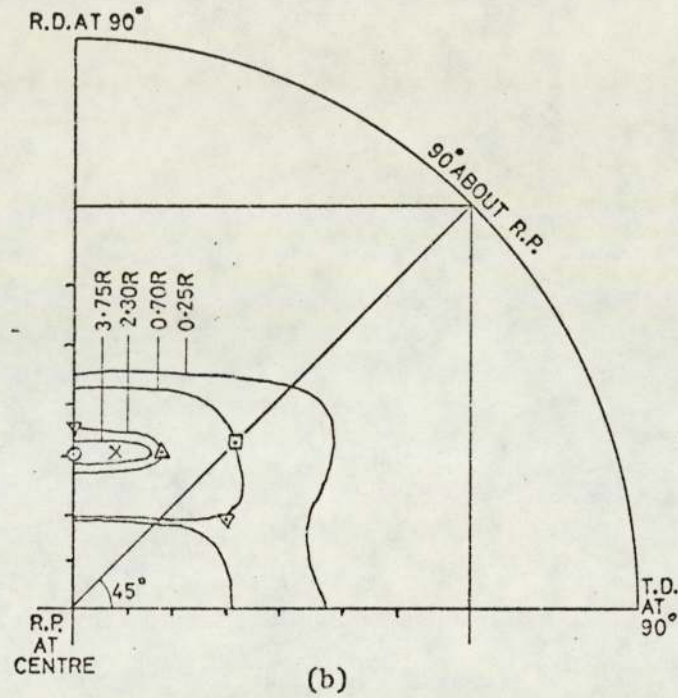
80% total rolling reduction + 6 hrs  
annealing + 20% tensile extension

85% total rolling reduction + 6 hrs  
annealing + 20% tensile extension.

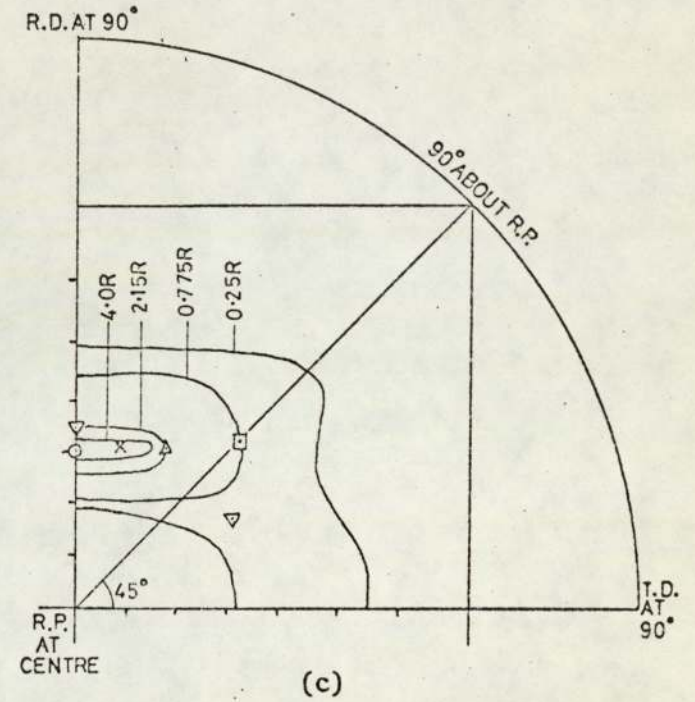
Fig. 5.5.b.6. One quadrant of (110) pole figures of specimens cold rolled using the 0.02 in/p schedule, annealed for 6 hrs, aged then subjected to 20% tensile extension.



70% total rolling reduction + 6 hrs annealing + 20% tensile extension

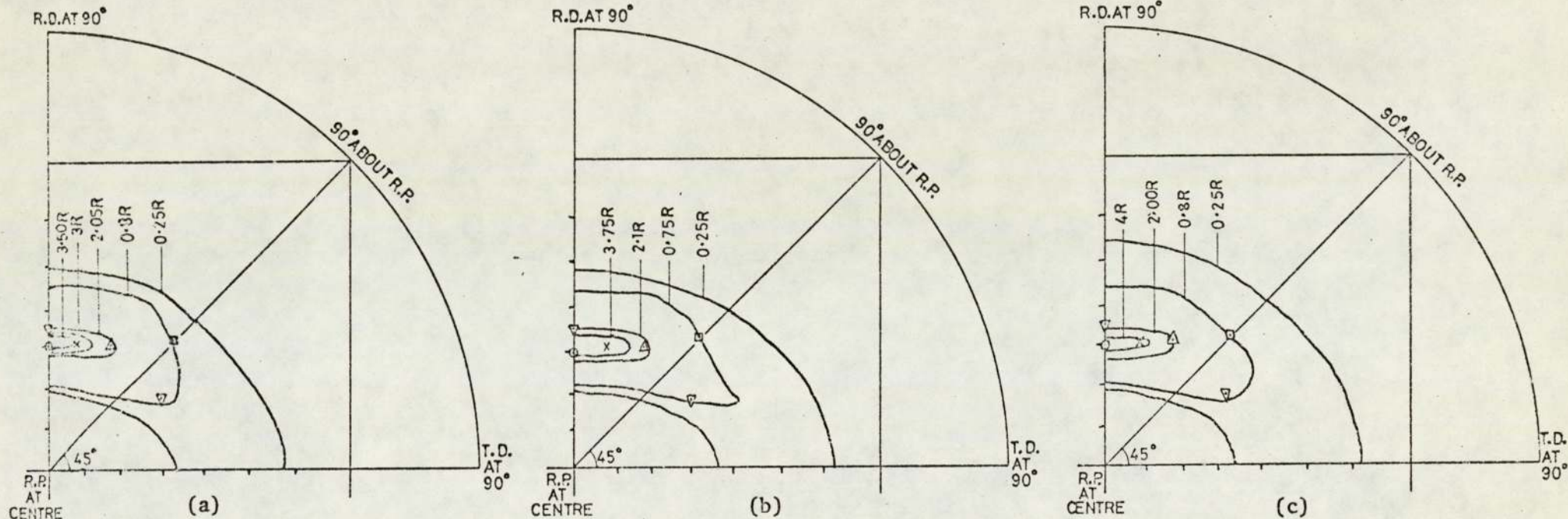


75% total rolling reduction + 6 hrs annealing + 20% tensile extension



80% total rolling reduction + 6 hrs annealing + 20% tensile extension.

Fig. 5.5.b.7. One quadrant of (110) pole figures of specimens cold rolled using the 0.005 in/p schedule, annealed for 6 hrs, aged then subjected to 20% tensile extension.



(a) 65% total rolling + 6 hrs annealing + 20% tensile extension

(b) 70% total rolling reduction + 6 hrs annealing + 20% tensile extension

(c) 75% total rolling reduction + 6 hrs annealing + 20% tensile extension.

Fig. 5.5.b.8. One quadrant of (110) pole figures of specimens cold rolled using the 0.001 in/p schedule , annealed for 6 hrs then subjected to 20% tensile extension.

0.02 in/p, 0.005 in/p and 0.001 in/p rolling schedule respectively. This is demonstrated in figure 5.5.b.4 and figure 5.5.b.5.

(110) pole figures of specimens cold rolled to 65, 70 and 75% using the pendulum mill, annealed for 6 hrs, aged then subjected to 20% tensile extension are shown in figure 5.5.b.9. (a,b,c). It is apparent that intensity of the  $\{112\}\langle 110\rangle$ ,  $\{113\}\langle 110\rangle$  and  $\{111\}\langle 112\rangle$  increased with increasing the total rolling reduction while intensity of the  $\{100\}\langle 110\rangle$  continued to increase. By calculating the difference in intensities of corresponding  $\{111\}$  and  $\{100\}$  components before and after tensile extension it appeared that the decrease in the  $\{111\}$  intensity and increase in the  $\{100\}$  intensity after tensile extension was enhanced when increasing the total rolling reduction as shown in figure 5.5.b.4 and figure 5.5.b.5.

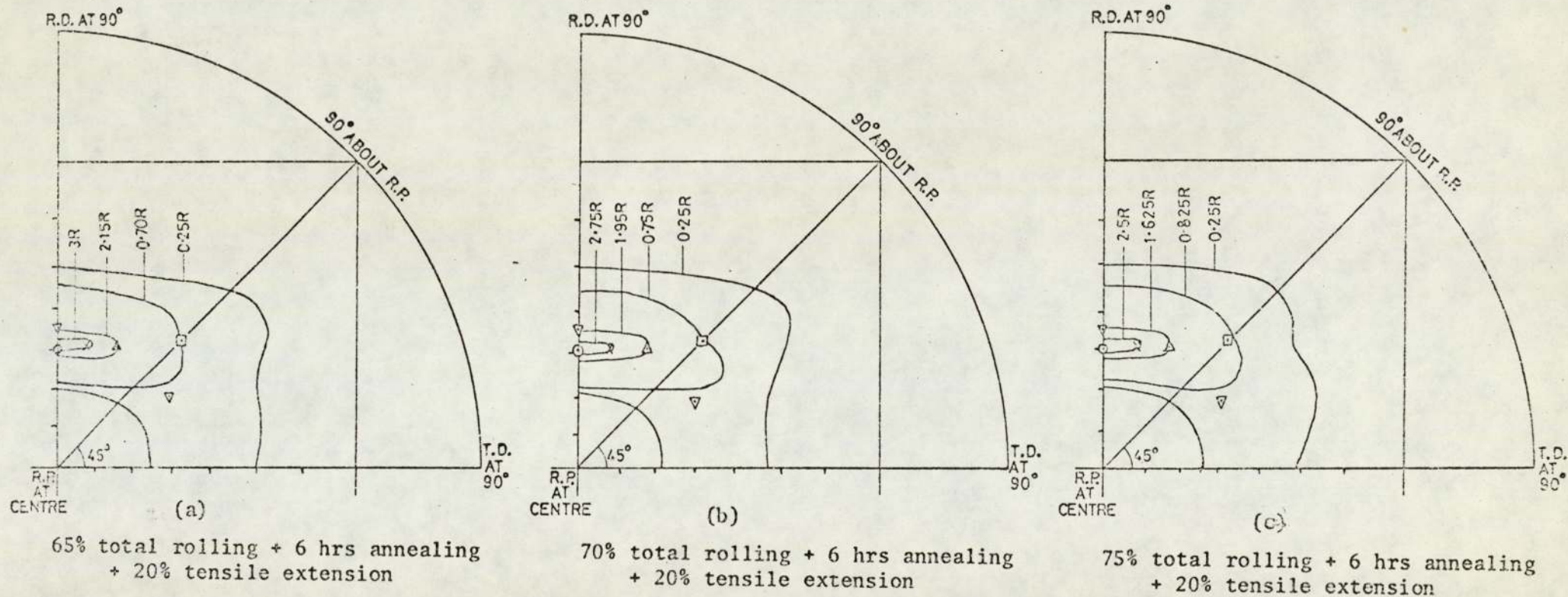


Fig. 5.5.b.9. One quadrant of (110) pole figures of specimens cold rolled using the pendulum schedule, annealed for 6 hrs, aged then subjected to 20% tensile extension.

6. DISCUSSION

## 6.1 INTRODUCTION

The results of the present investigation will be discussed in the order presented in the experimental results. It will be shown that the 25% total rolling reduction given to the initial material had no significant influence upon its final texture. The development of cold rolling and annealing textures will be accounted for. Texture before and after tensile extension is related to R value by the  $\frac{\{111\}}{\{100\}}$  texture ratio. The significance of the cold rolling geometry in the control of texture and R value is considered.

## 6.2 TEXTURE OF THE INITIAL MATERIAL

Deformation of low carbon steel, during hot rolling above the  $A_3$  temperature where austenite is the stable phase, occurs in a manner similar to that of high stacking fault f.c.c. metals at room temperature under similar friction condition<sup>(4)</sup>. Texture developed at that temperature should correspond to a weak f.c.c. pure metal and exhibit surface to centre segregation similar to that observed in copper and aluminium at room temperature under high frictions. A weak texture is to be expected since dynamic recrystallisation during hot rolling above the  $A_3$  temperature prohibits the formation of a strong austenitic texture. Phase transformation as dynamic recrystallisation occurs also reduced texture intensity in the ferritic phase<sup>(71)</sup>.

The surface and centre textures of ferritic steel were derived from the austenitic texture<sup>(42)</sup>, using the K-S transformation (G.Kurdjumov and G.Sachs, Z.Physik, 1930, 64, 325). Accordingly, the relationship between the transformed ferrite and the parent austenite can be described as follows:

- $\{101\}_\alpha$  orientation results from both  $\{100\}_\gamma$  and  $\{111\}_\gamma$  orientations<sup>(42,85)</sup>
- $\{100\}_\alpha$  orientation results from  $\{100\}_\gamma$  and  $\{110\}_\gamma$ <sup>(42,85)</sup>
- $\{111\}_\alpha$  orientation results from  $\{201\}_\gamma$  orientation<sup>(85)</sup>
- $\{112\}_\alpha$  orientation results from  $\{101\}_\gamma$  orientation<sup>(85)</sup>
- $\{312\}_\alpha$  orientation results from  $\{211\}_\gamma$  orientation<sup>(85)</sup>

The surface texture of the austenitic phase is expected to be a mixture of the  $\{100\}\langle 011\rangle$  and  $\{111\}\langle 110\rangle$  orientations, the latter being the prominent when rolling under high friction condition. Applying the above transformations, the  $\{110\}_\alpha$  orientation is the main ferritic texture at the sheet surface. Since the  $\{201\}_\gamma$  and  $\{101\}_\gamma$  orientations are of low intensities, therefore, the  $\{111\}_\alpha$  and  $\{112\}_\alpha$  orientation are expected to be of low intensity also. At the sheet mid-plane, the austenitic texture is expected to be a mixture of  $\{110\}\langle 112\rangle$  and  $\{112\}\langle 111\rangle$  orientations with the former predominating. Therefore, the  $\{100\}_\alpha$  is dominant at the centre of the sheet followed by the  $\{112\}_\alpha$  orientation. The  $\{111\}_\gamma$  and  $\{100\}_\gamma$  orientations, on the other hand, are of low intensity which results in a weak  $\{110\}_\alpha$  at the sheet mid-plane.

The observed texture of the initial material was weak but corresponded approximately with the predicted ferrite texture<sup>(70)</sup> as shown in Table 6.2.1. The surface texture however, is characterised by a higher ratio of  $\{110\}$  and lower ratio of  $\{112\}$  planes parallel to the surface. At the centre, intensity of the  $\{100\}$  was higher and intensity of the  $\{110\}$  planes was lower. The terms higher and lower refer to the relative magnitude of each texture component to each other. On the whole, texture of the initial material was relatively weak. This is in agreement with the previous measurements of texture of hot band rimmed steel<sup>(40,85)</sup>.

Texture components	Measured texture intensity X random	Predicted relative texture intensity
{110}	1.12	high
{100}	1.05	medium
{111}	1.00	low
{112}	0.97	low

(a) surface texture

Texture Components	Measured texture intensity X random	Predicted relative texture intensity
{100}	1.27	high
{112}	1.15	high
{123}	1.06	medium
{110}	0.70	low

(b) centre texture

Table 6.2.1. Illustrates the agreement between the surface and centre textures measured in the present study and the corresponding texture predicted<sup>(70)</sup>.

{hkl}	P values of the mid plane of the initial rimmed steel material used in the present study.	P values of the mid plane of a hot band rimmed steel abstracted from previous study
{110}	0.70	0.68
{200}	1.27	1.30
{211}	1.15	1.11
{310}	0.72	0.90
{222}	0.95	0.93
{321}	1.06	0.95
{411}	0.67	not given
{332}	0.77	0.98

Table 6.2.2. P values of the centre of the initial material used in the present study compared with the corresponding P values of the centre of a hot rolled rimmed steel band abstracted from the work of Hellewell<sup>(85)</sup>.

P values of the initial material mid-plane measured in the present study were comparable with the corresponding P values of a hot rolled rimmed steel band abstracted from the work of Hellewell<sup>(85)</sup> as shown in Table 6.2.2. It was, therefore, concluded that the 25% total cold rolling reduction and the annealing cycle previously given to the present initial material had no influence upon the final texture. This is also in agreement with a study by Thomson and Baker<sup>(72)</sup> in which it was stated that cold rolling of a hot rimmed steel band to a total reduction up to 40% had no effect upon its final texture.

### 6.3 THE EFFECT OF COLD ROLLING PROCEDURES UPON THE DEVELOPMENT OF COLD ROLLING TEXTURES

Development of the cold rolling texture is accounted for here on the basis of a theory<sup>(7)</sup> which has not found a wide-spread acceptance. Alternative approaches are possible<sup>(16,92)</sup>.

Analysis of (110) pole figures (section 5.4) revealed that texture developed after cold rolling was dependent upon the rolling procedures. After certain rolling reduction, intensities of the  $\{112\}\langle 110 \rangle$  and  $\{111\}\langle 112 \rangle$  orientations decreased when increasing the shear plane angle, decreasing the roll gap and using the pendulum mill. Conversely, intensity of the  $\{100\}\langle 110 \rangle$  orientation increased with altering the rolling procedures in the previous order. This is shown in figure 6.3.1.(a,b,c) derived from (110) pole figures of the cold rolled materials (figure 5.e.1.2(a,b,c), figure 5.4.1.3(a,b,c), figure 5.4.1.4(a,b,c), figure 5.4.1.5(a,b,c), figure 5.4.1.6(a,b,c), figure 5.4.1.7(a,b,c) and figure 5.4.1.8(a,b,c)).

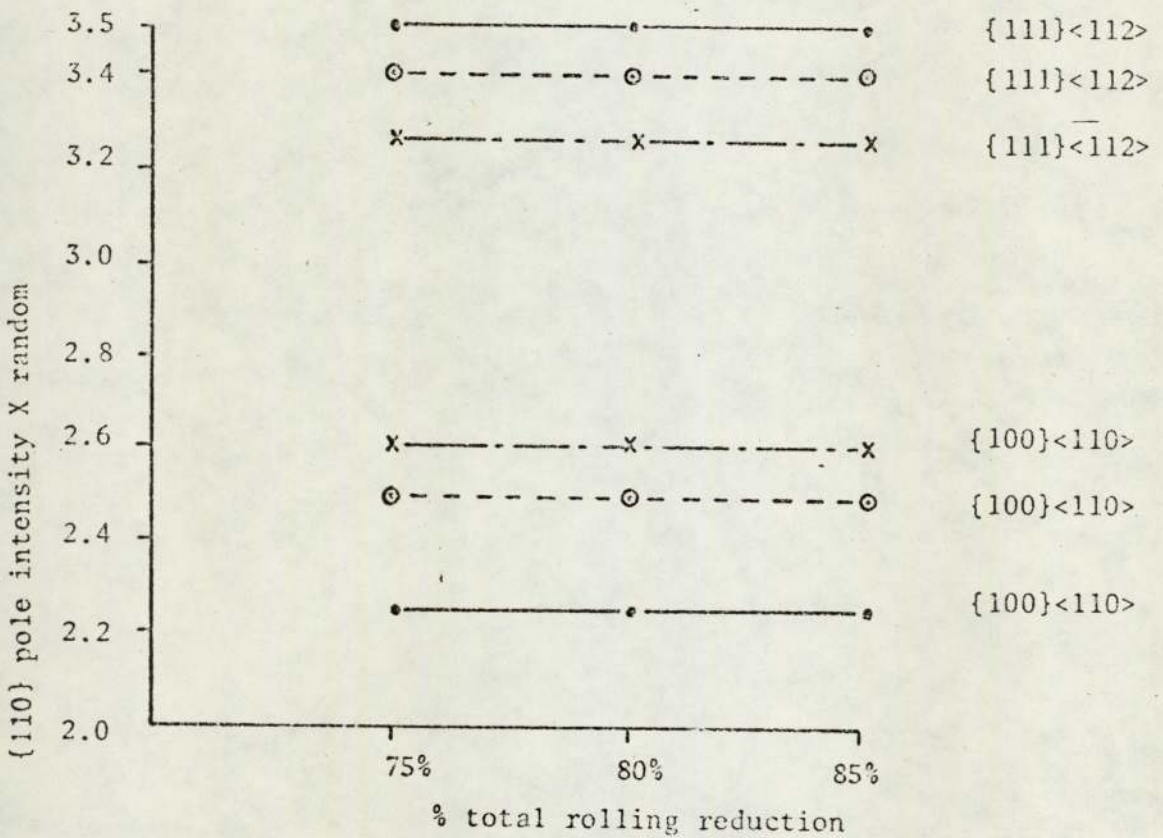
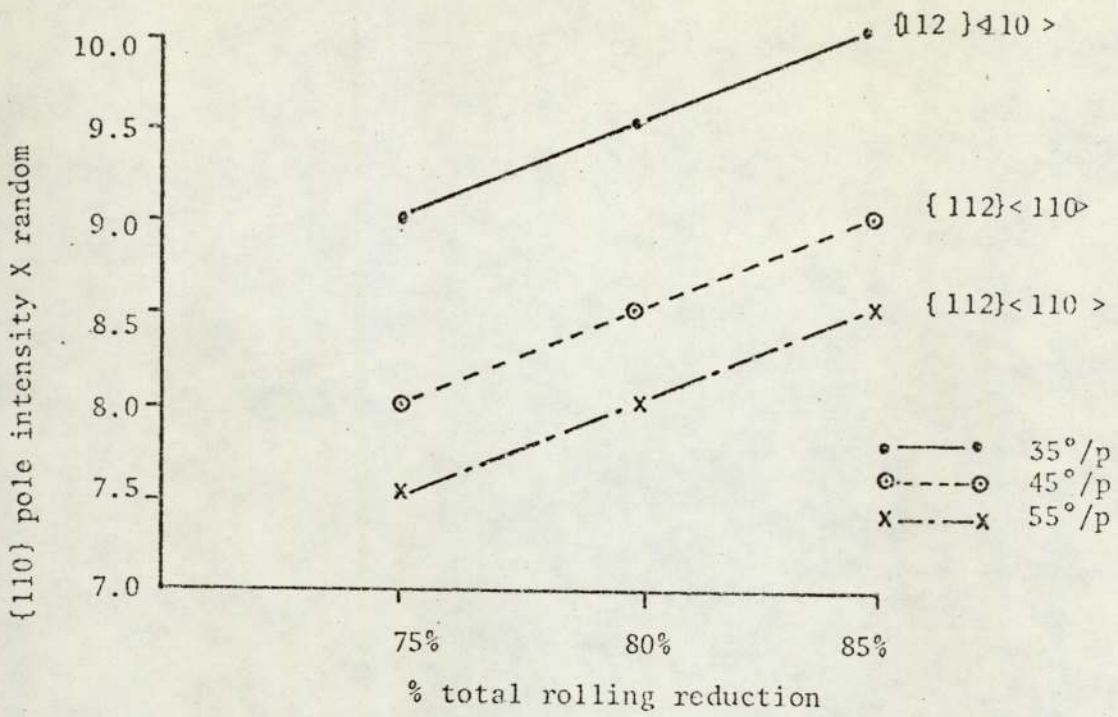


Fig.6.3.1.a Shows the variations in the {110} pole intensity at the ideal orientations {112}<110>, {111}<112> and {100}<110> with increasing the total rolling reduction using the 35°/p (•—•), 45°/p (○---○) and 55°/p (x-·-·-x) rolling schedules.

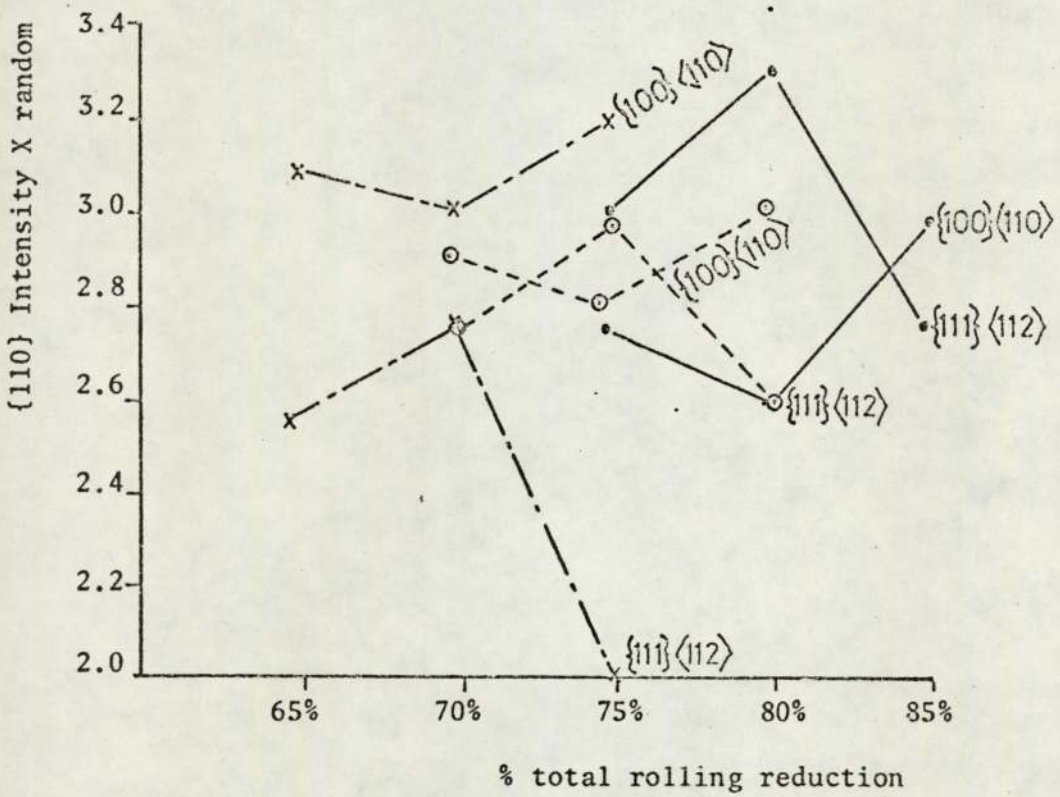
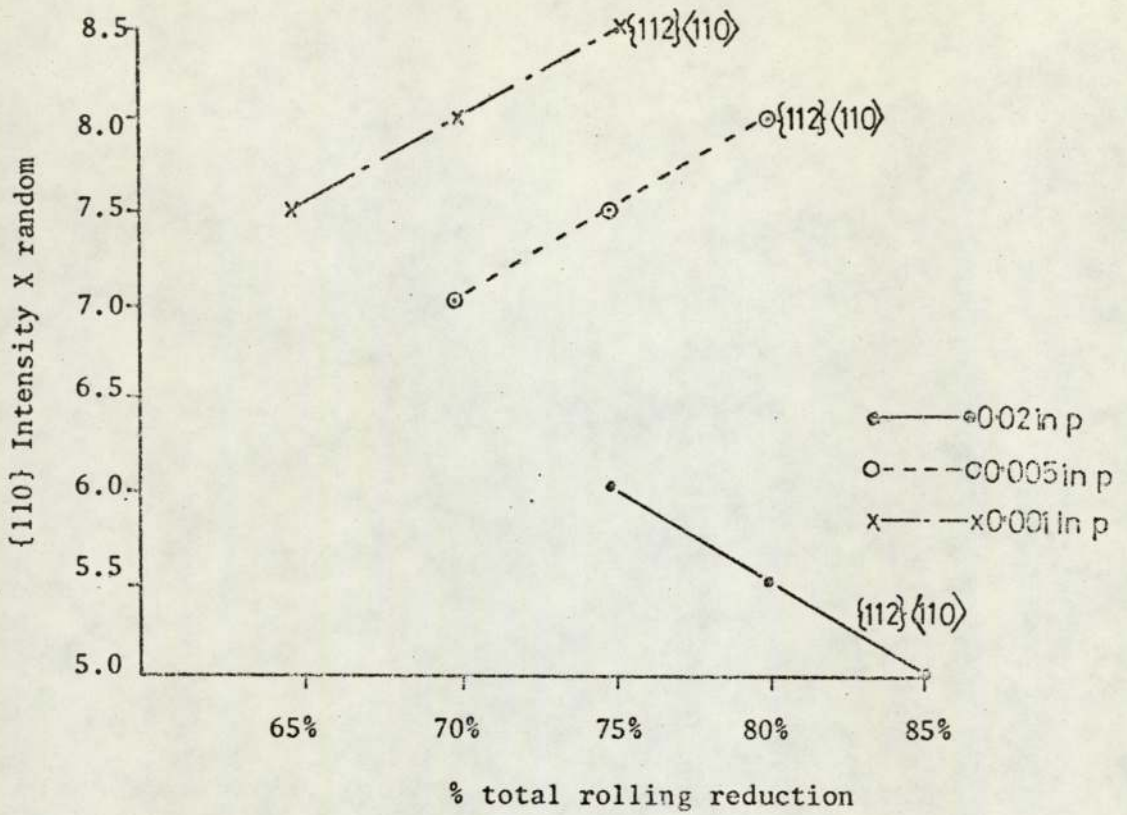


Fig. 6.3.1.b. Shows the variation in the {110} pole intensity at the ideal orientations {112}<110>, {111}<112> and {100}<110> with increasing the total rolling reduction using the 0.02 in/p (•—•), 0.005 in/p (⊙---⊙) and the 0.001 in/p (x---x) rolling schedules.

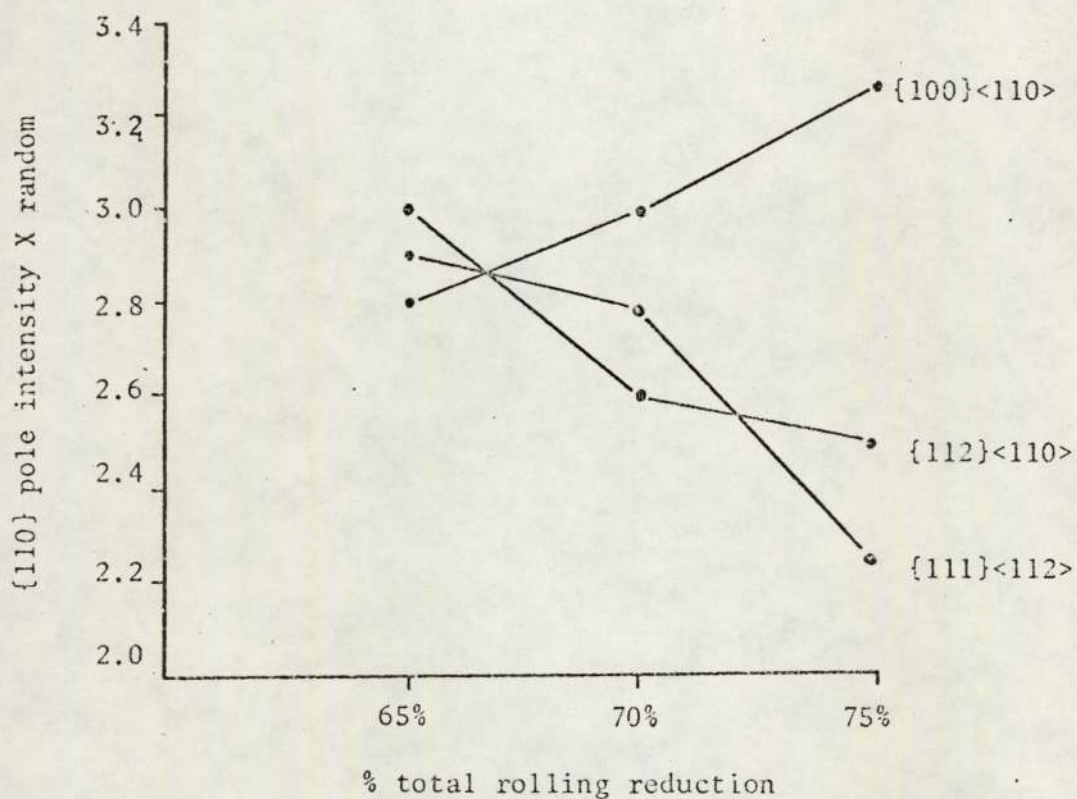


Fig. 6.3.1.c Shows the variation in the {110} pole intensity at the ideal orientations {112}<110>, {111}<112> and {100}<110> with increasing the total rolling reduction using the pendulum mill.

Cold rolling textures can be looked upon as symmetrically stable orientations under a biaxial stress system, compression normal to the rolling plane and tension in the rolling direction<sup>(7)</sup>. Furthermore, the crystallographic rotations during cold rolling can be represented stereographically by  $54^{\circ} 44'$  around the rolling direction and around the strip normal<sup>(7)</sup> as shown in figure 2.2.1. Accordingly in the early stages of cold rolling of a randomly orientated material, the  $\langle 111 \rangle$  slip direction rotates towards the rolling direction and stable on the  $54^{\circ} 44'$  around the strip normal. The  $\{110\}$  slip planes maintain contact with the compression circle likewise. The slip plane normal therefore, is stable on the tension circle and  $35^{\circ} 16'$  from the strip normal, figure 2.2.1. On this basis the  $\{100\}\langle 110 \rangle$  orientation is formed in the initial stages of cold rolling. In the  $\{100\}\langle 110 \rangle$  orientation figure 2.2.1, the  $\{111\}$  slip directions are symmetrically disposed around the rolling direction and the  $\{112\}$  pole lies on the tension circle. The  $\{112\}$  planes therefore, are active slip planes resulting in the formation of the  $\{112\}\langle 110 \rangle$  orientation. In addition the  $\{123\}$  slip planes which lie near the  $\{112\}$  slip planes as shown in figure 2.2.2. rotate around the  $\langle 111 \rangle$  direction to form the  $\{113\}\langle 110 \rangle$  orientation. Also, the four  $\{100\}$  poles rotate around the rolling direction to form the  $\{111\}\langle 110 \rangle$  orientation, figure 2.2.3. The  $\{111\}\langle 110 \rangle$  orientation rotates around the strip normal so as the  $\{110\}$  poles lie in the rolling direction and form the  $\{111\}\langle 112 \rangle$  orientation as in figure 2.2.4.

In a randomly orientated material where orientation of crystals may vary from one crystal to the next, deformation occurs by slip on those systems which lie parallel or near to the  $35^{\circ}$  and  $55^{\circ}$  from the

stress axes. The  $\{211\}$  poles lie  $35^\circ$  from the strip normal and the  $\{110\}$  poles rotate to the  $35^\circ$  position from the strip normal to form the  $\{111\}\langle 112 \rangle$  orientation. As a result, more  $\{112\}\langle 110 \rangle$  and  $\{111\}\langle 112 \rangle$  orientations are formed during cold rolling using the  $35^\circ/p$  rolling schedule in comparison with the  $45^\circ/p$  and  $55^\circ/p$  rolling schedules. During cold rolling using constant roll gap rolling schedules, the shear plane angle varies continuously, as shown in figure 6.3.2., to or away from the  $35^\circ$  position. Accordingly, less  $\{112\}\langle 110 \rangle$  and  $\{111\}\langle 112 \rangle$  orientations are formed during cold rolling using constant roll gap schedules. During cold rolling using the pendulum mill, the direction of rolling was reversed at the end of each stroke by reversing the stroke direction end for end before proceeding with the next stroke. Cold rolling using the pendulum mill is therefore equivalent to reverse rolling, see figure 6.3.3. Since the  $\{100\}\langle 110 \rangle$  component is the only texture component with four fold symmetry around the sheet normal, the development of the  $\{100\}\langle 110 \rangle$  component is enhanced at the expense of the  $\{112\}\langle 110 \rangle$  and  $\{111\}\langle 112 \rangle$  components during cold rolling using the pendulum mill.

During cold rolling using controlled geometry rolling schedules the rolling draughts and the percentage reduction per pass were very small after 75% total reduction (see Appendix III, IV and V). On increasing the total rolling reduction to 85% intensity of the  $\{112\}\langle 110 \rangle$  orientation increased while intensities of the  $\{111\}\langle 112 \rangle$  and  $\{100\}\langle 110 \rangle$  orientations remained constant (figure 6.3.1a).

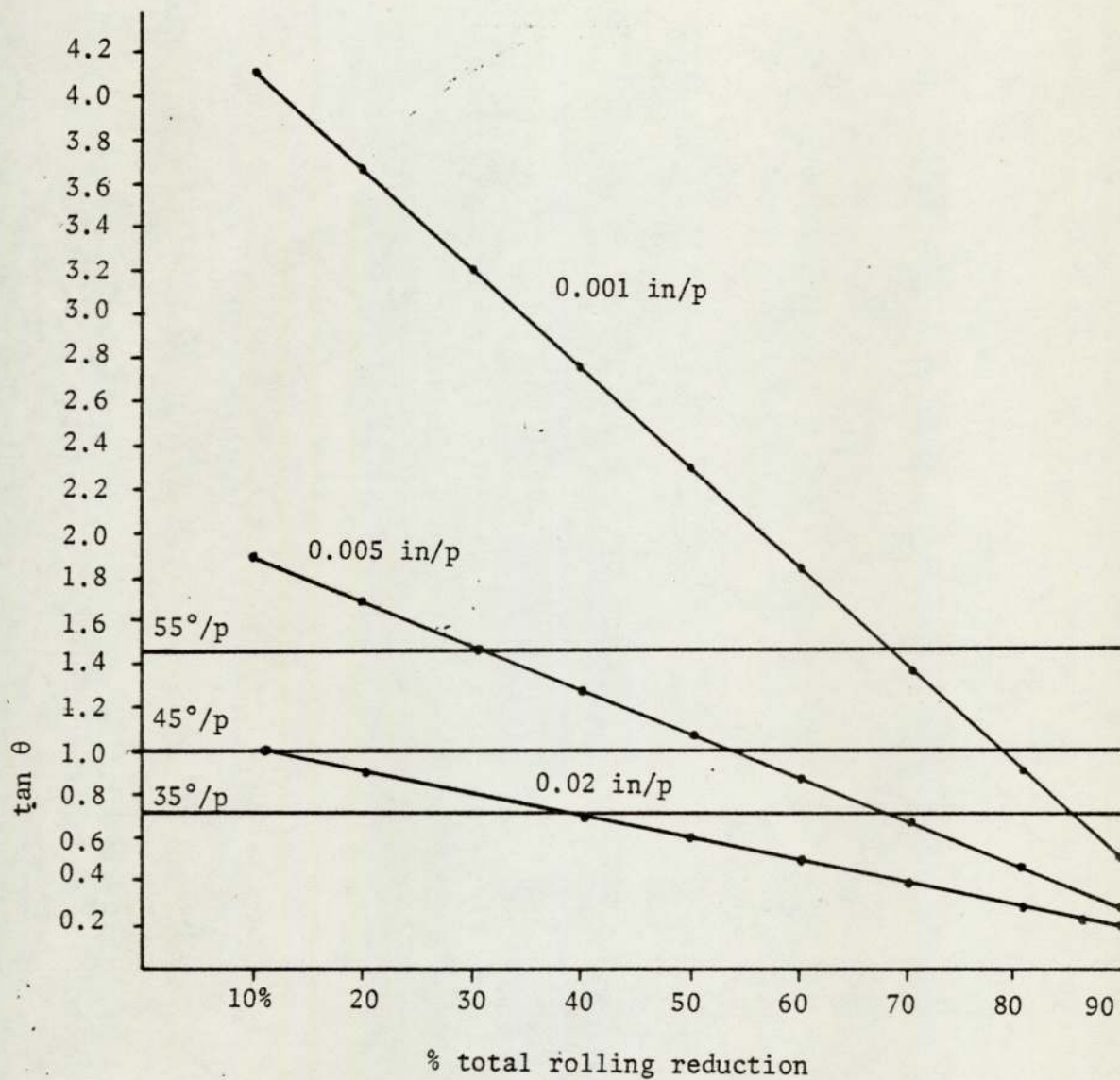


Fig. 6.3.2. The variation in  $\tan \theta$  versus the percentage total rolling reduction in the case of six rolling schedules,  $\theta$  is the shear angle in the material undergoing deformation.

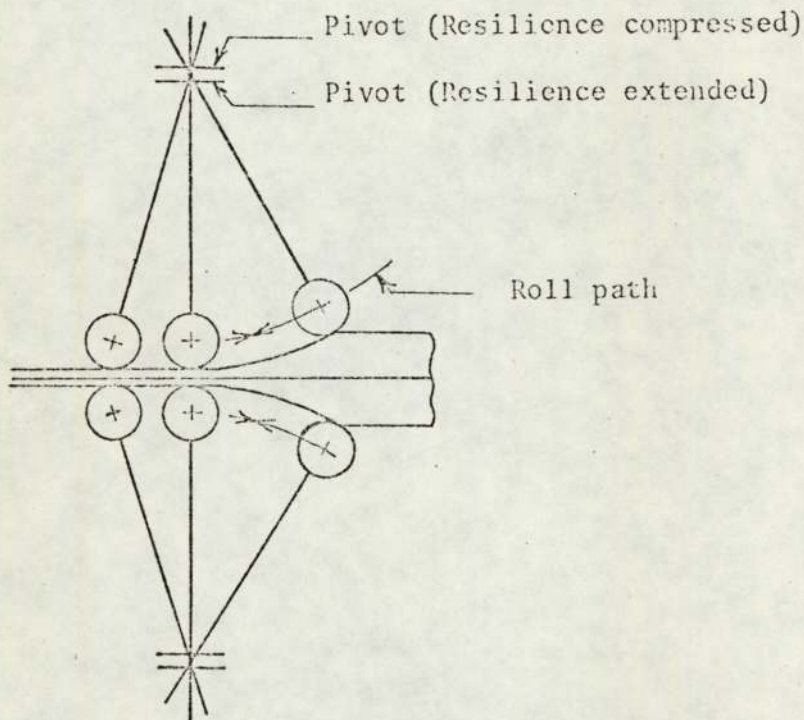


Fig. 6.3.3. A schematic representation of the pendulum cycle in which the rolls reverse their direction at the end of each stroke.

As cold rolling proceeds using 0.001 in/p rolling draughts, the angle  $\theta$  continues to decrease as shown in figure 6.3.2. towards the  $35^\circ$  position. This resulted in increasing the intensity of the  $\{112\}\langle 110\rangle$  and  $\{111\}\langle 112\rangle$  orientations at the expense of the  $\{100\}\langle 110\rangle$  orientation. After 70% total reduction, the percentage reduction per pass increased and the critical resolved shear stress on the  $\{100\}$  slip planes increased<sup>(7)</sup> so that the  $\{100\}$  planes become active slip planes. Accordingly the  $\{111\}\langle 112\rangle$  component rotates to the  $\{100\}\langle 110\rangle$  orientation and results in an increase in intensity of the second component at the expense of the first. During cold rolling using 0.005 in/p rolling draughts the percentage reduction per pass is higher. This increases the critical resolved shear stress on the  $\{100\}$  planes<sup>(7)</sup> which results in rotation of the  $\{112\}\langle 110\rangle$  component to the  $\{111\}\langle 112\rangle$  orientation. As a result, the reduction in intensity of the  $\{111\}\langle 112\rangle$  component is more noticeable after 75% total rolling reduction. Such a total rolling reduction is coincident with a stage at which the rotation of the  $\{112\}\langle 110\rangle$  component to the  $\{111\}\langle 112\rangle$  component is less than rotation of the second component to the  $\{100\}\langle 110\rangle$  orientation. In cold rolling using 0.02 in/p rolling draughts the situation is different in that the percentage reduction per pass is much higher and more  $\{112\}\langle 110\rangle$  orientation rotates to the  $\{111\}\langle 112\rangle$  orientation. Accordingly, intensity of the  $\{112\}\langle 110\rangle$  orientation decreased on increasing the total rolling reduction and the reduction in intensity of the  $\{111\}\langle 112\rangle$  occurred after higher total reductions (80%).

During cold rolling using the pendulum mill the deformation temperature and the coefficient of friction increased on increasing the total rolling reduction<sup>(66)</sup>. This can only increase the amount of {100}<110> orientation after heavy total rolling reduction as in figure 6.3.1.c. This is consistent with the previous analysis of cold rolling texture developed by conventional reverse rolling of b.c.c. metals<sup>(4,7,30,46)</sup>.

#### 6.4 THE EFFECT OF COLD ROLLING TEXTURE AND ANNEALING TIME UPON THE DEVELOPMENT OF THE ANNEALING TEXTURE

Analysis of the annealing texture after 0.5 hr annealing indicated a significant reduction in P value of the {100} component depending upon the rolling schedules. P values of the {111} component decreased also but remained dominant in the annealing texture, as shown in Table 5.4.2.1, figure 5.4.2.1 and figure 5.4.2.2. There was also an increase in intensity of the {110} orientation. The reduction in intensity of the {100} component after 0.5 hr annealing is due to its low stored energy of deformation<sup>(19)</sup>. On the same basis, the predominance of the {111} component in the annealing texture is to be expected because of its relatively high stored energy and its preponderance in the cold rolling texture. Although the stored energy of the {110} planes is higher than that of the {111} planes<sup>(19)</sup>, it is unlikely to dominate the annealing texture because of its low proportion in the cold rolling texture. The relatively low proportion of the {211}, {310}, {321}, {411}, and {332} planes in the annealing texture is also attributed to their low stored energies and proportions in the cold rolling texture.

Increasing the annealing time from 0.5 hr to 6 hrs was accompanied by an increase and a decrease in P values of the {111} and {100} orientations respectively. This is shown in Table 5.4.2.2, figure 5.4.2.1, and figure 5.4.2.2. The increase in P values of the {111} component after 6 hrs annealing in comparison with annealing for 0.5 hr is due to the normal growth of the {111} planes which are relatively strong in the primary recrystallisation texture at the expense of the weak {100} planes. With reference to the cold rolling texture, Table

5.4.1.1, P values of the {111} and {100} orientations of materials cold rolled to 75% using the 35°/p, 45°/p, 55°/p, 0.02 in/p, 0.005 in/p, 0.001 in/p and pendulum schedules decreased and increased respectively in that order. Accordingly, the growth of the {111} and {100} components after 6 hrs annealing varied with the rolling schedules in the same order of their magnitude in the cold rolling texture. After 6 hrs annealing, however, more {111} and less {100} components were developed on annealing of materials cold rolled using the 35°/p rolling schedules. In comparison less {111} and more {100} orientations were developed when materials cold rolled using the 45°/p, 55°/p, 0.02 in/p, 0.005 in/p, 0.001 in/p and pendulum schedules were annealed.

With reference to (110) pole figures of materials cold rolled to a range of total rolling reductions, figure 5.4.2.3 to figure 5.4.2.9, intensities of the {111} and {100} orientations depended upon the total rolling reductions. The growth of the {111} and {100} planes during annealing is, therefore, dependent upon the total rolling reduction prior to annealing. Accordingly, the variations in intensities of the {111} and {100} components after 6 hrs annealing with the total rolling reduction followed the same pattern as for prior to annealing though intensity of the {100} operation was greatly reduced. This is evident in figure 5.4.1.2 to figure 5.4.1.8 and figure 5.4.2.3 to figure 5.4.2.9.

## 6.5 THE RELATIONSHIP BETWEEN PROCESSING, TEXTURE AND R VALUE

It is well recognised that the average plastic strain ratio  $\bar{R}$  can be related to a texture parameter of the form  $\{111\}/\{100\}$ <sup>(87)</sup> as shown in figure 6.5.1. The theoretical reasons for this relationship have been given<sup>(23)</sup>. Because of the limited material width,  $\bar{R}$ , was not measured in the present investigation and  $R_0$  values only were obtained. For the materials investigated, there is also a good correlation between  $R_0$  value and the  $\{111\}/\{100\}$  texture parameter as shown in figure 6.5.2.

The measurements of the  $\{111\}/\{100\}$  ratios of materials cold rolled to 75% total rolling reductions using the 35°/p, 45°/p, 55°/p, 0.02 in/p, 0.005 in/p, 0.001 in/p and pendulum rolling schedules are shown in Table 6.5.1. The  $\{111\}/\{100\}$  ratios of the cold rolled materials are very low and below unity in the case of material cold rolled by the pendulum mill. These low values of the texture parameter are related to the very low  $R_0$  values of materials in the cold rolled conditions shown in figure 5.3.1. The  $\{111\}/\{100\}$  texture ratio decreased on increasing the shear plane angle, decreasing the roll gap and the lowest value of all is obtained by the pendulum schedule. Because of the experimental difficulty encountered in measuring  $R_0$  values of materials with very limited ductility, it was not possible to correlate these changes in texture parameter with changes in  $R_0$  value at these levels. Measurements of the  $\{111\}/\{100\}$  ratios after 75%, 80% and 85% total rolling reduction using the 35°/p schedule revealed no change in the texture parameter, as shown in figure 6.5.3. A similar observation is also evident in the case of materials cold rolled to the same total reductions using the 45°/p and 55°/p schedules. Cold rolling using the 0.02 in/p, 0.005 in/p and 0.001 in/p schedules resulted in increasing  $\{111\}/\{100\}$

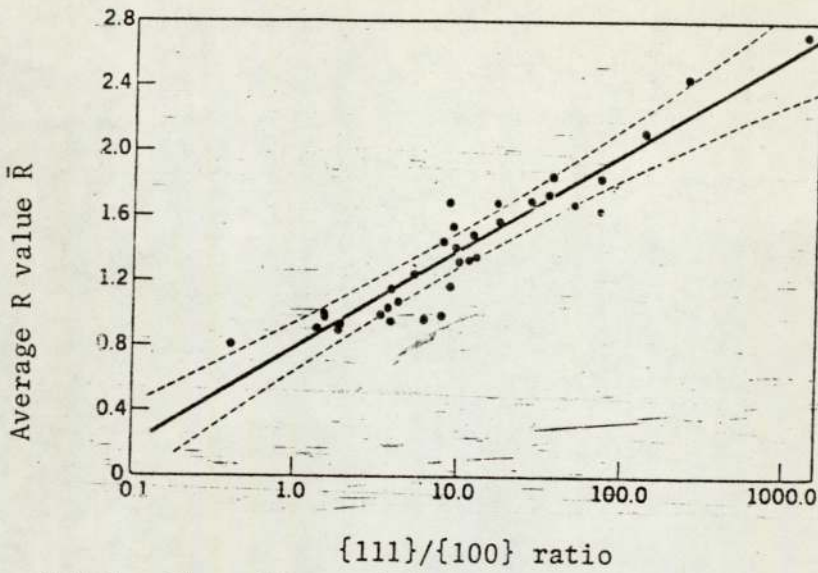


Fig. 6.5.1. The effect of the ratio of the intensity of the (111) component to the intensity of the (001) component on the average R value strain ratio of low-carbon steel.

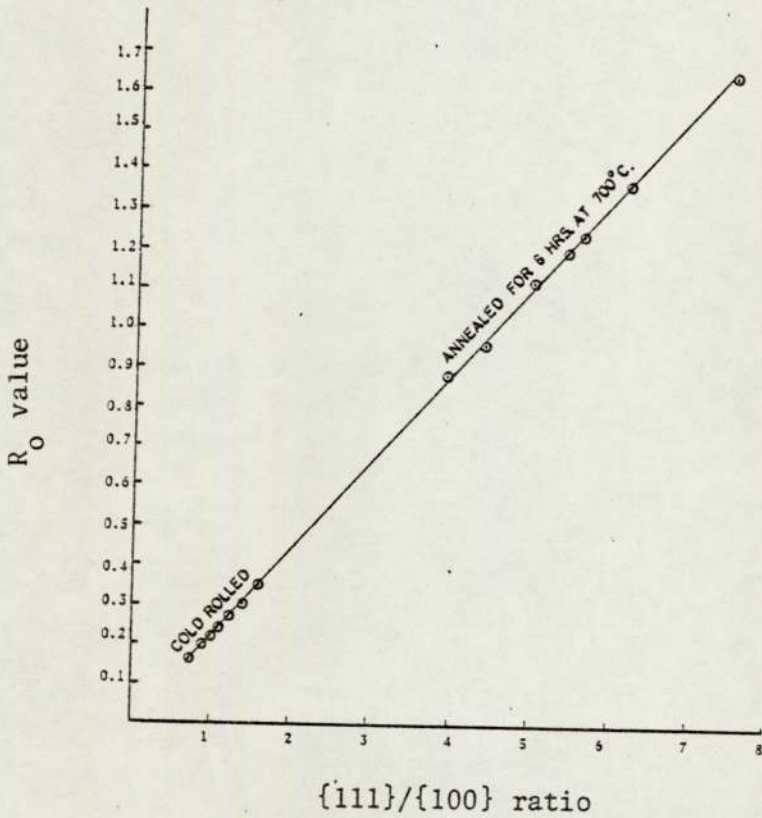


Fig. 6.5.2. The effect of the ratio {111}/{100} texture intensity upon  $R_0$  value measured in the present study.

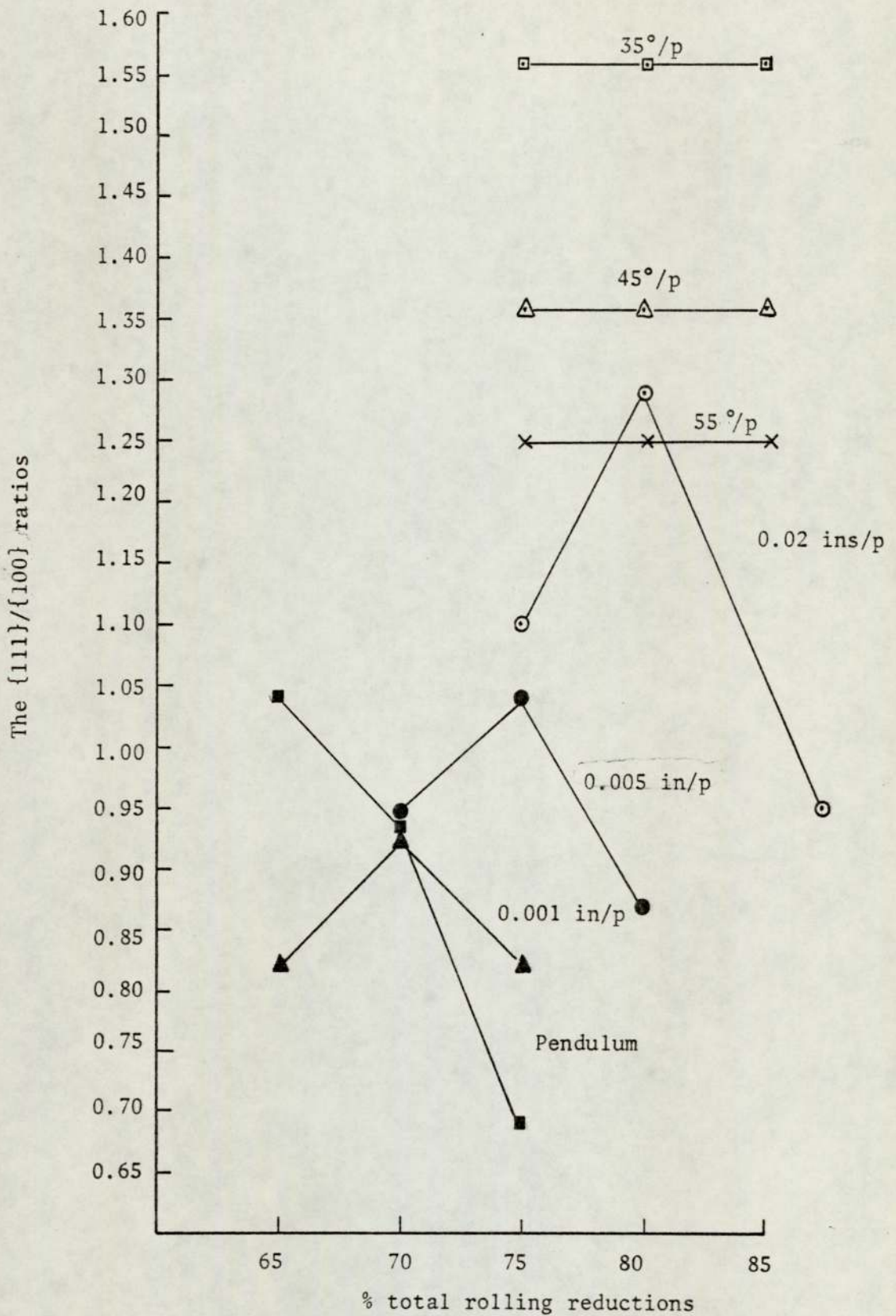


Fig. 6.5.3. The variations in the  $\{111\}/\{100\}$  ratios of materials cold rolled using the seven rolling schedules versus the percentage total rolling reduction

Rolling schedules	P values		{111}/{100} ratios
	{111} Planes	{100} Planes	
35°/p	3.49	2.20	1.59
45°/p	3.37	2.48	1.36
55°/p	3.26	2.60	1.25
0.02 in/p	3.01	2.71	1.11
0.005 in/p	2.92	2.81	1.04
0.001 in/p	2.72	3.01	0.90
Pendulum	2.39	3.20	0.75

Table 6.5.1. The variations in the {111}/{100} ratios and  $R_0$  values of materials cold rolled to 75% total reduction using the 35°/p, 45°/p, 55°/p, 0.02 in/p, 0.005 in.p, 0.001 in/p and pendulum schedules.

ratios with increasing total rolling reduction to a maximum at 80%, 75% and 70% respectively. In the case of materials cold rolled by the pendulum schedule, the  $\{111\}/\{100\}$  ratios decreased on increasing the total rolling reductions from 65% to 75%.

In order to demonstrate the significance of the reductions in intensity of the  $\{111\}$  and  $\{100\}$  components after 0.5 hr isothermal annealing at 700°C upon  $R_o$  value, the  $\{111\}/\{100\}$  ratios were measured and are listed in Table 6.5.2. By comparing Table 6.5.1 and Table 6.5.2, it is evident that the  $\{111\}/\{100\}$  ratios increased significantly after annealing. The improvement in the  $R_o$  values after annealing (see figure 5.3.2.a) is due to the relatively large reduction in P value of the  $\{100\}$  component.

The increase and decrease in P values of the  $\{111\}$  and  $\{100\}$  components respectively on increasing the annealing time from 0.5 hr to 6 hrs resulted in a significant increase in the  $\{111\}/\{100\}$  ratios of all materials. The magnitudes of the increases in the  $\{111\}/\{100\}$  ratios together with the percentage increase in their ratios are listed in Table 6.5.3. Accordingly, increasing the annealing time from 0.5 hr to 6 hrs resulted in 59% increase in the  $\{111\}/\{100\}$  ratio of a material previously cold rolled to 75% using the 35°/p rolling schedule. The corresponding values are 50%, 41% and 19% in the case of the materials cold rolled using the 45°/p, 55°/p and pendulum schedules. The increase in  $R_o$  value with increasing the annealing time is closely related to the increase in the corresponding  $\{111\}/\{100\}$  ratios. The variations in the  $\{111\}/\{100\}$  ratios of materials cold rolled to ranges of total rolling reductions using the 35°/p, 45°/p, 55°/p, 0.02 in/p,

Rolling schedules	P. values		{111}/{100} ratios
	{111} Planes	{100} Planes	
35°/p	2.20	0.50	4.39
45°/p	2.18	0.52	4.15
55°/p	2.17	0.54	3.98
0.02 in/p	2.15	0.55	3.89
0.005 in/p	2.14	0.57	3.74
0.001 in/p	2.14	0.58	3.66
Pendulum	2.01	0.61	3.31

Table 6.5.2. The variations in the {111}/{100} ratios and  $R_o$  values of materials cold rolled using the 35°/p, 45°/p, 55°/p and pendulum rolling schedules to 75% total reduction, annealed for 0.5 hr then aged.

Rolling Schedules	The $\frac{\{111\}}{\{100\}}$ ratios after 6 hrs annealing	The $\frac{\{111\}}{\{100\}}$ ratios after 0.5 hr annealing	% increase
35°/p	7.47	4.39	69
45°/p	6.22	4.15	50
55°/p	5.60	3.98	41
0.02 in/p	5.39	3.89	40
0.005 in/p	4.99	3.74	34
0.001 in/p	4.37	3.66	20
Pendulum	3.95	3.31	19

Table 6.5.3. The percentage increase in the  $\{111\}/\{100\}$  ratios after 6 hrs annealing in comparison with 0.5 hr annealing, the materials previously cold rolled to 75% total reduction using the 35°/p, 45°/p, 55°/p, 0.02 in/p, 0.005 in/p, 0.001 in/p and pendulum rolling schedules.

0.005 in/p, 0.001 in/p and pendulum schedules, annealed for 6 hrs then aged are shown in figure 6.5.4. It is evident that the variations in the  $\{111\}/\{100\}$  ratios correspond with the variations in  $R_o$  values (see figure 5.3.2.6).

An interesting comparison can be made between the present work and an earlier investigation by Mathur and Backofen<sup>(76)</sup>. These latter authors varied the deformation geometry by carrying out cold rolling and deep drawing with dies of varying angle. They characterised their deformation zone geometry by a term  $\Delta$  equivalent to the ratio between the entry thickness  $T_N$  and the roll diameter  $D$  which was used in the present study. They observed an effect of  $\Delta$  on the development of cold worked texture and also on the recrystallisation texture of Al killed steel. It was observed also that the microscopic shearing was associated with high  $\Delta$  geometry and that the occurrence of such shearing led to a reduction in the amount of the  $\{111\}$  component. Accordingly, repeated low  $\Delta$  reductions with possible intermediate annealing to restore work hardening capacity and further reduce the tendency for microscopic shearing was suggested as a process route for sheets with a high porportion of  $\{111\}$  oriented material. They were unable to associate the proportion of the  $\{100\}$  material with macro-shearing and their final statement regarding the effect of deformation geometry on  $\bar{R}$  value of finished sheet was inclusive. However, their results suggest a decreasing ratio of  $\{111\}/\{100\}$  as  $\Delta$  increases between 1 and 4 which is in agreement with the present observations.

The rolling schedules used in the present study can be expressed in terms of  $\Delta$  as shown in Table 6.5.4.

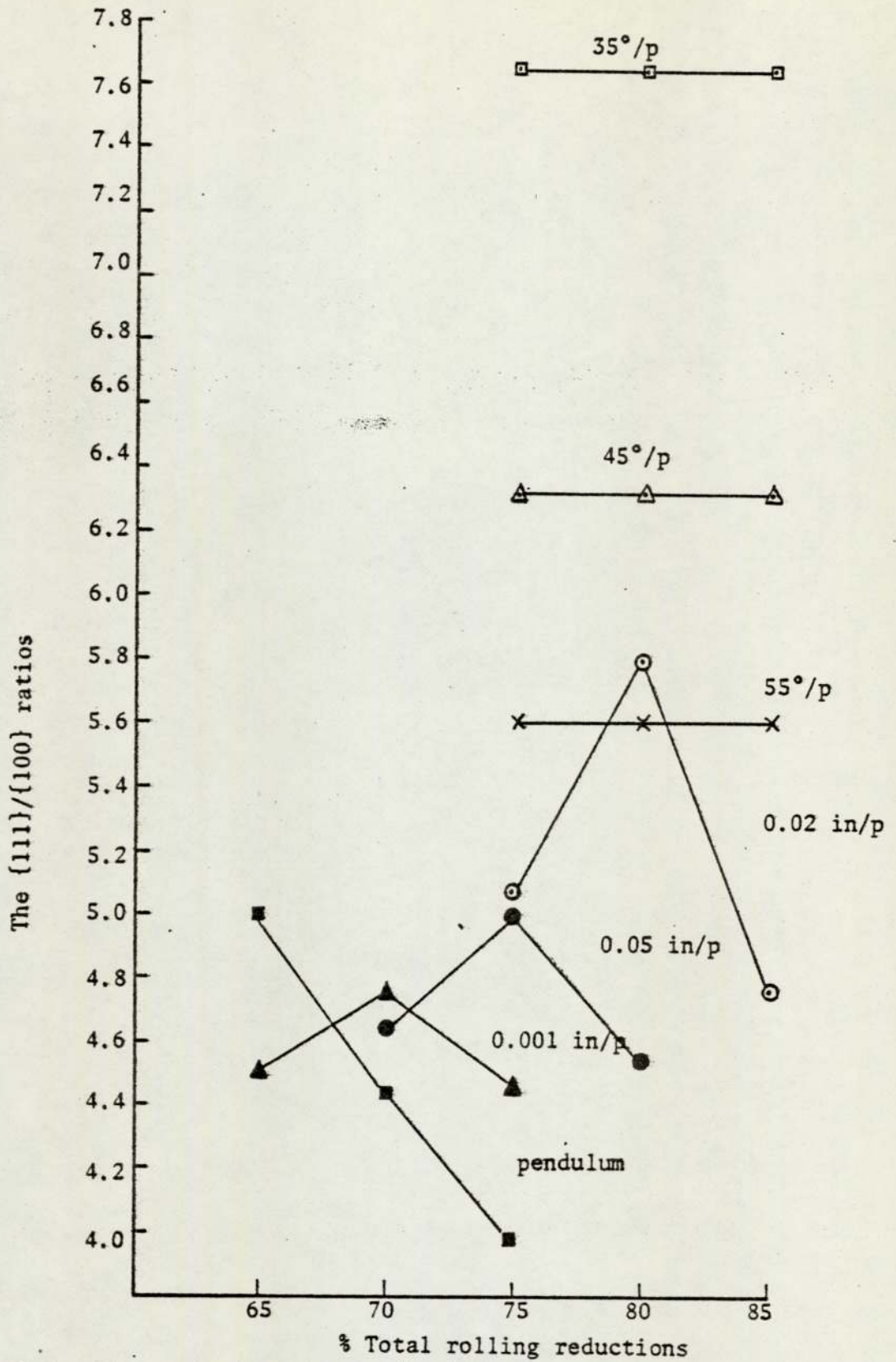


Fig. 6.5.4. The variations in the {111}/{100} ratios of materials cold rolled using the seven rolling schedules, annealed for 6 hrs then aged versus the total rolling reduction.

Table 6.5.4 shows the magnitude of  $\Delta$  at the beginning of rolling and after 90% total rolling reduction versus the constant geometry and constant roll gap schedules.

Rolling Schedules	$\Delta = T_N/D$	
	at the beginning of rolling	after 90% total rolling reduction
35°/p shear angle	0.7	0.7
45°/p shear angle	1.0	1.0
55°/p shear angle	1.4	1.4
0.02 in/p roll gap	0.8	0.14
0.005 in/p roll gap	1.6	0.18
0.001 in/p roll gap	3.5	0.35

Because of the varying geometry in the constant roll gap schedules, it is not possible to make a direct comparison with the results of Mathur and Backofen. On the other hand, deformation carried out with constant geometry demonstrates that a  $\Delta$  value of 0.7 leads to the production of sheets with a significantly higher ratio of  $\{111\}/\{100\}$ , and therefore a higher  $R_o$  value than those obtained, the higher  $\Delta$  values of 1.0 and 1.4.

The effects of the total rolling reduction were noted by Mathur and Backofen and they were also studied in the present work. Mathur and Backofen observed that the peak value of the  $\{111\}/\{100\}$  ratio occurred at high total reduction when  $\Delta$  was equal to 1 and at lower

total reductions as  $\Delta$  increased. It should be noted, however, that Mathur and Backofen measured only the  $\{111\}$  and  $\{100\}$  intensities and therefore their textural information was not as complete as that obtained in the present study. In the present investigation, it was observed that both the  $\{111\}/\{100\}$  texture ratio and  $R_0$  value were independent of the total rolling reduction over the range from 65% to 90% in the case of constant geometry schedules. On the other hand, the total reduction for a peak value of  $\{111\}/\{100\}$  and  $R_0$  decreased as the reduction per pass decreased for the constant roll gap schedules.

The evidence all points to the considerable importance of the deformation zone geometry in controlling the texture development in rolled and annealed low carbon steel. It suggests also that texture gradients arising from the frictional effects are not so important as they affect only a relatively small volume fraction of the sheet thickness.

Finally, of course, the annealing cycle itself can have a major influence on the development of the recrystallisation texture. Two annealing procedures were used in the present work and the beneficial effect of increasing the annealing time in order to promote the normal grain growth was demonstrated.

#### 6.6 THE RELATIONSHIP BETWEEN CRYSTAL REORIENTATION AFTER TENSILE EXTENSION AND R VALUE

As mentioned at the start of section 6.3, the rotations accompanying deformation can be analysed in various ways, and the method of analysis presented here is based on a particular viewpoint<sup>(7)</sup>.

According to (110) pole figures of materials cold rolled to 75% total reduction, annealed for 6 hrs, aged then subjected to 20% tensile extension intensities of the {112}, {113} and {100} planes of the <110> direction increased while intensity of the {111}<112> decreased after tensile extension. This is shown in figure 5.5.2.1 to figure 5.5.2.7. The increase and decrease in intensities of the {100} and {111} planes after tensile extension were dependent upon the rolling schedules. This indicates that crystals reorientation accompanying tensile extension resulted from different rotation mechanisms as shown in figure 6.6.1. The first mechanism decreases the texture intensity about the sheet normal resulting in increasing the intensities of the {112}, {113}, {100} planes of the <110> direction. The second mechanism accompanies the first and occurs by rotation away from the {111}<112> component resulting in a reduction in its intensity. The third mechanism occurs at the same time as the first and second and can be represented by rotation about the <110> rolling direction. This results in decreasing the intensity of the {111} planes parallel to the plane of the sheet and increasing the intensity of the {100} planes.

Measurements of P values of the {111} planes of materials cold rolled to 75% using the 35°/p, 45°/p, 55°/p, 0.02 in/p, 0.005 in/p, 0.001 in/p and pendulum schedules indicated that the {111} planes are not strongly represented in the 0.5 hr annealing texture (see Table 5.5.1.1). It is therefore rational that the third mechanism dominates resulting in a big reduction in P value of the {111} planes and a big increase in P value of the {100} planes after tensile extension. This is shown in Table 6.6.1. Since P values of the {111} planes decreased towards cold rolling using the pendulum mill, type 3 rotation becomes



more effective in the same direction. This resulted in more reduction and more increase in P values of the {111} and {100} planes in the order of the previous rolling schedules as shown in Table 5.5.1.1. Accordingly the corresponding {111}/{100} ratios decreased by increasing the angle  $\theta$  between the material and rolls, decreasing the rolling schedules and cold rolling using the pendulum mill as shown in Table 6.6.2. The difference in the {111}/{100} ratio before and after tensile extension decreased with altering the rolling procedure from 1.29 when cold rolling using 35°/p rolling schedules to 2.06 in the case of the pendulum mill. A big reduction in the {111}/{100} ratio as in the case of materials cold rolled by the pendulum indicates a through-thickness shear which results in more reduction in thickness than in width and hence low R values. On the other hand, a small reduction in the {111}/{100} ratio as in the case of material cold rolled using 35°/p rolling schedules indicates a through width shear. This results in more reduction in width than in thickness and higher R value.

Texture of materials annealed for 6 hrs were characterised by more {111} and less {100} planes parallel to the surface (Table 5.4.2.2.) in comparison with texture of materials annealed for 0.5 hr (Table 5.4.2.1). However, the reduction and increase in P values of the {111} and {100} planes of the first material were less relative to those annealed for 0.5 hr. This resulted in less reduction in the {111}/{100} ratios of materials annealed for 6 hrs after tensile extension as shown in Table 6.6.3 and Table 6.6.4 which indicates an improvement in R value after 6 hrs annealing.

Rolling Schedules	$P_{\{111\}}$	$P_{\{100\}}$	$P_{\{111\}}/P_{\{100\}}$
35°/p	1.92	0.62	3.10
45°/p	1.87	0.67	2.81
55°/p	1.81	0.70	2.57
0.02 in/p	1.73	0.78	2.24
0.005 in/p	1.69	0.83	2.04
0.001 in/p	1.66	0.91	1.82
Pendulum	1.39	1.11	1.25

Table 6.6.1. shows the  $\{111\}/\{100\}$  ratios of materials cold rolled for 75% total reduction, annealed for 0.5hr, aged, then subjected to 20% tensile extension as a function of the seven rolling schedules.

Rolling Schedules	$P_{\{111\}}/P_{\{100\}}$ (before ten.ext.)	$P_{\{111\}}/P_{\{100\}}$ (after ten.ext.)	Difference
35°/p	4.39	3.10	1.29
45°/p	4.15	2.81	1.34
55°/p	3.98	2.57	1.41
0.02 in/p	3.89	2.24	1.65
0.005 in/p	3.74	2.04	1.70
0.001 in/p	3.66	1.82	1.84
Pendulum	3.31	1.25	2.06

Table 6.6.2. shows the difference in the  $\{111\}/\{100\}$  ratios before and after 20% tensile extension of materials cold rolled to 75% total reduction using the seven rolling schedules, annealed for 0.5hrs then aged.

In the 6 hrs annealing texture of materials cold rolled using constant geometry rolling schedules, P values of the {111} and {100} planes increased and decreased respectively with decreasing the shear plane angle " $\theta$ " (Table 5.5.1.4.). Accordingly, the reduction and increase in P values of the {111} and {100} planes, after tensile extension, increased with increasing the angle  $\theta$ . The corresponding {111}/{100} ratios decreased also in the same order as shown in Table 6.6.3. The reduction in the {111}/{100} ratio after tensile extension increased on increasing the angle  $\theta$  as shown in Table 6.6.4. However, the reduction in thickness after tensile extension increases with increasing the angle  $\theta$  and therefore the R value decreases in this order. (figure 5.3.2). On increasing the total rolling reduction from 75% to 85%, the reduction in the {111}/{100} ratio after tensile extension remained constant as in figure 6.6.2 and figure 6.6.3. This indicates a constant R value when increasing the total rolling reduction.

In constant roll gap rolling schedules, the 6 hrs annealing texture contained less {111} and more {100} planes in comparison with constant geometry schedules. This resulted in more reductions in the {111} and more increases in the {100} P values after tensile extension, i.e. less {111}/{100} ratios as shown in Table 6.6.3. The corresponding reductions in the {111}/{100} ratios after tensile extension were relatively higher as shown in Table 6.6.4. This is in agreement with the relatively low R values in the case of materials previously cold rolled using constant roll gap schedules. The {111}/{100} ratios of materials cold rolled to 65%, 70% and 75%; 70%, 75% and 80%; and 75%, 80% and 85% using the 0.001 in/p, 0.005 in/p and 0.02 in/p respectively, annealed for 6 hrs, aged then subjected to 20% tensile extension are shown in figure 6.6.2.

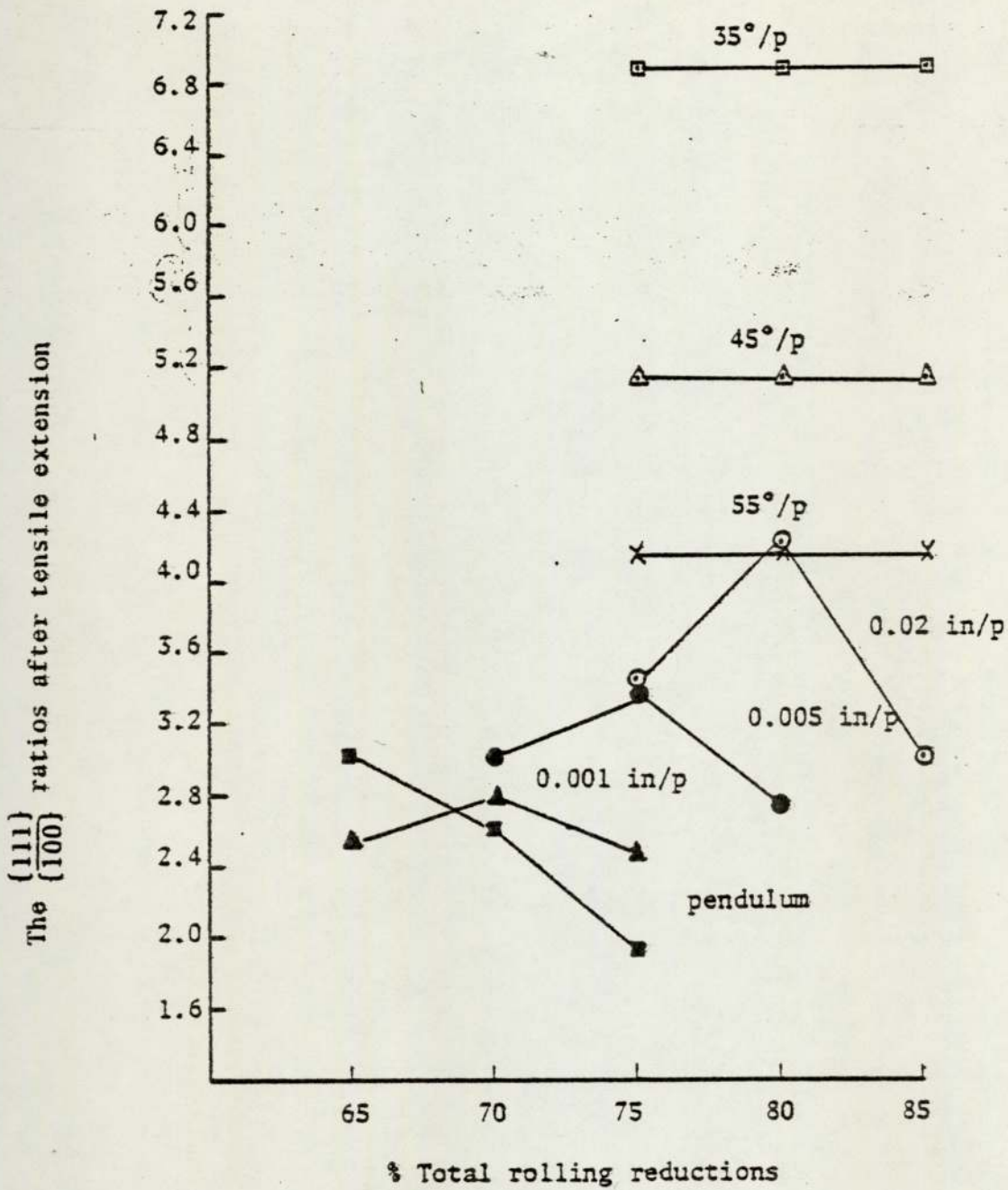


Fig. 6.6.2. The variation in the {111}/{100} ratios of materials cold rolled using the seven rolling schedules, annealed for 6 hrs aged then subjected to 20% tensile extension versus the total rolling reduction.

Rolling Schedules	$P_{\{111\}}$	$P_{\{100\}}$	$P_{\{111\}}/P_{\{100\}}$
35°/p	2.98	0.45	6.62
45°/p	2.77	0.54	5.13
55°/p	2.56	0.59	4.31
0.02 in/p	2.43	0.62	3.89
0.005 in/p	2.30	0.68	3.37
0.001 in/p	2.00	0.74	2.70
Pendulum	1.62	0.78	2.08

Table 6.6. 3. shows the  $\{111\}/\{100\}$  ratios of materials cold rolled for 75% total reduction, annealed for 6 hrs, aged then subjected to 20% tensile extension as a function of the seven rolling schedules.

Rolling Schedules	$P_{\{111\}}/P_{\{100\}}$ (before ten.ext.)	$P_{\{111\}}/P_{\{100\}}$ (after ten.ext.)	Difference
35°/p	7.47	6.62	0.85
45°/p	6.22	5.13	1.09
55°/p	5.60	4.31	1.29
0.02 in/p	5.39	3.89	1.50
0.005 in/p	4.99	3.37	1.62
0.001 in/p	4.37	2.70	1.63
Pendulum	3.95	2.08	1.87

Table 6.6.4. shows the difference in the  $\{111\}/\{100\}$  ratios before and after 20% tensile extension of materials cold rolled to 75% total reduction using the seven rolling schedules, annealed for 6 hrs then aged.

It is evident that the  $\{111\}/\{100\}$  ratios increased on increasing the total rolling reduction to a maximum at 70%, 75% and 80% total reduction in the case of material cold rolled using the 0.001 in/p, 0.005 in/p and 0.02 in/p rolling schedules. On the other hand, the reduction in the  $\{111\}/\{100\}$  ratios after tensile extension were minimum at 70%, 75% and 80%. On either side of the critical total rolling reduction the reduction in the  $\{111\}/\{100\}$  ratios were higher. R values of these materials increased on increasing the total rolling reduction to a maximum corresponding to a minimum reduction in the  $\{111\}/\{100\}$  ratios.

The 6 hrs annealing texture of material cold rolled to 75% using the pendulum mill contained less  $\{111\}$  and more  $\{100\}$  planes in comparison with controlled geometry and draughts rolling schedules, (see Table 5.5.1.4.). Accordingly, more reduction in intensity of the  $\{111\}$  and more increase in intensity of the  $\{100\}$  planes occurred after tensile strain. The corresponding  $\{111\}/\{100\}$  ratios were small in comparison with constant geometry and roll gap schedules, as shown in Table 6.6.3. The reductions in such ratios after tensile strain were higher as shown in Table 6.6.4. This indicates more reduction in thickness than in width and hence low R value. With reference to figure 6.6.2 the  $\{111\}/\{100\}$  ratios of materials cold rolled to 65%, 70% and 75% total reductions decreased with increasing the total rolling reduction. As a result, the thickness strain increased and hence R value decreased with increasing the total rolling reduction.

## 6.7 THE COLD ROLLING GEOMETRY

In the rolling process the arc of contact and hence the roll load increases with increasing roll diameter, rolling draughts and with decreasing the shear angle  $\theta$  (Section 4.2.1). During cold rolling using constant geometry schedules, the shear angle  $\theta$  was kept constant with the progress of rolling by reducing the rolling draughts from one pass to the next. This confines the deformation to certain zones in which crystallographic slip occurs under the same rolling condition. Three equations were therefore, derived (Section 4.2.1) in order to calculate the roll gap required to maintain  $55^\circ$ ,  $45^\circ$  and  $35^\circ$  shear angle during the rolling operations. These equations were based on the assumptions that the material in the roll gap is rectangular and that the entry thickness was equal to the difference between the exit of the previous pass and the next roll gap. A more accurate calculation is possible by considering the entry thickness to be equal to the difference between the average exit thickness and the roll gap.

Cold rolling to 80% total rolling reduction using the  $55^\circ/p$  and  $45^\circ/p$  schedules was reached in 77 and 39 passes respectively. In comparison, 20 passes were required by the  $35^\circ/p$  schedule to affect the same total rolling reduction. Besides being less favourable for high R value cold rolling by the  $55^\circ/p$  and  $45^\circ/p$  is not practicable relative to the  $35^\circ/p$  schedule. The number of passes corresponding to the  $35^\circ/p$  schedule is reduced to a certain extent by increasing the initial material thickness and decreasing the roll diameter. Decreasing the roll diameter is necessary<sup>(86)</sup> to decrease the amount of energy dissipated by the frictional losses, to decrease energy consumption and to improve the mill efficiency during cold rolling. The frictional losses were minimised

by reducing the rolling draughts. Following Orowan<sup>(75)</sup> cold rolling using lubricated, polished rolls and a small percentage reduction per pass is characterised by a low friction coefficient. The small draughts during the later stages of constant geometry schedules would therefore be associated with low frictional losses. Furthermore, cold rolling using the same percentage reduction per pass as in constant geometry schedules ensures that cold rolling was carried out under the frictional condition during each pass. The difficulty involved in using the present schedules on industrial scale is the high number of passes required to affect a heavy total rolling reduction.

With reference to Mathur and Backofen<sup>(76)</sup>, the deformation geometry ' $\Delta$ ' is determined by the material thickness, the roll diameter and the rolling draughts. In the present study, the rolling geometry is related to the previous variables together with a shear plane angle which is related to the deformation modes. The practical limitation involved in using Mathur and Backofen findings, and also the present work in strip rolling is that in order to keep a constant geometry the rolling draughts became very small and difficult to control. Nevertheless, the present study agrees with Mathur and Backofen in that the rolling geometry is an important factor in the control of texture and R value. Furthermore, the rolling draughts must be reduced with the progress of rolling in order to maintain a constant geometry.

In constant roll gap schedules, where the roll gap was kept constant during cold rolling, the percentage reduction per pass increased with the progress of rolling. The percentage reduction per pass, for example, increased from 8% at the beginning of rolling to 80% after 90% total

reduction using the 0.02 in/p schedules. Hence, as rolling proceeds and the material is reduced in thickness, the roll load varies from one pass to the next. The deformation during cold rolling occurs under different rolling geometry. In addition the energy dissipated and hence energy consumption is increased relative to a schedule involving small draughts. During cold rolling using constant roll gap schedules, the shear plane angle  $\theta$  decreases with increasing the roll gap and the total reductions as shown in figure 6.3.2.

Measurements of width of materials cold rolled using constant geometry and constant roll gap schedules revealed that the spread in width increased with decreasing the shear angle and increasing the roll gap.

In the pendulum schedule, the initial material is forced by feed rolls into a gap formed by converging paths of two work rolls. The rolls move backwards and forwards at about 2000 cycles/min. at very high speed reaching 400 ft/min. The entry strip moves at a low speed of 2 ft/min. and leaves the mill with a speed of 20 ft/min. Deformation of the strip takes place during both the up and down strokes of the cycle. The amount of reduction per stroke is small in comparison with that in conventional rolling, but the total reduction in the whole operation (many strokes) is a lot higher.

Since the percentage reduction per each operation of the pendulum schedule may be ten or twenty times greater than that in a conventional mill, the temperature rise during rolling is much higher and its effect on the strip properties is more important. Although the temperature distribution in the reduction zone is not known, it is locally high for

a very short period of time<sup>(66)</sup>. Empirical data related to the variation of the energy of deformation of annealed low carbon steel strip with the strain rate (rolling speed) at ambient temperature, indicated that deformation becomes more and more dependent upon the strain rate as it increases<sup>(88,89)</sup>. Holloman and Zener<sup>(90)</sup> pointed out that the yield strength is doubled by a thousandfold increase in the strain rate. The strip during the pendulum rolling schedule is at much higher temperature than ambient, and the resistance to deformation does not rise with the speed of deformation because of the temperature effect. Increasing the speed of deformation on the other hand, will reduce the effectiveness of cooling and temperature is bound to rise more with increasing the total reduction throughout the rolling operation, provided that the cooling condition remains unchanged.

The pendulum mill process in terms of conventional rolling mills is therefore equivalent to reverse rolling at high speed. Instead of reversing the direction of rolling by turning the strip end for end after each pass before re-entering the rolls as in conventional rolling, the direction of rolling in the pendulum process is reversed by reversing the direction of the pendulum oscillation after each stroke. A schematic representation of the pendulum cycle is shown in figure 6.3.3.

## 7. SUMMARY AND CONCLUSIONS

1. Texture of the initial material was relatively weak but similar to texture of the hot rolled rimmed steel band. This indicates that the interstage anneal given to the initially cold rolled material has not significantly affected the final texture.

2. Texture developed during cold rolling depended upon the rolling procedures as follows:

(a) Cold rolling using constant geometry schedules were characterised by higher proportions of the  $\{100\}\langle 110\rangle$  orientation relative to the constant roll gap and pendulum schedules. On increasing the total rolling reduction, using the controlled geometry schedules intensity of the  $\{112\}\langle 110\rangle$  orientation increased while intensity of the  $\{111\}\langle 112\rangle$  and  $\{100\}\langle 110\rangle$  orientations remained constant.

(b) In constant roll gap schedules, the percentage reduction per pass increases with the progress of rolling. As a result, the  $\{111\}\langle 112\rangle$  component rotates to the  $\{100\}\langle 110\rangle$  component. This contributes to the reduction in intensity of the  $\{111\}\langle 112\rangle$  orientation after certain total rolling reduction. During cold rolling using the 0.02 in/p schedule the percentage reduction per pass is higher relative to the 0.005 in/p and 0.001 in/p schedules. Accordingly, one  $\{112\}\langle 110\rangle$  component rotates to the  $\{111\}\langle 112\rangle$  which results in a decrease in intensity of the first component and an increase in intensity of the second when cold rolling using the 0.002 in/p schedule. Therefore, the critical total rolling reduction at which there is a turn over in intensities of the  $\{111\}\langle 112\rangle$  and  $\{100\}\langle 110\rangle$  orientations, decreases with decreasing the magnitude of the roll gap.

(c) Cold rolling using the pendulum schedule is equivalent to reverse rolling at high speed. It therefore, favours the development of more  $\{100\}\langle 110\rangle$  orientation since it is the only component with four fold symmetry around the rolling direction. Intensity of the  $\{100\}\langle 110\rangle$  orientation was therefore increased with the progress of rolling at the expense of the  $\{111\}\langle 112\rangle$  and  $\{112\}\langle 110\rangle$  components.

3. The low  $R_0$  values of the cold rolled materials is due to the relatively high proportion of the  $\{100\}$  oriented material in the cold rolled texture. The improvement in  $R_0$  values after 0.5 hr annealing is due to the big reduction in intensity of the  $\{100\}$  component. The increase in  $R_0$  value after 6 hrs annealing is attributed to the normal growth of the  $\{111\}$  oriented materials at the expense of the  $\{100\}$  component. The annealing texture developed is dependent upon texture of the matrix in which they grow. However,  $R_0$  value and texture developed after annealing varied with the total rolling reduction in the same manner as the cold rolling texture. Cold rolling using the  $35^\circ/p$  followed by annealing for 6 hrs then ageing resulted in higher  $\{111\}\langle 100\rangle$  texture ratio and hence higher  $R_0$  value in comparison with cold rolling using the  $45^\circ/p$ ,  $55^\circ/p$ , 0.02 in/p, 0.005 in/p, 0.001 in/p and pendulum schedules respectively. Furthermore, the  $\{111\}/\{100\}$  texture ratio and  $R_0$  value remained constant when the total rolling reduction was increased using the  $35^\circ/p$ ,  $45^\circ/p$  and  $55^\circ/p$  schedules. On the other hand, materials cold rolled using the 0.02 in/p, 0.005 in/p and 0.001 in/p schedules exhibited a maximum  $\{111\}/\{100\}$  ratio and a maximum  $R_0$  value at 80%, 75% and 70% total reduction respectively. The  $\{111\}/\{100\}$  ratio and  $R_0$  value of materials cold rolled using the pendulum mill schedule continued to decrease with increasing the total rolling reduction.

4. There is a linear relationship between  $R_0$  value and the  $\{111\}/\{100\}$  texture parameter.

5. Crystal orientation during subsequent tensile elongation is dependent upon the relative proportion of the  $\{111\}$  and  $\{100\}$  components in the texture prior to tensile extension. Texture of material cold rolled by the  $35^\circ/p$  schedule which is associated with high  $\{111\}/\{100\}$  ratio in the cold rolled and annealed condition changed only slightly after tensile extension. On the contrary texture of material cold rolled by the pendulum schedule which is characterised by a low  $\{111\}/\{100\}$  ratio, altered significantly during tensile extension.

6. The rolling geometry is an important factor in the control of texture and R value. It is defined by the rolling draughts, the material thickness, the roll diameter and a shear plane angle. For certain work roll diameter, the rolling draughts must be reduced with the progress of rolling in order to keep a constant geometry of deformation. Cold rolling using the  $35^\circ/p$  shear plane angle is favoured for a high  $\{111\}/\{100\}$  ratio and a high  $R_0$  value.

8. APPENDICES

## APPENDIX I

### CALCULATION OF THE SHEAR ANGLES IN PLASTIC DEFORMATION

The relative magnitudes of principal strains associated with an incremental strain by extension, compression and rolling was used to define the direction of extension and compression during plastic deformation. These directions were related to the direction of applied stress by an angle depending upon each mode of deformation as follows.

#### (a) Uniaxial extension

In a simple plastic extension, each incremental strain along the strain axis is associated with a strain of half the amount and of opposite sense in the transverse directions, on the assumption of no change in volume. Thus, an incremental plastic extension  $e$  in a direction  $OX$ , figure 10.1a, is accompanied by a contraction equivalent to  $\frac{1}{2}e$  in the  $OY$  and  $OZ$  directions. Considering a unit length in the direction  $OX$ , extended to a length  $(1 + e)$ . Let  $OP$  be the direction of zero extension in the  $XY$  plane making an angle  $\theta$  with the axis  $OX$ . Let the length of  $PX = L$ . Thus  $PX$  is contracted from  $L$  to  $L(1 - \frac{1}{2}e)$ . Therefore,

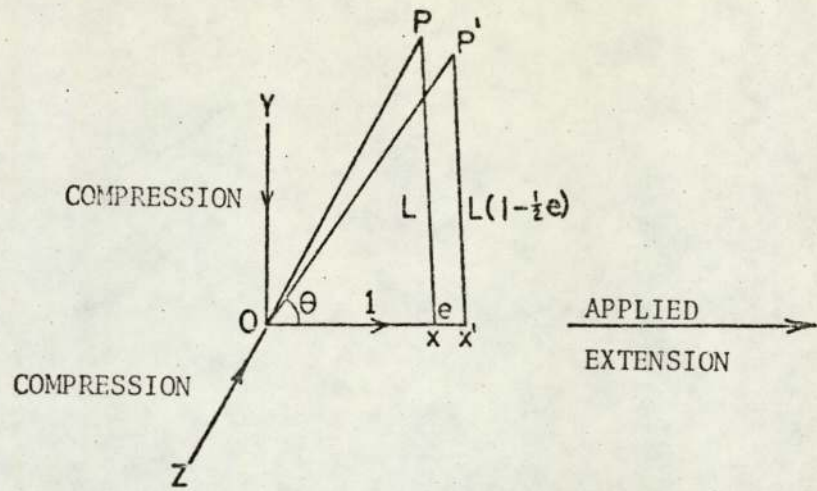
$$\begin{aligned}\overline{OP}^2 &= \overline{OX}^2 + \overline{PX}^2 \\ &= 1 + L^2\end{aligned}\quad \text{(before extension)}$$

and

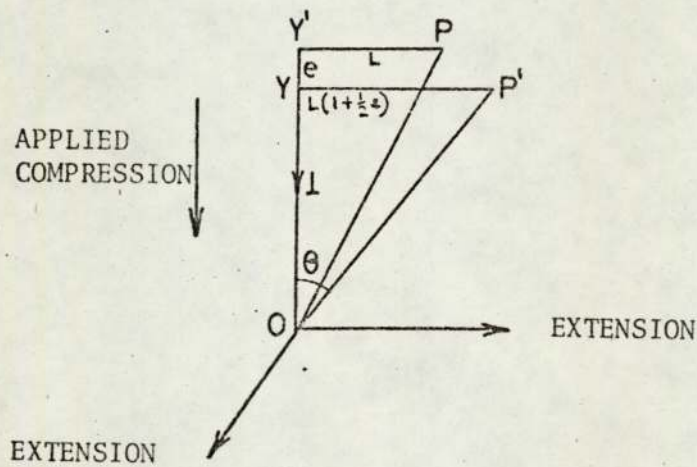
$$= (1+e)^2 + L^2(1 - \frac{1}{2}e)^2 \quad \text{(after extension)}$$

Therefore

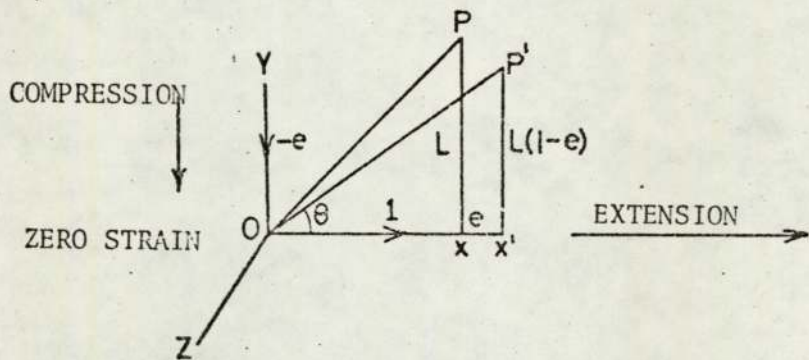
$$1 + L^2 = 1 + 2e + e^2 + L^2 - eL^2 + e^2L^2/4$$



(a) Tension parallel to OX



(b) Compression parallel to OY



(c) Rolling with tension component parallel to OX and compression component parallel to OY.

Fig. 10.1 Illustration of the incremental principal strain in plastic deformation by (a) tension, (b) compression, and (c) rolling.

Hence

$$L^2(1 - e/4)e = (2 + e)e$$

Accordingly

$$L^2 = \frac{2 + e}{1 - e/4}$$

For infinitesimally small  $e$ , hence,

$$L = \pm \sqrt{2}$$

Therefore

$$\text{Cot}\theta = \pm \sqrt{2}$$

That is

$$\theta = \pm 54^\circ 44'$$

(b) Uniaxial compression

This case is analogous to that of uniaxial extension but the incremental plastic extension- $e$  in the OY direction is accompanied by an extension of  $\frac{1}{2}e$  in the OX and OZ directions. Following the previous analysis the angle between the unextended direction OP and the compression axis is equivalent to  $54^\circ 44'$ , as shown in figure 10.I.b.

(c) Pure rolling

In the case of rolling, a small extension in the direction of OX (length) is accompanied by an equal contraction in OY (thickness) without change in OZ (width), on the assumption of constant volume. The angle between OP and OX directions, figure 10.I.c can be calculated as follows:

Considering a unit of unextended length OX, extended to a length  $(1 + e)$ . Let the strain in the direction OP in the XY plane be zero

and let  $PX = L$  then

$$\begin{aligned}\overline{OP}^2 &= \overline{OX}^2 + \overline{PX}^2 \\ &= 1 + L^2\end{aligned}\quad \text{(before extension)}$$

And

$$= (1 + e)^2 + L^2(1 - e)^2 \quad \text{(after extension)}$$

Hence

$$= 1 + 2e + e^2 + L^2 - 2eL^2 + e^2L^2$$

Therefore

$$L^2 = \frac{2 + e}{2 - e}$$

For infinitesimally small  $e$ , hence

$$L^2 = 1$$

That is

$$L = \pm 1$$

And

$$\text{Cot } \theta = \pm 1$$

$$\theta = \pm 45^\circ$$

APPENDIX II. A Computer programme for calculation of controlled  
geometry rolling draughts

```

0001      LIST (LP)
0002      PROGRAM (FXXX)
0003      INPUT 1 = CR0
0004      INPUT 3 = TR0
0005      INPUT 5 = CR1
0006      OUTPUT 2 = LP0
0007      OUTPUT 6 = LP1
0008      COMPRESS INTEGER AND LOGICAL
0009      COMPACT
0010      TRACE 2
0011      END
0012      TRACE 1
0013      READ FROM (CR)
0001      MASTER
0002      L = 0
0003      10 READ (1,60) THETA
0004      L = L + 1
0005      WRITE (2,80) THETA
0006      RAD = (3.14159*THETA)/180
0007      Z=TAN(RAD)
0008      TF=0.2500
0009      D=4.745
0010      20 R=(2.0*TE*TE)/(D*Z*Z+2.0*TE)
0011      PRCNT=(0.2500-TE)/0.2500*100
0012      TE=(TF-R)
0013      WRITE(2,70)R, TE, PRCNT
0014      IF(TE.GT.0.0088) GO TO 20
0015      IF(L.LT.3) GO TO 10
0016      60 FORMAT(F0.0)
0017      70 FORMAT(3(10X,F10.7))
0018      80 FORMAT(///,15X,7H THETA =,F10.5,
0019      1 //,15X,1HR,15X,7HNEXT TE,15X,5HPRCNT,/)
0020      STOP
0021      END

```

APPENDIX III. The calculated rolling draughts and % reduction per pass required to maintain a constant angle of 35° between the material rolled and rolls during cold rolling of the initial material to 90% total reduction.

R	NEXT TE	PRCNT
0.0432355	0.2067645	0.0000000
0.0304860	0.1762785	17.2942001
0.0226513	0.1536273	29.4885853
0.0174929	0.1361344	38.5490876
0.0139164	0.1222180	45.5462313
0.0113351	0.1108829	51.1128005
0.0094110	0.1014719	55.6468300
0.0079385	0.0935335	59.4112245
0.0067865	0.0867470	62.5866172
0.0058683	0.0808787	65.3012165
0.0051246	0.0757540	67.6485385
0.0045139	0.0712401	69.6983976
0.0040062	0.0672338	71.5039683
0.0035796	0.0636542	73.1064638
0.0032177	0.0604365	74.5383202
0.0029081	0.0575284	75.8254152
0.0026411	0.0548873	76.9886455
0.0024092	0.0524781	78.0450707
0.0022066	0.0502715	79.0087549
0.0020285	0.0482430	79.8913970
0.0018712	0.0463718	80.7028073
0.0017314	0.0446404	81.4512744
0.0016068	0.0430336	82.1438489
0.0014951	0.0415384	82.7865660
0.0013947	0.0401437	83.3846225
0.0013041	0.0388396	83.9425172
0.0012221	0.0376175	84.4641641
0.0011475	0.0364700	84.9529847
0.0010796	0.0353905	85.4119830
0.0010175	0.0343730	85.8438675
0.0009606	0.0334124	86.2508018
0.0009084	0.0325040	86.6350477
0.0008603	0.0316437	86.9984007
0.0008159	0.0308278	87.3425196
0.0007749	0.0300529	87.6688924
0.0007369	0.0293159	87.9788571
0.0007016	0.0286143	88.2736210
0.0006688	0.0279455	88.5542753
0.0006383	0.0273072	88.8218095
0.0006098	0.0266974	89.0771226
0.0005831	0.0261143	89.3210333
0.0005582	0.0255561	89.5542887
0.0005348	0.0250212	89.7775722
0.0005129	0.0245083	89.9915098
0.0004923	0.0240160	90.1966763

APPENDIX IV. The calculated rolling draughts and % reduction per pass required to maintain a constant angle of 45° between the material rolled and rolls during cold rolling of the initial material to 90% total reduction

R	NEXT TE	PRCNT
0.0236072	0.2263928	0.0000000
0.0195335	0.2068593	9.4428933
0.0164305	0.1904288	17.2562933
0.0140124	0.1764163	23.8284834
0.0120916	0.1643247	29.4334620
0.0105404	0.1537843	34.2701078
0.0092697	0.1445146	38.4862719
0.0082157	0.1362989	42.1941575
0.0073318	0.1289670	45.4804524
0.0065833	0.1223837	48.4131916
0.0059438	0.1164399	51.0465186
0.0053932	0.1110466	53.4240583
0.0049157	0.1061309	55.5813531
0.0044990	0.1016319	57.5476523
0.0041331	0.0974988	59.3472450
0.0038100	0.0936888	61.0004698
0.0035235	0.0901653	62.5244858
0.0032680	0.0868973	63.9338709
0.0030394	0.0838578	65.2410895
0.0028340	0.0810238	66.4568622
0.0026487	0.0783751	67.5904603
0.0024810	0.0758941	68.6499427
0.0023288	0.0735654	69.6423480
0.0021901	0.0713753	70.5738507
0.0020635	0.0693118	71.4498904
0.0019475	0.0673643	72.2752772
0.0018411	0.0655232	73.0542810
0.0017431	0.0637801	73.7907045
0.0016528	0.0621274	74.4879461
0.0015693	0.0605581	75.1490519
0.0014919	0.0590662	75.7767600
0.0014202	0.0576460	76.3735389
0.0013535	0.0562924	76.9416196
0.0012914	0.0550010	77.4830235
0.0012335	0.0537675	77.9995867
0.0011794	0.0525882	78.4929804
0.0011287	0.0514594	78.9647293
0.0010813	0.0503781	79.4162271
0.0010368	0.0493413	79.8487504
0.0009950	0.0483463	80.2634707
0.0009557	0.0473907	80.6614651
0.0009186	0.0464721	81.0437253
0.0008837	0.0455884	81.4111663
0.0008507	0.0447377	81.7646336
0.0008195	0.0439182	82.1049093
0.0007900	0.0431282	82.4327184
0.0007621	0.0423660	82.7487337
0.0007356	0.0416304	83.0535804
0.0007105	0.0409199	83.3478403
0.0006867	0.0402332	83.6320554
0.0006640	0.0395691	83.9067316

APPENDIX IV. continued

0.0006425	0.0389267	84.1723410
0.0006219	0.0383048	84.4293254
0.0006024	0.0377024	84.6780980
0.0005837	0.0371187	84.9190464
0.0005659	0.0365527	85.1525339
0.0005489	0.0360038	85.3789019
0.0005327	0.0354711	85.5984709
0.0005171	0.0349540	85.8115429
0.0005023	0.0344517	86.0184019
0.0004881	0.0339637	86.2193159
0.0004744	0.0334892	86.4145375
0.0004613	0.0330279	86.6043051
0.0004488	0.0325791	86.7880443
0.0004368	0.0321423	86.9683682
0.0004252	0.0317171	87.1430784
0.0004141	0.0313030	87.3131661
0.0004034	0.0308995	87.4788122
0.0003932	0.0305064	87.6401886
0.0003833	0.0301231	87.7974581
0.0003738	0.0297493	87.9507757
0.0003646	0.0293847	88.1002884
0.0003558	0.0290289	88.2461361
0.0003473	0.0286816	88.3884520
0.0003391	0.0283425	88.5273628
0.0003311	0.0280114	88.6629892
0.0003235	0.0276879	88.7954464
0.0003161	0.0273718	88.9248442
0.0003090	0.0270628	89.0512874
0.0003021	0.0267607	89.1748761
0.0002954	0.0264653	89.2957057
0.0002890	0.0261764	89.4138677
0.0002827	0.0258937	89.5294495
0.0002767	0.0256170	89.6425346
0.0002708	0.0253462	89.7532032
0.0002652	0.0250810	89.8615317
0.0002597	0.0248214	89.9675938
0.0002543	0.0245670	90.0714597

APPENDIX V. The calculated rolling draughts and % reduction per pass required to maintain a constant angle of 54°44' between the material rolled and rolls during cold rolling of the initial material to 90% total reduction.

<u>R</u>	<u>NEXT TF</u>	<u>PRCNT</u>
0.0123905	0.2376095	0.0000000
0.0112203	0.2263891	4.9562128
0.0102084	0.2161807	9.4443439
0.0093275	0.2068532	13.5277139
0.0085559	0.1982973	17.2587153
0.0078762	0.1904211	20.6810723
0.0072745	0.1831466	23.8315623
0.0067391	0.1764075	26.7413427
0.0062608	0.1701468	29.4369852
0.0058316	0.1643152	31.9412893
0.0054451	0.1588701	34.2739287
0.0050958	0.1537743	36.4519693
0.0047791	0.1489952	38.4902877
0.0044910	0.1445043	40.4019107
0.0042282	0.1402761	42.1982948
0.0039878	0.1362884	43.8895555
0.0037673	0.1325211	45.4846583
0.0035646	0.1289564	46.9915770
0.0033779	0.1255785	48.4174279
0.0032054	0.1223731	49.7685812
0.0030459	0.1193272	51.0507572
0.0028979	0.1164293	52.2691064
0.0027605	0.1136688	53.4282789
0.0026326	0.1110361	54.5324839
0.0025135	0.1085227	55.5855408
0.0024022	0.1061205	56.5909229
0.0022981	0.1038224	57.5517961
0.0022007	0.1016217	58.4710521
0.0021094	0.0995123	59.3513373
0.0020236	0.0974887	60.1950785
0.0019429	0.0955458	61.0045050
0.0018670	0.0936788	61.7816684
0.0017954	0.0918834	62.5284601
0.0017279	0.0901555	63.2466263
0.0016641	0.0884914	63.9377820
0.0016038	0.0868877	64.6034228
0.0015467	0.0853410	65.2449359
0.0014926	0.0838484	65.8636100
0.0014413	0.0824071	66.4606433
0.0013926	0.0810146	67.0371517
0.0013463	0.0796683	67.5941758
0.0013023	0.0783660	68.1326870
0.0012604	0.0771056	68.6535931
0.0012205	0.0758852	69.1577435
0.0011824	0.0747027	69.6459339
0.0011462	0.0735566	70.1189104
0.0011115	0.0724450	70.5773732
0.0010784	0.0713666	71.0219802
0.0010468	0.0703198	71.4533504
0.0010165	0.0693033	71.8720660
0.0009876	0.0683158	72.2786760

APPENDIX V. continued

0.0009598	0.0673560	72.6736978
0.0009332	0.0664227	73.0576198
0.0009077	0.0655150	73.4309034
0.0008832	0.0646318	73.7939848
0.0008597	0.0637721	74.1472766
0.0008372	0.0629349	74.4911694
0.0008155	0.0621195	74.8260333
0.0007946	0.0613248	75.1522195
0.0007745	0.0605503	75.4700607
0.0007552	0.0597951	75.7798733
0.0007366	0.0590585	76.0819577
0.0007187	0.0583398	76.3765994
0.0007014	0.0576384	76.6640702
0.0006847	0.0569537	76.9446288
0.0006687	0.0562850	77.2185213
0.0006531	0.0556319	77.4859827
0.0006382	0.0549938	77.7472368
0.0006237	0.0543701	78.0024973
0.0006097	0.0537604	78.2519680
0.0005962	0.0531642	78.4958437
0.0005831	0.0525811	78.7343106
0.0005704	0.0520107	78.9675466
0.0005582	0.0514525	79.1957220
0.0005463	0.0509062	79.4189997
0.0005349	0.0503713	79.6375357
0.0005237	0.0498476	79.8514796
0.0005130	0.0493346	80.0609744
0.0005025	0.0488321	80.2661576
0.0004924	0.0483397	80.4671609
0.0004825	0.0478572	80.6641108
0.0004730	0.0473842	80.8571286
0.0004637	0.0469204	81.0463310
0.0004548	0.0464657	81.2318299
0.0004460	0.0460196	81.4137331
0.0004375	0.0455821	81.5921441
0.0004293	0.0451528	81.7671625
0.0004213	0.0447315	81.9388842
0.0004135	0.0443180	82.1074014
0.0004059	0.0439121	82.2728030
0.0003986	0.0435135	82.4351746
0.0003914	0.0431221	82.5945987
0.0003844	0.0427377	82.7511549
0.0003776	0.0423601	82.9049199
0.0003710	0.0419891	83.0559676
0.0003646	0.0416245	83.2043694
0.0003583	0.0412662	83.3501943
0.0003522	0.0409141	83.4935088
0.0003462	0.0405672	83.6343772
0.0003404	0.0402274	83.7728616
0.0003347	0.0398927	83.9090219
0.0003292	0.0395635	84.0429162
0.0003238	0.0392397	84.1746006
0.0003186	0.0389211	84.3041294

APPENDIX V. continued

0.0003134	0.0386077	84.4315551
0.0003084	0.0382993	84.5569284
0.0003035	0.0379957	84.6802986
0.0002988	0.0376970	84.8017133
0.0002941	0.0374029	84.9212185
0.0002895	0.0371133	85.0388591
0.0002851	0.0368282	85.1546783
0.0002808	0.0365475	85.2687181
0.0002765	0.0362709	85.3810192
0.0002724	0.0359986	85.4916210
0.0002683	0.0357303	85.6005618
0.0002643	0.0354660	85.7078788
0.0002604	0.0352055	85.8136079
0.0002566	0.0349489	85.9177843
0.0002529	0.0346960	86.0204418
0.0002493	0.0344467	86.1216134
0.0002457	0.0342009	86.2213311
0.0002423	0.0339587	86.3196262
0.0002388	0.0337198	86.4165286
0.0002355	0.0334843	86.5120680
0.0002322	0.0332521	86.6062728
0.0002290	0.0330230	86.6991708
0.0002259	0.0327971	86.7907890
0.0002228	0.0325743	86.8811537
0.0002198	0.0323544	86.9702904
0.0002169	0.0321376	87.0582240
0.0002140	0.0319236	87.1449787
0.0002112	0.0317124	87.2305780
0.0002084	0.0315040	87.3150449
0.0002057	0.0312983	87.3984016
0.0002030	0.0310955	87.4806700
0.0002004	0.0308949	87.5618712
0.0001978	0.0306971	87.6420258
0.0001953	0.0305018	87.7211540
0.0001928	0.0303090	87.7992752
0.0001904	0.0301186	87.8764088
0.0001880	0.0299305	87.9525731
0.0001857	0.0297448	88.0277865
0.0001834	0.0295614	88.1020665
0.0001812	0.0293803	88.1754305
0.0001790	0.0292013	88.2478954
0.0001768	0.0290245	88.3194774
0.0001747	0.0288499	88.3901927
0.0001726	0.0286773	88.4600570
0.0001705	0.0285068	88.5290854
0.0001685	0.0283383	88.5972929
0.0001665	0.0281717	88.6646941
0.0001646	0.0280072	88.7313031
0.0001627	0.0278445	88.7971339
0.0001608	0.0276837	88.8622000
0.0001589	0.0275248	88.9265146
0.0001571	0.0273676	88.9900908
0.0001553	0.0272123	89.0529411
0.0001536	0.0270587	89.1150779

APPENDIX V. continued

0.0001519	0.0269069	89.1765133
0.0001502	0.0267567	89.2372591
0.0001485	0.0266082	89.2973269
0.0001469	0.0264613	89.3567279
0.0001453	0.0263161	89.4154731
0.0001437	0.0261724	89.4735735
0.0001421	0.0260303	89.5310394
0.0001406	0.0258897	89.5878814
0.0001391	0.0257507	89.6441094
0.0001376	0.0256131	89.6997334
0.0001361	0.0254770	89.7547630
0.0001347	0.0253423	89.8092078
0.0001333	0.0252091	89.8630770
0.0001319	0.0250772	89.9163796
0.0001305	0.0249467	89.9691247
0.0001291	0.0248176	90.0213208

APPENDIX VI. The computer programme used to calculate the P values of eight sets of  
crystallographic planes

```
LIST (LP)  
PROGRAM (FXYX)  
INPUT 1 = CR0  
INPUT 3 = IP0  
INPUT 5 = CR1  
OUTPUT 2 = IP0  
OUTPUT 4 = IP1  
COMPACT  
END
```

```
MASTER INVPGLEFIGST  
INTEGER TYPE,X,Y  
COMMON CURVE(2,20), M,N
```

```
DEPARTMENT OF METALLURGY, UNIVERSITY OF ASTON IN BIRMINGHAM  
THIS PROGRAM CALCULATES LINE INTENSITY RATIOS FROM A SERIES OF  
STRINGS OF PULSE COUNTS. IT ALLOWS FOR BACKGROUND AND ALSO  
TESTS FOR ERRORS IN THE DATA.  
DATA IS INPUT AS A SERIES OF INTEGER NUMBERS. EACH CURVE IS  
TERMINATED WITH A NEGATIVE INTEGER. EACH SERIES OF CURVES(SAMPLE  
AND RANDOM) IS TERMINATED WITH AN ADDITIONAL NEGATIVE INTEGER.  
FINALLY, THE WHOLE RUN IS TERMINATED WITH YET ANOTHER NEGATIVE  
INTEGER.
```

```
51 TYPE=1  
M=0  
SIGMA=0  
52 M=M+1  
70 READ(3,200)X  
200 FORMAT(13X,16)
```

APPENDIX VI. continued

```

IF(X)53,70,54
54 CURVE(TYPE,M)=TOTAL(X,TYPE )
WRITE(2,500)M
500 FORMAT(12)
GO TO 52
53 IF(TYPE-1)55,55,56
55 MA=M
TYPE=2
M=0
GO TO 52
56 IF(M.EQ.MA)GO TO 57
WRITE(2,151)
151 FORMAT(/56H THERE ARE DIFFERENT NUMBERS OF SAMPLE AND RANDOM CURVE
15)
GO TO 60
57 MA=MA-1
SIGMA=0
DO 58 M=1,MA
CURVE(1,M)=CURVE(1,M)/CURVE(2,M)
IF(N.F0.5000)GO TO 60
58 SIGMA=SIGMA+CURVE(1,M)
SIGMA=SIGMA/MA
WRITE(2,152)
152 FORMAT(//////40H LINE NUMBER RANDOM VALUE P,VALUE/)
DO 59 M=1,MA
CURVE(2,M)=CURVE(1,M)/SIGMA
59 WRITE(2,153)M,CURVE(1,M),CURVE(2,M)
153 FORMAT(/16,F16.4,F17.4)
READ(3,200)Y
IF(X)60,61,61
61 TYPE=1
M=1
SIGMA=0
GO TO 54
60 STOP
END

```

APPENDIX VI. continued

```

FUNCTION TOTAL(Y,TYPE )
DIMENSION X(1000),CURVE(2,20)
COMMON CURVE ,M,N
REAL MEAN
INTEGER Y,TYPE,ADD,TOP,ROT,X

C
C FUNCTION TO TEST AND TOTAL POINTS FROM TAPE PRODUCED BY X-RAY SCAN
C

XSQ=0
ADD=0
SIGSTART=0
SIGEND=0
N=2

SUMX=Y
X(1)=Y
1 LAST=X(N-1)
30 READ(3,201)X(N)
201 FORMAT(13X,16)
IF(X(N))2,30,3
3 IF(ABS(X(N)-LAST)-6000)4,5,5
5 IF(TYPE-1)6,6,7
6 WRITE(2,101)M, LAST, X(N)
101 FORMAT(/20H SAMPLE CURVE NUMBER,12,20H HAS ADJACENT VALUES,15,4H A
1ND,15)
GO TO 4
7 WRITE(2,102)M, LAST, X(N)
102 FORMAT(/20H RANDOM CURVE NUMBER,12,20H HAS ADJACENT VALUES,15,4H A
1ND,15)
4 SUMX=SUMX+X(N)
N=N+1
GO TO 1
2 DO 9 J=1,20
SIGSTART=SIGSTART+X(J)

```

APPENDIX VI. continued

```

9     XSQ=YSQ+FLOAT(Y(J))*FLOAT(X(J))
      N=N-1
      DO 10 J=21,24
10     ADD=ADD+Y(J)
      IF((0.25*ADD-0.05*SIGSTART)-0.318*SQRT(XSQ-0.05*SIGSTART*
1SIGSTART))11,11,12
12 IF(TYPE-1)13,13,14
13 WRITE(2,103)M
103 FORMAT(/20H SAMPLE CURVE NUMBER,12,60H APPEARS TO HAVE TOO LITTLE
1BACKGROUND SCAN AT THE BEGINNING)
      GO TO 11
14 WRITE(2,104)M
104 FORMAT(/20H RANDOM CURVE NUMBER,12,60H APPEARS TO HAVE TOO LITTLE
1BACKGROUND SCAN AT THE BEGINNING)
11 XSQ=0
      ADD=0
      DO 16 J=N-19,N
      SIGEND=SIGEND+X(J)
16     XSQ=YSQ+FLOAT(X(J))*FLOAT(X(J))
      DO 17 J=N-23,N-20
      ADD=ADD+Y(J)
      IF((0.25*ADD-0.05*SIGEND)-0.318*SQRT(XSQ-0.05*SIGEND*SIGEND))
118,18,17
17 IF(TYPE-1)19,19,20
19 WRITE(2,105)M
105 FORMAT(/20H SAMPLE CURVE NUMBER,12,54H APPEARS TO HAVE TOO LITTLE
1BACKGROUND SCAN AT THE END)
      GO TO 18
20 WRITE(2,106)M
106 FORMAT(/20H RANDOM CURVE NUMBER,12,54H APPEARS TO HAVE TOO LITTLE
1BACKGROUND SCAN AT THE END)
18 CONTINUE
22 TOTAL=SUMX-(SIGSTART+SIGEND)*0.125*N
      RETURN
      END

```

## REFERENCES

1. R.L.Whitely, D.E.Wise and D.J. Blickwede, *Steet Metal Industries* 1961, 38, 349.
2. B.N.Hellewell, T.Ll.Richards, *Metals Technology*, 1974, 1, 265.
3. F.A.Crane and J.M.Alexander, *J.Ins.Metals*, 1963/4, 92, 382.
4. I.L.Dillamore and W.T.Roberts, *J.Ins.Metals*, 1963/4, 92, 193.
5. G.E.Tucker, *Acta Met.*, 1964, 12, 1094.
6. R.A.Vandermeer and J.C.Ogle, *Trans.Met.Soc.AIME*, 1969, 245, 1511.
7. D.E.Yeomans and T.Ll.Richards, *Acta Cryst.* 1954, 7, 663.
8. R.V.Mises, *Z.Angew.Math.Mech.* 1928, 8, 161.
9. G.I.Taylor, *J.Ins.Metals*, 1938, 62, 307.
10. J.F.W.Bishop and R.Hill, *Phil.Mag.* 1951, 42, 414 and 1953, 44, 51.
11. W.Boas and E.Schmid, *Z.Tech.Physics*, 1931, 12, 71.
12. M.R.Pickus and E.H.Mathewson, *J.Ins.Metals*, 1939, 54, 237.
13. E.Schmid and W.Boas, *Plasticity of Crystals*, F.A.Hughes and Co.Ltd. London. 1950, 60 and 105.
14. G.I.Taylor and J.W.Christian, *Phil.Mag.* 1967, 15, 893.
15. E.A.Calnan and C.J.B.Clews, *Phil.Mag.* 1951, 42, 616.
16. I.L.Dillamore and W.T.Roberts, *Acta Met.*, 1964, 12, 281.
17. L.Clareborough and M.E.Hargreaves, *Prog.Metal Phys.* 1958, 8, 1.
18. G.E.G.Tucker, *Acta Met.*, 1964, 12, 1094.
19. I.L.Dillamore, C.J.E.Smith and T.W.Watson, *Met.Sci.J.* 1967, 1, 49.
20. I.L.Dillamore and W.B. Hutchinson, *Proc.I.C.S.T.I.S., Suppl. Trans. I.S.I.J.*, 1971, 11, 877.
21. M.Hillert, *Acta Met.* 1965, 13, 227.

22. R.S.Burns and R.H.Heyer, Sheet Metal Ind., 1958, 35, 261.
23. W.F.Hosford and W.A.Backofen, 9th Sagamore ~~ordance~~ of Material Research Conf., 1962, 28 - 31 Aug.
24. M.Fukuda, Trans.Jap. I.S.I., 1968, 8, 68.
25. S.Nagashima, H.Takechi and H.Kato, Texture in Research and Practice, Proc. ~~Claustal~~ Zellerfeld Symposium, 1968, Oct 2-5.
26. P.N.Richards and K.Ormay, Trans.Met.Soc.A.I.M.E., 1969, 245, 715.
27. T.M.Thomson and J.M.Baker, <sup>J. Aust. I. M.</sup> J. Ins. I. M., 1969, 14, 84.
28. R.Hill, Mathematical Theory of Plasticity, Oxford Univ. press, London, 1950, 315.
29. R.L.Whiteley, Trans.A.S.M., 1960, 52, 154.
30. L.W.Hu, J.App.Mechanics, 1956, 23, 444.
31. J.Willis, Deep Drawing, Butterworth Publication Ltd., London, 1954, 28.
32. D.H.Lloyd, Sheet Metal Ind., 1962, 39, 82.
33. J.C.Wright, Sheet Metal Ind., 1962, 39, 887.
34. I.Lilet, Sheet Metal Ind., 1966, 43, 949.
35. M.Atkinson and I.M.Maclean, I.D.D.R.G. Colloquium, London, 1964.
36. H.G.Rosenstock, H.F.Kläner and E.Schmidtman, Archiv fur das Eisenhüttenwesen, 1962, 33, 281.
37. J.E.Angele and W.F.McGarity, Trans.Amer.Soc.Mech.Eng. 1937, 5, 433.
38. H.Hoff and G.Masing, Stahl und Eisenhüttenwesen, 1956, 76, 1442.
39. S.D.Bhole, W.T.Roberts and D.V.Wilson, I.S.I./I.O.M.Meeting, 1973, Nov. 14 - 15. Met. Sci., 1974, 8, 277.
40. P.N.Richards and M.K.Ormay, J.Iron and Steel Ins., 1969, 239, 1857.
41. S.Nagashima, H.Takechi and H.Kato, Trans.Met.Soc.A.I.M.E., 1968, 242, 56.

42. A.Jones and B.Walker, ~~I.S.I./I.O.M. Meeting~~, <sup>Metals Technology</sup>, 1973, Nov.14 - 15.
43. P.N.Richards, J.Iron & Steel Ins., 1969, 207, 1333.
44. C.S.Barrett, Structure of Metals, McGraw Hill, N.Y. (2nd Edition).
45. G.Pomey and C.Crussard, Rev.Met., 1955, 52, 401.
46. F.Haessner and H.Weik, Arch. Eisenhuttenwesen, 1956, 27, 153.
47. J.Pugh and W.R.Wibbard, Trans.Am.Soc.Metals, 1956, 48, 526.
48. E.A.Calnan and C.J.B.Clews, Phil.Mag. 1950, 41, 1085.
49. L.R.Underwood, The Rolling of Metals, Chapman and Hall, London, 1958.
50. J.F.Held Trans.Met.Soc.A.I.M.E., 1967, 239, 573.
51. C.A.Stickels, Trans.Met.Soc.A.I.M.E., 1967, 239, 1857.
52. R.O.Williams, Trans.Met.Soc.A.I.M.E., 1962, 224, 129.
53. W.A.Backofen and B.B.Hundy, Trans.Met.Soc.A.I.M.E., 1953, 197, 61.
54. H.Möller and H.Stablein, Arch. Eisenhuttenwesen, 1958, 29, 377
55. J.Bennewitz, Arch. Eisenhuttenwesen, 1962, 33, 393.
56. S.Nagashima, H.Takechi and H.Kato, Texture in Research and  
Practice, Proc.Clausthal Zellerfeld Sym. 1968, Oct. 2 - 5.
57. I.L.Dillamore and W.T.Roberts, Metallurgical Review, 1965, 10, 39.
58. R.Whitely and D.Wise, 4th Mech.Working Conf. A.I.M.E., Chigaco,  
1962, Jan.
59. M.Atkinson, P.G.Brooks, A.O'Connor and T.G.Philips, Sheet Metal  
Ind., 1963, 40, 57.
60. R.F.Dewsnap, I.S.I. Special Report, 1963, 79, 112.
61. B.A.Kuznetsov, Metalloved. Term obra.Met. 1958, 2, 28.
62. J.D.Keller, A.I.S.E.Convention, Buffalo, N.Y., 1958, Apr.
63. A.F.Mohri, A.I.S.I. Convention, N.Y., 1956, May 23.
64. S.Garber, J.Iron and Steel Ins., 1962, 200, 460.
65. C.A.Stickels, Trans.Met.Soc. A.I.M.E., 1965, 233, 1550.

66. K.Saxl, Proc.Ins.Mech.Eng., 1964/5, 179.
67. W.T.Lankford, S.C.Snyder and J.A.Bauscher, Trans.Am.Soc.Metals, 1950, 42, 1197.
68. L. Schultz.App.Phys., 1949, 20, 1030.
69. G.B.Harris, Phil.Mag. 43, 113.
70. G.Kurdjumov and S.Sachs, Z.Phys., 1930, 64, 325.
71. M.Gensamer and P.A.Vukmanic, Trans.Met.Soc. A.I.M.E.,1937, 125, 507.
72. T.R.Thomson and J.M.Baker, J.Aus.I.M., 1969, 14, 84.
73. T.J.Lewis, The University of Aston in Birmingham, Ph.D.Thesis,1971.
74. R.J.Bentz and W.L.Roberts, Iron and Steel Eng., 1964, March, 101.
75. E.D.Orowan, Proc.Inst.Mech.Eng., 1943, 50, 140.
76. P.S.Mathur and W.A.Backofen, Met.Trans.1973, 4, 643.
77. J.T.Norton, J.Appl.Phys., 1948, 19, 1176.
78. M.Field and M.E.Merchant, J.Appl.Phys. 1949, 20, 741.
79. J.R.Holland, N.Engler and W.Powers, Editor W.Mueller, Advances in X ray Analysis, 1960, 4, 74.
80. J.J.Klappholz, S.Waxmann and C.Feno, Advances in X ray Analysis, 1972, 15, 365.
81. H.J.Bunge and W.T.Roberts, J.App.Crystallography, 1969, 2, 116.
82. L.K.Jetter, C.McHargue and R.O.Williams, J.Appl.Phys. 1956, 27,368.
83. R.O. Williams, A.I.M.E. Trans, 1968, 242, 105.
84. C.Feng, Advances in X ray Analysis, 1972, 15, 489.
85. B.N.Hellewell, Ph.D.Thesis, The University of Aston in Birmingham, 1971.
86. R.J.Benz and W.L.Roberts, Iron & Steel Eng., 1964, March, 101.

87. J.F.Held, Mechanical Working and Steel Processing IV, A.I.M.E. Conference, 1966, p.3.
88. F.A.Witt and W.L.Roberts, 5th Annual Conf. of the Mech.Working Committee, Iron and Steel Div. A.I.M.E., 1963, Jun.
89. W.C.F.Hessenburg and R.B.Smith, J.Iron and Steel Inst., 1951, June.
90. J.H.Hollomon and C.Zener, J.App.Physics, 1944, 15, 22.
91. M.H.Mueller, W.P.Chernock and P.A.Beck, Trans. of the Metallurgical Society of A.I.M.E., 1958, Feb., 39.
92. I.L.Dillamore and H.Katoh, Metal Science, 1974, 8, 73.

## ACKNOWLEDGEMENTS

The author would like to express his gratitude to the late Dr. T.Ll. Richards and Mr. D. Green for the encouragement and advice received during the present investigation.

Dr. W.T. Roberts has been especially helpful by his supervision during the preparation of the final manuscript and his help is greatly appreciated.

The guidance and discussion of Professor I.L. Dillamore and Professor J.T. Barnby are also acknowledged.

My thanks also to Mrs. G.M. Gado and Mr. H.J. Hyde for their help during the preparation of this thesis.